ADVANCEMENTS IN MOLECULAR DIAGNOSIS AND TREATMENT OF MELANOMA

EDITED BY: Giuseppe Palmieri, Paolo Antonio Ascierto, Daniela Massi and Igor Puzanov

PUBLISHED IN: Frontiers in Oncology

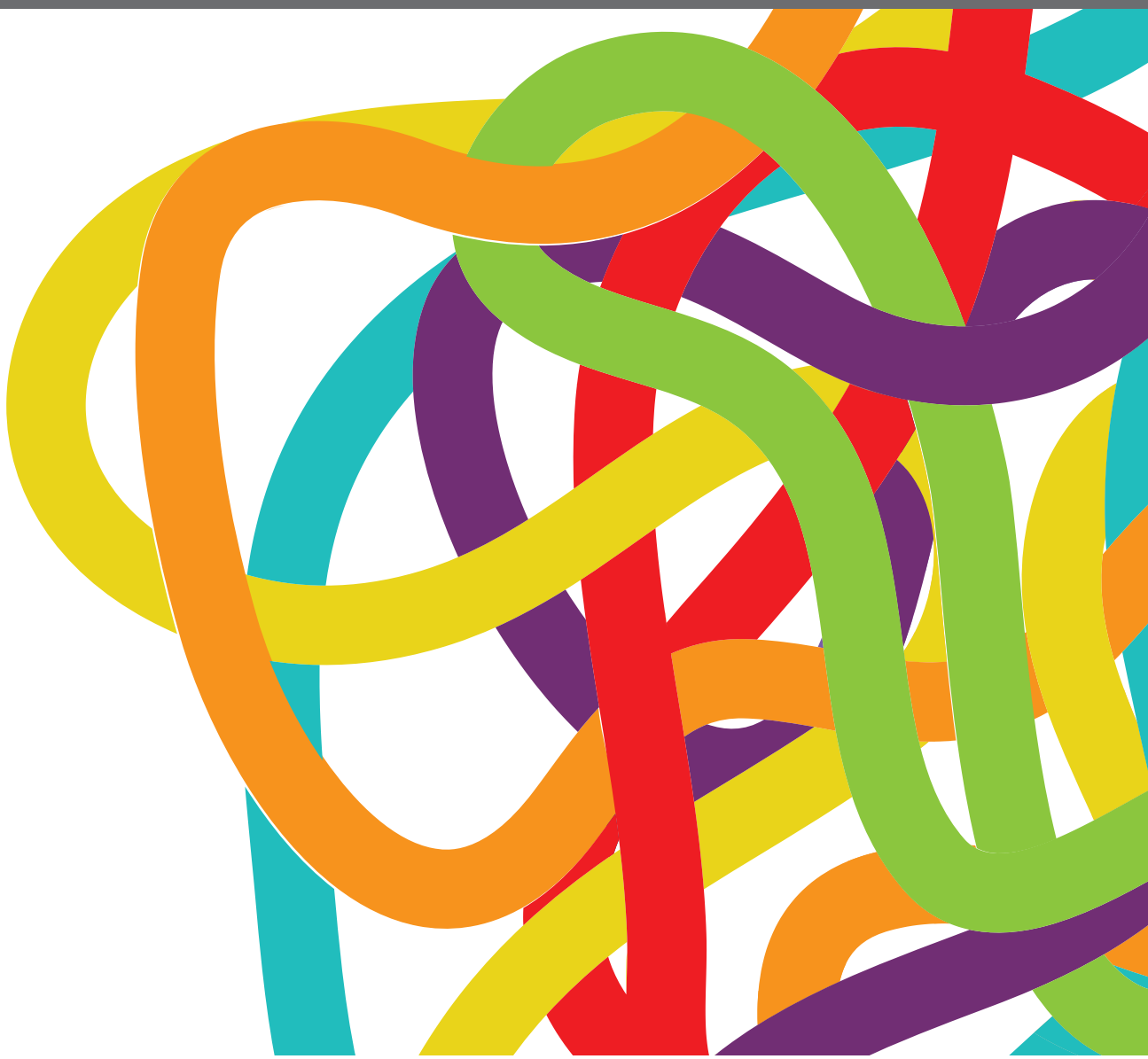

frontiers Research Topics

frontiers

ISSN 1664-8714
ISBN 978-2-88971-298-4
DOI 10.3389/978-2-88971-298-4

About Frontiers

Frontiers is more than just an open-access publisher of scholarly articles: it is a pioneering approach to the world of academia, radically improving the way scholarly research is managed. The grand vision of Frontiers is a world where all people have an equal opportunity to seek, share and generate knowledge. Frontiers provides immediate and permanent online open access to all its publications, but this alone is not enough to realize our grand goals.

Frontiers Journal Series

The Frontiers Journal Series is a multi-tier and interdisciplinary set of open-access, online journals, promising a paradigm shift from the current review, selection and dissemination processes in academic publishing. All Frontiers journals are driven by researchers for researchers; therefore, they constitute a service to the scholarly community. At the same time, the Frontiers Journal Series operates on a revolutionary invention, the tiered publishing system, initially addressing specific communities of scholars, and gradually climbing up to broader public understanding, thus serving the interests of the lay society, too.

Dedication to Quality

Each Frontiers article is a landmark of the highest quality, thanks to genuinely collaborative interactions between authors and review editors, who include some of the world's best academicians. Research must be certified by peers before entering a stream of knowledge that may eventually reach the public - and shape society; therefore, Frontiers only applies the most rigorous and unbiased reviews.
Frontiers revolutionizes research publishing by freely delivering the most outstanding research, evaluated with no bias from both the academic and social point of view. By applying the most advanced information technologies, Frontiers is catapulting scholarly publishing into a new generation.

What are Frontiers Research Topics?

Frontiers Research Topics are very popular trademarks of the Frontiers Journals Series: they are collections of at least ten articles, all centered on a particular subject. With their unique mix of varied contributions from Original Research to Review Articles, Frontiers Research Topics unify the most influential researchers, the latest key findings and historical advances in a hot research area! Find out more on how to host your own Frontiers Research Topic or contribute to one as an author by contacting the Frontiers Editorial Office: frontiersin.org/about/contact

ADVANCEMENTS IN MOLECULAR DIAGNOSIS AND TREATMENT OF MELANOMA

Topic Editors:
Giuseppe Palmieri, University of Sassari, Italy
Paolo Antonio Ascierto, Istituto Nazionale dei Tumori (IRCCS), Italy
Daniela Massi, University of Florence, Italy
Igor Puzanov, University at Buffalo, United States

Citation: Palmieri, G., Ascierto, P. A., Massi, D., Puzanov, I., eds. (2021). Advancements in Molecular Diagnosis and Treatment of Melanoma. Lausanne: Frontiers Media SA. doi: 10.3389/978-2-88971-298-4

Table of Contents

frontiers in Oncology

EDITORIAL
published: 09 July 2021
doi: 10.3389/fonc.2021.728113

Editorial: Advancements in Molecular Diagnosis and Treatment of Melanoma

Giuseppe Palmieri[1]*, *Igor Puzanov*[2], *Daniela Massi*[3] and *Paolo Antonio Ascierto*[4]

[1] University of Sassari & Unit of Cancer Genetics, National Research Council (CNR), Sassari, Italy, [2] Roswell Park Comprehensive Cancer Center, University of Buffalo, Buffalo, NY, United States, [3] Section of Pathology, Department of Health Sciences, University of Florence, Florence, Italy, [4] Melanoma, Cancer Immunotherapy and Development Therapeutics Unit, Istituto Nazionale Tumori Fondazione G. Pascale, Naples, Italy

Keywords: melanoma, molecular diagnosis, cancer progression, targeted therapy, immunotherapy

Editorial on the Research Topic

Advancements in Molecular Diagnosis and Treatment of Melanoma

OPEN ACCESS

Edited and Reviewed by:
Vladimir Spiegelman, Penn State Milton S. Hershey Medical Center, United States

***Correspondence:**
Giuseppe Palmieri
gpalmieri@yahoo.com
orcid.org/0000-0002-4350-2276

Specialty section:
This article was submitted to Skin Cancer, a section of the journal Frontiers in Oncology

Received: *20 June 2021*
Accepted: *28 June 2021*
Published: *09 July 2021*

Citation:
Palmieri G, Puzanov I, Massi D and Ascierto PA (2021) Editorial: Advancements in Molecular Diagnosis and Treatment of Melanoma. Front. Oncol. 11:728113. doi: 10.3389/fonc.2021.728113

Melanoma is characterized by a marked molecular heterogeneity, considerably greater than that highlighted so far from the histopathological and clinical points of view only. The development and progression of melanoma, like almost all other forms of malignant neoplasms, is based on the acquisition of sequential alterations in specific gene pathways or metabolic/molecular mechanisms involved in the regulation of cell functions (1, 2).

The role of genetic and epigenetic alterations in the onset and progression of tumors is being steadily established. Intracellular alterations occurring in molecular pathways have been found to even concur in interfering with the homeostasis of the tumor microenvironment (TME). As consequence, a tight interaction between intracellular changes and various extracellular factors participating in immune activity against the tumor is strongly involved in modulating neoplastic progression. One can summarize that cancer cells develop and progress under the pressure of an articulated network of intra- and extracellular growth stimuli.

In this complex scenario, several TME elements are progressively taking the stage: immune cells (including, in addition to the main effectors such as CD8+/CD4+ T lymphocytes and natural killer cells, a whole system of cells with regulatory and immunosuppressive activity), endothelial cells and vascular changes aimed at increasing angiogenesis, fibroblasts, components of the extracellular matrix (including those involved in epithelial-mesenchymal transition and/or stroma remodeling), and a variety of soluble molecules (such as growth factors, chemotactic factors, cytokines, etc.). On this latter aspect, several conditions may tip the scales in favor of an immunosuppressive or an immune reactive status. Here is a tentative list of examples of such conditions: altered levels of VEGF, interleukins, immune checkpoint effectors, cyto/chemokines, or enzymes such as IDO and arginase; variation of the TME concentration of immunosuppressive cells such as myeloid-derived suppressor cell/MDSC, tumor-associated macrophage/TAM, or regulatory T cell/Treg; unbalanced distribution of dendritic/mature dendritic cells (3). Overall, these elements form a complex

regulatory network that favors tumor growth by creating an environment that allows tumor cells to evade immune surveillance.

Among the events intrinsic to the cells, some molecular alterations may be able to profoundly affect the tumor sensitivity to T lymphocyte activity and, more in general, the capability of exerting an antitumor immune reaction. Again, here is an indicative and not fully comprehensive list of such molecular changes: silencing of PTEN, MAPK activation, enhanced PI3K activity, activated WNT/β-catenin signaling, JAK1/2 inactivating mutations, STAT1-3/STING/TBK1 signaling impairment, increased rates of chromosomal instability or aneuploidy, modifications in antigen/neoantigen presentation (3).

During the last decade, a real revolution has been registered for both management and treatment of melanoma. Before 2010, only one fourth of patients with metastatic disease were alive at 1 year (4). Current therapeutic strategies allowed the achievement of outstanding results represented by high response rates and prolonged disease control; to date, about half of patients with advanced melanoma is indeed alive at 5 years (5). Predominantly, therapeutic strategies that have contributed in recent years to change the outcome of melanoma patients with subsequent significant impact on long-term benefit include either a selective blocking of the BRAF-driven signal transduction (BRAF mutant inhibitors—vemurafenib, dabrafenib, encorafenib—given in combination with MEK inhibitors—cobimetinib, trametinib, binimetinib) either the immune checkpoint blockade therapy (targeting CTLA-4—ipilimumab—and the PD-1/PD-L1 axis—nivolumab, pembrolizumab). Moreover, the continuously improved experience of clinicians in managing sequence or combination of the above mentioned therapies as well as in appropriately integrating systemic treatments with specific loco-regional interventions (i.e. radiotherapy, metastasectomy, electrochemotherapy, etc.) significantly increased the chances of prolonged survival in ever larger groups of melanoma patients (5).

Unfortunately, the failure of the disease control into the remaining half of melanoma patients, who thus progress to death in the same time period, represents the disappointing other side of the coin. In this regard, several studies are ongoing in order to either investigate new treatment protocols either optimize the strategies for the best use of the currently available drugs. Trials are being conducted for defining the most effective sequence of targeted and immune checkpoint therapy in *BRAF*-mutated melanoma patients - also trying to clarify whether translational studies may be helpful in selecting distinct subsets of responders and non responders - as well as for determining the most appropriate regimens to be used after progression to the first-line treatments (6). Continuous efforts to strengthen the integration of surgical and medical interventions are likely to be the key in improving long-term outcomes in patients with melanoma.

The Research Topic "Advancements in molecular diagnosis and treatment of melanoma" provides an overview of the main strategic approaches aimed at improving the clinical benefits for the different patients' subsets, by including:

a. identification of additional molecular pathways and new available drugs, also considering preclinical and clinical data available for several targets under development (7). This will pave the way for further investigations on modalities of combining them with existing targeted or immune therapies as well as on evaluation of the safety and tolerability of such combination or sequential therapies;
b. development of methods capable of predicting patient response or resistance to different systemic treatment options (mostly, immunotherapy) by mainly providing circulating tumor-derived elements as non-invasive biomarkers (so-called "liquid biopsy"). In this sense, a clinical practice change into the management of melanoma patients would be represented by a "dynamic" characterization of the (epi)genetic and molecular signatures, to be assessed not only at baseline but also during the course of treatment or follow-up. In other words, the aim should be to monitor any biological variation of the disease behavior depending on intrinsic and acquired tumor heterogeneity (8);
c. assessment of the right time for therapy administration, when treatments may exert their maximal clinical benefit in terms of rates of patients alive with no evidence of disease (adjuvant and neoadjuvant approaches);
d. identification and translation into the clinical practice of deeper mutational profiling driven by new artificial intelligence tools (i.e. digitalization of tissue slides for recognizing all melanoma features to standardize diagnoses or better classify tumor microenvironment components as well as use of faster software for interpretation of multi-parametric data and development of bioinformatic algorithms). This would more accurately weight the specific contribution of any molecular feature to the disease behavior, in a patient-matched way;
e. methodological improvement of single-cell testing and multiplexed immunohistochemical or transcriptional assays for a more detailed evaluation of the functional roles of the genes associated with melanoma, toward a better understanding of their prognostic and/or predictive significance.

AUTHOR CONTRIBUTIONS

GP wrote the Editorial. IP, DM, and PAA helped in discussing the content. All authors contributed to the article and approved the submitted version.

FUNDING

We thank the Fondazione AIRC "Programma di ricerca 5 per Mille 2018-ID#21073" for partially funding this work.

REFERENCES

1. The Cancer Genome Atlas Network. Genomic Classification of Cutaneous Melanoma. *Cell* (2015) 161(7):1681–96. doi: 10.1016/j.cell.2015.05.044
2. Palmieri G, Colombino M, Casula M, Manca A, Mandalà M, Cossu A. Italian Melanoma Intergroup (IMI). Molecular Pathways in Melanomagenesis: What We Learned From Next-Generation Sequencing Approaches. *Curr Oncol Rep* (2018) 20(11):86. doi: 10.1007/s11912-018-0733-7
3. Ascierto PA, Agarwala SS, Botti G, Budillon A, Davies MA, Dummer R, et al. Perspectives in Melanoma: Meeting Report From the Melanoma Bridge (November 29th-1 December 1st, 2018, Naples, Italy). *J Transl Med* (2019) 17(1):234. doi: 10.1186/s12967-019-1979-z
4. Korn EL, Liu PY, Lee SJ, Chapman JA, Niedzwiecki D, Suman VJ, et al. Meta-Analysis of Phase II Cooperative Group Trials in Metastatic Stage IV Melanoma to Determine Progression-Free and Overall Survival Benchmarks for Future Phase II Trials. *J Clin Oncol* (2008) 26(4):527–34. doi: 10.1200/JCO.2007.12.7837
5. Curti BD, Faries MB. Recent Advances in the Treatment of Melanoma. *N Engl J Med* (2021) 384(23):2229–40. doi: 10.1056/NEJMra2034861
6. *ClinicalTrials.gov of the U.S. National Library of Medicine, National Institute of Health (NIH) in Bethesda*. Available at: https://clinicaltrials.gov/.
7. Coricovac D, Dehelean C, Moaca EA, Pinzaru I, Bratu T, Navolan D, et al. Cutaneous Melanoma - A Long Road From Experimental Models to Clinical Outcome: a Review. *Int J Mol Sci* (2018) 19(6):E1566. doi: 10.3390/ijms19061566
8. Palmieri G. Circulating Driver Gene Mutations: What is the Impact on Melanoma Patients' Management? *Ann Oncol* (2019) 30(5):669–71. doi: 10.1093/annonc/mdz090

Conflict of Interest: The authors declare that the research was conducted in the absence of any commercial or financial relationships that could be construed as a potential conflict of interest.

frontiers in Oncology

ORIGINAL RESEARCH
published: 20 August 2020
doi: 10.3389/fonc.2020.01559

Recognition of Cutaneous Melanoma on Digitized Histopathological Slides *via* Artificial Intelligence Algorithm

Francesco De Logu[1], Filippo Ugolini[2], Vincenza Maio[3], Sara Simi[2], Antonio Cossu[4], Daniela Massi[2], Italian Association for Cancer Research (AIRC) Study Group, Romina Nassini[1†] and Marco Laurino[5]*

[1] Section of Clinical Pharmacology and Oncology, Department of Health Sciences, University of Florence, Florence, Italy, [2] Section of Pathological Anatomy, Department of Health Sciences, University of Florence, Florence, Italy, [3] Histopathology and Molecular Diagnostics, Careggi University Hospital, Florence, Italy, [4] Department of Medical, Surgical, and Experimental Sciences, University of Sassari, Sassari, Italy, [5] Institute of Clinical Physiology, National Research Council, Pisa, Italy

OPEN ACCESS

Edited by:
Joshua Arbesman, Cleveland Clinic, United States

Reviewed by:
Ashley M. Holder, Houston Methodist Hospital, United States
Jacob Shreve, Cleveland Clinic, United States

***Correspondence:**
Romina Nassini
romina.nassini@unifi.it

†ORCID:
Romina Nassini
orcid.org/0000-0002-9223-8395

Specialty section:
This article was submitted to Skin Cancer, a section of the journal Frontiers in Oncology

Received: *23 May 2020*
Accepted: *20 July 2020*
Published: *20 August 2020*

Citation:
De Logu F, Ugolini F, Maio V, Simi S, Cossu A, Massi D, Italian Association for Cancer Research (AIRC) Study Group, Nassini R and Laurino M (2020) Recognition of Cutaneous Melanoma on Digitized Histopathological Slides via Artificial Intelligence Algorithm. Front. Oncol. 10:1559. doi: 10.3389/fonc.2020.01559

Increasing incidence of skin cancer combined with a shortage of dermatopathologists has increased the workload of pathology departments worldwide. In addition, the high intraobserver and interobserver variability in the assessment of melanocytic skin lesions can result in underestimated or overestimated diagnosis of melanoma. Thus, the development of new techniques for skin tumor diagnosis is essential to assist pathologists to standardize diagnoses and plan accurate patient treatment. Here, we describe the development of an artificial intelligence (AI) system that recognizes cutaneous melanoma from histopathological digitalized slides with clinically acceptable accuracy. Whole-slide digital images from 100 formalin-fixed paraffin-embedded primary cutaneous melanoma were used to train a convolutional neural network (CNN) based on a pretrained Inception-ResNet-v2 to accurately and automatically differentiate tumoral areas from healthy tissue. The CNN was trained by using 60 digital slides in which regions of interest (ROIs) of tumoral and healthy tissue were extracted by experienced dermatopathologists, while the other 40 slides were used as test datasets. A total of 1377 patches of healthy tissue and 2141 patches of melanoma were assessed in the training/validation set, while 791 patches of healthy tissue and 1122 patches of pathological tissue were evaluated in the test dataset. Considering the classification by expert dermatopathologists as reference, the trained deep net showed high accuracy (96.5%), sensitivity (95.7%), specificity (97.7%), F_1 score (96.5%), and a Cohen's kappa of 0.929. Our data show that a deep learning system can be trained to recognize melanoma samples, achieving accuracies comparable to experienced dermatopathologists. Such an approach can offer a valuable aid in improving diagnostic efficiency when expert consultation is not available, as well as reducing interobserver variability. Further studies in larger data sets are necessary to verify whether the deep learning algorithm allows subclassification of different melanoma subtypes.

Keywords: cutaneous melanoma, artificial intelligence, convolutional neural network, image analysis, diagnosis

Abbreviations: AI, artificial intelligence; CNNs, convolutional neural networks; FFPE, formalin fixed paraffin embedded; TIL, tumor infiltrating lymphocytes; WSIs, whole-slide images.

INTRODUCTION

Melanoma is one of the major causes of cancer-related death, and its incidence is increasing worldwide (1, 2). Histopathological diagnosis of melanoma is based on the assessment of cyto-architectural features on hematoxylin and eosin-stained slides, which has been recognized to be highly subjective. Recent observations have revealed a diagnostic discordance between histopathologists in distinguishing benign nevi and malignant melanomas (3, 4). A lack of access to dermatopathology expertise in this context can slow diagnostic turnaround times, resulting in delays in patient care and leading to potential adverse impacts on clinical outcomes. In this scenario, the computer-aided diagnosis (CAD) system reduces intraobserver and interobserver variability and improves the accuracy of pathology interpretation (5, 6).

In recent years, AI has attracted a lot of attention for digital imaging processing (7). The most commonly used and highly functioning AI approach for medical image processing (including histopathology) is based on deep learning algorithms and, in particular, on CNNs (8). CNNs are deep neural networks, trained for visual recognition tasks directly from pixel images with minimal preprocessing (9). CNNs require a considerable amount of data for training/validation, and the classification accuracy of CNN classifiers is mainly dependent on the quality and size of the image dataset (10). The training of a new CNN model with a new image dataset requires extensive effort to collect a large number of images. For this reason, a CNN architecture can be built from pretrained models (Transfer Learning approach) with a considerable reduction in the training image dataset (11). Several types of pretrained CNN architectures, including AlexNet, SqueezeNet, NASNet-Large, Inception-v3, ResNet-50, Vgg19, and Inception- ResNet-v2 (12–14), have been designed.

The deep learning applied to digital pathology is a continuing challenge for many reasons: (i) limited (labeled) dataset availability, (ii) complexity of pathological variability, (iii) large image sizes, and (iv) difficulty of implementation of CNN models due to a large number of setting parameters (15, 16).

In recent years, few studies that focus on deep learning algorithms have been proposed to automate the analysis of melanoma and skin lesions in WSIs (17–19). Since the sizes of WSIs are too large to be used as direct input to a CNN, the typical approach is to train, validate, and test the CNN, instead of using low-pixel-resolution patches of the WSI, obtaining tens to thousands of patches from each WSI (20). Although AI technology has achieved remarkable results for skin pathology analysis, in this field, the potential of CNNs has not been fully investigated, and their performances may be significantly improved. Future studies will focus on the development of different CNN architectures and training procedures, to finalize an optimal AI-based algorithm useful for clinical support.

In this study, we aimed to implement an annotation framework for the automated analysis of histopathological cutaneous melanoma images. We developed a CNN-based algorithm that allows us to build masks on scanned lesioned tissues, in order to define areas of healthy and pathological tissue, even in those samples for which identification by the pathologist is more complex due to the presence of a scarce tumoral component. Our data revealed a methodological approach to build a map reporting the topological distribution of melanoma and healthy tissues from analyzed WSIs.

MATERIALS AND METHODS

Sample Population and Data Set

The study included a retrospective collection of formalin-fixed paraffin-embedded (FFPE) cutaneous primary invasive melanomas (n = 100) from the Section of Pathology, Department of Health Sciences, University of Florence, Florence, Italy; the Center for Immuno-Oncology, Department of Oncology, University Hospital of Siena, Siena, Italy; and the Unit of Cancer Genetics, Institute of Biomolecular Chemistry (ICB), National Research Council (CNR), Sassari, Italy. Clinicopathological data of the patients are reported in **Table 1**. Two expert dermatopathologists (VM and DM) performed the histopathological reevaluation and confirmed the original diagnosis. Representative histopathological whole slides stained with hematoxylin and eosin were anonymized and digitalized using Pannoramic 250 Flash III (3D HISTECH) and Aperio AT2 (Leica) with × 20 power. From each scanned slide, a total of 8 ROIs (4 representatives of the tumor area and 4 of the adjacent healthy tissue) were extracted (**Figure 1**). The use of FFPE sections of human samples was approved by the Local Ethics Committee (#13676_bio and #17033_bio) according to the Helsinki Declaration.

AI Methodology

To adapt the data size of the input images to the CNN input layer size, smaller image patches were extracted from the labeled ROI. Each ROI was tiled in non-overlapping 299 × 299 pixel square patches (×20 magnification). The patch dimension of each pixel was about 0.2428 mm; therefore, the dimension of each patch was about 72.59 mm × 72.59 mm, corresponding to an area of about 5269.3 mm^2 (**Figure 2**). Patches were adjacent to each other and covered the entire tissue region of each ROI. Patches of the ROIs containing no more than 50% white background

TABLE 1 | Clinicopathological data of the patients.

Patients (n = 100)		
Age	Range (Mean ± SD)	24–89 (62.7 ±16.0)
Sex	Male (n)	62
	Female (n)	38
Location of primary tumor	Trunk (n)	56
	Extremity (n)	44
Tumor thickness	>2mm (n)	100
Clark's level	III (n)	47
	IV (n)	53
Ulceration	Present (n)	71
	Not present (n)	29
Stage	III (n)	47
	IV (n)	53
Mitotic rate/mm^2	Range	0–57

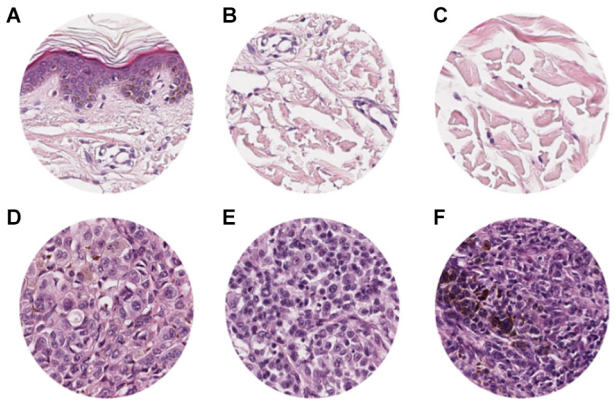

FIGURE 1 | ROI samples selected from healthy tissue **(A–C)** and invasive cutaneous melanoma **(D–F)** on a whole slide image. Each ROI was obtained at a magnification of 20×.

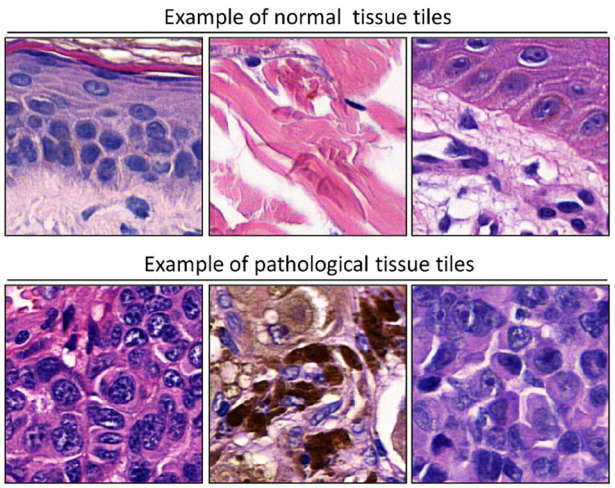

FIGURE 2 | Examples of patches cropped from ROIs. The first and second lines report sampled patches of normal and pathological tissues, respectively. Each patch has a size of 299 × 299 pixels (72.59 mm × 72.59 mm).

were used for further analysis. The patches obtained from ROIs of 60 slides (1377 patches for healthy tissue and 2141 patches for melanoma) were used as training/validation dataset; the patches from ROIs of 40 slides (791 for healthy tissue and 1122 patches for melanoma) were used as a test dataset. The training/validation and testing datasets were completely disjointed (i.e., extracted from different patients) in order to demonstrate the robustness of the trained CNN. The expansion of the image dataset for training and validation is useful for improving the capability of the model and to avoid overfitting. We augmented the training/validation dataset *via* affine transformations. The patches were horizontally or vertically shifted between 0 and 30 pixels and scaled by zoom-in and zoom-out operations with rate magnitude between 0 and 20%. The increased and original patches were used as training/validation sets.

A CNN based on a pretrained Inception-ResNet-v2 (12) with the training/validation dataset was trained by using 75% of the patches for training and 25% for validation. For training the net, stochastic gradient descent with momentum algorithm was used; the first 10 layers of the net were frozen, and for the residual layers, the learning rate was set to 0.003, and the momentum was set to 0.9. The maximum number of epochs for training was set to 15, and a mini-batch with 16 observations at each iteration was used. Then, the net performance with the test dataset was tested.

For binary (healthy tissue vs. melanoma) patch-level classification, the trained net performance was evaluated in terms of the following metrics:

1. Accuracy: the ratio between the number of correct predictions (both true positives and true negatives) and the overall number of samples.
2. Sensitivity (or recall): the number of true positives divided by the number of true positives and false negatives.
3. Specificity: the number of true negatives divided by the number of true negatives and false positives.
4. F_1 score: a measure of a classification accuracy often used in case of imbalanced data. This is the harmonic mean between precision and sensitivity. Precision is the number of true positives divided by the number of true positives and false positives.
5. Cohen's kappa: a measure of the agreement between the human and trained net classification (correcting for chance agreement). This is a statistical measure of inter-rater agreement. Kappa scores less than zero are interpreted as "no" agreement. Kappa scores ranging from 0.01 to 0.20 are considered "slight" agreement, 0.21 to 0.40 "fair" agreement, 0.41 to 0.60 "moderate" agreement, 0.61 to 0.80 "substantial" agreement, and 0.81 to 1.00 "almost perfect" agreement.

The trained net as a sliding window over the whole WSI was applied to evaluate the topological distribution of the melanoma and healthy tissue. A scheme of the methodological process, from raw WSI to trained CNN performance evaluation, is reported (**Figure 3**).

RESULTS

Training by using the curated image patches took approximately 18 h to complete 3200 iterations with Matlab software (R2019b, Natick, MA, United States: The MathWorks Inc.) and its Deep Learning Toolbox. As reported in the confusion matrix (**Figure 4**), the overall accuracy of our net in training set classification was 96.5% (1847 correct classification from a total of 1913). In particular, the misclassification rates were 2.3% for healthy tissue (18 patches of 791) and 4.3% for melanoma (48 patches of 1122). The obtained sensitivity, specificity, and F_1 score were 95.7, 97.7, and 97.0%, respectively, and Cohen's kappa was 0.929.

Misclassified patches were reviewed, and we found that, in 2/9 false-positive analyzed patches, signs of marked dermal solar elastosis (grade 3) (**Figure 5A**) and/or epidermal atrophy

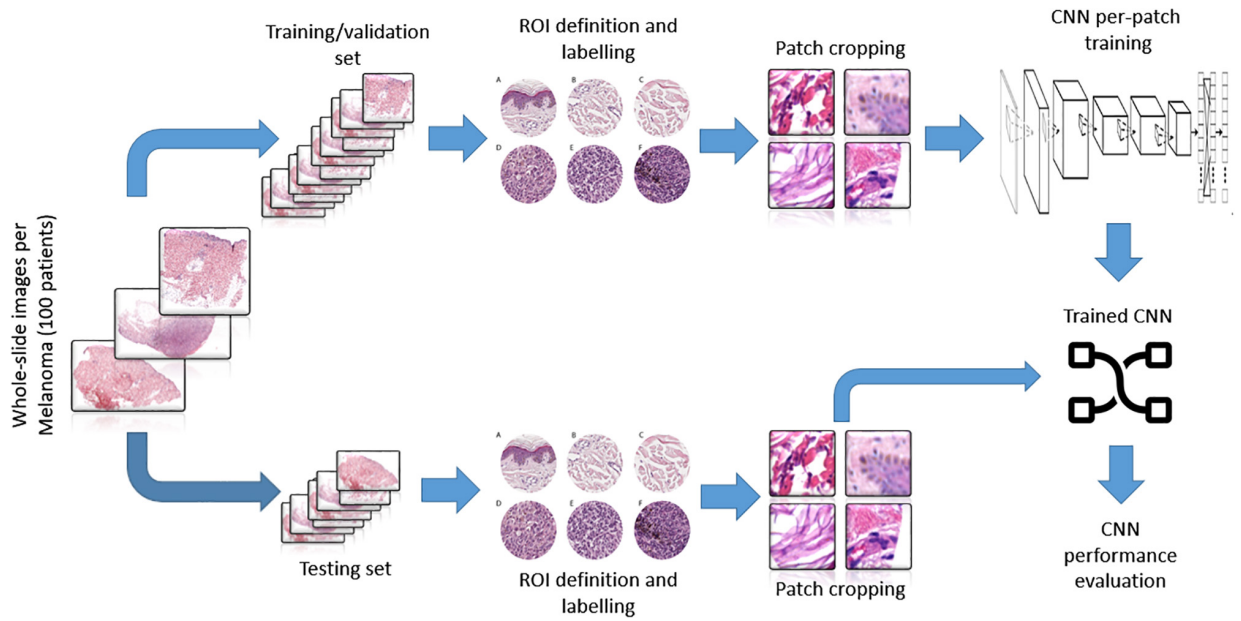

FIGURE 3 | Representative scheme of the methodological pipeline. The whole slide images of melanoma from 100 patients were split in training/validation and testing datasets that are disjointed during the process. ROIs of normal and pathological tissues were extracted from the two datasets and labeled. **(A–C)** Healthy tissue, **(D–F)** invasive cutaneous melanoma. Each ROI was tiled in 299 × 299 pixel patches. The patches of training/validation sets were used for the training of CNN. Finally, the performance indices of classification were estimated by applying the trained CNN to the testing set.

(**Figures 5A–C**) were observed. In the false-positive cases, the prevalence of dermal-based, instead of epidermal based or dermo-epidermal, patches was observed. In particular, in 3/9 of false-positive patches, an abnormal dilated small-to-medium-size vessel surrounded by normal dermal collagen was observed (**Figure 5D**). Extravasated erythrocytes in the dermis or within the adnexal epithelium were found in 3/9 cases (**Figures 5D,E**), and, in one case, normal sebaceous adnexal structures and follicular epithelium were detected (**Figure 5F**).

Histopathological reevaluation of the false-negative cases showed representative areas of pathological tissue with moderate-to-severe cytological atypia (melanoma cells) in all cases, with no significant areas of non-tumoral tissues. A known factor that negatively affects tumor classification by CNN is the presence of melanin (21); in our dataset, we observed that the level of pigmentation in false negatives was heterogeneous. In particular, it was absent in 5 cases (**Figure 6A**), mild in 8 cases (**Figures 6B–D**), and prominent (**Figure 6E**) in 18 cases, thus demonstrating that the trained neural network was not influenced by the presence or absence of melanin. Clear cell changes were detected in melanoma cells in two patches (**Figure 6F**). A more detailed analysis showed that, in 7/18 cases, tumor cells were arranged in large confluent aggregates (diffuse growth), with no nests. Tumor-infiltrating lymphocytes (TILs) were absent (16/18) or non-brisk (2/18), and none of the selected images showed a prominent (brisk) infiltration by TILs.

Finally, the classification maps obtained after the application of the trained net to five representative WSIs of invasive cutaneous melanoma were reported (**Figure 7**). The maps showed the topological distribution of patches of each WSI classified as healthy tissue (green area) or melanoma (red area).

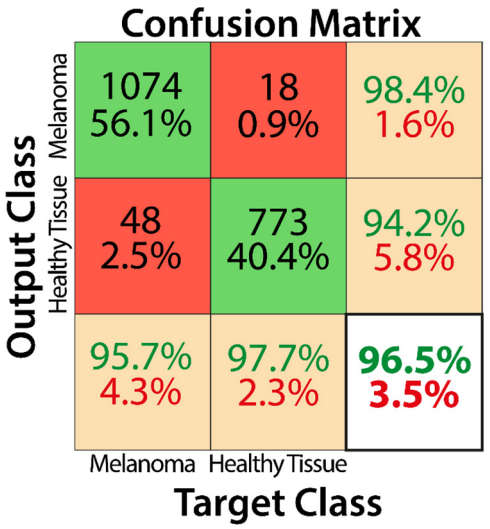

FIGURE 4 | Confusion matrix describing the classification performance of the trained CNN for the training dataset.

DISCUSSION

Since its development in the mid-twentieth century, research using AI has been subjected to transformation and criticism.

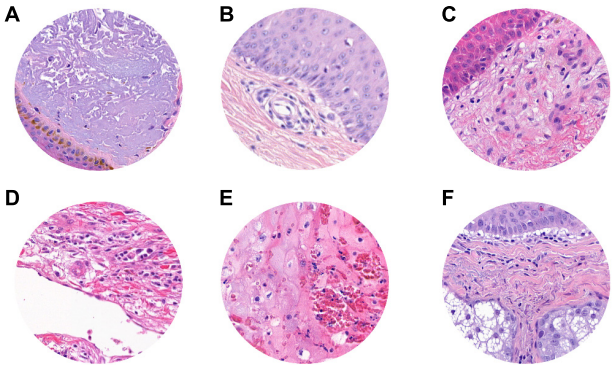

FIGURE 5 | ROI samples in which false-positive patches were identified. **(A)** Dermal solar elastosis (Grade 3). **(A–C)** Epidermal atrophy. **(D)** Abnormal dilated small-to-medium size vessels surrounded by normal dermal collagen. **(D,E)** Extravasated erythrocytes in the dermis or within adnexal epithelium. **(F)** Sebaceous adnexal structures and follicular epithelium.

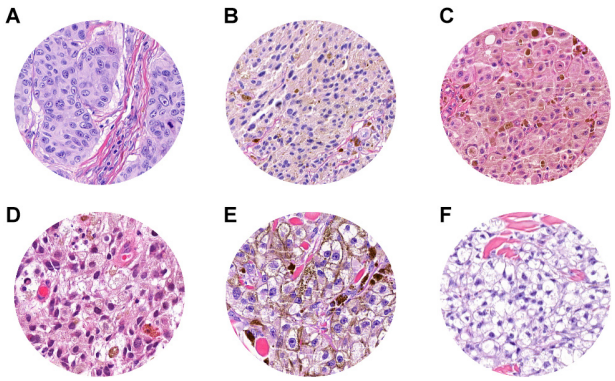

FIGURE 6 | ROI samples in which false-negative patches were identified. **(A)** Absent pigmentation. **(B–D)** Mild pigmentation. **(E)** Prominent pigmentation. **(F)** Clear cell changes in melanoma cell.

Using a powerful workstation, a large amount of data, and complex computer algorithms, AI can identify complex models in the real world, producing considerations, conclusions, extrapolations, associations, and forecasts that can match or exceed human capabilities. The analysis of histopathological images in general, and melanoma in particular, represent a natural application of this field.

In this study, we showed that an AI algorithm to recognize cutaneous melanoma can be a useful diagnostic tool for supporting dermatopathologists for diagnostic purposes. Although extensive research has been carried out on melanoma dermatoscopic images processing with AI (22–24), few studies have specifically shown the utility of AI in the recognition of melanoma compared to normal tissue in histopathological images (17–19).

Previous studies (18, 19) have proposed CNNs to distinguish between histopathological images of melanomas and benign tissue. First, a pretrained ResNet50 CNN with a randomly cropped area from 595 WSIs (300 nevi WSIs for 50152 patches; 295 melanoma WSIs for 55263 patches) and tested with a randomly cropped area from 100 WSIs (50 nevi WSIs for 50152 patches; 50 melanoma WSIs for 55263 patches) was used, and an overall accuracy of 81% with respect to the gold standard reference (i.e., classification by board-certified pathologists) was reported (18). Second, a CNN that automatically detected melanoma in WSIs and highlighted the lesion area on WSIs using a probabilistic heat map was reported by using a pretrained VGG16 CNN, trained with 38 WSI (27 healthy tissue WSIs for 50152 patches; 11 melanoma WSI for 55263 patches), and tested with an independent dataset of 76 WSIs (38 healthy tissue WSIs for 16904 patches; 38 melanoma WSI for 66222 patches). For patch diagnosis on an independent dataset, the proposed model also achieved accuracy, sensitivity, and specificity of 91.4, 91.0, and 92.8%, respectively (19).

Our data clearly show that the AI algorithm we built includes all the characteristics necessary for better recognition of tumor cells, including lesions that are not easily identified. The CNN proposed in this study has shown high performance in detecting cutaneous melanoma areas in histopathological slides. It can recognize portions of pathological and healthy tissues on independent testing datasets with an accuracy, sensitivity, specificity, and F_1 score of 96.5, 95.7, 97.7, and 97.0%, respectively. Unlike recently published data (18), our classification method does not aim to discriminate between melanoma and nevi, but rather to distinguish, within a WSI, healthy tissue from pathological tissue. Our aim is in line with the patch-level classification on an independent dataset (19). In addition, we obtained a classification performance higher than that reported (19), in terms of accuracy (96.5% vs. 91.4%), sensitivity (95.7% vs. 91.0%), and specificity (97.7% vs. 92.8%). In the previous study (19), the F_1 score was not estimated and, therefore, we cannot compare it with the F1 score of our net; nevertheless, the value obtained is high enough to demonstrate the high classification accuracy of our CNN.

The proposed CNN has the potential to quickly classify and give more detailed information on pathological cases, defining a heat map that distinguishes the malignant areas from the normal ones. A promising application would be for the pathologist to focus on a more accurate and faster identification of the tumor margin status, thus facilitating a heat map on the scan, to streamline the task in clinically critical decisions. Our results have also revealed that a dimension of about 5000 mm^2 per patch is sufficient to obtain a reliable patch-level recognition of pathological tissue in WSIs. The proposed CNN achieved a Cohen's kappa of 0.929 with respect to the reference classification of expert dermatopathologists, thus showing a high level of agreement between human and machine evaluation, as well as a higher inter-rater agreement with respect to the previous study (19), which reported a Cohen's kappa of 0.878 for patch-level classification on an independent dataset.

In our study, each misclassified patch was visually reanalyzed by expert dermatopathologists in search of possible explanations for the wrong classification by the trained CNN. In some of the false-positive patches, signs of marked dermal solar

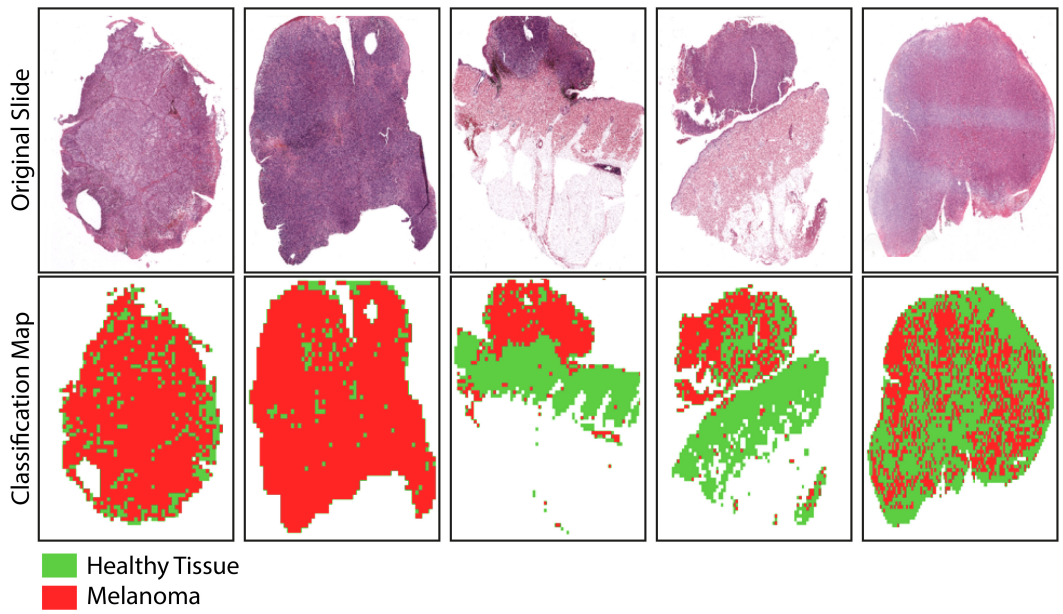

FIGURE 7 | Sample images showing the results of the trained-CNN application to five WSIs. Each WSI was associated with a classification binary map with texels representing classified patches: green area for non-melanoma patches and red area for melanoma patches. The background areas (corresponding to patches with more than 50% of the white background) were represented by the white areas.

elastosis and epidermal atrophy, as expected from UV-related melanomas arising on chronically sun-exposed anatomical sites, were observed. This finding is significant in light of the recent multidimensional classification for melanoma (25). The possibility that the AI algorithms implemented allow a better subclassification of Low-Cumulative Solar Damage (CSD) melanomas vs. High-CSD melanomas, which are different, as well as the genomic level and mutational status, should be further explored in larger data sets. In addition, a misdiagnosis could be attributed to the presence of more heterogeneous patches showing prominent dilated vessels and extravasated erythrocytes, or adnexal structures in the dermis. In all false-negative patches, areas of homogeneous pathological tissue with moderate–severe cytological atypia (melanoma cells), with no significant areas of non-tumoral tissues, were recognized. In about half of the cases, tumor cells were arranged in large confluent aggregates with no discrete nests. Whether or not the type of architectural tumor growth and cellular arrangement (confluent aggregates vs. small discrete nests) affects misclassification is currently a matter of investigation. None of the false-negative patches were associated with brisk TILs, thus avoiding the hypothesis that a prominent tumor-associated lymphocytic component in the tumor microenvironment could be responsible for the misclassification. Finally, tissue pigmentation did not affect classification.

The strength of our study is in the description of an AI that is proficient in working on a heterogeneous data set of melanomas, which reflects the cases usually inspected by dermatopathologists in daily clinical practice. However, this study has several limitations that will be addressed in future studies. First, the case series includes only pT3 and pT4 melanomas (Breslow thickness $>$ 2 mm). Indeed, the purpose of this study was to develop a CNN that works with high performance on thick melanomas; the second step will be to apply the neural network to melanomas with Breslow $<$2 mm, to evaluate its performance and, possibly, implement training with thinner melanomas. Second, a separate cohort of melanocytic nevi was not included in the comparison; we acknowledge that the ability to discriminate melanoma from nevi would increase the strength of the proposed AI approach. Third, additional studies incorporating larger datasets from clinical practice settings, as well as more general pathologists with a broader range of backgrounds, are necessary to further validate our data. Finally, the technical requirements for image acquisition should be validated in additional independent cohorts. In particular, the classification performance of the net could be reduced by the use of different digital WSI scanners.

CONCLUSION

In conclusion, Our data show that a deep learning system can be trained to recognize melanoma samples, achieving accuracies comparable to experienced dermatopathologists. This system could prove to be a valuable aid in improving diagnostic efficiency when expert consultation is not available, as well as reducing interobserver variability. Further studies in larger data sets are required to verify whether the deep learning algorithm allows subclassification of different melanoma subtypes.

MEMBERS OF THE ITALIAN ASSOCIATION FOR CANCER RESEARCH (AIRC) STUDY GROUP

The Italian Association for Cancer Research (AIRC) Study Group includes the following members who participated in this study and should be considered as co-authors: Michele Maio (MM), Azienda Ospedaliera Universitaria Senese, Siena, Italy. Andrea Anichini (AA), Istituto Nazionale Tumori, Milan, Italy. Giuseppe Palmieri (GP), Institute of Genetic and Biomedical Research, National Research Council, Sassari, Italy. Ulrich Pfeffer (UP), IRCCS Ospedale Policlinico San Martino, Genoa, Italy.

DATA AVAILABILITY STATEMENT

The raw data supporting the conclusions of this article will be made available by the authors, without undue reservation.

ETHICS STATEMENT

The studies involving human participants were reviewed and approved by the use of FFPE sections of human samples and the Local Ethics Committee (#13676_bio and #17033_bio) according to the Declaration of Helsinki. The patients/participants provided their written informed consent to participate in this study.

AUTHOR CONTRIBUTIONS

FD, FU, ML, RN, and DM: conceptualization, writing the original draft, and funding acquisition. DM: funding acquisition. ML: methodology. VM and SS: tissue collection and methodology. FD, FU, ML, RN, AC, and DM: review of draft. FD, FU, and ML: editing the draft. The Italian Association for Cancer Research (AIRC) Study Group, Michele Maio (MM), Andrea Anichini (AA), Giuseppe Palmieri (GP), Ulrich Pfeffer (UP), DM, and AC: resources. All authors contributed to the article and approved the submitted version.

FUNDING

This work was funded by the Associazione Italiana per la Ricerca sul Cancro (AIRC) "Programma di ricerca 5 per Mille 2018—ID#21073."

ACKNOWLEDGMENTS

We thank Marco Paterni and Davide Cini (Institute of Clinical Physiology, National Research Council, Pisa, Italy) for their technical assistance in data processing and AI development.

REFERENCES

1. Abbas O, Miller DD, Bhawan J. Cutaneous malignant melanoma. *Am J Dermatopathol.* (2014) 36:363–79. doi: 10.1097/DAD.0b013e31828a2ec5
2. Siegel RL, Miller KD, Jemal A. Cancer statistics, 2017. *CA Cancer J Clin.* (2017) 67:7–30. doi: 10.3322/caac.21387
3. Shoo BA, Sagebiel RW, Kashani-Sabet M. Discordance in the histopathologic diagnosis of melanoma at a melanoma referral center. *J Am Acad Dermatol.* (2010) 62:751–6. doi: 10.1016/j.jaad.2009.09.043
4. Elmore JG, Barnhill RL, Elder DE, Longton GM, Pepe MS, Reisch LM, et al. Pathologists' diagnosis of invasive melanoma and melanocytic proliferations: Observer accuracy and reproducibility study. *BMJ.* (2017) 357:2813. doi: 10.1136/bmj.j2813
5. Hekler A, Utikal JS, Enk AH, Solass W, Schmitt M, Klode J, et al. Deep learning outperformed 11 pathologists in the classification of histopathological melanoma images. *Eur J Cancer.* (2019) 118:91–6. doi: 10.1016/j.ejca.2019.06.012
6. Komura D, Ishikawa S. Machine learning approaches for pathologic diagnosis. *Virchows Arch.* (2019) 475:131–8. doi: 10.1007/s00428-019-02594-w
7. Acs B, Rimm DL. Not just digital pathology, intelligent digital pathology. *JAMA Oncol.* (2018) 4:403–4. doi: 10.1001/jamaoncol.2017.5449
8. Kulkarni S, Seneviratne N, Baig MS, Khan AHA. Artificial intelligence in medicine: where are we now? *Acad Radiol.* (2020) 27:62–70. doi: 10.1016/j.acra.2019.10.001
9. Anwar SM, Majid M, Qayyum A, Awais M, Alnowami M, Khan MK. Medical image analysis using convolutional neural networks: a review. *J Med Syst.* (2018) 42:1–13. doi: 10.1007/s10916-018-1088-1
10. Gao J, Jiang Q, Zhou B, Chen D. Convolutional neural networks for computer-aided detection or diagnosis in medical image analysis: an overview. *Math Biosci Eng.* (2019) 16:6536–61. doi: 10.3934/mbe.2019326
11. Shin HC, Roth HR, Gao M, Lu L, Xu Z, Nogues I, et al. Deep convolutional neural networks for computer-aided detection: CNN architectures, dataset characteristics and transfer learning. *IEEE Trans Med Imaging.* (2016) 35:1285–98. doi: 10.1109/TMI.2016.2528162
12. Szegedy C, Ioffe S, Vanhoucke V, Alemi AA. *Inception-v4, Inception-ResNet and the Impact of Residual Connections on Learning.* (2017). Available online at: www.aaai.org (accessed April 17, 2020).
13. Khosravi P, Kazemi E, Imielinski M, Elemento O, Hajirasouliha I. Deep convolutional neural networks enable discrimination of heterogeneous digital pathology images. *EBioMedicine.* (2018) 27:317–28. doi: 10.1016/j.ebiom.2017.12.026
14. Han T, Liu C, Yang W, Jiang D. Learning transferable features in deep convolutional neural networks for diagnosing unseen machine conditions. *ISA Trans.* (2019) 93:341–53. doi: 10.1016/j.isatra.2019.03.017
15. Madabhushi A, Lee G. Image analysis and machine learning in digital pathology: challenges and opportunities. *Med Image Anal.* (2016) 33:170–5. doi: 10.1016/j.media.2016.06.037
16. Dimitriou N, Arandjelović O, Caie PD. Deep learning for whole slide image analysis: an overview. *Front Med.* (2019) 6:264. doi: 10.3389/fmed.2019.00264
17. Acs B, Ahmed FS, Gupta S, Fai Wong P, Gartrell RD, Sarin Pradhan J, et al. An open source automated tumor infiltrating lymphocyte algorithm for prognosis in melanoma. *Nat Commun.* (2019) 10:5440. doi: 10.1038/s41467-019-13043-2
18. Hekler A, Utikal JS, Enk AH, Berking C, Klode J, Schadendorf D, et al. Pathologist-level classification of histopathological melanoma images with deep neural networks. *Eur J Cancer.* (2019) 115:79–83. doi: 10.1016/j.ejca.2019.04.021
19. Wang L, Ding L, Liu Z, Sun L, Chen L, Jia R, et al. Automated identification of malignancy in whole-slide pathological images: Identification of eyelid malignant melanoma in gigapixel pathological slides using deep learning. *Br J Ophthalmol.* (2020) 104:318–23. doi: 10.1136/bjophthalmol-2018-313706
20. Ghazvinian Zanjani F, Zinger S, Piepers B, Mahmoudpour S, Schelkens P. Impact of JPEG 2000 compression on deep convolutional neural networks for

metastatic cancer detection in histopathological images. *J Med Imaging.* (2019) 6:1. doi: 10.1117/1.jmi.6.2.027501

21. Dreiseitl S, Ohno-Machado L, Kittler H, Vinterbo S, Billhardt H, Binder M. A comparison of machine learning methods for the diagnosis of pigmented skin lesions. *J Biomed Inform.* (2001) 34:28–36. doi: 10.1006/jbin.2001.1004
22. Premaladha J, Ravichandran KS. Novel approaches for diagnosing melanoma skin lesions through supervised and deep learning algorithms. *J Med Syst.* (2016) 40:1–12. doi: 10.1007/s10916-016-0460-2
23. Esteva A, Kuprel B, Novoa RA, Ko J, Swetter SM, Blau HM, et al. Dermatologist-level classification of skin cancer with deep neural networks. *Nature.* (2017) 542:115–8. doi: 10.1038/nature21056
24. Gautam D, Ahmed M, Meena YK, Ul Haq A. Machine learning–based diagnosis of melanoma using macro images. *Int J Numer Method Biomed Eng.* (2018) 34:e2953. doi: 10.1002/cnm.2953
25. Elder DE, Bastian BC, Cree IA, Massi D, Scolyer RA. The 2018 world health organization classification of cutaneous, mucosal, and uveal melanoma: detailed analysis of 9 distinct subtypes defined by their evolutionary pathway. *Arch Pathol Lab Med.* (2020) 144:500–22. doi: 10.5858/arpa.2019-0561-ra

Conflict of Interest: The authors declare that the research was conducted in the absence of any commercial or financial relationships that could be construed as a potential conflict of interest.

frontiers in Oncology

SYSTEMATIC REVIEW
published: 15 October 2020
doi: 10.3389/fonc.2020.571135

Comparative Risks of High-Grade Adverse Events Among FDA-Approved Systemic Therapies in Advanced Melanoma: Systematic Review and Network Meta-Analysis

Ya-fang Huang[1]*, *Wen-jie Xie*[2], *Hai-yu Fan*[3] and *Juan Du*[1]*

[1] School of General Practice and Continuing Education, Capital Medical University, Beijing, China, [2] Department Clinical Research, University of Bern, Bern, Switzerland, [3] Center of Stroke, Beijing Institute for Brain Disorders, Capital Medical University, Beijing, China

OPEN ACCESS

Edited by:
Giuseppe Palmieri,
National Research Council (CNR), Italy

Reviewed by:
Francesco Spagnolo,
San Martino Hospital (IRCCS), Italy
Mahendra Pratap Kashyap,
University of Alabama at Birmingham, United States

***Correspondence:**
Ya-fang Huang
huangyafang85@163.com
Juan Du
cuckoo@ccmu.edu.cn

Specialty section:
This article was submitted to Skin Cancer, a section of the journal Frontiers in Oncology

Received: 10 June 2020
Accepted: 07 September 2020
Published: 15 October 2020

Citation:
Huang Y-f, Xie W-j, Fan H-y and Du J (2020) Comparative Risks of High-Grade Adverse Events Among FDA-Approved Systemic Therapies in Advanced Melanoma: Systematic Review and Network Meta-Analysis. Front. Oncol. 10:571135. doi: 10.3389/fonc.2020.571135

Background: Head-to-head evidence is lacking in comparative risks of high-grade adverse events (AEs) among different systemic treatment options for advanced melanoma.

Methods: An up-to-date systematic review and network meta-analysis (NMA) was performed. Randomized controlled trials (RCTs) of patients with advanced melanoma were eligible if at least one intervention was the Food and Drug Administration–approved targeted or immune checkpoint inhibitors. Risks of high-grade AEs were estimated by random-effects Bayesian NMAs, based on relative risks. Surface under the cumulative ranking probabilities was used to assess relative ranking of treatments. The summary incidences were calculated.

Results: Twenty-five RCTs (12,925 patients) comparing 10 different systemic treatment options were included. BRAF/MEK had the highest risk of overall high-grade AEs (pooled incidence: 32.11%). BRAF had the highest risk of high-grade arthralgia (0.39%), whereas MEK had the highest risk of high-grade hypertension (2.28%) and nausea (0.37%). Cytotoxic T-lymphocyte antigen 4 (CTLA-4)/chemo had the highest risk of high-grade diarrhea (1.31%), alanine aminotransferase (0.60%), and aspartate aminotransferase elevation (0.59%). Programmed cell death 1 (PD-1)/CTLA-4 had the highest risks of high-grade pyrexia (1.14%) and rash (0.94%). Using PD-1 inhibitor alone had the lowest risks of overall high-grade AEs.

Conclusions: Different systemic treatment options have varying high-grade AEs in advanced melanoma treatment. Current evidences highlight the important risks of BRAF/MEK, CTLA-4/chemo, and PD-1/CTLA-4.

Keywords: immune checkpoint inhibitor (ICI), targeted inhibitor, network meta-analysis, advanced melanoma, high-grade adverse event

INTRODUCTION

Systemic therapy is the main treatment modality for patients with advanced melanoma (1). The landscape of systemic treatment options is changing rapidly in recent years from traditional interferon α to novel mitogen-activated protein kinase pathway inhibitors (i.e., BRAF inhibitors and MEK inhibitors) and immune checkpoint inhibitors (ICIs) [i.e., programmed cell death 1 inhibitors (PD-1) and cytotoxic T-lymphocyte antigen 4 inhibitors (CTLA-4)] (2). Results from randomized controlled trials (RCTs) have shown that these new agents have drastically improved progression-free survival (PFS) and overall survival (OS) in patients with advanced melanoma (3, 4). However, high-grade adverse events (AEs) related to these targeted inhibitors and ICIs remain a concern in clinical practice (1).

Medical decision-making for patients with advanced melanoma is a major challenge for clinicians. It is important to balance between the clinical benefits and potential high-grade risks of each systemic treatment option during decision making (2, 5). Systematic review and network meta-analysis (NMA) have been conducted to provide high-quality evidences to support the medical decision-making. For example, previous studies found BRAF plus MEK combination was the most favorable therapy to improve PFS, whereas PD-1 was associated with improved OS benefit (5–9). However, these studies were mainly focused on the comparative efficacy. The risks of severe, life-threatening AEs or deaths related to the BRAF- or MEK-targeted inhibitors or ICIs treatments were not adequately summarized for patients with advanced melanoma (6, 9).

The decision about systemic therapies to patients with advanced melanoma should be informed not only by the reduction of recurrence risk or OS improvement, but also by careful management of high-grade risks (10). In the absence of a direct comparison among different systemic treatment options to guide the clinical decision-making, it has been unclear which treatment strategy has the highest high-grade AEs to patients with advanced melanoma. A comprehensive understanding of the high-grade AEs of these novel targeted and immunotherapy agents is needed for informed these clinical decisions. We conducted a NMA to compare high-grade AEs of the Food and Drug Administration (FDA)–approved ICIs and targeted inhibitors for patients with advanced melanoma.

MATERIALS AND METHODS

Study Design

This NMA was reported based on the Preferred Reporting Items for Systematic Reviews and Meta-Analyses guidelines (11, 12). *A priori* established review protocol was followed when the study was conducted. The review protocol was registered in the PROSPERO international prospective register of systematic reviews (CRD42020160453).

Abbreviations: ALT, alanine aminotransferase; AST, aspartate aminotransferase; CrIs, credible intervals; CTLA-4, cytotoxic T-lymphocyte antigen 4 inhibitors; FDA, Food and Drug Administration; ICIs, immune checkpoint inhibitors; PD-1, programmed cell death 1 inhibitors; RR, relative risk.

Search Strategy and Selection Criteria

The final searches of PubMed, EMBASE, and Cochrane Library were conducted up to December 20, 2019, using the combinations of the following terms: (melanoma OR melanocyte) AND (ipilimumab OR yervoy OR nivolumab OR opdivo OR pembrolizumab OR keytruda OR binimetinib OR mektovi OR cobimetinib OR cotellic OR dabrafenib OR tafinlar OR encorafenib OR braftovi OR trametinib OR mekinist OR vemurafenib OR zelboraf OR "cytotoxic T-lymphocyte antigen 4" OR "programmed cell death 1 receptor" OR "BRAF" OR "MEK") AND (random OR control OR phase II OR phase III OR placebo) without restriction on year of publication or language. The detailed search strategies are listed in **Supplementary Table 1**.

Trials were eligible if the following inclusion criteria were met: (1) patients with advanced melanoma regardless mutation status; (2) at least one of the interventions compared in the trial was either the FDA-approved ipilimumab, nivolumab, pembrolizumab, binimetinib, cobimetinib, dabrafenib, encorafenib, trametinib, vemurafenib, their combinations, or chemotherapy with their combinations; (3) high-grade AEs were extractable either from published articles or unpublished reports from clinicaltrial.gov; (4) phase II or III RCTs. We excluded (1) commentaries, letters, editorials, protocols or reviews; (2) trials only in conference abstracts/posters form; (3) phase I, dose escalation or single-arm trials; (4) *in vitro* or animal studies; and (5) studies of cost-effectiveness analyses or quality of life. The titles, abstracts and full texts were evaluated sequentially.

Data Extraction

Data from eligible trials were extracted by two investigators (HY and FH). The extracted information included trial name, line of treatment, study phase, blinding status, median age (range), sex, mutation status, resection status, treatment class [BRAF, MEK, BRAF, and MEK combination (BRAF/MEK), CTLA-4, PD-1, chemotherapy, PD-1 and CTLA-4 combination (PD-1/CTLA-4), CTLA-4, and chemotherapy combination (CTLA-4/chemo)], dosage of drugs, number of patients in each randomization arm, median length of follow-up in each treatment arm, number of patients in the safety dataset, and number of patients with the following: [1] overall high-grade AEs (grades 3–5 AEs); [2] general symptomatic high-grade AEs (fatigue, pyrexia); [3] general laboratory results–related high-grade AEs [alanine aminotransferase (ALT) elevation, aspartate aminotransferase (AST) elevation, hypertension]; [4] musculoskeletal/pain–related high-grade AEs (arthralgia, myalgia); [5] gastrointestinal high-grade AEs (diarrhea, nausea); and [6] cutaneous high-grade AEs (rash). Both published data from articles and unpublished data from clinicaltrial.gov were extracted. When discrepancies occurred between the published and unpublished data, we selected the data with higher number of events.

Quality Assessment

The risk of bias was assessed by two authors (HY and FH) independently. The domains assessed included random sequence generation (selection bias), allocation concealment (selection bias), blinding of participants and personnel (performance bias), blinding of outcome assessment (detection bias), incomplete

TABLE 1 | Characteristics of included trials (49 articles including 25 randomized controlled trials).

Trial name	Line of treatment	Study phase	Blinding	Median age (range)	Sex (Male)	Mutation status	Resection status	Treatment class	Treatment	Follow up (month)	No of patients in safety dataset	No of patients with grades 3–5 AEs
BREAK-3	First-line	Phase 3	Open-label	52 (21–93)	149	BRAF V600E mutation	Unresectable	BRAF	Dabrafenib 150 mg twice daily (187)	NA	187	64*
								Chemotherapy	Dacarbazine 1,000 mg/m² every 3 weeks (63)	NA	59	14*
BRF113220	First-line	Phase 2	Open-label	50 (18–85)	93	BRAF V600E or V600K mutations	Unresectable	BRAF/MEK	Trametinib 1 mg once daily plus dabrafenib 150 mg twice daily (54)**	Median 14.1	54	30
								BRAF/MEK	Trametinib 2 mg once daily plus dabrafenib 150 mg twice daily (54)	Median 14.1	55	42
								BRAF	Dabrafenib 150 mg twice daily (54)	Median 14.1	53	25
BRIM-3	First-line	Phase 3	Open-label	54 (17–86)	381	BRAF V600E mutation	Unresectable	BRAF	Vemurafenib 960 mg twice daily (337)	Median 13.4	336	165
								Chemotherapy	Dacarbazine 1,000 mg/m² every 3 weeks (338)	Median 9.2	293	52
BRIM-8	First-line	Phase 3	Double-blind	51 (38–61)	283	BRAF V600E mutation	Resected	BRAF	Vemurafenib 960 mg twice daily (250)	Median 30.8 in cohort 1; Median 33.5 in cohort 2	247	142
								Placebo	Placebo (248)	Median 30.8 in cohort 1; Median 33.5 in cohort 2	247	37
CA184-004	Not clear	Phase 2	Double-blind	55 (23–87)	52	Not clear	Unresectable	CTLA-4 low dose	Ipilimumab at 3 mg/kg every 3 weeks (40)	Median 8.9	40	7
								CTLA-4 high dose	Ipilimumab at 10 mg/kg every 3 weeks (42)	Median 8.6	42	14
CA184-022	Not clear	Phase 2	Double-blind	59 (19–85)	144	Not clear	Unresectable	CTLA-4	Ipilimumab 0.3 mg/kg every 3 weeks (73)**	Median 8.3	72	26
								CTLA-4 low dose	Ipilimumab 3 mg/kg every 3 weeks (72)	Median 8.7	71	35
								CTLA-4 high dose	Ipilimumab 10 mg/kg every 3 weeks (72)	Median 10.7	71	38
CA184-024	Not clear	Phase 3	Double-blind	57 (31–87)	301	Not clear	Unresectable	CTLA-4 plus chemotherapy	Ipilimumab 10 mg/kg plus dacarbazine 850 mg/m² (250)	Range: 36.6–54.0	247	170*
								Chemotherapy	Dacarbazine 850 mg/m² every 3 weeks (252)	Range: 36.6–54.0	251	121*
CA184-169	First-line	Phase 3	Double-blind	62 (49–71)	450	BRAF V600E,V600K, other mutation, or wild type	Unresectable	CTLA-4 high dose	Ipilimumab 10 mg/kg every 3 weeks (365)	Median 14.5	364	245*
								CTLA-4 low dose	Ipilimumab 3 mg/kg every 3 weeks (362)	Median 11.2	362	194*

(Continued)

TABLE 1 | Continued

Trial name	Line of treatment	Study phase	Blinding	Median age (range)	Sex (Male)	Mutation status	Resection status	Treatment class	Treatment	Follow up (month)	No of patients in safety dataset	No of patients with grades 3–5 AEs
CheckMate 037	Second-line	Phase 3	Open-label	60 (23–85)	261	BRAF V600E, V600K, or wild type	Unresectable	PD-1	Nivolumab 3 mg/kg every 2 weeks (272)	Median 8.4	268	156*
								Chemotherapy	Dacarbazine 1,000 mg/m² every 3 weeks or carboplatin AUC = 6 plus paclitaxel 175 mg/m² every 3 weeks (133)	Median 8.4	102	46
CheckMate 066	First-line	Phase 3	Double-blind	65 (18–87)	246	Wild type	Unresectable	PD-1	Nivolumab 3 mg/kg every 2 weeks (210)	Median 8.9	206	70
								Chemotherapy	Dacarbazine 1,000 mg/m² every 3 weeks (208)	Median 6.8	205	78
CheckMate 067	First-line	Phase 3	Double-blind	60 (18–90)	610	BRAF V600E, V600K, or wild type	Unresectable	PD-1	Nivolumab 3 mg/kg every 2 weeks (316)	Median 35.7	313	188
								CTLA-4 plus PD-1	Nivolumab 1 mg/kg every 3 weeks plus ipilimumab 3 mg/kg every 3 weeks (314)	Median 38.0	313	223*
								CTLA-4 low dose	Ipilimumab 3 mg/kg every 3 weeks (315)	Median 18.6	311	173
CheckMate 069	First-line	Phase 2	Double-blind	65 (27–87)	95	Not clear	Unresectable	CTLA-4 plus PD-1	Nivolumab 1 mg/kg plus ipilimumab 3 mg/kg every 3 weeks (95)	Minimum 11	94	58*
								CTLA-4 low dose	Ipilimumab 3 mg/kg every 3 weeks (47)	Minimum 11	46	18*
CheckMate 238	Not clear	Phase 3	Double-blind	55 (18–86)	527	BRAF V600E, V600K, or wild type	Resected	PD-1	Nivolumab 3 mg/kg every 2 weeks (453)	Median 19.5	452	115
								CTLA-4 high dose	Ipilimumab 10 mg/kg every 3 weeks (453)	Median 19.5	453	252
coBRIM	First-line	Phase 3	Double-blind	55 (23–88)	286	BRAF V600E mutation	Unresectable	BRAF/MEK	Vemurafenib 960 mg twice daily plus cobimetinib 60 mg once daily (247)	Median 7.3	247	186
								BRAF	Vemurafenib 960 mg twice daily (248)	Median 7.3	246	151
COLUMBUS	First-line	Phase 3	Open-label	56 (20–89)	334	BRAF V600E or V600K mutations	Unresectable	BRAF/MEK	Encorafenib 450 mg once daily plus binimetinib 45 mg twice daily (192)	Median 16.7	192	112
								BRAF	Encorafenib 300 mg once daily (194)**	Median 16.6	192	127
								BRAF	Vemurafenib 960 mg twice daily (191)	Median 14.4	186	118
COMBI-AD	First-line	Phase 3	Double-blind	50 (18–89)	388	BRAF V600E or V600K mutations	Resected	BRAF/MEK	Dabrafenib 150 mg twice daily plus trametinib 2 mg once daily (438)	Median 33.6	435	181
								Placebo	Placebo (432)	Median 33.6	432	61
COMBI-d	First-line	Phase 3	Double-blind	56 (22–89)	225	BRAF V600E or V600K mutations	Unresectable	BRAF/MEK	Dabrafenib 150 mg twice daily plus trametinib 2 mg once daily (211)	Median 9	209	104
								BRAF	Dabrafenib 150 mg twice daily (212)	Median 9	211	106

(Continued)

TABLE 1 | Continued

Trial name	Line of treatment	Study phase	Blinding	Median age (range)	Sex (Male)	Mutation status	Resection status	Treatment class	Treatment	Follow up (month)	No of patients in safety dataset	No of patients with grades 3–5 AEs
COMBI-v	First-line	Phase 3	Open-label	55 (18–91)	388	BRAF V600E mutation	Unresectable	BRAF/MEK	Dabrafenib 150 mg twice daily plus trametinib 2 mg once daily (352)	Median 11	350	173
								BRAF	Vemurafenib 960 mg twice daily (352)	Median 10	349	206
EORTC 18071	First-line	Phase 3	Double-blind	52 (18–84)	589	Not clear	Resected	CTLA-4 high dose	Ipilimumab 10 mg/kg every 3 weeks (475)	Median 63.6	471	260
								Placebo	Placebo (476)	Median 64.8	474	124
KEYNOTE-002	Second-line or more	Phase 2	Open-label	62 (15–89)	327	BRAF V600E, V600K, or wild type	Unresectable	PD-1	Pembrolizumab 2 mg/kg every 3 weeks (180)**	Median 10	178	94*
								PD-1	Pembrolizumab 10 mg/kg every 3 weeks (181)	Median 10	179	78*
								Chemotherapy	Paclitaxel plus carboplatin, paclitaxel, carboplatin, dacarbazine, or oral temozolomide (179)	Median 10	171	45
KEYNOTE-006	First-line or second-line	Phase 3	Open-label	62 (18–89)	497	BRAF V600E, V600K, or wild type	Unresectable	PD-1	Pembrolizumab 10 mg/kg every 2 weeks (279)**	Median 22.9	278	90*
								PD-1	Pembrolizumab 10 mg/kg every 3 weeks (277)	Median 22.9	277	84*
								CTLA-4 low dose	Ipilimumab 3 mg/kg every 3 weeks (278)	Median 22.9	256	81*
KEYNOTE-054	Second-line or more	Phase 3	Double-blind	54 (19–88)	628	BRAF V600E, V600K, other mutation, or wild type	Resected	PD-1	Pembrolizumab 200 mg every 3 weeks (514)	Median 15	509	161
								Placebo	Placebo (505)	Median 15	502	104*
MDX010-08	Not clear	Phase 2	Open-label	61 (25–82)	47	Not clear	Unresectable	CTLA-4 plus chemotherapy	Ipilimumab 3 mg/kg every 4 weeks plus dacarbazine 250 mg/m² every 3 weeks (36)	Median 20.9	35	9
								CTLA-4 low dose	Ipilimumab 3 mg/kg every 4 weeks (40)	Median 16.4	39	6
METRIC	Not clear	Phase 3	Open-label	54 (21–85)	173	BRAF V600E or V600K mutations	Unresectable	MEK	Trametinib 2 mg once daily (214)	Median 14.7	211	115
								Chemotherapy	Dacarbazine 1,000 mg/m² every 3 weeks or carboplatin AUC = 6 or paclitaxel 175 mg/m² every 3 weeks (108)	Median 8.7	99	40
NEMO	First-line	Phase 3	Open-label	64 (18–90)	251	NRAS mutation	Unresectable	MEK	Binimetinib 45 mg twice daily (269)	Median 1.7	269	91
								Chemotherapy	Dacarbazine 1,000 mg/m² every 3 weeks (133)	Median 1.7	114	25

AEs, adverse events; CTLA-4, cytotoxic T-lymphocyte-associated antigen-4 inhibitors; NA, not available; PD-1, programmed cell death protein 1 inhibitors.

**Data were extracted from clinicaltrial.gov.*

***The treatment was not included in the network meta-analysis.*

outcome data (attrition bias), selective reporting (reporting bias), and other bias (13).

Outcome Measures

The primary outcome was the incidence of overall high-grade AEs. The secondary outcome was the incidence of general symptomatic high-grade AEs (fatigue, pyrexia), general laboratory results–related high-grade AEs (ALT/AST elevation, hypertension), musculoskeletal/pain–related high-grade AEs (arthralgia, myalgia), gastrointestinal high-grade AEs (diarrhea, nausea), and cutaneous high-grade AEs (rash). Both the primary and secondary outcomes were defined as grades 3–5 AEs basing on the National Cancer Institute Common Terminology Criteria for Adverse Events (CTCAE) version 4.0.

Data Synthesis and Statistical Analysis

NMA was conducted based on the Bayesian framework using a Markov Chain Monte Carlo (MCMC) simulation technique. Non-informative priors were used to estimate the posterior distribution (14). The MCMC model was updated with 100,000 simulated draws after a burn-in of 20,000 iterations. We used a thinning interval of 10 for each chain. Brooks–Gelman–Rubin statistic was used to assess the adequacy of burn-in and convergence (15). Relative risks (RRs) along with corresponding 95% credible intervals were reported. Random-effects model was used because they generally show better goodness of fit. The posterior mean of the residual deviance was calculated to assess goodness of model fit. The incidence of both primary and secondary outcomes was estimated (incidence = 100 × assumed placebo risk × RR, the assumed placebo risk was generated by using traditional meta-analyses with random-effects model).

Hierarchy of both the primary and secondary outcomes was respectively estimated for all the treatment classes using median ranks and surface under the cumulative ranking curve (SUCRA). SUCRA was the percentage of drug safety on AEs that would be ranked first without uncertainty. When the drug safety was certain to be the best, the SUCRA value would equal one, whereas it would equal zero when the safety was certain to be the worst (16). The presence of inconsistency was evaluated by node splitting analysis in the entire network on particular comparisons (17, 18). The $P < 0.05$ was regarded as significant inconsistency. All the data analyses were conducted using STATA version 14.0 and WinBUGs version 1.4.3.

RESULTS

Selection of Trials

Initially, 2,955 unduplicated records were identified by literature search. After screening of titles and abstracts, 2,895 records were excluded. Sixty articles were assessed for eligibility. Finally, 49 articles involving 25 RCTs were included for qualitative and quantitative synthesis (3, 4, 19–65) (**Supplementary Figure 1**).

Characteristics of Trials and Patients

The 25 RCTs covered 10 treatment classes and included 12,925 patients with advanced melanoma (**Table 1** and **Supplementary Table 2**). **Supplementary Table 3** lists the arrangement of treatments into treatment classes. Among the 25 RCTs, 19 trials (76.0%) were phase III studies, and 15 trials (60.0%) included patients with first-line treatment. The median age of patients was between 50 and 65 years. **Supplementary Table 4** shows the details of risk-of-bias assessment based on each trial.

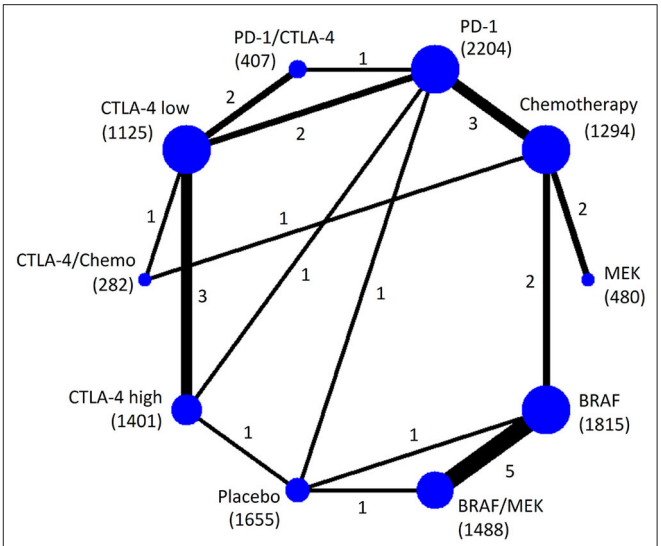

FIGURE 1 | Network plot of eligible comparisons for the Bayesian network meta-analysis of overall high-grade AEs. The size of the nodes is proportional to the number of trials that involved the connected treatment (nodes). The width of the lines is proportional to the number of comparisons (beside the line) comparing the connected treatment (nodes). The number of patients randomized to receive the treatment is in parentheses. A total of 27 comparisons were analyzed for overall high-grade AEs.

Overall High-Grade AEs

Twenty-five RCTs (n = 12,151) were involved in the NMA of overall high-grade AEs (**Figure 1**). Pooled incidence was highest for BRAF/MEK (incidence = 32.11%, 95% CrI = 28.25–34.68%, SUCRA = 5.5%), followed by using BRAF alone (incidence = 31.50%, 95% CrI = 27.51–34.12%, SUCRA = 9.8%). Among the therapeutic treatments, the pooled incidence of overall high-grade AEs was lowest for using chemotherapy alone (incidence = 22.21%, 95% CrI = 16.02–27.95%, SUCRA = 86.0%), followed by using PD-1 inhibitors alone (incidence = 24.70%, 95% CrI = 19.17–29.49%, SUCRA = 71.9%) (**Table 2**).

Using CTLA-4 at a low dose (i.e., ipilimumab at 3 mg/kg) was associated with decreased overall high-grade AEs compared with using CTLA-4 at a high dose (i.e., ipilimumab at 10 mg/kg) (RR = 0.84, 95% CrI = 0.68–0.96). Compared with using PD-1 inhibitor alone, BRAF/MEK, BRAF, and CTLA-4 at a high dose were associated with significantly increased overall high-grade AEs (**Figure 2**).

General Symptomatic High-Grade AEs

Twenty-four RCTs (n = 12,069) were involved in the NMA of high-grade fatigue (**Supplementary Figure 2A**). The incidence of fatigue was highest for CTLA-4/chemo (incidence = 0.94%, 95%

TABLE 2 | Median ranks and the pooled incidences of treatments in terms of high-grade AEs.

Types	Treatment	Rank (95% CrIs)	SUCRA	Incidence (95% CrIs)
OVERALL HIGH-GRADE AEs				
	Placebo	1 (1–3)	99.0	19.00%
	Chemo	2 (1–4)	86.0	22.21% (16.02–27.95%)
	PD-1	3 (2–6)	71.9	24.70% (19.17–29.49%)
	CTLA-4 low dose	4 (2–6)	65.5	25.37% (18.88–30.59%)
	MEK	5 (2–9)	49.4	27.28% (18.68–33.17%)
	CTLA-4/chemo	7 (3–10)	44.6	29.53% (21.45–34.45%)
	PD-1/CTLA-4	7 (4–10)	38.5	30.31% (23.37–34.56%)
	CTLA-4 high dose	7 (5–10)	29.7	30.46% (25.67–33.71%)
	BRAF	9 (5–10)	9.8	31.50% (27.51–34.12%)
	BRAF/MEK	9 (6–10)	5.5	32.11% (28.25–34.68%)
GENERAL, SYMPTOMATIC HIGH-GRADE AEs				
Fatigue	Placebo	1 (1–4)	91.4	0.50%
	CTLA-4 low dose	2 (1–4)	85.0	0.56% (0.27–0.82%)
	PD-1	2 (1–4)	83.6	0.58% (0.32–0.80%)
	CTLA-4 high dose	4 (2–6)	71.1	0.66% (0.43–0.84%)
	Chemo	6 (5–8)	43.9	0.86% (0.65–0.96%)
	PD-1/CTLA-4	6 (4–10)	37.8	0.87% (0.60–0.97%)
	MEK	7 (4–10)	37.3	0.88% (0.60–0.98%)
	BRAF	8 (5–10)	25.6	0.91% (0.77–0.98%)
	BRAF/MEK	9 (6–10)	13.0	0.93% (0.82–0.98%)
	CTLA-4/chemo	9 (6–10)	11.2	0.94% (0.78–0.99%)
Pyrexia	MEK	1 (1–5)	94.4	0.30% (0.03–0.95%)
	Placebo	3 (1–5)	82.8	0.60%
	Chemo	3 (1–5)	78.5	0.59% (0.18–0.98%)
	PD-1	4 (2–6)	71.2	0.72% (0.31–1.04%)
	BRAF	5 (2–7)	58.2	0.86% (0.42–1.10%)
	CTLA-4 low dose	7 (5–9)	33.4	1.08% (0.74–1.18%)
	CTLA-4/chemo	7 (4–10)	32.3	1.07% (0.58–1.19%)
	BRAF/MEK	8 (6–10)	19.8	1.13% (0.95%−1.18%)
	CTLA-4 high dose	9 (6–10)	15.9	1.14% (0.92–1.19%)
	PD-1/CTLA-4	9 (6–10)	13.5	1.14% (0.86–1.19%)
GENERAL, LABORATORY HIGH-GRADE AEs				
ALT elevation	Placebo	1 (1–3)	98.3	0.30%
	Chemo	3 (1–6)	76.3	0.51% (0.16–0.59%)
	PD-1	5 (2–7)	62.6	0.56% (0.38–0.60%)
	BRAF	4 (2–8)	62.5	0.55% (0.45–0.59%)
	MEK	4 (1–9)	60.8	0.55% (0.20–0.60%)
	CTLA-4 low dose	5 (2–8)	56.6	0.57% (0.37–0.60%)
	BRAF/MEK	6 (3–9)	42.7	0.57% (0.50–0.60%)
	CTLA-4 high dose	8 (6–10)	19.0	0.59% (0.55–0.60%)
	PD-1/CTLA-4	9 (6–10)	15.1	0.59% (0.55–0.60%)
	CTLA-4/chemo	10 (6–10)	6.2	0.60% (0.55–0.60%)
AST elevation	Placebo	1 (1–4)	94.6	0.30%
	Chemo	3 (1–6)	76.5	0.46% (0.06–0.59%)
	CTLA-4 low dose	4 (1–7)	71.1	0.51% (0.16–0.60%)
	PD-1	5 (2–7)	62.9	0.53% (0.26%−0.60%)
	BRAF	5 (2–8)	59.0	0.54% (0.37–0.59%)
	MEK	6 (2–10)	49.2	0.57% (0.15%−0.60%)
	BRAF/MEK	7 (3–10)	35.9	0.57% (0.47–0.60%)
	PD-1/CTLA-4	8 (5–10)	20.5	0.59% (0.47–0.60%)
	CTLA-4 high dose	9 (6–10)	15.6	0.59% (0.53–0.60%)
	CTLA-4/chemo	9 (4–10)	14.8	0.59% (0.39–0.60%)
Hypertension	Placebo	2 (1–7)	77.3	1.30%
	PD-1	4 (1–8)	65.0	1.66% (0.24–2.54%)
	Chemo	4 (1–8)	62.7	1.74% (0.22–2.54%)
	CTLA-4 low dose	4 (1–9)	61.4	1.68% (0–2.60%)
	BRAF	5 (2–9)	51.2	1.96% (1.14–2.46%)
	CTLA-4 high dose	8 (1–10)	40.7	2.39% (0.01–2.60%)
	PD-1/CTLA-4	8 (1–10)	38.2	2.37% (0.20–2.60%)
	BRAF/MEK	6 (2–10)	37.1	2.06% (1.28–2.46%)
	CTLA-4/chemo	8 (1–10)	36.1	2.40% (0.20–2.60%)
	MEK	7 (3–10)	30.3	2.28% (0.54–2.59%)
MUSCULOSKELETAL/PAIN RELATED HIGH-GRADE AEs				
Arthralgia	Placebo	1 (1–4)	94.4	0.20%
	PD-1	4 (2–8)	64.8	0.34% (0.18–0.39%)
	CTLA-4 high dose	4 (1–9)	59.2	0.34% (0.15–0.39%)
	Chemo	4 (2–8)	58.8	0.35% (0.18–0.39%)
	PD-1/CTLA-4	6 (1–10)	50.1	0.36% (0.13–0.40%)
	MEK	7 (1–10)	47.6	0.38% (0.07–0.40%)
	BRAF/MEK	6 (2–9)	40.7	0.37% (0.26–0.40%)
	CTLA-4 low dose	6 (2–10)	40.5	0.37% (0.18–0.40%)
	CTLA-4/chemo	9 (1–10)	32.2	0.39% (0.13–0.40%)
	BRAF	9 (5–10)	11.6	0.39% (0.34–0.40%)
Myalgia	PD-1/CTLA-4	1 (1–6)	82.8	NE
	CTLA-4 low dose	3 (1–8)	60.0	NE
	CTLA-4 high dose	3 (1–8)	59.3	NE
	Placebo	5 (1–7)	57.8	NE
	PD-1	4 (1–8)	54.4	NE
	Chemo	5 (2–8)	34.9	NE
	BRAF/MEK	7 (2–8)	34.1	NE
	BRAF	8 (3–8)	16.8	NE
GASTROINTESTINAL HIGH-GRADE AEs				
Diarrhea	MEK	2 (1–8)	84.6	0.56% (0.10–1.21%)
	PD-1	3 (1–5)	81.9	0.66% (0.34–1.02%)
	Chemo	3 (1–6)	78.6	0.66% (0.24–1.10%)
	Placebo	3 (1–6)	78.2	0.70%
	BRAF	5 (1–8)	55.3	0.93% (0.49–1.25%)
	CTLA-4 low dose	6 (4–8)	43.0	1.02% (0.66–1.25%)
	PD-1/CTLA-4	7 (4–9)	32.6	1.08% (0.66–1.30%)
	BRAF/MEK	8 (5–10)	23.9	1.18% (0.79–1.35%)
	CTLA-4 high dose	9 (7–10)	13.7	1.21% (1.02–1.33%)
	CTLA-4/chemo	10 (5–10)	8.3	1.31% (0.86–1.39%)
Nausea	Placebo	1 (1–5)	92.7	0.20%
	PD-1	3 (1–6)	78.3	0.28% (0.12–0.38%)
	CTLA-4 high dose	3 (1–9)	66.6	0.30% (0.14–0.38%)
	CTLA-4 low dose	4 (1–8)	63.5	0.30% (0.13–0.39%)
	BRAF	5 (2–9)	51.5	0.34% (0.19–0.39%)
	CTLA-4/chemo	6 (2–10)	46.4	0.34% (0.16–0.39%)

TABLE 2 | Continued

Types	Treatment	Rank (95% CrIs)	SUCRA	Incidence (95% CrIs)
	Chemo	8 (4–10)	26.7	0.36% (0.24–0.39%)
	BRAF/MEK	8 (3–10)	25.9	0.36% (0.25–0.40%)
	PD-1/CTLA-4	8 (3–10)	24.4	0.37% (0.22–0.40%)
	MEK	9 (3–10)	23.9	0.37% (0.22–0.40%)
CUTANEOUS HIGH-GRADE AEs				
Rash	Chemo	1 (1–4)	93.2	0.26% (0.03–0.81%)
	Placebo	2 (1–6)	79.1	0.50%
	PD-1	4 (1–7)	70.6	0.65% (0.18–0.95%)
	BRAF/MEK	5 (2–9)	54.5	0.75% (0.29–0.96%)
	CTLA-4 low dose	6 (2–9)	48.9	0.81% (0.28–0.98%)
	CTLA-4/chemo	6 (1–10)	45.6	0.82% (0.14–1.00%)
	CTLA-4 high dose	7 (4–10)	31.7	0.87% (0.45–0.99%)
	MEK	8 (2–10)	29.9	0.90% (0.21–1.00%)
	BRAF	8 (4–10)	27.5	0.88% (0.57–0.98%)
	PD-1/CTLA-4	9 (4–10)	19.0	0.94% (0.49–1.00%)

AEs, adverse events; ALT, alanine aminotransferase; AST, aspartate aminotransferase; CrIs, credible intervals; Chemo, Chemotherapy; CTLA-4, cytotoxic T-lymphocyte-associated antigen-4 inhibitors; NE, not estimable; PD-1, programmed cell death protein 1 inhibitors; SUCRA, surface under the cumulative ranking curve.

CrI = 0.78–0.99%, SUCRA = 11.2%), followed by BRAF/MEK (incidence = 0.93%, 95% CrI = 0.82–0.98%, SUCRA = 13.0%) and using BRAF alone (incidence = 0.91%, 95% CrI = 0.77–0.98%, SUCRA = 25.6%). CTLA-4/chemo increased high-grade fatigue significantly compared with PD-1 inhibitor (RR = 1.61, 95% CrI = 1.19–2.74). PD-1 inhibitor was not associated with increased high-grade fatigue compared with placebo (RR = 1.15, 95% CrI = 0.63–1.60) (**Supplementary Figure 3A**).

Twenty-three RCTs (n = 11,927) were involved in the NMA of high-grade pyrexia (**Supplementary Figure 2B**). The incidence was highest for PD-1/CTLA-4 (incidence = 1.14%, 95% CrI = 0.86–1.19%, SUCRA = 13.5%), followed by high-dose CTLA-4 (incidence = 1.14%, 95% CrI = 0.92–1.19%, SUCRA = 15.9%) and BRAF/MEK (incidence = 1.13%, 95% CrI = 0.95–1.18%, SUCRA = 19.8%). Compared with BRAF/MEK, BRAF was associated with decreased high-grade pyrexia (RR = 0.77, 95% CrI = 0.43–0.94). Using PD-1 inhibitor alone decreased high-grade pyrexia significantly compared with PD-1/CTLA-4 (RR = 0.65, 95% CrI = 0.32–0.90) (**Supplementary Figure 3B**).

General Laboratory Results–Related High-Grade AEs

Twenty RCTs (n = 11,196) were involved in the NMA of high-grade ALT and AST elevation, respectively (**Supplementary Figures 4A**,**B**). The incidence of high-grade ALT elevation was highest for CTLA-4/chemo (incidence = 0.60%, 95% CrI = 0.55–0.60%, SUCRA = 6.2%), followed by PD-1/CTLA-4 (incidence = 0.59%, 95% CrI = 0.55–0.60%, SUCRA = 15.1%). The incidence of high-grade AST elevation was highest for CTLA-4/chemo (incidence = 0.59%, 95% CrI = 0.39–0.60%, SUCRA = 14.8%), followed by high-dose CTLA-4 (incidence = 0.59%, 95% CrI = 0.53–0.60%, SUCRA = 15.6%). Compared with using chemotherapy alone, CTLA-4/chemo respectively increased the risks of high-grade ALT and AST elevation slightly (**Supplementary Figures 5A**,**B**).

Fourteen RCTs (n = 8,133) were involved in the NMA of high-grade hypertension (**Supplementary Figure 4C**). MEK had the lowest SUCRA value (30.3%) for high-grade hypertension, followed by CTLA-4/chemo (SUCRA = 36.1%) and BRAF/MEK (SUCRA = 37.1%). Compared with chemotherapy, MEK may increase the risk of high-grade hypertension (RR = 1.26, 95% CrI = 1.00–3.45) (**Supplementary Figure 5C**).

Musculoskeletal/Pain–Related High-Grade AEs

Twenty RCTs (n = 11,059) were involved in the NMA of high-grade arthralgia (**Supplementary Figure 6A**). The incidence of arthralgia was highest for BRAF (incidence = 0.39%, 95% CrI = 0.34–0.40%, SUCRA = 11.6%), followed by CTLA-4/chemo (incidence = 0.39%, 95% CrI = 0.13–0.40%, SUCRA = 32.2%). Compared with placebo, BRAF and BRAF/MEK increased high-grade arthralgia significantly (**Supplementary Figure 7A**).

Eleven RCTs (n = 5,655) were involved in the NMA of high-grade myalgia (**Supplementary Figure 6B**). The SUCRA value was lowest for BRAF (16.8%), followed by BRAF/MEK (SUCRA = 34.1%).

Gastrointestinal High-Grade AEs

Twenty-four RCTs (n = 12,069) were involved in the NMA of high-grade diarrhea (**Supplementary Figure 8A**). The incidence of diarrhea was highest for CTLA-4/chemo (incidence = 1.31%, 95% CrI = 0.86–1.39%, SUCRA = 8.3%), followed by high-dose CTLA-4 (incidence = 1.21%, 95% CrI = 1.02–1.33%, SUCRA = 13.7%) and BRAF/MEK (incidence = 1.18%, 95% CrI = 0.79–1.35%, SUCRA = 23.9%). Compared with PD-1 inhibitors, CTLA-4/chemo was associated with increased high-grade diarrhea (RR = 1.91, 95% CrI = 1.23–3.51). Using CTLA-4 at a low dose was associated with decreased high-grade diarrhea compared with using CTLA-4 alone at a high dose (RR = 0.85, 95% CrI = 0.61–0.98). Compared with BRAF/MEK, using BRAF alone was associated with decreased high-grade diarrhea (RR = 0.80, 95% CrI = 0.53–0.98) (**Supplementary Figure 9A**).

Twenty-four RCTs (n = 12,069) were involved in the NMA of high-grade nausea (**Supplementary Figure 8B**). The incidence of nausea was highest for MEK (incidence = 0.37%, 95% CrI = 0.22–0.40%, SUCRA = 23.9%), followed by PD-1/CTLA-4 (SUCRA = 24.4%), BRAF/MEK (SUCRA = 25.9%) and chemotherapy (SUCRA = 26.7%). Compared with chemotherapy, PD-1 inhibitors may be associated with decreased high-grade nausea (RR = 0.79, 95% CrI = 0.40–0.99) (**Supplementary Figure 9B**).

Cutaneous High-Grade AEs

Twenty-three RCTs (n = 11,823) were involved in the NMA of high-grade rash (**Supplementary Figure 10**). The incidence of rash was highest for PD-1/CTLA-4 (incidence = 0.94%, 95% CrI = 0.49–1.00%, SUCRA = 19.0%), followed by BRAF (incidence = 0.88%, 95% CrI = 0.57–0.98%, SUCRA = 27.5%)

BRAF									
0.98 (0.91 to 1.05)	BRAF/MEK								
1.24 (1.02 to 1.63)	**1.26 (1.03 to 1.68)**	CTLA-4 low							
1.03 (0.89 to 1.22)	1.05 (0.91 to 1.25)	**0.84 (0.68 to 0.96)**	CTLA-4 high						
1.07 (0.90 to 1.43)	1.09 (0.91 to 1.47)	0.86 (0.67 to 1.13)	1.03 (0.86 to 1.37)	CTLA-4/Chemo					
1.15 (0.95 to 1.63)	1.17 (0.96 to 1.68)	0.93 (0.70 to 1.31)	1.11 (0.90 to 1.58)	1.08 (0.81 to 1.50)	MEK				
1.27 (1.06 to 1.60)	**1.30 (1.08 to 1.64)**	1.03 (0.84 to 1.22)	**1.23 (1.06 to 1.49)**	1.19 (0.91 to 1.49)	1.10 (0.80 to 1.39)	PD-1			
1.04 (0.88 to 1.33)	1.06 (0.90 to 1.36)	0.84 (0.69 to 1.00)	1.01 (0.86 to 1.24)	0.98 (0.73 to 1.24)	0.90 (0.64 to 1.18)	0.82 (0.67 to 1.00)	PD-1/CTLA-4		
1.41 (1.15 to 1.86)	**1.44 (1.16 to 1.93)**	1.14 (0.89 to 1.49)	**1.36 (1.10 to 1.81)**	**1.32 (1.03 to 1.70)**	1.22 (0.95 to 1.53)	1.11 (0.92 to 1.39)	**1.35 (1.05 to 1.80)**	Chemo	
1.66 (1.45 to 1.80)	**1.69 (1.49 to 1.83)**	1.34 (0.99 to 1.61)	**1.60 (1.35 to 1.77)**	**1.55 (1.13 to 1.81)**	1.44 (0.98 to 1.75)	**1.30 (1.01 to 1.55)**	**1.60 (1.23 to 1.82)**	1.17 (0.84 to 1.47)	Placebo

FIGURE 2 | The Bayesian network meta-analysis of overall high-grade AEs. Comparisons should be read from the top treatment to the bottom treatment. Bold underline cells are significant. Results represent the pooled relative risks and 95% credible intervals for overall high-grade AEs. Relative risk >1 favors the bottom treatment.

and MEK (incidence = 0.90%, 95% CrI = 0.21–1.00%, SUCRA = 29.9%). PD-1/CTLA-4, BRAF, and MEK were associated with increased high-grade rash compared with chemotherapy (**Supplementary Figure 11**).

Model Fit and Inconsistence Check

The posterior mean values of the residual deviance were 47.0, 33.6, 36.4, 30.0, 30.0, 22.5, 29.2, 16.5, 35.3, 32.7, and 35.1 for overall high-grade AEs, fatigue, pyrexia, ALT elevation, AST elevation, hypertension, arthralgia, myalgia, diarrhea, nausea, and rash, respectively. The model's overall fit was relatively satisfactory. Node splitting analyses did not show inconsistency between direct and indirect results for all the outcomes (**Supplementary Table 5**).

DISCUSSION

Summary of Key Findings

This study fills a crucial knowledge gap regarding the comparative risks of high-grade AEs among the current FDA-approved systemic therapies in advanced melanoma. First, we found that the risk of overall high-grade AEs was highest for the BRAF/MEK inhibitor. Second, there were differences in the spectra of high-grade AEs among BRAF-targeted inhibitor (musculoskeletal toxicities and fatigue), MEK-targeted inhibitor (hypertension and nausea), CTLA-4 inhibitor (diarrhea and ALT/AST elevation), and PD-1/CTLA-4 inhibitors (pyrexia and rash). Third, using PD-1 inhibitor alone had the lowest risks of high-grade AEs for patients with advanced melanoma. Fourth, using CTLA-4 inhibitor alone at a low dose (i.e., ipilimumab at 3 mg/kg) decreased overall high-grade AEs significantly compared with using CTLA-4 inhibitor at a high dose (i.e., ipilimumab at 10 mg/kg).

Comparison With Other Studies

Our study agreed with the result from Franken et al. (5) that using PD-1 inhibitor alone was associated with the lowest risk of high-grade AEs. Devji et al. (7) showed that BRAF/MEK was associated with lower risk of high-grade AEs compared with using BRAF inhibitor alone despite the result was not significant. On the contrary, we found that BRAF/MEK inhibitors had the highest risk of overall high-grade AEs. The differences between our results and the results from Devji and colleagues' study may contribute to the updated trials included in our study (4, 44, 52, 56, 63). In addition, we focused on the FDA-approved targeted inhibitors and ICIs only. We considered that it would be more clinically relevant and would provide more useful evidence into clinical practice.

Previous studies combined high- and low-dose ipilimumab into one arm in analyses (5, 7). In this study, we classified the ipilimumab into the high-dose (10 mg/kg) and low-dose (3 mg/kg) arms when calculating the comparative risks of SAEs. We found that using CTLA-4 inhibitor alone at a high dose (i.e., ipilimumab at 10 mg/kg) was associated with increased risk of high-grade AEs compared with PD-1 or chemotherapy.

Strength and Limitations of Study

To our knowledge, this is the first and most comprehensive NMA that investigated high-grade AEs among the FDA-approved ICIs and targeted inhibitors for patients with advanced melanoma. Previous NMAs either focused only on treatment efficacy or provided limited information on high-grade AEs. In addition, we classified the treatments by mechanism of action rather than analyzing the drugs separately. Thus, multiple trials would contribute to the comparison between two treatment categories. The network would be concise. It avoided yielding very sparse networks in analyses because of the current limited number of available trials. Combining different drugs of the same class

within a single category may introduce heterogeneity. However, the values of the posterior mean of the residual deviance closely corresponded to the number of data points for the outcomes, indicating satisfactory model's fit.

Four limitations should be noted. First, this study provided evidence only on high-grade AEs with limited types. The tolerability of different treatments was not systematically investigated. In addition, because of limited information provided in each of the included studies and the very low incidence of grade 5 AEs (treatment-related deaths), we combined grades 3–4 AEs and grade 5 AEs. We used grades 3–5 AEs as the main outcome of this study. More clinically meaningful outcomes such as all-grade AEs, treatment-related deaths, or treatment discontinuation due to toxicities should be studied to compare the tolerability of different treatments in the future when more trials provide the detailed information. Further researches could also focus on other common AEs such as loss of weight, altered neurobehavioral responses, or other general laboratory results such as changes in blood or lipid profile. Second, the overall high-grade AEs investigated in this study included both non-immune-related reactions and immune-related reactions. The latter was usually late onset. Current clinical trials of ICIs may not have follow-up interval that is long enough to identify the potential risks. Therefore, the incidence of high-grade AEs of ICIs may be underestimated. Standardized method that specifies the clinical criteria for immune-related AEs would be suggested to be published in the future. Third, commentaries, letters, or trials only in conference abstracts were excluded in this study because of the limited information they provided. Publication bias would be a threat if only full-text articles with published data were extracted. Nevertheless, unpublished data from clinicaltrial.gov were obtained in this study to avoid publication bias. Last but not least, individual patient data (IPD) was not accessed in this study. Despite similar inclusion criteria across the included trials have added our confidence in the ability to estimate comparisons across the network of evidence, we still encourage IPD meta-analysis to be conducted in the future because it would provide more detailed patients' characteristics to identify the potential effect modifiers between the treatment options and the high-grade AEs.

Clinical and Research Implications

This study has obtained some unique clinical findings. First, we found a very similar overall high-grade AE risk between PD-1/CTLA-4 (i.e., nivolumab 1 mg/kg plus ipilimumab 3 mg/kg) and using ipilimumab at 10 mg/kg alone (RR = 1.00, 95% CrI = 0.86–1.24). However, the spectra of toxicity between them were different. Using ipilimumab at 10 mg/kg had a higher risk of diarrhea and ALT/AST elevation, whereas the combination of nivolumab 1 mg/kg and ipilimumab 3 mg/kg had a higher risk of high-grade pyrexia and rash. Second, the combination of ipilimumab and chemotherapy (CTLA-4/chemo) had the highest risk of high-grade fatigue, ALT/AST elevation, and diarrhea. CTLA-4/chemo was likely to be associated with increased overall high-grade AEs compared with using ipilimumab at 3 mg/kg alone, despite statistical significance was not detected. Third, focusing specifically on ipilimumab, we found that using ipilimumab at 3 mg/kg alone had a higher safety ranking compared with ipilimumab at 10 mg/kg. It is to be noted that ipilimumab at 3 mg/kg decreased high-grade diarrhea risk significantly, compared with using ipilimumab at 10 mg/kg (RR = 0.85, 95% CrI = 0.61–0.98). These findings presented above indicate that it is necessary for clinicians to be fully aware of these high-grade AEs and manage them appropriately according to the diagnosis criteria and treatment guidelines used across related trials. These comparative evidences of high-grade AEs could be used as important references when the clinicians balance against the improvements in clinical efficacy among different FDA-approved systemic therapeutic options and perform shared decision making with patients in advanced melanoma during clinical practice.

Two research implications could be noted. First, current RCTs conducted by pharmaceutical companies were mainly used as evidences to support the new drug application. Most RCTs would have chemotherapy as the control group. Direct evidence compared among targeted inhibitors and ICIs is still lacking. For example, BRAF inhibitors and PD-1 inhibitors have never been directly compared. We encourage more RCTs of real-world study be conducted in the future to focus on head-to-head comparisons among targeted inhibitors and ICIs. Second, the outcomes in this study were defined basing on CTCAE, because previous study showed that data from the analysis of AEs by severity to define serious AEs (SAEs) would be more informative (66). However, the safety data provided to FDA for new drug applications usually include only SAEs, which may not adequately reflect the safety signal. We encourage more data from the analysis of AEs by severity be reported in the future.

CONCLUSIONS

This current systematic review and NMA provides the most comprehensive comparison of high-grade AEs between targeted inhibitors and ICIs for the treatment of advanced melanoma. Our results show that different systemic treatment options have varying high-grade AEs and highlight the important risks of BRAF/MEK, CTLA-4/chemo and PD-1/CTLA-4 in advanced melanoma treatment.

DATA AVAILABILITY STATEMENT

All datasets generated for this study are included in the article/supplementary material.

AUTHOR CONTRIBUTIONS

Y-fH, W-jX, and JD: study conception and paper writing. Y-fH and JD: study design and discussion of the findings. Y-fH and H-yF: data extraction and elaboration. Y-fH, W-jX, and H-yF: data analysis and interpretation. Y-fH, W-jX, H-yF, and JD: all coauthors have read and approved the manuscript in its present form, agreed to be personally accountable for the author's own contributions and to ensure that questions related to the accuracy or integrity of any part of the work, even ones in

which the author was not personally involved, are appropriately investigated, resolved, and the resolution documented in the literature. All authors contributed to the article and approved the submitted version.

FUNDING

This study was supported by Capital Medical University Research and Cultivation Project (PYZ19087).

SUPPLEMENTARY MATERIAL

The Supplementary Material for this article can be found online at: https://www.frontiersin.org/articles/10.3389/fonc.2020.571135/full#supplementary-material

Supplementary Figure 1 | Literature search and selection.

Supplementary Figure 2 | Network plot of general symptomatic high-grade AEs. The size of the nodes is proportional to the number of trials that involving the connected treatment (nodes). The width of the lines is proportional to the number of comparisons (beside the line) comparing the connected treatment (nodes). The number of patients randomized to receive the treatment is in parentheses. A total of 26 comparisons were analyzed for high-grade fatigue **(A)**; a total of 25 comparisons were analyzed for high-grade pyrexia **(B)**.

Supplementary Figure 3 | The Bayesian network meta-analysis of general symptomatic high-grade AEs. Comparisons should be read from the top treatment to the bottom treatment. Bold underline cells are significant. Results represent the pooled relative risks and 95% credible intervals for high-grade fatigue **(A)** and high-grade pyrexia **(B)**. Relative risk >1 favors the bottom treatment.

Supplementary Figure 4 | Network plot of general laboratory results related high-grade AEs. The size of the nodes is proportional to the number of trials that involving the connected treatment (nodes). The width of the lines is proportional to the number of comparisons (beside the line) comparing the connected treatment (nodes). The number of patients randomized to receive the treatment is in parentheses. A total of 22 comparisons were analyzed for high-grade ALT elevation **(A)**; a total of 22 comparisons were analyzed for high-grade AST elevation **(B)**; a total of 16 comparisons were analyzed for high-grade hypertension **(C)**.

Supplementary Figure 5 | The Bayesian network meta-analysis of general laboratory results related high-grade AEs. Comparisons should be read from the top treatment to the bottom treatment. Bold underline cells are significant. Results represent the pooled relative risks and 95% credible intervals for high-grade ALT elevation **(A)**, high-grade AST elevation **(B)** and high-grade hypertension **(C)**. Relative risk >1 favors the bottom treatment.

Supplementary Figure 6 | Network plot of musculoskeletal/pain related high-grade AEs. The size of the nodes is proportional to the number of trials that involving the connected treatment (nodes). The width of the lines is proportional to the number of comparisons (beside the line) comparing the connected treatment (nodes). The number of patients randomized to receive the treatment is in parentheses. A total of 22 comparisons were analyzed for high-grade arthralgia **(A)**; a total of 13 comparisons were analyzed for high-grade myalgia **(B)**.

Supplementary Figure 7 | The Bayesian network meta-analysis of musculoskeletal/pain related high-grade AEs. Comparisons should be read from the top treatment to the bottom treatment. Bold underline cells are significant. Results represent the pooled relative risks and 95% credible intervals for high-grade arthralgia **(A)** and high-grade myalgia **(B)**. Relative risk >1 favors the bottom treatment.

Supplementary Figure 8 | Network plot of gastrointestinal high-grade AEs. The size of the nodes is proportional to the number of trials that involving the connected treatment (nodes). The width of the lines is proportional to the number of comparisons (beside the line) comparing the connected treatment (nodes). The number of patients randomized to receive the treatment is in parentheses. A total of 26 comparisons were analyzed for high-grade diarrhea **(A)**; a total of 26 comparisons were analyzed for high-grade nausea **(B)**.

Supplementary Figure 9 | The Bayesian network meta-analysis of gastrointestinal high-grade AEs. Comparisons should be read from the top treatment to the bottom treatment. Bold underline cells are significant. Results represent the pooled relative risks and 95% credible intervals for high-grade diarrhea **(A)** and high-grade nausea **(B)**. Relative risk >1 favors the bottom treatment.

Supplementary Figure 10 | Network plot of cutaneous high-grade AEs. The size of the nodes is proportional to the number of trials that involving the connected treatment (nodes). The width of the lines is proportional to the number of comparisons (beside the line) comparing the connected treatment (nodes). The number of patients randomized to receive the treatment is in parentheses. A total of 25 comparisons were analyzed for high-grade rash.

Supplementary Figure 11 | The Bayesian network meta-analysis of cutaneous high-grade AEs. Comparisons should be read from the top treatment to the bottom treatment. Bold underline cells are significant. Results represent the pooled relative risks and 95% credible intervals for high-grade rash. Relative risk >1 favors the bottom treatment.

Supplementary Table 1 | Search strategies.

Supplementary Table 2 | High-grade adverse events in the included trials (49 articles including 25 randomized controlled trials).

Supplementary Table 3 | Arrangement of treatments into treatment classes.

Supplementary Table 4 | Risk of bias summary.

Supplementary Table 5 | Nodesplit analysis of network meta-analysis in terms of the outcomes.

REFERENCES

1. Seth R, Messersmith H, Kaur V, Kirkwood JM, Kudchadkar R, McQuade JL, et al. Systemic therapy for melanoma: ASCO guideline. *J Clin Oncol*. (2020) Jco2000198. doi: 10.1200/jco.20.00198. [Epub ahead of print].
2. Coit DG, Thompson JA, Albertini MR, Barker C, Carson WE, Contreras C, et al. Cutaneous Melanoma, Version 2.2019, NCCN clinical practice guidelines in oncology. *J Natl Compr Canc Netw*. (2019) 17:367–402. doi: 10.6004/jnccn.2019.0018
3. Larkin J, Chiarion-Sileni V, Gonzalez R, Grob JJ, Rutkowski P, Lao CD, et al. Five-year survival with combined nivolumab and ipilimumab in advanced melanoma. *N Engl J Med*. (2019) 381:1535–46. doi: 10.1056/NEJMoa1910836
4. Robert C, Ribas A, Schachter J, Arance A, Grob JJ, Mortier L, et al. Pembrolizumab versus ipilimumab in advanced melanoma (KEYNOTE-006): post-hoc 5-year results from an open-label, multicentre, randomised, controlled, phase 3 study. *Lancet Oncol*. (2019) 20:1239–51. doi: 10.1016/S1470-2045(19)30388-2
5. Franken MG, Leeneman B, Gheorghe M, Uyl-de Groot CA, Haanen JBAG, van Baal PHM. A systematic literature review and network meta-analysis of effectiveness and safety outcomes in advanced melanoma. *Eur J Cancer*. (2019) 123:58–71. doi: 10.1016/j.ejca.2019.08.032
6. Zoratti MJ, Devji T, Levine O, Thabane L, Xie F. Network meta-analysis of therapies for previously untreated advanced BRAF-mutated melanoma. *Cancer Treat Rev*. (2019) 74:43–8. doi: 10.1016/j.ctrv.2019.02.001
7. Devji T, Levine O, Neupane B, Beyene J, Xie F. Systemic therapy for previously untreated advanced BRAF-mutated melanoma: a systematic review and network meta-analysis of randomized clinical trials. *JAMA Oncol*. (2017) 3:366–73. doi: 10.1001/jamaoncol.2016.4877
8. An Q, Liu Z. Comparative efficacy and safety of combination therapies for advanced melanoma: a network meta-analysis. *BMC Cancer*. (2019) 19:43. doi: 10.1186/s12885-018-5259-8

9. da Silveira Nogueira Lima JP, Georgieva M, Haaland B, de Lima Lopes G. A systematic review and network meta-analysis of immunotherapy and targeted therapy for advanced melanoma. *Cancer Med*. (2017) 6:1143–53. doi: 10.1002/cam4.1001
10. Brahmer JR, Lacchetti C, Schneider BJ, Atkins MB, Brassil KJ, Caterino JM, et al. Management of immune-related adverse events in patients treated with immune checkpoint inhibitor therapy: American Society of Clinical Oncology Clinical Practice Guideline. *J Clin Oncol*. (2018) 36:1714–68. doi: 10.1200/jco.2017.77.6385
11. Hutton B, Salanti G, Caldwell DM, Chaimani A, Schmid CH, Cameron C, et al. The PRISMA extension statement for reporting of systematic reviews incorporating network meta-analyses of health care interventions: checklist and explanations. *Ann Intern Med*. (2015) 162:777–84. doi: 10.7326/m14-2385
12. Liberati A, Altman DG, Tetzlaff J, Mulrow C, Gotzsche PC, Ioannidis JP, et al. The PRISMA statement for reporting systematic reviews and meta-analyses of studies that evaluate healthcare interventions: explanation and elaboration. *BMJ*. (2009) 339:b2700. doi: 10.1136/bmj.b2700
13. Higgins JPT, Green S, editors. *Cochrane Handbook for Systematic Reviews of Interventions Version 5.1.0 [updated March 2011]*. The Cochrane Collaboration (2011). Available online at: http://handbook.cochrane.org (accessed February 28, 2020).
14. Sutton AJ, Abrams KR. Bayesian methods in meta-analysis and evidence synthesis. *Stat Methods Med Res*. (2001) 10:277–303. doi: 10.1177/096228020101000404
15. Brooks SP, Gelman A. General methods for monitoring convergence of iterative simulations. *J Comput Graph Stat*. (1998) 7:434–55. doi: 10.1080/10618600.1998.10474787
16. Salanti G, Ades AE, Ioannidis JP. Graphical methods and numerical summaries for presenting results from multiple-treatment meta-analysis: an overview and tutorial. *J Clin Epidemiol*. (2011) 64:163–71. doi: 10.1016/j.jclinepi.2010.03.016
17. Dias S, Welton NJ, Caldwell DM, Ades AE. Checking consistency in mixed treatment comparison meta-analysis. *Stat Med*. (2010) 29:932–44. doi: 10.1002/sim.3767
18. Lu G, Ades AE. Assessing evidence inconsistency in mixed treatment comparisons. *J Am Stat Assoc*. (2006) 101:447–59. doi: 10.1198/016214505000001302
19. Ascierto PA, Long GV, Robert C, Brady B, Dutriaux C, Di Giacomo AM, et al. Survival outcomes in patients with previously untreated BRAF wild-type advanced melanoma treated with nivolumab therapy: three-year follow-up of a randomized phase 3 trial. *JAMA Oncol*. (2019) 5:187–94. doi: 10.1001/jamaoncol.2018.4514
20. Ascierto PA, McArthur GA, Dreno B, Atkinson V, Liszkay G, Di Giacomo AM, et al. Cobimetinib combined with vemurafenib in advanced BRAF(V600)-mutant melanoma (coBRIM): updated efficacy results from a randomised, double-blind, phase 3 trial. *Lancet Oncol*. (2016) 17:1248–60. doi: 10.1016/s1470-2045(16)30122-x
21. Carlino MS, Long GV, Schadendorf D, Robert C, Ribas A, Richtig E, et al. Outcomes by line of therapy and programmed death ligand 1 expression in patients with advanced melanoma treated with pembrolizumab or ipilimumab in KEYNOTE-006: A randomised clinical trial. *Eur J Cancer*. (2018) 101:236–43. doi: 10.1016/j.ejca.2018.06.034
22. Chapman PB, Hauschild A, Robert C, Haanen JB, Ascierto P, Larkin J, et al. Improved survival with vemurafenib in melanoma with BRAF V600E mutation. *N Engl J Med*. (2011) 364:2507–16. doi: 10.1056/NEJMoa1103782
23. Chapman PB, Robert C, Larkin J, Haanen JB, Ribas A, Hogg D, et al. Vemurafenib in patients with BRAFV600 mutation-positive metastatic melanoma: final overall survival results of the randomized BRIM-3 study. *Ann Oncol*. (2017) 28:2581–7. doi: 10.1093/annonc/mdx339
24. Dreno B, Ribas A, Larkin J, Ascierto PA, Hauschild A, Thomas L, et al. Incidence, course, and management of toxicities associated with cobimetinib in combination with vemurafenib in the coBRIM study. *Ann Oncol*. (2017) 28:1137–44. doi: 10.1093/annonc/mdx040
25. Dummer R, Ascierto PA, Gogas HJ, Arance A, Mandala M, Liszkay G, et al. Overall survival in patients with BRAF-mutant melanoma receiving encorafenib plus binimetinib versus vemurafenib or encorafenib (COLUMBUS): a multicentre, open-label, randomised, phase 3 trial. *Lancet Oncol*. (2018) 19:1315–27. doi: 10.1016/s1470-2045(18)30497-2
26. Dummer R, Ascierto PA, Gogas HJ, Arance A, Mandala M, Liszkay G, et al. Encorafenib plus binimetinib versus vemurafenib or encorafenib in patients with BRAF-mutant melanoma (COLUMBUS): a multicentre, open-label, randomised phase 3 trial. *Lancet Oncol*. (2018) 19:603–15. doi: 10.1016/s1470-2045(18)30142-6
27. Dummer R, Schadendorf D, Ascierto PA, Arance A, Dutriaux C, Di Giacomo AM, et al. Binimetinib versus dacarbazine in patients with advanced NRAS-mutant melanoma (NEMO): a multicentre, open-label, randomised, phase 3 trial. *Lancet Oncol*. (2017) 18:435–45. doi: 10.1016/s1470-2045(17)30180-8
28. Flaherty KT, Infante JR, Daud A, Gonzalez R, Kefford RF, Sosman J, et al. Combined BRAF and MEK inhibition in melanoma with BRAF V600 mutations. *N Engl J Med*. (2012) 367:1694–703. doi: 10.1056/NEJMoa1210093
29. Flaherty KT, Robert C, Hersey P, Nathan P, Garbe C, Milhem M, et al. Improved survival with MEK inhibition in BRAF-mutated melanoma. *N Engl J Med*. (2012) 367:107–14. doi: 10.1056/NEJMoa1203421
30. Gogas HJ, Flaherty KT, Dummer R, Ascierto PA, Arance A, Mandala M, et al. Adverse events associated with encorafenib plus binimetinib in the COLUMBUS study: incidence, course and management. *Eur J Cancer*. (2019) 119:97–106. doi: 10.1016/j.ejca.2019.07.016
31. Hauschild A, Dummer R, Schadendorf D, Santinami M, Atkinson V, Mandala M, et al. Longer follow-up confirms relapse-free survival benefit with adjuvant dabrafenib plus trametinib in patients with resected BRAF V600-mutant stage III melanoma. *J Clin Oncol*. (2018) 36:3441–9.. doi: 10.1200/jco.18.01219
32. Hauschild A, Grob JJ, Demidov LV, Jouary T, Gutzmer R, Millward M, et al. Dabrafenib in BRAF-mutated metastatic melanoma: a multicentre, open-label, phase 3 randomised controlled trial. *Lancet*. (2012) 380:358–65. doi: 10.1016/s0140-6736(12)60868-x
33. Larkin J, Ascierto PA, Dreno B, Atkinson V, Liszkay G, Maio M, et al. Combined vemurafenib and cobimetinib in BRAF-mutated melanoma. *N Engl J Med*. (2014) 371:1867–76. doi: 10.1056/NEJMoa1408868
34. Latimer NR, Bell H, Abrams KR, Amonkar MM, Casey M. Adjusting for treatment switching in the METRIC study shows further improved overall survival with trametinib compared with chemotherapy. *Cancer Med*. (2016) 5:806–15. doi: 10.1002/cam4.643
35. Long GV, Eroglu Z, Infante J, Patel S, Daud A, Johnson DB, et al. Long-term outcomes in patients with BRAF V600-mutant metastatic melanoma who received dabrafenib combined with trametinib. *J Clin Oncol*. (2018) 36:667–73. doi: 10.1200/jco.2017.74.1025
36. Long GV, Flaherty KT, Stroyakovskiy D, Gogas H, Levchenko E, de Braud F, et al. Dabrafenib plus trametinib versus dabrafenib monotherapy in patients with metastatic BRAF V600E/K-mutant melanoma: long-term survival and safety analysis of a phase 3 study. *Ann Oncol*. (2017) 28:1631–9. doi: 10.1093/annonc/mdx176
37. Long GV, Hauschild A, Santinami M, Atkinson V, Mandala M, Chiarion-Sileni V, et al. Adjuvant dabrafenib plus trametinib in stage III BRAF-mutated melanoma. *N Engl J Med*. (2017) 377:1813–23. doi: 10.1056/NEJMoa1708539
38. Long GV, Stroyakovskiy D, Gogas H, Levchenko E, de Braud F, Larkin J, et al. Combined BRAF and MEK inhibition versus BRAF inhibition alone in melanoma. *N Engl J Med*. (2014) 371:1877–88. doi: 10.1056/NEJMoa1406037
39. Long GV, Stroyakovskiy D, Gogas H, Levchenko E, de Braud F, Larkin J, et al. Dabrafenib and trametinib versus dabrafenib and placebo for Val600 BRAF-mutant melanoma: a multicentre, double-blind, phase 3 randomised controlled trial. *Lancet*. (2015) 386:444–51. doi: 10.1016/s0140-6736(15)60898-4
40. Maio M, Lewis K, Demidov L, Mandala M, Bondarenko I, Ascierto PA, et al. Adjuvant vemurafenib in resected, BRAF(V600) mutation-positive melanoma (BRIM8): a randomised, double-blind, placebo-controlled, multicentre, phase 3 trial. *Lancet Oncol*. (2018) 19:510–20. doi: 10.1016/s1470-2045(18)30106-2
41. McArthur GA, Chapman PB, Robert C, Larkin J, Haanen JB, Dummer R, et al. Safety and efficacy of vemurafenib in BRAF(V600E) and BRAF(V600K) mutation-positive melanoma (BRIM-3): extended follow-up of a phase 3, randomised, open-label study. *Lancet Oncol*. (2014) 15:323–32. doi: 10.1016/s1470-2045(14)70012-9
42. Robert C, Flaherty K, Nathan P, Hersey P, Garbe C, Milhem M, et al. Five-year outcomes from a phase 3 METRIC study in patients with BRAF

V600 E/K-mutant advanced or metastatic melanoma. *Eur J Cancer*. (2019) 109:61–9. doi: 10.1016/j.ejca.2018.12.015
43. Robert C, Karaszewska B, Schachter J, Rutkowski P, Mackiewicz A, Stroiakovski D, et al. Improved overall survival in melanoma with combined dabrafenib and trametinib. *N Engl J Med*. (2015) 372:30–9. doi: 10.1056/NEJMoa1412690
44. Hodi FS, Chiarion-Sileni V, Gonzalez R, Grob JJ, Rutkowski P, Cowey CL, et al. Nivolumab plus ipilimumab or nivolumab alone versus ipilimumab alone in advanced melanoma (CheckMate 067): 4-year outcomes of a multicentre, randomised, phase 3 trial. *Lancet Oncol*. (2018) 19:1480–92. doi: 10.1016/S1470-2045(18)30700-9
45. Robert C, Thomas L, Bondarenko I, O'Day S, Weber J, Garbe C, et al. Ipilimumab plus dacarbazine for previously untreated metastatic melanoma. *N Engl J Med*. (2011) 364:2517–26. doi: 10.1056/NEJMoa1104621
46. Weber JS, D'Angelo SP, Minor D, Hodi FS, Gutzmer R, Neyns B, et al. Nivolumab versus chemotherapy in patients with advanced melanoma who progressed after anti-CTLA-4 treatment (CheckMate 037): a randomised, controlled, open-label, phase 3 trial. *Lancet Oncol*. (2015) 16:375–84. doi: 10.1016/s1470-2045(15)70076-8
47. Robert C, Long GV, Brady B, Dutriaux C, Maio M, Mortier L, et al. Nivolumab in previously untreated melanoma without BRAF mutation. *N Engl J Med*. (2015) 372:320–30. doi: 10.1056/NEJMoa1412082
48. Postow MA, Chesney J, Pavlick AC, Robert C, Grossmann K, McDermott D, et al. Nivolumab and ipilimumab versus ipilimumab in untreated melanoma. *N Engl J Med*. (2015) 372:2006–17. doi: 10.1056/NEJMoa1414428
49. Eggermont AM, Chiarion-Sileni V, Grob JJ, Dummer R, Wolchok JD, Schmidt H, et al. Adjuvant ipilimumab versus placebo after complete resection of high-risk stage III melanoma (EORTC 18071): a randomised, double-blind, phase 3 trial. *Lancet Oncol*. (2015) 16:522–30. doi: 10.1016/s1470-2045(15)70122-1
50. Ribas A, Puzanov I, Dummer R, Schadendorf D, Hamid O, Robert C, et al. Pembrolizumab versus investigator-choice chemotherapy for ipilimumab-refractory melanoma (KEYNOTE-002): a randomised, controlled, phase 2 trial. *Lancet Oncol*. (2015) 16:908–18. doi: 10.1016/s1470-2045(15)00083-2
51. Maio M, Grob JJ, Aamdal S, Bondarenko I, Robert C, Thomas L, et al. Five-year survival rates for treatment-naive patients with advanced melanoma who received ipilimumab plus dacarbazine in a phase III trial. *J Clin Oncol*. (2015) 33:1191–6. doi: 10.1200/jco.2014.56.6018
52. Larkin J, Minor D, D'Angelo S, Neyns B, Smylie M, Miller WH Jr., et al. Overall survival in patients with advanced melanoma who received nivolumab versus investigator's choice chemotherapy in CheckMate 037: a randomized, controlled, open-label phase III trial. *J Clin Oncol*. (2018) 36:383–90. doi: 10.1200/jco.2016.71.8023
53. Hodi FS, Chesney J, Pavlick AC, Robert C, Grossmann KF, McDermott DF, et al. Combined nivolumab and ipilimumab versus ipilimumab alone in patients with advanced melanoma: 2-year overall survival outcomes in a multicentre, randomised, controlled, phase 2 trial. *Lancet Oncol*. (2016) 17:1558–68. doi: 10.1016/s1470-2045(16)30366-7
54. Eggermont AM, Chiarion-Sileni V, Grob JJ, Dummer R, Wolchok JD, Schmidt H, et al. Prolonged survival in stage III melanoma with ipilimumab adjuvant therapy. *N Engl J Med*. (2016) 375:1845–55. doi: 10.1056/NEJMoa1611299
55. Hamid O, Puzanov I, Dummer R, Schachter J, Daud A, Schadendorf D, et al. Final analysis of a randomised trial comparing pembrolizumab versus investigator-choice chemotherapy for ipilimumab-refractory advanced melanoma. *Eur J Cancer*. (2017) 86:37–45. doi: 10.1016/j.ejca.2017.07.022
56. Eggermont AMM, Blank CU, Mandala M, Long GV, Atkinson V, Dalle S, et al. Adjuvant pembrolizumab versus placebo in resected stage III melanoma. *N Engl J Med*. (2018) 378:1789–801. doi: 10.1056/NEJMoa1802357
57. Larkin J, Chiarion-Sileni V, Gonzalez R, Grob JJ, Cowey CL, Lao CD, et al. Combined nivolumab and ipilimumab or monotherapy in untreated melanoma. *N Engl J Med*. (2015) 373:23–34. doi: 10.1056/NEJMoa1504030
58. Robert C, Schachter J, Long GV, Arance A, Grob JJ, Mortier L, et al. Pembrolizumab versus ipilimumab in advanced melanoma. *N Engl J Med*. (2015) 372:2521–32. doi: 10.1056/NEJMoa1503093
59. Hamid O, Schmidt H, Nissan A, Ridolfi L, Aamdal S, Hansson J, et al. A prospective phase II trial exploring the association between tumor microenvironment biomarkers and clinical activity of ipilimumab in advanced melanoma. *J Transl Med*. (2011) 9:204. doi: 10.1186/1479-5876-9-204
60. Wolchok JD, Neyns B, Linette G, Negrier S, Lutzky J, Thomas L, et al. Ipilimumab monotherapy in patients with pretreated advanced melanoma: a randomised, double-blind, multicentre, phase 2, dose-ranging study. *Lancet Oncol*. (2010) 11:155–64. doi: 10.1016/s1470-2045(09)70334-1
61. Ascierto PA, Del Vecchio M, Robert C, Mackiewicz A, Chiarion-Sileni V, Arance A, et al. Ipilimumab 10 mg/kg versus ipilimumab 3 mg/kg in patients with unresectable or metastatic melanoma: a randomised, double-blind, multicentre, phase 3 trial. *Lancet Oncol*. (2017) 18:611–22. doi: 10.1016/s1470-2045(17)30231-0
62. Wolchok JD, Chiarion-Sileni V, Gonzalez R, Rutkowski P, Grob JJ, Cowey CL, et al. Overall survival with combined nivolumab and ipilimumab in advanced melanoma. *N Engl J Med*. (2017) 377:1345–56. doi: 10.1056/NEJMoa1709684
63. Weber J, Mandala M, Del Vecchio M, Gogas HJ, Arance AM, Cowey CL, et al. Adjuvant nivolumab versus ipilimumab in resected stage III or IV melanoma. *N Engl J Med*. (2017) 377:1824–35. doi: 10.1056/NEJMoa1709030
64. Schachter J, Ribas A, Long GV, Arance A, Grob JJ, Mortier L, et al. Pembrolizumab versus ipilimumab for advanced melanoma: final overall survival results of a multicentre, randomised, open-label phase 3 study (KEYNOTE-006). *Lancet*. (2017) 390:1853–62. doi: 10.1016/s0140-6736(17)31601-x
65. Hersh EM, O'Day SJ, Powderly J, Khan KD, Pavlick AC, Cranmer LD, et al. A phase II multicenter study of ipilimumab with or without dacarbazine in chemotherapy-naive patients with advanced melanoma. *Invest New Drugs*. (2011) 29:489–98. doi: 10.1007/s10637-009-9376-8
66. Smit M-AD, Casak SJ, Lemery S, Keegan P, McKee AE. FDA analysis of grade 3–4 safety events. *J Clin Oncol*. (2017) 35:2544. doi: 10.1200/JCO.2017.35.15_suppl.2544

Conflict of Interest: The authors declare that the research was conducted in the absence of any commercial or financial relationships that could be construed as a potential conflict of interest.

frontiers in Oncology

ORIGINAL RESEARCH
published: 16 October 2020
doi: 10.3389/fonc.2020.581985

Bioinformatic Analysis Identifies Potential Key Genes in the Pathogenesis of Melanoma

Yanjie Han[1], Xinxin Li[1], Jiliang Yan[1], Chunyan Ma[1], Xin Wang[1], Hong Pan[1], Xiaoli Zheng[2], Zhen Zhang[1], Biao Gao[1] and Xin-Ying Ji[3]**

[1] Clinical Laboratory, Functional Laboratory and Department of Stomatology, Kaifeng Central Hospital, Kaifeng, China, [2] Hospital Infection Control Office, First Affiliated Hospital of Henan University, Kaifeng, China, [3] Kaifeng Key Laboratory for Infectious Diseases and Biosafety, Henan International Joint Laboratory of Nuclear Protein Regulation, Henan School of Basic Medical Sciences, Henan University College of Medicine, Kaifeng, China

OPEN ACCESS

Edited by:
Igor Puzanov,
University at Buffalo, United States

Reviewed by:
Gagan Chhabra,
University of Wisconsin-Madison, United States
Ioana Cosgarea,
Newcastle University, United Kingdom

***Correspondence:**
Yanjie Han
hanyanjie86@163.com
Xin-Ying Ji
10190096@vip.henu.edu.cn

Specialty section:
This article was submitted to Skin Cancer, a section of the journal Frontiers in Oncology

Received: *10 July 2020*
Accepted: *24 September 2020*
Published: *16 October 2020*

Citation:
Han Y, Li X, Yan J, Ma C, Wang X, Pan H, Zheng X, Zhang Z, Gao B and Ji X-Y (2020) Bioinformatic Analysis Identifies Potential Key Genes in the Pathogenesis of Melanoma. Front. Oncol. 10:581985. doi: 10.3389/fonc.2020.581985

Melanoma is the deadliest skin tumor and is prone to distant metastases. The incidence of melanoma has increased rapidly in the past few decades, and current trends indicate that this growth is continuing. This study was aimed to explore the molecular mechanisms of melanoma pathogenesis and discover underlying pathways and genes associated with melanoma. We used high-throughput expression data to study differential expression profiles of related genes in melanoma. The differentially expressed genes (DEGs) of melanoma in GSE15605, GSE46517, GSE7553, and the Cancer Genome Atlas (TCGA) datasets were analyzed. Differentially expressed genes (DEGs) were identified by paired t-test. Then the DEGs were performed cluster and principal component analyses and protein–protein interaction (PPI) network construction. After that, we analyzed the differential genes through bioinformatics and got hub genes. Finally, the expression of hub genes was confirmed in the TCGA databases and collected patient tissue samples. Total 144 up-regulated DEGs and 16 down-regulated DEGs were identified. A total of 17 gene ontology analysis (GO) terms and 11 pathways were closely related to melanoma. Pathway of pathways in cancer was enriched in 8 DEGs, such as junction plakoglobin (JUP) and epidermal growth factor receptor (EGFR). In the PPI networks, 9 hub genes were obtained, such as loricrin (LOR), filaggrin (FLG), keratin 5 (KRT5), corneodesmosin (CDSN), desmoglein 1 (DSG1), desmoglein 3 (DSG3), keratin 1 (KRT1), involucrin (IVL), and EGFR. The pathway of pathways in cancer and its enriched DEGs may play important roles in the process of melanoma. The hub genes of DEGs may become promising melanoma candidate genes. Five key genes FLG, DSG1, DSG3, IVL, and EGFR were identified in the TCGA database and melanoma tissues. The results suggested that FLG, DSG1, DSG3, IVL, and EGFR might play important roles and potentially be valuable in the prognosis and treatment of melanoma. These hub genes might well have clinical significance as diagnostic markers.

Keywords: melanoma, differentially expressed genes, bioinformatics analysis, hub genes, tumor marker

INTRODUCTION

Melanoma is the most lethal tumor of skin tumors, and prone to distant metastasis (1, 2). The incidence of melanoma has increased rapidly over the past few decades, and current trends indicate that this growth has still been continuing (3–5). Despite encouraging trends related to improved screening and the introduction of new therapies, melanoma remains a major public health problem (6, 7). In 2020, there were approximately 100,350 newly diagnosed melanomas and 6850 deaths worldwide (8).

There are currently an estimated 1.2 million melanoma survivors in the United States alone (9). While many previous studies have examined factors associated with survival (10–13), exhaustive research on the pathogenic genes and markers of melanoma pathogenicity remain scarcely. Data on tumor markers of melanoma can generate important information that can guide treatment, monitoring plans, and point the way for future melanoma research.

In recent years, microarrays and high-throughput sequencing technologies that detect the expression levels of tens of millions of genes in humans have been widely used to predict potential targets for melanoma treatment (14, 15).

Most current studies only focus on the results of a single genetic event or a single cohort study of melanoma (16–18). However, there is still no comprehensive multi-factor analysis and treatment method (19–21). In this study, we have compiled the GEO and TCGA databases in order to explore the key genes and prognostic indicators of melanoma as comprehensively as possible. Our results will promote our cognition of the genetic etiology of melanoma and provide new insights into the clinical diagnosis and treatment of melanoma.

MATERIALS AND METHODS

Data Searches

We conducted a search of Gene Expression Omnibus (GEO: https://www.ncbi.nlm.nih.gov/geo/) for high-throughput functional genomics experiments of melanoma. GSE15605, GSE46517, and GSE7553 themicroarray expression profiling datasets were downloaded from Gene Expression Omnibus. These datasets were based on GPL570, GPL96, GPL570 Affymetrix Human Genome Array Platform, respectively. We used the following search terms: melanoma, primary melanoma, metastasis melanoma and skin cutaneous melanoma. Datasets were screened for dataset record following the criteria: (1) samples contained melanoma and normal skin tissue, (2) study type was restricted to expression profiling by array, (3) organism was restricted to Homo sapiens, (4) original data were accessible. We excluded studies of less than five samples in each group. The gene expression profiles meeting inclusion criteria were selected from GEO database and TCGA (https://cancergenome.nih.gov/abouttcga/overview) database. In addition, RNASeqV2 data for cutaneous melanoma can be downloaded from the TCGA database. Both GEO and TCGA have significantly increased our understanding of cancer. One very evident advantage of GEO and TCGA is that data from different independent studies can be integrated to get a large number of clinical samples based on TCGA HNSC RNA-seq data and indicated good performance for predicting 5-year overall survival. This powerful prognostic marker was successfully verified in another independent patients cohort.

Data Pre-Processing and Differential Expression Analysis

Robust multi-array average (RMA) approach was performed for background correction and normalization. Then, the original GEO data were converted into expression measures using Affy R package. Limma R package was subsequently employed for identifying DEGs. For TCGA data, edgeR package was used for DEGs screening. Adjusted $p < 0.05$ and (|logFC fold change|) >2 were chosen as the cut-off criteria based on Benjamini & Hochberg (BH) procedure (22). Intersect function in R was applied for identifying the common DEGs among GSE15605, GSE46517 and GSE7553 and TCGA. The Venn diagram was generated by Venn Diagram R package.

Gene Ontology and Pathway Enrichment Analyses

Gene ontology analysis (GO, http://www.geneontology.org/) was used to identify characteristic biological attributes for DEGs (23). Kyoto Encyclopedia of Genes and Genomes pathway (KEGG) enrichment analysis was performed to identify functional attributes for DEGs (24). We used online database for annotation, visualization and integrated discovery (DAVID) (25) and KEGG to access GO and pathway enrichment analysis. $p < 0.05$ was set as the cut-off criterion.

PPI Network Construction

Functional interactions between proteins can provide support for elucidating the molecular mechanisms of disease processes. In our study, the search tool for the retrieval of interacting gene (STRING) (26) database was utilized to construct PPI network. In addition, Cytoscape software was applied to construct protein interaction relationship network (27).

Hub Genes Identification

The Cytoscape was performed to scale degree and closeness of the PPI network. The degree of a node is the average number of edges (interactions) incident to this node. The genes at the top of the degree distribution (≥ 95% percentile) in the significantly perturbed networks were defined as hub genes.

Module Analysis of the PPI Network

Module analysis of the PPI network was performed with the parameters of minimum size > 3 and P-Value < 0.01 using ClusterONE, a Cytoscape plugin that unified different clustering techniques and displayed them in a single interface.

Hub Genes Expression Level and Survival Analysis

Gene-level correlations with patient survival were featured in UALCAN (http://ualcan.path.uab.edu/analysis.html) (28). Available TCGA patient survival data were used for Kaplan–Meier survival analysis and to generate overall survival plots.

Immunohistochemistry

All clinical specimens used in this research were from the First Affiliated Hospital of Henan University, including 63 cases of melanoma tissues and matched adjacent normal skin tissues obtained from patients who underwent surgery for melanoma or other non-melanoma diseases. Histological diagnosis and tumor stage were determined with immunohistochemical method according to the 2004 World Health Organization guidelines for classification. Paraffin sections (4 μm) were stained overnight with rabbit anti-LOR, anti-FLG, anti-KRT5, anti-CDSN, anti-DSG1, anti-DSG3, anti-KRT1, anti-IVL and anti-EGFR antibody (1: 50; Abcam, UK) at 4°C. Secondary staining was then performed with HRP-conjugated anti-rabbit or anti-mouse IgG using the MaxVision kit and DAB Peroxidase Substrate Kit (Maixin, China). Finally, all slides were stained with hematoxylin. The irrelevant rabbit IgG was used as a control for the primary antibody. All of these were evaluated by assessing staining intensity and percentage of positive cells as follows: no staining (0), weak staining (1), moderate staining (2), and strong staining (3); percentage of positive cells <1% (0), 1–33% (1), 34–66% (2), and 67–100% (3). The two scores for each slide were then combined to produce a final grade of the protein of target gene expression(PTGE): 0, total score = 0; 1+, total score = 1–2; 2+, total score = 3–4; 3+, total score = 5–6. The average score is used when there exists a difference between the two pathologists. This study was approved by the local ethics committee and written informed consent was obtained from each patient.

RESULTS

Search Results and Study Characteristics

According to the inclusion criteria, three GEO datasets and TCGA dataset were obtained in our study: GSE15605, GSE46517, GSE7553, and TCGA skin cutaneous melanoma data. DEGs 1,078, 407, 892, and 2,148 from the expression profile datasets GSE15605, GSE46517, GSE7553, and TCGA dataset were extracted, respectively. 160 consistently expressed genes were identified by Venn analysis (**Figure 1**). Among them, 144 genes were up-regulated while 16 were down-regulated compared to normal skin tissue (**Table 1**).

Gene Ontology Analysis

Gene ontology describes gene function and relationships between these concepts. $P < 0.01$ was used as the cut-off criterion. DEGs were classified into the biological process: pathways and larger processes made up of the activities of multiple gene products. After GO enrichment analysis, we found that 160 DEGs were enriched in 17 GO terms

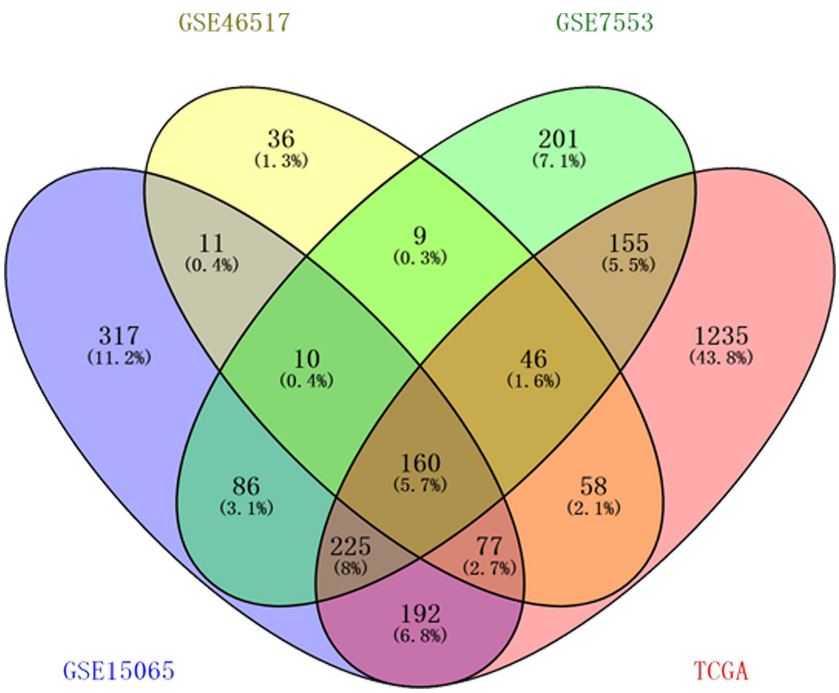

FIGURE 1 | One hundred sixty differentially expressed genes (DEGs) were identified from four datasets. Among them, 144 genes were up-regulated while 16 genes were down-regulated. Different color areas represented different datasets. The cross areas meant the commonly changed DEGs.

TABLE 1 | 160 differentially expressed genes (DEGs) were identified from datasets.

DEGs	
Up-regulated genes	LOR KRT15 GATA3 FLG PKP1 LGALS7B LGALS7 FGFR3 POF1B EFNA3 CST6 KRT2 CDSN COL17A1 DSG1 TRIM29 LY6D SCEL SERPINB5 TACSTD2 LCE2B PPL DSC1 SFN RAPGEFL1 CRCT1 KLK11 KRT23 CCL27 IL37 CA12 C1orf116 KRT1 KLF5 CALML5 PTK6 KRT5 DSC3 HOPX CLCA2 EVPL CHP2 FGFR2 JUP CWH43 ZNF750 POU2F3 ELOVL4 LYPD3 S100A14 KLK5 ANK3 EPHB6 SERPINB7 AIM1L RORA EGFR CXCL14 ANXA8 ANXA8L1 BBOX1 SCNN1A GJB5 ALDH3B2 CXADR PSORS1C2 ADIRF CYP4B1 PERP KLK10 AQP3 KLK7 HAL ASS1 SDC1 EPHX3 TP63 AZGP1 CYP3A5 RAB25 CALML3 KCNK7 EXPH5 TACC2 SPINK5 NEBL DSG3 ADH1B FERMT1 PKP3 DUOX1 CEBPA SLC24A3 ALOX15B CDS1 PTPRF HLA-DQB2 ARHGEF4 GJB3 PDZD2 CLEC3B NMU SPINT2 BCL11A LY6G6C MMP28 C1orf68 SCGB1D2 GPR87 F2RL1 DEFB1 LAD1 LAMB4 MAOA ALOXE3 PAMR1 NTRK2 SLC15A1 ARG1 KRT19 HLF C1orf106 PDZK1IP1 PALMD RNF39 PPP1R13L AIM1 ACSBG1 AKR1C2 PLLP NPY1R AP1M2 KRT31 KRT7 FAT2 PTGS1 IVL CDHR1 ZBTB16 SCNN1B IRF6 ATP2C2 IRX4 ACSL1
Down-regulated genes	TRIB2 SLC16A4 SNX10 BCL2A1 AP1S2 ALX1 UPP1 PHLDA1 SOX10 ETV5 PLAT LEF1 CITED1 IGF2BP3 SERPINE2 SPP1

Among them, 144 genes were up-regulated and 16 genes were down-regulated.

(biological process). Among them, the most enriched GO terms were epidermis development (p=1.88E-17), keratinocyte differentiation (p = 9.90E-10), keratinization (p = 3.40E-06) and establishment of skin barrier (p = 1.49E-05) (**Figure 2**).

Pathway Enrichment Analysis

Pathway enrichment analysis was carried out by online websites of KEGG, a database was applied to assign sets of DEGs to specific pathways. $p < 0.05$ was used as the cut-off criterion. After pathway enrichment analysis, we found that 160 DEGs were enriched in 11 pathways. Among them, DEGs were mainly enriched in the pathways in cancer (p = 0.03), transcriptional misregulation in cancer (p = 0.01), Rap1 signaling pathway (p = 0.02) and Ras signaling pathway (p = 0.03) (**Figure 3**).

PPI Network Analysis

We obtained a PPI network from STRING to describe protein interactions (**Figure 4**). Based on the information obtained from the STRING database, a PPI framework with 160 nodes and 385 edges was generated, and its local clustering coefficient was 0.45. The results of computed hub genes were shown in the **Table 2**, including LOR, FLG, KRT5, CDSN, DSG1, DSG3, KRT1, IVL, and EGFR.

Module Analysis of the PPI Network

To study and identify the function of the overlapping DEGs in detail, cluster analysis of the PPI network was conducted based on the ClusterONE Cytoscape plugin, an important tool for the analysis of densely connected and possibly overlapping regions within the Cytoscape network, which would contribute to the classification of protein network and relevant analysis. There were a total of 23 functional modules given and the most significant module (node = 29, density = 0.4335, p-value = 1.01E-8, **Figure 5A**) was selected for further analysis of functions and pathways to deeply understand the melanoma progression. To further verify the accuracy of this inference, the module genes were submitted into DAVID to perform the KEGG pathway enrichment analysis. The results showed that they were significantly enriched in the renin secretion signaling pathway, epidermal development, keratinocyte differentiation, peptide cross-linking, keratinization and single biological cell adhesion, among other processes shown, $p < 0.05$ (**Figure 5B**).

Hub Genes Expression Level and Survival Analysis

Using UALCAN, we verified gene expression level of hub genes in 1 normal tissue, 104 primary tissues, and 368 metastasis tissues from TCGA database. Through this analysis, we found that LOR, FLG, KRT5, CDSN, DSG1, DSG3, KRT1, and IVL were closely related to the metastasis of melanoma ($p < 0.01$) (**Figures 6A–I**). Kaplan–Meier survival analyses showed that FLG, KRT5, DSG1, DSG3, and IVL expression levels were significantly associated with melanoma patient survival ($p < 0.01$) (**Figures 6J–R**).

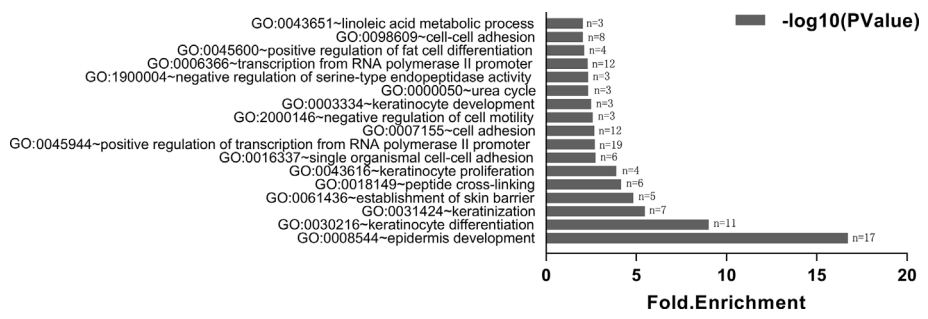

FIGURE 2 | Gene ontology analysis of DEGs. X-axis reflects gene count (n); Y-axis reflects different GO terms. The column value reflects p value (– log10(P Value)): the highest bar represents the biggest – log10(P Value) value (*p < 0.01). We only show terms with p-values less than 0.01 in the figure.

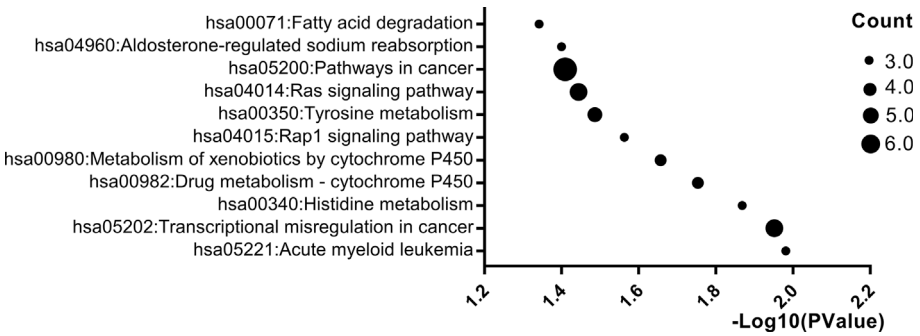

FIGURE 3 | Significantly enriched pathway terms of DEGs. X-axis reflects p value [– log10(p value)]. Y-axis reflects different passway terms. The node size reflects gene count: the bigger the gene count, the bigger the node size is (*p < 0.05). We only showed items with p-values less than 0.05 in the figure.

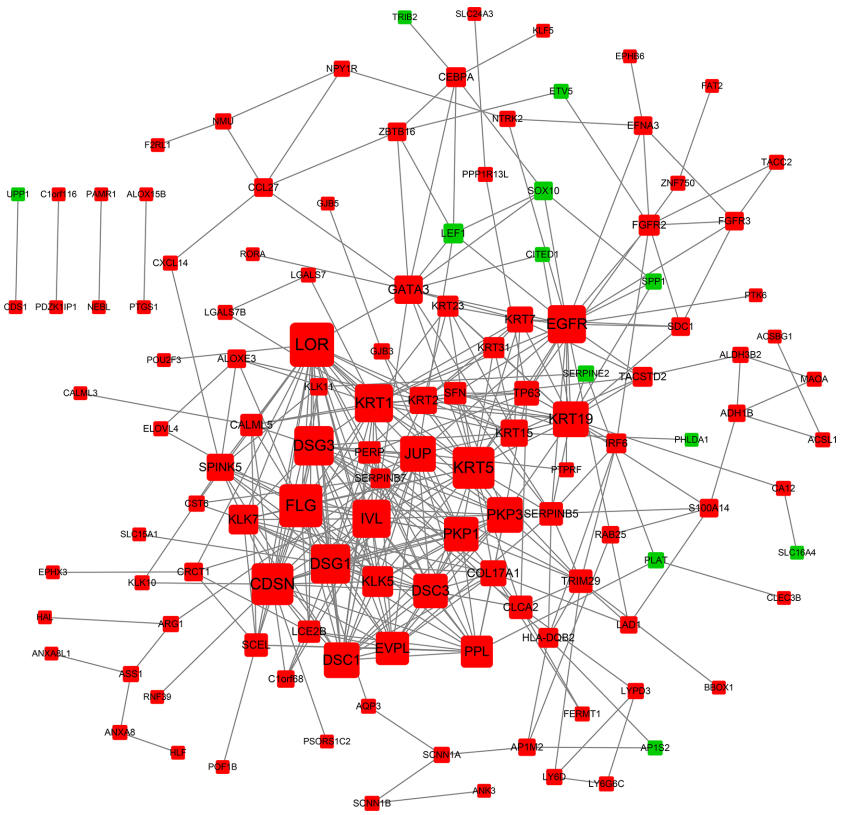

FIGURE 4 | PPI network of DEGs. Each node is a differentially expressed gene (protein). A red node represents an up-regulated gene (protein). A green node represents a down-regulated gene (protein). The node size reflects node degree: the bigger the degree value, the bigger the node size is.

Detection of Hub Genes Related Protein Expression by Immunohistochemistry

In order to determine the expression of hub genes in human melanoma, we used immunohistochemical methods to detect the expression of the protein corresponding to hub genes. We detected the expression level of hub genes in 63 pairs of melanoma specimens (melanoma and adjacent normal tissue) by immunohistochemistry (**Figure 7**). The results showed that the expressions of FLG, DSG1, DSG3, IVL, and EGFR were considerably higher than those of adjacent normal tissues (P <0.05) (**Figures 7B, E, F, H, I**).

TABLE 2 | The statistical results of connectivity degrees of the PPI network.

Gene	Degree
LOR	26
FLG	25
KRT5	24
CDSN	24
DSG1	22
DSG3	22
KRT1	21
IVL	21
EGFR	21

The gene in the table is the symbol of the protein (gene). Degree stands for the connectivity degree of the gene.

DISCUSSION

Melanoma is a progressive disease that requires effective prognostic indicators for diagnosis and treatment. In recent years, effective computational models have been constructed to identify disease-related mRNAs. However, most research has focused on using cell lines or animal models to intervene at the level of a single gene, protein, or miRNA (29, 30). Some commercial genetic testing kits for multi-center joint testing are still not comprehensive enough and still have deficiencies, and cannot effectively serve the purpose of detecting and discovering melanoma (31). For example, for clinicians currently using DecisionDx-melanoma, the integration of the results with the new AJCC staging standard is not clear, especially if the results of the 31 gene expression profile tests are inconsistent with the sentinel lymph node biopsy status (31). In our study, we used high-throughput expression data to study differential expression profiles of related genes in melanoma. We analyzed tumor and normal skin samples from patients in the GEO and TCGA databases to explore abnormally expressed genes in melanoma. The results showed that 160 differentially expressed genes were selected, including 144 up-regulated genes and 16 down-regulated genes. Later, we identified hub genes and pathways in melanoma based on the use of bioinformatics methods. We integrated 4 original microarray datasets and identified 160 frequently changed DEGs. DEGs were mainly enriched in 17 biological processes by GO terms, of which epidermis development, keratinocyte differentiation, keratinization, and establishment of skin barrier were the most obvious. KEGG pathway enrichment analysis showed that DEGs were mainly enriched in 5 signaling pathways, of which pathways in cancer, transcriptional misregulation in cancer, Rap1 signaling pathway and Ras signaling pathway were the most significant. In particular, the pathway of pathways in cancer was enriched by 8 DEGs, such as EGFR and JUP. EGFR (degree = 21) and JUP (degree = 19) were important key node genes in the PPI network. The results of our study suggested that these genes and pathways may play critical roles in the progression of melanoma. For instance, EGFR, as an essential receptor of transforming growth factor alpha, has attracted widespread attention. Previous studies have found that the frequency of oncogenic mutations in the EGFR gene is closely related to the occurrence of melanoma (32–34). In addition, EGFR has been proposed as an important molecular target for the treatment of cancer, which has promoted the development of EGFR pharmacological inhibitors (35, 36). Therefore, we speculated that EGFR may be a candidate gene in pathways in cancer of melanoma. Further, we used the TCGA database to detect the expression of hub genes. However, the sample size of non-melanoma normal tissues in the TCGA database is too small, with only one normal sample. When comparing tumor samples to normal samples, small sample sizes may cause inaccuracies, and we only compare primary and metastatic melanomas. The results showed that the expression of LOR, FLG, KRT5, CDSN, DSG1, DSG3, KRT1, and IVL in these nine hub genes were significantly different. In addition, we also explored the survival analysis of hub genes through the TCGA database. The results of the survival analysis showed that FLG, KRT5, DSG1, DSG3, and IVL of the nine central genes were notably

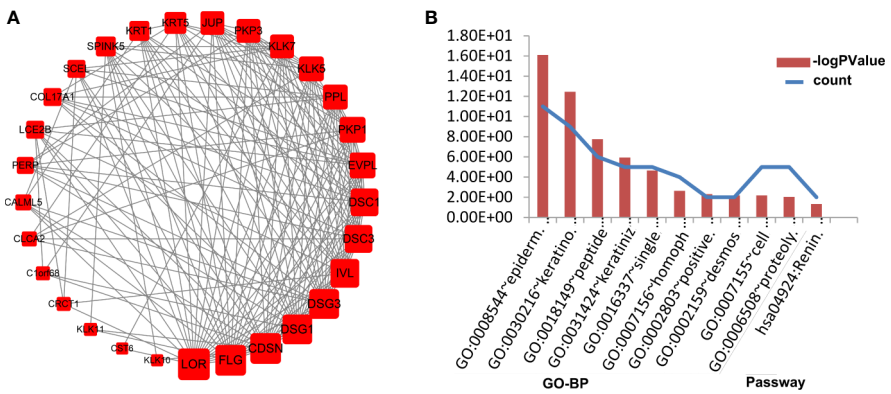

FIGURE 5 | Functional enrichment analysis of the most important modules in PPI networks. The most significant module in the PPI network **(A)**. Nodes stand for the proteins (genes), and edges stand for the interactions of proteins. The GO analysis of the most significant module **(B)**. The left ordinate of histogram represents the gene counts, and the right represents the p-value. BP stands for biological process; and Pathway stands for cell signaling pathway.

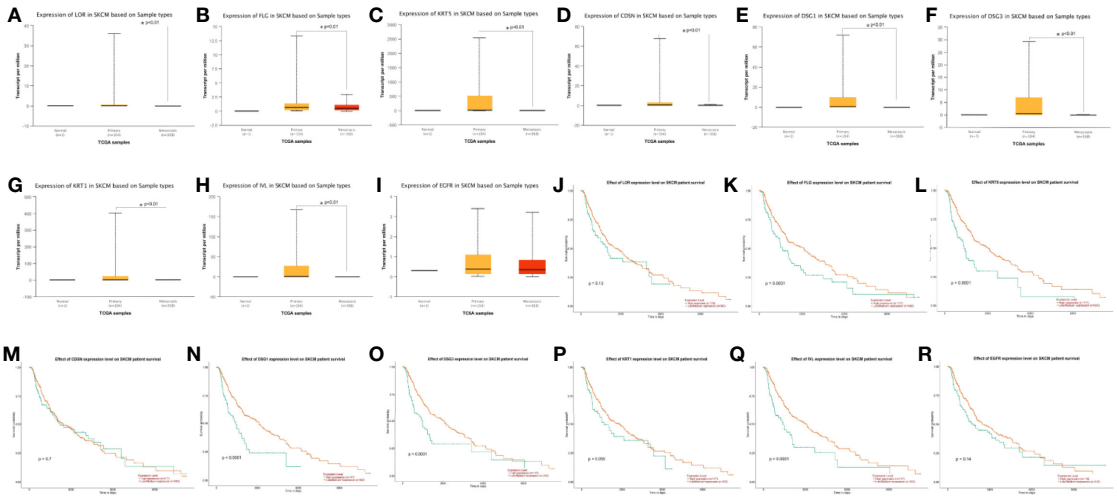

FIGURE 6 | **(A-I)** Expression profile based on major sample types of hub genes using 473 patients data from TCGA database (*p < 0.01). **(J-R)** Kaplan-Meier survival plot of hub genes using 459 melanoma patients data from TCGA database (*p < 0.01).

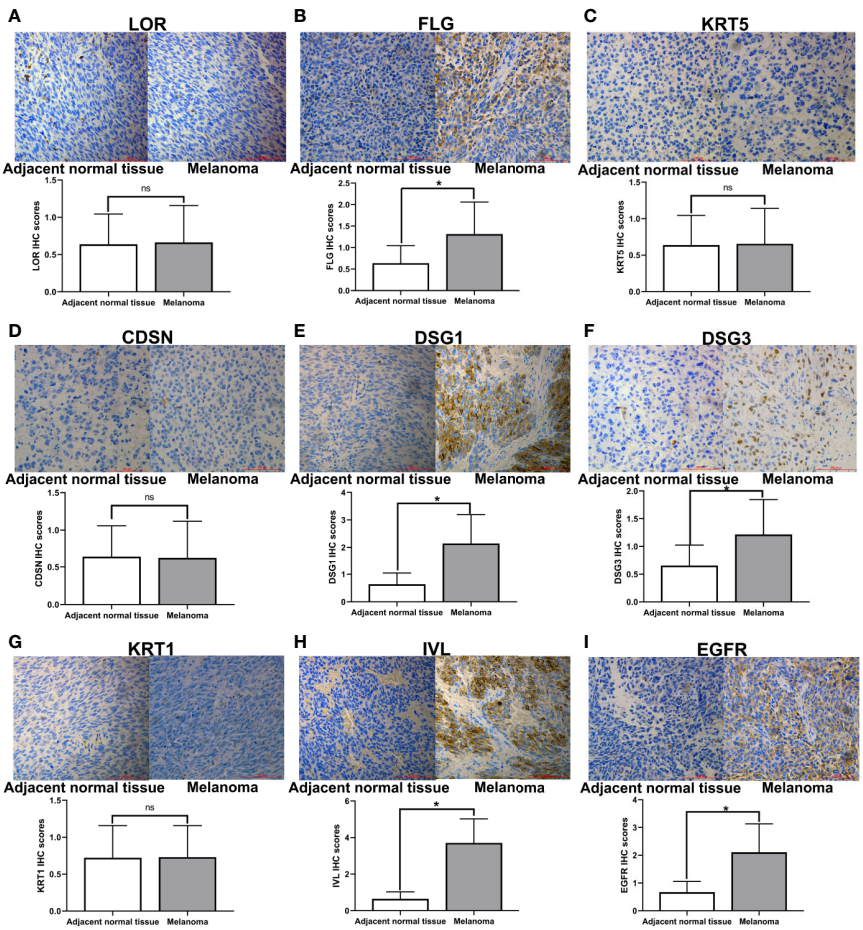

FIGURE 7 | Immunohistochemical staining of hub genes in melanoma tissues and matched adjacent normal tissues. Representative examples of immunohistochemical assessment of hub genes (proteins) expression in melanoma tissues and matched adjacent normal tissues (magnification 200x), *p < 0.05 (ns, no significance).

related to the survival time of patients. Finally, based on the survival analysis, we performed clinical specimen validation using immunohistochemistry. The results showed that the expressions of FLG, DSG1, DSG3, IVL, and EGFR were markedly higher than those of adjacent normal tissues. These studies indicated that we got the key genes FLG, DSG1, DSG3, IVL, and EGFR that could affect melanoma development. We further discussed hub genes expressed in melanoma patient tissues. Filaggrin, a highly abundant protein of the stratum corneum, draw considerable attention after the discovery of its role in the aetiology of atopic dermatitis (37). Currently, Kezic S. has reported that FLG may serve as a potential biomarker for a reduced risk of melanoma (38), however, there are limited reports about the associations between FLG and melanoma. Thus, we can speculate that FLG may also play an important role in the melanoma progression as well as EGFR. Desmoglein belongs to the cadherin family, DSG1 and DSG3 are both members, and its intracellular part binds to intracellular anchoring proteins (39, 40). Li G et al. found that desmoglein and E-cadherin together act as an adhesion between factors, especially when melanoma cells proliferate, the expression of desmoglein and E-cadherin decreases (41). Das A et al. found that T-type calcium channel blockers inhibit autophagy and promote apoptosis of malignant melanoma cells (42). Therefore, calcium signaling pathway may be a disease-targeting in melanoma clinical trials. IVL is a soluble cytosolic protein with a molecular weight of 68KD (43). It is a substrate for glutamine transferase of keratinocytes and plays a role in the formation of epidermal keratinizing envelope (43, 44). IVL is synthesized in the spinal cell layer and cross-linked with granulosa cells under the action of glutamine transferase to form an important structural support for the skin barrier (45). At present, IVL is mostly used as a marker protein to study skin keratinocyte differentiation (46, 47). However, there are few reports of the associations between integrin and melanoma (48, 49). In view of its important role in maintaining skin function, we can speculate that IVL may also play an important role in the progression of melanoma. Although the research on key genes of melanoma has been studied, they are not comprehensive enough and lack of experimental verification (50, 51). In this study, a combined analysis of biology and experiment was used in order to have a more comprehensive and in-depth understanding of melanoma.

These limitations should be recognized by the current research. Firstly, in this study, only 160 DEGs were included. The prognostic Hub genes identified here may not represent all DEGs candidates that were potentially correlated with melanoma overall survival. Furthermore, this consideration does not include the location and stage of melanoma, because the information was not available for a considerable proportion of cases. At the same time, the functions of these eight Hub genes were inferred by bioinformatics analysis, and their biological roles in the development of melanoma were still unclear and should be explored in further experimental demonstration.

CONCLUSION

In summary, we identified a signature of eight hub genes, which predicted the overall survival in four independent testing sets. Moreover, these hub genes were involved in cancer pathways, transcriptional dysregulation signaling pathways in cancer, Rap1 signaling pathway and Ras signaling pathway. These hub genes might well have clinical significance as diagnostic markers. This research was the first analysis of differential genes in melanoma and matched normal tissue samples. However, the biological roles of these eight hub genes in the occurrence and development of melanoma need further study.

DATA AVAILABILITY STATEMENT

Publicly available datasets were analyzed in this study. This data can be found here: https://www.ncbi.nlm.nih.gov/geo/, https://cancergenome.nih.gov/abouttcga/overview.

ETHICS STATEMENT

The studies involving human participants were reviewed and approved by: The pathological experimental protocol was approved by the ethics committee of Kaifeng Central Hospital. The patients/participants provided their written informed consent to participate in this study.

AUTHOR CONTRIBUTIONS

YH and X-YJ conceived and designed this article. JY, CM, XW, HP, XZ, ZZ and BG participated in the experimental data collection. YH and XL coordinated all research realization steps, revised the study draft, and contributed to crucial discussion. All authors contributed to the article and approved the submitted version.

FUNDING

This work was supported by the National Natural Science Foundation of China (No. 81670088 and No. 81602708); and the Henan Provincial Science Foundation Program (No.172102410019).

ACKNOWLEDGMENTS

Our article was published on the Research Square platform under the title of A Comprehensive Data Analysis of Differentially Regulated Genes in Melanoma.

REFERENCES

1. Wang Y, Leonard MK, Snyder DE, Fisher ML, Eckert RL, Kaetzel DM. NME1 Drives Expansion of Melanoma Cells with Enhanced Tumor Growth and Metastatic Properties. *Mol Cancer Res MCR* (2019) 17:1665–74. doi: 10.1158/1541-7786.MCR-18-0019
2. Han Y, Li X, Ma C, Ji X, Li T, Zheng X, et al. Seed targeting with tiny anti-miR-1297 inhibits EMT in melanoma cells. *J Drug Target* (2019) 27:75–81. doi: 10.1080/1061186X.2018.1481412
3. Li WQ, Cho E, Wu S, Li S, Matthews NH, Qureshi AA. Host Characteristics and Risk of Incident Melanoma by Breslow Thickness. Cancer epidemiology, biomarkers & prevention : a publication of the American Association for Cancer Research, cosponsored by the American Society of Preventive Oncology. (2019) 28:217–24. doi: 10.1158/1055-9965.EPI-18-0607
4. Liu-Smith F, Farhat AM, Arce A, Ziogas A, Taylor T, Wang Z, et al. Sex differences in the association of cutaneous melanoma incidence rates and geographic ultraviolet light exposure. *J Am Acad Dermatol* (2017) 76:499–505.e3. doi: 10.1016/j.jaad.2016.08.027
5. Gershenwald JE, Guy GP Jr. Stemming the Rising Incidence of Melanoma: Calling Prevention to Action. *J Natl Cancer Institute* (2016) 108:1–3. doi: 10.1093/jnci/djv381
6. Ferris LK, Saul MI, Lin Y, Ding F, Weinstock MA, Geller AC, et al. A Large Skin Cancer Screening Quality Initiative: Description and First-Year Outcomes. *JAMA Oncol* (2017) 3:1112–5. doi: 10.1001/jamaoncol.2016.6779
7. Wolchok JD, Chiarion-Sileni V, Gonzalez R, Rutkowski P, Grob JJ, Cowey CL, et al. Overall Survival with Combined Nivolumab and Ipilimumab in Advanced Melanoma. *N Engl J Med* (2017) 377:1345–56. doi: 10.1056/NEJMoa1709684
8. Siegel RL, Miller KD, Jemal A. Cancer statistics, 2020. *CA: Cancer J Clin* (2020) 70:7–30. doi: 10.3322/caac.21590
9. Miller KD, Siegel RL, Lin CC, Mariotto AB, Kramer JL, Rowland JH, et al. Cancer treatment and survivorship statistics, 2016. *CA: Cancer J Clin* (2016) 66:271–89. doi: 10.3322/caac.21349
10. Rachidi S, Wallace K, Li H, Lautenschlaeger T, Li Z. Postdiagnosis aspirin use and overall survival in patients with melanoma. *J Am Acad Dermatol* (2018) 78:949–956.e1. doi: 10.1016/j.jaad.2017.12.076
11. Helgadottir H, Tuominen R, Olsson H, Hansson J, Höiom V. Cancer risks and survival in patients with multiple primary melanomas: Association with family history of melanoma and germline CDKN2A mutation status. *J Am Acad Dermatol* (2017) 77:893–901. doi: 10.1016/j.jaad.2017.05.050
12. McDermott D, Lebbé C, Hodi FS, Maio M, Weber JS, Wolchok JD, et al. Durable benefit and the potential for long-term survival with immunotherapy in advanced melanoma. *Cancer Treat Rev* (2014) 40:1056–64. doi: 10.1016/j.ctrv.2014.06.012
13. Lemish WM, Heenan PJ, Holman CD, Armstrong BK. Survival from preinvasive and invasive malignant melanoma in Western Australia. *Cancer* (1983) 52:580–5. doi: 10.1002/1097-0142(19830801)52:3<580::AID-CNCR2820520334>3.0.CO;2-H
14. Marchione R, Laurin D, Liguori L, Leibovitch MP, Leibovitch SA, Lenormand JL. MD11-mediated delivery of recombinant eIF3f induces melanoma and colorectal carcinoma cell death. *Mol Ther Methods Clin Dev* (2015) 2:14056. doi: 10.1038/mtm.2014.56
15. Miao W, Li L, Wang Y. A Targeted Proteomic Approach for Heat Shock Proteins Reveals DNAJB4 as a Suppressor for Melanoma Metastasis. *Analyt Chem* (2018) 90:6835–42. doi: 10.1021/acs.analchem.8b00986
16. Zhan Y, Guo J, Yang W, Goncalves C, Rzymski T, Dreas A, et al. MNK1/2 inhibition limits oncogenicity and metastasis of KIT-mutant melanoma. *J Clin Invest* (2017) 127:4179–92. doi: 10.1172/JCI91258
17. Araiza-Olivera D, Feng Y, Semenova G, Prudnikova TY, Rhodes J, Chernoff J. Suppression of RAC1-driven malignant melanoma by group A PAK inhibitors. *Oncogene* (2018) 37:944–52. doi: 10.1038/onc.2017.400
18. Faraj BA, Camp VM, Murray DR, Kutner M, Hearn J, Nixon D. Plasma L-dopa in the diagnosis of malignant melanoma. *Clin Chem* (1986) 32:159–61. doi: 10.1093/clinchem/32.1.159
19. Sørensen BS, Schmidt H, von der Maase H, Straten PT, Nexø E. Quantification of melanoma cell-specific MART-1 mRNA in peripheral blood by a calibrated competitive reverse transcription-PCR. *Clin Chem* (2000) 46:1923–8. doi: 10.1093/clinchem/46.12.1923
20. Feigelson HS, Powers JD, Kumar M, Carroll NM, Pathy A, Ritzwoller DP. Melanoma incidence, recurrence, and mortality in an integrated healthcare system: A retrospective cohort study. *Cancer Med* (2019) 8:4508–16. doi: 10.1002/cam4.2252
21. Roger A, Finet A, Boru B, Beauchet A, Mazeron JJ, Otzmeguine Y, et al. Efficacy of combined hypo-fractionated radiotherapy and anti-PD-1 monotherapy in difficult-to-treat advanced melanoma patients. *Oncoimmunology* (2018) 7:e1442166. doi: 10.1080/2162402X.2018.1442166
22. Ward A, Balwierz A, Zhang JD, Küblbeck M, Pawitan Y, Hielscher T, et al. Re-expression of microRNA-375 reverses both tamoxifen resistance and accompanying EMT-like properties in breast cancer. *Oncogene* (2013) 32:1173–82. doi: 10.1038/onc.2012.128
23. Ashburner M, Ball CA, Blake JA, Botstein D, Butler H, Cherry JM, et al. Gene ontology: tool for the unification of biology. The Gene Ontology Consortium. *Nat Genet* (2006) 25(2000):25–9. doi: 10.1038/75556
24. Kanehisa M, Goto S. KEGG: kyoto encyclopedia of genes and genomes. *Nucleic Acids Res* (2000) 28:27–30. doi: 10.1093/nar/28.1.27
25. Dennis G Jr., Sherman BT, Hosack DA, Yang J, Gao W, Lane HC, et al. DAVID: Database for Annotation, Visualization, and Integrated Discovery. *Genome Biol* (2003) 4:P3. doi: 10.1186/gb-2003-4-5-p3
26. Szklarczyk D, Franceschini A, Wyder S, Forslund K, Heller D, Huerta-Cepas J, et al. STRING v10: protein-protein interaction networks, integrated over the tree of life. *Nucleic Acids Res* (2015) 43:D447–52. doi: 10.1093/nar/gku1003
27. Kohl M, Wiese S, Warscheid B. Cytoscape: software for visualization and analysis of biological networks. *Methods Mol Biol (Clifton N J)* (2011) 696:291–303. doi: 10.1007/978-1-60761-987-1_18
28. Chandrashekar DS, Bashel B, Balasubramanya SAH, Creighton CJ, Ponce-Rodriguez I, Chakravarthi B, et al. UALCAN: A Portal for Facilitating Tumor Subgroup Gene Expression and Survival Analyses. *Neoplasia (N Y N Y)* (2017) 19:649–58. doi: 10.1016/j.neo.2017.05.002
29. Randerson-Moor JA, Harland M, Williams S, Cuthbert-Heavens D, Sheridan E, Aveyard J, et al. A germline deletion of p14(ARF) but not CDKN2A in a melanoma-neural system tumour syndrome family. *Hum Mol Genet* (2001) 10:55–62. doi: 10.1093/hmg/10.1.55
30. Goldstein AM, Chan M, Harland M, Hayward NK, Demenais F, Bishop DT, et al. Features associated with germline CDKN2A mutations: a GenoMEL study of melanoma-prone families from three continents. *J Med Genet* (2007) 44:99–106. doi: 10.1136/jmg.2006.043802
31. Fried L, Tan A, Bajaj S, Liebman TN, Polsky D, Stein JA. Technological advances for the detection of melanoma: Advances in molecular techniques. *J Am Acad Dermatol* (2020) 83:996–1004. doi: 10.1016/j.jaad.2020.03.122
32. Pan SH, Su KY, Spiessens B, Kusuma N, Delahaye NF, Gruselle O, et al. Gene expression of MAGE-A3 and PRAME tumor antigens and EGFR mutational status in Taiwanese non-small cell lung cancer patients. *Asia Pacific J Clin Oncol* (2017) 13:e212–23. doi: 10.1111/ajco.12586
33. Koopmans I, Hendriks D, Samplonius DF, van Ginkel RJ, Heskamp S, Wierstra PJ, et al. A novel bispecific antibody for EGFR-directed blockade of the PD-1/PD-L1 immune checkpoint. *Oncoimmunology* (2018) 7:e1466016. doi: 10.1080/2162402X.2018.1466016
34. Katunarić M, Jurišić D, Petković M, Grahovac M, Grahovac B, Zamolo G. EGFR and cyclin D1 in nodular melanoma: correlation with pathohistological parameters and overall survival. *Melanoma Res* (2014) 24:584–91. doi: 10.1097/CMR.0000000000000123
35. Westphal M, Maire CL, Lamszus K. EGFR as a Target for Glioblastoma Treatment: An Unfulfilled Promise. *CNS Drugs* (2017) 31:723–35. doi: 10.1007/s40263-017-0456-6
36. Yang ZY, Shen WX, Hu XF, Zheng DY, Wu XY, Huang YF, et al. EGFR gene copy number as a predictive biomarker for the treatment of metastatic colorectal cancer with anti-EGFR monoclonal antibodies: a meta-analysis. *J Hematol Oncol* (2012) 5:52. doi: 10.1186/1756-8722-5-52
37. Thyssen JP, Kezic S. Causes of epidermal filaggrin reduction and their role in the pathogenesis of atopic dermatitis. *J Allergy Clin Immunol* (2014) 134:792–9. doi: 10.1016/j.jaci.2014.06.014
38. Kezic S. Loss-of-function mutations in filaggrin gene and malignant melanoma. *J Eur Acad Dermatol Venereol* (2018) 32:193. doi: 10.1111/jdv.14813
39. Schäfer S, Koch PJ, Franke WW. Identification of the ubiquitous human desmoglein, Dsg2, and the expression catalogue of the desmoglein subfamily

of desmosomal cadherins. *Exp Cell Res* (1994) 211:391–9. doi: 10.1006/excr.1994.1103
40. Klessner JL, Desai BV, Amargo EV, Getsios S, Green KJ. EGFR and ADAMs cooperate to regulate shedding and endocytic trafficking of the desmosomal cadherin desmoglein 2. *Mol Biol Cell* (2009) 20:328–37. doi: 10.1091/mbc.e08-04-0356
41. Li G, Schaider H, Satyamoorthy K, Hanakawa Y, Hashimoto K, Herlyn M. Downregulation of E-cadherin and Desmoglein 1 by autocrine hepatocyte growth factor during melanoma development. *Oncogene* (2001) 20:8125–35. doi: 10.1038/sj.onc.1205034
42. Das A, Pushparaj C, Herreros J, Nager M, Vilella R, Portero M, et al. T-type calcium channel blockers inhibit autophagy and promote apoptosis of malignant melanoma cells. *Pigment Cell Melanoma Res* (2013) 26:874–85. doi: 10.1111/pcmr.12155
43. Rorke EA, Eckert RL. Stable expression of transfected human involucrin gene in various cell types: evidence for in situ cross-linking by type I and type II transglutaminase. *J Invest Dermatol* (1991) 97:543–8. doi: 10.1111/1523-1747.ep12481579
44. Simon M, Green H. The glutamine residues reactive in transglutaminase-catalyzed cross-linking of involucrin. *J Biol Chem* (1988) 263:18093–8.
45. Steinert PM, Marekov LN. Direct evidence that involucrin is a major early isopeptide cross-linked component of the keratinocyte cornified cell envelope. *J Biol Chem* (1997) 272:2021–30. doi: 10.1074/jbc.272.3.2021
46. Joo YA, Chung H, Yoon S, Park JI, Lee JE, Myung CH, et al. Skin Barrier Recovery by Protease-Activated Receptor-2 Antagonist Lobaric Acid. *Biomol Ther* (2016) 24:529–35. doi: 10.4062/biomolther.2016.011
47. Inoue T, Toda S, Narisawa Y, Sugihara H. Subcutaneous adipocytes promote the differentiation of squamous cell carcinoma cell line (DJM-1) in collagen gel matrix culture. *J Invest Dermatol* (2001) 117:244–50. doi: 10.1046/j.0022-202x.2001.01431.x
48. Arias-Mejias SM, Warda KY, Quattrocchi E, Alonso-Quinones H, Sominidi-Damodaran S, Meves A. The role of integrins in melanoma: a review. *Int J Dermatol* (2020) 59:525–34. doi: 10.1111/ijd.14850
49. Leask A. A centralized communication network: Recent insights into the role of the cancer associated fibroblast in the development of drug resistance in tumors. *Semin Cell Dev Biol* (2020) 101:111–4. doi: 10.1016/j.semcdb.2019.10.016
50. Zhang Q, Wang Y, Liang J, Tian Y, Zhang Y, Tao K. Bioinformatics analysis to identify the critical genes, microRNAs and long noncoding RNAs in melanoma. *Med (Balt)* (2017) 96:e7497. doi: 10.1097/MD.0000000000007497
51. Li Q, Zhang LY, Wu S, Huang C, Liu J, Wang P, et al. Bioinformatics Analysis Identifies MicroRNAs and Target Genes Associated with Prognosis in Patients with Melanoma. *Med Sci Monitor Int Med J Exp Clin Res* (2019) 25:7784–94. doi: 10.12659/MSM.917082

Conflict of Interest: The authors declare that the research was conducted in the absence of any commercial or financial relationships that could be construed as a potential conflict of interest.

frontiers in Oncology

MINI REVIEW
published: 27 November 2020
doi: 10.3389/fonc.2020.576190

Dissecting the Lymphatic System to Predict Melanoma Metastasis

Rishi Suresh[1], *Arturas Ziemys*[2] *and Ashley M. Holder*[3]*

[1] Texas A&M College of Medicine, Bryan, TX, United States, [2] Department of Nanomedicine, Houston Methodist Research Institute, Houston, TX, United States, [3] Department of Surgery, Division of Surgical Oncology, University of Alabama at Birmingham, Birmingham, AL, United States

Melanoma is the most lethal form of skin cancer in the United States. Current American Joint Committee on Cancer (AJCC) staging uses Breslow depth and ulceration as the two primary tumor factors that predict metastatic risk in cutaneous melanoma. Early disease stages are generally associated with high survival rates. However, in some cases, patients with thin melanomas develop advanced disease, suggesting other factors may contribute to the metastatic potential of an individual patient's melanoma. This review focuses on the role of the lymphatic system in the metastasis of cutaneous melanoma, from recent discoveries in mechanisms of lymphangiogenesis to elements of the lymphatic system that ultimately may aid clinicians in determining which patients are at highest risk. Ultimately, this review highlights the need to integrate pathological, morphological, and molecular characteristics of lymphatics into a "biomarker" for metastatic potential.

Keywords: lymphatics, melanoma, metastasis, lymphangiogenesis, transport

OPEN ACCESS

Edited by:
Giuseppe Palmieri, Institute Genetic Biomedical Research (IRGB), Italy

Reviewed by:
Inna Smalley, Moffitt Cancer Center, United States
Gagan Chhabra, University of Wisconsin-Madison, United States

***Correspondence:**
Ashley M. Holder
ashleyholder@uabmc.edu

Specialty section:
This article was submitted to Skin Cancer, a section of the journal Frontiers in Oncology

Received: *25 June 2020*
Accepted: *28 October 2020*
Published: *27 November 2020*

Citation:
Suresh R, Ziemys A and Holder AM (2020) Dissecting the Lymphatic System to Predict Melanoma Metastasis. Front. Oncol. 10:576190. doi: 10.3389/fonc.2020.576190

INTRODUCTION

Melanoma is responsible for the majority of skin cancer related deaths in the United States. Despite an increased incidence in the United States, melanoma mortality has decreased significantly in the past few years (1). However, metastatic melanoma still carries a poor prognosis. The American Joint Committee on Cancer (AJCC) staging system, 8th edition, has identified Breslow depth and ulceration as important predictive factors of survival in patients with melanoma (2). When detected at an early stage, melanoma can be treated with wide local excision and staged with sentinel lymph node biopsy. However, more advanced disease requires a multidisciplinary approach that often includes systemic therapy—from targeted treatments (BRAFi) to checkpoint inhibitors (3). Nonetheless, up to 15% of patients who have thin melanomas ultimately develop metastatic disease (4, 5). The best way to identify these high-risk patients, manage their nodal basin, and improve their survival remains controversial (5). Therefore, further study is needed to improve risk stratification and staging of melanoma.

Melanoma preferentially metastasizes to lymph nodes, leading to hypotheses that it spreads through the lymphatic vasculature (4). However, the exact mechanisms of lymphatic invasion and metastasis are not well-defined. Recently, experimental models have been developed that explore the role of growth factors—such as VEGF-C—in lymphangiogenesis and eventual melanoma metastasis (6). Furthermore, several studies have closely analyzed the alterations that occur in the lymphatic system in response to melanoma, including changes in vessel size, density, and transport kinetics (7–9). Together, these studies have suggested that the lymphatic system likely has an essential

function in melanoma metastasis. This review will assess how the lymphatic system may contribute to metastasis of cutaneous melanoma, specifically focusing on factors that predict metastatic potential and can be integrated into a lymphatic "biomarker."

LYMPHATIC DENSITY, LYMPHATIC INVASION, AND MELANOMA METASTASIS

Given that melanomas often spread to lymph nodes, others have hypothesized that melanomas that are likely to metastasize would demonstrate increased lymphatic vessel density (LVD). Early attempts to study lymphatic vasculature in melanoma were limited by the challenge of distinguishing blood vessels from lymphatics, leading some initial studies to conclude that lymphatic density was unchanged in metastatic melanoma (10). Once antibodies specific for lymphatic vasculature in the skin, such as LYVE-1, were developed, investigating lymphatics was possible (7). To test the hypothesis that tumors that metastasize to the lymph nodes would show increased lymphatic density, Shields et al. compared lymphatic density in melanoma to: 1) normal dermis, 2) basal cell carcinoma (BCC), and 3) Merkel cell carcinoma (MCC). Both intratumoral and epitumoral lymphatic density were found to be substantially increased in melanoma relative to BCC or MCC, suggesting that lymphatic density is increased in tumors that preferentially metastasize to lymph nodes. Furthermore, increased lymphatic density was found to be associated with melanomas that were more likely to metastasize than those that were not. Finally, melanomas included in their study that had both vascular and lymphatic invasion were frequently metastatic. These results point to the possible value of utilizing both lymphatic vessel density and lymphovascular invasion as important predictive features in assessing metastatic potential.

Together, these observations were incorporated into the Shields index, a predictive metric based on lymphatic invasion, lymphatic density, and Breslow thickness to the metastatic potential of an individual melanoma. While the initial Shields et al. study had a relatively small sample size of 21 melanomas, several subsequent studies have reported that increased lymphatic density leads to a poor prognostic outcome (4, 7, 11, 12). Both Emmett et al. and Spiric et al. attempted to use the Shields index to predict whether a melanoma was likely to metastasize (**Table 1**). In a retrospective review of 102 melanomas, Emmett et al. found that the Shields index was the best technique for discriminating between metastatic and non-metastatic melanomas, followed by lymphatic vessel density alone, AJCC staging, and Breslow thickness (4). Similarly, Spiric et al. reviewed 100 melanoma specimens and found that the Shields index performed better than either melanoma thickness or AJCC staging at predicting metastatic potential of melanoma (7, 11).

Nonetheless, the role of lymphovascular invasion as a unique predictive value in determining metastasis is unclear. A review of 1,029 melanomas from the Melbourne Melanoma Project found lymphatic invasion to be a significant predictor of recurrence (13). However, other studies concluded that lymphatic invasion is not a significantly unique predictor of melanoma metastasis (14–19). More recent national cancer database analyses demonstrated that lymphovasacular invasion by histopathological analysis is an independent predictor of sentinel lymph node metastasis in patients with T2 (20) but not T1 (17) melanoma, while a European multi-institutional study suggested that lymphovascular invasion was an independent predictor of sentinel lymph node metastasis in patients with T1b melanoma (21). The discrepancies in these findings reveal the complexity of dissecting the role of lymphovascular invasion in metastasis. Notably, several studies that found no association between lymphatic invasion and metastasis had large sample sizes, further contributing to this controversy (**Table 2**).

These studies suggest that lymphatic vessel density (LVD) and the Shields index are valuable predictive tools. One possible reason that LVD has not been adopted as a predictive factor in clinical practice is the time-intensive nature of the procedure. In their comparison of different methods of identifying LVD, Emmett et al. compared the traditional Shields method to the "hot spot method." In the traditional Shields method, every lymphatic within 350 μm of the tumor edge is counted. The hot spot method requires that only three areas of subjective high lymphatic density are counted and then averaged. When compared, the time to complete the traditional Shields method was 19 min per slide, while the hot spot analysis was only 5.5 min (7). Despite being about four times faster, the hot spot method did not yield a Shields index that was significantly different than the traditional method. However, even the more cumbersome method of calculating lymphatic vessel density has the potential to provide important prognostic information for melanoma patients.

TABLE 1 | The Shields index to predict metastatic potential of cutaneous melanoma.

Authors	Sample size	Design	Epitumoral lymphatic vessel density method	Outcome
Shields et al. (7)	21	Retrospective	Complete • All lymphatics counted • x40 objective • 350 μm from tumor edge	Index predicted metastasis more effectively than thickness alone
Emmett et al. (4)	102	Retrospective	Complete and hotspot • x100 objective • Three areas of subjectively high density were counted and averaged	Hotspot faster but comparable to complete method Shields index (81% specific, 82% sensitive) predicted metastasis more effectively than lymphatic vessel density and AJCC staging
Spiric et al. (11)	100	Retrospective	Hotspot	Shields index (75% specific, 81.3% sensitive), performed better at predicting metastasis than thickness and AJCC staging

TABLE 2 | Studies concluding that lymphatic invasion does not predict metastasis.

Authors	Sample size	Staining technique	Outcome
Pettit et al. (16)	27 10 specimens with LI	D2-40/S-100 dual Immunohistochemistry	Lymphatic Invasion (LI) not associated with SLN metastasis
Egger et al. (17)	6894 T1b Melanoma specimens 107 specimens with LI	n/a	LI not a significant predictor of metastasis in T1b melanoma
Storr et al. (18)	202 specimens of thickness ≥ 0.75mm 27 specimens with LI	D2-40/CD34	No association with clinical outcome (relapse free or overall survival)
Rose et al. (19)	246 specimens (18% with LI)	D2-40/CD34	LI not significant predictor of SLN status

LI, lymphatic invasion.

MECHANISMS OF LYMPHANGIOGENESIS

The mechanism of tumor spread from the primary to the sentinel lymph node has been investigated in both animal models and patients (**Table 3**). Studies have demonstrated that tumor-draining lymph nodes enlarge prior to clinical evidence of metastasis (8). However, the specific alterations and mechanisms that lead to these changes are poorly understood.

VEGF-C has been studied extensively for its role in melanoma growth and metastasis. Hoshida et al. evaluated lymphatic drainage in C57BL/6 mice injected with the B16F10 murine melanoma cell line using intravital microscopy. To confirm prior reports that VEGF-C is involved in lymphangiogenesis, their team developed VEGF-C overexpressing cell lines and noticed that tumor cell delivery and lymph flow rate increased in the draining lymph nodes in models of this cell line (22). This finding was largely confirmed by Harrell et al. who injected B16F10 into the footpad of C57BL/6 mice and noted a dramatic increase in the size of lymphatic sinuses and flow in the draining lymph node (23). Interestingly, the study did not identify any alterations in the lymphatics immediately adjacent to the tumor. Their result is inconsistent with findings in human patients but may be related to the creation of the murine model compared to primary melanomas from patients (4, 7, 11). Finally, blocking the VEGF receptor-3 (a key receptor of VEGF-C) in a murine B16F10 melanoma model inhibited lymphangiogenesis and immunosuppressive cell infiltration, further suggesting that VEGF-C plays an important role in the growth of lymphatic vessels in response to tumor (6). Furthermore, in a similar murine model, the expression of VEGF-C was associated with infiltration of immunosuppressive cells, including regulatory T cells into the primary tumor (24). Tumors with VEGF-C expression were shown to suppress naïve T cell activation in the draining lymph node, even more strongly than preexisting vaccine-induced immunity (24).

It is important to note that several of the aforementioned studies employ a syngeneic B16F10 melanoma model, which have been previously shown to have differences in vascularity and other structural irregularities compared to human melanoma (27). In addition, differences in the immunogenicity and genetic background (lack of BRAF mutation) have called into question the applicability of this murine melanoma model (28, 29). Therefore, the biology revealed from research using these models may not translate to patients.

LYMPHATIC VESSELS AND THE TUMOR MICROENVIRONMENT

Given the role of lymphatic vessels in regulating immunologic tolerance in normal environments, Lane et al. hypothesized that they may regulate tumor environments (25). Their results from

TABLE 3 | Mechanistic studies evaluating melanoma metastasis.

Authors	Model	Key findings
Hoshida et al. (22)	B16F10 melanoma with C57BL/6 mice	VEGF-C overexpressing cell lines increased tumor cell delivery and flow rate
Qian et al. (8)	Human NPC cell line in BALB/c mice	Tumor-draining lymph nodes can enlarge prior to evidence of metastasis
Harrell et al. (23)	B16F10 melanoma with C57BL/6 mice	Increase in size of lymphatic sinuses and flow in draining lymph node of tumor
Fankhauser et al. (6)	B16F10 melanoma model	Blocking VEGF Receptor-3 inhibited lymphangiogenesis and immunosuppressive cell infiltration
Lund et al. (24)	B16F10 melanoma with C57BL/6 mice	VEGF-C associated with infiltration of Treg into primary tumor; tumors with VEGF-C expression suppressed naïve T cell activation
Lane et al. (25)	C57BL/6J mice with B16F10.OVA, MC38, YUMM1.7, YUMMER1.7 cells	Lymphatic endothelium plays a critical role in creating an immunosuppressive environment permitting tumor growth
Commerford et al. (26)	B16F10 melanoma with BALB/c and C57BL/6 mice	Adhesion genes such as Jam3 or integrin allb differentially regulated in tumor draining lymph nodes

murine models found that non-hematopoietic PD-L1 is expressed in lymphatic endothelial cells (LEC), limiting CD8+ T cell accumulation. They further established that IFNγ released by activated CD8+ T cells can induce PD-L1 expression in LECs and that loss of IFNγ receptor leads to increased T cell accumulation. These results suggest that the lymphatic endothelium has a critical function in developing an immunosuppressive environment that permits tumor growth. Implantation of B16F10 into B lymphocyte-deficient mice demonstrated that lymphatic network size and flow did not increase in the draining lymph nodes (23). Furthermore, primary tumors implanted into the footpad of mice were noted to attract myeloid cells and macrophages, but the tumor draining lymph nodes would accumulate T and B lymphocytes, suggesting that B lymphocytes are critical for the changes observed in distant lymph nodes (23). Together, these results suggest that immunosuppressive effects of melanoma are complex and mediated by B lymphocytes, lymphatic endothelium, and growth factors such as VEGF-C.

From these studies, targeting VEGF-C was considered to be a promising approach for decreasing metastasis in melanoma. However, the AVAST-M trial using adjuvant bevacizumab for melanoma patients failed to identify a significant difference in survival at 5 years (30, 31). Findings from studies, including Fankhauser et al., suggest that the effect of immunotherapy is potentiated in tumors that cause increased lymphangiogenesis. In a murine model, adoptively transferred *ex vivo* activated CD8+ T cells were able to respond to tumors in which VEGF-C was expressed compared to tumors where VEGFR-3 was blocked (6). To extrapolate their findings beyond mice, the sera of human metastatic melanoma patients were tested for VEGF-C. Consistent with their findings in murine models, higher VEGF-C concentrations correlated with response to immunotherapy and progression free survival.

Future studies may identify additional therapeutic targets of the lymphatic system in melanoma metastasis. Commerford et al. performed RNA sequencing of the LECs in the tumor draining lymph node of mice injected with B16F10 melanoma and compared it to normal LECs (26). Cell-cell and cell-matrix adhesion genes such as Jam3 or integrin αIIb were differentially regulated in the tumor-draining lymph node, suggesting that LECs in tumor-draining lymph nodes are altered at a transcriptional level. These results could identify potential future targets to prevent lymphangiogenesis in metastatic melanoma. Additional research needs to be performed to translate these mechanistic insights in routine clinical practice. Generally, the biomarkers associated with melanoma metastasis are diluted in a routine blood draw, limiting their use (32). Broggi et al. described use of postoperative lymphatic exudate and plasma in stage III melanoma patients as a way to collect biomarkers including factors not only associated with melanoma (LDH, S100B, S100A8) but also linked to metastatic potential (CSF-1, galectin-3, MMP2-MM-9). While this method could be used in patients with advanced disease, the difficulty of accessing lymphatic exudate limits its use in earlier stage melanomas in which extensive lymph node dissection is not typically performed.

Furthermore, recent research has shown that the tumor microenvironment could potentially be affected following surgical alterations. Following inoculation of B16F10 melanoma cells into BALB/c mice, Nakamura et al. performed bilateral inguinal lymph node resection or a U-incision and noted that tumor growth was significantly increased in mice with surgical damage (33). Upon further histologic analysis of the tumor, they noted that both the total number of CD4+ and CD8+ T cells and apoptotic cells were significantly reduced in the mice that underwent surgical intervention. These observations were also seen when using an immunogenic tumor cell line (MC38). Therefore, adaptive immunity mechanisms may be impaired by the disruption of lymphatic vasculature following surgery, due to impaired transit of tumor antigens through lymphatic vasculature to regional lymph nodes and subsequent expansion of tumor-specific T-cells.

LYMPHATIC TRANSPORT KINETICS

The kinetics of lymphatic transport have also been studied for prognostic applications in melanoma (**Table 4**). In a prospective trial of 276 patients, technetium-99m based lymphoscintigraphy was used to determine whether a patient had fast (less than 20 min) or slow (greater than 20 min) lymphatic transit (34). In this small feasibility study, all patients with slow drainage were found to be disease-free at 2 year follow-up. Later studies attempted to determine whether this scintigraphic appearance time (SAT) would be a reliable factor to distinguish melanomas based on their metastatic potential. Cammilleri et al. performed lymphoscintigraphy on 88 subjects with limb and trunk melanomas and retrospectively was able to determine that an SAT greater than 30 min correlated with a negative predictive value of 100% for the sentinel lymph node (35). These early studies suggested that a retrospective distinction could be made between SLN positive and SLN negative patients based on SAT time. However, when Mahieu-Renard et al. applied a SAT time of 30 min in a prospective cohort of 150 patients, the study yielded a negative predictive value of only 84.6% (65.1–95.6%) (36). It is slightly surprising that a lymph node containing tumor might have faster drainage, given that tumor infiltration of lymph nodes would theoretically cause an obstruction of flow (36), but likely the flow is unobstructed until large amounts of tumor are present. However, as shown previously, metastatic melanoma has been shown to significantly increase peritumoral lymphatic density (7) and increase the size of tumor draining lymph vasculature (23), factors that would likely contribute to increased transport flow capacity. Furthermore, metastatic melanoma is likely to result in an increase in activated macrophages (23), leading to increased scintigraphic uptake.

More recently, Fujiwara et al. described the use of the area extraction method to evaluate lymphatic kinetics in patients with truncal melanoma (9). The method utilizes technetium-99m phytate to perform dynamic lymphoscintigraphy and uses a gamma camera to acquire images and develop time activity curves (plotting tracer counts against time). Using this data, the researchers were able to identify a plateau, which they established as the scintigraphic saturation time (SST).

TABLE 4 | Studies evaluating lymphatic transport kinetics as predictive of sentinel lymph node metastasis.

Authors	Samplesize	Location of melanoma	Melanoma features	Type of melanoma[a]	Design	Colloid	Time cutoffs[b]	Variable[c]	Results[d]
Maza et al. (34)	276	Trunk, lower limbs, upper limbs, head/neck	pT1-T4	SS, NM, LM, AL	Prospective	Tc-99 nanocolloid	20 min	SAT	No SLN metastasis in slow drainage group
Cammilleri et al. (35)	88	Trunk, upper limb, lower limb	Stage I and II	n/a	Prospective	Tc-99m colloidal rhenium sulfide	30 min	SAT	No SLN metastasis in slow drainage group
Mahieu-Renard et al. (36)	Retro: 194 Prosp: 150	Limbs, trunk, hands/feet, head/neck	Breslow: ≤1mm->4mm	SS, NM, AL, LM	Retrospective, prospective	Tc-99m colloidal rhenium sulfide	30 min	SAT	Slow lymphatic drainage had a negative predictive value of 84.6%
Fujiwara et al. (9)	11	Trunk	n/a	SS	Retrospective	Tc-99m phytate	30 min	SST, LTR	All SLNs with <1.8cm/min LTR were non-metastatic
Toubert et al. (37)	160	Upper limb, lower limb, trunk, head/neck	Breslow >1mm	n/a	Prospective	Tc-99m colloidal rhenium sulfide	30 min	SAT	No significant difference based on speed of drainage

[a]*Superficial spreading (SS), lentigo maligna (LM), acral lentiginous (AL), nodular melanoma (NL).*
[b]*Lymphatic transport rate (LTR).*
[c]*Scintigraphic appearance time (SAT), scintigraphic saturation time (SST), lymphatic transport rate (LTR).*
[d]*Sentinel lymph node (SLN).*

Compared to the prior efforts of estimating SAT which were primarily based on researcher visualization, the SST represents a more reproducible method since it does not depend on the researcher's visualization. To determine the lymphatic transit rate (LTR), the distance between the primary tumor and the SLN (using real-time fluorescence navigation with indocyanine green) was calculated and then divided by the SST. Together, the LTR and SST were found to be significant in determining the status of the sentinel lymph node in patients with melanoma (9).

While there is evidence to support the notion that SAT can possibly determine the likelihood of sentinel lymph node positivity, some studies have contrarily suggested that there is no significant difference in SLN metastasis and speed of lymphatic transport. For example, Toubert et al. found in a cohort of 160 patients that there was no difference in metastatic SLN based upon speed of drainage using dynamic acquisition and static imaging divided into fast (<20 min), intermediate (20–30 min) or slow (>30 min) lymphatic drainage (37). Lymphoscintigraphy and lymphatic transport are factors that are difficult to standardize, which could account for the differences in procedures. Lymphatic transport can be affected broadly by several factors including age (38), weight (39), musculature, changes in Starling forces, and body position (40). The size of the colloid also significantly affects the SAT. Both Camilleri et al. and Toubert et al. used the same colloid (99mTc-rhenium sulfide) and therefore utilized the same SAT in their respective studies. Maza et al. used a 99mTc-nanocolloid, accounting for the difference in SAT (34). Both of these colloids were smaller than the 99mTc-phytate employed by Fujiwara et al. (9).

Furthermore, the transit time of lymphatic fluid varies greatly based on region of the body. Specifically, lymphatic drainage rates are significantly lower in the head and neck relative to the extremities (41). Additionally, the use of lymphoscintigraphy in the head and neck or perineal region can be obscured by shine-through (9). Therefore, any protocol developed regarding the use of SAT as a predictive marker of SLN metastasis will require an individualized approach based on these factors to yield consistent, reproducible results. The area extraction method developed by Fujiwara et al. appears to be a standardized way of evaluating SST and LTR (9). However, their technique required multiple and frequent imaging. Nonetheless, techniques for assessing lymphatic transport efficiency will require standardization prior to integration into staging guidelines for melanoma, as differences in technique would likely result in discrepancies in the predictive value of these approaches.

DISCUSSION

The lymphatic system makes a critical contribution in melanoma metastasis. Recent studies have suggested that factors like VEGF-C and the lymphatic endothelium itself play an important role in altering the immune system to support melanoma metastasis (22, 25). While these studies often rely on B16F10 melanoma models that may not accurately replicate human biology, their findings may ultimately yield important mechanistic insights. Several studies have suggested that using lymphatic vessel density and lymphatic invasion in the Shields index may aid in determining the metastatic potential of melanoma (4, 7, 11),. Furthermore, utilizing lymphatic transport kinetics as a predictive factor appears to be a promising area of research (9, 35).

While these studies represent important steps toward understanding the role that the lymphatic system plays in the growth and metastasis of cutaneous melanoma, there are still several areas that require further study. The original Shields index was validated as a meaningful predictor of melanoma metastasis by the work of Emmett et al. and Spiric et al. (4, 11). However, all studies to date performed on the Shields index are retrospective in nature; thus, a prospective study is needed to

establish the utility of the method. Furthermore, there are contradictory reports in the literature regarding features such as lymphatic invasion and their predictive potential, and future studies are needed to reconcile these differences. Additionally, while lymphatic transport kinetics have been shown to successfully identify metastatic melanomas, future research is needed to develop a reliable tool in clinical practice. The specific techniques utilized for analysis of lymphatic transport need to be refined to become more consistent and reproducible, and specialized protocols will need to be developed based on the type of colloid utilized and the affected body area. Finally, while experimental models have revealed significant findings in the role that melanoma plays in lymphangiogenesis, future study is required to translate these genetic and mechanistic insights into targeted therapies or biomarkers.

This review highlights several studies proposing the lymphatic system as a critical player in melanoma metastasis. Features such as lymphatic vessel density or lymphatic transport kinetics might eventually serve as adjuncts to current staging protocols to improve our ability to detect melanomas that are high-risk. Furthermore, future research on the lymphatic system and melanoma metastasis may aid in the development of biomarkers or novel targeted therapies. However, while the study of the lymphatic system may improve detection and management of melanomas that are likely to metastasize, there is the possibility of overtreating patients who otherwise could have been managed more conservatively. Future studies are necessary to develop a more accurate lymphatic "biomarker" that systematically integrates pathological, morphological, and molecular data to identify high-risk melanomas that are understaged with current techniques.

AUTHOR CONTRIBUTIONS

RS, AZ, and AH jointly conceived the review. RS and AH performed the literature review and wrote the manuscript. AZ analyzed the quality of the transport analysis performed by studies included in the literature review. RS, AZ, and AH edited the manuscript at all stages. All authors contributed to the article and approved the submitted version.

ACKNOWLEDGMENTS

The authors would like to gratefully acknowledge the manuscript review by Dr. Marshall Urist, Professor Emeritus, UAB Department of Surgery, Division of Surgical Oncology.

REFERENCES

1. Henley SJ, Ward EM, Scott S, Ma J, Anderson RN, Firth AU, et al. Annual report to the nation on the status of cancer, part I: National cancer statistics. *Cancer* (2020) 126(10):2225–49. doi: 10.1002/cncr.32802
2. Keung EZ, Gershenwald JE. The eight edition American Joint Committee on Cancer (AJCC) melanoma staging system: implications for melanoma treatment and care. *Expert Rev Anticancer Ther* (2018) 18(8):775–84. doi: 10.1080/14737140.2018.1489246
3. Joyce KM. Surgical Management of Melanoma. In: WH Ward, JM Farma, editors. *Cutaneous Melanoma: Etiology and Therapy*. Brisbane (AU): Codon Publications (2017). p. 91–100. doi: 10.15586/codon.cutaneousmelanoma.2017.ch7
4. Emmett MS, Symonds KE, Rigby H, Cook MG, Price R, Metcalfe C, et al. Prediction of melanoma metastasis by the Shields index based on lymphatic vessel density. *BMC Cancer* (2010) 10:1–8. doi: 10.1186/1471-2407-10-208
5. Raica M, Jitariu A-A, Cimpean AM. Lymphangiogenesis and Anti-lymphangiogenesis in Cutaneous Melanoma. *Anticancer Res* (2016) 36 (9):4427–35. doi: 10.21873/anticanres.10986
6. Fankhauser M, Broggi MAS, Potin L, Bordry N, Jeanbart L, Lund AW, et al. Tumor lymphangiogenesis promotes T cell infiltration and potentiates immunotherapy in melanoma. *Sci Trans Med* (2017) 9(407):1–12. doi: 10.1126/scitranslmed.aal4712
7. Shields J, Borsetti M, Rigby H, Harper S, Mortimer S, Levick J, et al. Lymphatic density and metastatic spread in human malignant melanoma. *Br J Cancer* (2004) 90(3):693–700. doi: 10.1038/sj.bjc.6601571
8. Qian C-N, Berghuis B, Tsarfaty G, Bruch M, Kort EJ, Ditlev J, et al. Preparing the "soil": the primary tumor induces vasculature reorganization in the sentinel lymph node before the arrival of metastatic cancer cells. *Cancer Res* (2006) 66(21):10365–76. doi: 10.1158/0008-5472.CAN-06-2977
9. Fujiwara M, Suzuki T, Takiguchi T, Fukamizu H, Tokura Y. Lymphatic transit rate as a novel predictive parameter for nodal metastasis in primary truncal skin cancers. *J Dermatol* (2016) 43:170–4. doi: 10.1111/1346-8138.13033
10. Waal RMD, Altena MCV, Erhard H, Weidle UH, Nooijen PTGA, Ruiter DJ. Lack of lymphangiogenesis in human primary cutaneous melanoma. Consequences for the mechanism of lymphatic dissemination. *Am J Pathol* (1997) 150(6):1951–57.
11. Spiric Z, Eric M, Eri Z. Lymphatic invasion and the Shields index in predicting melanoma metastases. *J Plast Reconstr Aesthetic Surg* (2017) 70(11):1646–52. doi: 10.1016/j.bjps.2017.05.056
12. Dadras SS, Paul T, Bertoncini J, Brown LF, Muzikansky A, Jackson DG, et al. A Novel Prognostic Indicator for Cutaneous Melanoma Metastasis and Survival. *Am J Pathol* (2003) 162(6):1951–60. doi: 10.1016/S0002-9440(10)64328-3
13. Matheson JAH, Marvelde LT, Mailer S, Speakman D, Spillane J, Henderson MA, et al. Prospective evaluation of prognostic indicators for early recurrence of cutaneous melanoma. *Melanoma Res* (2017) 27(1):43–9. doi: 10.1097/CMR.0000000000000302
14. Moy AP, Duncan LM, Kraft S. Lymphatic invasion and angiotropism in primary cutaneous melanoma. *Lab Invest* (2017) 97(2):118–29. doi: 10.1038/labinvest.2016.131
15. Pastushenko I, Vermeulen PB, Carapeto FJ, Eynden GVD, Rutten A, Ara M, et al. Blood microvessel density, lymphatic microvessel density and lymphatic invasion in predicting melanoma metastases: systematic review and meta-analysis. *Br J Dermatol* (2014) 170(1):66–77. doi: 10.1111/bjd.12688
16. Petitt M, Allison A, Shimoni T, Uchida T, Raimer S, Kelly B. Lymphatic invasion detected by D2-40/S-100 dual immunohistochemistry does not predict sentinel lymph node status in melanoma. *J Am Acad Dermatol* (2009) 61(5):819–28. doi: 10.1016/j.jaad.2009.04.026
17. Egger ME, Stevenson M, Bhutiani N, Jordan AC, Scoggins CR, Philips P, et al. Should Sentinel Lymph Node Biopsy Be Performed for All T1b Melanomas in the New 8(th) Edition American Joint Committee on Cancer Staging System? *J Am Coll Surg* (2019) 228(4):466–72. doi: 10.1016/j.jamcollsurg.2018.12.030
18. Storr SJ, Safuan S, Mitra A, Elliott F, Walker C, Vasko MJ, et al. Objective assessment of blood and lymphatic vessel invasion and association with macrophage infiltration in cutaneous melanoma. *Mod Pathol* (2012) 25 (4):493–504. doi: 10.1038/modpathol.2011.182
19. Rose AE, Christos PJ, Lackaye D, Shapiro RL, Berman R, Mazumdar M, et al. Clinical relevance of detection of lymphovascular invasion in primary melanoma using endothelial markers D2-40 and CD34. *Am J Surg Pathol* (2011) 35(10):1441–9. doi: 10.1097/PAS.0b013e31822573f5
20. Egger ME, Stevenson M, Bhutiani N, Jordan AC, Scoggins CR, Philips P, et al. Age and Lymphovascular Invasion Accurately Predict Sentinel Lymph Node Metastasis in T2 Melanoma Patients. *Ann Surg Oncol* (2019) 26(12):3955–61. doi: 10.1245/s10434-019-07690-4

21. Maurichi A, Miceli R, Camerini T, Mariani L, Patuzzo R, Ruggeri R, et al. Prediction of survival in patients with thin melanoma: results from a multi-institution study. *J Clin Oncol* (2014) 32(23):2479–85. doi: 10.1200/JCO.2013.54.2340
22. Hoshida T, Isaka N, Hagendoorn J, di Tomaso E, Chen YL, Pytowski B, et al. Imaging steps of lymphatic metastasis reveals that vascular endothelial growth factor-C increases metastasis by increasing delivery of cancer cells to lymph nodes: therapeutic implications. *Cancer Res* (2006) 66(16):8065–75. doi: 10.1158/0008-5472.CAN-06-1392
23. Harrell MI, Iritani BM, Ruddell A. Tumor-Induced Sentinel Lymph Node Lymphangiogenesis and Increased Lymph Node Precede Melanoma Metastasis. *Am J Pathol* (2007) 170(2):774–86. doi: 10.2353/ajpath.2007.060761
24. Lund AW, Duraes FV, Hirosue S, Raghavan VR, Nembrini C, Thomas SN, et al. VEGF-C Promotes Immune Tolerance in B16 Melanomas and Cross-Presentation of Tumor Antigen by Lymph Node Lymphatics. *Cell Rep* (2012) 1(3):191–9. doi: 10.1016/j.celrep.2012.01.005
25. Lane RS, Femel J, Breazeale AP, Loo CP, Thibault G, Kaempf A, et al. IFNγ-activated dermal lymphatic vessels inhibit cytotoxic T cells in melanoma and inflamed skin. *J Exp Med* (2018) 215(12):3057–74. doi: 10.1084/jem.20180654
26. Commerford CD, Dietrich LC, He Y, Hell T, Montoya-Zegarra JA, Noerrelykke SF, et al. Tumor lymphangiogenesis promotes T cell infiltration and potentiates immunotherapy in melanoma. *Cell Rep* (2018) 25(13):3554–63. doi: 10.1016/j.celrep.2018.12.002
27. Pautu V, Mellinger A, Resnier P, Lepeltier E, Martin L, Boussemart L, et al. Melanoma tumour vasculature heterogeneity: from mice models to human. *J Cancer Res Clin Oncol* (2019) 145(3):589–97. doi: 10.1007/s00432-018-2809-z
28. Hooijkaas A, Gadiot J, Morrow M, Stewart R, Schumacher T, Blank CU. Selective BRAF inhibition decreases tumor-resident lymphocyte frequencies in a mouse model of human melanoma. *Oncoimmunology* (2012) 1(5):609–17. doi: 10.4161/onci.20226
29. Becker JC, Houben R, Schrama D, Voigt H, Ugurel S, Reisfeld RA. Mouse models for melanoma: a personal perspective. *Exp Dermatol* (2010) 19 (2):157–64. doi: 10.1111/j.1600-0625.2009.00986.x
30. Corrie PG, Marshall A, Nathan PD, Lorigan P, Gore M, Tahir S, et al. Adjuvant bevacizumab for melanoma patients at high risk of recurrence: survival analysis of the AVAST-M trial. *Ann Oncol* (2018) 29(8):1843–52. doi: 10.1093/annonc/mdy299
31. Corrie PG, Marshall A, Dunn JA, Middleton MR, Nathan PD, Gore M, et al. Adjuvant bevacizumab in patients with melanoma at high risk of recurrence (AVAST-M): preplanned interim results from a multicentre, open-label, randomised controlled phase 3 study. *Lancet Oncol* (2014) 15(6):620–30. doi: 10.1016/S1470-2045(14)70110-X
32. Broggi MAS, Maillat L, Clement CC, Bordry N, Corthesy P, Auger A, et al. Tumor-associated factors are enriched in lymphatic exudate compared to plasma in metastatic melanoma patients. *J Exp Med* (2019) 216(5):1091–107. doi: 10.1084/jem.20181618
33. Nakamura Y, Fujisawa Y, Okiyama N, Watanabe R, Tanaka R, Ishitsuka Y, et al. Surgical damage to the lymphatic system promotes tumor growth via impaired adaptive immune response. *J Dermatol Sci* (2018) 90(1):46–51. doi: 10.1016/j.jdermsci.2017.12.016
34. Maza S, Valencia R, Geworski L, Sandrock D, Zander A, Audring H, et al. Influence of fast lymphatic drainage on metastatic spread in cutaenous malingant melanoma: a prospective feasibility study. *Eur J Nuclear Med Mol Imaging* (2003) 30(4):538–44. doi: 10.1007/s00259-003-1114-4
35. Cammilleri S, Jacob T, Rojat-Habib MC, Hesse S, Berthet B, Giorgi R, et al. High negative predictive value of slow lymphatic drainage on metastatic node spread detection in malignant head limb and trunk cutaneous melanoma. *Eur J Oncol* (2004) 91(7-8):225–8.
36. Mahieu-Renard L, Cammilleri S, Giorgi R, Gaudy-Marqueste C, Mundler O, Richard M-A, et al. Slow Dynamics of Lymphoscintigraphic Mapping Is Associated to the Negativity of the Sentinel Node in Melanoma Patients. *Ann Surg Oncol* (2008) 15(10):2878–86. doi: 10.1245/s10434-008-0080-2
37. Toubert M-E, Just P-A, Baillet G, Kerob D, Hindie E, Verola O, et al. Slow Dynamic Lymphoscintigraphy Is Not a Reliable Predictor of Sentinel-Node Negativity in Cutaneous Melanoma. *Cancer Biother Radiopharm* (2008) 23 (4):443–50. doi: 10.1089/cbr.2008.0468
38. Conway WC, Faries MB, Nicholl MB, Terando AM, Glass EC, Sim M, et al. Age-related lymphatic dysfunction in melanoma patients. *Ann Surg Oncol* (2009) 16(6):1548–52. doi: 10.1245/s10434-009-0420-x
39. Ogasawara Y, Ikeda H, Takahashi M, Kawasaki K, Doihara H. Evaluation of Breast Lymphatic Pathways with Indocyanine Green Fluorescence Imaging in Patients with Breast Cancer. *World J Surg* (2008) 32:1924–9. doi: 10.1007/s00268-008-9519-7
40. Stanton AWB, Patel HS, Levick JR, Mortimer PS. Increased Dermal Lymphatic Density in the Human Leg Compared with the Forearm. *Microvasc Res* (1999) 57(3):320–8. doi: 10.1006/mvre.1998.2141
41. Uren RF, Hawman-Giles R, Thompson JF. Variation in cutaneous lymphatic flow rates. *Ann Surg Oncol* (1997) 4(3):279–81. doi: 10.1007/BF02306624

Conflict of Interest: The authors declare that the research was conducted in the absence of any commercial or financial relationships that could be construed as a potential conflict of interest.

frontiers in Oncology

ORIGINAL RESEARCH
published: 30 November 2020
doi: 10.3389/fonc.2020.580029

Hierarchical Clustering of Cutaneous Melanoma Based on Immunogenomic Profiling

Jie Yu[†], *Minyue Xie*[†], *Shengfang Ge*, *Peiwei Chai*[*], *Yixiong Zhou*[*] *and Jing Ruan*[*]

Department of Ophthalmology, Shanghai Key Laboratory of Orbital Diseases and Ocular Oncology, Ninth People's Hospital, Shanghai JiaoTong University School of Medicine, Shanghai, China

Cutaneous melanoma is an aggressive malignancy with high heterogeneity. Several studies have been performed to identify cutaneous melanoma subtypes based on genomic profiling. However, few classifications based on assessments of immune-associated genes have limited clinical implications for cutaneous melanoma. Using 470 cutaneous melanoma samples from The Cancer Genome Atlas (TCGA), we calculated the enrichment levels of 29 immune-associated gene sets in each sample and hierarchically clustered them into Immunity High (Immunity_H, n=323, 68.7%), Immunity Medium (Immunity_M, n=135, 28.7%), and Immunity Low (Immunity_L, n=12, 2.6%) based on the ssGSEA score. The ESTIMATE algorithm was used to calculate stromal scores (range: -1,800.51–1,901.99), immune scores (range: -1,476.28–3,780.33), estimate scores (range: -2,618.28–5,098.14) and tumor purity (range: 0.216–0.976) and they were significantly correlated with immune subtypes (Kruskal–Wallis test, $P < 0.001$). The Immunity_H group tended to have higher expression levels of HLA and immune checkpoint genes (Kruskal–Wallis test, $P < 0.05$). The Immunity_H group had the highest level of naïve B cells, resting dendritic cells, M1 macrophages, resting NK cells, plasma cells, CD4 memory activated T cells, CD8 T cells, follicular helper T cells and regulatory T cells, and the Immunity_L group had better overall survival. The GO terms identified in the Immunity_H group were mainly immune related. In conclusion, immune signature-associated cutaneous melanoma subtypes play a role in cutaneous melanoma prognosis stratification. The construction of immune signature-associated cutaneous melanoma subtypes predicted possible patient outcomes and provided possible immunotherapy candidates.

Keywords: genomic profiling, ssGSEA, immune subtypes, prognosis, cutaneous melanoma

OPEN ACCESS

Edited by:
Igor Puzanov,
University at Buffalo, United States

Reviewed by:
Ioana Cosgarea,
Newcastle University, United Kingdom
Aurobind Vidyarthi,
Yale University, United States

***Correspondence:**
Peiwei Chai
chaipeiwei123@sjtu.edu.cn
Yixiong Zhou
zhouyixiong212@gmail.com
Jing Ruan
drjruan@163.com

[†]*These authors have contributed equally to this work*

Specialty section:
This article was submitted to Skin Cancer, a section of the journal Frontiers in Oncology

Received: *04 July 2020*
Accepted: *26 October 2020*
Published: *30 November 2020*

Citation:
Yu J, Xie M, Ge S, Chai P, Zhou Y and Ruan J (2020) Hierarchical Clustering of Cutaneous Melanoma Based on Immunogenomic Profiling. Front. Oncol. 10:580029. doi: 10.3389/fonc.2020.580029

INTRODUCTION

Cutaneous melanoma is one of the most aggressive types of cancer due to an elevated degree of heterogeneity in the aspects of clinical presentation, histopathological presentation and genomic profiles (1). Once spread, it becomes life threatening and causes 55,500 deaths every year (2). Due to its heterogeneity, many cutaneous melanoma classification studies have been carried out to lay the foundation for targeted therapies. Akbani R et al. divided 331 cutaneous melanoma patients into four subtypes based on three prevalent significantly mutated genes (BRAF, RAS, and NF1). Though there was no significant clinical correlation with this classification, a subclass whose genome was enriched in immune genes was associated with improved prognosis (3). Zhao Y et al., identified a 25-gene signature that was applied to calculate sample-specific leukocyte infiltration scores (LISs). A higher LIS proved to indicate a better prognosis in metastatic melanoma (4). Nie RC et al. developed an immunoscore based on eight immune subsets (naïve B cells, memory B cells, eosinophils, follicular helper T cells, regulatory T cells, M0 macrophages, plasma cells, and γδT cells), and cutaneous melanoma patients were divided into a high immunoscore group and a low immunoscore group to predict the anti-PD1 response (5). These efforts indicate the importance of classifying cutaneous melanoma for diagnosis and treatment.

To date, there are few treatment options available for cutaneous melanoma. Immunotherapy, such as immune checkpoint blockade, is one of the treatments that has recently increased hope for the survival outcomes of cutaneous melanoma patients (2). However, despite this tremendous advancement, immunotherapeutic strategies exhibit beneficial effects only in a subset of patients. Certain factors, such as tumor genomics, host germline genetics, and the PD-L1 level, influence the responsiveness of immunotherapy (6–8). Tumor microenvironment heterogeneity has been studied as a biomarker for prognosis and immunotherapy sensitivity in various cancers (9, 10). Of note, both infiltrating immune cells and tumor-related stromal cells, which play important roles in tumor growth, progression and drug resistance, are important components of the tumor immune microenvironment (11, 12). Therefore, an increasing number of studies have focused on these factors to provide novel insights into tumor biology and their prognostic value.

In our study, on the basis of immunogenomic profiling, we divided cutaneous melanoma patients into three groups: Immunity High (Immunity_H), Immunity Medium (Immunity_M), and Immunity Low (Immunity_L). We demonstrated that the classification was associated with immune infiltration and survival prognosis. Moreover, we identified subtype-specific genes and Gene Ontology (GO). The construction of immune signature-associated cutaneous melanoma subtypes may help identify possible candidates for immunotherapy.

Abbreviations: CIBERSORT, Cell-type Identification By Estimating Relative Subsets Of RNA Transcripts; ESTIMATE; Estimation of STromal and Immune cells in MAlignant Tumor tissues using Expression data; GO, Gene Ontology; Immunity_H, Immunity High; Immunity_L, Immunity Low; Immunity_M, Immunity Medium; LIS, leukocyte infiltration score.

METHODS

Database

The transcriptome profiles and clinical data of patients with cutaneous melanoma in this study were downloaded from The Cancer Genome Atlas (TCGA) database (https://portal.gdc.cancer.gov/). In total, 470 cutaneous melanoma patients were enrolled in the current study, and the clinical characteristics included sex, status and TNM stage.

Single Sample Gene Set Enrichment Analysis (ssGSEA)

For each cutaneous melanoma sample, we quantified the enrichment levels of the 29 immune-associated gene sets, representing immune cell types, functions, and pathways, as described in a previous study (13) by the ssGSEA score. On the basis of the ssGSEA scores of the 29 gene sets, we performed hierarchical clustering of cutaneous melanoma.

Estimation of STromal and Immune Cells in MAlignant Tumor Tissues Using Expression Data (ESTIMATE)

Stromal scores, immune scores, estimate scores, and the tumor purity of cutaneous melanoma patients were calculated with the ESTIMATE (14) algorithm using the estimate package in R version 3.6.2 (https://www.R-project.org/). All patients were divided into Immunity_H, Immunity_M, and Immunity_L groups.

Comparison of Immune Cell Infiltration Between Immune Subtypes

The fractions of 22 human immune cell subsets in cutaneous melanoma samples were calculated with Cell-type Identification By Estimating Relative Subsets Of RNA Transcripts (CIBERSORT) (15). One thousand permutations and $P < 0.05$ were set as the criteria to deconvolute each sample. Then, we compared the fractions of the immune cell subsets between immune subtypes with the Mann–Whitney U test.

Comparison of Survival Prognosis Between Immune Subtypes

With the survival data available, the survival R package was used to analyze the relationship between immune subtypes and the overall survival of patients. The survival differences were compared through a log-rank test, where $P < 0.05$ was regarded as statistically significant. Kaplan–Meier curves were plotted to visualize the differences in survival between immune subtypes.

Identification of Immune Subtype-Specific GO Terms

To identify the subtype-specific molecular features, we performed a weighted gene co-expression network (16) and identified the gene modules (GO terms) associated with the highly expressed genes in different immune subtypes.

RESULTS

Patient Characteristics and Immune Subtype Model Construction

We examined the gene expression profiles and clinical data of 470 cutaneous melanoma patients from TCGA database in this study. Selected patient characteristics are summarized in **Table 1**.

TABLE 1 | Clinical characteristics of the patients.

Characteristic	No. of patients (n = 470) (%)
Age	
median, range	58.2 (15-90)
Gender	
Male	290 (61.7)
Female	180 (38.3)
TNM stage	
I/II NOS	14 (3.0)
0	7 (1.5)
I	77 (16.4)
II	140 (29.8)
III	171 (36.4)
IV	23 (4.9)
Unknown	38 (8.1)
Prior treatment	
None	445 (94.7%)
Neoadjuvant treatment	25 (5.3%)
Survival status	
Death	211 (44.9)
Alive	259 (55.1)

The median age at diagnosis was 58.2 (range: 15.0–90.0) years, 290 (61.7%) patients were male, and 211 (44.9%) patients died. We first performed an unsupervised clustering analysis of 29 immune-associated gene sets. Based on the ssGSEA scores of the gene sets, there were three clear groups of samples: Immunity_H (n=323, 68.7%), Immunity_M (n=135, 28.7%) and Immunity_L (n=12, 2.6%) (**Figure 1**). As shown in the heatmap, the Immunity_H group expressed higher levels of immune-associated genes than the Immunity_L group. Cutaneous melanoma patients' stromal scores (ranging from -1,800.51 to 1,901.99), immune scores (ranging from -1,476.28 to 3,780.33), estimate scores (ranging from -2,618.28 to 5,098.14), and tumor purity (ranging from 0.216 to 0.976) data are shown in **Table S1** (according to the ESTIMATE algorithm). Particular, stromal and immune scores were calculated to predict infiltrating stromal and immune cells levels and to form the basis for the ESTIMATE score to infer tumor purity in tumor tissue (14). We found that the stromal scores, immune scores and estimate scores were significantly high in the Immunity_H group and significantly low in the Immunity_L group (Kruskal–Wallis test, $P < 0.001$) (**Figures 2A–C**), which suggested that these scores were meaningfully correlated with cutaneous melanoma. However, tumor purity showed the opposite trend (Kruskal–Wallis test, $P < 0.001$) (**Figure 2D**). Notably, these results indicate that Immunity_H samples contain the highest number of immune cells and stromal cells, Immunity_L samples contain the highest number of tumor cells, and Immunity_M samples are somewhere in between.

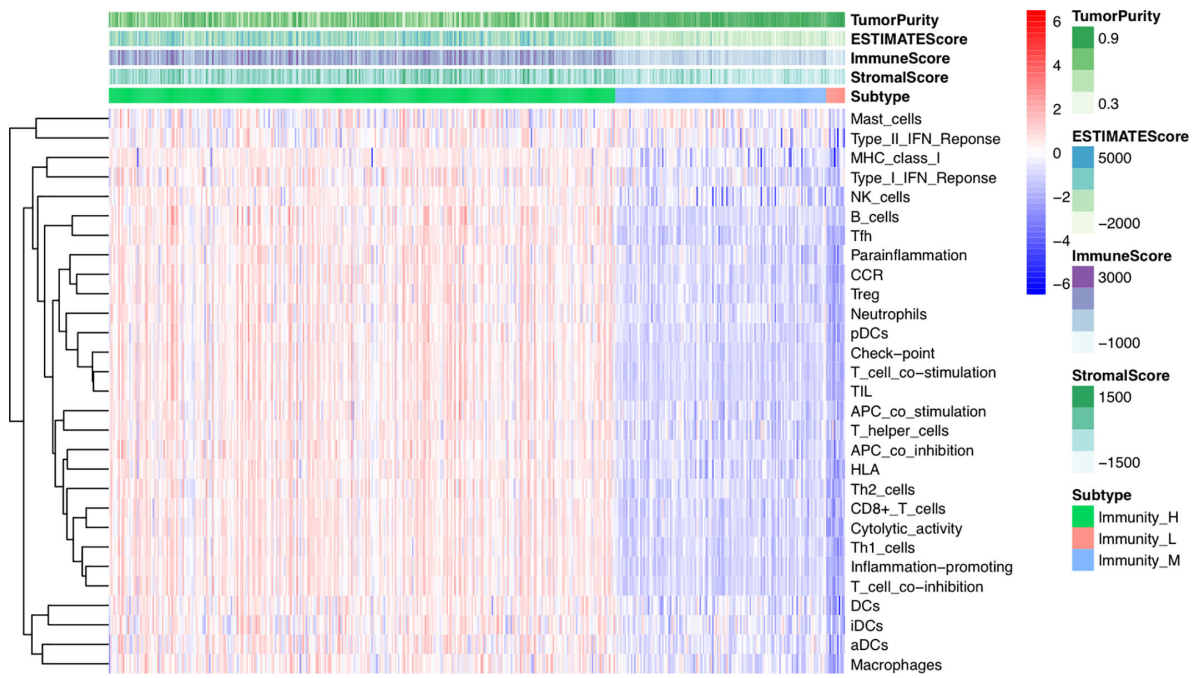

FIGURE 1 | Hierarchical clustering of Cutaneous melanoma into three subtypes. Hierarchical clustering of 470 tumors based on 29 immune-associated gene sets. Immunity_H, Immunity High; Immunity_M, Immunity Medium; Immunity_L, Immunity Low. Tumor purity, estimate scores, stromal scores, and immune scores were evaluated by ESTIMATE.

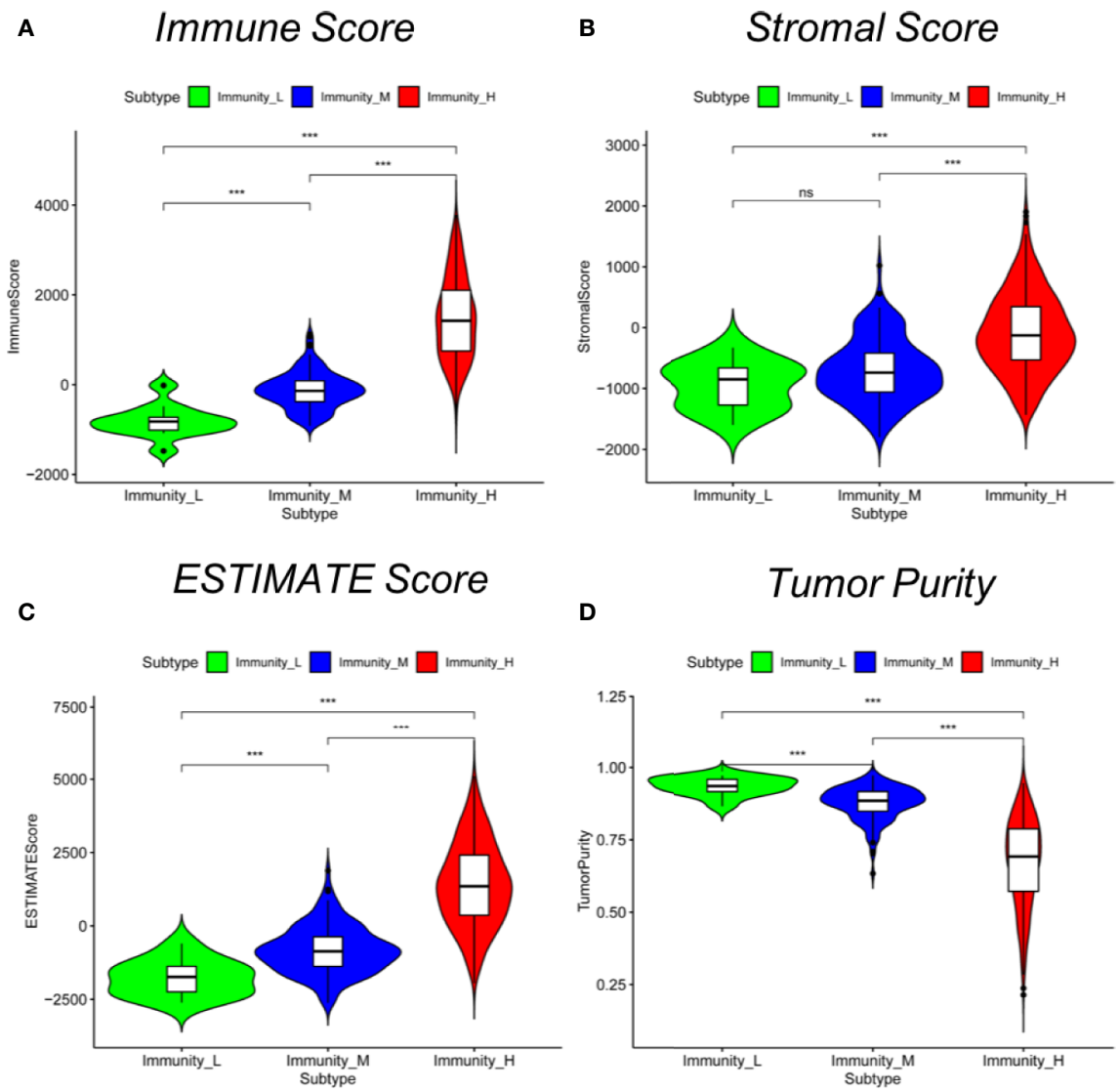

FIGURE 2 | Comparison of stromal scores, immune scores, estimated scores and tumor purity between cutaneous melanoma subtypes. Comparison of **(A)** stromal scores, **(B)** immune scores, **(C)** estimate scores, **(D)** and tumor purity between three subtypes (Mann–Whitney U test). *$P < 0.05$, ***$P < 0.001$.

Immune Subtypes Are Significantly Associated With HLA Genes and Immune Checkpoint Genes

To test the expression of immune-related genes in each group, we next explored the expression of HLA genes and the immune checkpoint genes in the three immune subtypes. Notably, the expression of all HLA genes was highest in the Immunity_H group and lowest in the Immunity_L group (ANOVA test, $P < 0.001$) (**Figure 3A**). Moreover, the expression levels of programmed cell death 1 ligand (PD-L1), also known as CD274, increased from the Immunity_L group to the Immunity_H group (Immunity_L < Immunity_M < Immunity_H) (Mann–Whitney U test, $P < 0.001$) (**Figure 3B**). The same was true for CTLA4 in the three subtypes (Mann–Whitney U test, $P < 0.05$) (**Figure 3C**). These results showed that these subgroups were significantly associated with the expression of immune-related genes.

Immune Subtypes Are Significantly Related to Immune Cell Infiltration and Clinical Outcomes

To further examine the tumor microenvironment, CIBERSORT was applied to assess the proportions of 22 human immune cell subsets in cutaneous melanoma. We found that the Immunity_H group had the highest level of naïve B cells, resting dendritic cells, M1 macrophages, resting NK cells, plasma cells, CD4 memory

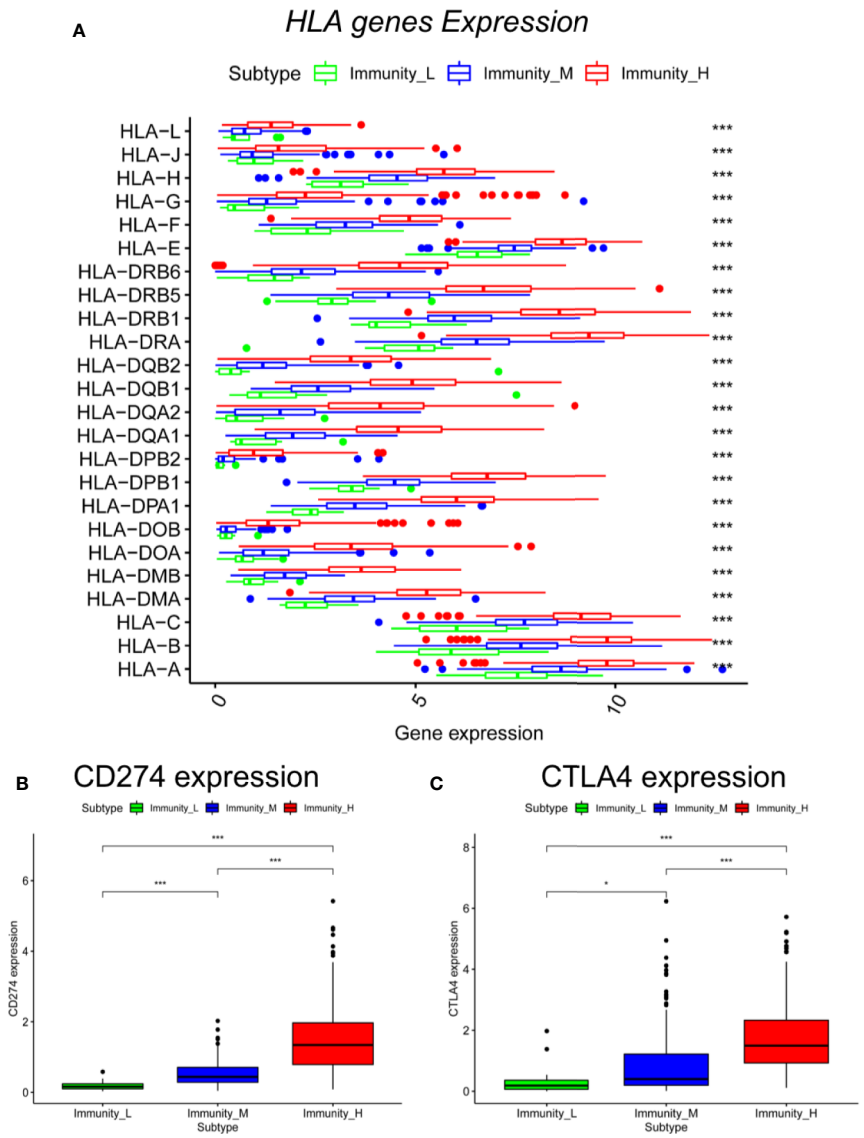

FIGURE 3 | Comparison of HLA genes and immune checkpoint genes between cutaneous melanoma subtypes. Comparison of **(A)** HLA genes (ANOVA test), **(B)** CD274, and **(C)** CTLA4 between three subtypes (Mann–Whitney U test). *$P < 0.05$, ***$P < 0.001$.

activated T cells, CD8 T cells, follicular helper T cells, and regulatory T cells, whereas the Immunity_L and Immunity_M groups had relatively low levels of these cell types. In addition, the Immunity_L group had higher levels of M0 macrophages and resting NK cells than the other two subtypes (Mann–Whitney U test, $P < 0.05$) (**Figure 4A**). This result indicated that the Immunity_H group had elevated anti-tumor immune activity.

Next, we investigated the prognostic value of the immune subtypes on patient survival. Interestingly, we found that the Immunity_H and Immunity_M groups had significantly worse overall survival than the Immunity_L group, indicating that these immunological features have distinct clinical outcomes in cutaneous melanoma (**Figure 4B**).

Identification of Specific GO Terms Associated With the Immune Subtypes

Finally, GSEA was performed to identify a number of GO terms enriched in the Immunity_H and Immunity_L groups. The top 10 GO terms identified in the Immunity_H group were mainly immune related (**Figure 5**, **Table S2**), including immunoglobulin complex; immunoglobulin complex, circulating; immunoglobulin receptor binding; complement activation; classical pathway; T cell receptor complex; humoral immune response mediated by circulating immunoglobulin; antigen binding; and immune response-regulating cell surface receptor signaling pathway involved in phagocytosis. This result also supported elevated immune activity in the Immunity_H group.

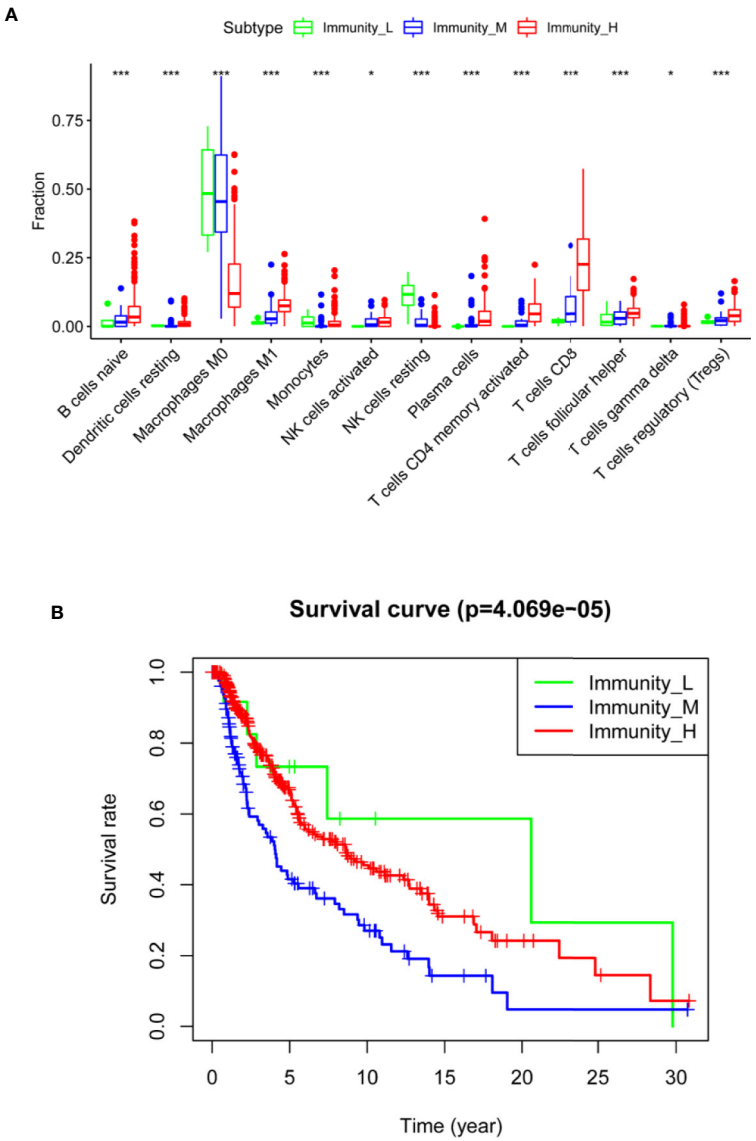

FIGURE 4 | Comparison of immune cell infiltration and clinical outcomes between cutaneous melanoma subtypes. **(A)** Comparison of immune cell infiltration in three subtypes (ANOVA test). **(B)** Comparison of survival prognosis between three subtypes (log-rank test). *$P < 0.05$, ***$P < 0.001$.

DISCUSSION

Genomic profiling has been used to determine the molecular subtypes in various cancers (17–19), including cutaneous melanoma (3, 4). Currently, accumulating evidence has suggested that the tumor microenvironment plays important roles in tumor progression and therapeutic responses (20, 21). The infiltration of immune cells as well as stromal cells in the tumor microenvironment has an impact on tumor progression and prognosis (22, 23). The development of cutaneous melanoma therapies, especially immunotherapy, has improved clinical outcomes (2). Therefore, an immune-related classification of cutaneous melanoma is needed. Our study found that cutaneous melanoma could be classified into three groups, Immunity_H, Immunity_M, and Immunity_L, using an unsupervised clustering analysis of 29 immune-associated gene sets. Using the ESTIMATE algorithm, we calculated stromal scores, immune scores, estimate scores, and the tumor purity of each patient. We found that stromal scores, immune scores and estimate scores were higher in the Immunity_H group than in the other groups. The Immunity_H group contained more immune cells and stromal cells than the other groups, which suggested elevated immune activity in this subtype. Moreover, GO analysis revealed that a set of gene modules in the Immunity_H group were mainly immune related, including immunoglobulin complex; immunoglobulin complex, circulating; immunoglobulin receptor binding; complement activation; classical pathway; T cell receptor complex; humoral

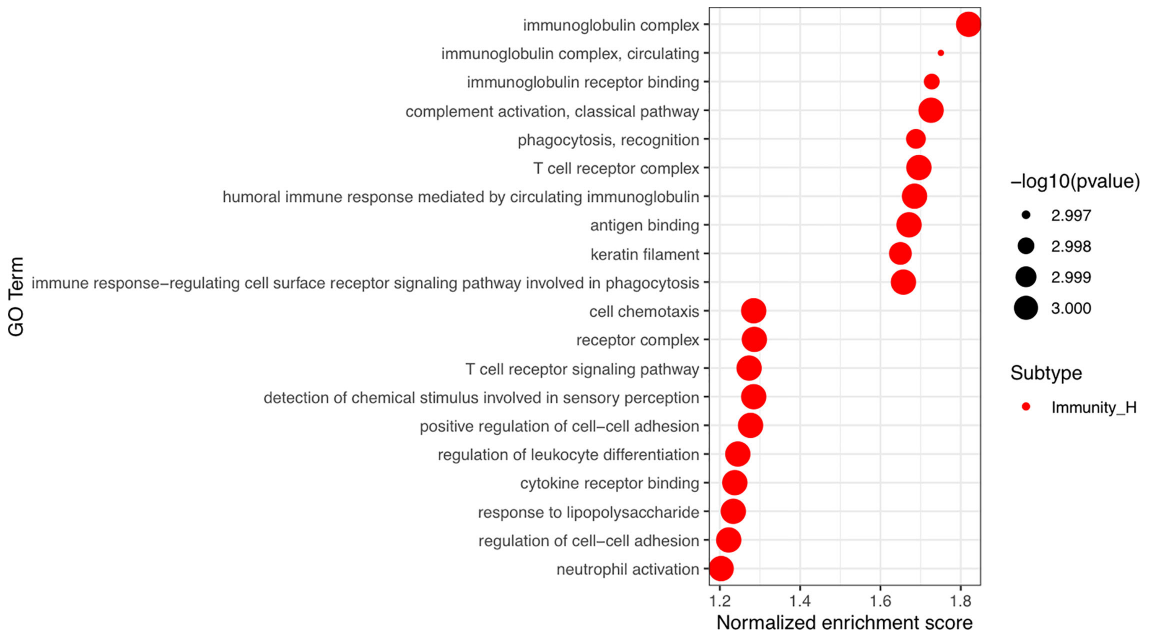

FIGURE 5 | Identification of cutaneous melanoma subtype-specific GO terms. Top 10 GO terms enriched in the Immunity_H and Immunity_L groups. GO, Gene Ontology.

immune response mediated by circulating immunoglobulin; antigen binding; and immune response-regulating cell surface receptor signaling pathway involved in phagocytosis. In the Immunity_L group, cell chemotaxis, receptor complex, detection of chemical stimulus involved in sensory perception, positive regulation of cell–cell adhesion, regulation of leukocyte differentiation, cytokine receptor binding, response to lipopolysaccharide and neutrophil activation. were observed. This further confirmed that immunity was activated in the Immunity_H group.

When we used CIBERSORT to assess the proportions of 22 human immune cell subsets, we found that most immune cells, including naïve B cells, resting dendritic cells, M1 macrophages, resting NK cells, plasma cells, CD4 memory activated T cells, CD8 T cells, follicular helper T cells and regulatory T cells, were significantly higher in the Immunity_H group than in the other groups. We also found that the expression levels of HLA genes and immune checkpoint genes were higher in the Immunity_H group than in the other groups. In addition, the immune checkpoint gene expression levels were significantly associated with the immune subtypes, suggesting that Immunity_H patients may have a good response to anti-PD-L1 or anti-CTLA4 immunotherapy, with evidence that PD-L1 and CTLA4 could serve as biomarkers for corresponding immunotherapeutic responsiveness (24).

The three distinct immune subtypes were strongly associated with clinical outcomes. Numerous studies have demonstrated that enhanced local immune activation contributes to a good prognosis in different kind of tumors (25, 26). In cutaneous melanoma, though several studies have reported that patients with high immune cell infiltration showed better prognosis (27–29), some types of immune cells are associated with worse prognosis, such as CD20-positive tumor-infiltrating lymphocytes, neutrophil granulocytes and mast cells (30, 31). In our study, based on the immunogenomic profiling of 29 immune signatures, we found that Immunity_L group was associated with better prognosis, which might be the infiltrated immune cells are non-tumor-specific and do not show the anti-tumor effect. Therefore, the underlying mechanism between strong immunogenicity and poor prognosis in cutaneous melanoma needs to be explored.

However, limitations in this study exist. First, it was a retrospective study, and all the data were retrieved from a publicly available database. Thus, external validations are needed to verify our findings. Second, though we identified the immune subtype-specific GO in different groups, further mechanistic studies are encouraged.

CONCLUSIONS

Immune signature-associated cutaneous melanoma subtypes may play a role in cutaneous melanoma prognosis stratification. The construction of immune signature-associated cutaneous melanoma subtypes predicted possible patient outcomes and provided possible candidates for immunotherapy.

DATA AVAILABILITY STATEMENT

We used publicly available cutaneous melanoma genomic dataset from the TCGA data portal (https://portal.gdc.cancer.gov/). We obtained 29 immune signatures (represented by 29 different gene sets, respectively) from the publications (32, 33).

AUTHOR CONTRIBUTIONS

YZ and JY conceptualized and designed the study. JR and YZ were in charge of the financial support. JR was in charge of the administrative support. PC and MX took part in the provision of the study materials and patients. JR and SG collected and assembled the data. JY and PC analyzed and interpreted the data. All authors helped in writing the manuscript. All authors contributed to the article and approved the submitted version.

FUNDING

This work was supported by the National Natural Science Foundation of China (No. 81972530, U1932135, 81802702), Fund for Excellent Young Scholars of Shanghai Ninth People's Hospital, Shanghai Jiao Tong University School of Medicine (JYYQ001), Shanghai Rising-Star Program (17QA1402000), a scholarship from the China Scholarship Council (201906235030), the Science and Technology Commission of Shanghai (17DZ2260100, 19JC1410200) and the pathogenesis and clinical study of orbital disease and eye tumor (SSMU-ZDCX20180400).

SUPPLEMENTARY MATERIAL

The Supplementary Material for this article can be found online at: https://www.frontiersin.org/articles/10.3389/fonc.2020.580029/full#supplementary-material

SUPPLEMENTARY FIGURE 1 | The mutational landscape of subgroups. Mutational landscape of Immunity_H **(A)** group, Immunity_M **(B)** group, and Immunity_L **(C)** group.

SUPPLEMENTARY TABLE 1 | Stromal scores, immune scores, estimate scores and tumor purity of each sample.

SUPPLEMENTARY TABLE 2 | GO terms enriched in Immunity_H and Immunity_L. GO, gene oncology.

REFERENCES

1. Coricovac D, Dehelean C, Moaca E-A, Pinzaru I, Bratu T, Navolan D, et al. Cutaneous Melanoma-A Long Road from Experimental Models to Clinical Outcome: A Review. *Int J Mol Sci* (2018) 19(6):1566. doi: 10.3390/ijms19061566
2. Schadendorf D, van Akkooi ACJ, Berking C, Griewank KG, Gutzmer R, Hauschild A, et al. Melanoma. *Lancet* (2018) 392(10151):971–84. doi: 10.1016/S0140-6736(18)31559-9
3. Akbani R, Akdemir KC, Aksoy BA, Albert M, Ally A, Amin SB, et al. Genomic Classification of Cutaneous Melanoma. *Cell* (2015) 161(7):1681–96. doi: 10.1016/j.cell.2015.05.044
4. Zhao Y, Schaafsma E, Gorlov IP, Hernando E, Thomas NE, Shen R, et al. A Leukocyte Infiltration Score Defined by a Gene Signature Predicts Melanoma Patient Prognosis. *Mol Cancer Res* (2019) 17(1):109–19. doi: 10.1158/1541-7786.MCR-18-0173
5. Nie RC, Yuan S-Q, Wang Y, Chen Y-B, Cai Y-Y, Chen S, et al. Robust immunoscore model to predict the response to anti-PD1 therapy in melanoma. *Aging (Albany NY)* (2019) 11(23):11576–90. doi: 10.18632/aging.102556
6. Havel JJ, Chowell D, Chan TA. The evolving landscape of biomarkers for checkpoint inhibitor immunotherapy. *Nat Rev Cancer* (2019) 19(3):133–50. doi: 10.1038/s41568-019-0116-x
7. Song BN, Kim S-K, Mun J-Y, Choi Y-D, Leem S-H, Chu I-S. Identification of an immunotherapy-responsive molecular subtype of bladder cancer. *EBioMedicine* (2019) 50:238–45. doi: 10.1016/j.ebiom.2019.10.058
8. Sugiyama E, Togashi Y, Takeuchi Y, Shinya S, Tada Y, Tada K, et al. Blockade of EGFR improves responsiveness to PD-1 blockade in EGFR-mutated non-small cell lung cancer. *Sci Immunol* (2020) 5(43):eaav3937. doi: 10.1126/sciimmunol.aav3937
9. Cesano A, Warren S. Bringing the next Generation of Immuno-Oncology Biomarkers to the Clinic. *Biomedicines* (2018) 6(1):14. doi: 10.3390/biomedicines6010014
10. Taube JM, Galon J, Sholl LM, Rodig SJ, Cottrell TR, Giraldo NA, et al. Implications of the tumor immune microenvironment for staging and therapeutics. *Mod Pathol* (2018) 31(2):214–34. doi: 10.1038/modpathol.2017.156
11. Gajewski TF, Schreiber H, Fu YX. Innate and adaptive immune cells in the tumor microenvironment. *Nat Immunol* (2013) 14(10):1014–22. doi: 10.1038/ni.2703
12. Kobayashi H, Enomoto A, Woods SL, Burt AD, Takahashi M, Worthley DL. Cancer-associated fibroblasts in gastrointestinal cancer. *Nat Rev Gastroenterol Hepatol* (2019) 16(5):282–95. doi: 10.1038/s41575-019-0115-0
13. He Y, Jiang Z, Chen C, Wang X. Classification of triple-negative breast cancers based on Immunogenomic profiling. *J Exp Clin Cancer Res* (2018) 37(1):327. doi: 10.1186/s13046-018-1002-1
14. Yoshihara K, Shahmoradgoli M, Martínez E, Vegesna R, Kim H, Torres-Garcia W, et al. Inferring tumour purity and stromal and immune cell admixture from expression data. *Nat Commun* (2013) 4:2612. doi: 10.1038/ncomms3612
15. Newman AM, Liu CL, Green MR, Gentles AJ, Feng W, Xu Y, et al. Robust enumeration of cell subsets from tissue expression profiles. *Nat Methods* (2015) 12(5):453–7. doi: 10.1038/nmeth.3337
16. Langfelder P, Horvath S. WGCNA: an R package for weighted correlation network analysis. *BMC Bioinf* (2008) 9(1):559. doi: 10.1186/1471-2105-9-559
17. Alessandrini F, Ceresa D, Appolloni I, Pagani F, Poliani PL, Marubbi D, et al. Glioblastoma models driven by different mutations converge to the proneural subtype. *Cancer Lett* (2020) 469:447–55. doi: 10.1016/j.canlet.2019.11.010
18. Chia NY, Tan P. Molecular classification of gastric cancer. *Ann Oncol* (2016) 27(5):763–9. doi: 10.1093/annonc/mdw040
19. Jiang YZ, Ma D, Suo C, Shi J, Xue M, Hu X. Genomic and Transcriptomic Landscape of Triple-Negative Breast Cancers: Subtypes and Treatment Strategies. *Cancer Cell* (2019) 35(3):428–440.e5. doi: 10.1016/j.ccell.2019.02.001
20. Rodriguez-Ruiz ME, Vitale I, Harrington KJ, Melero I, Galluzzi L. Immunological impact of cell death signaling driven by radiation on the tumor microenvironment. *Nat Immunol* (2020) 21(2):120–34. doi: 10.1038/s41590-019-0561-4
21. Wu T, Dai Y. Tumor microenvironment and therapeutic response. *Cancer Lett* (2017) 387:61–8. doi: 10.1016/j.canlet.2016.01.043
22. Cacho-Diaz B, García-Botello DR, Wegman-Ostrosky T, Reyes-Soto G, Ortiz-Sánchez E, Herrera-Montalvo LA, et al. Tumor microenvironment differences between primary tumor and brain metastases. *J Transl Med* (2020) 18(1):1. doi: 10.1186/s12967-019-02189-8
23. Thompson ED, Zahurak M, Murphy A, Cornish T, Cuka N, Abdelfatah E, et al. Patterns of PD-L1 expression and CD8 T cell infiltration in gastric adenocarcinomas and associated immune stroma. *Gut* (2017) 66(5):794–801. doi: 10.1136/gutjnl-2015-310839
24. Topalian SL, Taube JM, Anders RA, Pardoll DM. Mechanism-driven biomarkers to guide immune checkpoint blockade in cancer therapy. *Nat Rev Cancer* (2016) 16(5):275–87. doi: 10.1038/nrc.2016.36
25. Ali HR, Provenzano E, Dawson S-J, Blows FM, Liu B, Shah M, et al. Association between CD8+ T-cell infiltration and breast cancer survival in 12,439 patients. *Ann Oncol* (2014) 25(8):1536–43. doi: 10.1093/annonc/mdu191
26. Garnelo M, Tan A, Her Z, Yeon J, Lim CJ, Chen J, et al. Interaction between tumour-infiltrating B cells and T cells controls the progression of hepatocellular carcinoma. *Gut* (2017) 66(2):342–51. doi: 10.1136/gutjnl-2015-310814

27. Cursons J, Souza-Fonseca-Guimaraes F, Foroutan M, Anderson A, Hollande F, Hediyeh-Zadeh S, et al. A Gene Signature Predicting Natural Killer Cell Infiltration and Improved Survival in Melanoma Patients. *Cancer Immunol Res* (2019) 7(7):1162–74. doi: 10.1158/2326-6066.CIR-18-0500
28. Liu N, Liu Z, Liu X, Duan X, Huang Y, Jin Z, et al. Identification of an Immune-Related Prognostic Signature Associated With Immune Infiltration in Melanoma. *Front Genet* (2020) 11:1002. doi: 10.3389/fgene.2020.01002
29. Poźniak J, Nsengimana J, Laye JP, O'Shea SJ, Diaz JMS, Droop AP, et al. Genetic and Environmental Determinants of Immune Response to Cutaneous Melanoma. *Cancer Res* (2019) 79(10):2684–96. doi: 10.1158/0008-5472.CAN-18-2864
30. Ladányi A. Prognostic and predictive significance of immune cells infiltrating cutaneous melanoma. *Pigment Cell Melanoma Res* (2015) 28(5):490–500. doi: 10.1111/pcmr.12371
31. Martinez-Rodriguez M, Thompson AK, Monteagudo C. A significant percentage of CD20-positive TILs correlates with poor prognosis in patients with primary cutaneous malignant melanoma. *Histopathology* (2014) 65 (5):726–8. doi: 10.1111/his.12437
32. Bindea G, Mlecnik B, Tosolini M, Kirilovsky A, Waldner M, Obenauf AC, et al. Spatiotemporal dynamics of intratumoral immune cells reveal the immune landscape in human cancer. *Immunity* (2013) 39(4):782–95. doi: 10.1016/j.immuni.2013.10.003
33. Liu Z, Li M, Jiang Z, Wang X. A Comprehensive Immunologic Portrait of Triple-Negative Breast Cancer. *Transl Oncol* (2018) 11(2):311–29. doi: 10.1016/j.tranon.2018.01.011

Conflict of Interest: The authors declare that the research was conducted in the absence of any commercial or financial relationships that could be construed as a potential conflict of interest.

frontiers in Oncology

SYSTEMATIC REVIEW
published: 18 February 2021
doi: 10.3389/fonc.2020.637161

Adjuvant Therapy of High-Risk (Stages IIC–IV) Malignant Melanoma in the Post Interferon-Alpha Era: A Systematic Review and Meta-Analysis

Konstantinos Christofyllakis[1], Claudia Pföhler[2], Moritz Bewarder[1], Cornelia S. L. Müller[2], Lorenz Thurner[1], Torben Rixecker[1], Thomas Vogt[2], Stephan Stilgenbauer[1], Krista Yordanova[2†] and Dominic Kaddu-Mulindwa[1†]*

[1] Department of Hematology, Oncology, Clinical Immunology and Rheumatology, Medical School, University of Saarland, Homburg, Germany, [2] Department of Dermatology, Venerology and Allergology, Medical School, University of Saarland, Homburg, Germany

OPEN ACCESS

Edited by:
Igor Puzanov,
University at Buffalo, United States

Reviewed by:
Piotr Rutkowski,
Maria Sklodowska-Curie National Research Institute of Oncology, Poland
Ioana Cosgarea,
Newcastle University, United Kingdom

***Correspondence:**
Konstantinos Christofyllakis
konstantinos.christofyllakis@uks.eu

†These authors have contributed equally to this work

Specialty section:
This article was submitted to Skin Cancer, a section of the journal Frontiers in Oncology

Received: 02 December 2020
Accepted: 30 December 2020
Published: 18 February 2021

Citation:
Christofyllakis K, Pföhler C, Bewarder M, Müller CSL, Thurner L, Rixecker T, Vogt T, Stilgenbauer S, Yordanova K and Kaddu-Mulindwa D (2021) Adjuvant Therapy of High-Risk (Stages IIC–IV) Malignant Melanoma in the Post Interferon-Alpha Era: A Systematic Review and Meta-Analysis. Front. Oncol. 10:637161. doi: 10.3389/fonc.2020.637161

Introduction: Multiple agents are approved in the adjuvant setting of completely resected high-risk (stages IIC–IV) malignant melanoma. Subgroups may benefit differently depending on the agent used. We performed a systematic review and meta-analysis to evaluate the efficiency and tolerability of available options in the post interferon era across following subgroups: patient age, stage, ulceration status, lymph node involvement, BRAF status.

Methods: The PubMed and Cochrane Library databases were searched without restriction in year of publication in June and September 2020. Data were extracted according to the PRISMA Guidelines from two authors independently and were pooled according to the random-effects model. The predefined primary outcome was recurrence-free survival (RFS). Post-data extraction it was noted that one trial (BRIM8) reported disease-free survival which was defined in the exact same way as RFS.

Results: Five prospective randomized placebo-controlled trials were included in the meta-analysis. The drug regimens included ipilimumab, pembrolizumab, nivolumab, nivolumab/ipilimumab, vemurafenib, and dabrafenib/trametinib. Adjuvant treatment was associated with a higher RFS than placebo (HR 0.57; 95% CI= 0.45–0.71). Nivolumab/ipilimumab in stage IV malignant melanoma was associated with the highest RFS benefit (HR 0.23; 97.5% CI= 0.12–0.45), followed by dabrafenib/trametinib in stage III BRAF-mutant melanoma (HR 0.49; 95% CI= 0.40–0.59). The presence of a BRAF mutation was associated with higher RFS rates (HR 0.30; 95% CI= 0.11–0.78) compared to the wildtype group (HR 0.60; 95% CI= 0.44–0.81). Patient age did not influence outcomes (≥65: HR 0.50; 95% CI= 0.36–0.70, <65: HR 0.58; 95% CI= 0.46–0.75). Immune checkpoint inhibitor monotherapy was associated with lower RFS in non-ulcerated melanoma. Patients with stage IIIA benefited equally from adjuvant treatment as those with stage IIIB/C. Nivolumab/ipilimumab and ipilimumab monotherapy were associated with higher toxicity.

Conclusion: Adjuvant therapy should not be withheld on account of advanced age or stage IIIA alone. The presence of a BRAF mutation is prognostically favorable in terms of RFS. BRAF/MEK inhibitors should be preferred in the adjuvant treatment of BRAF-mutant non-ulcerated melanoma.

Keywords: melanoma, adjuvant, immunotherapy, BRAF mutation, meta-analysis, checkpoint inhibitors, BRAF/MEK inhibitors

INTRODUCTION

The incidence of malignant melanoma (MM) increases consistently (39% between 2006 and 2016) with a current incidence of over 132.000 estimated cases worldwide each year (1, 2). Low risk MM (stages I-IIB) can be effectively treated with surgical excision only (3, 4). In contrast, high-risk MM (stages IIC-IV) with no evidence of disease (NED) after excision is associated with a worse survival rate (5) and therefore an efficient and tolerable adjuvant therapy is needed (4, 6). Interferon alpha (IFN-α) has lost its relevance in the wake of new therapeutic options due to its inconsistent impact on overall survival (OS) and high toxicity (7–9). After IFN-α, ipilimumab was the first agent to be approved for stage III (10). However, due to its unfavorable side effect profile, it was soon replaced by nivolumab and pembrolizumab (11). A recent phase II trial demonstrated the superior efficacy of the nivolumab/ipilimumab combination versus nivolumab or placebo in stage IV MM with NED (12). For patients with *BRAF*-V600 mutant (BRAF*mut*) MM, targeted adjuvant therapy is another option. While initial results with the BRAFi vemurafenib were not encouraging, the combination of the BRAFi dabrafenib with the MEKi trametinib demonstrated a clear benefit versus placebo in stage III disease (13, 14). Despite these significant developments, there is still no standard of care for the adjuvant therapy of high-risk MM, especially in the presence of a BRAF driver mutation (15).

Previous meta-analyses of adjuvant therapy for MM either included IFN-α, did not include subgroup-specific data or lacked a direct comparison of nivolumab versus placebo within a randomized placebo-controlled trials (RCT) (8, 16).

MATERIALS AND METHODS

Objective

This systematic review and meta-analysis aimed to compare the efficacy of modern agents in the adjuvant setting of cutaneous MM versus placebo with specific regard to different subgroups [patient age, stage, primary tumor ulceration, number of involved lymph nodes (LN), type of LN involvement (micro- or macrometastases) and BRAF mutational status]. Methodology and reporting follow the PRISMA guidelines (Preferred Reporting Items for Systematic Reviews and Meta-Analysis) (17), a checklist is provided in **eTable 1, supplement**. The meta-analysis is registered on the Open Science Framework (Registration DOI: 10.17605/OSF.IO/SGPHN, protocol accessible on: https://osf.io/m9vr5)

Data Sources, Search Strategy, and Data Extraction

The PubMed and Cochrane Library databases were searched in June 2020 using the terms "melanoma" AND "adjuvant" and the filter "clinical trial". An updated search was performed on September 14th, 2020 (search strategy in **eFigure 1, supplement**). RCT (phase 2 or 3) comparing adjuvant treatment with placebo or an FDA- or EMA approved agent in patients with MM with NED published in English were included. We excluded systematic reviews, meta-analyses, abstracts, trials including neoadjuvant treatment, IFN-α as well as non-placebo-controlled RCT. Baseline participant demographics and outcome data were extracted including: type and name of the trial, primary outcome for the whole population, and separately for the following subgroups: patients <65 and ≥65 years of age, ulceration status, number of positive LN, presence of micro- or macrometastases, stage and BRAF status. Two authors (KC and KY) conducted the systematic review and data extraction independently. Conflicts were resolved by a third author (DK-M).

Comparators and Data Analysis

We conducted a meta-analysis of the summary statistic hazard ratio (HR) with corresponding 95% confidence intervals (CI) for each trial. Data from each trial were pooled using the random effects (DerSimonian-Laird) model. Statistical heterogeneity between the trials was assessed using Cochran´s Q test and I^2. All statistical analyses were conducted using StatsDirect version 3.3.0. Results were presented with forest plots. Two-sided $P < 0.05$ was deemed statistically significant.

Risk of Bias

Trial quality and risk of bias on study level were assessed using the revised Cochrane tool for assessing risk of bias in randomized trials (RoB2 tool) (18) by two authors independently (KC and KY). Conflicts were referred to a third author (DK-M). A potential presence of publication bias was assessed visually with funnel plots and formally using Egger's regression asymmetry test (19).

RESULTS

Study Selection

We identified 1,404 studies in total. After assessment for eligibility, five randomized, double blind, placebo-controlled trials were included in the meta-analysis. A flowchart is provided in **Figure 1** and an overview of these trials in **Table 1**.

Study Characteristics

The following drug regimens were compared versus placebo: pembrolizumab (EORTC-1325), ipilimumab (EORTC-18071), vemurafenib (BRIM8), nivolumab/ipilimumab, nivolumab (IMMUNED) and dabrafenib/trametinib (COMBI-AD). The BRIM8 trial incorporated two cohorts of patients based on the tumor stage: cohort 1 (IIC-IIIB) and cohort 2 (IIIC). In total, data from 3505 patients were evaluated. For the EORTC-18071 and COMBI-AD trials, updated data published in 2016 and 2018 were used, respectively. Staging was performed according to the 7th edition of the American Joint Committee on Cancer (AJCC) in the COMBI-AD, EORTC-1325 and BRIM8 trials. The EORTC-18071 trial included only patients with stage III disease according to the 6th AJCC edition. However, there are no differences in stage III definition between 6th and 7th edition. Only nodal micrometastatic disease size > 1 mm was included in the EORTC-1325, EORTC-18071, BRIM8, and COMBI-AD trials. The IMMUNED trial included only patients with stage IV with NED, whose distinction from stage III does not differ between the 7th and 8th editions. Thus, cross-trial comparability is warranted. Taken together, all trials enrolled patients with completely resected stage IIC to IV cutaneous MM. The median follow-up of the studies ranged from 15 months to 2.9 years. The primary endpoint of three of the studies was RFS defined as the time from randomization to disease recurrence or death. The BRIM8 trial used disease-free survival (DFS) as the primary endpoint defined as the time from randomization until the date of the first disease recurrence or death. As those two definitions are identical, RFS will be used from now on for purposes of simplicity. All trials except BRIM8 met their primary endpoint. All patients included in the COMBI-AD and BRIM8 trials had BRAF*mut* melanoma. In the EORTC-1325 and IMMUNED trials 49% and 45% of patients respectively had BRAF*mut* MM. The EORC-18071 did not report BRAF mutational status (**eTable 2, supplement**).

Recurrence-Free Survival

Adjuvant treatment resulted consistently in longer RFS compared to placebo (HR 0.57; 95% CI= 0.45–0.7) (**Figure 2**). Patients in stage IV treated with nivolumab/ipilimumab derived the highest benefit (HR 0.23; 97.5% CI= 0.12–0.45). Pembrolizumab and nivolumab demonstrated similar efficacy, (HR 0.57; 95% CI= 0.43–0.74 and HR

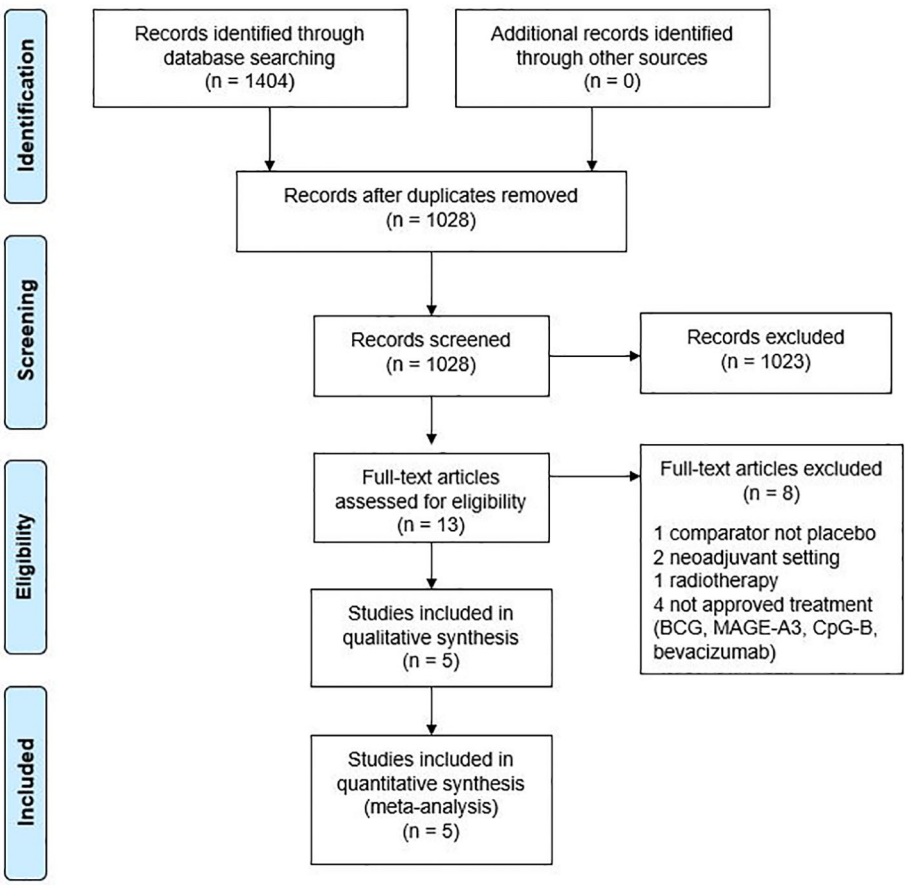

FIGURE 1 | Meta-analysis flowchart. BCG, bacillus Calmette-Guerin; MAGE-A3, melanoma antigen A3.

TABLE 1 | Overview of the characteristics of the included studies.

Trial	Comparison	Randomised patients (n)	Dose schedule	Duration of treatment	Median follow up	Primary endpoint HR, (95% CI)
EORC-18071	Ipilimumab versus placebo	951	10 mg/kg i.v. q3w for four doses, then every 3 months for 3 years	3 years	2.74 years	RFS, 0.76 (0.64–0.89)
COMBI-AD	Dabrafenib plus Trametinib versus placebo	870	Dabrafenib 150 mg 2× day + trametinib 2 mg 1× day	1 year	2.9 years	RFS, 0.49 (0.40–0.59)
BRIM8	Vemurafenib versus placebo	Cohort 1: 314	Vemurafenib tablets (960 mg 2× day for 52 weeks [13 × 28-day cycles])	52 weeks	33.5 months	DFS, 0.55 (0.38–0.80)
		Cohort 2: 184	as Cohort 1	52 weeks	30.8 months	DFS, 0.81 (0.55–1.19)
EORTC-1325	Pembrolizumab versus placebo	1019	200 mg i.v. q3w for a total of 18 doses	Approximately 1 year	15 months	RFS, 0.57 (0.43–0.74)
IMMUNED	Nivolumab versus placebo	167	3 mg/kg nivolumab q3w	Up to 1 year	28.4 months	RFS, 0.56 (0.33–0.94)
	Nivolumab plus Ipilimumab versus placebo		1 mg/kg i.v. nivolumab q3w plus 3 mg/kg i.v. ipilimumab q3w for four doses, followed by 3 mg/kg i.v. nivolumab q2w			RFS, 0.23 (0.12–0.45)*

* *97.5% CI.*

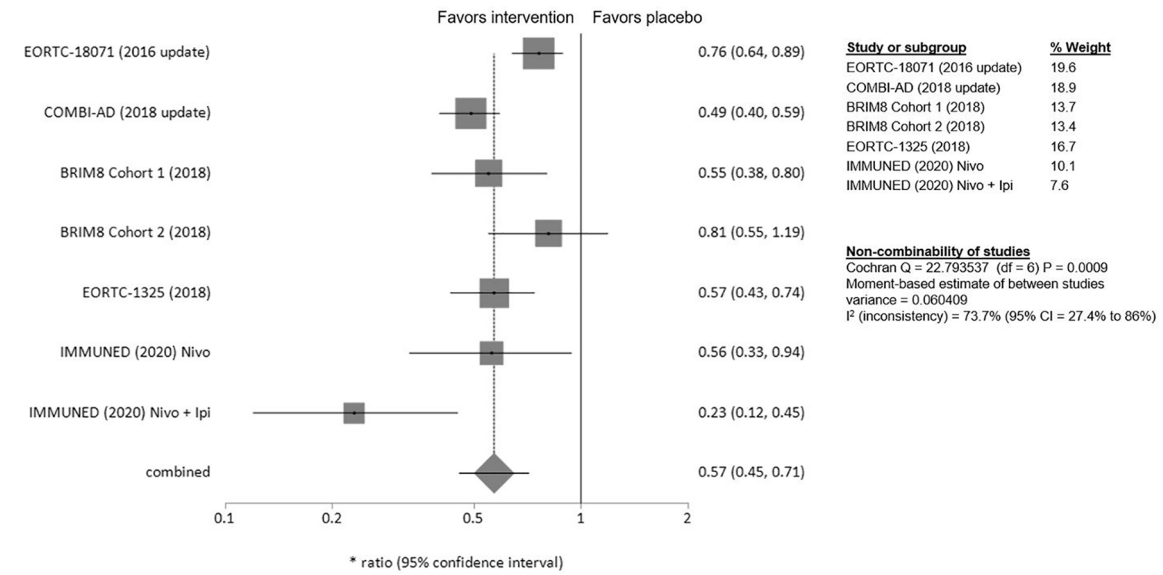

FIGURE 2 | Forest plot for primary outcome analysis on relapse free survival. Notes: Hazard ratio for relapse, or death along the x-axis, and results from all trials on the y axis with gray squares representing effect estimates and lines through them representing 95% CIs. The gray diamond represents the overall effect measure, which lies clear off the line of no effect and shows a benefit for the treatment groups compared to placebo with a summary hazard ratio of 0.57 (95% CI: 0.45–0.71). The percentage weight for each study is separately listed on the right side of the graph as well as the data on the heterogeneity of the meta-analysis, with the relevant measure being the I^2 score. CI, confidence interval.

0.56; 95% CI= 0.33–0.94 respectively). Patients with stage III BRAF*mut* MM treated with dabrafenib/trametinib had a 51% lower risk of relapse (HR 0.49; 95% CI= 0.40–0.59). Adjuvant therapy with ipilimumab was less effective (HR 0.76; 95% CI= 0.64–0.89). BRIM8 did not reach its primary endpoint in cohort 2 (stage IIIC MM, HR 0.81; 95%CI= 0.55–1.19). In cohort 1 however, treatment with vemurafenib resulted in longer RFS (stages IIC–IIIA, HR 0.55; 95% CI= 0.38–0.80).

Subgroup Analyses

An overview of patient characteristics and demographics is provided in **eTables 2** and **3** in the **supplement**.

Age

No difference in adjuvant treatment benefit for patients aged over and under 65 years could be observed [≥65: HR 0.50 (95% CI= 0.36–0.70), <65: HR 0.58 (95% CI= 0.46–0.75)]. The greatest

benefit of adjuvant therapy over placebo for patients ≥65 years was shown in the IMMUNED trial (HR 0.26; 95% CI= 0.07–0.92) (**Figure 3**).

Lymph Node Involvement

Neither the number of involved LN, nor the presence of macro- or micrometastases alone had significant influence on RFS. (**eFigures 2** and **3, supplement**).

Ulceration Status

In patients with ulcerated MM pembrolizumab and ipilimumab appeared to be more effective than in patients with non-ulcerated melanomas (pembrolizumab: HR 0.52; 95% CI 0.35–0.79 vs 0.68; 95% CI= 0.45–1.05, ipilimumab: HR 0.64, 95% CI= 0.44–0.94, vs 0.80, 95%CI= 0.54–1.20) (**Figure 4**). Interestingly, clinical benefit from dabrafenib/trametinib was consistent regardless of LN involvement or ulceration. Adjuvant therapy in non-ulcerated melanomas with macro-metastases was associated with the smallest RFS benefit and did not reach statistical significance (HR 0.73; 95%CI= 0.50–1.05) (**eFigure 4, supplement**).

Stage

In stage IIIA, while none of the examined substances alone reach statistical significance in the corresponding trials, our meta-analysis demonstrates a clear RFS-benefit for treatment versus placebo in stage IIIA, which in fact is numerically equivalent to that shown for stages IIIB/C. Dabrafenib/trametinib were associated with a consistent improvement in RFS, apart from stage IIIA where the upper confidence interval is marginally crossed (HR 0.58; 95% CI= 0.32–1.06). In contrast, ipilimumab had limited efficacy in patients with stage IIIA/B whereas a clear benefit with treatment was seen only in stage IIIC with >4 LN

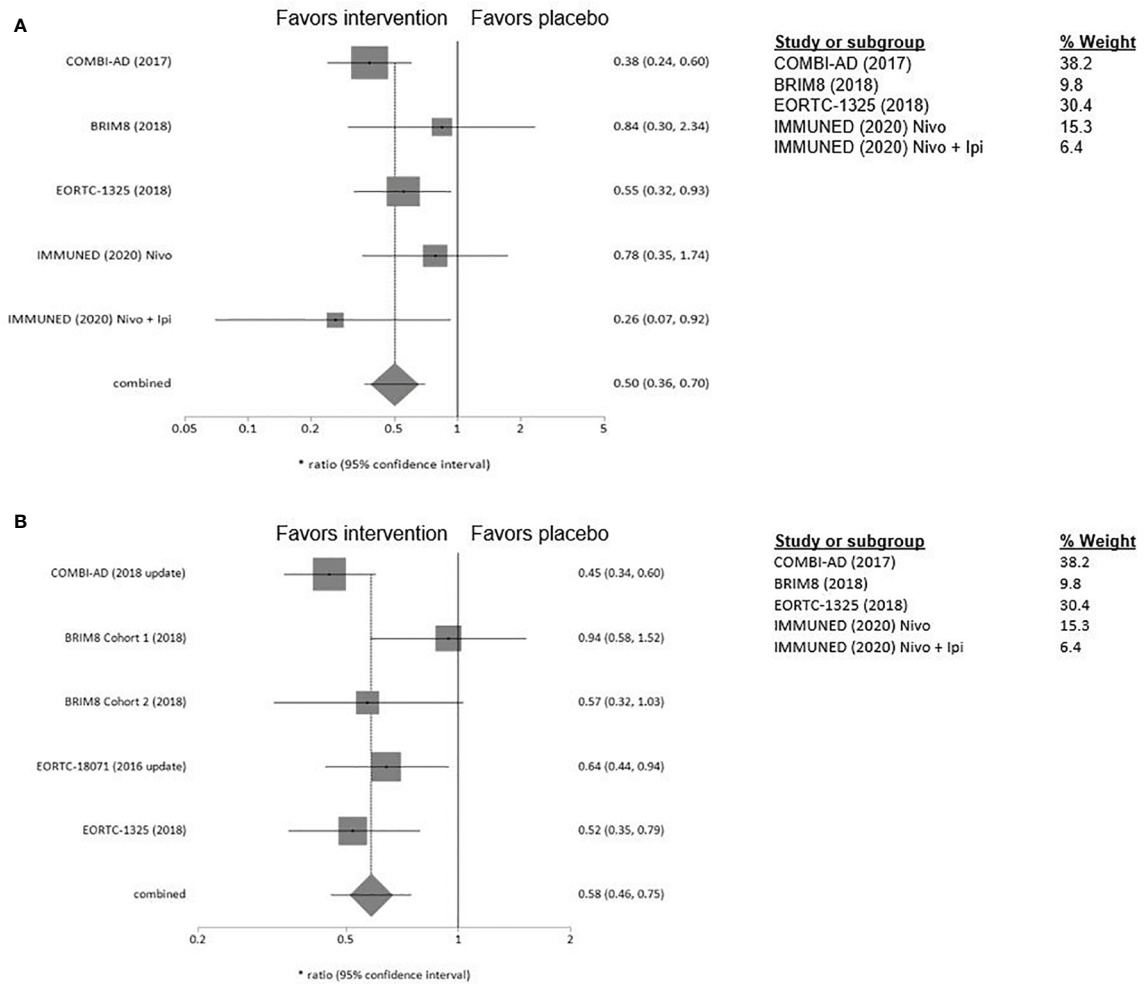

FIGURE 3 | **(A)** Forest plot for primary outcome analysis on relapse free survival for patients ≥**65 years old**. **(B)** Forest plot for primary outcome analysis on survival for patients <**65 years old**. Notes: Hazard ratio for relapse or death along the x-axis, and results from the different studies, with gray squares representing effect estimates and lines through them representing 95% CIs. The gray diamond represents the overall effect measure which lies clear off the line of no effect, showing a benefit for the treatment groups compared to placebo. The percentage weight for each study is separately listed on the right of the graph. CI, confidence interval.

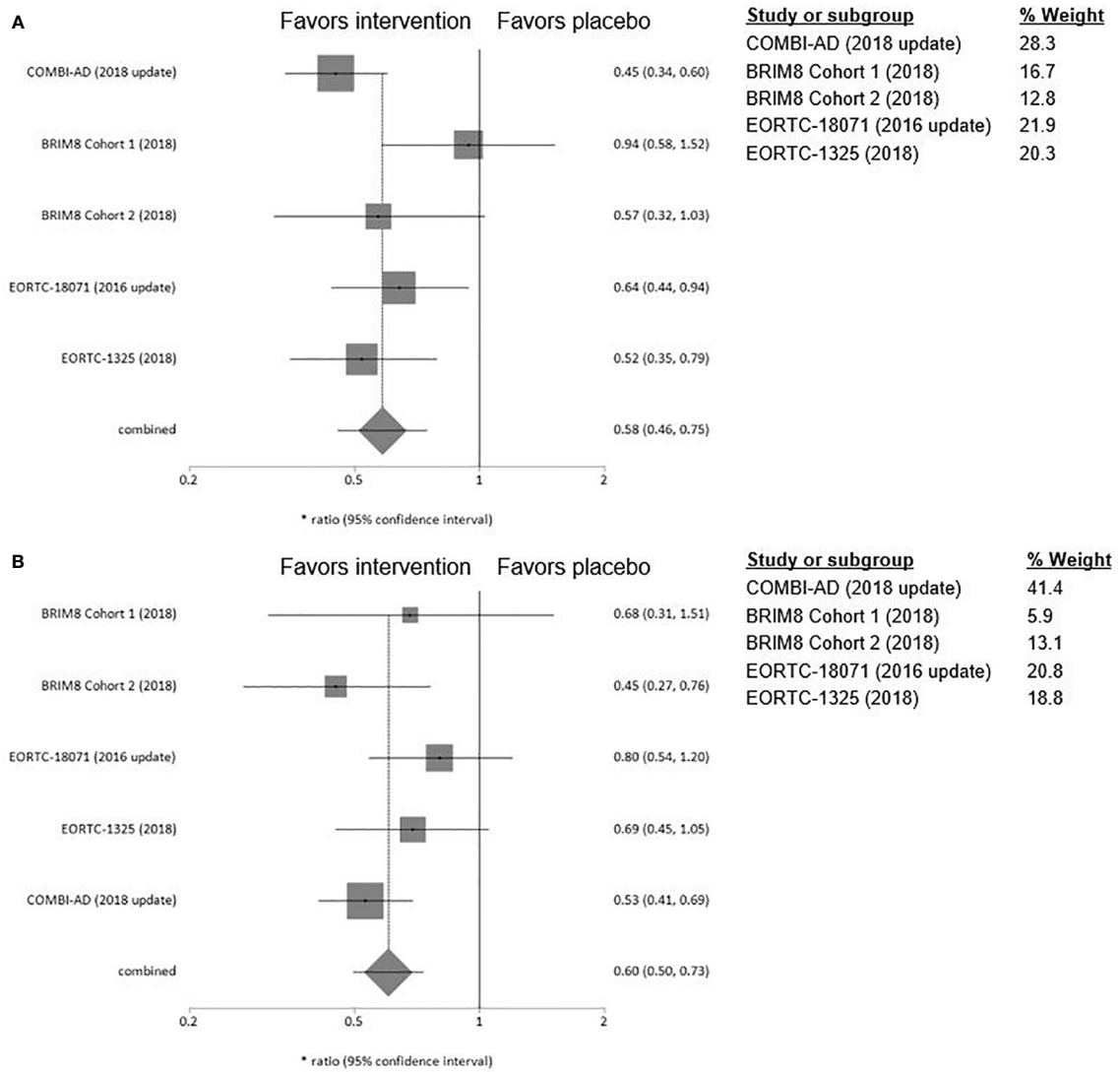

FIGURE 4 | **(A)** Forest plot for primary outcome analysis on relapse free survival for patients **with ulcerated primary tumor**. **(B)** for patients **with non-ulcerated primary tumor.** Hazard ratio for relapse or death along the x-axis, and trial results on the y axis, with gray squares representing effect estimates and lines through them representing 95% CIs. The gray diamond represents the overall effect measure which lies clear of the line off no effect, showing a benefit for the treatment groups compared to placebo. The percentage weight for each study is separately listed on the right of the graph. CI, confidence interval.

(HR 0.48; 95%CI= 0.28–0.81). Consistently, pembrolizumab also demonstrated a non-statistically significant benefit in stage IIIA (HR 0.38; 95%CI= 0.11–1.31) while higher stages (IIIB/C) clearly profit from adjuvant pembrolizumab treatment (**Figure 5**). The BRIM8 trial was the only to include patients with stage IIC. Here, median RFS was not reached in the vemurafenib arm.

BRAF Mutation

The IMMUNED and EORTC-1325 trials reported separate outcomes as per BRAF mutational status. The presence of a BRAF mutation was associated with higher RFS rates (HR 0.30; 95% CI= 0.11–0.78) compared to the BRAF wildtype group (HR 0.60; 95% CI= 0.44–0.81). Nivolumab/ipilimumab was associated with the highest benefit in BRAF*mut* MM (HR 0.07; 95% CI= 0.02–0.23) (**eFigure 5, supplement**).

Secondary Endpoints

Cross-trial comparison of secondary end points like OS and distant metastases free survival (DMFS) was not possible due to considerable variability in endpoint selection and reporting. In the EORTC-18071 trial, adjuvant therapy with ipilimumab significantly prolonged DMFS and most importantly OS (HR 0.72; 95.1% CI= 0.58–0.88) (20). In the COMBI-AD trial, data on OS were only reported for the first interim analysis. Treatment with BRAF/MEKi demonstrated higher 3-years OS-rates than with placebo (86% vs. 77% HR 0.57; 95%CI= 0.42–0.79) (21).

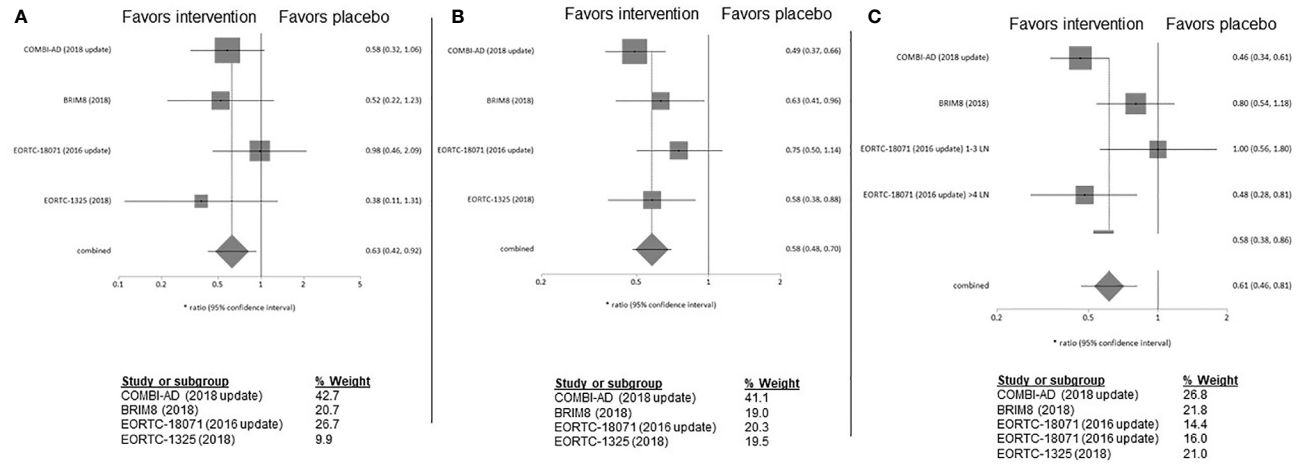

FIGURE 5 | **(A)** Forest plot for primary outcome analysis on relapse free survival for patients with stage **IIIA**; **(B)** melanoma stage **IIIB** and **C** stage **IIIC** Hazard ratio for relapse or death along the x-axis, and results from all four studies; in **(C)** upper value for the EORTC18071 study includes patients in stage IIC with 1–3 LN, lower value with 4 LN, with gray squares representing effect estimates and lines through them representing 95% CIs. The gray diamond represents the overall effect measure which lies clear of the line off no effect, showing a benefit for the treatment groups compared to placebo. The percentage weight for each study is separately listed underneath the graph. CI, confidence interval; LN, lymph nodes.

EORTC-1325 demonstrated that pembrolizumab has maintained the health-related quality of life (22). The BRIM8 study demonstrated a DMFS of 37.2 months; in cohort 1, the DMFS was not reached.

Adverse Events

The highest rate of grades 3–4 adverse events (AE) was observed with the nivolumab/ipilimumab combination (82%) with a treatment discontinuation rate of up to 62% (**eTable 4, supplement**). Ipilimumab monotherapy and vemurafenib were also associated with high grade 3-4 AE rates (54% and 59%, respectively) and discontinuation rates of 52% and 20%, respectively. Five deaths were attributed to ipilimumab monotherapy. 26% of patients treated with dabrafenib/trametinib went off study due to AE. One fatal serious AE (pneumonia) was reported in the combination-therapy group. In the EORTC-1325 trial, 13.8% of the patients discontinued pembrolizumab due to AE, which were equal to or higher than grade 3 in 31.6% of cases. There was one pembrolizumab related death due to myositis. Similar AE rates were observed with nivolumab monotherapy, with grades 3–4 toxicity up to 41% and 13% treatment discontinuation rate.

Risk of Bias

The funnel plot (**eFigure 6, supplement**) and the result from Egger's test (p = 0.311) showed indication of a publication bias. However, due to the limited number of studies included in the meta-analysis, this should be interpreted with caution. Overall, the trials were deemed to be at low risk for bias, except for "deviation of intended intervention" bias, for which it was unclear, whether participants with missing outcome data were excluded. In the COMBI-AD trial RFS was the prespecified outcome measurement however its estimation at 3 years was not prespecified (**eFigures 7** and **8, supplement**).

DISCUSSION

The RFS-benefit of modern adjuvant therapy (HR 0.57, 95% CI= 0.45–0.71) is higher than that shown for IFN-α in previous meta-analyses (HR 0.82, 95% CI = 0.77–0.87) (23).

Immune checkpoint inhibitor (ICi) monotherapy with pembrolizumab or nivolumab is similarly effective in improving RFS and both agents seem to be superior to ipilimumab while being less toxic, as previously demonstrated for nivolumab in the Checkmate-238 trial (24). This trial was not included in the current meta-analysis because of the lack of a placebo arm. An indirect analysis of adjuvant nivolumab versus placebo in stage III MM based on the Checkmate-238 and EORC-18071 trials calculated a HR for RFS of 0.53 (95% CI = 0.41–0.68) which is similar to the HR for RFS in the IMMUNED trial in stage IV (25).

The BRAF/MEKi combination therapy in the COMBI AD trial was associated with a clinical benefit across all subgroups with a tolerable adverse effect profile. In fact, the combination therapy demonstrated the highest numerical RFS-benefit in stage III melanoma (HR 0.49; 95% CI= 0.40–0.59). In stage IV melanoma with NED, nivolumab/ipilimumab demonstrated an impressive RFS benefit (HR 0.23; 97.5% CI= 0.12–0.45). The superiority of the combination versus ipilimumab or nivolumab monotherapy has also been demonstrated in metastatic melanoma, although at the cost of more grades 3–4 AE [24, 32]. However, only interim results from the rather small IMMUNED trial are currently published, and thus they must be interpreted with caution. Furthermore, stage IV patients with NED are per se at a higher risk of relapse, thus RFS benefits with adjuvant therapy between stages III and IV are not comparable.

In the interferon era, BRAF*mut* MM has been independently associated with a worse overall survival with HR of 1.7 (95% CI= 1.37–2.12) (26). Another, more recent meta-analysis of 52 trials

also found that the presence of a BRAF mutation was associated with a reduced OS (HR 1.23, 95% CI= 1.09–1.38) (27). Most trials however included neither BRAF/MEKi nor ICi therapy. Prognosis of BRAF*mut* MM is expected to be crucially influenced by modern therapeutic agents. ICi have dramatically improved outcomes in the adjuvant and metastatic setting and additionally, patients with a BRAF mutation have now the option of targeted therapy. Thus, their prognosis can be expected to improve in the context of modern therapy. Interestingly, in our analysis, BRAF*mut* resectable MM was associated with higher RFS in trials which reported outcomes according to BRAF mutational status (IMMUNED and EORTC-1325). In contrast, in advanced melanoma, Puzanov and colleagues found in a pooled analysis of three RCTs with ICi (pembrolizumab) that BRAF*mut* patients had similar OS as patients with BRAF wild-type MM (PFS; 19.8% and 22.9% and OS; 35.1% and 37.5%). Patients with BRAF*mut* MM who did not receive BRAFi +/- MEKi therapy had a worse prognosis than those who did (28). This contradiction could be explained through the fact that, while BRAF mutations are early events in their evolution (29), metastatic melanomas accumulate further genomic alterations such as whole-genome duplication over time, which may account for resistance to treatment (30). Furthermore, the higher tumor burden of unresected melanomas might lead to increased potential of developing resistant clones under BRAF/MEKi compared to completely resected melanoma. These two factors could account for the discordance in the prognostic influence of BRAF mutations between completely resected stage III/IV in our meta-analysis and advanced/unresectable melanoma in the meta-analysis by Puzanov et al.

Age does not influence outcomes after adjuvant therapy. Specifically, the HR for RFS in patients ≥65 years old is even numerically lower than that of their younger counterparts. Therefore, advanced age alone should not discourage administration of adjuvant therapy. Recently published data on elderly patients with MM receiving ICi also demonstrated good clinical outcomes without increased toxicity (31).

Ulceration status of the primary tumor may be predictive of RFS when ICi are used. Several studies have shown that ulcerated melanomas have distinct biologic characteristics (32, 33). In our study, ipilimumab and pembrolizumab are both associated with a significant RFS benefit in patients with ulcerated melanoma, but not in those with primary tumors without ulceration. In contrast, dabrafenib/trametinib showed benefit regardless of ulceration status, while vemurafenib is also associated with superior RFS in non-ulcerated stage IIIC MM. A *post hoc* meta-analysis of the EORTC-18952 (IFN α-2b versus observation in stages IIB–III) and -18991 trials (pegylated-IFN versus observation in stage III) also demonstrated that the absence of ulceration was predictive for inefficacy of adjuvant treatment with IFN-α (34). Therefore, it would be reasonable to prefer a BRAF/MEKi combination in non-ulcerated BRAF*mut* MM.

Adjuvant treatment in stage IIIA is associated with a similar RFS-benefit as in stages IIIB/C. Thus, our meta-analysis supports administration of adjuvant therapy in stage IIIA. However, all the above trials are powered for DFS/RFS and OS data have only been reported for the first interim analysis of the COMBI-AD trial and for the EORC-18071 trial, where a benefit could be demonstrated in favor of treatment. The recently reported update of the Checkmate-238 trial (35) showed no difference in OS between ipilimumab and nivolumab despite a significant RFS benefit. This and the general lack of OS data pose the issue of early vs late treatment, particularly in stages II/IIIA. Further data on OS are needed to guide treatment decisions. The influence of toxicity in decision making in earlier stages is discussed below.

As IFN-α has been associated with substantial AE and drug related fatalities, modern adjuvant therapeutics have to meet high expectations (23, 36, 37). The highest toxicity was seen with the nivolumab/ipilimumab combination in stage IV MM with NED. Pembrolizumab toxicity in the adjuvant setting (31.6% grade ≥3 AE) was lower compared to the AE rate of nivolumab (41%). However, data on nivolumab toxicity in our meta-analysis are derived from stage IV MM, while pembrolizumab was tested in stage III patients. The Checkmate238 trial, which also included stage III patients demonstrated a 25.4% rate of grades 3–4 AE in patients treated with nivolumab (11). Monotherapy with pembrolizumab or nivolumab have been shown to have a considerably better tolerability profile than ipilimumab (10, 24, 38). The dabrafenib/trametinib combination demonstrated similar grades 3–4 AE rates as pembrolizumab and nivolumab (26%) and less than half compared to vemurafenib (59%), as in previous trials comparing BRAF/MEKi combinations to BRAFi monotherapy (39, 40). The ICi combination and ipilimumab monotherapy were associated with the highest toxicity. In the context of the curative adjuvant setting, potentially permanent toxicities involved with ICi become particularly relevant. The incidence is higher with ICi combination than with PD-1 monotherapy (hypophysitis: 8.0% vs. 1.1, hypothyroidism: 13.2% vs. 7.0%). Primary adrenal insufficiency and insulin dependent diabetes are rare events (cumulative incidence after ICi: 0.7% and 0.2% respectively) (41–43). Because of this potentially long-lasting toxicity and the lack of consistent data on OS as discussed above we generally prefer BRAF/MEKi as adjuvant treatment in the context of BRAF-mutant MM, especially in stages IIIA/B.

An important unanswered clinical question is adjuvant therapy for patients with stage II MM, where rates of distant recurrence after resection can reach 44% (44, 45). Vemurafenib monotherapy is not approved in the adjuvant therapy of MM, however, BRIM8 was the only trial to include patients with stage IIC. In this subgroup, no events occurred in the vemurafenib arm (0/15) whereas six patients suffered a relapse in the placebo arm (6/12) (13). Although IFN-α remains an adjuvant therapeutic option for patients with stages IIB and IIC melanoma, it is rarely used in daily practice due to its significant toxicity (9). Currently ongoing trials are comparing pembrolizumab and nivolumab vs. placebo in resected stage II MM (45, 46).

Neoadjuvant approaches with both BRAF/MEKi and ICi in high-risk resectable MM are also currently under investigation (47, 48).

Although based on well-designed trials with robust results, our meta-analysis still has some limitations. First, it does not address the

contemporary question of a comparison between adjuvant and neoadjuvant therapy. Second, it was restricted to placebo-controlled studies and thus forced the exclusion of relevant trials like those comparing two agents (e.g., ipilimumab versus nivolumab). Moreover, due to the significant trial variability regarding endpoint reporting and lacking consistent OS data reporting/availability, our meta-analysis is based on RFS and not on OS data. On this matter, significant inter-trial heterogeneity is also noted in the stages included. Furthermore, comparisons between subgroups were not possible for all the included RCTs, as subgroup-definition as well as data availability for each subgroup varied across the trials. Another limitation is the inconsistent representation of BRAF*mut* MM across trials. In addition, treatment and definition of stage III within the included RCTs does not correspond completely to current standards. Moreover, complete lymph node dissection was required for trial enrollment in the EORTC-1325, EORTC-18071 and COMBI-AD trials. This practice has been meanwhile replaced by sentinel lymph node biopsy according to results from RCTs (49, 50). Additionally, it must be kept in mind, that the current definition of stage III disease according to the 8th edition of AJCC is different than the one used in the RCTs above. Stages IIIA/B/C as defined in the 7th edition carry a worse prognosis, and may therefore benefit more from adjuvant therapy (51).

In conclusion, contemporary adjuvant therapy in the post interferon-alpha era for patients with high-risk completely resected MM is effective and tolerable and should be recommended in all patients in the absence of contraindications. BRAF*mut* MM was associated with higher RFS. Furthermore, some subgroups may benefit more from specific treatments and this can guide treatment choice. Advanced age and stage IIIA should not discourage adjuvant treatment. Options in BRAF wildtype melanoma are limited to ICi. In BRAF*mut* MM, BRAF/MEKi should be preferred, especially in the absence of ulceration and stage IIIA. Adjuvant treatment should be adapted to patient preference like the intake schedule or pre-existing conditions.

DATA AVAILABILITY STATEMENT

The data sets presented in this study can be found in online repositories. The names of the repository/repositories and accession number(s) can be found below: "The Open Science Framework—Center for OpenScience" (https://osf.io/m9vr5).

AUTHOR CONTRIBUTIONS

KC, KY, and DK-M performed the systematic review. KC, KY, MB, LT, and TR performed the data analysis. KC, CP, CM, TV, SS, and DK-M evaluated the data. KC, KY, and DK-M drafted the manuscript. All authors contributed to the article and approved the submitted version.

SUPPLEMENTARY MATERIAL

The Supplementary Material for this article can be found online at: https://www.frontiersin.org/articles/10.3389/fonc.2020.637161/full#supplementary-material

REFERENCES

1. World Health Organization. *Skin cancers*. Available at: https://www.who.int/uv/resources/FAQ/skincancer/en/index1.html (Accessed June 14, 2020).
2. Fitzmaurice C, Akinyemiju TF, Al Lami FH, Alam T, Alizadeh-Navaei R, Allen C, et al. Global, regional, and national cancer incidence, mortality, years of life lost, years lived with disability, and disability-adjusted life-years for 29 cancer groups, 1990 to 2016 a systematic analysis for the global burden of disease study global burden of disease cancer collaboration. *JAMA Oncol* (2018) 4:1553–68. doi: 10.1001/jamaoncol.2018.2706
3. Balch CM, Gershenwald JE, Soong SJ, Thompson JF, Atkins MB, Byrd DR, et al. Final version of 2009 AJCC melanoma staging and classification. *J Clin Oncol* (2009) 27:6199–206. doi: 10.1200/JCO.2009.23.4799
4. Michielin O, Van Akkooi ACJ, Ascierto PA, Dummer R, Keilholz U. Cutaneous melanoma: ESMO Clinical Practice Guidelines for diagnosis, treatment and follow-up. *Ann Oncol* (2019) 30(12):1884–901. doi: 10.1093/annonc/mdz411
5. Gershenwald JE, Scolyer RA. Melanoma Staging: American Joint Committee on Cancer (AJCC) 8th Edition and Beyond. *Ann Surg Oncol* (2008) 25 (8):2105–110. doi: 10.1245/s10434-018-6513-7
6. Verma S, Quirt I, McCready D, Bak K, Charette M, Iscoe N. Systematic review of systemic adjuvant therapy for patients at high risk for recurrent melanoma. *Cancer* (2006) 106:1431–42. doi: 10.1002/cncr.21760
7. Malczewski A, Marshall A, Payne MJ, Mao L, Bafaloukos D, Si L, et al. Intravenous high-dose interferon with or without maintenance treatment in melanoma at high risk of recurrence: meta-analysis of three trials. *Cancer Med* (2016) 5:17–23. doi: 10.1002/cam4.563
8. Mocellin S, Lens MB, Pasquali S, Pilati P, Chiarion Sileni V. Interferon alpha for the adjuvant treatment of cutaneous melanoma. *Cochrane Database Syst Rev* (2013) 6:CD008955. doi: 10.1002/14651858.CD008955.pub2
9. Ives NJ, Suciu S, Eggermont AMM, Kirkwood J, Lorigan P, Markovic SN, et al. Adjuvant interferon-α for the treatment of high-risk melanoma: An individual patient data meta-analysis. *Eur J Cancer* (2017) 82:171–83. doi: 10.1016/j.ejca.2017.06.006
10. Eggermont AMM, Chiarion-Sileni V, Grob JJ, Dummer R, Wolchok JD, Schmidt H, et al. Adjuvant ipilimumab versus placebo after complete resection of high-risk stage III melanoma (EORTC 18071): A randomised, double-blind, phase 3 trial. *Lancet Oncol* (2015) 16:522–30. doi: 10.1016/S1470-2045(15)70122-1
11. Weber JS, Mandala M, Del Vecchio M, Gogas H, Arance AM, Cowey CL, et al. Adjuvant therapy with nivolumab (NIVO) versus ipilimumab (IPI) after complete resection of stage III/IV melanoma: updated results from a phase III trial (CheckMate 238). *J Clin Oncol* (2018) 36(15_suppl):9502–9502. doi: 10.1200/JCO.2018.36.15-suppl.9502
12. Zimmer L, Livingstone E, Hassel JC, Fluck M, Eigentler T, Loquai C, et al. Adjuvant nivolumab plus ipilimumab or nivolumab monotherapy versus placebo in patients with resected stage IV melanoma with no evidence of disease (IMMUNED): a randomised, double-blind, placebo-controlled, phase 2 trial. *Lancet (Lond Engl)* (2020) 395:1558–68. doi: 10.1016/S0140-6736(20)30417-7
13. Maio M, Lewis K, Demidov L, Mandalà M, Bondarenko I, Ascierto PA, et al. Adjuvant vemurafenib in resected, BRAF(V600) mutation-positive melanoma (BRIM8): a randomised, double-blind, placebo-controlled, multicentre, phase 3 trial. *Lancet Oncol* (2018) 19:510–20. doi: 10.1016/S1470-2045(18)30106-2
14. Long GV, Hauschild A, Santinami M, Atkinson V, Mandal M, Chiarion-Sileni V, et al. Adjuvant dabrafenib plus trametinib in stage III BRAF-mutated melanoma. *N Engl J Med* (2017) 377:1813–23. doi: 10.1056/NEJMoa1708539
15. Ward WH, Lambreton F, Goel N, Yu JQ, Farma JM. Clinical Presentation and Staging of Melanoma. In: *Cutaneous Melanoma: Etiology and Therapy*. Singapore: Codon Publications (2017). p. 79–89. doi: 10.15586/codon.cutaneousmelanoma.2017.ch6

16. Longo C, Pampena R, Lallas A, Kyrgidis A, Stratigos A, Peris K, et al. Adjuvant therapy for cutaneous melanoma: a systematic review and network meta-analysis of new therapies. *J Eur Acad Dermatol Venereol* (2020) 34:956–66. doi: 10.1111/jdv.16074
17. Moher D, Liberati A, Tetzlaff J, Altman DG. Preferred reporting items for systematic reviews and meta-analyses: the PRISMA statement. *J Clin Epidemiol* (2009) 62:1006–12. doi: 10.1016/j.jclinepi.2009.06.005
18. Sterne JAC, Savović J, Page MJ, Elbers RG, Blencowe NS, Boutron I, et al. RoB 2: A revised tool for assessing risk of bias in randomised trials. *BMJ* (2019) 366:l4898. doi: 10.1136/bmj.l4898
19. Egger M, Smith GD, Schneider M, Minder C. Bias in meta-analysis detected by a simple, graphical test. *Br Med J* (1997) 315:629–34. doi: 10.1136/bmj.315.7109.629
20. Eggermont AMM, Chiarion-Sileni V, Grob J-J, Dummer R, Wolchok JD, Schmidt H, et al. Adjuvant ipilimumab versus placebo after complete resection of stage III melanoma: long-term follow-up results of the European Organisation for Research and Treatment of Cancer 18071 double-blind phase 3 randomised trial. *Eur J Cancer* (2019) 119:1–10. doi: 10.1016/j.ejca.2019.07.001
21. Hauschild A, Dummer R, Schadendorf D, Santinami M, Atkinson V, Mandalà M, et al. Longer Follow-Up Confirms Relapse-Free Survival Benefit With Adjuvant Dabrafenib Plus Trametinib in Patients With Resected BRAF V600-Mutant Stage III Melanoma. *J Clin Oncol* (2018) 36:3441–9. doi: 10.1200/JCO.18.01219
22. Coens C, Bottomley A, Blank CU, Mandala M, Long GV, Atkinson VG, et al. Health-related quality-of-life results for pembrolizumab versus placebo after complete resection of high-risk stage III melanoma from the EORTC 1325-MG/Keynote 054 trial: An international randomized double-blind phase III trial. *Ann Oncol* (2018) 29:viii456. doi: 10.1093/annonc/mdy289.034
23. Mocellin S, Pasquali S, Rossi CR, Nitti D. Interferon alpha adjuvant therapy in patients with high-risk melanoma: A systematic review and meta-analysis. *J Natl Cancer Inst* (2010) 102:493–501. doi: 10.1093/jnci/djq009
24. Weber J, Mandala M, Del Vecchio M, Gogas HJ, Arance AM, Cowey CL, et al. Adjuvant nivolumab versus ipilimumab in resected stage III or IV melanoma. *N Engl J Med* (2017) 377:1824–35. doi: 10.1056/NEJMoa1709030
25. Freeman M, Betts KA, Jiang S, Du EX, Gupte-Singh K, Lu Y, et al. Indirect Treatment Comparison of Nivolumab Versus Observation or Ipilimumab as Adjuvant Therapy in Resected Melanoma Using Pooled Clinical Trial Data. *Adv Ther* (2019) 36:2783–96. doi: 10.1007/s12325-019-01060-y
26. Safaee Ardekani G, Jafarnejad SM, Tan L, Saeedi A, Li G. The Prognostic Value of BRAF Mutation in Colorectal Cancer and Melanoma: A Systematic Review and Meta-Analysis. *PloS One* (2012) 7(10):e47054. doi: 10.1371/journal.pone.0047054
27. Ny L, Hernberg M, Nyakas M, Koivunen J, Oddershede L, Yoon M, et al. BRAF mutational status as a prognostic marker for survival in malignant melanoma: a systematic review and meta-analysis. *Acta Oncol (Madr)* (2020) 59:833–44. doi: 10.1080/0284186X.2020.1747636
28. Puzanov I, Ribas A, Robert C, Schachter J, Nyakas M, Daud A, et al. Association of BRAF V600E/K Mutation Status and Prior BRAF/MEK Inhibition with Pembrolizumab Outcomes in Advanced Melanoma: Pooled Analysis of 3 Clinical Trials. *JAMA Oncol* (2020) 6:1256–64. doi: 10.1001/jamaoncol.2020.2288
29. Pollock PM, Harper UL, Hansen KS, Yudt LM, Stark M, Robbins CM, et al. High frequency of BRAF mutations in nevi. *Nat Genet* (2003) 33:19–20. doi: 10.1038/ng1054
30. Birkeland E, Zhang S, Poduval D, Geisler J, Nakken S, Vodak D, et al. Patterns of genomic evolution in advanced melanoma. *Nat Commun* (2018) 9:2665. doi: 10.1038/s41467-018-05063-1
31. Perier-Muzet M, Gatt E, Péron J, Falandry C, Amini-Adlé M, Thomas L, et al. Association of immunotherapy with overall survival in elderly patients with melanoma. *JAMA Dermatol* (2018) 154:82–7. doi: 10.1001/jamadermatol.2017.4584
32. Bønnelykke-Behrndtz ML, Schmidt H, Christensen IJ, Sam CME. Prognostic Stratification of Ulcerated Melanoma Not Only the Extent Matters. *Am J Clin Pathol* (2014) 142(6):845–56. doi: 10.1309/AJCPW56PHGLFTKZC
33. Eggermont AMM, Spatz A, Lazar V, Robert C. Is ulceration in cutaneous melanoma just a prognostic and predictive factor or is ulcerated melanoma a distinct biologic entity? *Curr Opin Oncol* (2012) 24:137–40. doi: 10.1097/CCO.0b013e32834fcb0d
34. Eggermont AMM, Suciu S, Testori A, Kruit WH, Marsden J, Punt CJ, et al. Ulceration and stage are predictive of interferon efficacy in melanoma: Results of the phase III adjuvant trials EORTC 18952 and EORTC 18991. *Eur J Cancer* (2012) 48:218–25. doi: 10.1016/j.ejca.2011.09.028
35. Weber J, Del Vecchio M, Mandala M, Gogas H, Fernandez AMA, Dalle S, et al. 1076O Adjuvant nivolumab (NIVO) vs ipilimumab (IPI) in resected stage III/IV melanoma: 4-y recurrence-free and overall survival (OS) results from CheckMate 238. *Ann Oncol* (2020) 31:S731–2. doi: 10.1016/j.annonc.2020.08.1200
36. Bottomley A, Coens C, Suciu S, Santinami M, Kruit W, Testori A, et al. Adjuvant therapy with pegylated interferon alfa-2b versus observation in resected stage III melanoma: A phase III randomized controlled trial of health-related quality of life and symptoms by the European Organisation for Research and Treatment of Cancer. *J Clin Oncol* (2009) 27:2916–23. doi: 10.1200/JCO.2008.20.2069
37. Eggermont AM, Suciu S, Santinami M, Testori A, Kruit WH, Marsden J, et al. Adjuvant therapy with pegylated interferon alfa-2b versus observation alone in resected stage III melanoma: final results of EORTC 18991, a randomised phase III trial. *Lancet* (2008) 372:117–26. doi: 10.1016/S0140-6736(08)61033-8
38. Eggermont AMM, Blank CU, Mandala M, Long GV, Atkinson V, Dalle S, et al. Adjuvant pembrolizumab versus placebo in resected stage III melanoma. *N Engl J Med* (2018) 378:1789–801. doi: 10.1056/NEJMoa1802357
39. Boespflug A, Thomas L. Cobimetinib and vemurafenib for the treatment of melanoma. *Expert Opin Pharmacother* (2016) 17:1005–11. doi: 10.1517/14656566.2016.1168806
40. Larkin J, Ascierto PA, Dréno B, Atkinson V, Liszkay G, Maio M, et al. Combined Vemurafenib and Cobimetinib in BRAF-Mutated Melanoma. *N Engl J Med* (2014) 371:1867–76. doi: 10.1056/NEJMoa1408868
41. Barroso-Sousa R, Barry WT, Garrido-Castro AC, Hodi FS, Min L, Krop IE, et al. Incidence of endocrine dysfunction following the use of different immune checkpoint inhibitor regimens a systematic review and meta-analysis. *JAMA Oncol* (2018) 4:173–82. doi: 10.1001/jamaoncol.2017.3064
42. Samuel E, Moore M, Voskoboynik M, Shackleton M, Haydon A. An update on adjuvant systemic therapies in melanoma. *Melanoma Manag* (2019) 6:MMT28. doi: 10.2217/mmt-2019-0009
43. Cousin S, Seneschal J, Italiano A. Toxicity profiles of immunotherapy. *Pharmacol Ther* (2018) 181:91–100. doi: 10.1016/j.pharmthera.2017.07.005
44. Jang JK, Khawli LA, Canter DC, Hu P, Zhu TH, Wu BW, et al. Systemic delivery of chTNT-3/CpG immunoconjugates for immunotherapy in murine solid tumor models. *Cancer Immunol Immunother* (2016) 65:511–23. doi: 10.1007/s00262-016-1813-x
45. Luke JJ, Ascierto PA, Carlino MS, Gershenwald JE, Grob J-J, Hauschild A, et al. KEYNOTE-716: Phase III study of adjuvant pembrolizumab versus placebo in resected high-risk stage II melanoma. *Future Oncol* (2020) 16:4429–38. doi: 10.2217/fon-2019-0666
46. ClinicalTrials.gov. NCT04309409. *Adjuvant Nivolumab Treatment in Stage II (IIA, IIB, IIC) High-risk Melanoma*. (2020). Available at: https://clinicaltrials.gov/show/NCT04309409 (Accessed June 14, 2020).
47. Amaria RN, Prieto PA, Tetzlaff MT, Reuben A, Andrews MC, Ross MI, et al. Neoadjuvant plus adjuvant dabrafenib and trametinib versus standard of care in patients with high-risk, surgically resectable melanoma: a single-centre, open-label, randomised, phase 2 trial. *Lancet Oncol* (2018) 19:181–93. doi: 10.1016/S1470-2045(18)30015-9
48. Blank CU, Rozeman EA, Fanchi LF, Sikorska K, van de Wiel B, Kvistborg P, et al. Neoadjuvant versus adjuvant ipilimumab plus nivolumab in macroscopic stage III melanoma. *Nat Med* (2018) 24:1655–61. doi: 10.1038/s41591-018-0198-0
49. Leiter U, Stadler R, Mauch C, Hohenberger W, Brockmeyer N, Berking C, et al. Complete lymph node dissection versus no dissection in patients with sentinel lymph node biopsy positive melanoma (DeCOG-SLT): a multicentre, randomised, phase 3 trial. *Lancet Oncol* (2016) 17:757–67. doi: 10.1016/S1470-2045(16)00141-8
50. Faries MB, Thompson JF, Cochran AJ, Andtbacka RH, Mozzillo N, Zager JS, et al. Completion Dissection or Observation for Sentinel-Node Metastasis in Melanoma. *N Engl J Med* (2017) 376:2211–22. doi: 10.1056/nejmoa1613210

51. Keung EZ, Gershenwald JE. The eighth edition American Joint Committee on Cancer (AJCC) melanoma staging system: implications for melanoma treatment and care. *Expert Rev Anticancer Ther* (2018) 18:775–84. doi: 10.1080/14737140.2018.1489246

Conflict of Interest: The authors declare that the research was conducted in the absence of any commercial or financial relationships that could be construed as a potential conflict of interest.

frontiers in Oncology

REVIEW
published: 01 March 2021
doi: 10.3389/fonc.2021.640314

Beyond PD-1: The Next Frontier for Immunotherapy in Melanoma

Anjali Rohatgi and John M. Kirkwood *

Hillman Cancer Center, University of Pittsburgh Medical Center, Pittsburgh, PA, United States

The advent of first and second-generation immune checkpoint blockade (ICI) has resulted in improved survival of patients with metastatic melanoma over the past decade. However, the majority of patients ultimately progress despite these treatments, which has served as an impetus to consider a range of subsequent therapies. Many of the next generation of immunotherapeutic agents focus on modifying the immune system to overcome resistance to checkpoint blockade. ICI resistance can be understood as primary, or acquired—where the latter is the most common scenario. While there are several postulated mechanisms by which resistance, particularly acquired resistance, occurs, the predominant escape mechanisms include T cell exhaustion, upregulation of alternative inhibitory checkpoint receptors, and alteration of the tumor microenvironment (TME) into a more suppressive, anti-inflammatory state. Therapeutic agents in development are designed to work by combating one or more of these resistance mechanisms. These strategies face the added challenge of minimizing immune-related toxicities, while improving antitumor efficacy. This review focuses upon the following categories of novel therapeutics: 1) alternative inhibitory receptor pathways; 2) damage- or pathogen-associated molecular patterns (DAMPs/PAMPs); and 3) immune cell signaling mediators. We present the current state of these therapies, including preclinical and clinical data available for these targets under development.

Keywords: melanoma, checkpoint inhibition/blockade, pathogen recognition receptor (PRR), cytokines, TLR (Toll-like receptors)

OPEN ACCESS

Edited by:
Giuseppe Palmieri,
National Research Council (CNR), Italy

Reviewed by:
Inna Smalley,
Moffitt Cancer Center, United States
Kathleen Marie Kokolus,
University at Buffalo, United States

***Correspondence:**
John M. Kirkwood
kirkwoodjm@upmc.edu

Specialty section:
This article was submitted to Skin Cancer, a section of the journal Frontiers in Oncology

Received: *11 December 2020*
Accepted: *07 January 2021*
Published: *01 March 2021*

Citation:
Rohatgi A and Kirkwood JM (2021) Beyond PD-1: The Next Frontier for Immunotherapy in Melanoma. Front. Oncol. 11:640314. doi: 10.3389/fonc.2021.640314

INTRODUCTION

The use of checkpoint inhibitors in melanoma has dramatically changed treatment options for patients with melanoma. Prior to 2011 and the FDA approval of ipilimumab, standard of care options included chemotherapy and high dose IL-2, and in the adjuvant setting, high-dose interferon alpha-2, all of which were associated with limited efficacy and significant toxicity. Targeted therapy with BRAF and MEK inhibition has also been approved for the 50% of melanoma patients with activating BRAF mutations. Despite a promising overall response rate and evidence of durable responses for some, the majority of patients with advanced melanoma have ultimately exhibited progression of disease on or after checkpoint blockade (1). Further, while the majority of patients tolerate therapy, there is risk of significant and sometimes fatal toxicity.

Significant effort has been put into finding ways to re-sensitize tumors after immunotherapy resistance has developed as well as alternative strategies for checkpoint blockade. In fact, the number

of trials of combination inhibitors has increased significantly each year, though success of this approach remains to be seen (2). In this review, we will profile some of the most promising strategies in broad categories, including 1) alternative checkpoint receptors 2) DAMPs/PAMPs and 3) immune cell signaling modulators of the TME.

In order to understand the rationale for many of these novel therapies, mechanisms of anti-PD-1/PDL-1 resistance need to be discussed. Resistance is characterized as primary or secondary. The Society for Immunotherapy of Cancer taskforce recently published consensus guidelines to define these terms (3). Primary resistance is defined as progression of disease or at best stable disease for less than 6 months for patients who received a minimum of 6 weeks of therapy. Secondary resistance is defined as nonresponse with progression of disease after initial response to therapy with at least complete response (CR), partial response (PR) or stable disease (SD) of greater than 6 months duration. The mechanisms of resistance to anti-PD-1 therapy are postulated to be diverse, but this remains an area of exploration. In particular, identifying which mechanism or mechanisms are responsible for disease progression in individual patients is an area of ongoing interest.

A full review of immunotherapy escape mechanisms is outside the scope of this review; this topic has been reviewed extensively elsewhere and is summarized briefly here (4–7). Mechanisms attributed to resistance include a lack of target tumor neoantigens, or impaired antigen presentation in the tumor. Further, a lack of tumor immune cell infiltration described as a "cold" tumor, within which the non-inflamed tumor lacks the effector T cell populations that are the basis of benefit from ICI has been reported. Further, impairment of IFNγ secretion or signaling or other inflammatory cytokine responses can lead to resistance (8). This is often accompanied by presence of other types of suppressive immune cells, including M2 macrophages, T regulatory cells (Tregs), and myeloid derived suppressor cells (MDSCs). Alternative checkpoints that may govern the antitumor function of T cells, such as LAG3, TIM3 and other inhibitory receptors are also discussed here, as they can lead to reduction of antitumor cytotoxicity of T cells and are observed in exhausted T cells after chronic antigen stimulation. We will focus on strategies for which clinical data from ongoing trials are anticipated.

A combinatorial approach with ICI has been favored for many of these therapies, both because of limited efficacy seen thus far with many of the single agents being explored, and also because of postulated mechanisms of resistance to immunotherapy. For example, an alternative inhibitory receptor may reduce T-cell exhaustion, but may not be sufficient to promote T effector cytotoxicity without the concurrent administration of anti-PD-1. An example of successful combinatorial therapy is seen with dual-checkpoint inhibition using nivolumab and ipilimumab, as seen in several disease types including melanoma, lung cancer, and renal cell carcinoma. However, increases in response rates compared to ipilimumab monotherapy have come at the expense of increased toxicity (9). Where available, efficacy and toxicity with combination therapy are reported in this review.

ALTERNATIVE CHECKPOINT RECEPTOR PATHWAYS

Additional inhibitory checkpoint receptors are being explored as a potential avenue for single agent or combined therapy with anti-PD-1. Many of these receptors were identified in the setting of chronic viral infection, which leads to T cell exhaustion and unresponsiveness to stimuli. Therapies targeting inhibitory receptors are postulated to augment anti-tumor response, perhaps by reversing T cell exhaustion. Most of these are monoclonal antibodies that act *via* inhibitory receptors to relieve inhibition of T cell activity. This review will focus on effector T cell receptors, however it is worth noting that additional strategies for targeting other suppressive immune cell actors including MDSCs and Tregs are under development.

Lymphocyte Activation Gene-3

Lymphocyte activation gene-3 (LAG3) (CD223) is a type I membrane protein found on the surface of activated T cells, T regulatory cells, NK cells, and plasmacytoid dendritic cells (10). LAG3 demonstrates homology to the costimulatory membrane protein CD4 and binds major histocompatibility complex II (MHCII) (11). LAG3 expression on T cells is upregulated after continued antigenic stimulation, and often co-expressed with additional inhibitory receptors such as PD-1 and TIGIT (12). LAG3 can also be proteolytically cleaved, releasing the external portion to become soluble LAG3, the role of which remains unclear (13). LAG3 has multiple functions in suppressing the immune response, as elucidated by murine knockout models. First, LAG3 decreases CD4+ T cell proliferation and secretion of inflammatory cytokines such as IL-2, IFNγ, and TNFα (14). LAG3 also affects the development of memory CD4+ T cells (15). LAG3 promotes the suppressive activity of Tregs, and inhibition of LAG3 can reduce Treg formation (16, 17). Similar immunosuppressive properties of LAG3 have been observed in human tumor samples (18). These data support LAG3 as an additional promising clinical immunotherapy target.

LAG3-targetting agents are currently under clinical investigation from several companies. Soluble LAG3 peptide (IMP321; eftilagimod alpha) has been tested in several early phase clinical trials for patients with solid tumors, both as monotherapy and as an adjuvant to vaccine development. In a phase I/IIa trial in resected melanoma, IMP321 was used as an adjuvant with a peptide vaccine in which the primary objective was to evaluate the T cell response and toxicity of the therapy (19). Indeed, CD8+ and CD4+ T cell responses were induced in the majority of patients. Additional studies have been conducted in combination with gemcitabine in patients with pancreatic cancer with a best response of stable disease (20), and in combination with paclitaxel for breast cancer with an objective tumor response rate of 50% (partial responses in 15/30 patients) (21). Partial responses have also been seen in combination with pembrolizumab in head and neck carcinoma in a phase II trial (22). Ongoing combinatorial strategies for IMP321 are under investigation.

Further, a number of anti-LAG3 monoclonal antibodies is under development, including BMS-986016 (relatlimab), LAG525, TSR-033, REGN3767, and MK-4280. These antibodies are under therapeutic evaluation in patients with melanoma, both as monotherapy and in combination with anti-PD-1. Further, they are being explored in the neoadjuvant and metastatic settings. Recruitment is ongoing for the majority of these studies. Preliminary data from NCT01968109, reporting the results of relatlimab plus nivolumab in melanoma patients who have received prior immunotherapy was reported at ESMO 2019 with an ORR of 11.5% (23). In a Phase I study of advanced solid tumors, LAG525 was given with or without spartalizumab resulting in the majority of patients discontinuing treatment for progressive disease (79% and 67% respectively) (24). Efficacy was reported as 11 PRs and 1 CR in the combination arm. Together, these data demonstrate less success with second line LAG3 inhibition than had been anticipated, but larger phase II studies in the treatment refractory and treatment naïve setting are needed to assess the potential role of this agent and are forthcoming.

T Cell Immunoglobulin and Mucin-Domain Containing-3

T cell immunoglobulin and mucin-domain containing-3 (Tim-3) is a type I transmembrane protein found on the surface of T cells, NK cells, dendritic cells and macrophages (25). Tim-3 has several ligands including galactin-9, engagement of which results in cell death of Th1 cells (26). Other ligands include ceacam1, which may stabilize Tim-3 on the cell surface, and HMGB1 and phosphatidylserine (27). Tim-3 is also a marker of exhausted T cells, and is often co-expressed on CD8+ T cells with PD-1 (28). Tim-3 is associated with decreased inflammatory cytokine production of IFNγ, and can also enhance the immunosuppressive activity of Foxp3 Tregs, (29) (30). Tim-3 can also contribute to the suppressive TME by promoting the generation of MDSCs (31). In humans, Tim-3 is implicated in autoimmunity as well as chronic viral infections (29, 32). Patients whose tumors exhibit high levels of Tim-3 expression are more likely to have worse prognosis in several tumor types (27).

Similar to LAG3, Tim-3 is an attractive clinical target and several monoclonal antibodies targeting Tim-3 are under investigation including MGB453, TSR-022, Sym023, BGBA425, RO7121661, ICAGN02390, LY3321367, and BMS-986258. Ongoing trials with these antibodies were recently summarized in the review by Acharya, et al (33). Clinical data is forthcoming. LY3321367 alone, or with an anti-PD-L1 therapy, did not produce any dose-limiting toxicities, and was associated with >20% tumor regression (1 PR) in the monotherapy arm (NCT03099109) (34). For patients with NSCLC and melanoma treated with prior anti-PD-1/PD-L1, MBG453 was given with spartalizumab in a phase II study. Of the 33 patients in that study, 15.2% were being treated at the time of abstract presentation, with the remainder discontinuing study due to progressive disease. Grade 3/4 adverse effects including pruritis, amylase and lipase elevation, increased ALT were noted (35). As with the studies of LAG3, mature data and larger studies are in development.

T Cell Immunoreceptor With Immunoglobulin and ITIM Domain

T cell immunoreceptor with immunoglobulin and ITIM domain (TIGIT) is another inhibitory receptor on T cells, as its name implies. TIGIT is a found on activated CD8+ and CD4+ T cells, NK cells, Tregs and T follicular cells (36). TIGIT binds to multiple ligands including CD155 and CD112, for which binding competes with the co-stimulatory receptor CD226/DNAM-1 (37). TIGIT is highly expressed in tumor samples and T cells that also express PD-1, suggesting a role in T cell exhaustion (38). In murine models of CT26 colorectal carcinoma, monotherapy with anti-TIGIT therapy did not effect tumor growth; however, when introduced with anti-PD-1 it resulted in a reduction of tumor growth (38). Further, this combination increased percent of tumor-infiltrating IFNγ+ CD8+ T cells (38). The anti-tumor effect of TIGIT may also be mediated by NK cells and enhanced by IL-15 (39).

A number of anti-TIGIT monoclonal antibodies are under development as listed in **Table 1**. A recent review by Chauvin, et al. lists ongoing Phase I/II clinical trials involving TIGIT, which are primarily being conducted with anti-PD-1/PD-L1 therapies (36). Results from the CITYSCAPE Phase II trial of anti-TIGIT tiragolumab and atezolizumab in patients with PD-L1+ advanced NSCLC demonstrated grade >=3 TRAE in 15% of patients. ORR was higher in patients receiving tiragolumab and atezolizumab (37.3% (CI 25–49.6) compared to those receiving placebo and atezoliumab (20.6% (CI 10.2–30.9), with an odds ratio of 2.57 (CI 1.07–6.14) (40). Tiragolumab with or without atezolizumab was also tested in patients with advanced solid tumors, in a Phase Ia/Ib dose escalation trial with TRAE of ≥ grade 3 in 4% of patients in each phase (41). There were three responses greater than stable disease in the Phase 1b portion, all of which occurred in PD-L1 positive patients. In an additional NSCLC expansion cohort ORR was 50%. Results are not yet available for additional clinical trials.

Additional Inhibitory Receptors

Additional inhibitory receptors under current clinical investigation include V-domain Ig-containing suppressor of T cell Activation (VISTA) (42). VISTA has homology to CD28 family members including PD-1 (43). Data is primarily available in the preclinical setting, but suggests VISTA blockade may reduce tumor growth in melanoma models, and alter the TME by reducing MDSCs and Tregs (44). The small molecule CA-170 which binds both VISTA and PD-1 has been evaluated in phase I trials with patients with advanced solid tumors, lymphomas and mesotheliomas (45, 46). Phase I trials with anti-VISTA monoclonal antibody is also currently underway.

Neuropilin-1 (NRP1) is another inhibitory receptor under investigation for its clinical potential (47). NRP1 may play a role in T cell dysfunction and is highly expressed on PD1+ intratumoral CD8+ T cells. Murine melanoma models exhibited decreased tumor growth with treatment of

TABLE 1 | Summary of inhibitory receptors in clinical trials.

Receptor	Binding Partners	Therapies under development	Clinical trials
LAG3	MHC II	IMP321 Relatlimab LAG525 TSR-033 REGN3767 MK-4280	IMP321: Vaccine adjuvant With gemcitabine for pancreatic cancer With paclitaxel in breast cancer With pembrolizumab in HNSCC Relatlimab: With nivolumab in melanoma LAG525: With Spartalizumab in advanced solid tumors
TIM-3	Galectin-9 Ceacam1 HMGB1 Phosphatidylserine	MGB453 TSR-022 Sym023 BGBA425 RO7121661 ICAGN02390 LY3321367 BMS-986258	LY3321367: With and without anti-PD-L1 in advanced solid tumors MBG453: With spartalizumab in NSCLC and melanoma
TIGIT	CD155 CD112	BMS-986207 BGB-A1217 Tiragolumab AB154 ASP8374 MK-7684 COM701 LY3435151	Tiragolumab: With atezolizumab in NSCLC With atezolizumab in advanced solid tumors
VISTA	Unknown	JNJ-61610588 (CI-8993) CA-170 W0180	CA170: In advanced solid tumors and lymphoma In mesothelioma
NRP-1	Class 3 Semaphorins Growth factors (VEGF, TGF, HPF and others)	MNRP1685A ASP1948 CEND1	MNRP1685A: with bevacizumab, with or without paclitaxel in advanced solid tumors CEND1: with gemcitabine and nab-paclitaxel in pancreatic cancer

combination anti-PD-1 and anti-Nrp-1 (48). Early phase clinical trials with two anti-NRP1 agents were published, but do not appear to have been pursued further, in part due to toxicity (49, 50). An anti-NRP1 monoclonal antibody is currently under clinical development in a Phase 1b trial.

Co-Stimulatory Receptors

Another strategy has been to target co-stimulatory receptors with monoclonal antibodies that behave as receptor agonists, with or without anti-PD-1 blockade. These receptors include OX40, CD27, 4-1BB, and GITR. Co-stimulatory receptors are present on T cells and counter-act the negative regulation of inhibitory receptors such as PD-1 and CTLA-4 (51). Phase I studies of anti-OX40 agonists have yielded disappointing results, with a single partial response noted in the trial of MEDI0562 in advanced solid tumors, and best response of stable disease with GSK998 (52, 53). When combined with pembrolizumab in a trial enrolling 96 patients, anti-OX40, gave 2 CRs and 7PRs (53). 4-1BB targeted therapy was complicated by hepatic toxicity that was mitigated at lower doses (54). However, efficacy of monotherapy and combination treatment with anti-PD-1 was not particularly impressive (55). Several companies have dropped their pursuit of co-stimulatory monoclonal antibodies, such as OX40 from their pipelines.

DAMAGE- OR PATHOGEN-ASSOCIATED MOLECULAR PATTERNS

Pattern recognition receptors (PRRs) were identified as part of the innate immune system as a first line defense to pathogens. These receptors can recognize pathogen-associated molecular patterns (PAMPs) and include a family of receptors called toll-like receptors (TLRs). Additional receptors have been identified to recognize damage-associated molecular patterns (DAMPs). TLRs are present on both immune and non-immune cell types. Presence of a PAMP/DAMP leads to TLR activation, and downstream activation of transcription factors that result in the production of interferons, and interferon-stimulated responses. In addition to triggering the production of inflammatory cytokines and chemokines, the IFN response is also important for antigen presentation and the priming of an adaptive immune response. Interferon triggers maturation of antigen-presenting cells, leading to presentation of proteins in the context of MHC. This ultimately leads to the induction of specific T and B cell responses. Preclinical work with tumor cell lines and murine models however, have also shown data suggesting TLR stimulation can lead to tumor proliferation (56, 57). Whether the anti-tumor effects of TLR-stimulation can be specifically harnessed is a work in progress.

Although the mechanisms were not known at the time, TLR-agonists were used in early cancer therapy by William Coley (58). In his historic experiments, patients with cancer were injected with lipopolysaccharide (LPS)-containing bacterial concoctions, and tumor regression was occasionally noted. Unsurprisingly, these patients also developed high fevers and other intolerable side effects. LPS was ultimately identified in these bacterial cocktails as the active agent. Since that time many strategies to utilize PRRs in cancer therapy have been exploited as described below and summarized in **Table 2**.

TABLE 2 | Toll-like receptor (TLR) agonists under investigation.

Receptor	PAMP	Therapies under development	Clinical trials
TLR3	polyinosinic:polycytidylic acid (poly(I:C))	Rintatolimod	Rintatolimod: with IFN for melanoma, colorectal cancer, prostate cancer
		ARNAX	With pembrolizumab and cisplatin for ovarian cancer
			With IFN and neoadjuvant chemotherapy for breast cancer
TLR4	Lipopolysaccharide	MPLA	GLA-SE: Vaccine adjuvant
		GLA-SE	GSK1795091: With immunotherapy in advanced solid tumors
		GSK1795091	
TLR7	Single-stranded RNA	Imiquimods	Imiquimod: With tumor lysate vaccine in grade II gliomas
TLR8		Resiquimod	With dendritic cell vaccine in malignant gliomas
		Motolimod	With dendritic cell and GM-CSF vaccine in ovarian cancer
			Resiquimod: Vaccine adjuvant
			Motolimod: With nivolumab in HNSCC
			With doxorubicin and durvalumab in ovarian cancer
TLR9	Double-stranded DNA	Lefitolimod	Lefitolimod: With ipilimumab in advanced solid tumors
		SD-101	SD-101: With anti-Ox40 for NHL
		CMP-001	With ibrutinib and radiation for follicular lymphoma
		Tilsotolimod	With nivolumab and radiation for pancreatic cancer
			With pembrolizumab in prostate cancer
			With pembrolizumab in breast cancer
			CMP-001: With pembrolizumab in HNSCC
			With Pembrolizumab in melanoma
			With nivolumab, ipilimumab and radiation in colorectal cancer
			With immunotherapies in advanced solid tumors

Toll-Like Receptor Agonists

Toll-Like Receptors That Bind Nucleic Acids

TLRs recognizing nucleic acids have been under investigation and promising for some time as therapeutic agents for cancer. These include TLR3, TLR7, TLR8, and TLR9. TLR3 recognizes dsRNA, and a common synthetic nucleic acid used for stimulation is polyinosinic:polycytidylic acid (poly(I:C)). Early studies had issues with toxicity and stability and were discontinued (59). Further, phase I studies with poly(I:C) monotherapy appeared to have little clinical efficacy (60). Since that time, several compounds modified to enhance stability have been produced and are being studied in various malignancies in combination with immunotherapy and as adjuvants in vaccine-based strategies (61). Early phase clinical trials are ongoing with the formulations rintatolimod and ARNAX.

TLR7 and TLR8 recognize single-stranded RNA. Stimulation results in activation of MyD88, and secretion of cytokines, including type I interferons. The synthetic imidazoquinolones have been tested as antiviral treatments, and now derivatives are being explored as cancer therapeutics. Imiquimod is compound used topically to treat several skin conditions, including basal cell carcinomas and is being explored in pre-cancerous lesions, such as cervical intraepithelial neoplasia. Imiquimod has also been used in early phase clinical trials for treatment of cutaneous metastases for breast cancer and melanoma, however has not been pursued further (62, 63). Imiquimods have been explored as an adjuvant cancer vaccines and is being used in a variety of these trials (NCT01678352, NCT00799110, NCT01792505) (64). Resiquimod binds both TLR7 and TLR8 and is similarly being explored as an adjuvant in cancer vaccines (65). Motolimod (VTX-2337) is another imidazoquinolone with preclinical evidence supporting activation of NK cells and priming of CD8+ T cells when given with cetuximab (66, 67). A phase 1b clinical trial of motolimod and cetuximab in patients with head and neck squamous cell carcinoma resulted in demonstration of maximum tolerated dose with 2/13 patients achieving partial responses (68). Studies are ongoing with motolimod in combination with anti-PD1 for patients with head and neck cancer (NCT03906526), as well as with doxorubicin and durvalumab in patients with ovarian cancer (NCT02431559).

TLR9 recognizes double-stranded DNA, typically in the form of unmethylated cytidine phosphate guanosine (CpG) oligonucleotides (ODN) present in pathogens. Several synthetic CpG-ODNs have been investigated for cancer therapy, including in combination with chemotherapy, immunotherapy or as vaccine adjuvants. Lefitolimod (MGN1703) is a DNA molecule tested in a phase I dose escalation with ipilimumab, with planned dose escalation (NCT02668770) (69). SD-101 is another CpG-ODN that has been tested intratumorally in combination with pembrolizumab in a phase 1b clinical trial with an ORR of 15% (70). A number of trials are ongoing evaluating SD-101 in hematologic malignancies, as well as in pancreatic cancer (NCT04050085) and prostate cancer (NCT03007732). CMP-001 is a CpG-A virus-like particle that stimulates TLR9. Intratumoral CMP-001 with pembrolizumab has been shown in a Phase 1b trial demonstrating 24% ORR in melanoma patients who have previously progressed on anti-PD-1 therapy (71). Additional trials are evaluating CMP-001 by subcutaneous administration (NCT03084640), in the neoadjuvant setting (NCT04401995), and in other solid tumors and hematologic malignancies. Tilsotolimod (IMO-2125) is another TLR9 agonist being investigated in combination with nivolumab and ipilimumab for patients with solid tumors (NCT03865082), with preliminary data from a phase 1/2 trial only available by press release thus far.

Toll-Like Receptors That Recognize Other Bacterial Products

Additional TLRs target bacterial components. TLR1,2,6, and 4 bind bacterial cell wall products and TLR5 binds flagellin. TLR2 is found on the cell surface and forms a heterodimer with either TLR1 or TLR6 that recognized lipoproteins (72). Although there are several synthetic lipoproteins targeting these receptors being explored in autoimmunity or as adjuvants in therapy of viral infection, none are actively explored in malignancies. BCG is used to treat non-muscle-invasive bladder cancers, and may work in part by inducing inflammation through TLR2 and TLR4 (73). TLR4 agonists have been explored extensively since Coley's initial observations. An LPS derivative of Salmonella, monophosphoryl lipid A (MPLA) is a TLR4 agonist that is currently used as an adjuvant in the Cervarix HPV vaccine (74). A dose escalation studies of lipid A formulations as monotherapy for were tolerated at lower doses, but did not demonstrate anti-tumor responses as monotherapy (75, 76). TLR4 agonists such as GLA-SE have been used as adjuvants in vaccines directed at malignancies or infectious agents, but are not actively being developed in oncologic trials (77). Currently, GSK1795091 synthetic agonist was tested in healthy volunteers, and a planned trial in combination with immunotherapy in advanced solid tumors is planned (NCT03447314) (78). TLR5 binds flagella, and has been targeted by Mobilan, an adenoviral vector expressing flagellin. Mobilan has been tested in a phase I trial with intratumoral injection for prostate cancer, though has not been pursued further (79).

Additional Pathogen Recognition Receptors

Additional PRRs have been identified since the initial discovery of TLRs and include RIG-I like receptors (RLRs), NOD-like receptors (NLRs) and C-type lectin receptors (CLRs). The work on these receptors has not been as well-developed as for the TLRs, but are now being explored in cancer immunity. RLRs include two receptors, retinoic acid-inducible gene I protein (RIG-I) and melanoma differentiation associated protein 5 (MDA5) that bind viral RNA molecules. Downstream signaling results in interferon secretion. The RIG-I agonist, MK4621, was tested in a phase I/II trial for advanced solid tumors without dose-limiting toxicities observed (80) and is planned for study in combination with pembrolizumab (NCT03739138). NLRs recognize bacterial products and lead to activation of the inflammasome and IL-1β production. NLR activation may contribute to carcinogenesis, and is being explored for potential therapeutic targets (81, 82). CLRs are a large group of PRRs that bind a wide variety of ligands and can result in pro-inflammatory and anti-inflammatory responses, and are trying to be understood (83). STING is an additional nucleic acid PRR located in the endoplasmic reticulum (84). Many early phase clinical trials are underway with STING agonists as monotherapy, in combination with immunotherapy, chemotherapy, or radiation (85).

IMMUNE SIGNALING MEDIATORS

Cytokines

Cytokines in the TME are produced by infiltrating tumor and stromal cells, and can contribute to either a pro-inflammatory or anti-inflammatory milieu (86). Cytokine therapy has FDA approved indications with IL-2 for renal cell carcinoma and melanoma, and type I interferon for adjuvant therapy of melanoma, and in CML and MPNs. While these therapies are used infrequently in melanoma in favor of current ICI immunotherapy, a small number of patients do well, and may have been cured with IL-2 in metastatic RCC (87). GM-CSF has also been investigated for its potential benefits in cancer therapy. The GM-CSF modality is currently an underlying basis of the benefits of talimogene laherparepvec, an FDA-approved oncolytic immunotherapy for melanoma (88). The body of literature discussing the many functions of cytokines in cancer therapy is vast, and this review will focus on those therapies currently under development.

Toxicity has been a significant issue with cytokine administration in clinical trials and standard therapies, as evidenced by the experience with IL-12. Preclinical data demonstrated the anti-tumor effects of IL-12 by multiple mechanisms and in several murine tumor models (89). However, although a dose was selected in phase I trials to minimize toxicity, the phase II study was halted after significant toxicity and 2 patient deaths (90, 91). The additional toxicities seen in the phase II trial were thought to be a result of a change in the dosing schedule, when a priming initial dose was no longer given. Interest in IL-12 persists, with formulations such as NHS-IL12, an IL12 heterodimer fused to an antibody, tested in a phase I trial (92). A number of ongoing trials with this compound are ongoing, as monotherapy and in combination with immunotherapy. Additional studies use IL-12 expressing viral or CART constructs.

IL-15 shares part of the IL-2 receptor and signaling pathway, and similarly results in NK and T cell proliferation (93). Unlike IL-2, however, IL-15 is not thought to stimulate T regulatory cells, making it an attractive target. Recombinant IL-15 (rhIL15) has been studied in patients with advanced solid tumors in a phase I study, notable for increased NK and CD8 + T cell proliferation seen in the peripheral blood (94). Subcutaneous rhIL15 along with haploidentical NK cell infusion was used to treat patients with acute myeloid leukemia, demonstrating NK cell proliferation and 40% remission rates, though cytokine release syndrome was noted in 56% of these patients (95). ALT-803 is a IL-15/IL-15Ra Fc fusion complex, referred to a superagonist, that has been tested in PD-1 refractory NSCLC patients evaluated in phase Ib study, with additional studies ongoing (96). Other formulations of IL-15 have been developed and are undergoing clinical trials, including recombinant proteins BJ-001, PF-07209960, NIZ985, and N-803. Additional combinations of IL-15 products are being conducted with immunotherapy, and as part of adoptive cell therapy products.

Interferon-γ is a type III interferon potently induced by IL-12, whose expression is associated with immunotherapy response in

melanoma (8). However, IFNγ has been associated with both anti-tumor and pro-tumor effects (97). Clinical trials with IFNγ as monotherapy have not been fruitful, perhaps due to its seemingly contradictory role in the TME. Other cytokines initially pursued and since abandoned for toxicity and lack of efficacy include IL-21 and IL-7 (98).

Small Molecule Inhibitors

In addition to traditional cytokines and chemokines, the TME also contains a number of small molecules that effect the inflammatory state of the tumor. Indoleamine 2,3-dioxygenase 1 (IDO1) helps convert tryptophan to kynurenine, which has an immunosuppressive effect on the TME. Kynurenine promotes development of Tregs and MDSCs (99). Epacadostat is an IDO1 inhibitor that has been studied in combination with pembrolizumab. Although the initial phase I/II trial in advanced solid tumors showed promise, the phase III trial in melanoma did not show a difference in progression-free survival or overall survival versus placebo with pembrolizumab (100, 101). Many of the ongoing trials of IDO1 inhibitors have since been terminated, though a few trials with IDO1 inhibitor BMS-986205 are still recruiting.

The phosphoinositide 3-kinase (PI3K) signaling pathway functions at many stages of cancer biology including cell division, differentiation, motility and metabolism (102). Inhibitors downstream of the PI3K pathway are active in some solid tumors, including everolimus in neuroendocrine tumors (103) and everolimus with exemestane in breast cancer (104). Targeting the PI3K isoforms γ and δ, that are specifically expressed in hematopoietic cells, is an area of investigation supported by preclinical work showing alterations in the TME to a pro-inflammatory phenotype (105). PI3Kγ and γ/δ inhibition are being studied in clinical trials.

CONCLUDING REMARKS

The strategies discussed in this review highlight a number of promising approaches for overcoming immunotherapy resistance, a significant treatment dilemma for patients with advanced melanoma. These therapies all aim to increase local inflammation in the TME but by drastically different mechanisms, with varying routes of administration and toxicities. Of these, use of DAMPs/PAMPs are of particular promise, and early phase trials have shown intratumoral and administration with anti-PD-1 to be tolerable with early signs of efficacy. Development of intravenous formulations or formulations compounded with anti-PD-1 monoclonal antibodies could be an interesting avenue to explore. We look forward to more data in this field and with other tumor types.

One major challenge in the development and testing of novel immunotherapeutics is the heterogeneity of mechanisms of resistance. Patients have varying expression of inhibitory receptors after immunotherapy, differing levels and types of immune infiltrates, and differences in mutational profiles and epigenetic changes that can all alter response to immunotherapy (106). This heterogeneity may also contribute to the limited efficacy observed in some trials. However, without definitive biomarkers to reliably sort patients by mechanism, this truly personalized approach remains currently out of reach. While some biomarkers are certainly helpful, such as TMB and PD-L1 expression, even these do not always correlate with response (107).

Ongoing efforts to identify biomarkers are underway, including with gene-expression profiling, such as those signatures associated with IFNγ (8, 108). Until robust biomarkers are identified and then correlated with response to specific therapies, an all-comers approach must be utilized. After validation of a biomarker-based treatment approach, these therapies could also be explored in the front-line setting, perhaps identifying those at risk for primary resistance to immunotherapy, and ultimately leading to greater portion of those with durable responses. Cost-benefit analysis would also be an important factor in the design of a biomarker-driven, personalized medicine approach to avoid contributing to the already egregious cost of oncologic care that may benefit a small portion of patients.

The strategies discussed in this review are only a part of the approach being considered for overcoming immunotherapy resistance, and a number of other promising strategies that are under development. These include vaccine development with tumor-associated antigens, in part with the adjuvants mentioned here. Other strategies that may in the near future gain regulatory approval include adoptive cell transfer, both with the use of TILs and perhaps with CAR-T therapies. Finally, targeting other elements of the TME that are a more fundamental basis of immunotherapy resistance, such as myeloid derived suppressor cells and T regulatory cells are also under development. There is much reason for excitement given the breadth and pace of development of immunonotherapeutics and forthcoming results in the next several years will dictate the future of the field.

AUTHOR CONTRIBUTIONS

AR contributed to the design, concept, research, writing, and critical review of this review. JK contributed to the design, concept, critical review, and supervision of this review. All authors contributed to the article and approved the submitted version.

FUNDING

The work of the authors is supported by the NIH National Cancer Institute SPORE in Skin CAncer grant P50 CA-121973.

REFERENCES

1. Larkin J, Chiarion-Sileni V, Gonzalez R, Grob JJ, Cowey CL, Lao CD, et al. Combined nivolumab and ipilimumab or monotherapy in untreated Melanoma. *N Engl J Med* (2015) 373:23–34. doi: 10.1056/NEJMc1509660
2. Tang J, Yu JX, Hubbard-Lucey VM, Neftelinov ST, Hodge JP, Lin Y. The clinical trial landscape for PD1 / PD-L1 immune checkpoint inhibitors. *Nat Rev Drug Discov* (2018) 17:854–55. doi: 10.1038/nrd.2018.210
3. Kluger HM, Zito CR, Barr ML, Baine MK, Chiang VLS, Sznol M, et al. Characterization of PD-L1 expression and associated T-cell infiltrates in metastatic melanoma samples from variable anatomic sites. *Clin Cancer Res* (2015) 21:3052–60. doi: 10.1158/1078-0432.CCR-14-3073
4. Jenkins RW, Barbie DA, Flaherty KT. Mechanisms of resistance to immune checkpoint inhibitors. *Br J Cancer* (2018) 118:9–16. doi: 10.1038/bjc.2017.434
5. Kim TK, Herbst RS, Chen L. De fi ning and Understanding Adaptive Resistance in Cancer Immunotherapy. *Trends Immunol* (2018) 39:624–31. doi: 10.1016/j.it.2018.05.001
6. Pitt JM, Vétizou M, Daillère R, Roberti MP, Yamazaki T, Routy B. Tumor-Intrinsic and -Extrinsic Factors. *Cancer* (2016) 28:1255–69. doi: 10.1016/j.immuni.2016.06.001
7. Havel JJ, Chowell D, Chan TA. The evolving landscape of biomarkers for checkpoint inhibitor immunotherapy. *Nat Rev Cancer* (2019) 19:133–50. doi: 10.1038/s41568-019-0116-x
8. Ayers M, Lunceford J, Nebozhyn M, Murphy E, Loboda A, Kaufman DR, et al. IFN-γ-related mRNA profile predicts clinical response to PD-1 blockade. *J Clin Invest* (2017) 127:2930–40. doi: 10.1172/JCI91190
9. Hodi FS, Chiarion-Sileni V, Gonzalez R, Grob JJ, Rutkowski P, Cowey CL, et al. Nivolumab plus ipilimumab or nivolumab alone versus ipilimumab alone in advanced melanoma (CheckMate 067): 4-year outcomes of a multicentre, randomised, phase 3 trial. *Lancet Oncol* (2018) 19:1480–92. doi: 10.1016/S1470-2045(18)30700-9
10. Workman CJ, Rice DS, Dugger KJ, Kurschner C, Vignali DAA. Phenotypic analysis of the murine CD4-related glycoprotein, CD223 (LAG-3). *Eur J Immunol* (2002) 32:2255–63. doi: 10.1002/1521-4141(200208)32:8<2255::AID-IMMU2255>3.0.CO;2-A
11. Huard B, Mastrangeli R, Prigent P, Bruniquel D, Donini S, El-Tayar N, et al. Characterization of the major histocompatibility complex class II binding site on LAG-3 protein. *Proc Natl Acad Sci U S A* (1997) 94:5744–9. doi: 10.1073/pnas.94.11.5744
12. Wherry EJ, Ha SJ, Kaech SM, Haining WN, Sarkar S, Kalia V, et al. Molecular Signature of CD8+ T Cell Exhaustion during Chronic Viral Infection. *Immunity* (2007) 27:670–84. doi: 10.1016/j.immuni.2007.09.006
13. Li N, Wang Y, Forbes K, Vignali KM, Heale BS, Saftig P, et al. Metalloproteases regulate T-cell proliferation and effector function via LAG-3. *EMBO J* (2007) 26:494–504. doi: 10.1038/sj.emboj.7601520
14. Huard B, Tournier M, Hercend T, Triebel F, Faure F. Lymphocyte-activation gene 3/major histocompatibility complex class II interaction modulates the antigenic response of CD4+ T lymphocytes. *Eur J Immunol* (1994) 24:3216–21. doi: 10.1002/eji.1830241246
15. Workman CJ, Cauley LS, Kim I-J, Blackman MA, Woodland DL, Vignali DAA, et al. Lymphocyte Activation Gene-3 (CD223) Regulates the Size of the Expanding T Cell Population Following Antigen Activation In Vivo. *J Immunol* (2004) 172:5450–5. doi: 10.4049/jimmunol.172.9.5450
16. Huang CT, Workman CJ, Flies D, Pan X, Marson AL, Zhou G, et al. Role of LAG-3 in regulatory T cells. *Immunity* (2004) 21:503–13. doi: 10.1016/j.immuni.2004.08.010
17. Durham NM, Nirschl CJ, Jackson CM, Elias J, Kochel CM, Anders RA, et al. Lymphocyte activation gene 3 (LAG-3) modulates the ability of CD4 T-cells to be suppressed In Vivo. *PloS One* (2014) 9:1–13. doi: 10.1371/journal.pone.0109080
18. Andrews LP, Marciscano AE, Drake CG, Vignali DAA. LAG3 (CD223) as a cancer immunotherapy target. *Immunol Rev* (2017) 276:80–96. doi: 10.1111/imr.12519
19. Legat A, Maby-El Hajjami H, Baumgaertner P, Cagnon L, Maillard SA, Geldhof C, et al. Vaccination with LAG-3Ig (IMP321) and peptides induces specific CD4 and CD8 T-cell responses in metastatic melanoma patients-report of a phase I/IIa clinical trial. *Clin Cancer Res* (2016) 22:1330–40. doi: 10.1158/1078-0432.CCR-15-1212
20. Wang-Gillam A. A phase i study of IMP321 and gemcitabine as the front-line therapy in patients with advanced pancreatic adenocarcinoma. *Invest New Drugs* (2013) 31:707–13. doi: 10.1007/s10637-012-9866-y
21. Brignone C, Gutierrez M, Mefti F, Brain E, Jarcau R, Cvitkovic F, et al. First-line chemoimmunotherapy in metastatic breast carcinoma: Combination of paclitaxel and IMP321 (LAG-3Ig) enhances immune responses and antitumor activity. *J Transl Med* (2010) 8:1–11. doi: 10.1186/1479-5876-8-71
22. Felip E, Doger B, Majem M, Carcereny E, Krebs M, Peguero JA, et al. Initial results from a phase II study (TACTI-002) in metastatic non-small cell lung or head and neck carcinoma patients receiving eftilagimod alpha (soluble LAG-3 protein) and pembrolizumab. *J Clin Oncol* (2020) 38:3100. doi: 10.1200/JCO.2020.38.15_suppl.3100
23. Ascierto PA, Bono P, Bhatia S, Melero I, Nyakas MS, Svane I-M, et al. Efficacy of BMS-986016, a monoclonal antibody that targets lymphocyte activation gene-3 (LAG-3), in combination with nivolumab in pts with melanoma who progressed during prior anti–PD-1/PD-L1 therapy (mel prior IO) in all-comer and biomarker-enriched popu. *Ann Oncol* (2017) 28:v611–2. doi: 10.1093/annonc/mdx440.011
24. Hong DS, Schoffski P, Calvo A, Sarantopoulos J, Ochoa De Olza M, Carvajal RD, et al. Phase I/II study of LAG525 ± spartalizumab (PDR001) in patients (pts) with advanced malignancies. *J Clin Oncol* (2018) 36:3012. doi: 10.1200/JCO.2018.36.15_suppl.3012
25. Monney L, Sabatos CA, Gaglia JL, Ryu A, Waldner H, Chernova T, et al. Th1-specific cell surface protein Tim-3 regulates macrophage activation and severity of an autoimmune disease. *Nature* (2002) 415:536–41. doi: 10.1038/415536a
26. Zhu C, Anderson AC, Schubart A, Xiong H, Imitola J, Khoury SJ, et al. The Tim-3 ligand galectin-9 negatively regulates T helper type 1 immunity. *Nat Immunol* (2005) 6:1245–52. doi: 10.1038/ni1271
27. Das M, Zhu C, Kuchroo VK. Tim-3 and its role in regulating anti-tumor immunity. *Immunol Rev* (2017) 276:97–111. doi: 10.1111/imr.12520
28. Fourcade J, Sun Z, Benallaoua M, Guillaume P, Luescher IF, Sander C, et al. Upregulation of Tim-3 and PD-1 expression is associated with tumor antigen-specific CD8+ T cell dysfunction in melanoma patients. *J Exp Med* (2010) 207:2175–86. doi: 10.1084/jem.20100637
29. Koguchi K, Anderson DE, Yang L, O'Connor KC, Kuchroo VK, Hafler DA. Dysregulated T cell expression of TIM3 in multiple sclerosis. *J Exp Med* (2006) 203:1413–8. doi: 10.1084/jem.20060210
30. Sakuishi K, Ngiow SF, Sullivan JM, Teng MWL, Kuchroo VK, Smyth MJ, et al. TIM3+FOXP3+ regulatory T cells are tissue-specific promoters of T-cell dysfunction in cancer. *Oncoimmunology* (2013) 2. doi: 10.4161/onci.23849
31. Dardalhon V, Anderson AC, Karman J, Apetoh L, Chandwaskar R, Lee DH, et al. Tim-3/Galectin-9 Pathway: Regulation of Th1 Immunity through Promotion of CD11b + Ly-6G + Myeloid Cells. *J Immunol* (2010) 185:1383–92. doi: 10.4049/jimmunol.0903275
32. Jones RB, Ndhlovu LC, Barbour JD, Sheth PM, Jha AR, Long BR, et al. Tim-3 expression defines a novel population of dysfunctional T cells with highly elevated frequencies in progressive HIV-1 infection. *J Exp Med* (2008) 205:2763–79. doi: 10.1084/jem.20081398
33. Acharya N, Acharya N, Sabatos-Peyton C, Anderson AC, Anderson AC. Tim-3 finds its place in the cancer immunotherapy landscape. *J Immunother Cancer* (2020) 8:1–11. doi: 10.1136/jitc-2020-000911
34. Harding JJ, Patnaik A, Moreno V, Stein M, Jankowska AM, Velez de Mendizabal N, et al. A phase Ia/Ib study of an anti-TIM-3 antibody (LY3321367) monotherapy or in combination with an anti-PD-L1 antibody (LY3300054): Interim safety, efficacy, and pharmacokinetic findings in advanced cancers. *J Clin Oncol* (2019) 37:12. doi: 10.1200/JCO.2019.37.8_suppl.12
35. Mach N, Curigliano G, Santoro A, Kim D-W, Tai DWM, Hodi S, et al. Phase (Ph) II study of MBG453 + spartalizumab in patients (pts) with non-small cell lung cancer (NSCLC) and melanoma pretreated with anti–PD-1/L1 therapy. *Ann Oncol* (2019) 30:v491–2. doi: 10.1093/annonc/mdz253.028
36. Chauvin JM, Zarour HM. TIGIT in cancer immunotherapy. *J Immunother Cancer* (2020) 8:1–7. doi: 10.1136/jitc-2020-000957

37. Bottino C, Castriconi R, Pende D, Rivera P, Nanni M, Carnemolla B, et al. Identification of PVR (CD155) and Nectin-2 (CD112) as cell surface ligands for the human DNAM-1 (CD226) activating molecule. *J Exp Med* (2003) 198:557–67. doi: 10.1084/jem.20030788
38. Johnston RJ, Comps-Agrar L, Hackney J, Yu X, Huseni M, Yang Y, et al. The Immunoreceptor TIGIT Regulates Antitumor and Antiviral CD8+ T Cell Effector Function. *Cancer Cell* (2014) 26:923–37. doi: 10.1016/j.ccell.2014.10.018
39. Chauvin J-M, Ka M, Pagliano O, Menna C, Ding Q, DeBlasio R, et al. IL15 Stimulation with TIGIT Blockade Reverses CD155-mediated NK-Cell Dysfunction in Melanoma. *Clin Cancer Res* (2020) 26:5520–33. doi: 10.1158/1078-0432.CCR-20-0575
40. Rodriguez-Abreu D, Johnson ML, Hussein MA, Cobo M, Patel AJ, Secen NM, et al. Primary analysis of a randomized, double-blind, phase II study of the anti-TIGIT antibody tiragolumab (tira) plus atezolizumab (atezo) versus placebo plus atezo as first-line (1L) treatment in patients with PD-L1-selected NSCLC (CITYSCAPE). *J Clin Oncol* (2020) 38:9503. doi: 10.1200/JCO.2020.38.15_suppl.9503
41. Bendell JC, Bedard P, Bang Y-J, LoRusso P, Hodi S, Gordon M, et al. CT302 - Phase Ia / Ib dose-escalation study of the anti-TIGIT antibody tiragolumab as a single agent and in combination with atezolizumab in patients with advanced solid tumors. *Cancer Res* (2020) 80:CT302–CT302. doi: 10.1158/1538-7445. AM2020-CT302
42. Nowak EC, Lines JL, Varn FS, Deng J, Sarde A, Mabaera R, et al. Immunoregulatory functions of VISTA. *Immunol Rev* (2017) 276:66–79. doi: 10.1111/imr.12525
43. Wang L, Rubinstein P, Lines JL, Wasiuk A, Ahonen C, Guo Y, et al. VISTA, a novel mouse Ig superfamily ligand that negatively regulates T cell responses. *J Exp Med* (2011) 208:577–92. doi: 10.1084/jem.20100619
44. Mercier I, Chen W, Lines JL, Day M, Li J, Sergent P, et al. VISTA Regulates the Development of Protective Antitumor Immunity. *Cancer Res* (2014) 74:1933–45. doi: 10.1158/0008-5472.CAN-13-1506
45. Zauderer M, Brody J, Marron T, Pacey S, Martell R, Wang H, et al. First-in-class small molecule CA-170 targeting VISTA: a report on efficacy outcomes from a cohort of 12 malignant pleural mesothelioma (MPM) patients in study CA170-101. *J Immunother Cancer* (2019) 7:283. doi: 10.1186/s40425-019-0764-0
46. Bang Y-L, Sosman JA, Daud A, Meric-Bernstam F, Garcia-Corbacho J, Patel MR, et al. Phase 1 study of CA-170, a first-in-class, orally available, small molecule immune checkpoint inhibitor (ICI) dually targeting VISTA and PD-L1, in patients with advanced solid tumors or lymphomas. in P341. (2018) 6:175. doi: 10.1186/s40425-018-0422-y
47. Chuckran CA, Liu C, Bruno TC, Workman CJ, Vignali DAA. Neuropilin-1: a checkpoint target with unique implications for cancer immunology and immunotherapy. *J Immunother Cancer* (2020) 8:1–12. doi: 10.1136/jitc-2020-000967
48. Leclerc M, Voilin E, Gros G, Corgnac S, de Montpréville V, Validire P, et al. Regulation of antitumour CD8 T-cell immunity and checkpoint blockade immunotherapy by Neuropilin-1. *Nat Commun* (2019) 10:1–14. doi: 10.1038/s41467-019-11280-z
49. Weekes CD, LoRusso P, Ramakrishnan V, Shih LM, Darbonne WC, Hegde P, et al. A phase Ib study for MNRP1685A (anti-NRP1) administered intravenously with bevacizumab with or without paclitaxel to patients with advanced solid tumors. *J Clin Oncol* (2011) 29:3050. doi: 10.1200/jco.2011.29.15_suppl.3050
50. Dean A, Gill S, McGregor M, Broadbridge V, Jarvelainen HA, Price TJ. 1528P Phase I trial of the first-in-class agent CEND-1 in combination with gemcitabine and nab-paclitaxel in patients with metastatic pancreatic cancer. *Ann Oncol* (2020) 31:S941. doi: 10.1016/j.annonc.2020.08.2011
51. Krummel BMF, Allison JR. CD28 and CTLA-4 have opposing effects on the response of T cells to stimulation. *J Exp Med* (1995) 182:459–65. doi: 10.1084/jem.182.2.459
52. Glisson B, Leidner R, Ferris RL, Powderly J, Rizvi NA, Keam B, et al. Safety and clinical activity of MEDI0562, a humanized OX40 agonist monoclonal antibody, in adult patients with advanced solid tumors. *Ann Oncol* (2018) 29:viii410. doi: 10.1093/annonc/mdy288.025
53. Postel-Vinay S, Lam VK, Ros W, Bauer TM, Hansen AR, Cho DC, et al. Abstract CT150: A first-in-human phase I study of the OX40 agonist GSK3174998 (GSK998) +/- pembrolizumab in patients (Pts) with selected advanced solid tumors (ENGAGE-1). *Tumor Biol* (2020) 3174998:CT150–0. doi: 10.1158/1538-7445.AM2020-CT150
54. Segal NH, He AR, Doi T, Levy TM, Bhatia S, Pishvaian MJ, et al. Phase i study of single-agent utomilumab (PF-05082566), a 4-1bb/cd137 agonist, in patients with advanced cancer. *Clin Cancer Res* (2018) 24:1816–23. doi: 10.1158/1078-0432.CCR-17-1922
55. Massarelli E. Clinical safety and efficacy as- sessment of the CD137 agonist urelumab alone and in combination with nivolumab in patients with hematologic and solid tumor malignancies. In: *Proceeding of the 31st Annual Meeting and Associated Programs of the Society for Immunotherapy of Cancer* (2016) 4:5. Available at: https://jitc.biomedcentral.com/articles/10.1186/s40425-016-0172-7
56. Pinto A, Morello S, Sorrentino R. Lung cancer and toll-like receptors. *Cancer Immunol Immunother* (2011) 60:1211–20. doi: 10.1007/s00262-011-1057-8
57. Rakoff-nahoum S, Medzhitov R. Toll-like receptors and cancer. *Nat Rev Cancer* (2009) 9:57–63. doi: 10.1038/nrc2541
58. Birbriar A. Tumor Microenvironment. In: *Tumor Microenvironment* DW Siemann (ed.). Chichester, UK: John Wiley and Sons, Ltd (2010). doi: 10.1002/9780470669891
59. Vanpouille-Box C, Hoffmann JA, Galluzzi L. Pharmacological modulation of nucleic acid sensors — therapeutic potential and persisting obstacles. *Nat Rev Drug Discovery* (2019) 18:845–67. doi: 10.1038/s41573-019-0043-2
60. Stevenson HC, Abrams PG, Schoenberger CS, Smalley RB, Herberman RB, Foon KA. A phase I evaluation of poly(I,C)-LC in cancer patients. *J Biol Response Mod* (1985) 4:650–5.
61. Takeda Y, Kataoka K, Yamagishi J, Ogawa S, Seya T, Matsumoto M. A TLR3-Specific Adjuvant Relieves Innate Resistance to PD-L1 Blockade without Cytokine Toxicity in Tumor Vaccine Immunotherapy. *Cell Rep* (2017) 19:1874–87. doi: 10.1016/j.celrep.2017.05.015
62. Green DS, Bodman-Smith MD, Dalgleish AG, Fischer MD. Phase I/II study of topical imiquimod and intralesional interleukin-2 in the treatment of accessible metastases in malignant melanoma. *Br J Dermatol* (2007) 156:337–45. doi: 10.1111/j.1365-2133.2006.07664.x
63. Adams S, Kozhaya L, Martiniuk F, Meng TC, Chiriboga L, Liebes L, et al. Topical TLR7 agonist imiquimod can induce immune-mediated rejection of skin metastases in patients with breast cancer. *Clin Cancer Res* (2012) 18:6748–57. doi: 10.1158/1078-0432.CCR-12-1149
64. Adams S, O'Neill DW, Nonaka D, Hardin E, Chiriboga L, Siu K, et al. Immunization of Malignant Melanoma Patients with Full-Length NY-ESO-1 Protein Using TLR7 Agonist Imiquimod as Vaccine Adjuvant. *J Immunol* (2008) 181:776–84. doi: 10.4049/jimmunol.181.1.776
65. Sabado RL, Pavlick A, Gnjatic S, Cruz CM, Vengco I, Hasan F, et al. Resiquimod as an immunologic adjuvant for NY-ESO-1 protein vaccination in patients with high-risk melanoma. *Cancer Immunol Res* (2015) 3:278–87. doi: 10.1158/2326-6066.CIR-14-0202
66. Lu H, Dietsch GN, Matthews MAH, Yang Y, Ghanekar S, Inokuma M, et al. VTX-2337 is a novel TLR8 agonist that activates NK cells and augments ADCC. *Clin Cancer Res* (2012) 18:499–509. doi: 10.1158/1078-0432.CCR-11-1625
67. Stephenson RM, Lim CM, Matthews M, Dietsch G, Hershberg R, Ferris RL. TLR8 stimulation enhances cetuximab-mediated natural killer cell lysis of head and neck cancer cells and dendritic cell cross-priming of EGFR-specific CD8+ T cells. *Cancer Immunol Immunother* (2013) 62:1347–57. doi: 10.1007/s00262-013-1437-3
68. Chow LQM, Morishima C, Eaton KD, Baik CS, Goulart BH, Anderson LN. Phase Ib trial of the toll-like receptor 8 agonist, motolimod (VTX-2337), combined with cetuximab in patients with recurrent or metastatic SCCHN. *Clin Cancer Res* (2017) 23:2442–50. doi: 10.1158/1078-0432.CCR-16-1934
69. Reilley M, Tsimberidou AM, Piha-Paul SA, Yap TA, Fu S, Naing A. Phase 1 trial of TLR9 agonist lefitolimod in combination with CTLA-4 checkpoint inhibitor ipilimumab in advanced tumors. *J Clin Oncol* (2019) 37:TPS2669–TPS2669. doi: 10.1200/JCO.2019.37.15_suppl.TPS2669

70. Ribas A, Medina T, Kummar S, Amin A, Kalbasi A, Drabick JJ, et al. Sd-101 in combination with pembrolizumab in advanced melanoma: Results of a phase ib, multicenter study. *Cancer Discovery* (2018) 8:1250–7. doi: 10.1158/2159-8290.CD-18-0280
71. Milhem M, Zakharia Y, Davar D, Buchbinder E, Medina T, Daud A, et al. Durable responses in anti-PD-1 refractory melanoma following intratumoral injection of a Toll-like receptor 9 (TLR9) agonist, CMP-001, in combination with pembrolizumab. *SITC 2019 Annu Meet* (2019) O85. doi: 10.1136/LBA2019.4
72. Oliveira-Nascimento L, Massari P, Wetzler LM. The role of TLR2 ininfection and immunity. *Front Immunol* (2012) 3:1–17. doi: 10.3389/fimmu.2012.00079
73. Méndez-Samperio P, Belmont L, Miranda E. Mycobacterium bovis BCG Toll-Like Receptors 2 and 4 Cooperation Increases the Innate Epithelial Immune Response. *Arch Med Res* (2008) 39:33–9. doi: 10.1016/j.arcmed.2007.06.019
74. Vacchelli E, Galluzzi L, Eggermont A, Fridman WH, Galon J, Sautès-Fridman C, et al. Trial watch: FDA-approved toll-like receptor agonists for cancer therapy. *Oncoimmunology* (2012) 1:894–907. doi: 10.4161/onci.20931
75. Vosika GJ, Barr C, Gilbertson D. Phase-I study of intravenous modified lipid A. *Cancer Immunol Immunother* (1984) 18:107–12. doi: 10.1007/BF00205743
76. Isambert N, Fumoleau P, Paul C, Ferrand C, Zanetta S, Bauer J, et al. Phase I study of OM-174, a lipid A analogue, with assessment of immunological response, in patients with refractory solid tumors. *BMC Cancer* (2013) 13:1–10. doi: 10.1186/1471-2407-13-172
77. Mahipal A, Ejadi S, Gnjatic S, Kim-Schulze S, Lu H, ter Meulen JH, et al. First-in-human phase 1 dose-escalating trial of G305 in patients with advanced solid tumors expressing NY-ESO-1. *Cancer Immunol Immunother* (2019) 68:1211–22. doi: 10.1007/s00262-019-02331-x
78. Hug BA, Matheny CJ, Burns O, Struemper H, Wang X, Washburn ML, et al. Safety, Pharmacokinetics, and Pharmacodynamics of the TLR4 Agonist GSK1795091 in Healthy Individuals: Results from a Randomized, Double-blind, Placebo-controlled, Ascending Dose Study. *Clin Ther* (2020) 42:1519–1534.e33. doi: 10.1016/j.clinthera.2020.05.022
79. Eremina NV, Kazey VI, Mishugin SV, Leonenkov RV, Pushkar DY, Mett VL, et al. First-in-human study of anticancer immunotherapy drug candidate mobilan: Safety, pharmacokinetics and pharmacodynamics in prostate cancer patients. *Oncotarget* (2020) 11:1273–88. doi: 10.18632/oncotarget.27549
80. Middleton MR, Wermke M, Calvo E, Chartash E, Zhou H, Zhao X, et al. Phase I/II, multicenter, open-label study of intratumoral/intralesional administration of the retinoic acid–inducible gene I (RIG-I) activator MK-4621 in patients with advanced or recurrent tumors. *Ann Oncol* (2018) 29:viii712. doi: 10.1093/annonc/mdy424.016
81. Saxena M, Yeretssian G. NOD-like receptors: Master regulators of inflammation and cancer. *Front Immunol* (2014) 5:1–16. doi: 10.3389/fimmu.2014.00327
82. Moossavi M, Parsamanesh N, Bahrami A, Atkin SL, Sahebkar A. Role of the NLRP3 inflammasome in cancer. *Mol Cancer* (2018) 17:158. doi: 10.1186/s12943-018-0900-3
83. Brown GD, Willment JA. & Whitehead, L. C-type lectins in immunity and homeostasis. *Nat Rev Immunol* (2018) 18:374–89. doi: 10.1038/s41577-018-0004-8
84. Ishikawa H, Barber GN. STING is an endoplasmic reticulum adaptor that facilitates innate immune signalling. *Nature* (2008) 455:674–8. doi: 10.1038/nature07317
85. Le Naour J, Zitvogel L, Galluzzi L, Vacchelli E, Kroemer G. Trial watch: STING agonists in cancer therapy. *Oncoimmunology* (2020) 9:1–12. doi: 10.1080/2162402X.2020.1777624
86. Dranoff G. Cytokines in cancer pathogenesis and cancer therapy. *Nat Rev Cancer* (2004) 4:11–22. doi: 10.1038/nrc1252
87. Fyfe G, Fisher RI, Rosenberg SA, Sznol M, Parkinson DR, Louie AC. Results of treatment of 255 patients with metastatic renal cell carcinoma who received high-dose recombinant interleukin-2 therapy. *J Clin Oncol* (1995) 13:688–96. doi: 10.1200/JCO.1995.13.3.688
88. Andtbacka RHI, Kaufman HL, Collichio F, Amatruda T, Senzer N, Chesney J, et al. Talimogene laherparepvec improves durable response rate in patients with advanced melanoma. *J Clin Oncol* (2015) 33:2780–8. doi: 10.1200/JCO.2014.58.3377
89. Lasek W, Zagożdżon R, Jakobisiak M. Interleukin 12: Still a promising candidate for tumor immunotherapy? *Cancer Immunol Immunother* (2014) 63:419–35. doi: 10.1007/s00262-014-1523-1
90. Atkins MB, Robertson MJ, Gordon M, Lotze MT, DeCoste M, DuBois JS, et al. Phase I evaluation of intravenous recombinant human interleukin 12 in patients with advanced malignancies. *Clin Cancer Res* (1997) 3:409–17.
91. Leonard JP, Sherman ML, Fisher GL, Buchanan LJ, Larsen G, Atkins MB, et al. Effects of Single-Dose Interleukin-12 Exposure on Interleukin-12–Associated Toxicity and Interferon-γ Production. *Blood* (1997) 90:2541–8.
92. Strauss J, Heery CR, Kim JW, Jochems C, Donahue RN, Montgomery AS, et al. First-in-human phase I trial of a tumor-targeted cytokine (NHS-IL12) in subjects with metastatic solid tumors. *Clin Cancer Res* (2019) 25:99–109. doi: 10.1158/1078-0432.CCR-18-1512
93. Ma A, Koka R, Burkett P. Diverse functions of IL-2, IL-15, and IL-7 in lymphoid homeostasis. *Annu Rev Immunol* (2006) 24:657–79. doi: 10.1146/annurev.immunol.24.021605.090727
94. Miller JS, Morishima C, McNeel DG, Patel MR, Kohrt HEK, Thompson JA, et al. A first-in-human phase I study of subcutaneous outpatient recombinant human IL15 (rhIL15) in adults with advanced solid tumors. *Clin Cancer Res* (2018) 24:1525–35. doi: 10.1158/1078-0432.CCR-17-2451
95. Cooley S, He F, Bachanova V, Vercellotti GM, DeFor TE, Curtsinger JM, et al. First-in-human trial of rhIL-15 and haploidentical natural killer cell therapy for advanced acute myeloid leukemia. *Blood Adv* (2019) 3:1970–80. doi: 10.1182/bloodadvances.2018028332
96. Wrangle JM, Velcheti V, Patel MR, Garrett-Mayer E, Hill EG, Ravenel JG, et al. ALT-803, an IL-15 superagonist, in combination with nivolumab in patients with metastatic non-small cell lung cancer: a non-randomised, open-label, phase 1b trial. *Lancet Oncol* (2018) 19:694–704. doi: 10.1016/S1470-2045(18)30148-7
97. Burke JD, Young HA. IFN-Γ: A cytokine at the right time, is in the right place. *Semin Immunol* (2019) 43:101280. doi: 10.1016/j.smim.2019.05.002
98. Conlon KC, Miljkovic MD, Waldmann TA. Cytokines in the Treatment of Cancer. *J Interf Cytokine Res* (2019) 39:6–21. doi: 10.1089/jir.2018.0019
99. Le Naour J, Galluzzi L, Zitvogel L, Kroemer G, Vacchelli E. Trial watch: IDO inhibitors in cancer therapy. *Oncoimmunology* (2020) 9:1–16. doi: 10.1080/2162402X.2020.1777625
100. Mitchell TC, Hamid O, Smith CD, Bauer TM, Wasser JS, Olszanski AJ, et al. Epacadostat plus pembrolizumab in patients with advanced solid tumors: Phase I results from a multicenter, open-label phase I/II trial (ECHO-202/KEYNOTE-037). *J Clin Oncol* (2018) 36:3223–30. doi: 10.1200/JCO.2018.78.9602
101. Long GV, Dummer R, Hamid O, Gajewski TF, Caglevic C, Dalle S, et al. Epacadostat plus pembrolizumab versus placebo plus pembrolizumab in patients with unresectable or metastatic melanoma (ECHO-301/KEYNOTE-252): a phase 3, randomised, double-blind study. *Lancet Oncol* (2019) 20:1083–97. doi: 10.1016/S1470-2045(19)30274-8
102. Fruman DA, Chiu H, Hopkins BD, Bagrodia S, Cantley LC, Abraham RT. The PI3K Pathway in Human Disease. *Cell* (2017) 170:605–35. doi: 10.1016/j.cell.2017.07.029
103. Yao JC, Shah MH, Ito T, Bohas CL. Everolimus for advanced pancreatic neuroendocrine tumors. *N Engl J Med* (2011) 364:514–23. doi: 10.1056/NEJMoa1009290
104. Baselga J, Campone M, Piccart M, Burris HA, Rugo HS, Sahmoud T, et al. Everolimus in postmenopausal hormone-receptor-positive advanced breast cancer. *N Engl J Med* (2012) 366:520–9. doi: 10.1056/NEJMoa1109653
105. Horwitz SM, Koch R, Porcu P, Oki Y, Moskowitz A, Perez M, et al. Activity of the PI3K-δ,g inhibitor duvelisib in a phase 1 trial and preclinical models of T-cell lymphoma. *Blood* (2018) 131:888–98. doi: 10.1182/blood-2017-08-802470
106. Huang Q, Lei Y, Li X, Guo F. & Liu, M. A Highlight of the Mechanisms of Immune Checkpoint Blocker Resistance. *Front Cell Dev Biol* (2020) 8:1–12. doi: 10.3389/fcell.2020.580140
107. Chae YK, Oh MS, Giles FJ. Molecular Biomarkers of Primary and Acquired Resistance to T-Cell-Mediated Immunotherapy in Cancer: Landscape,

Clinical Implications, and Future Directions. *Oncologist* (2018) 23:410–21. doi: 10.1634/theoncologist.2017-0354

108. Grasso CS, Tsoi J, Onyshchenko M, Abril-Rodriguez G, Ross-Macdonald P, Wind-Rotolo M, et al. Conserved Interferon-γ Signaling Drives Clinical Response to Immune Checkpoint Blockade Therapy in Melanoma. *Cancer Cell* (2020) 38:500–515.e3. doi: 10.1016/j.ccell.2020.08.005

Conflict of Interest: JK has received grants and personal fees for consultancy from Amgen, Bristol-Myers Squibb, Checkmate and Novartis, and grants from Castle Biosciences, Immunocore, and Iovance.

The remaining author declares that the research was conducted in the absence of any commercial or financial relationships that could be construed as a potential conflict of interest.

frontiers in Oncology

ORIGINAL RESEARCH
published: 09 March 2021
doi: 10.3389/fonc.2021.619003

CXC Chemokines as Therapeutic Targets and Prognostic Biomarkers in Skin Cutaneous Melanoma Microenvironment

Xuezhi Zhou, Manjuan Peng, Ye He, Jingjie Peng, Xuan Zhang, Chao Wang, Xiaobo Xia and Weitao Song**

Hunan Key Laboratory of Ophthalmology, Eye Center of Xiangya Hospital, Central South University, Changsha, China

OPEN ACCESS

Edited by:
Paolo Antonio Ascierto, Istituto Nazionale dei Tumori (IRCCS), Italy

Reviewed by:
Chandra K. Singh, University of Wisconsin-Madison, United States
Sanjay Premi, Moffitt Cancer Center & Research Institute, United States

***Correspondence:**
Xiaobo Xia
xbxia123123@163.com
Weitao Song
wtsong123@163.com

Specialty section:
This article was submitted to Skin Cancer, a section of the journal Frontiers in Oncology

Received: *19 October 2020*
Accepted: *22 January 2021*
Published: *09 March 2021*

Citation:
Zhou X, Peng M, He Y, Peng J, Zhang X, Wang C, Xia X and Song W (2021) CXC Chemokines as Therapeutic Targets and Prognostic Biomarkers in Skin Cutaneous Melanoma Microenvironment. Front. Oncol. 11:619003. doi: 10.3389/fonc.2021.619003

Background: Skin Cutaneous Melanoma (SKCM) is a tumor of the epidermal melanocytes induced by gene activation or mutation. It is the result of the interaction between genetic, constitutional, and environmental factors. SKCM is highly aggressive and is the most threatening skin tumor. The incidence of the disease is increasing year by year, and it is the main cause of death in skin tumors around the world. CXC chemokines in the tumor microenvironment can regulate the transport of immune cells and the activity of tumor cells, thus playing an anti-tumor immunological role and affecting the prognosis of patients. However, the expression level of CXC chemokine in SKCM and its effect on prognosis are still unclear.

Method: Oncomine, UALCAN, GEPIA, STRING, GeneMANIA, cBioPortal, TIMER, TRRUST, DAVID 6.8, and Metascape were applied in our research.

Result: The transcription of CXCL1, CXCL5, CXCL8, CXCL9, CXCL10, and CXCL13 in SKCM tissues were significantly higher than those in normal tissues. The pathological stage of SKCM patients is closely related to the expression of CXCL4, CXCL9, CXCL10, CXCL11, CXCL12, and CXCL13. The prognosis of SKCM patients with low transcription levels of CXCL4, CXCL9, CXCL10, CXCL11, and CXCL13 is better. The differential expression of CXC chemokines is mainly associated with inflammatory response, immune response, and cytokine mediated signaling pathways. Our data indicate that the key transcription factors of CXC chemokines are RELA, NF-κB1 and SP1. The targets of CXC chemokines are mainly LCK, LYN, SYK, MAPK2, MAPK12, and ART. The relationship between CXC chemokine expression and immune cell infiltration in SKCM was closed.

Conclusions: Our research provides a basis for screening SKCM biomarkers, predicting prognosis, and choosing immunotherapy.

Keywords: CXC chemokine, therapeutic targets, prognostic biomarkers, skin cutaneous melanoma, microenvironment

INTRODUCTION

Skin Cutaneous Melanoma is a common skin tumor caused by abnormal hyperproliferation of melanocytes (1). Its incidence varies with race, region, and age. The incidence of white people is much higher than that of black people, with the incidence of white people living in Queensland, Australia reaching 17/100,000 (2). In recent decades, the incidence of melanoma has continued to increase worldwide. It is the fastest-growing malignant disease in men and second only to lung cancer in women, with annual growth rates of 3–5% (3). Melanoma ranks 5th and 6th in malignant diseases in males and females, respectively, second only to adult leukemia in terms of risk of death (4). The median age of onset was 45–55 years old. Risk factors for melanoma include clear family history, melanoma history, multiple atypical or dysplastic nevi, and congenital genetic mutations (5). Sun exposure may also promote the development of melanoma (5). The association between molecular biological indicators and tumor prognosis has aroused great attention of researchers lately. Studies have revealed the relationship between the expression of S-100, Vimentin, and other proteins and tumor metastasis and prognosis (6). However, more effective therapeutic targets and more sensitive markers related to prognosis are still to be developed.

Chemokines are a superfamily composed of small molecules of cytokine-like proteins (7). CXC chemokines are an important member of this family (8). They occupy a major position in inflammation and damage repair and are closely linked with the occurrence, development, invasion, and metastasis of tumors (9). The function of CXC chemokines in tumors is deep association with the existence of ELR domains (10). CXC chemokines containing ELR domains are mainly concerned with the growth, proliferation, metastasis, and angiogenesis regulation of tumor cells. The diversity of functions of CXC chemokines without ELR domains in tumors may be related to the difference of ELR-CXC chemokine binding receptors. Therefore, we therefore speculate that CXC chemokines may also occupy and major position in various biological processes of SKCM.

In SKCM there are many updated reviews on molecular factors important for biology, drug targeting, and prognosis (BRAF, MEK, PD-1 et. al) (11–13). However, few studies have focused on the mechanism of CXC chemokine in SKCM and its potential value. Studies have reported the expression and function of some members of CXC chemokines in SKCM. However, so far it is still unknown which CXC can be used as a biomarker for prognosis and a target for immunotherapy for SKCM. With the continuous update and iteration of a variety of biological detection methods, it is possible to comprehensively analyze CXC chemokines.

Hence, the focus of this research is to find biological targets from CXC that can be used as the diagnosis and treatment of SKCM. In addition, we hope to discover the specific molecular mechanism of CXC affecting prognosis of SKCM through bioinformatics analysis.

MATERIALS AND METHODS

ONCOMINE

ONCOMINE (http://www.oncomine.org) is a great tumor gene chip database, which contains multiple functions include finding outliers, predicting co-expressed genes, and analyzing gene expression differences (14). It can also be classified according to clinical information such as tumor stage, grade, and tissue type, and can also be used to search for possible diagnostic biomarkers and therapeutic targets. In this study, figure was exported to show the expression difference of CXC chemokines in SKCM through analysis from this website. The expression differences of CXC chemokines in SKCM were analyzed by a Student t-test. ONCOMINE contains 715 datasets and 86,733 samples.

UALCAN

UALCAN (http://ualcan.path.uab.edu/index.html) can effectively analyze and mine cancer data on-line (15). The tumor-related data of the TCGA database is the basis of data mining on this website. The function of UALCAN includes biomarker identification, expression profile analysis, survival analysis, *etc*. In our study, the SKCM data set was import into UALCAN Expression Analysis module to evaluate the CXC chemokines expression. Student t-test was used to analyzed SKCM data.

GEPIA

GERIA (http://gepia.cancer-pku.cn/index.html) is a newly developed interactive web server for analyzing the RNA sequencing expression data of 9,736 tumors and 8,587 normal samples from the TCGA and the GTEx projects, using a standard processing pipeline (16). It fills the gap of big data information in cancer genomics. GEPIA analyzed RNA sequencing expression data from 9,736 tumors and 8,587 normal samples from the TCGA and GTEx projects. The expression data of TCGA and GTEx are calculated under the same pipeline, which can be directly analyzed in a very comprehensive way. The database is an open public database. In this study, we used GEPIA's "Single Gene Analysis" to analyze the differential expression of CXC chemokines in tumor tissues and normal tissues, as well as pathological stage Analysis and prognosis Analysis. "Multiple Gene Comparison" was used for the polygenic comparative analysis of CXC chemokines in the "SKCM" data set. Student t-test was used to explore SKCM data.

STRING

STRING (https://string-db.org/) is a database that searches for known interactions between proteins and predicts their interactions (17). The database, available for 2,031 species, contains 9.6 million proteins and 13.8 million protein–protein interactions. It contains experimental data, PubMed abstracts, and other database data, as well as results predicted by bioinformatics methods. In this study, STRING was used for PPI analysis of CXC chemokines and peripheral interaction gene.

GeneMANIA

The function of GeneMANIA (http://www.genemania.org) is to predict the interactions between proteins, including Predicted, Physical Interactions, co-location, co-expression, Pathway, Shared protein domains, and Genetic Interactions (18). GeneMANIA has almost 2,277 networks that collectively contain nearly 600 million interactions covering almost 163,599 genes.

cBioPortal

cBioPortal (www.cbioportal.org) integrates data from 126 tumor genome studies (19). These included large tumor research projects such as TCGA and ICGC, which included data from 28,000 samples, and some samples with phenotypic information such as clinical prognosis. Genetic variation, gene network, and co-expression of CXC chemokines in SKCM were analyzed by cBioPortal.

TIMER

TIMER (https://cistrome.shinyapps.io/timer/) using a deconvolution algorithm from the gene expression profile (TIICs) concluded that tumor-infiltrating immune cells in abundance (20). Gene expression data of 10,897 TCGA samples from 32 cancer types were reanalyzed to estimate the abundance of six TIIC subsets (B cells, CD4+T cells, CD8+T cells, macrophages, neutrophils, and dendritic cells) to establish a link between tumor immunity and genomic data. The web server provides the abundance of immune infiltrates estimated by multiple immune-deconvolution methods and allows users to dynamically generate high-quality graphics to fully explore the immunological, clinical, and genomic characteristics of tumors.

TRRUST

TRRUST (https://www.grnpedia.org/trrust/) is a record of transcription factors regulating the relationship database (21). TRRUST contains 8,444 and 6,552 TF-target regulatory relationships of 800 human TFs and 828 mouse TFs (21). It includes not only the corresponding target genes of transcription factors but also the regulatory relationship between transcription factors. At present, the database only stores regulatory information related to humans and mice, and these regulatory relations are sorted out from the literature through text mining.

DAVID 6.8

DAVID 6.8 integrates biological data and analysis tools to provide systematic and comprehensive biological functional annotation information for the large-scale gene or protein lists (hundreds of gene or protein ID lists) to help users extract biological information from DAVID 6.8 (https://david.ncifcrf.gov/summary.jsp) (22). GO enrichment analysis and KEGG analysis on CXC chemokines and 50 closely related genes were performed by applying DAVID.

METASCAPE

Metascape (http://metascape.org) integrates more than 40 bioinformatics databases (23). It not only includes bio-pathway enrichment analysis, protein interaction network structure analysis, and abundant gene annotation functions but also presents the results in high-quality graphical language that biologists can easily understand. The enrichment analysis of CXC chemokines and highly interacting genes were verified by the Express Analysis module.

QRT-PCR ANALYSIS

10 SKCM tissues and 12 normal tissues were enrolled in our research to verify the CXC chemokines expression. We obtained consent of patients and ethical approval from the Xiangya hospital ethics committee. All procedures were executed by the ethics guidelines and regulations. We extracted total RNA of the tissue by using Trizol reagent (Invitrogen, CA, USA). qRT-PCR was performed with SYBR® Green dye (TaKaRa, Shiga, Japan). The primer sequences of relative genes are provided in **Supplementary Table 1**.

RESULTS

CXC Chemokines in SKCM Patients

The expression differences of 16 CXC chemokines between SKCM patients and controls were analyzed in the Oncomine database (**Figure 1** and **Table 1**). Analysis results showed that the transcription levels of CXCL1, CXCL5, CXCL8, CXCL9, CXCL10, and CXCL13 in SKCM patients were significantly increased compared with normal skin tissues. Risker et al. confirmed that the transcription level of CXCL1, CXCL5, CXCL8, and CXCL13 in SKCM patients were significantly higher than those in normal skin tissues (24). Haqq et al. also proved that the transcription of CXCL1, CXCL9, and CXCL10 in melanoma patients is significantly higher than that in normal skin tissues with a P-value of 0.005, 6.75E-4, and 2.52E-4 (25). Talatov et al. also confirmed that the transcription level of CXCL8 was significantly increased with a P-value of 0.004 (26). There was no significant difference in the transcriptional levels of SKCM patients and normal people among CXCL2, CXCL3, CXCL4, CXCL6, CXCL7, CXCL11, CXCL12, CXCL14, CXCL16, and CXCL17.

Relationship between 16 CXC chemokines and the pathological stage of SKCM was assessed by GEPIA. The results showed that CXCL4 (P = 0.0349), CXC9 (P = 7.74E-05), CXC10 (P = 0.000105), CXC11 (P = 0.000664), CXC12 (P =0.00989), and CXC13 (P =0.000815) were notably associated with the pathological stage of SKCM (**Figure 2**). High expression of CXCL4, CXCL9, CXCL10, CXCL11, CXCL12, and CXCL13 promotes the progress of SKCM. It concluded that CXC chemokines are extremely closely connected with the pathological progress of SKCM.

CXC Chemokines in Primary SKCM and Metastasis SKCM Patients

The difference in CXC chemokine expression levels between primary SKCM and metastatic SKCM patients was analyzed by

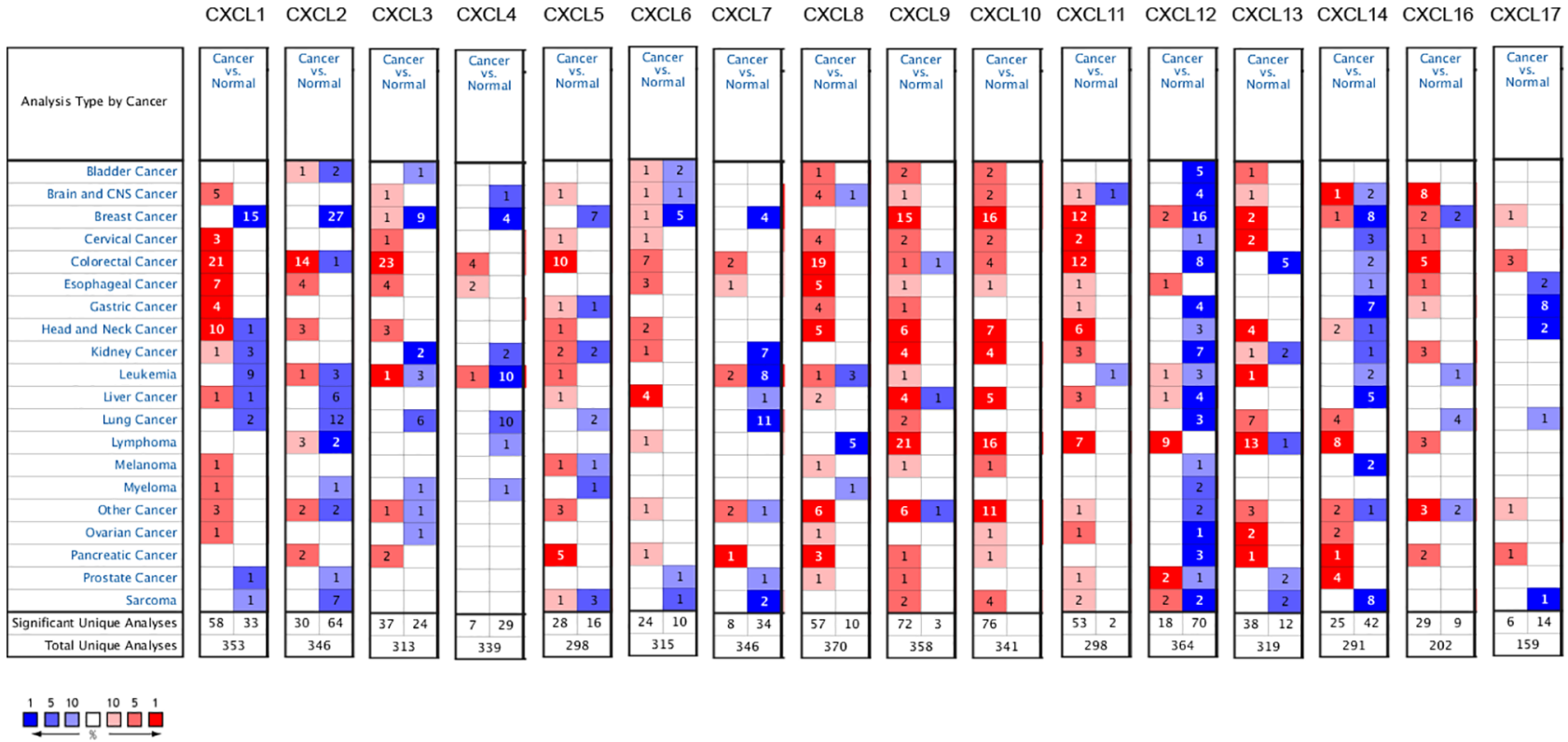

FIGURE 1 | mRNA levels of CXC chemokines in SKCM (ONCOMINE). The panel shows the numbers of datasets with statistically significant mRNA over-expression (red) or downregulated expression (blue) of CXC chemokines.

TABLE 1 | The mRNA levels of CXC in SKCM and normal skin tissues at transcriptome level.

TLR	Type	Fold change	*P*-value	*t*-test	References
CXCL1	SKCM	4.096	0.003	3.535	(21)
	Melanoma	12.232	0.004	4.100	(22)
CXCL5	SKCM	6.945	1.73E-4	4.528	(21)
CXCL8	SKCM	5.651	0.004	3.239	(21)
	SKCM	2.559	0.004	2.837	(23)
CXCL9	SKCM	5.144	6.75E-4	6.321	(22)
CXCL10	SKCM	5.651	2.52E-4	6.311	(22)
CXCL13	SKCM	11.238	0.037	2.166	(21)

UALCAN (**Figure 3**). Analysis results indicated that the CXCL1 (P = 4.16E-02) and CXCL7 (P = 1.46E-02) level in primary SKCM patients was remarkably higher than metastasis SKCM patients (P = 4.16E-02). However, the expression level of CXCL9 (P = 1.37E-11), CXCL10 (P = 3.04E-03), CXCL12 (P = 5.05E-11), CXCL13 (P = 3.52E-06), and CXCL16 (P =1.18E-04) in patients with metastasis SKCM is notably higher than that of patients with primary SKCM. We concluded that CXCL1, CXCL 7, CXCL 9, CXCL 10, CXCL 12, CXCL 13, and CXCL 16 have obvious differences in expression in patients with primary SKCM and metastasis SKCM. No obvious difference has been seen in the expression levels of CXCL2, CXCL3, CXCL4, CXCL5, CXCL6, CXCL8, CXCL11, CXCL14, and CXCL17 in patients with primary SKCM and metastasis SKCM. We also analyzed the expression levels of each gene of the CXC chemokine family in SKCM tissue through the GEPIA website (**Figure 4**). The analysis results revealed that CXCL12 and CXCL16 level in SKCM patients were highest.

CXC Chemokines Affect Prognostic of SKCM Patients

We evaluated the worth of different CXC chemokines in SKCM clinical outcomes by using GEPIA. No obvious correlation between the level of CXC chemokine family transcription and disease-free survival time in SKCM patients was found (**Figure 5**). The worth of CXC chemokines with different expressions in the total survival of SKCM patients was assessed (**Figure 6**). The results showed that low expression of CXCL4 (p = 0.0028), CXCL9 (P = 0.00024), CXCL10 (P = 2.8E-05), CXCL11 (P =1.9e-05), and CXCL13 (P = 2.7e-05) was remarkably related to longer overall survival in SKCM.

Gene Changes, Adjacent Gene Networks, and Interaction of CXC Chemokines in SKCM

An exhaustive molecular characterization excavation of CXC chemokines differentially expressed was performed. The genetic changes of differentially expressed CXC chemokines were analyzed applying the TCGA data set. The analytical results showed that CXCL1, CXCL2, CXCL3, CXCL4, CXCL5, CXCL6, CXCL7, CXCL8, CXCL9, CXCL10, CXCL11, CXCL12, CXCL13, CXCL14, CXCL16, CXCL17 were changed in 4, 1.4, 2.5, 4, 2.2, 4, 5, 4, 7, 5, 4, 2.8, 2.2, 5,5, and 2.2% of the queried SKCM samples, respectively (**Figures 7A, B**). The most common change in these samples was increased mRNA expression. Also, PPI network analysis was performed for CXC chemokines and Strings with different expressions to explore their possible interactions. Several 16 nodes and several 11 edges were acquired from the PPI network (**Figure 7C**). PPI analysis results showed that the PPI enrichment P-value was <1.0e-16. GeneMANIA analysis showed that the effect of 16 CXC chemokines was mainly associated with chemokine receptor binding and activity (**Figure 7D**). Besides, String analyzed the top 50 most regularly interacting neighboring genes related to 16 CXC chemokines. The results showed that CXCR4, CXCR2, CCR5, IL10, CXCR1, CXCR5, CCL5, ACKR3, CCL19, CXCR6, IL4, IL1B, CCL21, CCL11, CCL11, CCL20, CCL25, RELA, CCL1, IL6, IL13, STAT3, MMP9, CCR4, CCR3, ACKR1, CCL2, CCR5, CCL4L1, CCR2, MAPK14, TNF, VEGFA, CCR7, CC R1, FPR2, JUN, CX3CL1, CEBPB, CCR10, VWF, PTPRC, MAPK1, JAK2, CX3CR1, MAPK3, CCR9, LCN2, and EP300 are mainly related to the regulation and capability of CXC chemokines in SKCM patients (**Figure 7E**).

Biological Process Analysis of CXC Chemokines

The enrichment analysis of CXC chemokines and its closely interacting neighboring genes is performed by DAVID 6.8 and Metascape. **Figure 8A** shows the first 10 items using DAVID 6.8 for the functional enrichment analysis. In the BP category, inflammatory response, immune response, cytokine-mediated signaling pathway, leukocyte chemotaxis, positive regulation of ERK1 and ERK2, and cellular response to interferon-γ, interleukin-1, and tumor necrosis factor were associated with SKCM oncogenesis and progression. In the CC category, the extracellular space, external side of the plasma membrane, extracellular region, cell, and Pseudopodium are the five functional enrichment projects. In the MF category, the CXC chemokines and its adjacent genes are mostly enriched in CXC chemokine receptor binding, C-C chemokine receptor activity, C-X-C chemokine receptor activity, CXCR Chemokine receptor binding, MAP kinase activity, cytokine activity, heparin-binding, and growth factor activity. KEGG pathway analysis was also performed, and the results showed the chemokine signaling pathway, cytokine receptor interaction, TNF signaling pathway, toll-like receptor signaling pathway, Leishmaniasis, Intestinal Immune Network for IgA production, Influenza, and NOD-like receptor signaling Pathway, Chagas disease, inflammatory disease, tuberculosis, T cell signaling pathway are closely related to tumor formation (**Figure 8B**).

We also used Metascape for enrichment analysis. The functions of CXC chemokines and their adjacent genes are mostly focused on

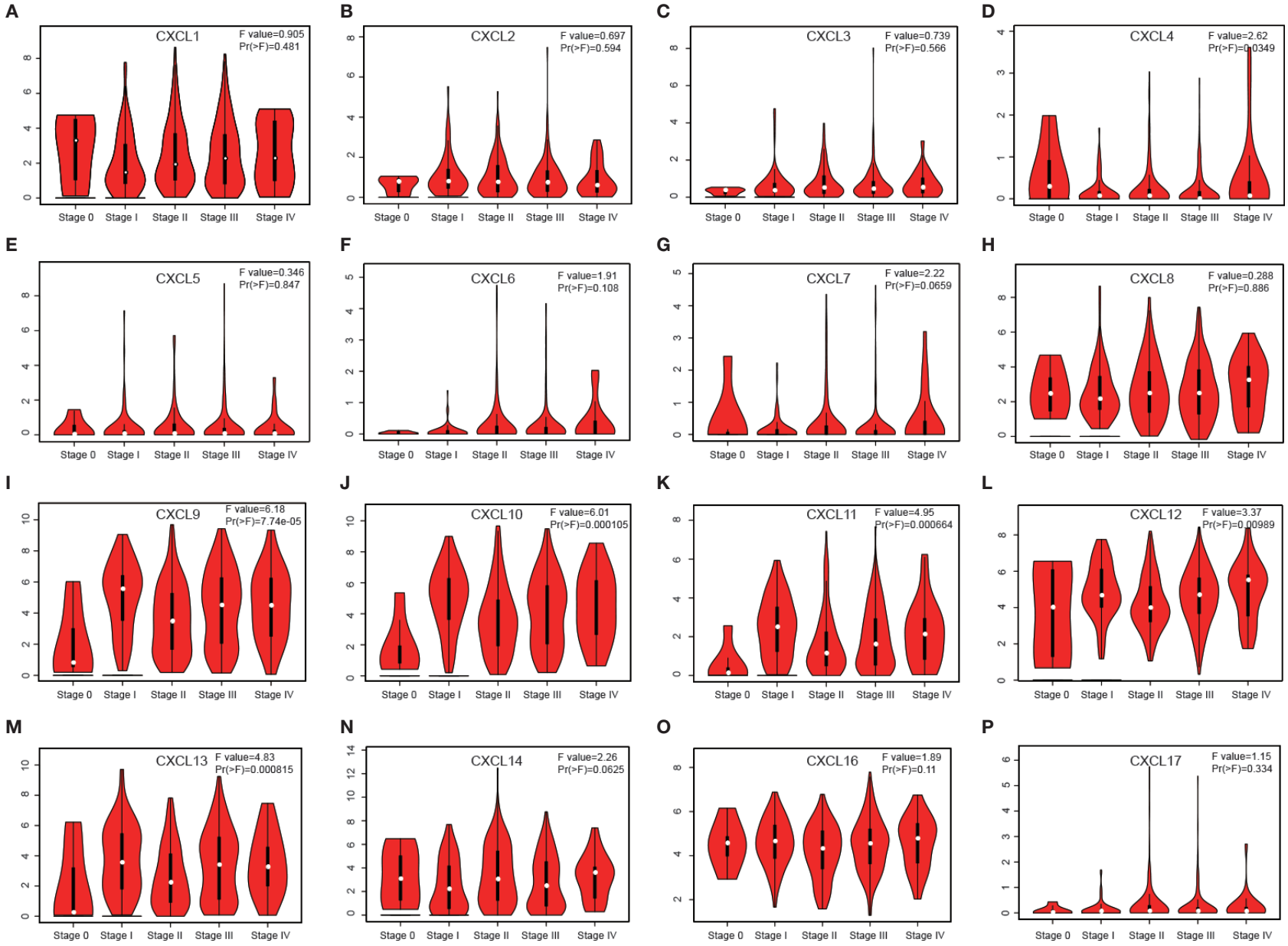

FIGURE 2 | Correlation between different expressed CXC chemokines and the pathological stage of SKCM patients **(A–P)** (GEPIA). *P* value less than 0.05 indicate significant difference.

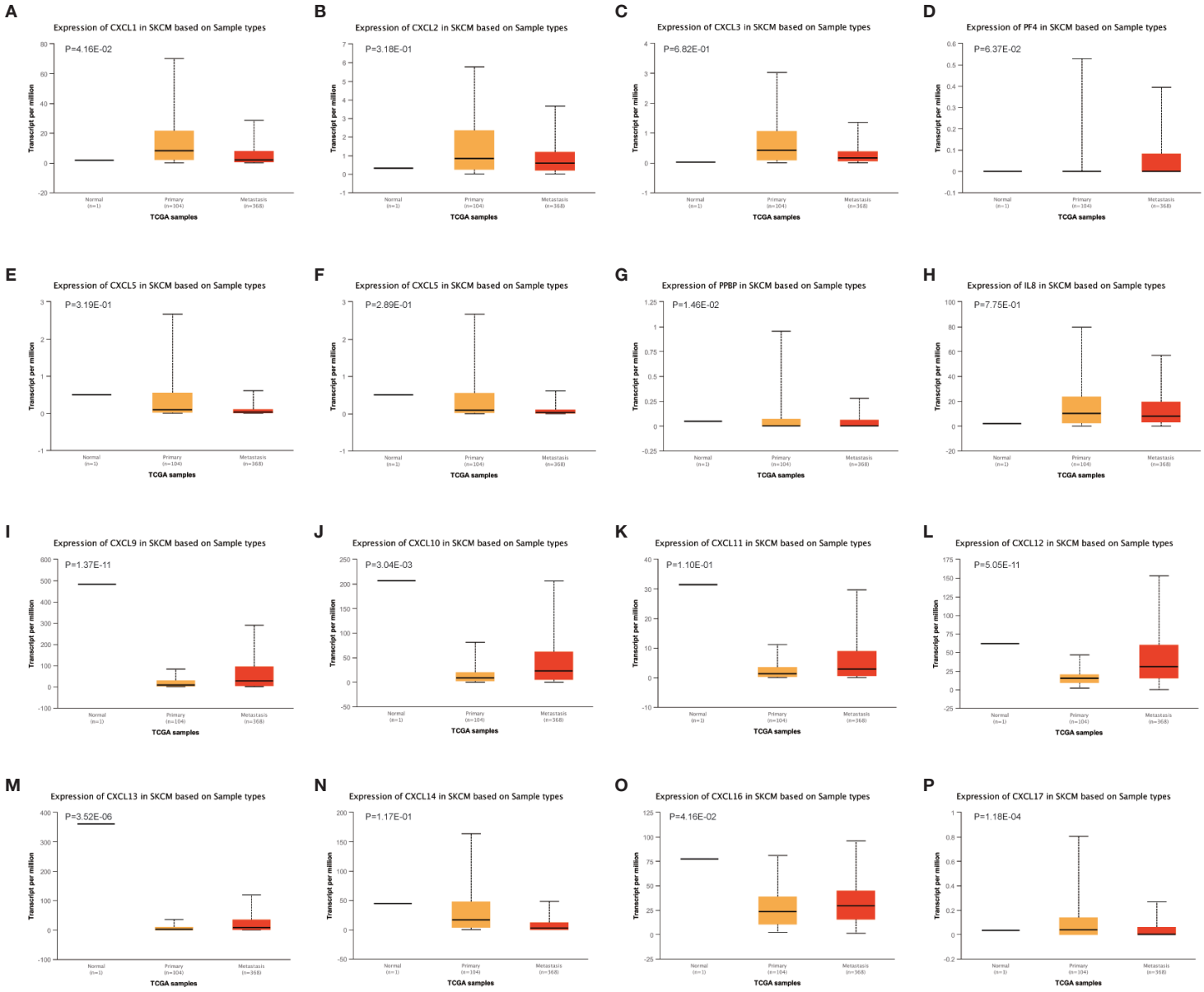

FIGURE 3 | The transcription of CXC chemokines in SKCM (UALCAN). The transcriptional levels of **(A)** CXCL1 and **(G)** CXCL7 in primary SKCM tissues were significantly elevated compared with metastasis SKCM patients while the transcriptional levels of **(I)** CXCL 9, **(J)** CXCL 10, **(L)** CXCL 12, **(M)** CXCL 13, and **(O)** CXCL 16 were significantly reduced. The p value was set at 0.05. There were no differences in transcriptional levels of **(B)** CXCL 2, **(C)** CXCL 3, **(D)** PF4, **(E)** CXCL 5, **(F)** CXCL6, **(H)** IL 8, **(K)** CXCL11, **(N)** CXCL 14, and **(P)** CXCL 17 between primary SKCM and metastasis SKCM patients. The p value was set at 0.05.

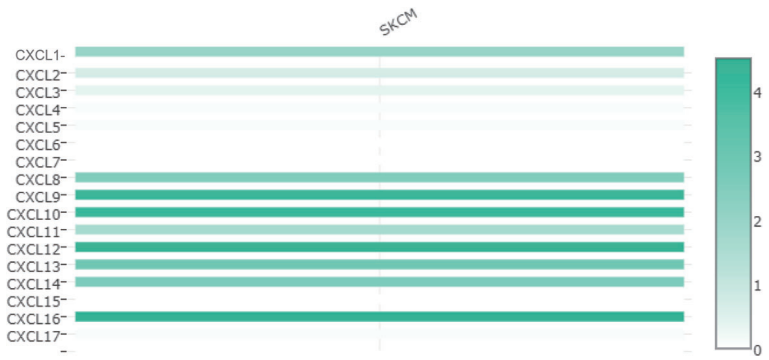

FIGURE 4 | The relative level of CXC chemokines in SKCM.

chemokines bind chemokines, positive regulation of locomotion, response to lipopolysaccharide, mononuclear cell migration, cellular calcium ion homeostasis, Interleukin-10 signaling, Toll-like receptor signaling pathway, *etc.* (**Figures 9A, B**). In order to explore the interaction between 16 CXC chemokines and its closely related gene, we analyzed the related data using the PPI network and mCODE components (**Figures 9C, D**). The result showed that the CXC chemokines biological functions are mainly associated with chemokine receptors bind chemokines, chemokine-mediated signaling pathways, cellular response to chemokine, IL-7 signaling pathway, AGE-RAGE signaling pathway, and TNF signaling pathway (**Figure 9E**).

Transcription Factor Targets and Kinase Target Analysis

TRRUST and LinkedOmics databases were used to explore possible transcription factors and kinase targets for differential expression of CXC chemokines. TRRUST contains CXCL 1, CXCL 2, CXCL 5, CXCL 8, CXCL 10, CXCL 12, and CXCL 14. Three transcription factors (RELA, NF-KB1, and SP1) were found to significantly regulated CXC chemokines in SKCM (**Table 2**). The transcription factors RELA and NFKB1were identified as key regulators of CXCL1, CXCL2, CXCL5, CXCL 8, CXCL10, and CXCL12. One of the main transcription factors regulating CXCL1, CXCL5, and CXCL 14 transcription in SKCM is SP1. LinkedOmics was utilized to analyze the kinase target of CXC chemokines (**Table 3**). ROCK1 and RPS6KB1 are among the most significant kinase targets for CXCL1. LCK and IKBKB are the most important kinase targets for CXCL2. MAPK12 and MYLK are the most important kinase targets for CXCL3. Both PAK1 and MAPK2 are key kinase targets of CXCL4. FER and JAK3 are most major kinase targets for CXCL5. BCR and MAPK14 are considered the key targets of the CXCL6 kinase target network. ADRBK2 and EIF2AK4 are considered as major targets of the CXCL8. LCK and SYK are the two largest targets in CXCL10, CXCL11, and CXCL9 kinase target network. LCK and LYN are mostly linked with CXCL12 and CXCL16. The CXCL13 kinase target network is mostly related to LCK and CSNK1E, while the CXCL14 kinase target network is mostly related to ART and PLK1. ART and NEK2 are considered as key targets of the CXCL17 kinase target network.

The Association of CXC Chemokines With Immune Cell Infiltration

Clinical outcome is related to inflammatory response and immune cell infiltration in SKCM patients, in which CXC chemokines are also involved. Timer database was applied to comprehensively quest whether CXC chemokines expression is associated with immune infiltration in SKCM patients (**Figrues 10A–P** and **Table 4**). The analysis results showed the correlation between CXCL1 expression and CD4+ T cell infiltration was negative in SKCM-primary patients (Cor = −0.207, P = 3.79E-02). The expression of CXCL2 was positively correlated with Neutrophil cell invasion in SKCM-primary patients (Cor = 0.293, P = 3.12E-03). CXCL2 is positively correlated with CD8+ T cells (Cor = 0.155, P = 4.32E-03) and Neutrophil cells (Cor = 0.215, P = 4.81e-05) infiltrates in SKCM-metastasis patients. CXCL3 is mostly related to Neutrophil cell invasion (Cor = 0.122, P = 2.22E-02) in SKCM-metastasis patients (**Figure 10C**). The correlation between the expression of CXCL4 and CD4+ T cell infiltration was negative in SKCM-primary patients (Cor = −0.266, P = 7.16E-03). In SKCM-metastasis, CXCL4 is negatively correlated with CD8+ T cells (Cor = −0.129, P = 1.81e-02) and Neutrophil cells (Cor = −0.119, P = 2.62e-02) and Dendritic cell (Cor = −0.131, P = 1.53e-02) infiltrates. CXCL5 was definitely related to Neutrophil cell infiltration in SKCM-primary patients (Cor = 0.228, P = 2.26E-02). In SKCM-metastasis, CXCL5 is positively correlated with invasion of B cells (Cor = 0.157, P = 3.51E-03) and Neutrophil cells (Cor = 0.163, P = 2.14e-03). The expression of CXCL7 in SKCM-primary was negatively correlated with Dendritic cells infiltration (Cor = −0.207, P = 3.82E-02). In SKCM-metastasis patients, CXCL7 is negatively correlated with B cells (Cor = −0.127, P = 1.79e-02) and Dendritic cells (Cor = −0.134, P = 1.30e-02) infiltrate. CXCL8's expression was positively correlated with Neutrophil cell infiltration in SKCM-primary patients (Cor = 0.374, P = 1.26E-04). In SKCM-metastasis patients, CXCL8 is positively correlated with the infiltration of CD8 + T cells (Cor = 0.135, P = 1.34e-02), Macrophage cells (Cor = 0.15, P = 4.79e-03), and Neutrophil cells

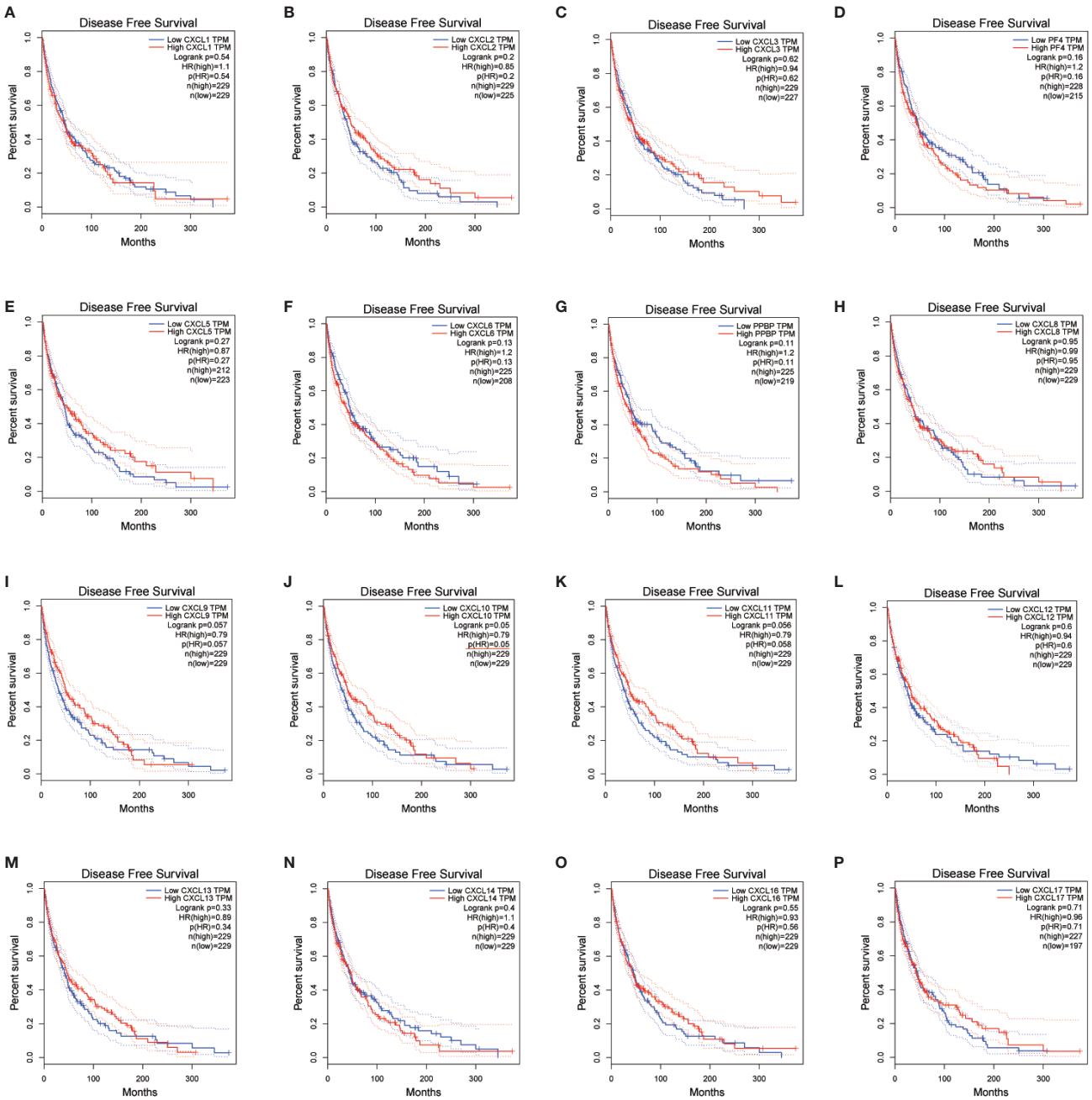

FIGURE 5 | The prognostic value of different expressed CXC chemokines in SKCM patients in the disease free survival curve **(A–P)** (GEPIA).

(Cor = 0.303, P = 7.27e-09) and Dendritic cells (Cor = 0.147, P = 6.31e-03). In SKCM-primary patients, down-regulation of CXCL9 enhanced infiltration of CD8 + T cells (COR = 0.573, *P* = 3.65e-10), CD4 + T cells (COR = 0.349, *P* = 3.44e-04), Neutrophil cells (COR = 0.488, *P* = 2.52e-07), and dendritic cells (COR = 0.535, *P* = 7.93E-49). In SKCM-metastasis patients, CXCL9 was positively correlated with infiltration of B cells (COR = 0.201, *P* = 1.73e-04), CD8+ T cells (COR = 0.679, *P* = 8.20e-47), CD4+ T cells (COR = 0.255, *P* = 1.71e-06), Macrophage cells (COR = 0.255, *P* = 1.27e-06), Neutrophil cells (Cor = 0.68, *P* = 6.05E-49) and Dendritic cells (Cor = 0.672, P = 1.48e-46). In SKCM-primary patients, CXCL10 was certainly related to infiltration of CD8 + T cells (COR = 0.584, *P* = 1.40e-10), CD4 + T cells (COR = 0.326, *P* = 8.87e-04), Neutrophil cells (COR = 0.637, *P* = 1.08e-12), and dendritic cells (COR = 0.58, *P* = 2.14e-10). In SKCM-metastasis, CXCL10 was positively correlated with infiltration of B cells

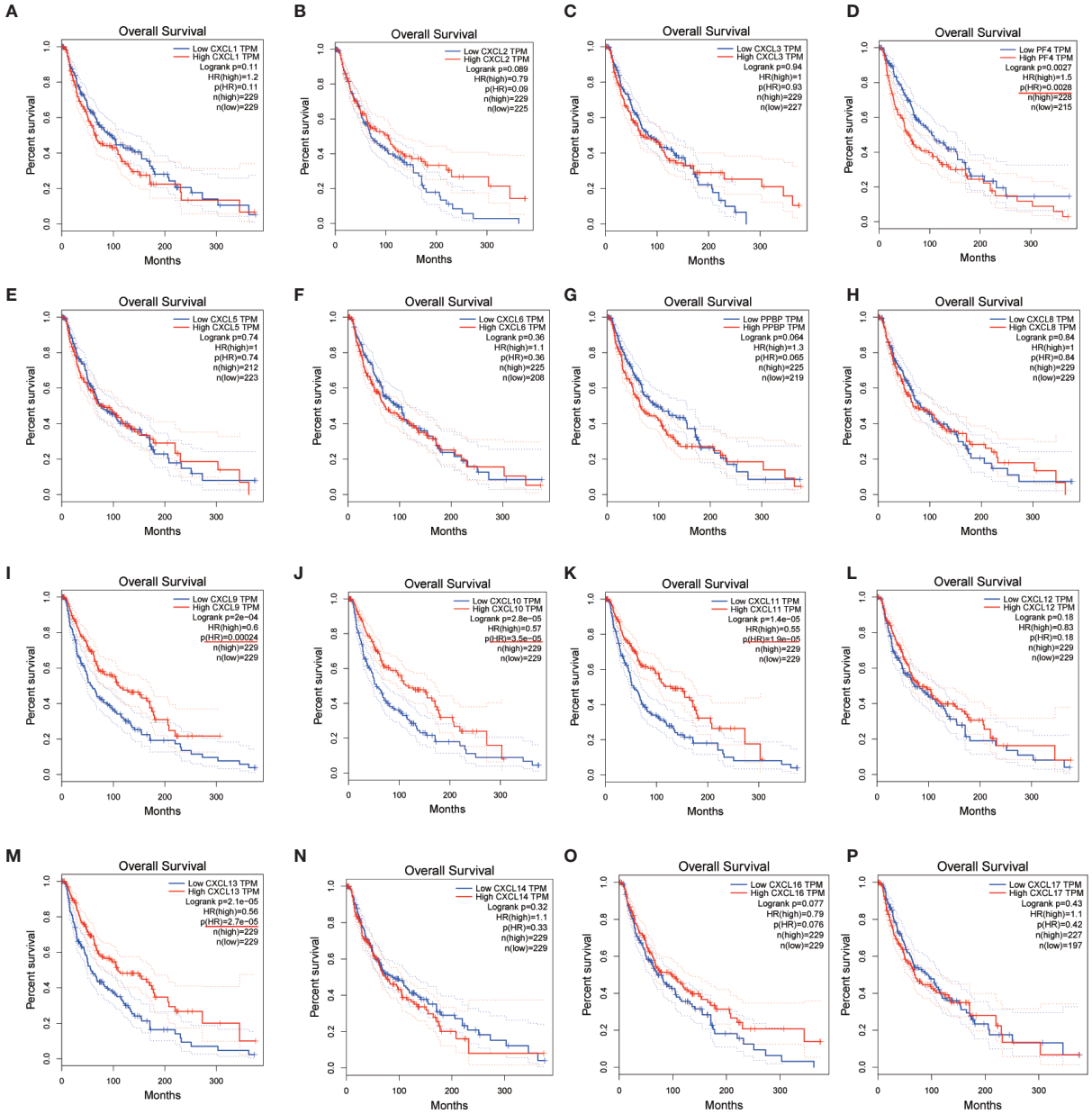

FIGURE 6 | The prognostic value of CXC chemokines in SKCM patients in the overall survival curve **(A–P)** (GEPIA).

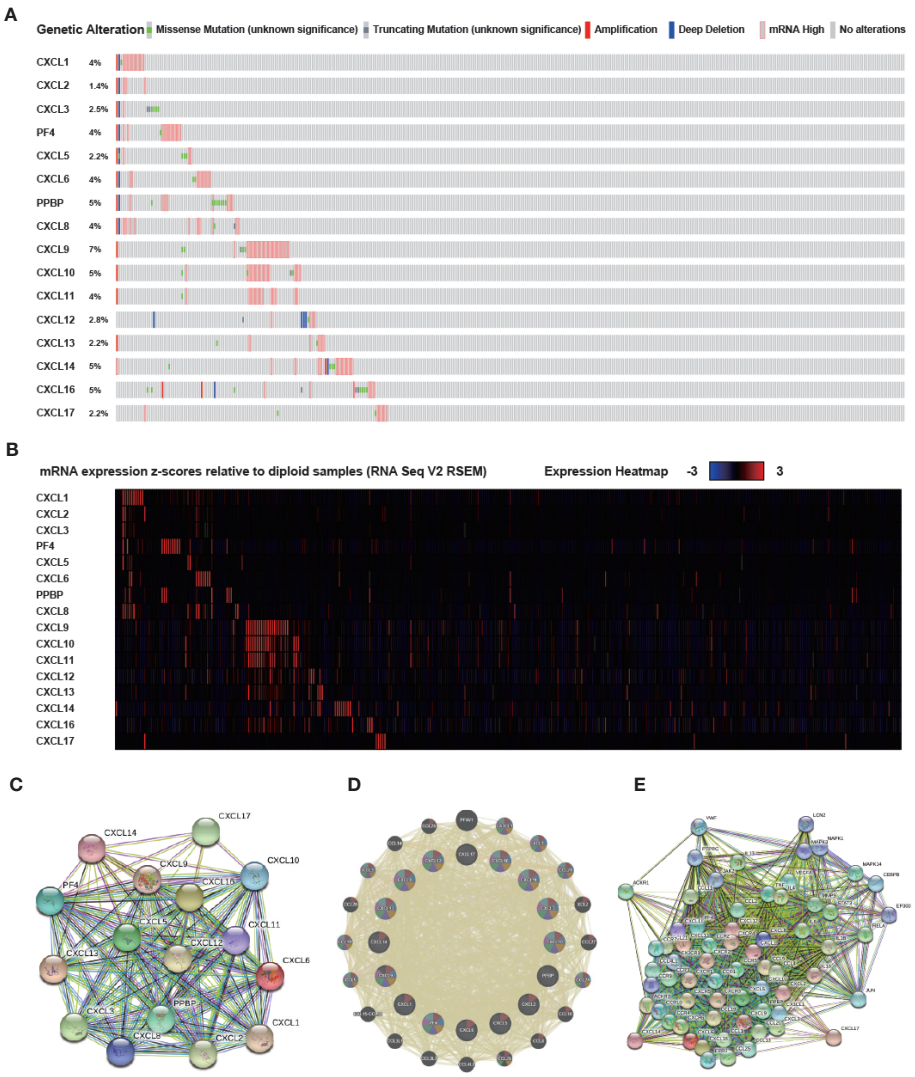

FIGURE 7 | Genetic alteration, mRNA expression, and interaction analyses of different expressed CXC chemokines in SKCM patients. **(A)** Summary of alterations in different expressed CXC chemokines in SKCM. **(B)** mRNA expression heat map of different expressed CXC chemokines in SKCM. **(C, D)** Protein-protein interaction network of different expressed CXC chemokines. **(E)** Gene-gene interaction network of different expressed CXC chemokines and 50 most frequently altered neighboring genes.

(COR = 0.143, *P* = 7.51e-03), CD8+ T cells (COR = 0.613, *P* = 4.29e-36), CD4+ T cells (COR = 0.244, *P* = 4.49e-06), Macrophage cells (COR = 0.226, *P* = 1.94e-05), Neutrophil cells (Cor = 0.697, *P* = 2.32E-52) and Dendritic cells (Cor = 0.614, P = 4.83e-37).

Similar results were found in CXCL11, CXCL12, CXCL13, CXCL14, and CXCL16. The upregulation of these CXC chemokines enhanced infiltration of B cells, CD8+ T cells, CD4+ T cells, Macrophage cells, Neutrophils cells, and Dendritic cells (**Figures 10H–L**). There is no linear correlation between CXCL17 and various immune cells in SKCM-primary and SKCM-metastasis patients. The confounding factors were corrected by using a Cox proportional hazard model. Macrophage (P = 0.055), CXCL2 (P = 0.051), CXCL14 (P = 0.075), and CXCL17 (P = 0.018) were closed related to the clinical outcome of SKCM patients (b).

Validation of CXC Chemokines in Clinical Samples

To further determine which genes might play a significant role in the progression of SKCM, real-time PCR was used to detect the expression of CXC chemokines using clinical samples, including CXCL1, CXCL2, CXCL3, CXCL4, CXCL5, CXCL6, CXCL7, CXCL8, CXCL9, CXCL10, CXCL11, CXCL12, CXCL13, CXCL14, CXCL16, and CXCL17 (**Figures 11A–P**). The analysis results showed that CXCL1, CXCL5, CXCL8, CXCL9, CXCL10, and CXCL13 were usually upregulated in SKCM tissues comparing to normal skin tissues, which is consistent

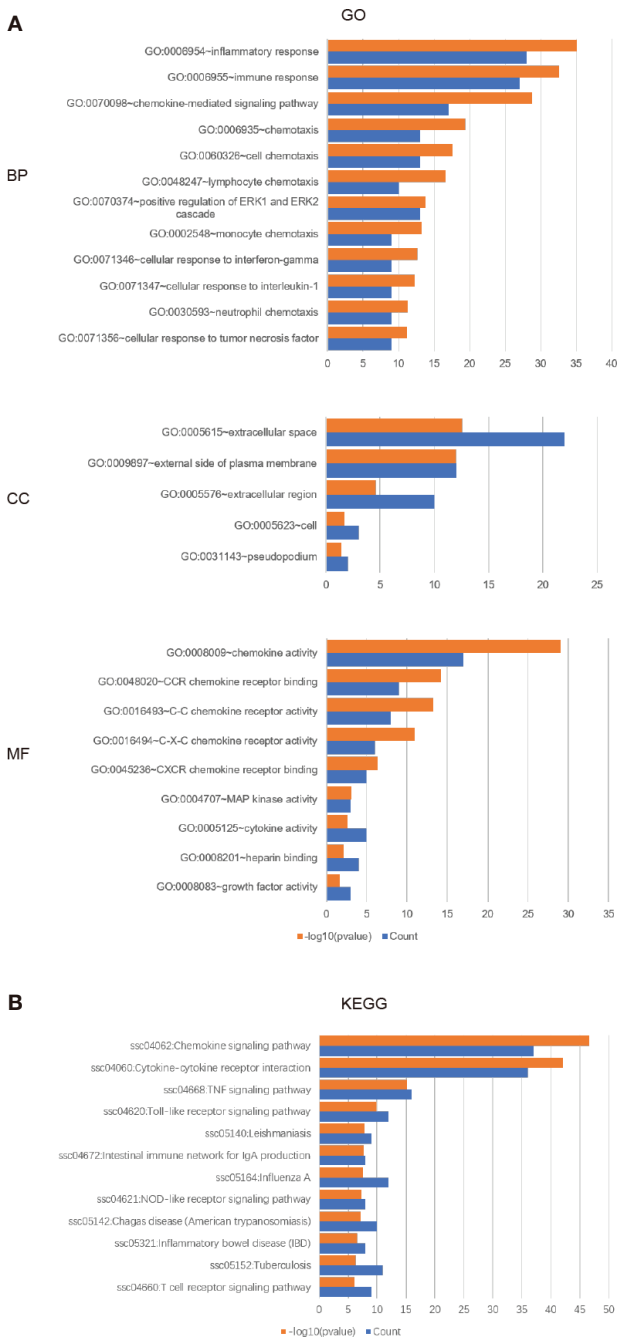

FIGURE 8 | The enrichment analysis of different expressed CXC chemokines and 50 most frequently altered neighboring genes in SKCM (David 6.8). **(A)** Bar plot of GO enrichment in biological process terms, cellular component terms, and molecular function terms. **(B)** Bar plot of KEGG enriched terms.

with the results of bioinformatics analysis above. There was no significant difference in CXCL2, CXCL3, CXCL4, CXCL6, CXCL7, CXCL11, CXCL12, CXCL14, CXCL16, and CXCL17 between SKCM tissues and normal skin tissues, which is also consistent with the Oncomine analysis results.

DISCUSSION

Chemokines are tiny protein molecules whose main function is associated with inflammation and immunity (27). Chemokines have been divided into five main subfamilies: CXC, CC, CX3C, XC, and CX (28). CXC chemokines occupy a vital position in the chemokine family. They have been classified into ELR + CXC and ELR − CXC according to the motif with or without Glu leu-ARG (ELR) (29). Chemokine receptors are G-protein-coupled transmembrane receptors that mediate the function of chemokines and contain 7 transmembrane regions (30, 31). CXC chemokines and their receptors are expressed in a variety of cells and play an important role in the generation, differentiation, development regulation, immune response regulation of immune cells, and bone marrow hematopoietic cells (32). They can promote angiogenesis, tumor cell proliferation, survival, and dissemination. They also participate in the process of organ-specific metastasis of malignant tumors and play an important role in the occurrence and development of tumors (33, 34). However, there are few studies on the potential value of CXC's clinical diagnosis and treatment guidance in SKCM. Therefore, exploring the pathological and molecular mechanisms of CXC chemokines in SKCM is basis for clinical diagnosis and treatment.

To probe CXC chemokines and its relationship with the pathological stage in SKCM patients, mRNA analyses were performed for the 16 CXC chemokines using ONCOMINE and GEPIA. Among the 16 CXC chemokines, six chemokines (CXCL1, CXCL5, CXCL8, CXCL9, CXCL10, and CXCL13) were identified as being expression difference between SKCM patient tissues and normal tissues. ONCOMINE database analysis results showed that the expression levels of these six CXC chemokines in SKCM tissues were significantly higher than that in normal tissues. Further validation by clinical samples, the mRNA level of CXCL1, CXCL5, CXCL8, CXCL9, CXCL10, and CXCL13 was considerably adjusted. One research has pointed out that CXCL1 down-regulation leads to reduced colorectal cell viability, invasion, and proliferation. *In vivo*, knockdown of CXCL1 resulted in the prevention of tumor growth in nude mice (35). CXCL1 promotes tumor growth through VEGF pathway activation and is associated with inferior survival in gastric cancer (36). Therefore, the high expression of CXCL1 might promote melanoma cell viability, invasion, and proliferation. Neutrophils may be the cause of elevated CXC5 expression in primary melanoma (37). The up-regulation of CXCL8 and its receptors CXCR1 and CXCR2 may be one of the reasons for the development of SKCM. CXCL8 promotes tumor angiogenesis by maintaining the proliferation and activity of endothelial cells, and CXCR1 and CXCR2 are the basis of this function (38). CXCL9 promotes the metastasis of melanoma cells through its combination with CXCR3 to enhance the permeability of tumor blood vessels (39). High expression of CXCL10 will inhibit the immune response mediated by T cells, leading to an increase in tumor growth rate (40). The CXCL13: CXCR5 axis is an fundamental regulatory component in the biological process of SKCM (41). Overall, these findings match the results of our data mining. Besides, GEPIA was used to explore whether there is a connection between CXC with the

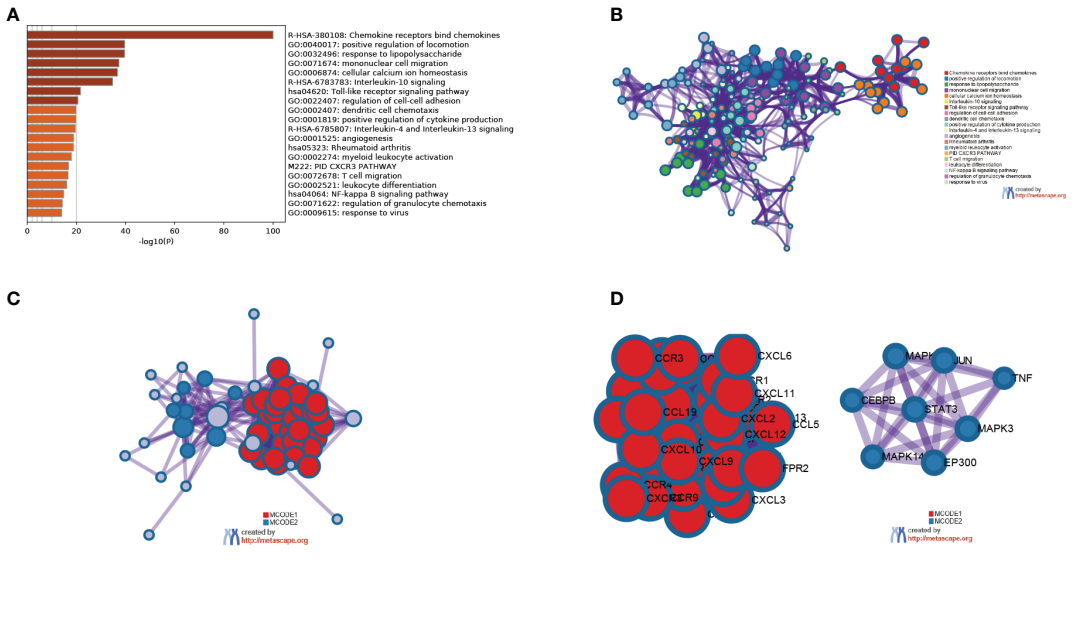

E

Color	MCODE	GO	Description	Log10(P)
	MCODE_1	R-HSA-380108	Chemokine receptors bind chemokines	-92.6
	MCODE_1	GO:0070098	chemokine-mediated signaling pathway	-80.8
	MCODE_1	GO:1990869	cellular response to chemokine	-79.1
	MCODE_2	hsa04657	IL-17 signaling pathway	-13.1
	MCODE_2	hsa04933	AGE-RAGE signaling pathway in diabetic complications	-13.0
	MCODE_2	hsa04668	TNF signaling pathway	-12.7

FIGURE 9 | The enrichment analysis of different expressed CXC chemokines and 50 most frequently altered neighboring genes in SKCM patients (Metascape). **(A)** Bar graph of top 20 enriched terms across different expressed CXC chemokines and 50 most frequently altered neighboring genes, colored by p-values. **(B)** Network of enriched terms, colored by cluster ID. **(C–E)** Protein–protein interaction network and MCODE components identified in different expressed CXC chemokines and 50 most frequently altered neighboring genes.

TABLE 2 | Key regulated factor of CXC chemokines in SKCM (TRRUST).

Key TF	Description	Regulated gene	*P*-value	FDR
RELA	v-rel reticuloendotheliosis viral oncogene homolog A (avian)	CXCL1, CXCL2, CXCL5, CXCL8, CXCL10, CXCL12	1.09E-07	1.71E-07
NFKB1	nuclear factor of kappa light polypeptide gene enhancer in B-cells 1	CXCL1, CXCL2, CXCL5, CXCL8, CXCL10, CXCL12	1.14E-07	1.71E-07
SP1	Sp1 transcription factor	CXCL1, CXCL5, CXCL14	0.00683	0.00683

survival rate in SKCM. The increased expression of six CXC chemokines (CXCL4, CXCL9, CXCL10, CXCL11, CXCL12, and CXCL13) was related to tumor progression. The SKCM patients with low expression of them had better overall survival. Previous studies have demonstrated that CXC chemokines may also play an important role in the progression of SKCM (42, 43).

The expression differences of CXC chemokines between primary SKCM and metastatic SKCM were explored by using UALCAN database. The result showed that CXCL1 and CXCL7 were higher in the primary SKCM than in the metastatic SKCM. One research indicates that primary melanoma cells might down-regulate the invasion activity of metastatic melanoma

TABLE 3 | The Kinase target networks of CXC chemokines in SKCM (LinkedOmics).

CXC chemokines	Enriched kinase target	Description	Leading EdgeNum	*P*-value
CXCL 1	Kinase_ROCK1	Rho associated coiled-coil containing protein kinase 1	14	0
	Kinase_RPS6KB1	ribosomal protein S6 kinase B1	8	0
CXCL 2	Kinase_LCK	LCK proto-oncogene, Src family tyrosine kinase	26	0
	Kinase_IKBKB	inhibitor of nuclear factor kappa B kinase subunit beta	8	0.0030030
CXCL 3	Kinase_MAPK12	mitogen-activated protein kinase 12	8	0.023569
	Kinase_MYLK	myosin light chain kinase	3	0.015936
CXCL 4	Kinase_PAK1	p21 (RAC1) activated kinase 1	19	0
(PF 4)	Kinase_MARK2	microtubule affinity regulating kinase 2	6	0
CXCL 5	Kinase_FER	FER tyrosine kinase	4	0.023256
	Kinase_JAK3	Janus kinase 3	4	0.034843
CXCL 6	Kinase_BCR	BCR, RhoGEF and GTPase activating protein	8	0.0031746
	Kinase_MAPK14	mitogen-activated protein kinase 14	26	0
CXCL 8	Kinase_ADRBK2	G protein-coupled receptor kinase 3	1	0.0042735
(IL 8)	Kinase_EIF2AK4	eukaryotic translation initiation factor 2 alpha kinase 4	2	0.058366
CXCL 9	Kinase_LCK	LCK proto-oncogene, Src family tyrosine kinase	24	0
	Kinase_SYK	spleen associated tyrosine kinase	17	0
CXCL 10	Kinase_LCK	LCK proto-oncogene, Src family tyrosine kinase	22	0
	Kinase_SYK	spleen associated tyrosine kinase	15	0
CXCL 11	Kinase_LCK	LCK proto-oncogene, Src family tyrosine kinase	20	0
	Kinase_SYK	spleen associated tyrosine kinase	16	0
CXCL 12	Kinase_LCK	LCK proto-oncogene, Src family tyrosine kinase	26	0
	Kinase_LYN	LYN proto-oncogene, Src family tyrosine kinase	23	0
CXCL 13	Kinase_LCK	LCK proto-oncogene, Src family tyrosine kinase	23	0
	Kinase_CSNK1E	casein kinase 1 epsilon	9	0
CXCL 14	Kinase_ATR	ATR serine/threonine kinase	21	0
	Kinase_PLK1	polo like kinase 1	45	0
CXCL 16	Kinase_LCK	LCK proto-oncogene, Src family tyrosine kinase	21	0
	Kinase_LYN	LYN proto-oncogene, Src family tyrosine kinase	23	0
CXCL 17	Kinase_ATR	ATR serine/threonine kinase	27	0
	Kinase_NEK2	NIMA related kinase 2	5	0

cells through CXCL1 signaling (44). Therefore, we speculated that the high expression of CXCL1 in primary SKCM can inhibit tumor metastasis. So far, no studies on CXCL7 in primary and metastatic SKCM have been found. The studies of other tumors showed that CXCL7 was closely related to tumor metastasis, and the high expression of CXCL7 would cause tumor metastasis. This contradicts the results of our analysis. There are two possible reasons for considering UALCAN database analysis results. The first reason is that the amount of data collected by the UALCAN database is insufficient, so there is a deviation in the analysis results. The second reason is that CXCL7 expression may be higher in primary SKCM than in metastatic SKCM, but there is no specific mechanism to explain. In the future study, samples will be collected for verification and related mechanism exploration.

As suggested by the results of the DAVID analysis, the CXC chemokines and 50 most closely interacting genes were enriched for the terms inflammatory response and immune response in the "biological process" category, the term extracellular space and external side of the plasma membrane in the "cellular component" category, chemokine activity and chemokine receptor binding in the "molecular function" category. The KEGG pathway analysis showed the enrichment of 50 most closely interacting genes for the terms of the chemokine signaling pathway, cytokine-cytokine receptor interaction, and TNF signaling pathway. The enrichment analysis results of Metascape were similar with DAVID. This is following the results reported before, which have shown that CXC chemokines signaling pathways occupy a mayor position in multiple biological activities of tumors (45, 46). A large number of clinical and epidemiological studies have shown that 15–20% of a malignant tumor is caused by infection and inflammation of the controllability, such as inflammatory bowel disease associated with colon cancer, chronic hepatitis B virus infection can lead to liver cancer, *Helicobacter pylori* infection was significantly associated with gastric cancer, EB virus infection can cause nasopharyngeal carcinoma, the human papillomavirus infection can cause cervical cancer or Burkitt lymphoma, *etc.* (47). Chronic inflammation is involved in the pathogenesis, development, invasion, and metastasis of malignant tumors (48). These results indicate that CXC chemokines regulate the progress of SKCM by regulating inflammation and immune responses.

TRRUST database was used to explore the transcription factor targets of CXC chemokines with different expressions. The analysis results showed that the transcription factors which play an important in regulating CXC chemokine are RELA, NFKB1, and SP1. NF-KB pathway was regulated by Phosphorylated RELA which is related to the course of tumor, and inflammation-related diseases (49). RELA has been shown to play a key role in mediating cancer-induced senescence in precancerous lesions (50). NF-kB1 inhibits the occurrence and development of a variety of cancers by reducing the overexpression of the NF-kB signaling pathway (51). Some research has showed that Sp1 is overexpressed in cancer cells and contributes to the formation of cancer (52). Inhibiting the expression level of Sp1 can significantly inhibit the proliferation

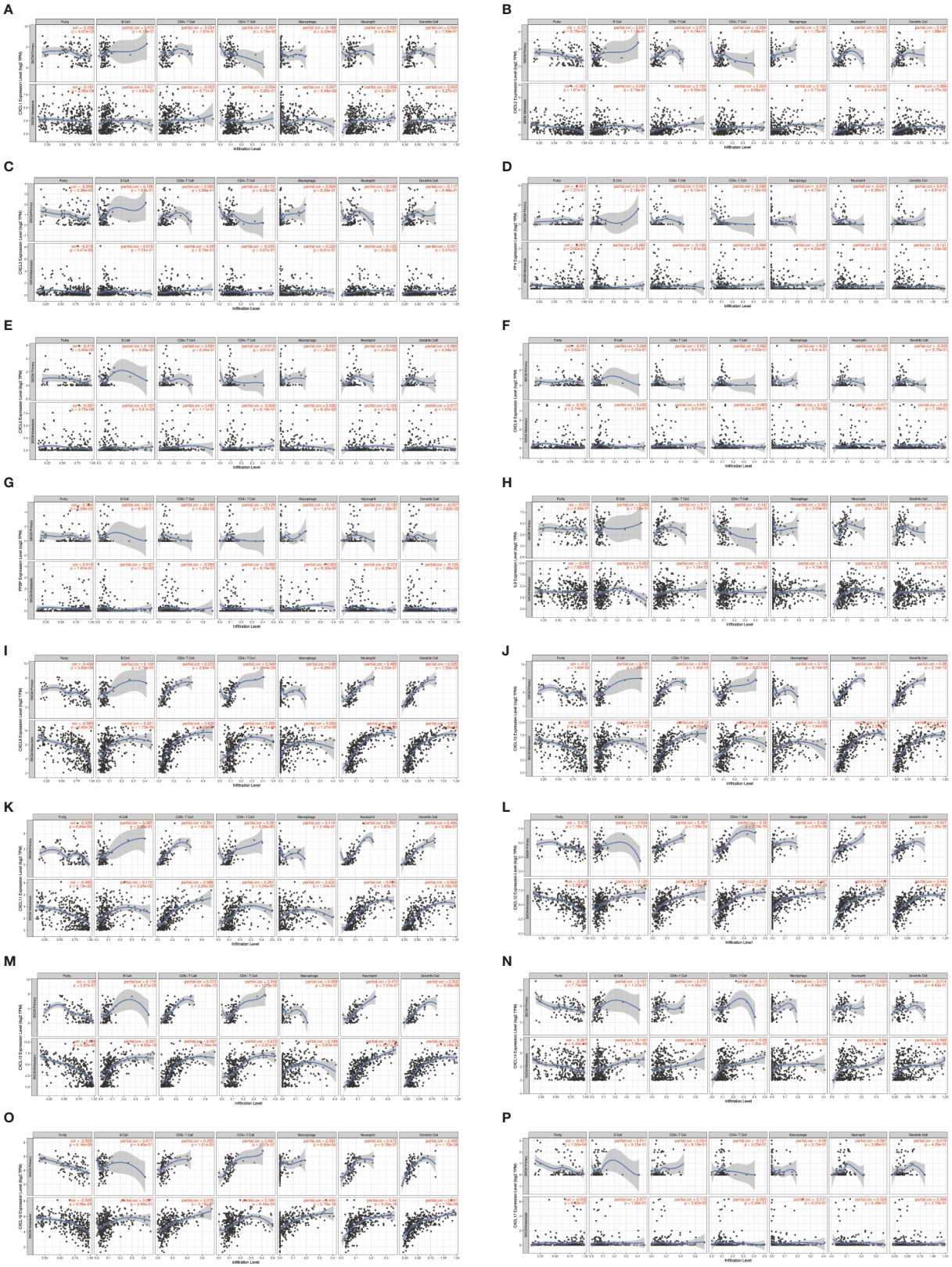

FIGURE 10 | The correlation between different expressed CXC chemokines and immune cell infiltration in primary and metastasis SKCM patients **(A–P)** (TIMER).

TABLE 4 | The Cox proportional hazard model of CXC chemokines and six tumor-infiltrating immune cells in SKCM (TIMER).

	coef	HR	95%CI_l	95% CI_u	*p*-value	sig
B_cell	−2.678	0.069	0.001	3.178	0.171	
CD8_Tcell	−0.137	0.872	0.070	10.780	0.915	
CD4_Tcell	2.554	12.859	0.409	403.809	0.146	
Macrophage	2.543	12.722	0.951	170.184	0.055	*
Neutrophil	−4.938	0.007	0.000	26.239	0.238	
Dendritic	−0.115	0.891	0.105	7.544	0.916	
CXCL1	0.060	1.062	0.946	1.193	0.310	
CXCL2	−0.319	0.727	0.528	1.001	0.051	*
CXCL3	0.104	1.109	0.725	1.697	0.633	
CXCL4	0.108	1.114	0.850	1.461	0.433	
CXCL5	0.093	1.098	0.930	1.296	0.269	
CXCL6	−0.077	0.926	0.693	1.236	0.600	
CXCL7	0.062	1.064	0.837	1.352	0.612	
CXCL8	0.089	1.093	0.975	1.224	0.127	
CXCL9	0.049	1.050	0.865	1.273	0.622	
CXCL10	−0.075	0.928	0.724	1.190	0.556	
CXCL11	−0.071	0.932	0.688	1.261	0.647	
CXCL12	−0.013	0.987	0.864	1.127	0.845	
CXCL13	0.013	1.013	0.880	1.166	0.858	
CXCL14	0.068	1.070	0.993	1.154	0.075	*
CXCL16	−0.145	0.865	0.726	1.031	0.105	
CXCL17	0.175	1.192	1.030	1.378	0.018	*

*$P < 0.05$.

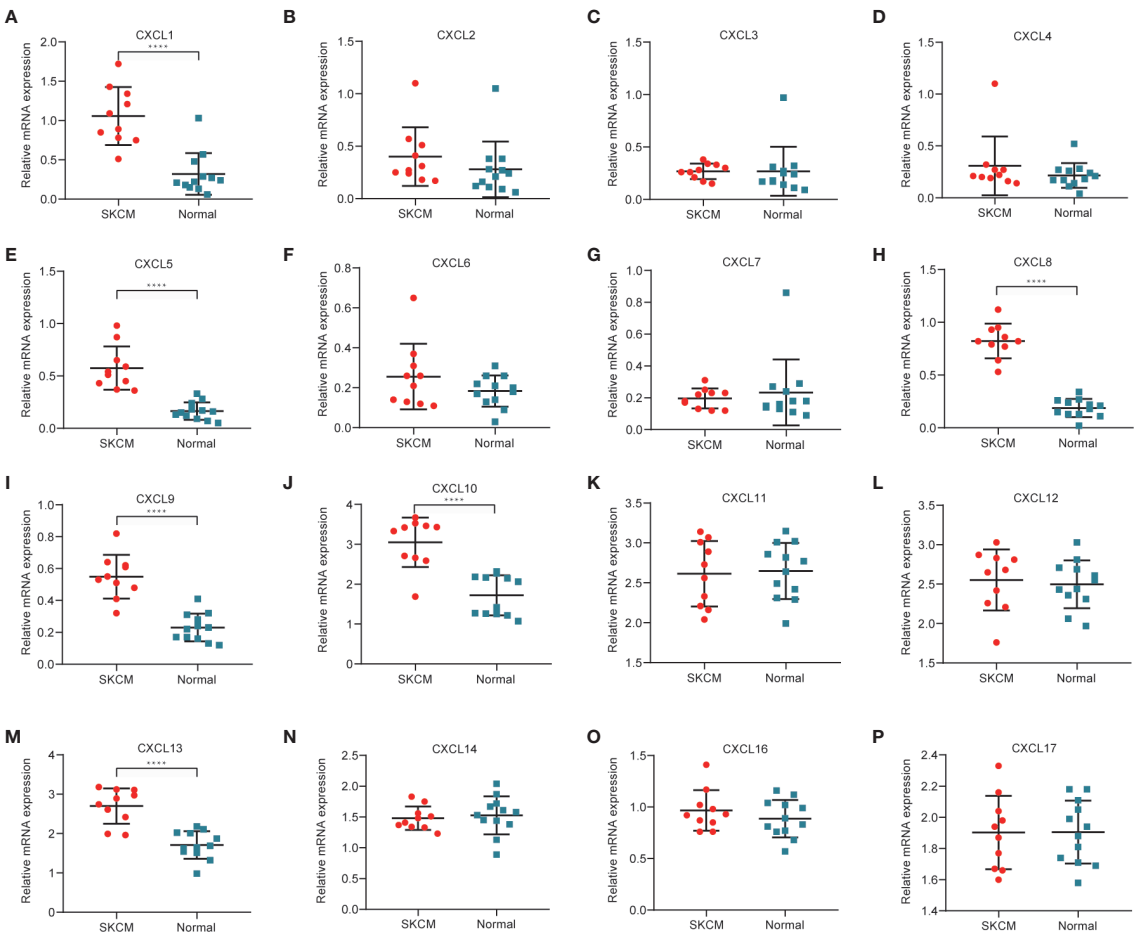

FIGURE 11 | Real-time qPCR validation of CXC chemokines in 10 SKCM and 12 normal skin tissues **(A–P)**. ****P < 0.05, analysis by non-paired tested.

of human malignant melanoma cells (53). The above results confirmed that RELA, NF-KB, and Sp1 play an important role in CXC chemokines regulation of SKCM. LinkedOmics database was applied to explore the kinase target networks of CXC chemokines in SKCM. The result suggested that LCK, LYN, FYN, MAPK1, MAPK3, and CSNK1D may be targets for differential expression of CXC chemokines. These kinases influence cancer formation and progress by modulating cancer cell migration, invasion, and apoptosis. The results of our observation indicated that these kinases were the important regulator of CXC chemokines in SKCM.

CXC chemokines can mediate the migration and localization of immune cells (54, 55). Timer database was applied to analyze the association between CXC chemokines and immune cells. There is growing confirmation showed that immune cell infiltration may influence cancer development and recurrence and is an important determinant of immunotherapy response and clinical outcome (56, 57). The results showed that CXC chemokines and immune cell infiltration levels were positively correlated in SKCM. Macrophage, CXCL2, CXCL14, and CXCL17 were closely related to the clinical outcome of SKCM patients. These strongly confirmed the positive correlation between CXC chemokines and immune infiltration in SKCM. Thus, it is likely that CXC chemokines not only as being diagnostic biomarkers but also affect the immune condition in SKCM.

There are some limitations in our research. Analysis of transcription can indicate immune condition but not integrated status. Also, vivo and vitro research should be conducted to verify our results. Our findings will offer new understanding to support the program of new immunotherapy, assist doctors select efficacious drugs and prognostic biomarkers for SKCM patients and identify biomarkers to precisely estimate prognosis.

DATA AVAILABILITY STATEMENT

The original contributions presented in the study are included in the article/**Supplementary Material**. Further inquiries can be directed to the corresponding authors.

AUTHOR CONTRIBUTIONS

Conceptualization, XX, WS, and XZZ. Data curation, MP, JP, and CW. Methodology, WS, XZ, and XZZ. Writing, WS, YH, and XZZ. All authors contributed to the article and approved the submitted version.

FUNDING

This work was supported by National Nature Science Foundation (No. 81974132, No. 81974134, and No. 81770927). Hunan province also provided financial support in the form of the Human Nature Science Foundation (No. 2018JJ2624).

SUPPLEMENTARY MATERIAL

The Supplementary Material for this article can be found online at: https://www.frontiersin.org/articles/10.3389/fonc.2021.619003/full#supplementary-material

Supplementary Table 1 | The primers used for quantitative RT-PCR.

REFERENCES

1. Bertolotto C. Melanoma: from melanocyte to genetic alterations and clinical options. *Sci (Cairo)* (2013) 2013:635203. doi: 10.1155/2013/635203
2. Gupta AK, Bharadwaj M, Mehrotra R. Skin Cancer Concerns in People of Color: Risk Factors and Prevention. *Asian Pac J Cancer Prev* (2016) 17:5257–64. doi: 10.22034/APJCP.2016.17.12.5257
3. Erdei E, Torres SM. A new understanding in the epidemiology of melanoma. *Expert Rev Anticancer Ther* (2010) 10:1811–23. doi: 10.1586/era.10.170
4. Ferlay J, Soerjomataram I, Dikshit R, Eser S, Mathers C, Rebelo M, et al. Cancer incidence and mortality worldwide: sources, methods and major patterns in GLOBOCAN 2012. *Int J Cancer* (2015) 136:E359–86. doi: 10.1002/ijc.29210
5. Goldstein AM, Tucker MA. Dysplastic nevi and melanoma. *Cancer Epidemiol Biomarkers Prev* (2013) 22:528–32. doi: 10.1158/1055-9965.EPI-12-1346
6. Satelli A, Li S. Vimentin in cancer and its potential as a molecular target for cancer therapy. *Cell Mol Life Sci* (2011) 68:3033–46. doi: 10.1007/s00018-011-0735-1
7. Martins-Green M, Petreaca M, Wang L. Chemokines and Their Receptors Are Key Players in the Orchestra That Regulates Wound Healing. *Adv Wound Care (New Rochelle)* (2013) 2:327–47. doi: 10.1089/wound.2012.0380
8. Miller MC, Mayo KH. Chemokines from a Structural Perspective. *Int J Mol Sci* (2017) 18:2. doi: 10.3390/ijms18102088
9. Chow MT, Luster AD. Chemokines in cancer. *Cancer Immunol Res* (2014) 2:1125–31. doi: 10.1158/2326-6066.CIR-14-0160
10. Barbieri F, Bajetto A, Florio T. Role of chemokine network in the development and progression of ovarian cancer: a potential novel pharmacological target. *J Oncol* (2010) 2010:426956. doi: 10.1155/2010/426956
11. Guan J, Gupta R, Filipp FV. Cancer systems biology of TCGA SKCM: efficient detection of genomic drivers in melanoma. *Sci Rep* (2015) 5:7857. doi: 10.1038/srep07857
12. Bailey MH, Tokheim C, Porta-Pardo E, Sengupta S, Bertrand D, Weerasinghe A, et al. Comprehensive Characterization of Cancer Driver Genes and Mutations. *Cell* (2018) 174:1034–5. doi: 10.1016/j.cell.2018.07.034
13. Danilova L, Wang H, Sunshine J, Kaunitz GJ, Cottrell TR, Xu H, et al. Association of PD-1/PD-L axis expression with cytolytic activity, mutational load, and prognosis in melanoma and other solid tumors. *Proc Natl Acad Sci U.S.A.* (2016) 113:E7769–77. doi: 10.1073/pnas.1607836113
14. Rhodes DR, Yu J, Shanker K, Deshpande N, Varambally R, Ghosh D, et al. ONCOMINE: a cancer microarray database and integrated data-mining platform. *Neoplasia* (2004) 6:1–6. doi: 10.1016/S1476-5586(04)80047-2
15. Chandrashekar DS, Bashel B, Balasubramanya SAH, Creighton CJ, Ponce-Rodriguez I, Chakravarthi B, et al. UALCAN: A Portal for Facilitating Tumor Subgroup Gene Expression and Survival Analyses. *Neoplasia* (2017) 19:649–58. doi: 10.1016/j.neo.2017.05.002
16. Tang Z, Kang B, Li C, Chen T, Zhang Z. GEPIA2: an enhanced web server for large-scale expression profiling and interactive analysis. *Nucleic Acids Res* (2019) 47:W556–60. doi: 10.1093/nar/gkz430
17. Szklarczyk D, Gable AL, Lyon D, Junge A, Wyder S, Huerta-Cepas J, et al. STRING v11: protein-protein association networks with increased coverage, supporting functional discovery in genome-wide experimental datasets. *Nucleic Acids Res* (2019) 47:D607–13. doi: 10.1093/nar/gky1131
18. Warde-Farley D, Donaldson SL, Comes O, Zuberi K, Badrawi R, Chao P, et al. The GeneMANIA prediction server: biological network integration for gene prioritization and predicting gene function. *Nucleic Acids Res* (2010) 38: W214–20. doi: 10.1093/nar/gkq537

19. Gao J, Aksoy BA, Dogrusoz U, Dresdner G, Gross B, Sumer SO, et al. Integrative analysis of complex cancer genomics and clinical profiles using the cBioPortal. *Sci Signal* (2013) 6:pl1. doi: 10.1126/scisignal.2004088
20. Li T, Fan J, Wang B, Traugh N, Chen Q, Liu JS, et al. TIMER: A Web Server for Comprehensive Analysis of Tumor-Infiltrating Immune Cells. *Cancer Res* (2017) 77:e108–10. doi: 10.1158/0008-5472.CAN-17-0307
21. Han H, Cho JW, Lee S, Yun A, Kim H, Bae D, et al. TRRUST v2: an expanded reference database of human and mouse transcriptional regulatory interactions. *Nucleic Acids Res* (2018) 46:D380–6. doi: 10.1093/nar/gkx1013
22. Huang da W, Sherman BT, Lempicki RA. Systematic and integrative analysis of large gene lists using DAVID bioinformatics resources. *Nat Protoc* (2009) 4:44–57. doi: 10.1038/nprot.2008.211
23. Zhou Y, Zhou B, Pache L, Chang M, Khodabakhshi AH, Tanaseichuk O, et al. Metascape provides a biologist-oriented resource for the analysis of systems-level datasets. *Nat Commun* (2019) 10:1523. doi: 10.1038/s41467-019-09234-6
24. Riker AI, Enkemann SA, Fodstad O, Liu S, Ren S, Morris C, et al. The gene expression profiles of primary and metastatic melanoma yields a transition point of tumor progression and metastasis. *BMC Med Genomics* (2008) 1:13. doi: 10.1186/1755-8794-1-13
25. Haqq C, Nosrati M, Sudilovsky D, Crothers J, Khodabakhsh D, Pulliam BL, et al. The gene expression signatures of melanoma progression. *Proc Natl Acad Sci U.S.A.* (2005) 102:6092–7. doi: 10.1073/pnas.0501564102
26. Talantov D, Mazumder A, Yu JX, Briggs T, Jiang Y, Backus J, et al. Novel genes associated with malignant melanoma but not benign melanocytic lesions. *Clin Cancer Res* (2005) 11:7234–42. doi: 10.1158/1078-0432.CCR-05-0683
27. Sokol CL, Luster AD. The chemokine system in innate immunity. *Cold Spring Harb Perspect Biol* (2015) 7:13. doi: 10.1101/cshperspect.a016303
28. Vilgelm AE, Richmond A. Chemokines Modulate Immune Surveillance in Tumorigenesis. *Metastasis Response to Immunother Front Immunol* (2019) 10:333. doi: 10.3389/fimmu.2019.00333
29. Boshagh MA, Foroutan P, Moloudi MR, Fakhari S, Malakouti P, Nikkhoo B, et al. ELR positive CXCL chemokines are highly expressed in an animal model of ulcerative colitis. *J Inflammation Res* (2019) 12:167–74. doi: 10.2147/JIR.S203714
30. Lodowski DT, Palczewski K. Chemokine receptors and other G protein-coupled receptors. *Curr Opin HIV AIDS* (2009) 4:88–95. doi: 10.1097/COH.0b013e3283223d8d
31. Stone MJ, Hayward JA, Huang C, Huma ZE, Sanchez J. Mechanisms of Regulation of the Chemokine-Receptor Network. *Int J Mol Sci* (2017) 18:13. doi: 10.3390/ijms18020342
32. Hughes CE, Nibbs RJB. A guide to chemokines and their receptors. *FEBS J* (2018) 285:2944–71. doi: 10.1111/febs.14466
33. Keeley EC, Mehrad B, Strieter RM. CXC chemokines in cancer angiogenesis and metastases. *Adv Cancer Res* (2010) 106:91–111. doi: 10.1016/S0065-230X(10)06003-3
34. Singh S, Sadanandam A, Singh RK. Chemokines in tumor angiogenesis and metastasis. *Cancer Metastasis Rev* (2007) 26:453–67. doi: 10.1007/s10555-007-9068-9
35. Bandapalli OR, Ehrmann F, Ehemann V, Gaida M, Macher-Goeppinger S, Wente M, et al. Down-regulation of CXCL1 inhibits tumor growth in colorectal liver metastasis. *Cytokine* (2012) 57:46–53. doi: 10.1016/j.cyto.2011.10.019
36. Wei ZW, Xia GK, Wu Y, Chen W, Xiang Z, Schwarz RE, et al. CXCL1 promotes tumor growth through VEGF pathway activation and is associated with inferior survival in gastric cancer. *Cancer Lett* (2015) 359:335–43. doi: 10.1016/j.canlet.2015.01.033
37. Forsthuber A, Lipp K, Andersen L, Ebersberger S, Grana C, Ellmeier W, et al. CXCL5 as Regulator of Neutrophil Function in Cutaneous Melanoma. *J Invest Dermatol* (2019) 139:186–94. doi: 10.1016/j.jid.2018.07.006
38. Singh S, Singh AP, Sharma B, Owen LB, Singh RK. CXCL8 and its cognate receptors in melanoma progression and metastasis. *Future Oncol* (2010) 6:111–6. doi: 10.2217/fon.09.128
39. Amatschek S, Lucas R, Eger A, Pflueger M, Hundsberger H, Knoll C, et al. CXCL9 induces chemotaxis, chemorepulsion and endothelial barrier disruption through CXCR3-mediated activation of melanoma cells. *Br J Cancer* (2011) 104:469–79. doi: 10.1038/sj.bjc.6606056
40. Gorbachev AV, Kobayashi H, Kudo D, Tannenbaum CS, Finke JH, Shu S, et al. CXC chemokine ligand 9/monokine induced by IFN-gamma production by tumor cells is critical for T cell-mediated suppression of cutaneous tumors. *J Immunol* (2007) 178:2278–86. doi: 10.4049/jimmunol.178.4.2278
41. Kazanietz MG, Durando M, Cooke M. CXCL13 and Its Receptor CXCR5 in Cancer: Inflammation, Immune Response, and Beyond. *Front Endocrinol (Lausanne)* (2019) 10:471. doi: 10.3389/fendo.2019.00471
42. Xiong TF, Pan FQ, Liang Q, Luo R, Li D, Mo H, et al. Prognostic value of the expression of chemokines and their receptors in regional lymph nodes of melanoma patients. *J Cell Mol Med* (2020) 24:3407–18. doi: 10.1111/jcmm.15015
43. Lazennec G, Richmond A. Chemokines and chemokine receptors: new insights into cancer-related inflammation. *Trends Mol Med* (2010) 16:133–44. doi: 10.1016/j.molmed.2010.01.003
44. Hatano T, Yashiro M, Fujikawa H, Motomura H. C-X-C Motif Ligand 1 (CXCL1) from melanoma cells down-regulates the invasion of their metastatic melanoma cells. *Oncotarget* (2018) 9:31090–7. doi: 10.18632/oncotarget.25783
45. Grivennikov SI, Greten FR, Karin M. Immunity, inflammation, and cancer. *Cell* (2010) 140:883–99. doi: 10.1016/j.cell.2010.01.025
46. Sarvaiya PJ, Guo D, Ulasov I, Gabikian P, Lesniak MS. Chemokines in tumor progression and metastasis. *Oncotarget* (2013) 4:2171–85. doi: 10.18632/oncotarget.1426
47. Axelrad JE, Lichtiger S, Yajnik V. Inflammatory bowel disease and cancer: The role of inflammation, immunosuppression, and cancer treatment. *World J Gastroenterol* (2016) 22:4794–801. doi: 10.3748/wjg.v22.i20.4794
48. Multhoff G, Molls M, Radons J. Chronic inflammation in cancer development. *Front Immunol* (2011) 2:98. doi: 10.3389/fimmu.2011.00098
49. Hoesel B, Schmid JA. The complexity of NF-kappaB signaling in inflammation and cancer. *Mol Cancer* (2013) 12:86. doi: 10.1186/1476-4598-12-86
50. Lesina M, Wormann SM, Morton J, Diakopoulos KN, Korneeva O, Wimmer M, et al. RelA regulates CXCL1/CXCR2-dependent oncogene-induced senescence in murine Kras-driven pancreatic carcinogenesis. *J Clin Invest* (2016) 126:2919–32. doi: 10.1172/JCI86477
51. Xia Y, Shen S, Verma IM. NF-kappaB, an active player in human cancers. *Cancer Immunol Res* (2014) 2:823–30. doi: 10.1158/2326-6066.CIR-14-0112
52. Hsu TI, Wang MC, Chen SY, Yeh YM, Su WC, Chang WC, et al. Sp1 expression regulates lung tumor progression. *Oncogene* (2012) 31:3973–88. doi: 10.1038/onc.2011.568
53. Bang W, Jeon YJ, Cho JH, Lee RH, Park SM, Shin JC, et al. beta-lapachone suppresses the proliferation of human malignant melanoma cells by targeting specificity protein 1. *Oncol Rep* (2016) 35:1109–16. doi: 10.3892/or.2015.4439
54. Stein JV, Nombela-Arrieta C. Chemokine control of lymphocyte trafficking: a general overview. *Immunology* (2005) 116:1–12. doi: 10.1111/j.1365-2567.2005.02183.x
55. Griffith JW, Sokol CL, Luster AD. Chemokines and chemokine receptors: positioning cells for host defense and immunity. *Annu Rev Immunol* (2014) 32:659–702. doi: 10.1146/annurev-immunol-032713-120145
56. Havel JJ, Chowell D, Chan TA. The evolving landscape of biomarkers for checkpoint inhibitor immunotherapy. *Nat Rev Cancer* (2019) 19:133–50. doi: 10.1038/s41568-019-0116-x
57. Zappasodi R, Merghoub T, Wolchok JD. Emerging Concepts for Immune Checkpoint Blockade-Based Combination Therapies. *Cancer Cell* (2018) 33:581–98. doi: 10.1016/j.ccell.2018.03.005

Conflict of Interest: The authors declare that the research was conducted in the absence of any commercial or financial relationships that could be construed as a potential conflict of interest.

frontiers in Oncology

REVIEW
published: 18 March 2021
doi: 10.3389/fonc.2021.645069

The Promise of Liquid Biopsy to Predict Response to Immunotherapy in Metastatic Melanoma

Luigi Fattore[1], Ciro Francesco Ruggiero[2], Domenico Liguoro[3], Vittorio Castaldo[3], Angiolina Catizone[4], Gennaro Ciliberto[5] and Rita Mancini[3]*

[1] SAFU Laboratory, Department of Research, Advanced Diagnostics and Technological Innovation, Translational Research Area, IRCCS Regina Elena National Cancer Institute, Rome, Italy, [2] Department of Experimental and Clinical Medicine, University "Magna Graecia" of Catanzaro, Catanzaro, Italy, [3] Department of Clinical and Molecular Medicine, Sapienza University of Rome, Rome, Italy, [4] Department of Anatomy, Histology, Forensic- Medicine and Orthopedics, Sapienza University of Rome, Rome, Italy, [5] Scientific Directorate, IRCSS Regina Elena National Cancer Institute, Rome, Italy

Metastatic melanoma is the deadliest form of skin cancer whose incidence has been rising dramatically over the last few decades. Nowadays, the most successful approach in treating advanced melanoma is immunotherapy which encompasses the use of immune checkpoint blockers able to unleash the immune system's activity against tumor cells. Immunotherapy has dramatically changed clinical practice by contributing to increasing long term overall survival. Despite these striking therapeutic effects, the clinical benefits are strongly mitigated by innate or acquired resistance. In this context, it is of utmost importance to develop methods capable of predicting patient response to immunotherapy. To this purpose, one major step forward may be provided by measuring non-invasive biomarkers in human fluids, namely Liquid Biopsies (LBs). Several LB approaches have been developed over the last few years thanks to technological breakthroughs that have allowed to evaluate circulating components also when they are present in low abundance. The elements of this so-called "circulome" mostly encompass: tumor DNA, tumor and immune cells, soluble factors and non-coding RNAs. Here, we review the current knowledge of these molecules as predictors of response to immunotherapy in metastatic melanoma and predict that LB will soon enter into routine practice in order to guide clinical decisions for cancer immunotherapy.

Keywords: melanoma, immunotherapy, drug resistance, liquid biopsy, biomarkers

OPEN ACCESS

Edited by:
Igor Puzanov,
University at Buffalo, United States

Reviewed by:
Pamela Bond Cassidy,
Oregon Health and Science University, United States
Ioana Cosgarea,
Newcastle University, United Kingdom

***Correspondence:**
Gennaro Ciliberto
gennaro.ciliberto@ifo.gov.it

Specialty section:
This article was submitted to Skin Cancer, a section of the journal Frontiers in Oncology

Received: *22 December 2020*
Accepted: *01 March 2021*
Published: *18 March 2021*

Citation:
Fattore L, Ruggiero CF, Liguoro D, Castaldo V, Catizone A, Ciliberto G and Mancini R (2021) The Promise of Liquid Biopsy to Predict Response to Immunotherapy in Metastatic Melanoma. Front. Oncol. 11:645069. doi: 10.3389/fonc.2021.645069

BACKGROUND

Melanoma is a highly malignant tumor originating from melanocytes and is characterized by high metastatic propensity and high mortality rates (1). The development of melanoma involves several dynamic processes in which the immune system plays a key role (2). It is well known that tumor cells activate different mechanisms to escape immune surveillance: a process known as "cancer-

Abbreviations: LB, liquid biopsy; PD-1, Programmed Cell Death Protein 1; PD-L1, Programmed Cell Death Ligand 1; ctDNA, circulating tumor DNA; ctRNA, circulating tumor RNA; CTCs, circulating tumor cell; EV, and extracellular vesicle; ICB, immune checkpoint blockers; cfDNA, cell-free DNA; ddPCR, Droplet Digital PCR; TMB, tumor mutation burden; OS, overall survival; PFS, progression free survival; MST, mixed solid tumors; LDH, Lactate Dehydrogenase; NLR, neutrophil-to-lymphocyte ratio; PBMC, peripheral blood mononuclear cell; HNSCC, head and neck squamous cell carcinoma; MDSC, myeloid-derived suppressor cell.

immunoevasion" (1). In this review, we will not probe into describing these complex processes that are the focus of several other excellent reviews (1, 3–6). The most effective therapeutic approach for advanced melanoma relies on the possibility to reactivate immune cells on recognizing tumor cells as foreign components and on controlling their growth. This concept lies at the basis of immuno-oncology. Historically, this approach has been pursued through the use of interferon and interleukin cytokines (like IL-2), but clinical benefits were very modest and laden by substantial toxicities (7). However, the experiences derived from those drugs paved the way for more successful immunotherapies. The first of them was the development of ipilimumab as an anti-CTLA-4 antibody which was then later on followed by the discovery of inhibitors of PD-1/PD-L1 receptor-ligand couple (3, 7). These monoclonal antibodies, initially nivolumab and pembrolizumab and subsequently atezolizumab and durvalumab, represent the main therapeutic breakthroughs over the last few years (8). These molecules have radically changed the therapeutic scenario contributing to increasing overall survival not only in patients with metastatic melanoma but also in a growing number of cancer types (3, 7, 9). Furthermore, due to their non-overlapping mechanisms of action, combinations of nivolumab together with ipilimumab led to longer progression-free survival and a higher proportion of objective response rate as compared to monotherapies (10, 11). Unfortunately, cancer immunotherapy with checkpoint inhibitors is efficacious only in a subset of cases because 40–60% of patients do not achieve any significant therapeutic benefit (12, 13). In this scenario, it would be important to develop biomarkers capable of predicting response to immunotherapy, also in light of the elevated costs as well as the high degree of toxicity and severe adverse events of this type of therapy. Furthermore, it is worth considering that the therapeutic landscape of metastatic melanoma has been also improved by the availability of target therapy based on the combination of BRAF and MEK inhibitors in approximately 50% of patients carrying mutations in the amino acid V600 of the BRAF oncogene (14). Hence, in this subset of patients the choice of first line therapy, i.e. target therapy with BRAFi/MEKi vs. immunotherapy is still highly debated. These lines of evidence taken together stress the need to identify novel biomarkers that are able to predict the response to a given treatment. In the last few years, the use of liquid biopsies has provided major opportunities(LBs) (15, 16). LBs are a non-invasive approach which agreeably complement tumor biopsies in acquiring important information about tumor progression and response to therapy. Among the main advantages of LBs there is the possibility to follow disease evolution over time by collecting longitudinal sampling during the course of disease as well as during therapy. LBs can be represented by several human fluids, among them the most commonly evaluated is the blood (17). They are a source of different biological circulating tumor elements (defined "circulome") that include proteins, circulating tumor DNA and RNA (ctDNA and ctRNA), circulating tumor cells (CTCs) and extracellular vesicles (EVs) (18, 19). Interestingly, these elements could derive from cancer cells themselves as well as from the tumor microenvironment. During the last few years thanks to significant technological advances and improvements in sensitivity, LBs have become a valuable tool from both diagnostic and prognostic points of view not only in melanoma but also across other cancer types. In this narrative review, we will focus on the state-of-the-art of liquid biopsies as predictors of response to immunotherapy in metastatic melanoma. In particular, we will focus on three main aspects a) circulating tumors DNA, b) circulating tumor cells (CTCs)/immune cells and soluble factors and c) non coding RNAs. These analytes are represented in **Figure 1**.

CIRCULATING TUMOR DNA (ctDNA)

ctDNA is one of the most reliable biomarkers available in LBs (20) and its potential to predict response to immune checkpoint blockers (ICB) in melanoma has been investigated in several relevant studies over the last few years. They will be summarized in this section. From a biological point of view, ctDNA is constituted by DNA fragments released into the bloodstream by apoptotic or necrotic cancer cells and its amount in general adequately correlates with tumor stage and prognosis (21–24). The absolute amount of ctDNA varies along with the number of cancer cells and the total tumor burden. Furthermore, its evaluation is able to provide information on the genetic

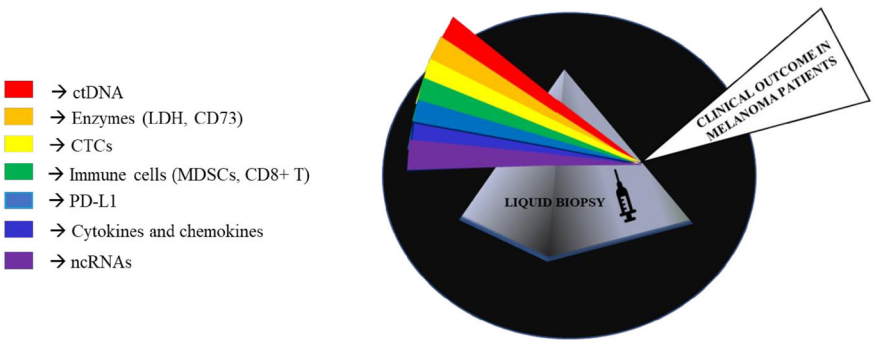

FIGURE 1 | Representative image of non-invasive biomarkers available in liquid biopsies to manage metastatic melanoma.

mutational profile of the tumor and can be a mirrored image of the heterogeneous complexity of advanced metastatic cancer (20). Besides ctDNA, the presence of cell-free DNA (cfDNA), a broader term that describes DNA that circulates freely in the bloodstream, but is not necessarily of tumor origin must also be reported (25). However, the evaluation of cfDNA, unlike ctDNA has not yet been considered a prognostic parameter *per se*.

The dosage of ctDNA has been made possible in the last decade thanks to modern advances in genomic and non-genomic technologies. One of the main issues to overcome is the limitation to detect ctDNA concentrations that are in general very low in the blood. In recent years, very sensitive multi-gene testing panels have been developed to measure ctDNA in LBs. Recently the FoundationOne Liquid CDx (https://www.foundationmedicine.com/test/foundationone-liquid-cdx) and Guardant360 CDx (https://guardant360cdx.com/) have recently been approved by the FDA for comprehensive tumor mutation profiling across solid cancers through LB sampling (26). In addition to large NGS panels, one of the most reliable methods in detecting ctDNA is through the use of Droplet Digital PCR (ddPCR) (27). This technology is able to provide ultrasensitive and absolute nucleic acid quantification and is particularly useful for low-abundant targets and for the design of patient-specific customized tests. Nowadays, the most accepted metric system for measuring ctDNA in LBs is to assess tumor-specific variant as copies/ml plasma through ddPCR.

Another potential biomarker of response to immunotherapy in melanoma is the emerging tumor mutation burden (TMB). This arises from the assumption that melanoma carries one of the highest mutational loads among human tumors. Even though TMB has been proposed as an independent predictor of response to immunotherapy (28), the most promising results have been obtained in combination with plasmatic ctDNA evaluation. This was the focus of the following study. In particular, it has taken advantage of a tumor panel comprised of 710 tumor-associated genes to reliably calculate TMB in liquid biopsies deriving from 35 melanoma patients treated with ipilimumab (as anti-CTLA-4) and nivolumab (as anti-PD-1) (27). The patients enrolled in this prospective study were almost equally divided into BRAF mutated (n=16) and BRAF wild type (n=19). The results demonstrated that TMB in the tumor biopsy was significantly higher (TMB > 23.1 Mut/Mb) in responders than in non-responders (TMB ≤ 23.1 Mut/Mb) before starting therapy (27). Furthermore, the same authors also evaluated TMB in combination with ctDNA (measured as copies/ml plasma) in the same experimental cohort. Their results demonstrated that the simultaneous reduction of both these parameters after 3 weeks of starting treatment was able to better distinguish patients who respond to combined immunotherapy (27). In particular, these authors measured as ctDNA markers not only mutated driver genes such as BRAF and NRAS, but also additional somatic variants like CDK4, GNAQ, STAT1 and others. It is important to point out that one limitation of this study relies on the fact that only a part of the patients enrolled (i.e. 63%) had ipilimumab or nivolumab as their first line systemic treatment whereas 13 patients received targeted therapy or PD-1 antibodies before.

The importance of ctDNA in predicting response to immunotherapy has also been demonstrated in another prospective study carried out by Seremet and colleagues (29). This study tested plasma samples from 85 patients undergoing anti-PD-1 therapy evaluating $BRAF^{V600E/K}$ or $NRAS^{Q61/G12/G13}$ in ctDNA (copies/ml plasma). Patients with undetectable ctDNA at baseline showed a better overall and progression free survival (OS and PFS) as compared to those patients with detectable ctDNA (29). Along the same line, another prospective study demonstrated that the assessment of ctDNA at baseline and during therapy was predictive for tumor response and clinical outcome in metastatic melanoma patients with a $BRAF^{V600E/K}$ or $NRAS^{Q61/G12/G13}$ mutation. In particular, the levels of ctDNA were evaluated in a prospective cohort of 40 advanced melanoma patients subjected to PD-1 inhibitors alone or in combination with ipilimumab at baseline and early during therapy. The objective was to assess the potential of ctDNA in predicting response and clinical outcome. Results showed that patients with higher basal levels of ctDNA (copies/ml plasma) and a persistently elevated ctDNA levels during therapy had a worse progression free survival (PFS) and overall survival (OS) (30). Similar results were achieved also in another prospective study which evaluated the clinical validity of ctDNA before and during ICB treatment (i.e. pembrolizumab) as a prognostic and predictive tool (31). In this prospective phase II study, ctDNA was measured in five distinct cohorts of patients with advanced solid tumors such as high-grade serous ovarian cancer (HGSOC), malignant melanoma and mixed solid tumors (MST) (31). ctDNA levels were measured in 316 plasma samples before (at basal levels) and during treatment with pembrolizumab. In particular, an early reduction in ctDNA (measured as mean tumor molecules per mL of plasma; MTM/mL) after two cycles of pembrolizumab and on-treatment ctDNA clearance distinguished patients with good prognosis independently from tumor types.

Along the same line, another study (32) assessed the levels of ctDNA ($BRAF^{mut}$ or $NRAS^{mut}$) as an indicator of response during anti-PD-1 treatment. In particular, these authors observed that the reduction of ctDNA levels in the blood after 2-3 weeks upon the first administration of nivolumab predicted the best response. In contrast, the anti-PD-1 antibody was ineffective in those patients where ctDNA did not decrease after starting treatment (32). This study also highlighted how ctDNA is a better predictor of response to therapy compared to other well-known clinical parameters such as Lactate Dehydrogenase (LDH).

Altogether these studies clearly demonstrated that ctDNA is a novel parameter in assessing response to immunotherapy both at baseline and during treatment and pave the way to propose the clinical practice of the ctDNA-based surveillance in melanoma patients treated with immune-checkpoint inhibitors.

Finally, ctDNA is useful in addition to being a novel parameter for assessing response to targeted therapy (BRAF/MEK inhibitors). Indeed, several studies have demonstrated that the fluctuations of this biomarker were generally correlated with treatment response to such inhibitors (33, 34). For example,

Schreuer et al. analyzed $BRAF^{V600}$ ctDNA in liquid biopsies deriving from 36 melanoma patients before and during treatment with dabrafenib and trametinib. Most of these samples showed detectable levels of ctDNA at baseline (75%) which rapidly decreased upon initiating targeted therapy and became undetectable in about 50% of those patients after 6 weeks of treatment (34). Most importantly, 27 out of 36 patients underwent disease progression (PD) and this was associated with an increase of ctDNA levels.

In summary, the results of this section (also summarized in **Table 1**) if further validated in larger prospective Phase III studies, provide the rationale for monitoring ctDNA at basal level to better stratify melanoma patients capable of responding to immunotherapy or also during administration of checkpoint inhibitors in order to early identify non-responding patients and stop therapy.

CIRCULATING TUMOR CELLS (CTCs), SOLUBLE FACTORS AND IMMUNE CELLS

LBs can be interrogated both for cellular and non-cellular components which can be exploited as promising biomarkers for monitoring and predicting response to immunotherapy in metastatic melanoma. This paragraph will focus on these aspects.

CTCs are cells that derive from primary/metastatic tumor sites, whose presence within the peripheral blood can predict the development of new metastatic lesions (51). During the last few decades, CTCs demonstrated to be suitable non-invasive biomarkers for studying the response to different types of therapies in melanoma in several studies, including target therapies and immunotherapies. One must consider that CTC reliability is challenged by the lack of standardized methodologies for their evaluation as well as for inter-patient heterogeneity that is responsible for the different levels of detectability of these cells in the blood (52). The methods for CTCs enrichment from peripheral blood are mainly divided into two categories: 1) enrichment for physical properties, i.e. size, and 2) enrichment for specific markers (53). The first method is based on microfilters that separate CTCs from other blood cells such as leukocytes. This is the approach recently used by our group. Briefly, we took advantage of ScreenCell® size exclusion technology to isolate CTCs from blood samples taken from melanoma patients. In this way, cells entrapped on absorbent membrane can be processed by immunofluorescence for specific markers of interest. In our study, we demonstrated that increased phosphorylation of the ErbB3 receptor on CTC surface early occurs upon patient treatment with BRAFi and MEKi. Importantly, the activation of this receptor has been identified as an early mechanism of escape from therapies in melanoma. These findings open the possibility to further investigate the role of CTCs as predictors of response to targeted therapy (54).

The second approach to quantify CTCs was based on the detection of specific markers on their surface like MCSP, MCAM or MLANA (55). Taking advantage of this approach, CTCs were evaluated in the blood from a prospective cohort of 49 melanoma patients treated with immune checkpoint inhibitors (16 treated with ipilimumab, 33 with pembrolizumab). Interestingly, authors observed a strong decrease in CTC score within 7 weeks of therapy correlating with marked improvement in progression-free and overall survival (35).

Furthermore, the study of CTCs can also take advantage of the recent advent of genomic and non-genomic technologies in order to further increase sensitivity (55, 56). For example, in a recent study CTCs deriving from melanoma patients were identified using a multi-marker immunostaining panel for melanocytic proteins like gp100, S100 and MLANA. Thanks to this approach, CTCs were identified in the blood deriving from 52 melanoma patients who received immune checkpoints and their number positively correlated with high LDH levels. Thereby, authors designed a "disease outcome panel," in which "high-risk" and "low-risk" melanoma patient subgroups were defined. Accordingly, patients belonging to the first subgroup were characterized by worse disease-free and overall survival (36).

These findings suggest that a valuable tool for evaluating response to immune-checkpoint inhibitors is the association between CTCs and LDH. LDH evaluation in the blood is one of the longstanding biomarkers for cancer progression and response to therapy in human cancers (57). Recently, the levels of this enzyme have also been tested for predicting response to immunotherapy in melanoma. For instance, in the recent Checkmate-067 study, patients treated with nivolumab were still alive at 4 years if the baseline LDH values were lower than those compared to patients who had higher levels before starting therapy, showing a worse overall survival (58).

Even though a significant proportion (about 27%) of PD-L1 negative melanoma patients may benefit from anti-PD-1/PD-L1 antibodies (59), its evaluation through immunohistochemistry (IHC) from tissue sections has been historically considered one of the most valuable biomarkers capable of predicting response to immunotherapy (60). However, this practice is limited to the primary tumors rendering the longitudinal sampling to monitor disease progression and response to therapy very difficult.

From here on, a potential biomarker of response to anti-PD-1/anti-PD-L1 therapy can be considered the expression of PD-L1 on CTC surface, as proposed for breast cancer, non-small cell lung cancer (NCLS) and also metastatic melanoma (61, 62). Initial findings promoted the activation of prospective clinical trials testing PD-L1 expression on CTCs for monitoring the response to immune-checkpoint inhibitors. For instance, it has been demonstrated that melanoma patients with high levels of CTCs that are positive for PD-L1 had better progression-free survival (PFS) after treatment with pembrolizumab as compared to patients with high CTCs with low PD-L1 levels. Furthermore, in the same study it was also shown that the ratio of PD-L1+/PD-L1- CTCs decreases upon treatment in responder patients whereas increases or remains unchanged in most non-responders. These data suggest that the detection of those cells may help stratify responder and non-responder patients to immunotherapy (37). The limitation of this pioneering study is related to the small cohort of patients tested and highlights the

TABLE 1 | List of predictive biomarkers of response to immunotherapy in metastatic melanoma coming from liquid biopsies.

LIQUID BIOPSY SOURCE	REFERENCES	N° ENROLLED PATIENTS/ TREATMENTS	MARKERS	MAIN RESULTS
ctDNA	Forschner et al. (27)	- 35 treated with ipilimumab and nivolumab: - 16 BRAF mutated - 19 BRAF wild type	- *BRAF V600-* - *NRAS Q61-* - *CDK4, GNAQ, STAT1*	ctDNA levels is associated with tumor mutation burden (TMB)
ctDNA	Seremet et al. (29)	- 85 treated with pembrolizumab - 63 BRAF V600 mut - 22 NRAS mut	- *BRAF* V600E/K- - *NRAS* Q61/G12/G13	Undetectable pre-treatment ctDNA levels correspond to better OS and PFS
ctDNA	J H Lee et al. (30)	- 86 total: - 50 received anti PD-1 (pembrolizumab or nivolumab) - 36 received anti-PD1 + ipilimumab	- *BRAF* V600E/K- - *NRAS* Q61/G12/G13	Higher basal levels of ctDNA match up with poor prognosis
ctDNA	Bratman et al. (31)	- Pembrolizumab-treated Melanoma cohort (n=12)	- Personalized ctDNA based on 16 clonal somatic mutations	Baseline ctDNA levels correlate with PFS, OS, clinical response and clinical benefit
ctDNA	Ashida et al. (32)	5 treated with nivolumab: - 4 BRAF V600-mutated - 1 NRASQ61K	*BRAF* V600E/K NRAS Q61K	Reduction of ctDNA levels during treatment is predictive of best response to therapy
Circulating Tumor Cells	Hong et al. (35)	- 49 total - 33 treated with pembrolizumab - 16 treated with ipilimumab	Circulating tumor cells (CTCs) number	Low CTCs number during treatment improve PFS
Circulating Tumor Cells Soluble plasma protein	Lin et al. (36)	-52 total - 36 pembrolizumab - 5 ipilimumab - 8 nivolumab - 2 combination with ipilimumab/ nivolumab 1 – ipilimumab/ pembroluzumab	- CTCs number - Lactate dehydrogenase (LDH) levels	"Non-responders" patients are correlated to elevated CTCs number and LDH levels.
Circulating Tumor Cells	Khattak et al. (37)	- 40 treated with pembrolizumab	Identification of PDL-1 on CTCs	Melanoma patients with CTCs/PD-L1+ had better PFS in response to pembrolizumab
Soluble plasma proteins	Zhou et al. (38)	- 42 treated with ipilimumab plus bevacizumab - 23 ipilimumab - 35 pembrolizumab	Soluble PDL-1	Higher sPD-L1 levels at baseline had poorer in response to ipilimumab-based therapy.
Soluble plasma proteins	Weber et al. (39)	- 119 nivolumab treated melanoma patients - 101 nivolumab + pembrolizumab - 48 ipilimumab - 21 ipilimumab + nivolumab	209 circulating plasma protein. Most of which are involved in of acute phase of inflammation, complement activation and wound healing phenotypes.	High levels of identified 209 circulating plasma protein are correlated with worst response to immune-checkpoint inhibitors.
Soluble plasma proteins	Lim et al (40).	- 98total: - 40 anti-PD1 - 58 anti-CTLA-4 + anti-PD1	11 circulating cytokines (G-CSF, GM-CSF, Fractalkine, FGF-2, IFNα2, IL12p70, IL1a, IL1B, IL1RA, IL2, and IL13)	- Increased levels of 11 circulating cytokines are associated with the development of high-grade immune-related toxicity - TNF-a, IL-8 or IP-10 increase in non-responder patients to immunotherapy
Soluble plasma proteins	Sanmamed et al. (41)	- 29 treated with nivolumab and	IL-8	Increased levels of IL-8 match up with worst response to immunotherapy

(Continued)

TABLE 1 | Continued

LIQUID BIOPSY SOURCE	REFERENCES	N° ENROLLED PATIENTS/ TREATMENTS	MARKERS	MAIN RESULTS
		pembrolizumab - 19 treated with nivolumab and pembrolizumab		
Soluble plasma proteins	Morello et al. (42)	- 37 treated with nivolumab and ipilimumab	Soluble CD73	Elevated levels at baseline of CD73 correlate with lower response rate, shorter survival and higher rates of progression disease (PD)
Lymphocytes	Capone et al. (43)	- 100 nivolumab-treated melanoma patients	CD8+ CD73+ subset lymphocytes	High presence of CD8+CD73+ lymphocytes correlate with worse response to immunotherapy
Myeloid-derived suppressor cell (MDSc)	Meyer et al. (44)	- 49 treated with ipilimumab	Myeloid-derived suppressor cell (MDSc) levels	Lower baseline levels of MDSC correlate with better response to ipilimumab
Myeloid-derived suppressor cell (MDSc)	Tarhini et al. (45)	- 35 treated with ipilimumab	Myeloid-derived suppressor cell (MDSc) levels	Low MDSCs levels predicts better PFS after neoadjuvant ipilimumab treatment
Neutrophil and lymphocyte	Capone et al. (46)	- 97 treated with nivolumab	Neutrophil to lymphocyte ratio (NLR)	Elevated NLR at baseline was associated with worst OS, PFS, and clinical response to immunotherapy
Extracellular Vesicles (EVs) Non coding RNAs	Huber et al. (47)	87 total; - 49 received nivolumab or ipilimumab	miR-146a, miR-155, miR-125b, miR-100, let-7e, miR-125a, miR-146b, miR-99b	High levels of specific microRNAs signature is related to not response to immunotherapies
Exosomes Non coding RNAs	Vignard et al. (48)	No patients were enrolled	miR-181, miR-498	miR-181-miR-498 impact on immune response through TNFa down-regulation
Extracellular Vesicles (EVs) Non coding RNAs	Shi et al. (49)	- 50 treated with immune checkpoint inhibitors	miR-551a, miR-4519 and miR-4674	-High levels of miR-551a were found in extracellular vesicles (EVs) of non-responder patients - High levels miR-4519 and miR-4674 were found in EVs of responder patients to immunotherapy
Non coding RNAs	Bustos et al. (50)	- 47 total -31 received Anti-PD1 -16 received Anti-PD1 plus Anti-CTLA4	miR-4649-3p, miR-615-3p and miR-1234-3p, miR-615-3p	- miR-4649-3p, miR-615-3p and miR-1234-3p signature are up-regulated in responder patient - miR-615-3p increased levels correlate with progression disease (PD)

OS, Overall Survival; PFS, Progression Free Survival; PD, Progression Disease; CTCs, Circulating Tumor Cells; LDH, Lactate Dehydrogenase; MDSc, Myeloid-derived suppressor cells; EVs, Extracellular Vesicles.

need to strengthen those findings in larger studies. However, because CTCs are usually very rare, fragile and difficult to capture, PD-L1 assessment on their surface remains a technical challenge.

A second method used to evaluate PD-L1 as a biomarker of response to immunotherapy relies on the discovery of its existence in a soluble form in the blood, known as sPD-L1 (63). This molecule has been identified in different human cancers, including renal cell carcinoma, multiple myeloma, large B-cell lymphoma and also in melanoma (64–66). In this context, Zhou and colleagues have demonstrated that melanoma patients with higher sPD-L1 levels at baseline had poorer outcome as compared to those patients with moderate/low sPD-L1 in response to ipilimumab-based therapy (38). In this context, *in vitro* studies have highlighted that sPD-L1 retains the signaling domain necessary for interacting with PD-1 on T cells and delivering immune-inhibitory signals (67). This could be the reason why, in the same study, a further increase of sPD-L1 levels in the blood has been observed in those patients who did not respond to immunotherapy as compared to those that did (responders).

Besides PD-L1, also different chemokines and cytokines have been proposed to be able to predict response to immunotherapy in melanoma in LBs. For example, due to the use of MALDI-TOF mass spectroscopy, a panel of 209 serum proteins that are associated with a better response to immune-checkpoint inhibitors, nivolumab and pembrolizumab has been identified (39). These circulating proteins, such as C reactive protein, serum amyloid A and P and angiostatin A are the indicators of a massive involvement of acute phase response, inflammation, complement activation and wound healing.

The detection of specific chemokines and cytokines in the blood has also been correlated to immune-mediated toxicity, an adverse event that requires interrupting immunotherapy

treatment in melanoma patients. Along the same line, another study tested the expression levels of 65 cytokines in longitudinal plasma samples collected from melanoma patients treated with nivolumab or pembrolizumab alone or in combination with ipilimumab (40). Results showed that the increased levels of 11 circulating cytokines, such as IL1a, IL2, and IFNα2 were significantly associated with the development of high-grade immune-related toxicity. Furthermore, the same authors also demonstrated that other cytokines, like TNF-a, IL-8 or IP-10 increased their levels in the blood in patients who do not respond to immunotherapy as compared to those who did (responders).

The increased levels of IL-8 as a negative biomarker of response to either anti-PD-1 and anti-CTLA-4 was confirmed in another independent study carried out on metastatic melanoma (n=29) and NSCLC (n=19) patients (41).

Furthermore, recent studies have also focused on circulating levels of the CD73 enzyme which is expressed by different cellular populations of the tumor microenvironment such as the cancer cells themselves, endothelial and immune cells (68). This enzyme facilitates the establishment of a immunosuppressive tumor microenvironment inhibiting NK and T cell-mediated anti-tumor responses through producing extracellular adenosine (69). Increased levels of CD73 have been associated with worse prognosis in many types of cancers, including melanoma (70). In this context, a recent study has demonstrated that elevated serum levels at baseline of CD73 correlated with lower response rate, shorter survival and higher rates of progression disease in melanoma patients treated with nivolumab (42).

Besides non-cellular elements which circulate freely in the bloodstream a relevant prognostic role in cancer has certainly been attributed to the deregulation of specific immune subpopulation of cells. This suggests the possibility to evaluate them as predictors of response to immunotherapy as well.

In this regard, Capone and colleagues analyzed peripheral blood mononuclear cells (PBMCs) in samples deriving from 100 nivolumab-treated melanoma patients (43). Among the different subpopulation of immune cells tested, these authors identified CD8+/CD73+ subset of lymphocytes as the strongest associated with worse survival and poor clinical benefits. Indeed, their low baseline percentages were associated with clinical benefits and better survival as compared to non-responsive patients. Even though the biological role of CD8+/CD73+ lymphocytes in the immune response against melanoma cells during nivolumab treatment is still unknown, the expression of CD73 on T cells has been suggested capable of promoting an exhausted phenotype in pre-clinical mouse models of head and neck squamous cell carcinoma (HNSCC) (64). Another class of immune cells associated with the response to immunotherapy in melanoma is myeloid-derived suppressor cells (MDSCs). Ipilimumab-treated melanoma patients with better response to therapy have lower baseline levels of these cells compared to those that do not (non-responders) (44). Importantly, a reduction of MDSCs in the blood also predicts better progression-free survival after neoadjuvant ipilimumab treatment (45).

Finally, the potential consequences of immune-checkpoint inhibitor administration such as the cytotoxic effect as well as local and systemic inflammation should be considered (71). These events are frequently associated with alterations in peripheral blood leukocytes that can be highlighted by evaluating the neutrophil-to-lymphocyte ratio (NLR) (71). Various studies have highlighted that in patients with unresectable stage III-IV melanoma, elevated NLR at baseline was associated with worse overall survival, progression-free survival, and clinical response following ipilimumab and nivolumab treatments (46, 72). Altogether the findings reviewed in this paragraph strongly suggest that liquid biopsies based on the evaluation of cellular and non-cellular elements may be valuable tools in predicting response to immunotherapy in melanoma to the same extent as compared to ctDNA. The results described in this paragraph are schematically summarized in **Table 1**.

NON CODING RNAs (ncRNAs)

Over the last two decades ncRNAs have emerged as key players in the development of human cancers as well as in the establishment of resistance to several anticancer treatments (73–75). In this review, we will not discuss their biological roles as this topic has already been widely discussed in outstanding recent reviews (76, 77).

It is important to point out tha9t the development of ncRNA signatures in the blood is a more challenging field of research as compared to the other biomarkers already described in the previous sections. Some of the main limitations are due to three issues: 1) their low abundance in body fluids; 2) the difficulty in normalizing the results as there are no suitable endogenous ncRNAs that can be used as "housekeeping" reference analytes at the moment and 3) the great intra-patient variability limiting the possibility of finding consistency between biomarkers identified in different studies (78). However, it has to be considered that thanks to their great stability in body fluids, ncRNAs are emerging in several studies as novel potential biomarkers. A large part of these studies focused on the most abundant class of ncRNAs, namely microRNAs (miRNAs). The stability of these molecules in the blood is preserved by their association with proteins such as AGO1/AGO2, proteolipid complexes and above all extracellular vesicles (EVs) (79, 80).

EVs are broadly classified into four subtypes based upon vesicle size: 1) exosomes (30-150 nm), 2) microvesicles (50-1000 nm), 3) large vesicles (>1000 nm) and 4) apoptotic bodies (>1000 nm) (81). As to metastatic melanoma, most studies have assessed the role of miRNAs as predictors of response to targeted therapies in BRAF-mutant patients (82–85). For example, we have demonstrated that a mini-signature composed of four miRNAs, i.e. miR-199b-5p, miR-204-5p, miR-4443 and miR-4488, is able to distinguish drug-sensitive from drug-resistant patients (83). In contrast, much less is known about miRNAs as biomarkers of response to immunotherapy. For some time, the only data available focused on solid biopsies and provided only

indirect information about circulating biomarkers. For example, miR-17-5p levels were shown to be anti-correlated with those of PD-L1 in melanoma tissue biopsies from patients resistant to BRAFi or MEKi therapy (86). Likewise, plasma levels of this miRNA were shown to be higher in patients with PD-L1+ tissues as compared to PD-L1- 9lesions. Along the same line, the expression levels of the oncogenic miR-222 were shown to be higher in solid biopsies from melanoma patients who had no clinical benefit from ipilimumab as compared to patients who responded to such therapy (87). These findings suggest that miR-222 could be a biomarker for predicting response to anti-CTLA-4 checkpoint inhibitors. To the best of our knowledge, the first study demonstrating that a signature of circulating miRNAs is potentially able to predict response to immunotherapy in melanoma was performed by Huber and colleagues (47). These authors showed that a set of 8 miRNAs, i.e. miR-146a, miR-155, miR-125b, miR-100, let-7e, miR-125a, miR-146b, miR-99b are significantly higher in the plasma of patients who did not respond to immunotherapy (i.e. ipilimumab or nivolumab) as compared to responders. Interestingly, the same study also demonstrated that this signature of miRNAs correlated with increased levels of MDSCs in the blood of non-responding patients (47). The subpopulation of immune cells represents a major obstacle to effective immunotherapy in melanoma and is considered a valuable biomarker of response as well (see previous section). Afterwards, miRNA contents of melanoma-derived exosomes were correlated with response to immunotherapy. In taking advantage of flow cytometry and microscopy techniques, it was demonstrated that CD8+ T cells actively internalize specific miRNAs carried by melanoma exosomes (48). Among them, miR-3187-3p, miR-498 and miR-181a/b were found to be able to regulate TCR signaling and TNFa secretion reducing immune response against the tumor. These findings suggest that those miRNAs could be measured in the blood and potentially correlate with the response to immunotherapy in melanoma. Along the same line, a recent comprehensive transcriptomic profiling performed on plasma-derived extracellular vesicles (EVs) from 50 patients with metastatic melanoma underwent immunotherapy and were divided into responders (n= 33) and non-responders (n= 17) (49) 9. Results demonstrated that EVs deriving from non-responding patients are enriched for transcriptional signatures belonging to immune- and tumor-related pathways such as CD1A, MAP2K4, TRBV7-2 and IGFL1. In regards to the miRNA content, authors found some miRNAs enriched in the EVs from non-responding patients, such as miR-551a; in contrast, other miRNAs such as miR-4519 and miR-4674 were enriched in the EVs derived from responding patients (49). Finally, a pilot study identified a signature composed of three circulating miRNAs, namely miR-4649-3p, miR-615-3p and miR-1234-3p as potentially capable of distinguishing melanoma patients who better respond to immunotherapy (ipilimumab, nivolumab, pembrolizumab, or the combination of ipilimumab and nivolumab as first line therapy) (50). In particular, the levels of these miRNAs significantly decreased in the post-treatment samples derived from patients who had a complete response (CR) as compared to patients who progressed from immunotherapy. Interestingly, the increased levels of one of these miRNA, i.e. miR-615-3p showed a superior statistic capability in predicting PD in post-therapy plasma samples as compared to LDH levels (50).

Unlike miRNAs, the other classes of ncRNAs have not been studied as much as circulating biomarkers that predict cancer management and response to therapy. Emerging findings indicate that long non coding RNAs (lncRNAs) and circular RNAs (circRNAs) may be involved in resistance to immunotherapy because they regulate immune cell-specific gene signatures that mediate immune escape (11, 88, 89). However, up until now no studies have investigated their deregulation in liquid biopsies as predictors of response to checkpoint inhibitors in melanoma. So far only one study has tried to correlate lncRNA alterations to the prediction of immunotherapy response. This study used 9data available from The Cancer Genome Atlas (TCGA) belonging to bladder cancer and melanoma patients treated with immunotherapy for identifying lncRNA profiles associated with immune response (89). These bioinformatics analyses led to identifying a signature composed of 49 lncRNAs that are potentially capable of distinguishing cancer patients who benefit from immunotherapy. Among them, the low expression levels of a specific lncRNA, called NKILA were found to be able to

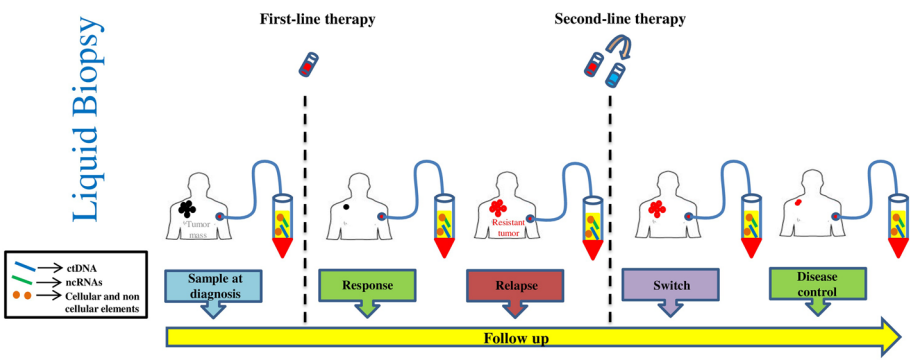

FIGURE 2 | Schematic representation of liquid biopsy sampling.

distinguish patients who respond to immunotherapy as compared to those that do not (non-responders). These initial findings warrant future validation in additional confirmatory studies.

Altogether the results of this section highlight the potential role of ncRNAs as predictors of response to immunotherapy in melanoma. However, it is evident that compared to CTCs and ctDNA for example, their development as robust biomarkers is still in its infant stage.

The main findings described in the above paragraphs are schematically summarized in **Table 1**.

FINAL CONSIDERATIONS

One major therapeutic breakthrough over the past ten years in medical oncology has been the introduction of immunotherapy with checkpoint inhibitors targeting CTLA-4 and PD-1/PD-L1 axis (7). After its initial suc9cess in the treatment of metastatic melanoma, the clinical application of checkpoint inhibitors has rapidly spread to the majority of cancer cases with varying degrees of success. Among several cancer types, melanoma remains one of the most positively impacted by the use of these molecules, most likely because of its high mutational rate as well as to the frequent generation of an inflammatory microenvironment which together help establish appropriate conditions for the immune-system to respond (90, 91). In stage IV melanoma, five year overall survival rates obtained with the combination of ipilimumab and nivolumab are currently up to 52% (92). Three Phase III combination studies in the subset of patients with BRAF V600 mutation using a BRAF plus a MEK inhibitor and immunotherapy with anti-PD-1 or anti-PD-L1 have been carried out (93–95). Although we have not yet obtained data about long term outcomes from these studies, in two out of three trials, progression free survival did not improve in the combo therapy arm of immunotherapy plus targeted therapy over targeted therapy alone and in the third trial there was a modest improvement. Hence, the issue still remains that a significant proportion of patients do not benefit from existing therapies both alone or in combination.

Significant efforts are being devoted to understanding the biological and immunological basis of drug resistance and several clinical trials are being conducted with combinations of additional checkpoint inhibitors i9n the attempt to improve response rates (94, 95). At the same time, it is important to develop biomarkers capable of identifying responders from non-responders to current therapy. The main reasons being the elevated costs and the high rate of serious immunological adverse events, in particular those observed with the combination of anti-CTLA4 and anti-PD-1/anti-PD-L1 antibodies (10). In this regard, a significant contribution has been provided by the discovery that the combination of interferon signature and mutational burden in tumor biopsies is a better, albeit not absolute predictor, of response than the simple detection of PD-L1 (96). In principle however, an ideal predictive biomarker should have the following features: a) require minimally invasive procedures to be measured, b) allow real-time longitudinal monitoring during the course of therapy and c) be easy to be measured and standardized. LBs using blood samples provide the ideal solution (**Figure 2**). This approach has the potential to overcome the shortcomings of repeated re-biopsies of tumors that are often difficult to obtain (97). Furthermore, the issue with sensitivity of liquid biopsies has been solved thanks to major technological advancements reached in the last few years. As it has been reviewed in this paper, several analytes can be detected in the blood: 1) nucleic acids like ctDNA and ncRNAs, 2) cellular elements like CTCs and immune cells and 3) soluble factors like cytokines and enzymes. Clinical data are more mature with ctDNA based assays and is relevant to consider that a ctDNA assay based on the simultaneous measure of 16 different patient-specific tumor mutations in the blood, has recently been approved in the US by Medicare to monitor minimal residual disease in Stage II and III colorectal cancer and to guide therapeutic decisions (Signatera™ MRD Test) (98, 99). Very promising data have been obtained using the same technology for predicting response to pembrolizumab in patients with various solid cancers (31). Hence, we may expect in future years a prominent increase in ctDNA validation studies and registratio9n of several blood based assays. The outcome of these studies will allow to set up new companion diagnostics able to direct/guide precision medicine in oncology.

AUTHOR CONTRIBUTIONS

LF conceptualized and revised the manuscript. CFR did figures and drafted the manuscript. DL did table and drafted the manuscript. VC did figures and revised bibliography. AC helped to draft the manuscript. GC supervised and revised the manuscript and provided critical suggestions. RM revised the manuscript and provided critical suggestions. All authors have read and agreed to the published version of the manuscript. All authors contributed to the article and approved the submitted version.

FUNDING

This work was supported by: 1) Italian Association for Cancer Research (AIRC) grants IG15216 to GC and IG17009 to RM; 2) the Lazioinova grant 2018 n.85-2017-13750 to RM; 3) PRIN Bando 2017 (Prot. 2017HWTP2K) to GC and RM.

ACKNOWLEDGMENTS

We thank Tania Merlino for the editing of the manuscript.

REFERENCES

1. Rodríguez-Cerdeira C, Carnero Gregorio M, López-Barcenas A, Sánchez-Blanco E, Sánchez-Blanco B, Fabbrocini G, et al. Advances in Immunotherapy for Melanoma: A Comprehensive Review. *Mediators Inflamm* (2017) 2017:3264217. doi: 10.1155/2017/3264217
2. Jamal-Hanjani M, Quezada SA, Larkin J, Swanton C. Translational implications of tumor heterogeneity. *Clin Cancer Res* (2015) 21:1258–66. doi: 10.1158/1078-0432.CCR-14-1429
3. O'Donnell JS, Teng MWL, Smyth MJ. Cancer immunoediting and resistance to T cell-based immunotherapy. *Nat Rev Clin Oncol* (2019) 16:151–67. doi: 10.1038/s41571-018-0142-8
4. Bruschini S, Ciliberto G, Mancini R. The emerging role of cancer cell plasticity and cell-cycle quiescence in immune escape. *Cell Death Dis* (2020) 11:471. doi: 10.1038/s41419-020-2669-8
5. Bai X, Fisher DE, Flaherty KT. Cell-state dynamics and therapeutic resistance in melanoma from the perspective of MITF and IFNγ pathways. *Nat Rev Clin Oncol* (2019) 16:549–62. doi: 10.1038/s41571-019-0204-6
6. Tucci M, Passarelli A, Mannavola F, Felici C, Stucci LS, Cives M, et al. Immune System Evasion as Hallmark of Melanoma Progression: The Role of Dendritic Cells. *Front Oncol* (2019) 9:1148. doi: 10.3389/fonc.2019.01148
7. Luke JJ, Flaherty KT, Ribas A, Long GV. Targeted agents and immunotherapies: optimizing outcomes in melanoma. *Nat Rev Clin Oncol* (2017) 14:463–82. doi: 10.1038/nrclinonc.2017.43
8. Simeone E, Grimaldi AM, Festino L, Trojaniello C, Vitale MG, Vanella V, et al. Immunotherapy in metastatic melanoma: a novel scenario of new toxicities and their management. *Melanoma Manage* (2019) 6:MMT30. doi: 10.2217/mmt-2019-0005
9. Topalian SL, Taube JM, Anders RA, Pardoll DM. Mechanism-driven biomarkers to guide immune checkpoint blockade in cancer therapy. *Nat Rev Cancer* (2016) 16:275–87. doi: 10.1038/nrc.2016.36
10. Larkin J, Hodi FS, Wolchok JD. Combined Nivolumab and Ipilimumab or Monotherapy in Untreated Melanoma. *N Engl J Med* (2015) 373:1270–1. doi: 10.1056/NEJMc1509660
11. Fattore L, Mancini R, Ascierto PA, Ciliberto G. The potential of BRAF-associated non-coding RNA as a therapeutic target in melanoma. *Expert Opin Ther Targets* (2019) 23:53–68. doi: 10.1080/14728222.2019.1554057
12. Imbert C, Montfort A, Fraisse M, Marcheteau E, Gilhodes J, Martin E, et al. Resistance of melanoma to immune checkpoint inhibitors is overcome by targeting the sphingosine kinase-1. *Nat Commun* (2020) 11:437. doi: 10.1038/s41467-019-14218-7
13. Sharma P, Hu-Lieskovan S, Wargo JA, Ribas A. Primary, Adaptive, and Acquired Resistance to Cancer Immunotherapy. *Cell* (2017) 168:707–23. doi: 10.1016/j.cell.2017.01.017
14. Sun J, Carr MJ, Khushalani NI. Principles of Targeted Therapy for Melanoma. *Surg Clin North Am* (2020) 100:175–88. doi: 10.1016/j.suc.2019.09.013
15. Huynh K, Hoon DSB. Liquid Biopsies for Assessing Metastatic Melanoma Progression. *Crit Rev Oncog* (2016) 21:141–54. doi: 10.1615/CritRevOncog.2016016075
16. De Rubis G, Rajeev Krishnan S, Bebawy M. Liquid Biopsies in Cancer Diagnosis, Monitoring, and Prognosis. *Trends Pharmacol Sci* (2019) 40:172–86. doi: 10.1016/j.tips.2019.01.006
17. Corcoran RB. Liquid biopsy versus tumor biopsy for clinical-trial recruitment. *Nat Med* (2020) 26:1815–6. doi: 10.1038/s41591-020-01169-6
18. Qi Z-H, Xu H-X, Zhang S-R, Xu J-Z, Li S, Gao H-L, et al. The Significance of Liquid Biopsy in Pancreatic Cancer. *J Cancer* (2018) 9:3417–26. doi: 10.7150/jca.24591
19. Lim SY, Lee JH, Diefenbach RJ, Kefford RF, Rizos H. Liquid biomarkers in melanoma: detection and discovery. *Mol Cancer* (2018) 17:8. doi: 10.1186/s12943-018-0757-5
20. Heitzer E. Circulating Tumor DNA for Modern Cancer Management. *Clin Chem* (2019) 66:143–5. doi: 10.1373/clinchem.2019.304774
21. Papadopoulos N. Pathophysiology of ctDNA Release into the Circulation and Its Characteristics: What Is Important for Clinical Applications. *Recent Results Cancer Res* (2020) 215:163–80. doi: 10.1007/978-3-030-26439-0_9
22. Song Y, Hu C, Xie Z, Wu L, Zhu Z, Rao C, et al. Circulating tumor DNA clearance predicts prognosis across treatment regimen in a large real-world longitudinally monitored advanced non-small cell lung cancer cohort. *Transl Lung Cancer Res* (2020) 9:269–79. doi: 10.21037/tlcr.2020.03.17
23. Calapre L, Warburton L, Millward M, Gray ES. Circulating tumour DNA (ctDNA) as a biomarker in metachronous melanoma and colorectal cancer- a case report. *BMC Cancer* (2019) 19:1109. doi: 10.1186/s12885-019-6336-3
24. Gray JE, Okamoto I, Sriuranpong V, Vansteenkiste J, Imamura F, Lee JS, et al. Tissue and Plasma EGFR Mutation Analysis in the FLAURA Trial: Osimertinib versus Comparator EGFR Tyrosine Kinase Inhibitor as First-Line Treatment in Patients with EGFR-Mutated Advanced Non-Small Cell Lung Cancer. *Clin Cancer Res* (2019) 25:6644–52. doi: 10.1158/1078-0432.CCR-19-1126
25. Barbany G, Arthur C, Liedén A, Nordenskjöld M, Rosenquist R, Tesi B, et al. Cell-free tumour DNA testing for early detection of cancer - a potential future tool. *J Intern Med* (2019) 286:118–36. doi: 10.1111/joim.12897
26. Paik PK, Felip E, Veillon R, Sakai H, Cortot AB, Garassino MC, et al. Tepotinib in Non-Small-Cell Lung Cancer with MET Exon 14 Skipping Mutations. *N Engl J Med* (2020) 383:931–43. doi: 10.1056/NEJMoa2004407
27. Forschner A, Battke F, Hadaschik D, Schulze M, Weißgraeber S, Han C-T, et al. Tumor mutation burden and circulating tumor DNA in combined CTLA-4 and PD-1 antibody therapy in metastatic melanoma - results of a prospective biomarker study. *J Immunother cancer.* (2019) 7:180. doi: 10.1186/s40425-019-0659-0
28. Goodman AM, Kato S, Bazhenova L, Patel SP, Frampton GM, Miller V, et al. Tumor Mutational Burden as an Independent Predictor of Response to Immunotherapy in Diverse Cancers. *Mol Cancer Ther* (2017) 16:2598–608. doi: 10.1158/1535-7163.MCT-17-0386
29. Seremet T, Jansen Y, Planken S, Njimi H, Delaunoy M, El Housni H, et al. Undetectable circulating tumor DNA (ctDNA) levels correlate with favorable outcome in metastatic melanoma patients treated with anti-PD1 therapy. *J Transl Med* (2019) 17:303. doi: 10.1186/s12967-019-2051-8
30. Lee JH, Long GV, Boyd S, Lo S, Menzies AM, Tembe V, et al. Circulating tumour DNA predicts response to anti-PD1 antibodies in metastatic melanoma. *Ann Oncol* (2017) 28:1130–6. doi: 10.1093/annonc/mdx026
31. Bratman SV, Yang SYC, Iafolla MAJ, Liu Z, Hansen AR, Bedard PL, et al. Personalized circulating tumor DNA analysis as a predictive biomarker in solid tumor patients treated with pembrolizumab. *Nat Cancer* (2020) 1:873–81. doi: 10.1038/s43018-020-0096-5
32. Ashida A, Sakaizawa K, Uhara H, Okuyama R. Circulating Tumour DNA for Monitoring Treatment Response to Anti-PD-1 Immunotherapy in Melanoma Patients. *Acta Derm Venereol* (2017) 97:1212–8. doi: 10.2340/00015555-2748
33. Gray ES, Rizos H, Reid AL, Boyd SC, Pereira MR, Lo J, et al. Circulating tumor DNA to monitor treatment response and detect acquired resistance in patients with metastatic melanoma. *Oncotarget* (2015) 6:42008–18. doi: 10.18632/oncotarget.5788
34. Schreuer M, Meersseman G, Van Den Herrewegen S, Jansen Y, Chevolet I, Bott A, et al. Quantitative assessment of BRAF V600 mutant circulating cell-free tumor DNA as a tool for therapeutic monitoring in metastatic melanoma patients treated with BRAF/MEK inhibitors. *J Transl Med* (2016) 14:95. doi: 10.1186/s12967-016-0852-6
35. Hong X, Sullivan RJ, Kalinich M, Kwan TT, Giobbie-Hurder A, Pan S, et al. Molecular signatures of circulating melanoma cells for monitoring early response to immune checkpoint therapy. *Proc Natl Acad Sci U S A* (2018) 115:2467–72. doi: 10.1073/pnas.1719264115
36. Lin SY, Chang S-C, Lam S, Irene Ramos R, Tran K, Ohe S, et al. Prospective Molecular Profiling of Circulating Tumor Cells from Patients with Melanoma Receiving Combinatorial Immunotherapy. *Clin Chem* (2020) 66:169–77. doi: 10.1373/clinchem.2019.307140
37. Khattak MA, Reid A, Freeman J, Pereira M, McEvoy A, Lo J, et al. PD-L1 Expression on Circulating Tumor Cells May Be Predictive of Response to Pembrolizumab in Advanced Melanoma: Results from a Pilot Study. *Oncologist* (2019) 25:e520–7. doi: 10.1634/theoncologist.2019-0557
38. Zhou J, Mahoney KM, Giobbie-Hurder A, Zhao F, Lee S, Liao X, et al. Soluble PD-L1 as a Biomarker in Malignant Melanoma Treated with Checkpoint Blockade. *Cancer Immunol Res* (2017) 5:480–92. doi: 10.1158/2326-6066.CIR-16-0329
39. Weber JS, Sznol M, Sullivan RJ, Blackmon S, Boland G, Kluger HM, et al. A Serum Protein Signature Associated with Outcome after Anti-PD-1 Therapy

in Metastatic Melanoma. *Cancer Immunol Res* (2018) 6:79–86. doi: 10.1158/2326-6066.CIR-17-0412
40. Lim SY, Lee JH, Gide TN, Menzies AM, Guminski A, Carlino MS, et al. Circulating Cytokines Predict Immune-Related Toxicity in Melanoma Patients Receiving Anti-PD-1-Based Immunotherapy. *Clin Cancer Res* (2019) 25:1557–63. doi: 10.1158/1078-0432.CCR-18-2795
41. Sanmamed MF, Perez-Gracia JL, Schalper KA, Fusco JP, Gonzalez A, Rodriguez-Ruiz ME, et al. Changes in serum interleukin-8 (IL-8) levels reflect and predict response to anti-PD-1 treatment in melanoma and non-small-cell lung cancer patients. *Ann Oncol* (2017) 28:1988–95. doi: 10.1093/annonc/mdx190
42. Morello S, Capone M, Sorrentino C, Giannarelli D, Madonna G, Mallardo D, et al. Soluble CD73 as biomarker in patients with metastatic melanoma patients treated with nivolumab. *J Transl Med* (2017) 15:244. doi: 10.1186/s12967-017-1348-8
43. Capone M, Fratangelo F, Giannarelli D, Sorrentino C, Turiello R, Zanotta S, et al. Frequency of circulating CD8+CD73+T cells is associated with survival in nivolumab-treated melanoma patients. *J Transl Med* (2020) 18:121. doi: 10.1186/s12967-020-02285-0
44. Meyer C, Cagnon L, Costa-Nunes CM, Baumgaertner P, Montandon N, Leyvraz L, et al. Frequencies of circulating MDSC correlate with clinical outcome of melanoma patients treated with ipilimumab. *Cancer Immunol Immunother* (2014) 63:247–57. doi: 10.1007/s00262-013-1508-5
45. Tarhini AA, Edington H, Butterfield LH, Lin Y, Shuai Y, Tawbi H, et al. Immune monitoring of the circulation and the tumor microenvironment in patients with regionally advanced melanoma receiving neoadjuvant ipilimumab. *PLoS One* (2014) 9:e87705. doi: 10.1371/journal.pone.0087705
46. Capone M, Giannarelli D, Mallardo D, Madonna G, Festino L, Grimaldi AM, et al. Baseline neutrophil-to-lymphocyte ratio (NLR) and derived NLR could predict overall survival in patients with advanced melanoma treated with nivolumab. *J Immunother Cancer* (2018) 6:74. doi: 10.1186/s40425-018-0383-1
47. Huber V, Vallacchi V, Fleming V, Hu X, Cova A, Dugo M, et al. Tumor-derived microRNAs induce myeloid suppressor cells and predict immunotherapy resistance in melanoma. *J Clin Invest* (2018) 128:5505–16. doi: 10.1172/JCI98060
48. Vignard V, Labbé M, Marec N, André-Grégoire G, Jouand N, Fonteneau J-F, et al. MicroRNAs in Tumor Exosomes Drive Immune Escape in Melanoma. *Cancer Immunol Res* (2020) 8:255–67. doi: 10.1158/2326-6066.CIR-19-0522
49. Shi A, Kasumova GG, Michaud WA, Cintolo-Gonzalez J, Diaz-Martinez M, Ohmura J, et al. Plasma-derived extracellular vesicle analysis and deconvolution enable prediction and tracking of melanoma checkpoint blockade outcome. *Sci Adv* (2020) 6. doi: 10.1126/sciadv.abb3461
50. Bustos MA, Gross R, Rahimzadeh N, Cole H, Tran LT, Tran KD, et al. A Pilot Study Comparing the Efficacy of Lactate Dehydrogenase Levels Versus Circulating Cell-Free microRNAs in Monitoring Responses to Checkpoint Inhibitor Immunotherapy in Metastatic Melanoma Patients. *Cancers (Basel)* (2020) 12. doi: 10.3390/cancers12113361
51. Fabisiewicz A, Grzybowska E. CTC clusters in cancer progression and metastasis. *Med Oncol* (2017) 34:12. doi: 10.1007/s12032-016-0875-0
52. Attard G, de Bono JS. Utilizing circulating tumor cells: challenges and pitfalls. *Curr Opin Genet Dev* (2011) 21:50–8. doi: 10.1016/j.gde.2010.10.010
53. Gkountela S, Castro-Giner F, Szczerba BM, Vetter M, Landin J, Scherrer R, et al. Circulating Tumor Cell Clustering Shapes DNA Methylation to Enable Metastasis Seeding. *Cell* (2019) 176:98–112.e14. doi: 10.1016/j.cell.2018.11.046
54. Ruggiero CF, Malpicci D, Fattore L, Madonna G, Vanella V, Mallardo D, et al. ErbB3 Phosphorylation as Central Event in Adaptive Resistance to Targeted Therapy in Metastatic Melanoma: Early Detection in CTCs during Therapy and Insights into Regulation by Autocrine Neuregulin. *Cancers (Basel)* (2019) 11. doi: 10.3390/cancers11101425
55. Marsavela G, Aya-Bonilla CA, Warkiani ME, Gray ES, Ziman M. Melanoma circulating tumor cells: Benefits and challenges required for clinical application. *Cancer Lett* (2018) 424:1–8. doi: 10.1016/j.canlet.2018.03.013
56. Bankó P, Lee SY, Nagygyörgy V, Zrínyi M, Chae CH, Cho DH, et al. Technologies for circulating tumor cell separation from whole blood. *J Hematol Oncol* (2019) 12:48. doi: 10.1186/s13045-019-0735-4
57. Schadendorf D, Long GV, Stroiakovski D, Karaszewska B, Hauschild A, Levchenko E, et al. Three-year pooled analysis of factors associated with clinical outcomes across dabrafenib and trametinib combination therapy phase 3 randomised trials. *Eur J Cancer* (2017) 82:45–55. doi: 10.1016/j.ejca.2017.05.033
58. Hodi FS, Chiarion-Sileni V, Gonzalez R, Grob J-J, Rutkowski P, Cowey CL, et al. Nivolumab plus ipilimumab or nivolumab alone versus ipilimumab alone in advanced melanoma (CheckMate 067): 4-year outcomes of a multicentre, randomised, phase 3 trial. *Lancet Oncol* (2018) 19:1480–92. doi: 10.1016/S1470-2045(18)30700-9
59. Gandini S, Massi D, Mandalà M. PD-L1 expression in cancer patients receiving anti PD-1/PD-L1 antibodies: A systematic review and meta-analysis. *Crit Rev Oncol Hematol* (2016) 100:88–98. doi: 10.1016/j.critrevonc.2016.02.001
60. Nowicki TS, Hu-Lieskovan S, Ribas A. Mechanisms of Resistance to PD-1 and PD-L1 Blockade. *Cancer J* (2018) 24:47–53. doi: 10.1097/PPO.0000000000000303
61. Guibert N, Delaunay M, Lusque A, Boubekeur N, Rouquette I, Clermont E, et al. PD-L1 expression in circulating tumor cells of advanced non-small cell lung cancer patients treated with nivolumab. *Lung Cancer* (2018) 120:108–12. doi: 10.1016/j.lungcan.2018.04.001
62. Roscilli G, De Vitis C, Ferrara FF, Noto A, Cherubini E, Ricci A, et al. Human lung adenocarcinoma cell cultures derived from malignant pleural effusions as model system to predict patients chemosensitivity. *J Transl Med* (2016) 14:61. doi: 10.1186/s12967-016-0816-x
63. Gu D, Ao X, Yang Y, Chen Z, Xu X. Soluble immune checkpoints in cancer: production, function and biological significance. *J Immunother Cancer* (2018) 6:132. doi: 10.1186/s40425-018-0449-0
64. Frigola X, Inman BA, Lohse CM, Krco CJ, Cheville JC, Thompson RH, et al. Identification of a soluble form of B7-H1 that retains immunosuppressive activity and is associated with aggressive renal cell carcinoma. *Clin Cancer Res* (2011) 17:1915–23. doi: 10.1158/1078-0432.CCR-10-0250
65. Rossille D, Gressier M, Damotte D, Maucort-Boulch D, Pangault C, Semana G, et al. High level of soluble programmed cell death ligand 1 in blood impacts overall survival in aggressive diffuse large B-Cell lymphoma: results from a French multicenter clinical trial. *Leukemia* (2014) 28:2367–75. doi: 10.1038/leu.2014.137
66. Wang L, Wang H, Chen H, Wang W, Chen X-Q, Geng Q-R, et al. Serum levels of soluble programmed death ligand 1 predict treatment response and progression free survival in multiple myeloma. *Oncotarget* (2015) 6:41228–36. doi: 10.18632/oncotarget.5682
67. Lu D, Ni Z, Liu X, Feng S, Dong X, Shi X, et al. Beyond T Cells: Understanding the Role of PD-1/PD-L1 in Tumor-Associated Macrophages. *J Immunol Res* (2019) 2019:1919082. doi: 10.1155/2019/1919082
68. Allard B, Longhi MS, Robson SC, Stagg J. The ectonucleotidases CD39 and CD73: Novel checkpoint inhibitor targets. *Immunol Rev* (2017) 276:121–44. doi: 10.1111/imr.12528
69. Neo SY, Yang Y, Record J, Ma R, Chen X, Chen Z, et al. CD73 immune checkpoint defines regulatory NK cells within the tumor microenvironment. *J Clin Invest* (2020) 130:1185–98. doi: 10.1172/JCI128895
70. Wang R, Zhang Y, Lin X, Gao Y, Zhu Y. Prognositic value of CD73-adenosinergic pathway in solid tumor: A meta-analysis and systematic review. *Oncotarget* (2017) 8:57327–36. doi: 10.18632/oncotarget.16905
71. Zahorec R. Ratio of neutrophil to lymphocyte counts–rapid and simple parameter of systemic inflammation and stress in critically ill. *Bratisl Lek Listy* (2001) 102:5–14.
72. Weide B, Martens A, Hassel JC, Berking C, Postow MA, Bisschop K, et al. Baseline Biomarkers for Outcome of Melanoma Patients Treated with Pembrolizumab. *Clin Cancer Res* (2016) 22:5487–96. doi: 10.1158/1078-0432.CCR-16-0127
73. Fattore L, Costantini S, Malpicci D, Ruggiero CF, Ascierto PA, Croce CM, et al. MicroRNAs in melanoma development and resistance to target therapy. *Oncotarget* (2017) 8:22262–78. doi: 10.18632/oncotarget.14763
74. Fattore L, Sacconi A, Mancini R, Ciliberto G. MicroRNA-driven deregulation of cytokine expression helps development of drug resistance in metastatic melanoma. *Cytokine Growth Factor Rev* (2017) 36:39–48. doi: 10.1016/j.cytogfr.2017.05.003
75. Varrone F, Caputo E. The miRNAs Role in Melanoma and in Its Resistance to Therapy. *Int J Mol Sci* (2020) 21. doi: 10.3390/ijms21030878
76. Panni S, Lovering RC, Porras P, Orchard S. Non-coding RNA regulatory networks. *Biochim Biophys Acta Gene Regul Mech* (2020) 1863:194417. doi: 10.1016/j.bbagrm.2019.194417

77. Acunzo M, Romano G, Wernicke D, Croce CM. MicroRNA and cancer–a brief overview. *Adv Biol Regul* (2015) 57:1–9. doi: 10.1016/j.jbior.2014.09.013
78. Mumford SL, Towler BP, Pashler AL, Gilleard O, Martin Y, Newbury SF. Circulating MicroRNA Biomarkers in Melanoma: Tools and Challenges in Personalised Medicine. *Biomolecules* (2018) 8. doi: 10.3390/biom8020021
79. Salehi M, Sharifi M. Exosomal miRNAs as novel cancer biomarkers: Challenges and opportunities. *J Cell Physiol* (2018) 233:6370–80. doi: 10.1002/jcp.26481
80. Cui M, Wang H, Yao X, Zhang D, Xie Y, Cui R, et al. Circulating MicroRNAs in Cancer: Potential and Challenge. *Front Genet* (2019) 10:626. doi: 10.3389/fgene.2019.00626
81. Butler JT, Abdelhamed S, Kurre P. Extracellular vesicles in the hematopoietic microenvironment. *Haematologica* (2018) 103:382–94. doi: 10.3324/haematol.2017.183335
82. Fattore L, Mancini R, Acunzo M, Romano G, Laganà A, Pisanu ME, et al. miR-579-3p controls melanoma progression and resistance to target therapy. *Proc Natl Acad Sci U S A* (2016) 113:E5005–13. doi: 10.1073/pnas.1607753113
83. Fattore L, Ruggiero CF, Pisanu ME, Liguoro D, Cerri A, Costantini S, et al. Reprogramming miRNAs global expression orchestrates development of drug resistance in BRAF mutated melanoma. *Cell Death Differ* (2019) 26:1267–82. doi: 10.1038/s41418-018-0205-5
84. Caporali S, Amaro A, Levati L, Alvino E, Lacal PM, Mastroeni S, et al. miR-126-3p down-regulation contributes to dabrafenib acquired resistance in melanoma by up-regulating ADAM9 and VEGF-A. *J Exp Clin Cancer Res* (2019) 38:272. doi: 10.1186/s13046-019-1238-4
85. Tupone MG, D'Aguanno S, Di Martile M, Valentini E, Desideri M, Trisciuoglio D, et al. microRNA-378a-5p iS a novel positive regulator of melanoma progression. *Oncogenesis* (2020) 9:22. doi: 10.1038/s41389-020-0203-6
86. Audrito V, Serra S, Stingi A, Orso F, Gaudino F, Bologna C, et al. PD-L1 up-regulation in melanoma increases disease aggressiveness and is mediated through miR-17-5p. *Oncotarget* (2017) 8:15894–911. doi: 10.18632/oncotarget.15213
87. Galore-Haskel G, Nemlich Y, Greenberg E, Ashkenazi S, Hakim M, Itzhaki O, et al. A novel immune resistance mechanism of melanoma cells controlled by the ADAR1 enzyme. *Oncotarget* (2015) 6:28999–9015. doi: 10.18632/oncotarget.4905
88. Xu Z, Li P, Fan L, Wu M. The Potential Role of circRNA in Tumor Immunity Regulation and Immunotherapy. *Front Immunol* (2018) 9:9. doi: 10.3389/fimmu.2018.00009
89. Yu Y, Zhang W, Li A, Chen Y, Ou Q, He Z, et al. Association of Long Noncoding RNA Biomarkers With Clinical Immune Subtype and Prediction of Immunotherapy Response in Patients With Cancer. *JAMA Netw Open* (2020) 3:e202149–e202149. doi: 10.1001/jamanetworkopen.2020.2149
90. Grzywa TM, Paskal W, Włodarski PK. Intratumor and Intertumor Heterogeneity in Melanoma. *Transl Oncol* (2017) 10:956–75. doi: 10.1016/j.tranon.2017.09.007
91. Di Martile M, Farini V, Consonni FM, Trisciuoglio D, Desideri M, Valentini E, et al. Melanoma-specific bcl-2 promotes a protumoral M2-like phenotype by tumor-associated macrophages. *J Immunother Cancer* (2020) 8. doi: 10.1136/jitc-2019-000489
92. Larkin J, Chiarion-Sileni V, Gonzalez R, Grob J-J, Rutkowski P, Lao CD, et al. Five-Year Survival with Combined Nivolumab and Ipilimumab in Advanced Melanoma. *N Engl J Med* (2019) 381:1535–46. doi: 10.1056/NEJMoa1910836
93. Ascierto PA, Ferrucci PF, Stephens R, Del Vecchio M, Atkinson V, Schmidt H, et al. KEYNOTE-022 Part 3: phase II randomized study of 1L dabrafenib (D) and trametinib (T) plus pembrolizumab (Pembro) or placebo (PBO) for BRAF-mutant advanced melanoma. *Ann Oncol* (2018) 29:viii442–. doi: 10.1093/annonc/mdy289
94. Gutzmer R, Stroyakovskiy D, Gogas H, Robert C, Lewis K, Protsenko S, et al. Atezolizumab, vemurafenib, and cobimetinib as first-line treatment for unresectable advanced $BRAF^{V600}$ mutation-positive melanoma (IMspire150): primary analysis of the randomised, double-blind, placebo-controlled, phase 3 trial. *Lancet* (2020) 395:1835–44. doi: 10.1016/S0140-6736(20)30934-X
95. Nathan P, Dummer R, Long GV, Ascierto PA, Tawbi HA, Robert C, et al. LBA43 Spartalizumab plus dabrafenib and trametinib (Sparta-DabTram) in patients (pts) with previously untreated BRAF V600–mutant unresectable or metastatic melanoma: Results from the randomized part 3 of the phase III COMBI-i trial. *Ann Oncol* (2020) 31:S1172. doi: 10.1016/j.annonc.2020.08.2273
96. Cristescu R, Mogg R, Ayers M, Albright A, Murphy E, Yearley J, et al. Pan-tumor genomic biomarkers for PD-1 checkpoint blockade{\textendash}based immunotherapy. *Science* (2018) 362. doi: 10.1126/science.aar3593
97. Fattore L, Ruggiero CF, Liguoro D, Mancini R, Ciliberto G. Single cell analysis to dissect molecular heterogeneity and disease evolution in metastatic melanoma. *Cell Death Dis* (2019) 10. doi: 10.1038/s41419-019-2048-5
98. Reinert T, Henriksen TV, Christensen E, Sharma S, Salari R, Sethi H, et al. Analysis of Plasma Cell-Free DNA by Ultradeep Sequencing in Patients With Stages I to III Colorectal Cancer. *JAMA Oncol* (2019) 5:1124–31. doi: 10.1001/jamaoncol.2019.0528
99. Christensen E, Birkenkamp-Demtröder K, Sethi H, Shchegrova S, Salari R, Nordentoft I, et al. Early Detection of Metastatic Relapse and Monitoring of Therapeutic Efficacy by Ultra-Deep Sequencing of Plasma Cell-Free DNA in Patients With Urothelial Bladder Carcinoma. *J Clin Oncol* (2019) 37:1547–57. doi: 10.1200/JCO.18.02052

Conflict of Interest: The authors declare that the research was conducted in the absence of any commercial or financial relationships that could be construed as a potential conflict of interest.

frontiers in Oncology

ORIGINAL RESEARCH
published: 25 March 2021
doi: 10.3389/fonc.2021.636057

A Multi-Omics Analysis of Metastatic Melanoma Identifies a Germinal Center-Like Tumor Microenvironment in HLA-DR-Positive Tumor Areas

Laura Gadeyne[1†], Yannick Van Herck[2†], Giorgia Milli[3], Zeynep Kalender Atak[4], Maddalena Maria Bolognesi[5], Jasper Wouters[4], Lukas Marcelis[3], Angeliki Minia[6], Vaia Pliaka[6], Jan Roznac[6,7], Leonidas G. Alexopoulos[6,8], Giorgio Cattoretti[5], Oliver Bechter[2], Joost Van Den Oord[3], Frederik De Smet[3], Asier Antoranz[3‡] and Francesca Maria Bosisio[3‡]*

[1] Department of Pathology, UZ Leuven, Leuven, Belgium, [2] Department of General Medical Oncology, University Hospitals Leuven, Leuven, Belgium, [3] Translational Cell and Tissue Research, Department of Imaging and Pathology, KU Leuven, Leuven, Belgium, [4] Laboratory of Computational Biology, KU Leuven, Leuven, Belgium, [5] Pathology, Department of Medicine & Surgery, University of Milano-Bicocca, Milan, Italy, [6] ProtATonce Ltd, Athens, Greece, [7] Life Sciences Research Unit, University of Luxembourg, Belvaux, Luxembourg, [8] Biomedical Systems Laboratory, Department of Mechanical Engineering, National Technical University of Athens, Athens, Greece

The emergence of immune checkpoint inhibitors has dramatically changed the therapeutic landscape for patients with advanced melanoma. However, relatively low response rates and a high incidence of severe immune-related adverse events have prompted the search for predictive biomarkers. A positive predictive value has been attributed to the aberrant expression of Human Leukocyte Antigen-DR (HLA-DR) by melanoma cells, but it remains unknown why this is the case. In this study, we have examined the microenvironment of HLA-DR positive metastatic melanoma samples using a multi-omics approach. First, using spatial, single-cell mapping by multiplexed immunohistochemistry, we found that the microenvironment of HLA-DR positive melanoma regions was enriched by professional antigen presenting cells, including classical dendritic cells and macrophages, while a more general cytotoxic T cell exhaustion phenotype was present in these regions. In parallel, transcriptomic analysis on micro dissected tissue from HLA-DR positive and HLA-DR negative areas showed increased IFNγ signaling, enhanced leukocyte adhesion and mononuclear cell proliferation in HLA-DR positive areas. Finally, multiplexed cytokine profiling identified an increased expression of germinal center cytokines CXCL12, CXCL13 and CCL19 in HLA-DR positive metastatic lesions, which, together with IFNγ and IL4 could serve as biomarkers to discriminate tumor samples containing HLA-DR overexpressing tumor cells from HLA-DR negative samples. Overall, this suggests that HLA-DR positive areas in melanoma attract the anti-tumor immune cell infiltration by creating a dystrophic germinal center-like microenvironment where an enhanced antigen presentation leads to an exhausted microenvironment, nevertheless representing a fertile ground for a better efficacy of anti-PD-1 inhibitors due to

OPEN ACCESS

Edited by:
Igor Puzanov,
University at Buffalo, United States

Reviewed by:
Camelia Quek,
Melanoma Institute Australia, Australia
Yuhang Zhang,
University of Cincinnati, United States

***Correspondence:**
Francesca Maria Bosisio
francescamaria.bosisio@kuleuven.be

[†]These authors share first authorship

[‡]These authors share last authorship

Specialty section:
This article was submitted to Skin Cancer, a section of the journal Frontiers in Oncology

Received: *30 November 2020*
Accepted: *26 February 2021*
Published: *25 March 2021*

Citation:
Gadeyne L, Van Herck Y, Milli G, Atak ZK, Bolognesi MM, Wouters J, Marcelis L, Minia A, Pliaka V, Roznac J, Alexopoulos LG, Cattoretti G, Bechter O, Oord JVD, De Smet F, Antoranz A and Bosisio FM (2021) A Multi-Omics Analysis of Metastatic Melanoma Identifies a Germinal Center-Like Tumor Microenvironment in HLA-DR-Positive Tumor Areas. Front. Oncol. 11:636057. doi: 10.3389/fonc.2021.636057

simultaneous higher levels of PD-1 in the immune cells and PD-L1 in the HLA-DR positive melanoma cells.

Keywords: melanoma, single-cell, multi-omics, multiplex, HLA-DR

INTRODUCTION

Primary Cutaneous Melanoma (PCM) is characterized by an aggressive course including metastatic spread directly proportional to the depth of invasion of the tumor cells into the skin (typically defined as the Breslow thickness) (1). In addition, PCM is also characterized by one of the highest somatic mutation rates (2), from which only a minority are driver mutations, while rest are passenger mutations that do not play a role in tumor development or progression. Yet, this high tumor mutational burden (TMB) can translate into a high amount of neo-antigens available for antigen recognition by the immune system, a feature that has been attributed to the strong immunogenicity of melanoma and the clinical effect of immunotherapy in these patients. Indeed, immune checkpoint inhibitor (ICI) therapy aimed at blocking the PD-1/PD-L1 axis was approved by the FDA in 2014 for the treatment of PCM and is now being used as a standard of care for patients with irresectable stage III or stage IV disease, and as adjuvant therapy in stage III melanoma (3). Unfortunately, ICI response rates are still relatively low, at least when given in monotherapy, and a significant percentage of patients suffers from severe, immune-related adverse events, which in rare cases can even be fatal (4–6). Therefore a great demand exists for predictive biomarkers to allow a better patient selection before exposing them to ineffective, potentially toxic therapies, for which a number of markers have already been proposed. For example, the density of CD8+ T cells in both the border and bulk of the tumor have been correlated with a higher response to ICI (7, 8). Likewise, the presence of a high TMB, an interferon-gamma (IFNγ)-related mRNA profile and a T cell-inflamed gene expression profile have also been proven to have a positive predictive value (9–12). Interestingly, the expression of Human Leukocyte Antigen-DR (HLA-DR), which is a Major Histocompatibility Complex (MHC) class II molecule, has also been associated with outcome in ICI-treated melanoma patients (13–16). Nevertheless, despite the plethora of different markers, none of those mentioned can predict response with acceptable accuracy and none of them have been prospectively evaluated in the context of a clinical trial which is why they have not found their way to daily clinical practice.

HLA-DR molecules are dimeric surface receptors that are mainly expressed in professional antigen presenting cells to present antigen peptides to CD4+ T cells in order to elicit an adaptive immune response. HLA-DR, HLA-DQ and HLA-DP are the three major MHC class II genes. Among these, HLA-DR is the most ubiquitously expressed. Expression of HLA-DR molecules requires the expression of CIITA, a transcriptional coactivator known as the master regulator of MHC II transcription. In an inflammatory microenvironment, MHC II molecules can be aberrantly expressed by non-hematopoietic cells, including melanoma cells (17), which, similar to PD-L1 expression in melanoma, can occur following secretion of IFNγ by NK cells and cytotoxic T cells (18, 19). Binding of IFNγ to its receptor induces JAK/STAT signaling, which initiates transcription of CIITA *via* binding of STAT-1 to the CIITA promoter IV (20). Intuitively, it could therefore be hypothesized that the aberrant MHC II expression by melanoma cells would stimulate the immune response by increasing the presentation of tumor-specific antigens. However, other interactions are needed to elicit T cell activation, in particular the expression of co-stimulatory receptors (21, 22). Contrary to that, MHC II is also a ligand to Lymphocyte-activation gene 3 (LAG3), a checkpoint molecule that is expressed by activated T lymphocytes. Upon sustained interaction with MHC II positive melanoma cells, activated lymphocytes will evolve into exhaustion, and thus become inactivated (23). These different mechanisms and the additional cofactors may explain why MHC II expression is associated with an unfavorable prognosis in some studies, but with tumor regression and longer survival in others (18, 24–28).

Although some features such as enhanced tumor infiltrating lymphocytes (TILs), the presence of a lymphocytic activation pathway and the occurrence of tumor-specific CD4+ T cells preventing the activation of cytotoxic T cells through production of tumor necrosis factor α (TNFα) have been reported in HLA-DR+ melanoma (13, 29, 30), relatively little is known about the underlying mechanisms and the actual composition of the tumor microenvironment in these areas. The goal of our study was therefore to explore the tumor microenvironment in HLA-DR positive areas of malignant melanoma in order to get deeper insights into the composition of the infiltrate and the possible interactions between the local inflammatory cells. To this aim, we characterized the immune microenvironment in HLA-DR positive and negative areas using a multi-omics approach, combining spatial single-cell profiling using multiplexed immunohistochemistry, but also RNA sequencing (RNA-seq) from micro dissected material and cytokine profiling (**Figure 1**). As such, we identified in HLA-DR positive tumors a concentration of immune cells specifically in HLA-DR-expressing areas of the tumor, and this was due to a germinal center-like microenvironment. We found evidence at multiple levels that this microenvironment was also characterized by T cell exhaustion, hyperactivity of the antigen presentation pathways, and simultaneous higher levels of PD-1 in the immune cells and PD-L1 in the HLA-DR+ melanoma cells.

MATERIALS AND METHODS

Patient Selection

The clinical features of the patients included in the study are summed up in **Supplementary Table 1**. A first data set of 9

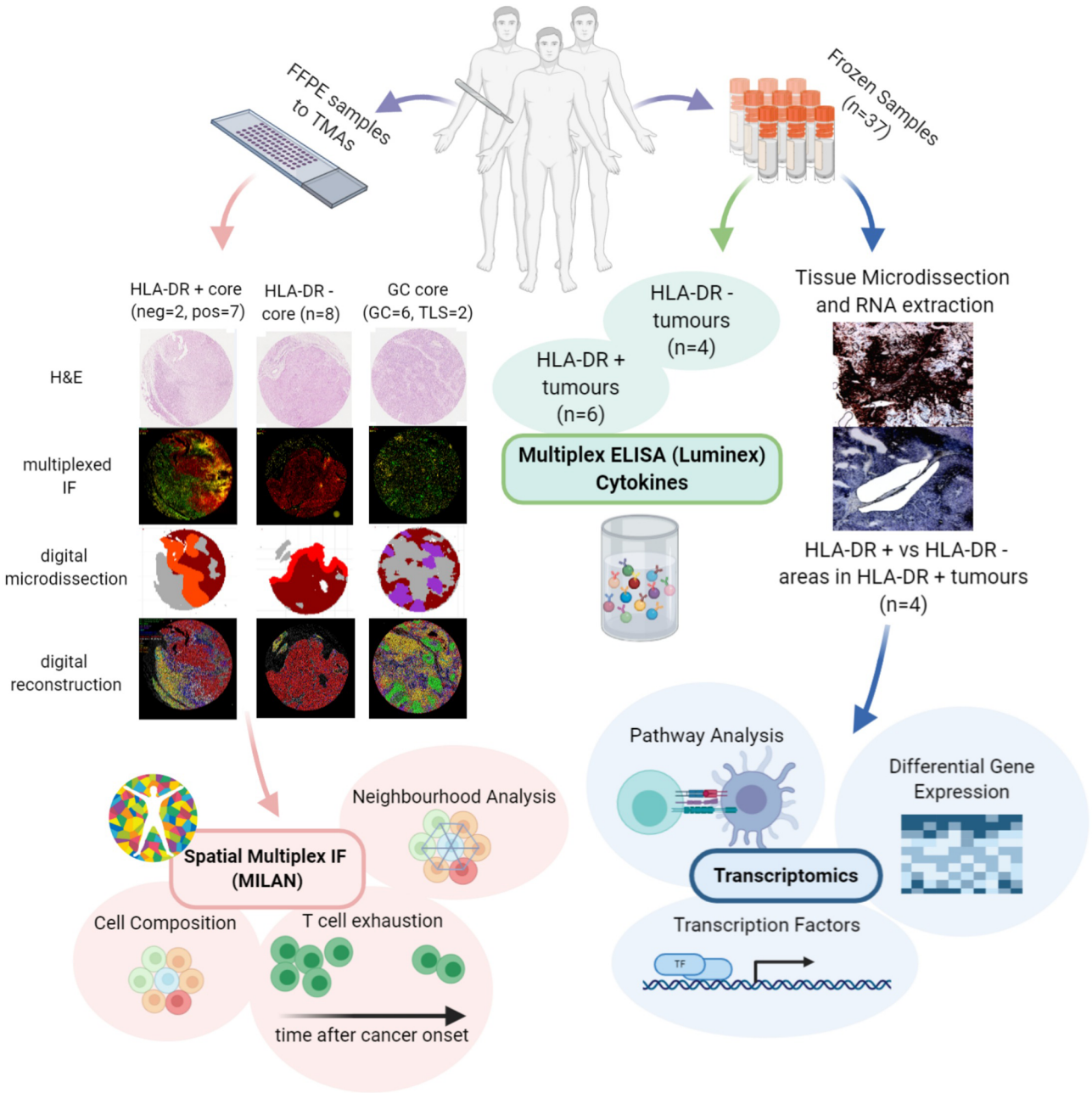

FIGURE 1 | Investigation of the microenvironment of HLA-DR positive metastatic melanoma samples using multi-omics approach. FFPE samples from patients expressing HLA-DR+ metastatic melanoma were selected and transferred to TMAs. Then, MILAN was performed on HLA-DR+ and HLA-DR- areas in order to characterize the immune microenvironment at single-cell level. The data extracted allowed investigating the cell composition, performing the neighborhood analysis and revealed presence of T cell exhaustion. The cell composition and neighborhood analyses was repeated for germinal centers/tertiary lymphoid structures to provide more evidence about the similarity between the features characterizing the immune microenvironment of HLA-DR + and HLA-DR- areas and the germinal centers. In parallel, Multiplexed immunohistochemistry was applied to the frozen samples of HLA-DR+ tumors to reveal HLA-DR+ regions. The regions were micro dissected to compare Pos and NegInPos areas of selected cases with adequate RNA quality. Gene expression analysis, transcription activity and pathway analysis revealed signatures related to both pro-inflammatory and anti-inflammatory roles and an upregulation of multiple biological pathways primarily involving the immune system function. Finally, multiplexed ELISA was performed on HLA-DR+ and HLA-DR- tumors taken from the frozen sample dataset to investigate which cytokines predominantly drive the composition of the tumour microenvironment.

melanoma metastases (4 HLA-DR+, 5 HLA-DR-), 4 lymph nodes from completion lymphadenectomies and 1 case with tertiary lymphoid structures adjacent to a cutaneous melanoma metastasis with available FFPE material were collected from the archive of the Department of Pathology of the UZ Leuven (Leuven, Belgium) and assembled in a Tissue Micro Array (TMA) with a variable number (1–3) of 2-mm cores per patient according to the size of the tumor and the extension of the HLA-DR+ areas in order to achieve a satisfactory representation of the HLA-DR+ and HLA-DR- areas. A second data set of 37 fresh frozen melanoma metastases was collected in order to select cases for laser microdissection and NGS sequencing. HLA-DR immunohistochemistry (Abcam, SPM289, 1:1000, 4 µ slides, targeting the alpha subunit of HLA-DR molecule) was performed, and 4 HLA-DR+ cases were selected for microdissection on the basis of a higher RNA quality obtained after RNA extraction. Other 10 frozen samples (6 HLA-DR+ and 4 HLA-DR-) from this data set were used as a validation cohort for multiplex ELISA analysis.

Multiplexed Immunohistochemistry Using the MILAN Method

Multiplexed immunofluorescence staining was performed according to the previously published MILAN protocol (31, 32), which makes use of a cyclic staining-stripping approach. An overview of the panel of markers and antibodies used can be found in **Supplementary Table 2**. Immunofluorescence images were scanned using the NanoZoomer S60 Digital slide scanner (Hamamatsu, Japan) at 20X objective with resolution of 0,45 micron/pixel. Image analysis, feature extraction and phenotypic identification of the main cell types was performed following the procedure described in Bosisio et al. (33). Briefly, DAPI images from consecutive rounds were aligned (registered) using the Turboreg and MultiStackReg plugins from Fiji/ImageJ (version 1.51 u). The coordinates of the registration were saved as Landmarks and applied to the rest of the channels. Tissue autofluorescence was subtracted from an acquired image in a dedicated channel, for FITC, TRITC and Pacific Orange. The TMA was segmented into tissue cores using a custom macro. Cell segmentation, and feature extraction were performed using a custom pipeline in CellProfiler (version 2014-07-23T17:45:00 6c2d896). MFIs were further normalized to Z-scores as recommended in Caicedo JC et al. (34). Z-scores were trimmed between −5 and +5 to avoid a strong influence of any possible outliers in the downstream analysis. Cell subpopulations were identified by applying in a subset of all cells (25,000) three different clustering methods: PhenoGraph, ClusterX and K-means over the 38 included phenotypic markers: CD138, CD14, CD141, CD16, CD163, CD1A, CD1C, CD2, CD20, CD21, CD23, CD248, CD25, CD27, CD3, CD303, CD31, CD34, CD4, CD5, CD56, CD64, Cd68, CD79A, CD8, CK, FOXP3, GRB7, HLA-DR, IRF4, IRF8, LYZ, MELANA, PAX5, PNAD, PODOPLANIN, PRDM1, and S100B. A fingerprint for each cluster was constructed by averaging the expression of all their cells for each marker. These fingerprints were associated with known cell phenotypes by manual annotation from domain experts (FMB, YVH). This way we have three annotations for each cell, one per clustering method. The final annotation was obtained by applying a consensus-based approach: if two or more of the clustering methods agreed on the assigned phenotype, then the cell was labelled as such. If all three clustering methods assigned different cell phenotypes, the cells were labelled as "other". In **Supplementary Figure 1A** are shown the fingerprints with the expression of all the markers used for clustering in relation to every identified cell type *via* the consensus-based approach. These fingerprints were used to label the cell phenotype of the remaining cells in the entire dataset (minimum of Euclidean distance). We further characterized specific cell types by applying manual gating to the expression (asinh transformed) of specific markers, as indicated in **Supplementary Figures 1B–D**. We identified T Follicular Helpers based on PD-1 expression in the T helpers (Th) cluster (TFH, PD-1 high); based on expression of BCL6 and BCL2, B cells were sub classified into germinal center B cells (BCL6+/BCL2-, BC_GerminalCenter), early germinal center B cells (BCL6+/BCL2+, BC_EarlyGerminalCenter) and B cells not further specified (BCL6-/BCL2- and BCL6-/BCL2+, BC); finally, melanoma cells were stratified into HLA-DR+ and HLA-DR- melanoma cells (HLADRpos_mel and HLADRneg_mel).

In Silico Tissue Microdissection

We digitally micro dissected the tissue cores by fragmenting the tissue into 50x50 pixel tiles (~22 sq micrometers). Tiles with at least 1 cell identified as tumor were initially defined as tumor areas. To reduce the impact of potential outliers a median filter was applied to the obtained tumor masks. Similarly, to define germinal centers we created a mask for the tiles containing at least 50% of follicular dendritic cells (fDC), germinal center B cells (BC_GerminalCenter) or B cells not further specified (BC) in the tile. Then, we filtered out all the objects in the mask smaller than 10 tiles (~220 sq micrometers). Finally, we removed those objects not containing all three cell types used to define the mask (fDC, BC_GerminalCenter, BC).

To reproduce as much as possible the conditions that we would have applied during real life microdissection, in a second step we manually dissected the tumor areas of HLA-DR+ tumors into HLA-DR+ areas ("Pos") and HLA-DR- areas ("NegInPos"). Given that HLA-DR+ areas were always in the tumor edge, only HLA-DR- areas at the tumor border were included. In addition, we manually micro dissected the tumor borders of HLA-DR- tumors ("NegTum"). Finally, we micro dissected germinal centers from reactive lymph nodes ("GC") and germinal centers from tertiary lymphoid structures ("TLS") from a cutaneous melanoma metastasis.

Cell Composition Analysis

We compared the cell proportion and density (cell counts per square millimeter) of the different micro dissected areas using Wilcoxon's rank sum test. The reader should note that we removed the "other", "stroma", and "epithelial" cell phenotypes from the comparison due to the lack of relevance of these cell types for our analysis. An overview of the p-values derived from all these comparisons can be found in **Supplementary Table 4**.

P-values were not adjusted for multiple comparisons due to the relatively low number of samples and the exploratory nature of the study.

Neighborhood Analysis

We characterized the immune landscape of the different dissected tissue types by neighborhood analysis (35). We focused on short distance cell-cell interactions by selecting a kernel of radius = 50px (~22 micrometers) and assigned an empirical p-value by a permutation test (N = 1000). The size of the kernel that defines the neighborhood of a cell is a user-defined parameter and depends on whether we want to see short/medium/long-distance interactions. For this particular study, we are interested in short-distance interactions and have set the radius of the neighborhood kernel to 50 pixels (~22 micrometers). Considering that the average cell-radius size in this dataset is of 7 micrometers and that the distance between two cells is calculated from their centers, this corresponds to less than 1 cell diameter from the edge of the cell. In brief, the neighborhood analysis method described by Schapiro et al. (35) counts specific cell pairs at a user-defined distance and compares them with the counts that could be found in the random case. This random case is built by permuting the labels of all the cells a number of times (N=1000). This approach allows us to compare the number of interactions observed in the real tissue and compare them with randomized cases to assign a significance value to a cell-cell interaction representative of the spatial organization of the cells. Neighborhood analysis was limited to the in-silico micro dissected areas (Pos, NegInPos, NegTum, GC and TLS). In the tumor areas (Pos, NegInPos and NegTum), the large majority of cells are melanoma cells. Therefore, we did not randomize the position of melanoma cells in the permutations since the melanoma cells are organized in large clusters with relatively few interactions to the rest of the cells. A complete randomization would thus exaggerate all the other cell-cell interactions which can lead to misleading results. Interaction scores across different samples were integrated using a weighted average. The weight for each sample was defined as the log10 of the geometric average of the counts for the two cell types being considered. Finally we classified the nature of the interaction between two cells types into "strong interaction" if the number of counts in the observed tissue was higher than 950 random cases (p-value < 0.05), "moderate interaction" if the number of counts in the observed tissue was higher than 900 random cases (p-value < 0.1), and "no interaction" otherwise (p-value > 0.1). "Other", "stroma", and "epithelial" cell phenotypes were not included in the neighborhood analysis due to the lack of relevance of these cell types.

Laser Capture Microdissection and RNA Sequencing

HLA-DR+ tumor/areas were identified by screening all the mentioned data sets *via* conventional immunohistochemical staining for HLA-DR (Abcam, SPM289, 1:1000). A tumor was considered positive if showing tumor areas with HLA-DR expression in melanoma cells. HLA-DR expression in our data sets was generally zonal, as expected, and located at the margin of the tumors at the tumor-stroma interface. Two expert dermatopathologists (LG, FB) evaluated the HLA-DR positivity and classified the tumors as positive, distinguishing HLA-DR expression in inflammatory cells (e.g. macrophages/dendritic cells) from real expression in melanoma cells in a similar way as it is done in the clinics for PD-L1 evaluation, that is considered to be the gold standard. In this way, only areas with real HLA-DR expression in melanoma cells (and not exclusively in inflammatory cells) were microdissected. Laser microdissection was executed by the expert dermatopathologists on the section immediately consecutive to the one that was stained for HLA-DR (**Figure 2**). Laser microdissection (LMD) of HLA-DR+ and HLA-DR- tumor areas was performed in HLA-DR+ tumors. The microdissection was restricted to the marginal zone of the tumors both in positive and negative areas limiting the amount of stroma included to strictly peri-tumor. An average of around 2000 tumor cells was dissected per vial. RNA extraction from the LMD samples was performed by usage of a special RNA extraction kit for LMD samples (RNAqueous®-Micro Kit, Life

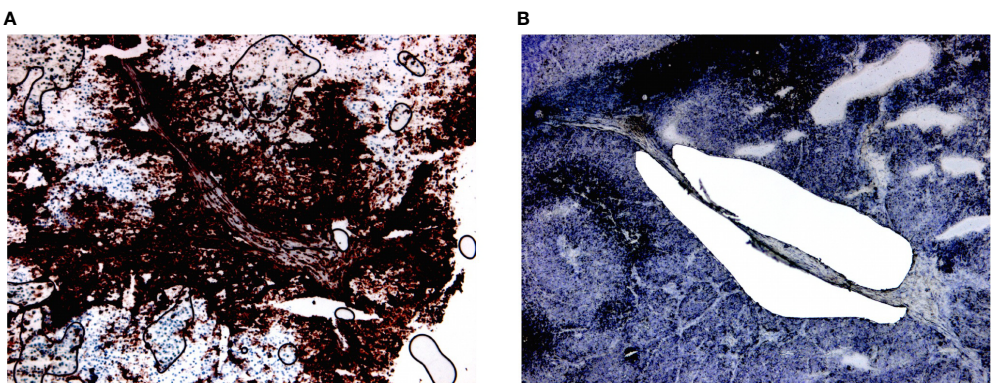

FIGURE 2 | Laser microdissection of HLA-DR+ areas in HLA-DR+ tumors. **(A)** HLA-DR+ areas were identified using conventional immunohistochemical staining for HLA-DR. HLA-DR expression in melanoma cells located at the margin of the tumors at margins of the tumour nodules, at the so-called tumour-stromal interface. **(B)** Laser microdissection was executed on the immediately consecutive section after morphological recognition of the HLA-DR+ region.

Technologies Corporation). Before submission to RNA sequencing analysis, RNA quality of the LMD samples was assessed using the Bioanalyzer RNA 6000 pico assay (Agilent). Four cases with acceptable RNA Integrity Number (RIN between 3,90-6,90) were selected. RNA sequencing analysis was performed using the Quantseq protocol (Lexogen).

Computational Analysis of Gene Expression Data

RNA-Seq.fastq files were aligned to the reference genome (CRCh38.p12, gencode.v31) using STAR v2.7. Raw counts were then obtained using the featureCounts function from the RSubread R package. Counts were normalized using the DESeq2 R package. The sequencing data is available at the European Nucleotide Archive (ENA) under the accession number PRJEB41749. Next, samples were grouped and we compared the expression of HLA-DR+ vs HLA-DR- areas in matched patients. For differential gene expression analysis we applied the DESeq2 R package with standard thresholds (p-value = 0.05, logFC = ± 1). Since transcription factors might only become active in a phosphorylated state or in the presence of coactivators, differential mRNA expression cannot provide us with information about their activation. Therefore, the activity of the transcription factors was predicted based on the expression of their targets using DOROTHEA (36). Only transcription factors with a confidence level of A, B, and C were kept for this analysis. Because complex and heterogeneous phenotypes are often not the answer to large changes in individual genes but rather smaller changes in functionally correlated genes, we subsequently performed pathway analysis using Piano (37). Implementing the Piano framework, we used the following 10 pathway analysis methods and gene-level-statistics: Fisher (p-value), Stouffer (p-value), Reporter (p-value), tailStrength (p-value), Page (t-value), GSEA (t-value), maxmean (t-value), Mean (FC), Median (FC), Sum (FC). The molecular Signatures Database (MSigDB), curated pathways (c2), canonical pathways (cp) version 7.0 was used for the definition of the gene sets. This database contains 11763 genes mapping to 2199 pathways.

Luminex Analysis

Proteins were extracted from five 10 micrometers-thick cryostat sections according to the protocol of Allred et al. (38). We built and validated a customized Multiplex ELISA panel for the Luminex Flexmap 3D at Protavio (Athens, Greece), coupling different magnetic beads from Luminex with the capture antibody of the duoset ELISA from R&D Systems and Standard ABTS ELISA Development Kit from Peprotech against human INFγ, IL6, IL10, TNFα, IL4, CXCL10, IL17, IL13, CCL18, TGFβ, IL23, CXCL13, CXCL12, and CCL19. Initially, we explored the information content of these 14 markers using unsupervised dimensionality reduction (hierarchical clustering and uMap). Next, we trained machine-learning models (linear discriminant analysis, LDA) using panels of 1 to 14 markers at the time. We fitted each model following a leave-one-out cross-validation scheme. Mean Fluorescence Intensities (MFIs) were normalized (z-scores) before training the LDA models. For each panel size, the best panel was selected as the one maximizing accuracy. Models with the same accuracy were prioritized by minimizing the residual probabilities. Following Ockham's razor, we want the simplest model that explains the data. To that end, we finally selected the optimal model by applying the elbow criterion on the generated Pareto front to select the smallest panel size that provides a good predictive ability.

RESULTS

Single Cell Characterization of the Tumor Microenvironment of HLA-DR Positive and Negative Areas in Metastatic Melanoma

The main goal of this study was aimed at defining the composition and characteristics of the tumor microenvironment of HLA-DR+ metastatic melanoma samples compared to HLA-DR- negative areas/tumors at single cell and spatial level. As a first step, we screened a cohort of metastatic melanoma tissue samples for HLA-DR expression. By performing IHC for HLA-DR in these samples, we identified samples in which the melanoma cells did not express HLA-DR (HLA-DR-) and samples in which tumor cells were expressing high levels of HLA-DR (HLA-DR+) (**Supplementary Table 1**). Importantly, in this second group, HLA-DR expression in the tumor cells was mostly not homogeneous but expressed mainly at the borders of the tumor where tumor cells were interacting with the adjacent stromal tissue. The borders of the HLA-DR+ tumors were not circumferentially positive but positive areas and negative areas could both be present at the borders of a HLA-DR+ tissue sample (**Figure 1**). Therefore, in HLA-DR+ tumors we analyzed and compared the microenvironment of HLA-DR+ areas ("Pos") and HLA-DR- areas ("NegInPos") and in HLA-DR- tumors we sampled the border zone ("NegTum"). As the next step, we wished to understand the cellular composition of each of these regions, with a strong focus on the immune infiltrates and their interactions. To achieve this, we performed spatially-resolved, single-cell, multiplexed immunohistochemistry using the MILAN method (see methods) using a broad panel of inflammatory, tumor and other stromal cell markers (**Supplementary Table 2**). Following quality control and cell clustering of ~544k DAPI+ cells using the main phenotypic markers across the included samples, the large majority could be unequivocally mapped and identified as tumor, endothelial, myeloid (macrophage or dendritic cells), T, B, NK, and stromal cells (**Supplementary Figure 1A**). These were subsequently combined with a number of functional markers, resulting in the identification of 23 robust cell types (**Figure 3A**, **Table 1**). Using this approach, we observed that ~7% of the identified MelanA +/S100B+ melanoma cells were also positive for HLA-DR (13497 HLA-DR+ vs 177829 HLA-DR- cells). Areas enriched in HLA-DR + melanoma cells ("Pos") showed the same zonal distribution as described for the conventional immunohistochemically staining for HLA-DR (**Figure 2**). In each of the samples, we subsequently defined the different areas ("Pos", "NegInPos" and "NegTum"), including also non-tumor lymphoid areas (Germinal centers "GC" and tertiary lymphoid structures "TLS") for

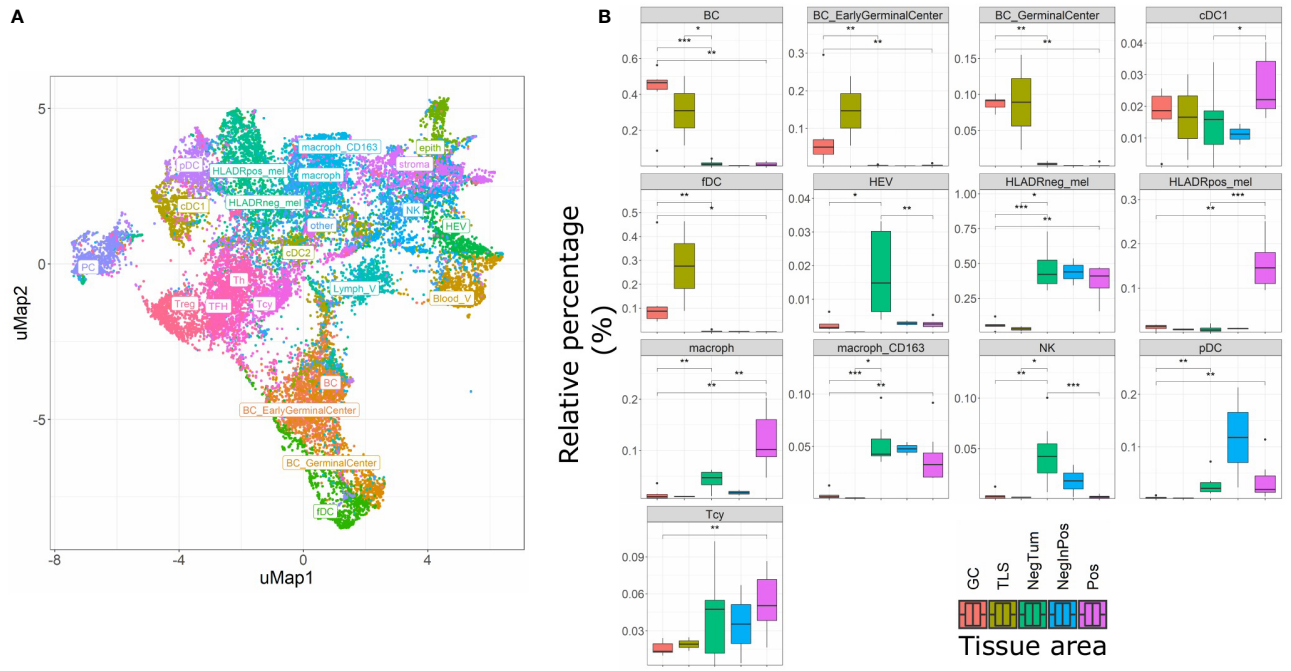

FIGURE 3 | Single cell composition of HLA-DR+ areas, HLA-DR- areas in positive tumors, HLA-DR- tumors, germinal centers and tertiary lymphoid structures. **(A)** uMap of a subset of cells (22,000) from the complete dataset included in this analysis (544,910 cells). BC= B cell not further specified; BC_EarlyGerminalCenter= Early germinal center B cell; BC_GerminalCenter= Germinal center B cell; cDC1 = Classical dendritic cell type I; fDC= Follicular dendritic cell; HEV= High endothelial venule; HLAneg_mel= HLA-DR negative melanoma cell; HLADRpos_mel= HLA-DR positive melanoma cell; macrop= Macrophage; macrop_CD163= CD163 positive macrophage; NK= Natural Killer cell; pDC= Plasmacytoid dendritic cell; Tcy= Cytotoxic T cell; Treg= Regulatory T cell; TFH = T Follicular Helper cells; Th= T helper cell; PC = Plasma cell; cDC2 = Classical dendritic cell type II; Stroma= Stromal cell; epith= Epithelial cell; Lymph_V= Lymphatic vessel; other= Cells not further specified. **(B)** Boxplots indicating the relative proportion of different cell-types in the different micro dissected areas, from left to right: 'GC' (Germinal center from reactive lymph nodes; orange), TLS (germinal centers from tertiary lymphoid structures, ochre), 'NegTum' (Tumour border of HLA-DR negative tumors, green), 'NeginPos' (HLA-DR negative area of HLA-DR positive tumors, blue) and 'Pos' (HLA-DR positive area of HLA-DR positive tumors, pink). Significance levels indicate: *p-value ≤ 0.05, **p-value ≤ 0.01, ***p-value ≤ 0.001. P-values are derived from Wilcoxon tests (not fdr corrected).

comparison. Next, we determined both the relative distribution as well as the cell density of the identified cell types across these different areas (**Figure 3B**, **Supplementary Figures 2–3** and **Supplementary Table 3**). In the lymphoid compartment, Tcy were generally more present in tumor than GC/TLS, with a significant difference between Pos and GC, while Th, Treg did not show significant differences. All subtypes of B cells were enriched as expected in GC/TLS compared to the tumor. NK cells were strongly enriched in NegTum compared to HLA-DR+ tumors. Among dendritic cells, the main differences were the expected high abundance of fDC in GC; an enrichment of cDC1 in Pos compared to both the NegTum and NegInPos; a higher density, but not proportion, of cDC1 in GC in comparison with Neg; and a general enrichment of pDC in the tumor compared to GC. The macrophage compartment showed a peculiar distribution among the different areas: M1-like macrophages were abundantly present in Pos compared to NegTum, while NegInPos had a lower proportion of them (though this difference was non-significant for density). M2-like macrophages, on the other hand, were entirely absent in the GC/TLS areas, while they were present in all tumor areas. We found differences also in the vascular composition of the areas: high endothelial venules (HEV) were significantly more present in NegTum compared to GC/TLS or HLA-DR+ tumors, in which HEVs were equally less represented in both Pos and NegInPos. There were also some trends that did not reach significance but for which borderline p-values were observed. In particular, we found an enrichment of plasma cells in Pos compared to the adjacent NegInPos, of lymph vessels in NegInPos and of blood vessels in the tumor areas, while Pos tended to have less TFH than NegTum and GC/TLS. **Supplementary Table 4** includes the p-values for all comparisons in terms of cell density as well as cell proportion.

Next, we evaluated the activation status of the Tcy located in the different areas according to a defined algorithm that makes use of a panel of activation and exhaustion markers including CD69, TIM3, OX40, LAG3 as previously published (**Figure 4A**) (33). We compared activation levels in the different areas using a t-test with false-discovery-rate (fdr) correction. We found levels of exhaustion of the Tcy to be higher in HLA-DR+ tumors compared to the HLA-DR- ones (p-adj=5.80×10^{-61}), and within the positive tumors, the Tcy were particularly exhausted in Pos compared to NegInPos (p-adj=9.92×10^{-7}). Moreover, since HLA-DR overexpression was found to be associated with response to anti-PD-1 therapy (13, 16), we also evaluated the

TABLE 1 | Main cell types identified with MILAN.

Cell type	Cell subtype	Abbreviation	# cells	% overall	% subtype	Cell density(cells/mm²)
B cell	Not further specified	BC	39 600	7.27	61.09	13 356
	Early germinal center	BC_EarlyGerminalCenter	6 920	1.27	10.67	2 334
	Germinal center	BC_GerminalCenter	7 161	1.31	11.05	2 415
Plasma cell	N/A	PC	11 146	2.05	17.19	3 759
T cell	T helper	Th	38 308	7.03	41.34	12 920
	Regulatory T cell	Treg	13 074	2.4	14.11	4 410
	T Follicular Helper	TFH	16 845	3.09	18.18	5 681
	Cytotoxic T cell	Tcy	24 432	4.48	26.37	8 240
Natural Killer cell	N/A	NK	7 581	1.39	100	2 557
Dendritic cell	Classical dendritic cell type I	cDC1	22 736	4.17	47.14	7 668
	Classical dendritic cell type II	cDC2	11 841	2.17	24.55	3 994
	Follicular dendritic cell	fDC	5 325	0.98	11.04	1 796
	Plasmacytoid dendritic cell	pDC	8 329	1.53	17.27	2 809
Macrophage	Macrophage	Macroph	23 776	4.36	49.46	8 019
	CD163 positive macrophage	Macroph_CD163	24 291	4.46	50.54	8 193
Melanoma	HLA-DR+ melanoma	HLADRpos_mel	13 497	2.48	7.05	4 552
	HLA-DR- melanoma	HLADRneg_mel	177 829	32.63	92.95	59 977
Vasculature	Blood vessel	Blood_V	16 388	3.01	44.77	5 527
	High Endothelial Venule	HEV	6 460	1.19	17.65	2 179
	Lymphatic vessel	Lymph_V	13 757	2.52	37.58	4 640
Epithelial cell	N/A	Epith	1 941	0.36	100	655
Stromal cells	N/A	Stroma	10 546	1.94	100	3 557
Other	N/A	other	43 127	7.91	100	14 546

Overview of the number of cells detected and both the relative proportion (% of all cells and the % of each subtype) as well as the cell density (cells/mm²) of all identified cell types in the MILAN analysis, not discriminating between the different micro dissected areas. For the expression/marker profile of each cell type, we refer to ***Supplementary Figure 1****. N/A, not applicable.*

expression of PD-1 in the different areas, thereby observing that Pos also had higher levels of PD-1 expression (Wilcoxon rank sum test, fdr corrected, $p\text{-}adj_{NegTum}=4.22\times10^{-7}$, $p\text{-}adj_{NegInPos}=3.54\times10^{-4}$) (**Figure 4B**). In addition, considering higher PD-L1 expression being described in HLA-DR+ melanoma cell lines and that HLA-DR mediated signaling increases the expression of PD-L1 in melanoma cells (13, 39), we compared the expression of PD-L1 between HLA-DR- and HLA-DR+ melanoma cells and could observe significant higher expression levels in the HLA-DR+ melanoma cells (Wilcoxon rank sum test, fdr corrected, p-adj < $1x\ e^{-16,}$**Figure 4C**). Summarizing the above, we could show simultaneous higher PD-1 expression on the immune cells surrounding the HLA-DR+ melanoma cells that have higher PD-L1 expression compared to the HLA-DR- melanoma cells.

Finally, we investigated the various cell-cell interactions between all the identified cellular subtypes in each of the defined areas (**Figures 5A, B**). As positive control, we found that the GC had a florid interaction network, including the ones that we expected in the B cell (where the various B cell and plasma cells are interacting with the fDCs cells) and T cell zones (with a network of TFH, Th, Tcy and Treg cells) (**Figures 5A, B**, left panels). In the tumor areas, we mainly found interactions of M1-like macrophages with either HLA-DR+ and HLA-DR- melanoma cells. Though, the strength of interaction and the other actors involved in the interactions with the two melanoma cell types were different in positive and negative tumors: while in NegTum HLA-DR- melanoma cells strongly interacted with M1-like macrophages and also had interactions with pDC (**Figures 5A, B**, central panels), in Pos the interaction between HLA-DR- melanoma cells and M1-like macrophages was weaker and accompanied by interactions with cDC2, while the stronger interaction was between M1-like macrophages and HLA-DR+ melanoma cells (**Figures 5A, B**, right panels). In addition, specifically in Pos, small communities of mixed T and B cells were found, where in particular Treg interacted with TFH and Tcy, TFH with Th, and Tcy with BC_GerminalCenter. HLA-DR negative tumors presented instead a smaller T community composed of Tcy in contact with TFH.

Gene Expression Analysis, Transcription Factor Activity Analysis and Pathway Analysis Identify Signatures Related to a Mixed B-T Microenvironment, With Upregulation of IFNγ and Antigen Presentation but Also With Clues Towards Immunosuppression in HLA-DR+ Tumor Areas

To further corroborate and further expand the previous findings, we also performed a transcriptome analysis of micro dissected samples comparing Pos and NegInPos areas of selected cases with adequate RNA quality of the data set with frozen samples. From the 55,401 genes included in the analysis, we found 162 genes significantly overexpressed and 66 genes significantly under expressed (abs(logFC)>1, p-value<0,05) (**Figure 6A**, **Supplementary Table 5**). We identified the gene functions of the most expressed genes using the Genecards and Uniprot database (40, 41). The overexpressed genes in HLA-DR+ versus HLA-DR- areas were divided into 8 subgroups: (1) HLA class II and related genes (HLA-DPB1, HLA-DRB1, HLA-DPA1, CIITA, CTSS), (2) cytokines, chemokines and cell signaling

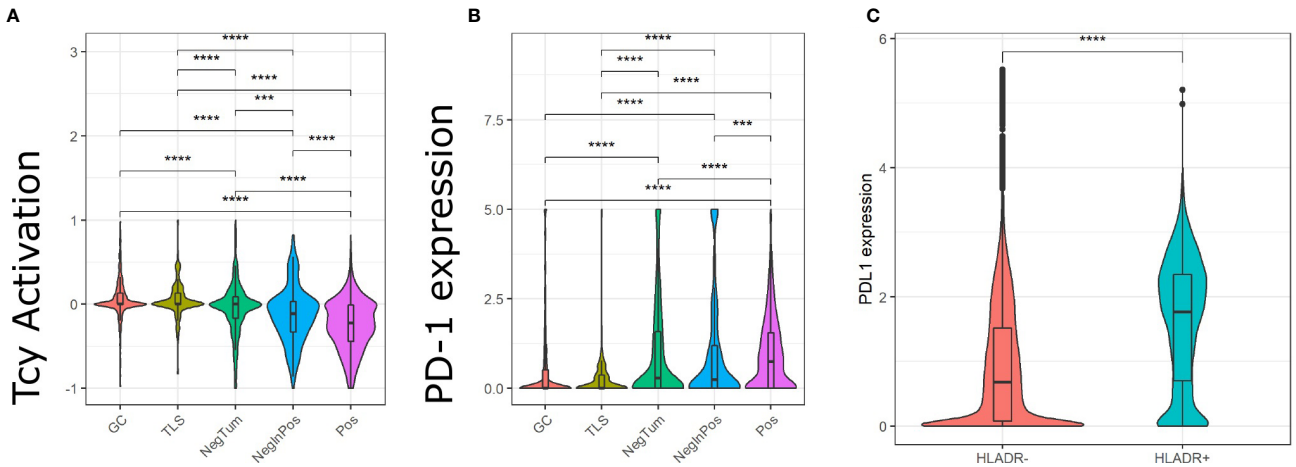

FIGURE 4 | Analysis of Tcy activation status, TIM3 and PD-1 in the *in-silico* micro dissected areas. Violin plots of the activation score **(A)** and PD-1 **(B)** for the cytotoxic T cells (Tcys) in the different micro dissected areas. P-values are derived from pairwise t-test **(A)** and Wilcoxon test **(B)**. **(C)** Difference in expression of PD-L1 in HLA-DR+ melanoma versus HLA-DR- melanoma. P-values are derived from Wilcoxon Rank Sum and Signed Rank Test. Significance levels indicate: *** p-value ≤ 0.001, **** p-value ≤ 0.0001. P-values were adjusted using the false discovery rate (fdr) method

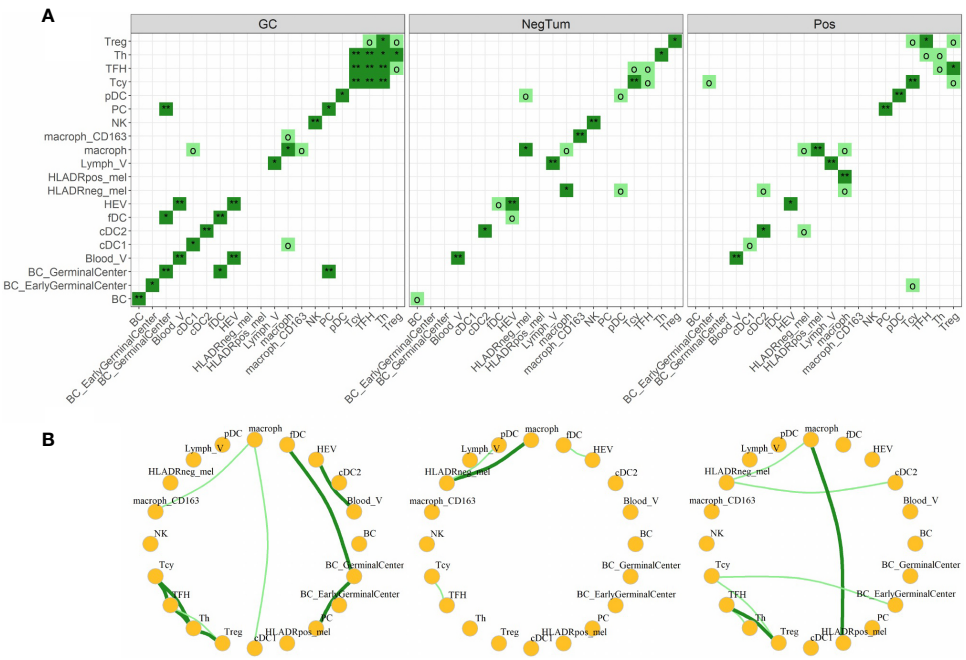

FIGURE 5 | Neighborhood analysis. **(A)** Heat maps indicating the significance of cell-cell interactions in the different micro dissected areas. Interactions go from "strong interaction" (dark green, p-value < 0.05), "moderate interaction" (light green, p-value < 0.1), to "no interaction" (white, p-value ≥ 0.1). Significance levels indicate: o p-value < 0.1, *p-value < 0.05, **p-value < 0.01. **(B)** Social networks obtained from moderate and strong interactions. Each node in the graph represents a cell-type and each edge an interaction.

receptors (TGFB1, TLR10, ZFP36, CXCL14, KIR2DL4, TNFSF15), (3) T and NK cell function related genes (KIR2DL4, CYTIP, TIM3/HAVCR2, FASLG, SLAMF7, BHLHE41, LGALS9), (4) B cell function related genes (BANK1, IGHM), (5) myeloid and monocyte related genes (MNDA, APOBEC3A), (6) cell growth and differentiation related genes (ST14, SPINT2, PRKCB, JUNB, MIXL1, ADIRF, RELB), (7) cell structure, motility and metabolic genes (APOL1, SNCG, SYTL3, CAPG, STAC3, MYOM1, DSP, DSC3, TINAGL1, BVES, FMO2, PLA2G4A, ALOX5) and (8) cell

A

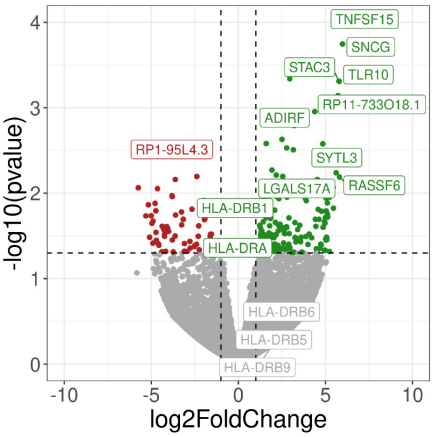

B

Pathway ID	Brief description	Rank	p.value
KEGG_ANTIGEN_PROCESSING_AND_PRESENTATION	Antigen processing and presentation	7	1.06E-04
KEGG_NATURAL_KILLER_CELL_MEDIATED_CYTOTOXICITY	Natural killer cell mediated cytotoxicity	10	1.07E-04
KEGG_B_CELL_RECEPTOR_SIGNALING_PATHWAY	B cell receptor signaling pathway	11	1.07E-04
KEGG_ALLOGRAFT_REJECTION	Allograft rejection	12	1.08E-04
KEGG_GRAFT_VERSUS_HOST_DISEASE	Graft-versus-host disease	15	1.08E-04
PID_IL12_2PATHWAY	IL12-mediated signaling events	20	1.55E-04
PID_TCR_PATHWAY	TCR signaling in naïve CD4+ T cells	22	1.68E-04
BIOCARTA_CTL_PATHWAY	CTL mediated immune response against target cells	24	1.88E-04
BIOCARTA_DC_PATHWAY	Dendritic cells in regulating TH1 and TH2 Development	26	2.17E-04
BIOCARTA_IL2RB_PATHWAY	IL-2 Receptor Beta Chain in T cell Activation	27	2.24E-04
PID_CD8_TCR_PATHWAY	TCR signaling in naïve CD8+ T cells	28	2.81E-04
BIOCARTA_TCRA_PATHWAY	Lck and Fyn tyrosine kinases in initiation of TCR Activation	29	2.81E-04
BIOCARTA_NO2IL12_PATHWAY	NO2-dependent IL 12 Pathway in NK cells	30	2.81E-04

FIGURE 6 | Transcriptomic analysis. **(A)** Volcano plot showing differential gene expression between HLA-DR+ and HLA-DR- tumour areas. The x-axis represents the log2 of the fold change while the y-axis represents the -log10 of the p-value derived from a t-test. P-values here are not corrected for multiple comparisons given the low number of samples included in the analysis. Dashed lines represent the typical thresholds used in differential gene expression to define significance (1 and -1 for the log2FoldChange and -log10(0.05) for the p-value). Genes in the top-right corner (green) are overexpressed in HLA-DR+ areas compared to HLA-DR- areas while genes in the top-left corner (red) are overexpressed in HLA-DR- areas. The gene names for the top 10 most significant genes are also included in their respective position. Differential gene expression of different HLA-DR genes are also included among the gene names. **(B)** Pathway analysis of HLA-DR+ areas compared to HLA-DR- areas. Interesting pathways from the top 30 up-regulated pathways are included.

cycle related genes (RASSF2, RASSF6, WIF1, JUNB). The overexpression of several HLA class II genes of group 1 served as an internal control, confirming the correct location of the laser-micro dissected areas. The most interesting groups for our study are number 2, 3, 4, and 5, picturing a mixed inflammatory microenvironment including B cells, T cells, NK cells and monocytes. In all these groups we could distinguish genes exerting both anti-inflammatory roles (TGFB1, TLR10, ZFP36, CYTIP, TIM3/HAVCR2) as well as genes with pro-inflammatory and activating roles (CXCL14, KIR2DL4, KIR2DL4, FASLG, SLAMF7, BANK1). Moreover, genes that inhibit angiogenesis were also present (TNFSF15, CXCL14). In addition to TIM3/HAVCR2 overexpression, also LGALS9, encoding galectin-9, a main ligand of TIM3, was found to be overexpressed. Interestingly, the genes in the myeloid-related group (number 5) are mainly IFN-induced genes. In addition, we checked the expression of specific genes associated with immunosuppression/immune checkpoints that were not included in the MILAN panel, in particular PD-L1/CD274, IDO1 and CTLA4. Both PD-L1 and IDO1 were close to the significance threshold set for this study (PD-L1: p-value=0,067; IDO1: p-value=0,051). Instead, we did not find a significant differential expression for CTLA4. Finally, among the significantly under expressed genes we identified genes involved in more general cell functions such as cell cycle regulation and metabolism but no specific immune-related genes. The functions of the genes listed in this paragraph are further discussed in **Supplementary Table 6**.

In addition, we selected the 30 transcription factors predicted to be the most differentially active between Pos and NegInPos areas and divided them in 7 groups (**Supplementary Data 4**): (1) NFKB-signaling related transcription factors (RELA, RELB, NFKB1, LYL1), (2) IFNγ-signaling related transcription factors (STAT1, STAT2, USF1, IRF1, RFXANK, RFXAP, RFX5), (3) immune cell function-related transcription factors related to T cell (TBX21/T-bet), B cell (PAX5, POU2F2), both T and B cell (BATF, IKZF1) and more various immune cell (IRF4, SPI1, SPIB), (4) cell growth and differentiation-related transcription factors (FOS, JUN, JUND, SMAD3, ELF3, GRHL2, KLF5, SP1, ETS1, ERG) and (5) a transcription factor that is in normal circumstances restricted to ovarian tissue, that will not further be discussed (FOXL2). Also the transcription factor analysis supported the idea of a mixed immune microenvironment in the HLA-DR positive areas, with predominant IFNγ signature. The functions of the transcription factors listed in this paragraph are further discussed in **Supplementary Table 7**.

Finally, we performed pathway analysis and demonstrated an upregulation of multiple interesting biological pathways primarily involving the immune system function. In **Supplementary Table 8**, all the 2119 pathways included in the database used for pathways analysis are shown. Among these, 332 pathways were significantly upregulated in the HLA-DR positive areas compared to the HLA-DR negative areas. Among these, we looked for pathways that were relevant for immune-related processes and disregarded those not adding any relevant information to our study because they were linked to general biologic pathways (**Figure 6B**, **Supplementary Table 8**). Interestingly, we found again most of these pathways to be involved in B cell activation, NK and T cell functions (both helper and cytotoxic), plus upregulation of pathways involving dendritic cells and antigen presentation and of the PD-1 signaling pathway. From a cytokine point of view, the IFNγ and the IL-12 pathway were predicted to be the most active.

Since some of the upregulated pathways show a significant number of overlapping genes, crosstalk between these pathways will definitely be present. The gene signatures of the pathways implicated in IFNγ (REACTOME_REGULATION_OF_IFNG_SIGNALING, BIOCARTA_IFNG_PATHWAY, PID_IFNG_PATHWAY) and IL-12/IL4 signaling (PID_IL12_2PATHWAY, BIOCARTA_NO2IL12_PATHWAY, PID_IL12_STAT4_PATHWAY, BIOCARTA_IL12_PATHWAY, PID_IL4_2PATHWAY), in particular, showed some overlapping genes (**Supplementary Figure 4**). Some of these were significantly overexpressed in our gene expression analysis in HLA-DR positive areas. In the IFNγ pathway, the only significantly overexpressed gene was IRF1, a downstream regulator of IFN-signaling that is rapidly induced by IFN-α, IFN-β and IFN-γ, and regulates the transcription of several IFN-γ-induced genes (20). In the case of IFN-γ-stimulation, this gene, together with USF1 cooperate in the STAT1-mediated transcription of CIITA, the master regulator of MHC II transcription (20). Concerning the IL12-pathway, CD247, FASLG, HLA-DRA, IL2RB and RELB were significantly overexpressed. CD247 encodes the protein T-cell receptor zeta, which is a subunit of the T-cell receptor-CD3 complex. The zeta chain plays an important role in coupling antigen recognition to several intracellular signal-transduction pathways and thus plays an essential role in the adaptive immune system. FASLG is the gene that encodes the protein FAS ligand, a membrane anchored protein of the TNF family that is present on activated T cells and NK cells and is essential for their cytotoxic function and T cell homeostasis. HLA-DRA encodes the alpha-subunit of HLA-DR, and is thus important for antigen presentation. IL2RB encodes the beta-subunit of the IL-2 receptor that plays a role in CD8+ T cell and NK cell mediated immune responses (42). RELB encodes a transcription factor that is involved in the alternative pathway of NFκB signaling, stimulated by a small number of TNF receptor superfamily members (such as CD40) (43). Finally, in the IL4 pathway the differential gene expression analysis showed that COL1A1, DOK2 and SOCS3, of which only SOCS3 is interesting enough to discuss. It encodes for a STAT-induced STAT inhibitor that suppresses cytokine signaling. Its expression is induced by IL6, IL10 and IFNG. This protein can inhibit the activity of JAK2 kinase, another gene in common between the IFNγ and the IL12 pathways (44).

Cytokine Expression Profiling Suggests a Germinal Center-Like Environment in HLA-DR+ Areas

Finally, we investigated which cytokines predominantly drive the composition of the tumor microenvironment in HLA-DR+ metastases. Therefore, we performed a customized Multiplex ELISA panel for the Luminex Flexmap 3D including IFNγ, IL6, IL10, TNFα, IL4, CXCL10, IL17, IL13, CCL18, TGFβ, IL23, CXCL13, CXCL12, and CCL19 comparing HLA-DR+ and entirely HLA-DR/- samples. Because sufficient material was needed to measure robust cytokine levels, we could not perform laser-assisted microdissection, but rather compared the overarching groups. The normalized (z-score) Mean Fluorescence Intensity (MFI) values of the different cytokines in each sample are summarized in **Figure 7A**. Initially, we explored the information content of these 14 markers using unsupervised dimensionality reduction (uMap). Unsupervised clustering separated only partially the HLA-DR+ and HLA-DR- cases (**Figure 7B**). This means that we had some informative markers that allowed us to distinguish HLA-DR+ from HLA-DR- melanomas, and uninformative markers that an unsupervised analysis cannot dismiss. In order to find the optimal discriminative panel, we trained Linear Discriminant Analysis (LDA) models as described in the methods, which identified a panel of 5 cytokines as the optimal panel (**Figure 7C**). These 5 markers included IFNγ, IL4, and the three germinal center cytokines CCL19, CXCL12 and CXCL13 (**Figure 7D**), highlighting a germinal center-like microenvironment in HLA-DR+ tumors. This limited 5-plex cytokine panel separated completely the melanoma metastases expressing HLA-DR from ones completely negative for HLA-DR (**Figures 7E, F**).

DISCUSSION

The MHC II complex is one of the main routes for antigen presentation and immune system activation, yet expression by melanoma cells is associated with a controversial role in literature, being described as an unfavorable prognostic factor in some studies and with longer survival in others (18, 24–28). Recently, MHC II expression, HLA-DR in particular, has also been correlated with response to anti-PD-1 therapy (13–16), nevertheless little is known about the biology behind this finding. To investigate the inflammatory microenvironment in HLA-DR positive melanoma, we first characterized at single cell level the immune microenvironment in HLA-DR positive and negative areas, then we investigated the upregulated genes and pathways in these areas and finally we confirmed the hypothesis generated by the first two levels of analysis by determining which cytokines are determinant in driving HLA-DR expression in melanoma.

Using MILAN, we identified in HLA-DR positive tumors a higher variety of inflammatory cell types compared to negative areas in the same tumor, where in particular a very low amount of B cells, cDC1, M1-like macrophages and TFH were present. This finding was also supported by the transcriptomic analysis that depicted a mixed immune microenvironment in the HLA-DR positive areas in comparison with HLA-DR negative areas, with overexpression of several genes, predicted upregulation of multiple transcription factors and activation of pathways linked to an increased presence of T cells, B cells and monocytes. Yet, comparing HLA-DR positive areas with HLA-DR negative tumors, the former showed a similar degree of variety in the inflammatory subtypes present, suggesting us that in HLA-DR positive tumors the HLA-DR positive areas will have the function of attract and concentrate most of the inflammatory cells infiltrating the tumor, pauperizing the HLA-DR negative areas instead.

Concentration and attraction of inflammatory cells is usually a feature of primary and secondary lymphoid organs, where a precise loco regional organization of lymphoid and myeloid cells is also

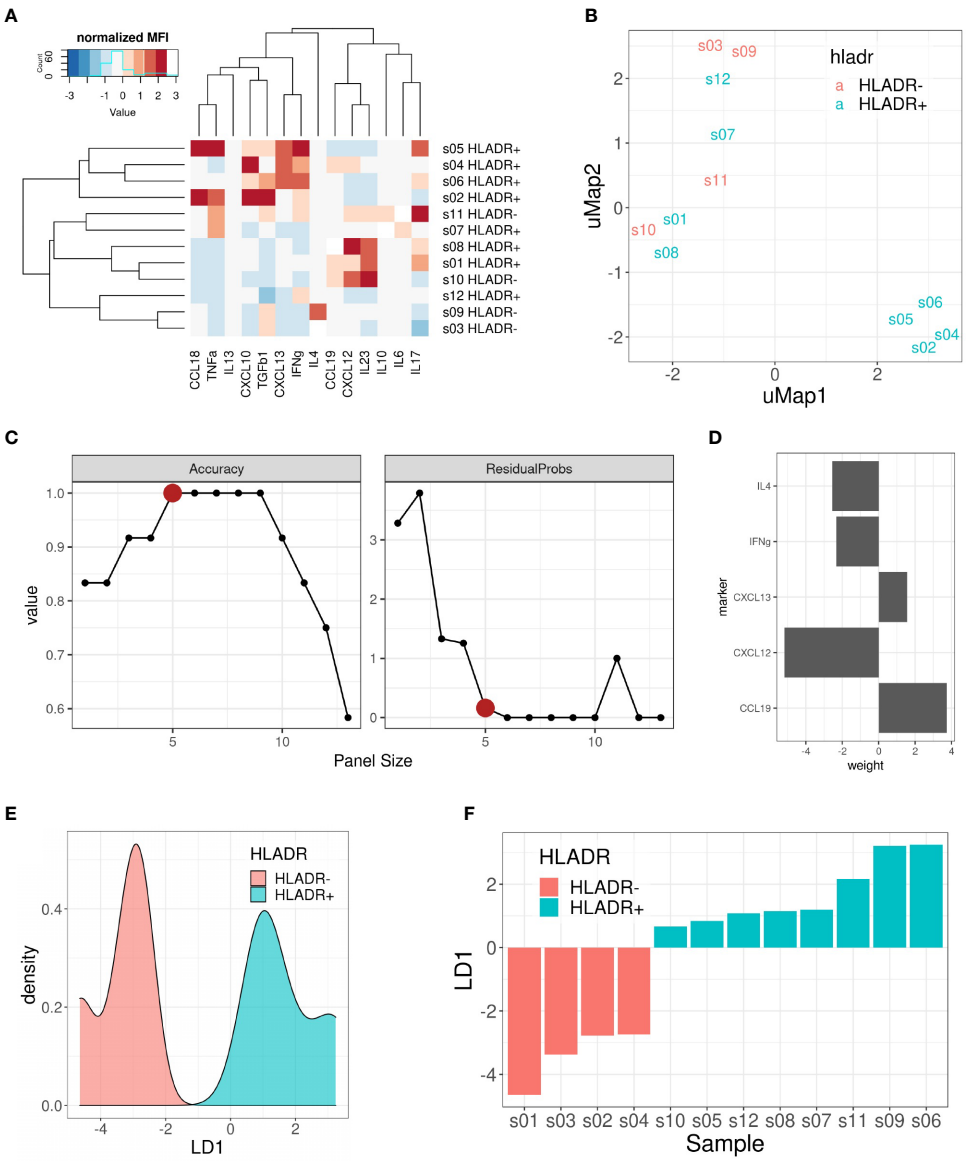

FIGURE 7 | Multiplex ELISA assay. **(A)** Heat map representing the normalized (z-score) mean fluorescence intensity (MFI) of the 14 measured cytokines (columns) in the 12 samples included (rows). Both rows and columns are sorted based on hierarchical clustering. **(B)** uMap representing the partial separation of HLA-DR+ and HLA-DR- samples by unsupervised dimensionality reduction. **(C)** Pareto front representing model accuracy (left) and residual probability (right) of the best LDA model for each panel size (x-axis). Elbow criterion identified a panel size of 5 markers as the optimal one. **(D)** Weights of the 5 included cytokines for the optimal LDA model: CCL19, CXCL12, CXCL13, IFNγ and IL4. **(E)** Density plot on LD1 for the included samples. **(F)** Bar plot showing the separation of HLA-DR+ and HLA-DR- samples following the predictions made with the 5 cytokine panel.

present. It was therefore surprising for us to find in HLA-DR positive areas small communities of mixed T and B cells, in particular with Treg-TFH, TFH-Th and Tcy-BC_GerminalCenter interactions. Moreover, additional upregulated genes and pathways pointed at the presence of enhanced antigen presentation, B cell activation and B cell-specific processes. In particular, the *Bystander B cell pathway* regulates apoptosis of those B cells that are not activated by antigens, a process that usually takes place in the germinal centers of lymph nodes. Furthermore, transcription factor analysis showed upregulation of BATF and IRF4, that cooperatively regulate IL-4 production in TFH cells (45). Moreover, IRF4 is expected in plasma cells, B cell activation and germinal center B centrocytes (46). An immune microenvironment with these features could be comparable to a germinal center.

To provide more evidences about this, we went back to the single cell data and compared the cell-cell interaction profiles of negative tumors and HLA-DR positive areas in positive tumors with germinal centers/tertiary lymphoid structures, by performing a neighborhood analysis on our spatial single-cell data. Here, we found that our positive control, the germinal

center itself, had a very specific interaction pattern involving a B cell community and a T cell community, and in comparison the close interactions in the positive areas also involved both T and B cells (BC_GerminalCenter-Tcy-Treg-TFH-Th) while in negative tumors only the T cell compartment showed significant cell-cell interactions (Tcy-TFH). Finally, we checked on a broad panel of cytokines which ones were in combination the most efficient in discriminating between negative and positive cases. The Luminex assay confirmed that the ones expressed in the germinal center microenvironment, together with IFNγ and IL4, best separated HLA-DR positive and negative cases.

This germinal-center-like microenvironment seems to be supported by the presence of pro-inflammatory cytokines. In particular, we found to be enriched in the HLA-DR positive microenvironment: IL12, at transcriptomic level, a cytokine that is secreted by phagocytic cells and stimulates the production of IFNγ and TNFα by NK cells and T cells, thereby enhancing their cytotoxic activity (47); and IFNγ both at transcriptomic and cytokine level, providing a nice and solid validation of our approach and confirming the well-known role of IFNγ in stimulating HLA-DR expression.

Nevertheless, the end result of this germinal center-like microenvironment appeared to have a dystrophic orientation towards immune suppression. First of all, overexpression of multiple immunomodulatory genes (TGFβ, HMOX1, TIM3) and pathways (*PD-1 pathway*) was found at transcriptomic level. In particular, TGFβ, inhibits the function of effector T cells and favors differentiation of naïve T cells into Tregs, and activity of the PD-1 pathway can lead to T cell exhaustion. This was already confirmed at single cell level, where not only overexpression of PD-1 was present in HLA-DR positive areas, but also higher levels of T cell exhaustion, significantly higher than in HLA-DR negative tumors and definitely more than in germinal centers, used as control for an area of generation of an efficient immune response.

Additional evidence points towards an hyper stimulation of the Tcy as the possible explanation for this exhaustion and immunosuppression enhancement in HLA-DR positive areas. Specifically, HLA-DR positive areas were found to be enriched in antigen-presenting cells (cDC1 and M1-like macrophages) at single cell level and associated with an enhanced activity of pathways linked to antigen presentation and dendritic cell functions in the transcriptomic analysis. Besides that, M1-like macrophages are found both in negative and positive tumors to be close neighbors of the melanoma cells. Though, while in negative tumors they are strongly close to HLA-DR negative melanoma cells, in positive tumors they have a preferential strong interaction with HLA-DR positive cells, and this may represent an overstimulating/confounding microenvironment in terms of antigen presentation leading to exhaustion and/or to a immunosuppressive shift in the microenvironment as a control mechanism to hyper immunity.

Finally, the high levels of PD-1 expression in these areas could also explain why anti-PD-1 therapy would be more efficient in HLA-DR positive tumors. In addition, the earlier described pan-tumor T-cell inflamed gene expression signature correlating with clinical benefit to anti-PD-1 treatment seems to partially overlap with the micro environmental changes specific for HLA-DR positive melanoma areas described here. This 18-gene immune panel contains among others CIITA, STAT1, HLA-DRA, CXCL13 and IFNγ (10). Although being described as an immune-specific signature, based on our findings a similar gene expression profile is to be expected in HLA-DR positive melanoma and hence could partially explain the high efficacy rate of checkpoint blockade in these patients. In addition, we could observe, in line with others (13, 39), higher PD-L1 expression in HLA-DR+ melanoma compared to HLA-DR- melanoma. Johnson and colleagues previously described a higher PD-1/PD-L1 interaction score to be predictive for response to immunotherapy, not considering the underlying type of cell-cell interaction or the cell types expressing these markers and independent of HLA-DR expression by the melanoma cells (14). Our findings, showing higher PD-1 expression levels in the immune cells in the tumor areas containing HLA-DR+ melanoma cells in addition to higher PD-L1 expression in the HLA-DR+ melanoma cells themselves, highlight a similar PD-1/PD-L1 proximity, potentially driven by HLA-DR expression in the melanoma cells that could explain the predictive potential of the expression of HLA-DR.

Despite its novelty, our study is not exempt of limitations. First of all, the number of patients with HLA-DR+ and HLA-DR- melanoma included in our analysis is rather limited. Although the aim of the study was to investigate the specific microenvironment of HLA-DR expressing melanomas to elucidate an explanation for the predictive potential of HLA-DR for response to immunotherapy observed by others rather than producing a patient classifier, the validity of our findings would be certified if applicable on a larger patient cohort. Nonetheless, the main conclusion of the germinal center-like microenvironment in HLA-DR + melanoma is corroborated using multi-omics applied on different (small) patient cohorts. In addition, the predictive potential of HLA-DR expression for response to immunotherapy has been described in literature by others (13, 16, 48). Independent of this observation, tumor microenvironmental analysis in melanoma and even more so in HLA-DR+ melanoma has not been given sufficient attention within literature. Driven by these 2 aforementioned observations, in our analysis we had the intent to explore the local microenvironment of HLA-DR expressing melanoma and particularly what is different from the tumor microenvironment of melanoma cells that do not express HLA-DR, and by doing so potentially provide a first insight on why there is an improved response to immunotherapy. Hence, because our samples were selected using only the expression of HLA-DR in melanoma metastases without considering treatment history prior or after sampling during this selection, as it was not the primary objective of our study, we cannot correlate our findings with response to therapy. Therefore, it remains unclear and speculative whether our findings in the specific local microenvironment are in fact the reason why these patients tend to respond better to immunotherapy. Moreover, in a small subset of pretreatment biopsy or resection specimens from 30 patient treated with

anti-PD-1 or anti-PD-L1, objective response rate was significantly higher in the HLA-DR + subset (79% versus 38%), yet still lacking response in 21% of the patients (13). Although further validation of these findings is needed in a bigger patient cohort, micro environmental differences between responding HLA-DR+ melanoma and non-responding HLA-DR+ melanoma still remain to be elucidated.

In conclusion, we found that HLA-DR positive areas in melanoma attract and concentrate the anti-tumor immune cell infiltration creating a germinal center-like microenvironment, though presenting dystrophic features. This microenvironment in fact seems to lead to an exhausted microenvironment through hyperactivity of the antigen presentation pathways, nevertheless representing a fertile ground for a better efficacy of anti-PD1 inhibitors.

DATA AVAILABILITY STATEMENT

The data presented in the study are deposited in the European Nucleotide Archive (ENA) repository, accession number PRJEB41749.

ETHICS STATEMENT

Ethical approval was obtained from the Ethical Committee/IRB OG032 of the University Hospital of Leuven. After the approval, the study was identified with the number S57266. According to the Clinical Trial regalement no informed consent was needed due to the use of post-diagnostic left-over material. Written informed consent for participation was not required for this study in accordance with the national legislation and the institutional requirements. Written informed consent was not obtained from the individual(s) for the publication of any potentially identifiable images or data included in this article.

AUTHOR CONTRIBUTIONS

LG performed microdissection, RNA extraction, transcriptomics interpretation and wrote the paper. YH collected clinical data, reviewed the processed images, participated in the MILAN analysis, prepared the images and wrote the paper. GM participated in the data analysis, prepared images and reviewed the paper. ZK performed the RNAseq data processing and analysis. MB reviewed and processed the raw images. JW performed the RNAseq data analysis. LM supervised LG in the experiments and reviewed the paper. AM supervised FB in the preparation of the samples and the design of the Luminex. VP executed part of the Luminex. JR executed part of the Luminex. LA provided reagents, machines and guidance for the Luminex. GC executed the stainings according to the MILAN protocol and provided guidance for MILAN. OB collected clinical data, gave clinical guidance and reviewed the paper. JO designed the project. FS gave critical insight to the project and reviewed the paper. AA coordinated all the dry lab analysis, performing the transcription factor and pathways analysis, the Luminex analysis, all the MILAN downstream analysis and wrote the paper FB designed the project, performed part of the wet lab analysis, guided the first co-authors, interpreted the results, and wrote the paper. All authors contributed to the article and approved the submitted version.

FUNDING

This work was funded by the MEL-PLEX research training program ('Exploiting MELanoma disease comPLEXity to address European research training needs in translational cancer systems biology and cancer systems medicine', Grant agreement no: 642295, MSCA-ITN-2014-ETN, Project Horizon 2020, in the framework of the MARIE SKŁODOWSKA-CURIE ACTIONS), the SyMBioSys research training programme ('Systematic Modeling of Biological Systems'), grant agreement no: 675585, MSCA-ITN-2015-ETN, Project Horizon 2020, in the framework of the MARIE SKŁODOWSKA-CURIE ACTIONS, and the Regione Lombardia POR FESR 2014-2020, Call HUB Ricerca ed Innovazione: ImmunHUB to GC.

ACKNOWLEDGMENTS

We want to express our gratitude to Prof. Stein Aerts, for giving us lots of useful inputs, knowledge and personnel to bring this research to its fruitful conclusion. Furthermore, we like to thank Mario Faretta (European Institute of Oncology, Milan) for image registration software and suggestions.

SUPPLEMENTARY MATERIAL

The Supplementary Material for this article can be found online at: https://www.frontiersin.org/articles/10.3389/fonc.2021.636057/full#supplementary-material

Supplementary Figure 1 | Phenotypic identification. **(A)** Expression fingerprints. Average expression profile of the identified cell phenotypes after clustering and manual annotation (see *Methods*). M indicates the mean expression of a given marker for a given cell phenotype. **(B)** Histogram showing the distribution of HLA-DR expression in melanoma cells (asinh transformed) used for their manual gating. A threshold of 2 was selected to separate HLA-DR positive from HLA-DR negative melanoma cells. **(C)** Histogram showing the distribution of PD1 expression in CD3+ CD4+ T cells (asinh transformed) used for manual gating. A threshold of 2 was selected to separate T Follicular Helpers (TFH, PD1+) from wild-type T Helpers (TH, PD1-). **(D)** 2D histogram showing the distribution of BCL2 and BCL6 in B cells (asinh transformed) used for their manual gating. A threshold of 2 was selected in both markers to separate germinal center B cells (BCL6+/BCL2-), early germinal center B cells (BCL6+/BCL2+) and B cells not further specified (BCL6-/BCL2- or BCL6-/BCL2+).

Supplementary Figure 2 | Cell proportion single cell composition of HLA-DR+ areas, HLA-DR- areas in positive tumours, HLA-DR- tumours, germinal centers and

tertiary lymphoid structures. Boxplots indicating the relative proportion of different cell-types in the different micro dissected areas, from left to right: 'GC' (Germinal centre from reactive lymph nodes; orange), TLS (germinal centers from tertiary lymphoid structures, ochre), 'NegTum' (Tumour border of HLA-DR negative tumours, green), ' NeginPos' (HLA-DR negative area of HLA-DR positive tumours, blue) and 'Pos' (HLA-DR positive area of HLA-DR positive tumours, pink). Blood_V= Blood vessel; cDC2= Classical dendritic cell type II; Th= T helper cell; TFH= T follicular helper cell; Treg= Regulatory t cell; Lymph_V= Lymphatic vessel; PC= Plasma cell. Significance levels indicate: * p-value ≤ 0.05, ** p-value ≤ 0.01, *** p-value ≤ 0.001, **** p-value ≤ 0.0001. P-values are derived from Wilcoxon tests (no fdr corrected).

Supplementary Figure 3 | Cell density single cell composition of HLA-DR+ areas, HLA-DR- areas in positive tumours, HLA-DR- tumours, germinal centers and tertiary lymphoid structures. Boxplots indicating the cell density (cells/mm²) of different cell-types in the different micro dissected areas, from left to right: 'GC' (Germinal centre from reactive lymph nodes; orange), TLS (germinal centers from tertiary lymphoid structures, ochre), 'NegTum' (Tumour border of HLA-DR negative tumours, green), ' NeginPos' (HLA-DR negative area of HLA-DR positive tumours, blue) and 'Pos' (HLA-DR positive area of HLA-DR positive tumours, pink). BC= B cell not further specified; BC_EarlyGerminalCenter= Early germinal center B cell; BC_GerminalCenter= Germinal center B cell; PC= Plasma cell; Th= T helper cell; Treg= Regulatory t cell; TFH= T follicular helper cell; Tcy= Cytotoxic t cell; NK= Natural killer cell; cDC1= Classical dendritic cell type I; cDC2= Classical dendritic cell type II; fDC= Follicular dendritic cell; pDC= Plasmacytoid dendritic cell; macrop= Macrophage; macrop_CD163= CD163 positive macrophage; HLApos_mel= HLA-DR positive melanoma cell; HLADRneg_mel= HLA-DR negative melanoma cell; Blood_V= Blood vessel; HEV= High endothelial venule; Lymph_V= Lymphatic vessel. Significance levels indicate: * p-value ≤ 0.05, ** p-value ≤ 0.01, *** p-value ≤ 0.001, **** p-value ≤ 0.0001. P-values are derived from Wilcoxon tests (no fdr corrected).

Supplementary Figure 4 | Volcano plots showing the differential expression between HLA-DR+ and HLA-DR- areas of genes included in different IGNy and IL-4/IL-12 pathways obtained from the Molecular Signatures Database. **(A)** BIOCARTA_IL12_PATHWAY, **(B)** PID_IFNG_PATHWAY, **(C)** BIOCARTA_IFNG_PATHWAY, **(D)** PID_IL12_STAT4_PATHWAY, **(E)** REACTOME_REGULATION_OF_IFNG_SIGNALING, **(F)** BIOCARTA_NO2IL12_PATHWAY, **(G)** PID_IL12_2PATHWAY, **(H)** PID_IL4_2PATHWAY. The x-axis represents the log2 of the fold change in expression between HLA-DR positive and HLA-DR negative areas while the y-axis represents the -log10 of the p-value of a t-test comparing the expression values of these areas.

REFERENCES

1. Gershenwald JE, Scolyer RA, Hess KR, Sondak VK, Long GV, Ross MI, et al. Melanoma staging: Evidence-based changes in the American Joint Committee on Cancer eighth edition cancer staging manual. *CA Cancer J Clin* (2017) 67 (6):472–92. doi: 10.3322/caac.21409
2. Alexandrov LB, Nik-Zainal S, Wedge DC, Aparicio SA, Behjati S, Biankin AV, et al. Signatures of mutational processes in human cancer. *Nature* (2013) 500 (7463):415–21. doi: 10.1038/nature12477
3. Coit DG, Thompson JA, Albertini MR, Barker C, Carson WE, Contreras C, et al. Cutaneous Melanoma, Version 2.2019, NCCN Clinical Practice Guidelines in Oncology. *J Natl Compr Canc Netw* (2019) 17(4):367–402. doi: 10.6004/jnccn.2019.0018
4. Ascierto PA, Long GV, Robert C, Brady B, Dutriaux C, Di Giacomo AM, et al. Survival Outcomes in Patients With Previously Untreated BRAF Wild-Type Advanced Melanoma Treated With Nivolumab Therapy: Three-Year Follow-up of a Randomized Phase 3 Trial. *JAMA Oncol* (2019) 5(2):187–94. doi: 10.1001/jamaoncol.2018.4514
5. Schachter J, Ribas A, Long GV, Arance A, Grob JJ, Mortier L, et al. Pembrolizumab versus ipilimumab for advanced melanoma: final overall survival results of a multicentre, randomised, open-label phase 3 study (KEYNOTE-006). *Lancet* (2017) 390(10105):1853–62. doi: 10.1016/S0140-6736(17)31601-X
6. Postow MA, Sidlow R, Hellmann MD. Immune-Related Adverse Events Associated with Immune Checkpoint Blockade. *N Engl J Med* (2018) 378 (2):158–68. doi: 10.1056/NEJMra1703481
7. Tumeh PC, Harview CL, Yearley JH, Shintaku IP, Taylor EJ, Robert L, et al. PD-1 blockade induces responses by inhibiting adaptive immune resistance. *Nature* (2014) 515(7528):568–71. doi: 10.1038/nature13954
8. Taube JM, Klein A, Brahmer JR, Xu H, Pan X, Kim JH, et al. Association of PD-1, PD-1 ligands, and other features of the tumor immune microenvironment with response to anti-PD-1 therapy. *Clin Cancer Res* (2014) 20(19):5064–74. doi: 10.1158/1078-0432.CCR-13-3271
9. Van Allen EM, Miao D, Schilling B, Shukla SA, Blank C, Zimmer, et al. Genomic correlates of response to CTLA-4 blockade in metastatic melanoma. *Science* (2015) 350(6257):207–11. doi: 10.1126/science.aad0095
10. Ayers M, Lunceford J, Nebozhyn M, Murphy E, Loboda A, Kaufman D, et al. IFNγ-related mRNA profile predicts clinical response to PD-1 blockade. *J Clin Invest* (2017) 127(8):2930–40. doi: 10.1172/JCI91190
11. Jiang P, Gu S, Pan D, Fu J, Sahu A, Hu X, et al. Signatures of T cell dysfunction and exclusion predict cancer immunotherapy response. *Nat Med* (2018) 24 (10):1550–8. doi: 10.1038/s41591-018-0136-1
12. Auslander N, Zhang G, Lee JS, Frederick DT, Miao B, Moll T, et al. Robust prediction of response to immune checkpoint blockade therapy in metastatic melanoma. *Nat Med* (2018) 24(10):1545–9. doi: 10.1038/s41591-018-0157-9
13. Johnson DB, Estrada MV, Salgado R, Sanchez V, Doxie DB, Opalenik SR, et al. Melanoma-specific MHC-II expression represents a tumour-autonomous phenotype and predicts response to anti-PD-1/PD-L1 therapy. *Nat Commun* (2016) 7:10582. doi: 10.1038/ncomms10582
14. Johnson DB, Bordeaux J, Kim JY, Vaupel C, Rimm DL, Ho TH, et al. Quantitative Spatial Profiling of PD-1/PD-L1 Interaction and HLA-DR/IDO-1 Predicts Improved Outcomes of Anti-PD-1 Therapies in Metastatic Melanoma. *Clin Cancer Res* (2018) 24(21):5250–60. doi: 10.1158/1078-0432.CCR-18-0309
15. Toki MI, Merritt CR, Wong PF, Smithy JW, Kluger HM, Syrigos KN, et al. High-Plex Predictive Marker Discovery for Melanoma Immunotherapy-Treated Patients Using Digital Spatial Profiling. *Clin Cancer Res* (2019) 25 (18):5503–12. doi: 10.1158/1078-0432.CCR-19-0104
16. Rodig SJ, Gusenleitner D, Jackson DG, Gjini E, Giobbie-Hurder A, Jin C, et al. MHC proteins confer differential sensitivity to CTLA-4 and PD-1 blockade in untreated metastatic melanoma. *Sci Transl Med* (2018) 10(450):eaar3342. doi: 10.1126/scitranslmed.aar3342
17. Pollack MS, Heagney SD, Livingston PO, Fogh J. HLA-A, B, C and DR alloantigen expression on forty-six cultured human tumour cell lines. *J Natl Cancer Inst* (1981) 66:1003–12. doi: 10.1093/jnci/66.6.1003
18. Degenhardt Y, Huang J, Greshock J, Horiates G, Nathanson K, Yang X, et al. Distinct MHC gene expression patterns during progression of melanoma. *Genes Chromosomes Cancer* (2010) 49(2):144–54. doi: 10.1002/gcc.20728
19. Taube JM, Anders RA, Young GD, Xu H, Sharma R, McMiller TL, et al. Colocalization of inflammatory response with B7-h1 expression in human melanocytic lesions supports an adaptive resistance mechanism of immune escape. *Sci Transl Med* (2012) 4(127):127ra37. doi: 10.1126/scitranslmed.3003689
20. Muhlethaler-Mottet A, Di Berardino W, Otten LA, Mach B. Activation of the MHC class II transactivator CIITA by interferon-gamma requires cooperative interaction between Stat1 and USF-1. *Immunity* (1998) 8(2):157–66. doi: 10.1016/s1074-7613(00)80468-9
21. Deffrennes V, Vedrenne J, Stolzenberg MC, Piskurich J, Barbieri G, Ting JP, et al. Constitutive expression of MHC class II genes in melanoma cell lines results from the transcription of class II transactivator abnormally initiated from its B cell-specific promoter. *J Immunol* (2001) 167(1):98–106. doi: 10.4049/jimmunol.167.1.98
22. Becker JC, Brabletz T, Czerny C, Termeer C, Bröcker EB. Tumor escape mechanisms from immunosurveillance: induction of unresponsiveness in a specific MHC-restricted CD4+ human T cell clone by the autologous MHC class II+ melanoma. *Int Immunol* (1993) 5(12):1501–8. doi: 10.1093/intimm/5.12.1501
23. Andrews LP, Marciscano AE, Drake CG, Vignali DA. LAG3 (CD223) as a cancer immunotherapy target. *Immunol Rev* (2017) 276(1):80–96. doi: 10.1111/imr.12519
24. Martins I, Sylla K, Deshayes F, Lauriol J, Ghislin S, Dieu-Nosjean MC, et al. Coexpression of major histocompatibility complex class II with chemokines and nuclear NFkappaB p50 in melanoma: a rational for their association with poor prognosis. *Melanoma Res* (2009) 19(4):226–37. doi: 10.1097/CMR.0b013e32832e0bc3

25. Barbieri G, Rimini E, Costa MA. Effects of human leukocyte antigen (HLA)-DR engagement on melanoma cells. *Int J Oncol* (2011) 38(6):1589–95. doi: 10.3892/ijo.2011.988
26. Carretero R, Wang E, Rodriguez AI, Reinboth J, Ascierto ML, Engle AM, et al. Regression of melanoma metastases after immunotherapy is associated with activation of antigen presentation and interferon-mediated rejection genes. *Int J Cancer* (2012) 131(2):387–95. doi: 10.1002/ijc.26471
27. Bernsen MR, Håkansson L, Gustafsson B, Krysander L, Rettrup B, Ruiter D, et al. On the biological relevance of MHC class II and B7 expression by tumour cells in melanoma metastases. *Br J Cancer* (2003) 88(3):424–31. doi: 10.1038/sj.bjc.6600703
28. Chen YY, Chang WA, Lin ES, Chen YJ, Kuo PL. Expressions of HLA Class II Genes in Cutaneous Melanoma Were Associated with Clinical Outcome: Bioinformatics Approaches and Systematic Analysis of Public Microarray and RNA-Seq Datasets. *Diagn (Basel)* (2019) 9(2):59. doi: 10.3390/diagnostics 9020059
29. Donia M, Andersen R, Kjeldsen JW, Fagone P, Munir S, Nicoletti F, et al. Aberrant Expression of MHC Class II in Melanoma Attracts Inflammatory Tumor-Specific CD4+ T- Cells, Which Dampen CD8+ T-cell Antitumor Reactivity. *Cancer Res* (2015) 75(18):3747–59. doi: 10.1158/0008-5472.CAN-14-2956
30. Donia M, Kjeldsen JW, Svane IM. The controversial role of TNF in melanoma. *Oncoimmunology* (2015) 5(4):e1107699. doi: 10.1080/2162402X.2015.1107699
31. Bolognesi MM, Manzoni M, Scalia CR, Zannella S, Bosisio FM, Faretta M, et al. Multiplex Staining by Sequential Immunostaining and Antibody Removal on Routine Tissue Sections. *J Histochem Cytochem* (2017) 65 (8):431–44. doi: 10.1369/0022155417719419
32. Cattoretti C, Bosisio FM, Marcelis L, Bolognesi MM. Multiple Iterative Labeling by Antibody Neodeposition (MILAN). PROTOCOL (Version 5) available at Research Square. (2019). doi: 10.21203/rs.2.1646/v5
33. Bosisio FM, Antoranz A, van Herck Y, Bolognesi MM, Marcelis L, Chinello C, et al. Functional heterogeneity of lymphocytic patterns in primary melanoma dissected through single-cell multiplexing. *Elife* (2020) 9:e53008. doi: 10.7554/eLife.53008
34. Caicedo JC, Cooper S, Heigwer F, Warchal S, Qiu P, Molnar C, et al. Data-analysis strategies for image-based cell profiling. *Nat Methods* (2017) 14 (9):849–63. doi: 10.1038/nmeth.4397
35. Schapiro D, Jackson HW, Raghuraman S, Fischer JR, Zanotelli VRT, Schulz D, et al. HistoCAT: analysis of cell phenotypes and interactions in multiplex image cytometry data. *Nat Methods* (2017) 14(9):873–6. doi: 10.1038/nmeth.4391
36. Garcia-Alonso L, Holland CH, Ibrahim MM, Turei D, Saez-Rodriguez J. Benchmark and integration of resources for the estimation of human transcription factor activities. *Genome Res* (2019) 29(8):1363–75. doi: 10.1101/gr.240663.118
37. Väremo L, Nielsen J, Nookaew I. Enriching the gene set analysis of genome-wide data by incorporating directionality of gene expression and combining statistical hypotheses and methods. *Nucleic Acids Res* (2013) 41(8):4378–91. doi: 10.1093/nar/gkt111
38. Allred CC, Krennmayr T, Koutsari C, Zhou L, Ali AH, Jensen MD. A novel ELISA for measuring CD36 protein in human adipose tissue. *J Lipid Res* (2011) 52(2):408–15. doi: 10.1194/jlr.M008995
39. Costantini F, Barbieri G. The HLA-DR mediated signalling increases the migration and invasion of melanoma cells, the expression and lipid raft recruitment of adhesion receptors, PD-L1 and signal transduction proteins. *Cell Signal* (2017) 36:189–203. doi: 10.1016/j.cellsig.2017.05.008
40. Stelzer G, Rosen N, Plaschkes I, Zimmerman S, Twik M, Fishilevich S, et al. The GeneCards Suite: From Gene Data Mining to Disease Genome Sequence Analyses. *Curr Protoc Bioinf* (2016) 54:1.30.1–1.30.33. doi: 10.1002/cpbi.5
41. UniProt Consortium. UniProt: a worldwide hub of protein knowledge. *Nucleic Acids Res* (2019) 47(D1):D506–15. doi: 10.1093/nar/gky1049
42. Boyman O, Sprent J. The role of interleukin-2 during homeostasis and activation of the immune system. *Nat Rev Immunol* (2012) 12(3):180–90. doi: 10.1038/nri3156
43. Mineva ND, Rothstein TL, Meyers JA, Lerner A, Sonenshein GE. CD40 ligand-mediated activation of the de novo RelB NF-kappaB synthesis pathway in transformed B cells promotes rescue from apoptosis. *J Biol Chem* (2007) 282(24):17475–85. doi: 10.1074/jbc.M607313200
44. Kershaw NJ, Murphy JM, Liau NP, Varghese LN, Laktyushin A, Whitlock EL, et al. SOCS3 binds specific receptor-JAK complexes to control cytokine signaling by direct kinase inhibition. *Nat Struct Mol Biol* (2013) 20(4):469–76. doi: 10.1038/nsmb.2519
45. Sahoo A, Alekseev A, Tanaka K, Obertas L, Lerman B, Haymaker C, et al. Batf is important for IL-4 expression in T follicular helper cells. *Nat Commun* (2015) 6:7997. doi: 10.1038/ncomms8997
46. Willis SN, Good-Jacobson KL, Curtis J, Light A, Tellier J, Shi W, et al. Transcription factor IRF4 regulates germinal center cell formation through a B cell-intrinsic mechanism. *J Immunol* (2014) 192(7):3200–6. doi: 10.4049/jimmunol.1303216
47. Zundler S, Neurath MF. Interleukin-12: Functional activities and implications for disease. *Cytokine Growth Factor Rev* (2015) 26(5):559–68. doi: 10.1016/j.cytogfr.2015.07.003
48. Sidaway P. MHC expression predicts response. *Nat Rev Clin Oncol* (2018) 15 (10):591. doi: 10.1038/s41571-018-0082-3

Conflict of Interest: Authors AM, VP, JR, and LA were employed by the company ProtATonce Ltd.

The remaining authors declare that the research was conducted in the absence of any commercial or financial relationships that could be construed as a potential conflict of interest.

frontiers in Oncology

REVIEW
published: 29 March 2021
doi: 10.3389/fonc.2021.636681

Multiplexed Immunohistochemistry and Digital Pathology as the Foundation for Next-Generation Pathology in Melanoma: Methodological Comparison and Future Clinical Applications

Yannick Van Herck[1†], Asier Antoranz[2†], Madhavi Dipak Andhari[2], Giorgia Milli[2], Oliver Bechter[1], Frederik De Smet[3‡] and Francesca Maria Bosisio[2‡]*

[1] Department of Oncology, KU Leuven, Leuven, Belgium, [2] Laboratory for Translational Cell and Tissue Research, Department of Imaging and Pathology, KU Leuven, Leuven, Belgium, [3] Laboratory for Precision Cancer Medicine, Translational Cell and Tissue Research Unit, Department of Imaging and Pathology, KU Leuven, Leuven, Belgium

The state-of-the-art for melanoma treatment has recently witnessed an enormous revolution, evolving from a chemotherapeutic, "one-drug-for-all" approach, to a tailored molecular- and immunological-based approach with the potential to make personalized therapy a reality. Nevertheless, methods still have to improve a lot before these can reliably characterize all the tumoral features that make each patient unique. While the clinical introduction of next-generation sequencing has made it possible to match mutational profiles to specific targeted therapies, improving response rates to immunotherapy will similarly require a deep understanding of the immune microenvironment and the specific contribution of each component in a patient-specific way. Recent advancements in artificial intelligence and single-cell profiling of resected tumor samples are paving the way for this challenging task. In this review, we provide an overview of the state-of-the-art in artificial intelligence and multiplexed immunohistochemistry in pathology, and how these bear the potential to improve diagnostics and therapy matching in melanoma. A major asset of in-situ single-cell profiling methods is that these preserve the spatial distribution of the cells in the tissue, allowing researchers to not only determine the cellular composition of the tumoral microenvironment, but also study tissue sociology, making inferences about specific cell-cell interactions and visualizing distinctive cellular architectures - all features that have an impact on anti-tumoral response rates. Despite the many advantages, the introduction of these approaches requires the digitization of tissue slides and the development of standardized analysis pipelines which pose substantial challenges that need to be addressed before these can enter clinical routine.

Keywords: melanoma, multiplex, single cell, digital pathology, spatial proteomics

OPEN ACCESS

Edited by:
Igor Puzanov,
University at Buffalo, United States

Reviewed by:
Selma Ugurel,
University of Duisburg-Essen, Germany
Matthew D. Vesely,
Yale University, United States

****Correspondence:***
Francesca Maria Bosisio
francescamaria.bosisio@kuleuven.be

†These authors share first authorship

‡These authors share last authorship

Specialty section:
This article was submitted to Skin Cancer, a section of the journal Frontiers in Oncology

Received: *01 December 2020*
Accepted: *12 March 2021*
Published: *29 March 2021*

Citation:
Van Herck Y, Antoranz A, Andhari MD, Milli G, Bechter O, De Smet F and Bosisio FM (2021) Multiplexed Immunohistochemistry and Digital Pathology as the Foundation for Next-Generation Pathology in Melanoma: Methodological Comparison and Future Clinical Applications.11:636681. doi: 10.3389/fonc.2021.636681

INTRODUCTION

Next-Generation Pathology and Personalized Medicine in Melanoma

The oncological treatment of melanoma has radically changed over the past 10 years: it evolved from a "one-fits-all" chemotherapeutic treatment with DTIC (1) to a more tailored setting where therapies are only given when patient- and tumor-specific features are present. This evolution toward personalized therapy was ignited by the observation that specific drugs were only clinically effective in the presence of a specific mutation (2–10). In addition, following the first successes with IL-2 therapy (11–13), immunotherapy was re-evaluated leading to the identification and implementation of checkpoint inhibitor therapy, a type of immunotherapy based on blocking the breaks that normally prevent the immune system from becoming hyperactivated (14–17). While oncology is gradually moving toward personalized treatments, also pathological assessments need to progress to cope with the need for in-depth characterizations of tumor tissues from individual patients. Salto-Tellez et al. have previously discussed how pathology, a discipline originally based on the evaluation of tissue morphology by hematoxylin-eosin (HE) staining, witnessed 3 main revolutions: first, the introduction of immunohistochemistry (IHC) in the 80s; second, the adoption of molecular techniques in pathology (molecular pathology, MP; mostly next-gen sequencing); and, most recently, the development of artificial intelligence (AI) tools to support the pathologist to evaluate and interpret the different features (18). While tools from the first two revolutions are nowadays fully embedded in routine clinical work and represent the earliest steps toward personalized medicine, the third revolution is still awaiting its breakthrough.

From the available tools, MP is the most advanced as it reached the required level of specificity to represent the state-of-the-art. It is mostly based on next-generation sequencing through which it allows the identification of genetic aberrations, either by analyzing focused gene panels or whole genome sequencing. In melanoma, the mutational profile is nowadays used to support diagnostics but also to select the most appropriate treatment. For the former, the new WHO Skin Cancer classification has identified 9 molecular pathways in which the melanocytic lesions can be classified based on the type and number of genetic alterations involved (19). Each of these pathways is further divided in 3 categories with different biological behavior (benign, intermediate and malignant) that can also be predicted according to the number of genetic alterations (≤1, 2 and >2 respectively) (19). The choice of treatment, on the other hand, is primarily based on the presence of targetable mutations, such as BRAF V600 mutations, for which specific therapies are available (2–10).

While NGS methods are constantly improving and evolving, the use of IHC hardly changed over the past 20 years. Indeed, as opposed to NGS analyses that typically cover 10-100 genes simultaneously, conventional IHC allows to stain tissue sections one marker at the time. As such, the analysis of multiple biomarkers typically requires the analysis of serial sections which may be a limiting step in small biopsies where only small amounts of materials are available. Moreover, by its inability to investigate the co-expression of several markers in the same cell, important information is systematically missed. A workaround has been to analyze marker expression patterns in serial sections, but this approach does not achieve sufficient detail to get to a robust interpretation. As a consequence, conventional IHC has become largely insufficient to cope with the required level and depth by which tumor tissues for each individual patients should be analyzed. A striking example involves the use of PD-L1 as a single-plex marker for the prediction of immunotherapy response: even though it has been implemented in routine pathological assessments, its detection suffers from significant technical hurdles making it largely insufficient as a good predictive marker. Moreover, recent research suggests that the cell types that express PD-L1 and their location in the tissue is also of major importance. However, gaining such insights cannot be addressed by old pathological practices where a semi-quantitative eye-balling interpretation of the staining is used for subjective evaluation, and therefore requires the implementation of single cell-technologies that preserve the spatial distribution of the various cell types and their original state (20). Multiplexed IHC, a technological approach that harbors the potential to collect exactly this type of data, has witnessed major progress over the past 2-3 years, but still requires several adaptations. For instance, it relies on full image digitalization and extended computational analysis, a limitation (but also opportunity) that multiplexed IHC and artificial intelligence (AI) have in common for their further implementation in a clinical setting.

Even though digital pathology-based AI tools have already been developed and have shown some diagnostic, prognostic, and predictive potential comparable to standard molecular and genomic-based tests, digital pathology (i.e. the process of digitizing whole-slide images using advanced slide-scanning techniques) has not yet been introduced in hospitals at large scale. Recent advancements in multiplexed IHC anticipate an even more important role for AI in pathology. The plethora of data generated by multiplexed IHC where tens to hundreds of markers are measured in thousands to millions of cells in their spatial context, provides the ideal setting to exploit AI and deep learning methods in particular. One of the strongest aspects of deep learning is to discover hidden features (and their combinations) otherwise invisible by purely visual inspection, and correlate them with clinical data. The parallel advancement of multiplexed IHC and AI-based computational models represent an unprecedented scenario for the introduction of next-generation pathology in clinical practice, characterized by the more widespread usage of digital images and the introduction of artificial intelligence and deep learning tools on histopathological images.

In this review we discuss the state-of-the-art, the potential and the challenges linked to the introduction of next-generation pathology to the clinical practice of melanoma patients. All the studies considered in this review are summarized in **Table 1**.

TABLE 1 | Overview of recent studies using digital pathology in melanoma. All studies are ordered according to time of publication.

Study	Main Objective	Study population	Method(s)	Main finding(s)/results
Makhzami et al. 2012 (21)	Improve the cell-type purity by performing laser-microdissection and investigate tissue-based transcriptomic data	Transgenic mice	IHC-guided laser microdissection	Optimized workflow of laser microdissection & stronger expression of five genes (M-MITF, TYR, STAT3, CCND1 and PAX3) in primary than metastatic melanoma
Bifulco et al. 2014 (22)	Investigate prognostic and predictive value of immunoscore in advanced melanoma patients treated with ipilimumab	190 FFPE metastatic samples from melanoma patients treated with ipilimumab	IHC expression of CD3, CD8, CD20 and FOXP3 on serial tissue sections	No relationship between CD3, CD8, CD20, CD163, FoxP3 both intratumoral (CT) and peritumoral (IM) with response/benefit; Only a trend for the CD163 positive PD-L1 positive population ($p = 0.07$)
Capone et al. 2014 (23)	Potential prognostic value of CD3, CD8, CD20, and FOXP3 as an 'Immunoscore' for melanoma	150 lymph nodes from 34 melanoma patients	IHC expression of CD3, CD8, CD20 and FOXP3 on serial tissue sections	Significant higher ratio of peri/intra tumoral CD3 and CD8 in patients without recurrence
Tumeh et al. 2014 (24)	Investigate adaptive immune resistance as predictor of response to anti-PD-1 therapy	Discovery cohort of 46 patients with FFPE material treated with anti-PD1 monotheray; Validation cohort of 15 patients	multiplex IF triple stainings, including S100, CD8, CD4, CD80, Ki67, pSTAT1, PD-1 and PD-L1	Predictive model for response to therapy based on CD8 expression at the invasive margin (after multivariate analysis)
Xu et al. 2017 (25)	Technique for measuring melanoma DoI in microscopic images digitized from MART1 (i.e., meleanoma-associated antigen recognized by T cells) stained skin histopathological sections	29 histopathological melanoma images (1 training, 28 validation images)	Four modules technique, including robust Bayesian based method for skin granular detection and multiresolution method using Hausdorff distance to measure melanoma invasion depth.	Superior performance in measuring the melanoma DoI of proposed multi-resolution approach compared to two closely related techniques.
Fertig et al. 2017 (26)	Compare concordance in differentiating spongiotic dermatitis (SD) and mycosis fungoides (MF) between digital whole-slide imaging (WSI) and traditional microscopy (TM)	20 cases of subacute SD and 20 cases of MF	WSI versus TM	Similar inter- and intraobserver discordance between WSI and TM
Kent et al. 2017 (27)	Compare accuracy/ reproducibility of pathologist in diagnosing dermatopathology cases between digital whole-slide imaging (WSI) and traditional microscopy (TM)	499 dermatopathology cases representing spectrum of diagnoses seen in the laboratory	WSI versus TM	Accuracy and reproducibility similar for WSI/TM
Xu et al. 2018 (28)	computer-aided technique for automated analysis and classification of melanocytic tumor on skin whole slide biopsy images.	66 H&E stained skin WSIs including 17 normal skin tissues, 17 nevi and 32 melanomas	multi-class support vector machine (mSVM) with extracted epidermis and dermis features	More than 95% accuracy for classifying a melanocytic image into different categories such as melanoma, nevus or normal tissue
Edwards et al. 2018 (29)	Prognostic value of tumor-resident CD8+ T cells in metastatic melanoma patients prior to immunotherapy and in patients undergoing anti–PD-1 immunotherapy	52 melanoma patients	multiplex IF using OPAL (CD8, CD103, SOX10, PD-1) & FACS	Increased numbers of CD69+CD103+ tumor-resident CD8+ T cells were associated with improved melanoma-specific survival in immunotherapy-naïve melanoma patients.
Halse et al. 2018 (30)	Prospective study explored the heterogeneous nature of metastatic melanoma using Multiplex immunohistochemistry (IHC) and flow cytometry (FACS)	FFPE from 21 melanoma patients	FACS & multiplex IF using OPAL (CD4, CD3, CD8, FOXP3, PD-L1, SOX10, CD20, CD68 and CD11c)	Model to define metastatic melanoma immune context into four categories using the presence or absence of PDL1+ melanoma cells and/or macrophages, combined with the presence or absence of IT CD8+ T cells
Onega et al. 2018 (31)	Compare accuracy/reproducibility of pathologist in diagnosing melanocytic lesions between digital whole-slide imaging (WSI) and traditional microscopy (TM)	180 skin biopsy cases including 90 invasive melanoma	WSI versus TM	Accuracy and reproducibility similar for WSI/TM
Thrane et al. 2018 (32)	Optimize and apply spatial transcriptomics (ST) technology for the in situ and quantitative detection of gene expression in stage III melanoma lymph node metastases	4 lymph node melanoma metastases	Spatial Transcriptomics AB	A detailed landscape of melanoma metastases was revealed by applying the ST technology to generate gene expression profiles, not evident through morphologic annotation

(Continued)

TABLE 1 | Continued

Study	Main Objective	Study population	Method(s)	Main finding(s)/results
Johnson et al. 2018 (33)	Quantify immunosupression mechanisms within the tumor microenvironment by multiparameter algorithms to identify strong predictors of anti-PD1 response	Discovery cohort of 24 melanoma patients with FFPE material; Validation cohort of 142 melanoma patients with FFPE material	multiplex IF using OPAL (PD-1 & PD-L1, HLA-DR & IDO-1 and CD11b & S100); Analysis using AQUAnalysis ™	Patients with high PD-1/PD-L1 and/or IDO-1/ HLA-DR more likely to respond (P = .0096) and have significantly improved progression free survival (hazard ratio [HR] = 0.36; P = .0004) and overall survival (HR = 0.39; P = .0011)
Alheejawi et al. 2019 (34)	Automatic measurement of proliferation index in Ki-67 stained biopsy image using deep learning algorithm	9 melanoma WSI	Convolutional neural network using SegNet architecture to segment and classify the Ki-67 stained image into three classes (i.e., background, active and passive nuclei	Robust segmentation/nuclei classification with average error rate less than 0.7%
Alheejawi et al. 2019 (35)	Computer Aided Diagnosis (CAD) method to segment the lymph nodes and melanoma regions in a biopsy image and measure the proliferation index	39 WSIs include 9 H&E, 9 MART-1, 9 KI-67, 5 CD-45, and 7 S-100 images	Local frequency features and SVM classifier for lymph node segmentation & Thresholding and SVM classification to determine active/passive nuclei	Segmentation of lymph nodes with more than 90% accuracy & proliferation index calculation with average error rate of less than 1.5%
Fu et al. 2019 (36)	systematic review of articles about the prognostic roles of TIL responses and CD3+, CD4+, CD8+, FOXP3+, and CD20+ TIL subsets in the prognosis of melanoma	41 studies included in final analysis	Systematic review & meta-analysis	Favorable prognostic role of CD3+, CD4+, CD8 +, FOXP3+ and CD20+ TILs in melanoma
Wong et al. 2019 (37)	Are pretreatment tumor-infiltrating lymphocyte (TIL) profiles associated with response?	Study cohort of 94 anti-PD-1 treated melanoma patients; Historical cohort 100 untreated melanoma	5-plex IF using OPAL (including CD4, CD8, CD20, Ki67, GZMB)	Pretreatment lymphocytic infiltration is associated with anti–PD-1 response in metastatic melanoma
Robinson et al. 2019 (38)	Deep Neural Network (DNN) for quantitative prediction of melanoma recurrence from a H&E stained tissue	Training set of 75 melanoma patients; Validation cohort of 115 melanoma patients	Deep neural net (DNN) architecture consisting of convolutional and recurrent neural networks (CNN, RNN).	DNN recurrence prediction is independent prognostic factor in a multivariable Cox proportional hazard model
Wong et al. 2019 (39)	Test the hypothesis that CAF profiles in pretreatment tumor specimens are associated with response to anti-PD-1	Discovery cohort: 117 anti-PD1 treated melanoma patients; Control group: 194 melanoma patients	5-plex IF using OPAL (including Thy1, SMA, FAP, S100 and HMB45)	Pretreatment CAF profiles are associated with melanoma immunotherapy outcome
Gide et al. 2019 (40)	Examine the spatial distribution of immune and tumor cells to predict response to anti-PD-1-based therapies and patient outcomes	61 melanoma patients with FFPE material (27 monotherapy anti-PD1 treated; 34 combined anti-PD1 and anti-CTLA4)	multiplex IF using OPAL (PD-1, SOX10, PD-L1 and CD8)	Best model for 12-month progression-free survival for anti-PD-1 monotherapy included PD-L1+ cells within proximity to tumor cells and intratumoral CD8+ density (AUC = 0.80), and for combination therapy included CD8+ cells in proximity to tumor cells, intratumoral PD-L1+ density and LDH (AUC = 0.85)
Baltzarsen et al. 2020 (41)	Evaluate the diagnostic or prognostic marker of hTERT mRNA in melanoma	17 melanoma and 13 benign naevi	RNAscope	hTERT mRNA was more abundantly expressed in melanomas compared with benign naevi and correlated with the prognostic markers Breslow thickness and the Ki67 index
Cabrita et al. 2020 (42)	Investigate the role of B cells in antitumor responses in melanoma	177 melanoma patients	multiplex IF & Nanostring GeoMx Digital Spatial Profiler	Tertiary lymphoid structures have a key role in the immune microenvironment in melanoma, by conferring distinct T cell phenotypes & co-occurrence of tumour-associated CD8+ T cells and CD20+ B cells is associated with improved survival
Helmink et al. 2020 (43)	Investigate the role of B cells in antitumour responses in melanoma	Discovery cohort of 23 melanoma patients; Validation cohort of 18 melanoma patients	Gene expression profiling, multiplex IF using OPAL (CD20, CD21, CD4,	Potential role of B cells and tertiary lymphoid structures in the response to ICB treatment

(Continued)

TABLE 1 | Continued

Study	Main Objective	Study population	Method(s)	Main finding(s)/results
			CD8, FOXP3), Nanostring GeoMx Digital Spatial Profiler & CytOF	
Bosisio et al. 2020 (44)	Characterize the immune landscape in primary melanoma	29 primary cutaneous melanoma (23 non-brisk, 6 brisk)	multiplex IF using MILAN (39 plex), shotgun proteomics & qPCR	Brisk and non-brisk patterns are heterogeneous functional categories that can be further sub-classified into active, transitional or exhausted, and have an improved prognostic value when compared to that of the brisk classification
Ianni et al. 2020 (45)	deep learning system to classify digitized dermatopathology slides into 4 diagnostically-relevant classes (Basaloid, Squamous, Melanocytic and Other)	Training set of 5070 H&E stained skin biopsies; Validation set of 13 537 H&E stained skin biopsies	Deep learning system using a cascade of three independently-trained convolutional neural networks (CNNs)	Deep-learning-based confidence scoring classification system with accuracy of up to 98%
Chou et al. 2020 (46)	Compare the prognostic accuracy of an automated % TIL score using the NN192 algorithm to that of Clark's grading	453 melanoma patients	TIL-quantifying neural network: NN192 algorithm	Automated % TIL scoring significantly differentiated survival using an estimated cutoff of 16.6% TIL, whereas TIL did not associate with RFS between groups ($P > 0.05$) when categorized as brisk, nonbrisk, or absent.
Kucharski et al. 2020 (47)	semi-supervised solution using convolutional autoencoders to to segment nests of melanocytes in histopathological images of H&E-stained skin specimens	Training set of 70 H&E stained WSIs of selected melanocytic lesions including 22 lentigo maligna, 20 junctional dysplastic nevi, 13 melanoma in situ and 15 superficial spreading melanoma (15); Validation set (of manually labeled ground truth images) of	Computer-vision based deep learning tool: Convolutional autoencoder neural network architecture with two semi-supervised training stages for the encoding and decoding parts	Segmentation of nests areas with Dice similarity coefficient 0.81, sensitivity 0.76, and specificity 0.94
Figueriredo et al. 2020 (48)	Investigate the mechanisms that supress tumor infiltrating lymphocyte in uveal melanoma	1 patient with uveal melanoma for Digital Spatial profiler,	Nanostring GeoMx Digital Spatial Profiler, CytOF and mRNA expression analysis	Loss of BAP1 expression is associated with an immunosuppressive microenvironment in uveal melanoma
Dikshit et al. 2020 (49)	Develop a novel workflow to combine the single molecule and single cell visualization capabilities of the RNAscope in situ hybridization (ISH) assay with the highly multiplexed spatial profiling capabilities of the GeoMx™ Digital Spatial Profiler (DSP) RNA assays	3 melanoma & 3 prostate tumors	RNAscope & Nanostring GeoMx Digital Spatial Profiler	Transcriptionally profiling of regions of high and low CTNNB1 expression within melanoma and prostate tumors and identify genes potentially regulated by the WNT- β-catenin pathway
Klein et al. 2021 (50)	Evaluate the predictive value of tumor infiltrating lymphocyte (TIL) clusters in primary MM and its association to molecular subtypes to predict response to CPI treatment.	H&E stained slides: Discovery cohort of 90 immune checkpoint therapy treated melanoma and a validation cohort of 351 patients from TGCA database	Deep-convolutional-neural network (U-Net) to detect viable tumor areas; following a quantitative TIL detection using a separate additional neural network	TIL clusters are associated with response to immunotherapy in BRAF V600E/K mutated MM.
Moore et al. 2021 (51)	Test whether automated digital (TIL) analysis (ADTA) improves accuracy of prediction of disease specific survival (DSS) based on current pathology standards	Training cohort of 80 melanoma patients, validation cohort of 145 melanoma patients	automated digital (TIL) analysis (ADTA) using a convolutional neural network (CNN)	After multivariable Cox proportional hazards analysis, ADTA contributed to DSS prediction (HR: 4.18, CI 1.51–11.58, $p = 0.006$).
Martinez-Morilla et al. 2021 (52)	Characterize the tumor microenvironment of patients with metastatic melanoma to find indicative factors of treatment response	Not reported	Imaging Mass Cytometry (IMC) (25 markers)	Identification of a series of potentially indicative biomarkers for immunotherapy in metastatic melanoma, including B2M.

The New Morphological Evaluation: AI-Based

Historically, the role of the dermatopathologist in malignant melanoma concerned mainly 3 aspects: (i) find the right histopathological diagnosis of pigmented lesions; (ii) define the pathological staging for the primary malignant melanoma on the basis of Breslow thickness and ulceration; and (iii) list all the other relevant prognostic parameters not included in the staging process such as regression, inflammatory infiltrate, microsatellites, etc. This evaluation has always been done using a simple hematoxylin-eosin (HE) staining and a visual interpretation of the morphometric features of the tissue by the pathologist. The first task listed above is definitely the most challenging and still impossible to be performed by the machine autonomously. For the last two monotonous tasks, instead, the pathologist can be more effectively assisted by digital pathology where these parameters can be objectively quantified by the computer on digitized whole-slide images leaving more time to the pathologist for the diagnostic process.

First of all, finding the right histopathological diagnosis of pigmented lesions is known to be one of the most challenging tasks in pathology, requiring extended training and expertise. This is further highlighted by the fact that there can be a high degree of discordance when the same lesion gets evaluated by different pathologists (53). Even though discordance is still present among the more experienced dermatopathologists (54), experience and specific training in dermatopathology do improve the diagnosis of difficult cases (55). In fact, digital pathology can be used to virtually share slides between peripheral hospitals and reference centers, facilitating the process of second opinion and expert review. As such, both AI and digital pathology can provide a more standardized level of diagnostic accuracy, ensuring patients get access to the most reliable diagnostic assessments. Digitized whole scan images of a histological slide have been found to have similar effectiveness, both in terms of accuracy and diagnostic workflow, to traditional microscopy for the evaluation melanocytic lesions (26, 27, 56). Moreover, artificial intelligence can also bring its experience, namely its machine learning training, to the side of less experienced pathologists to assist them with more complex diagnostics. In this direction, even before the introduction of machine learning, feature extraction-based algorithms had already proven to be efficient to distinguish melanocytic lesions with an accuracy of 95% (28). Even more recently, a first machine learning algorithm was developed to evaluate the degree of uniformity and symmetry of melanocytic nests as a first step to discriminate between benign and malignant lesions (47). Nevertheless, it is very unlikely that the application of digital pathology and AI will replace the pathologist in the diagnostic process, especially for melanocytic lesions. Since the use of deep learning allows the mining of complex morphometric features that go beyond mere visual identification, these can be applied in the form of an augmented reality rather than of an autonomously working AI, in order to suggest elements in favor and against the diagnosis of melanoma that will necessarily need to be reviewed by the pathologist itself. The augmented reality will bring to the attention of the pathologist features that should not be missed, helping him to recognize the trivial case (all the features pointing in one direction) from the more complex one (more contrasting/ambiguous features), speeding up the work of the pathologist, thanks to a triage process but not substituting him in making the definitive diagnosis. Therefore, it is also more realistic that the role of digital pathology and machine learning will be assisting the general pathologists with less experience in melanocytic lesions rather than the experienced dermatopathologist (**Figure 1**).

Interestingly, artificial intelligence could also be used to organize collections of digitized tissue slides by image similarity, and, as such, go far beyond the use of mere text-based searches. This can have various applications: (i) matching new cases to archived morphologically similar cases to propose a putative diagnosis and potentially improve the diagnostic accuracy; (ii) groups of similar images can more efficiently be retrieved from the archives for training purposes, not only to develop new or improved algorithms, but also for pathologists-in-training (57).

Software packages that are able to apply automated measurements, can also make diagnostics more efficient by automatically retrieving the required parameters and adding them to clinical reports. One of the first studies to use deep learning in histopathology allowed to recognize and count mitotic cells in breast cancer with higher accuracy compared to manual assessment (58). As manual counting mitotic nuclei is a highly time-consuming tasks, it could be easily replaced by AI in melanoma reporting as well. Other practical examples involve the measurement of the Breslow thickness (25), the evaluation of the proliferation index or the detection of lymph node metastasis (34, 35), for which deep learning algorithms are already available. In addition to this, deep learning has been proven useful as an alternative way to the most traditional pathological report to predict the risk of melanoma recurrence, on the basis of features extracted from HE images (38). Moreover, image analysis and machine learning were also applied to quantify tumor infiltrating lymphocytes (TILs) on HE, revealing to be a better tool than the actual semiquantitative classification in brisk, non-brisk and absent to estimate survival for melanoma patients (46, 50, 51) and to be associated with response to checkpoint inhibitors in BRAF V600E/K mutated malignant melanomas (50)

Finally, on top of assisting the pathologist with the diagnostic process and the definition of the prognosis, there are additional advantages to the introduction of digital pathology (**Figure 1**). The number of cases in dermatopathology has been rising over the last decade, and as such also the workload of the dermatopathologists (59). Most of these lesions are benign and easy to recognize, yet require dedicated time for evaluation. This reduces the available time for the more challenging/difficult cases. Software packages have recently entered the market that can assign a "class" to a skin lesion (e.g. epithelial vs melanocytic), detect easy, benign lesions, that can be prioritized and quickly diagnosed, and assign a particular flag to cases recognized as "complex", onto which the pathologist can focus longer (45). In this way, artificial intelligence can help to

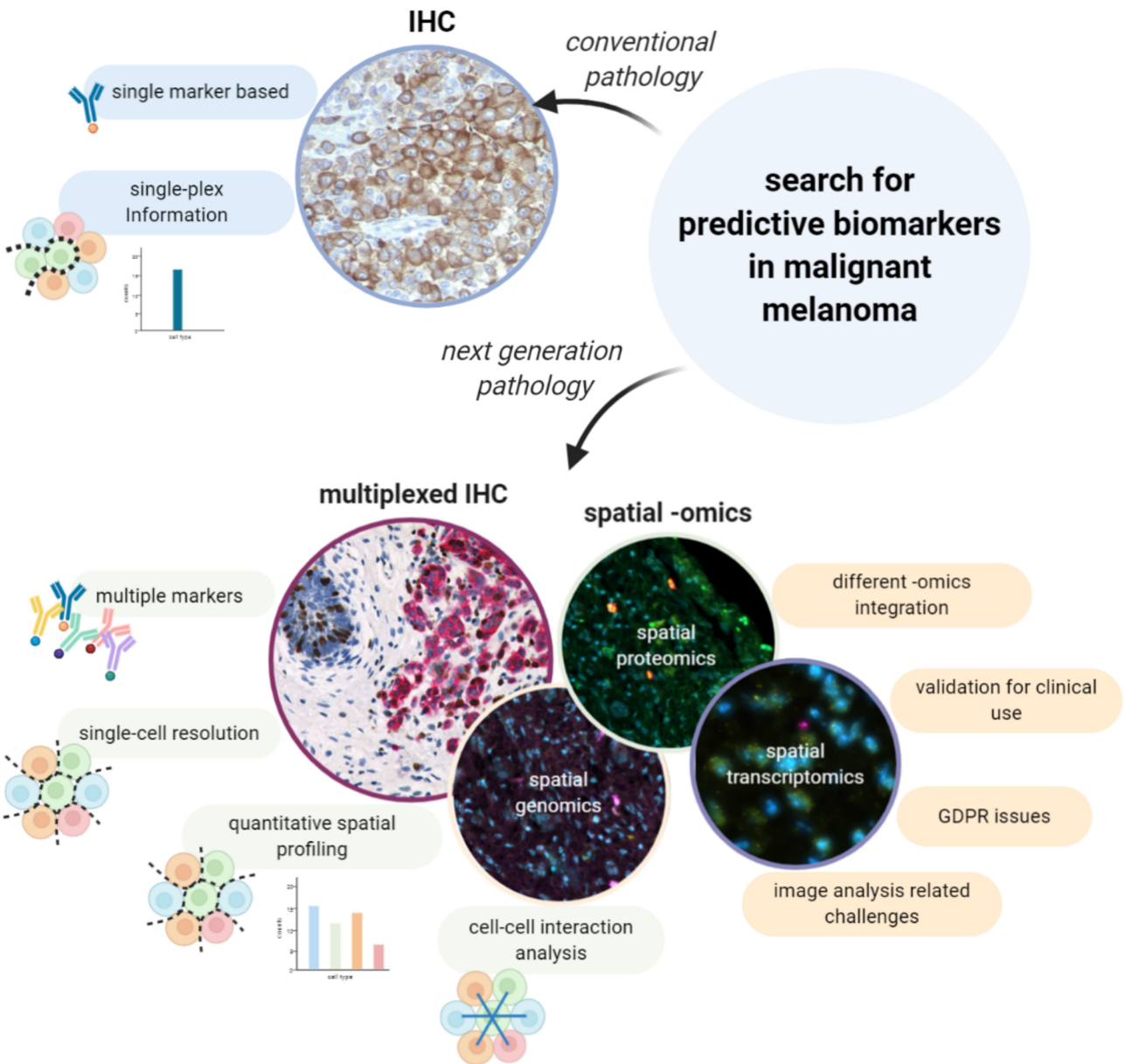

FIGURE 1 | Digital Pathology and AI for a new morphological evaluation. The limitations related to the visual inspection-based diagnosis made by the pathologist on HE stained samples can be overcome with digital pathology and the support of AI and image analysis. Thanks to such computational tools it is possible to achieve more accurate diagnoses, based on a quantitative and more detailed analysis rather than a qualitative assessment, to support pathologists in their work, to automate time-consuming and repetitive tasks and to also improve the organization and the way cases are stored.

optimize the flow of the daily work of the pathologist and improve the robustness and efficiency to come to a proper diagnosis.

Beyond Morphology: The Spatial Omics

As stated higher, the evolving treatment landscape in malignant melanoma has resulted in an increased demand for more and better predictive evaluations on top of the already available prognostic ones. The combination of both is a prerequisite to move toward personalized approaches in which treatments are matched to the right patients. Within metastatic melanoma, the use of checkpoint inhibitor therapy has revolutionized the outcome for patients with an objective response rate between 33.7-45%. Interestingly, the clinical efficacy of anti-PD1 antibodies as monotherapy (15, 16, 60), was slightly improved when combined with anti-CTLA-4 antibodies (up to 58%) (60, 61), but at the cost of higher toxicity rates. To avoid the biological, ethical and economical costs of administering

non-effective treatments to patients, we will need to find predictive biomarkers that can guide clinicians to make informed decisions. In this light, several biomarkers have been described, such as a minimal expression of PD-L1 by conventional IHC (62), a minimal level of tumor mutational burden (TMB) (63), and gene expression profiling (GEP) using the IPRES or IMPRES signatures (64, 65), but none of these have provided the required sensitivity and/or specificity to be implemented in the clinic. This could be due to the limited amounts of information on the tumor and its microenvironment that are gathered by these assays, and which turned out to be insufficient to efficiently predict response to therapy. Indeed, understanding the conditions in which the immune system can be reinvigorated by ICB turns out to be complex and requires the integration of multiple parameters and features. Next-generation pathology using spatially resolved single-cell assessments of a tissue has the potential to shed more light on the complex role of the TME in a patient response to therapy, as it integrates functional information of each individual cell while adding information about their spatial context (**Figure 2**) and as such the interactions between different cell types.

As anticipated in the introduction, conventional IHC cannot provide a multiparametric in-depth characterization of the tissue at single cell level. To overcome the limitations of conventional IHC, multiple approaches have been tested. A first example involves the use of virtual multiplexing which vertically aligns digital images from serial sections. Virtual multiplexing has been made (commercially) available by VisioPharm and HistogGeneX (66) among others. An example is the Tissuealign™ analysis module from VisioPharm that has been validated for *in vitro* diagnostic use (CE-IVD) in Europe in combination with the CE IVD APPs from VisioPharm (67, 68). Nevertheless, vertical registration still does not allow detailed single-cell phenotyping which requires insights in the co-expression of different markers in exactly the same cell. In addition, to identify all the inflammatory subpopulations that are present in a histological sample, the evaluation of more than 20 markers is needed, ideally on the same tissue section ("high-plexing"). Nowadays, several methods for tissue multiplexing are available (69) and any technique representing a surrogate to investigate co-expression of markers at single cell level should be replaced by multiplexed IHC. First investigated in the context of colorectal cancer (70), the implementation of the concept of an 'Immunoscore' or immunoprofiling into a renewed cancer staging system incorporating the effects of the host immune response based on the numeration of specific lymphocyte populations alongside with the tumor cell-autonomous characteristics has been proven useful in the context of advanced melanoma as well (23). The colorectal Immunoscore, which involved a quantitative assessment of $CD3^+$ and $CD8^+$ T cells both at the invasive margin and bulk of the tumor, was already published in 2006 and encouraged the adoption of digital pathology tools for biomarker discovery (70, 71). Specific for melanoma, the definition of a comparable Immunoscore seems to be a more difficult challenge (72). In many patients, metastatic lymph nodes are the only available tissue samples and concerns are raised about the applicability of an Immunoscore in lymph nodes because they are constitutively rich in CD3 and CD20 lymphocytes. In a first effort, an Immunoscore constructed based on the expression of CD8, CD3, CD20 and FOXP3, was applied on a small cohort of stage III melanoma patients showing significant differences in the peri/intratumoral ratio for both CD3 and CD8, with the ratio being higher in patients without recurrence compared to patients with melanoma recurrence, with similar trends for both FOXP3 and CD20 were observed (71). In a more recently published systematic review, a favorable prognostic role of the $CD3^+$, $CD4^+$, $CD8^+$, $FOXP3^+$, and $CD20^+$ TILs on the overall survival of melanoma patients was confirmed. In addition, in a subgroup analysis, brisk TILs were associated with overall survival, recurrence-free survival, and melanoma-specific survival (36). Likewise, the predictive performance of an alternative Immunoscore, using a digital image analysis application to characterize immune infiltrate expression of CD3, CD8, CD20, FOXP3 and CD163 and of PD-L1, was tested in a metastatic melanoma cohort of patients treated with Ipilimumab in the MISIPI trial (22, 72). Unfortunately, this trial was unable to confirm the relationship between intra/peritumoral expression of CD3, CD8, CD20, CD163, FOXP3 and a response/benefit to therapy, apart from a trend for the CD163-PD-L1 double positive population (22). Another study, using a low-plex with only 6 markers found instead that the quantity but not the activation of CD8+ TILs was associated with anti-PD-1 response in metastatic melanoma (37). In an attempt to categorize the intrinsic heterogeneous nature of metastatic melanoma, Halse and colleagues used multiplex immunohistochemistry to provide a model which defines the immune context into four categories, using the presence or absence of $PD\text{-}L1^+$ melanoma cells and/or macrophages, and their location within or around the tumor, combined with the presence or absence of intratumoral $CD8^+$ T cells. This model values the melanoma TME as a spectrum between tumor escape and tumor (immune) control within the space of a tissue (30), encouraging others to investigate the spatial distribution of both immune and tumoral cells when interpreting the response to immunotherapy. Confirming the latter, whereas no association with response or survival could be observed in the expression of individual biomarkers (PD-1, PD-L1, IDO-1, HLA-DR), a spatially-resolved low-plex PD-1/PD-L1 interaction score and/or IDO-1/HLA-DR co-expression was strongly associated with an anti–PD-1 response, highlighting the importance of quantitative spatial profiling for multiple features (33). Furthermore, Gide and colleagues examined the spatial distribution of immune and tumor cells using a 5-plex immunofluorescence approach in samples of patients prior to a treatment with either anti-PD-1 monotherapy or a combination of anti-CTLA-4 and anti-PD-1. In a multivariate analysis, the best predictor for a 12-month progression-free survival upon anti-PD-1 monotherapy involved the quantification of the proximity of $PD\text{-}L1^+$ immune cells to tumor cells and the density of intratumoral $CD8^+$ T-cell, as such achieving an AUC of 0.80. For the combination therapy, the authors identified that a correlation with the proximity of $CD8^+$ T-cells

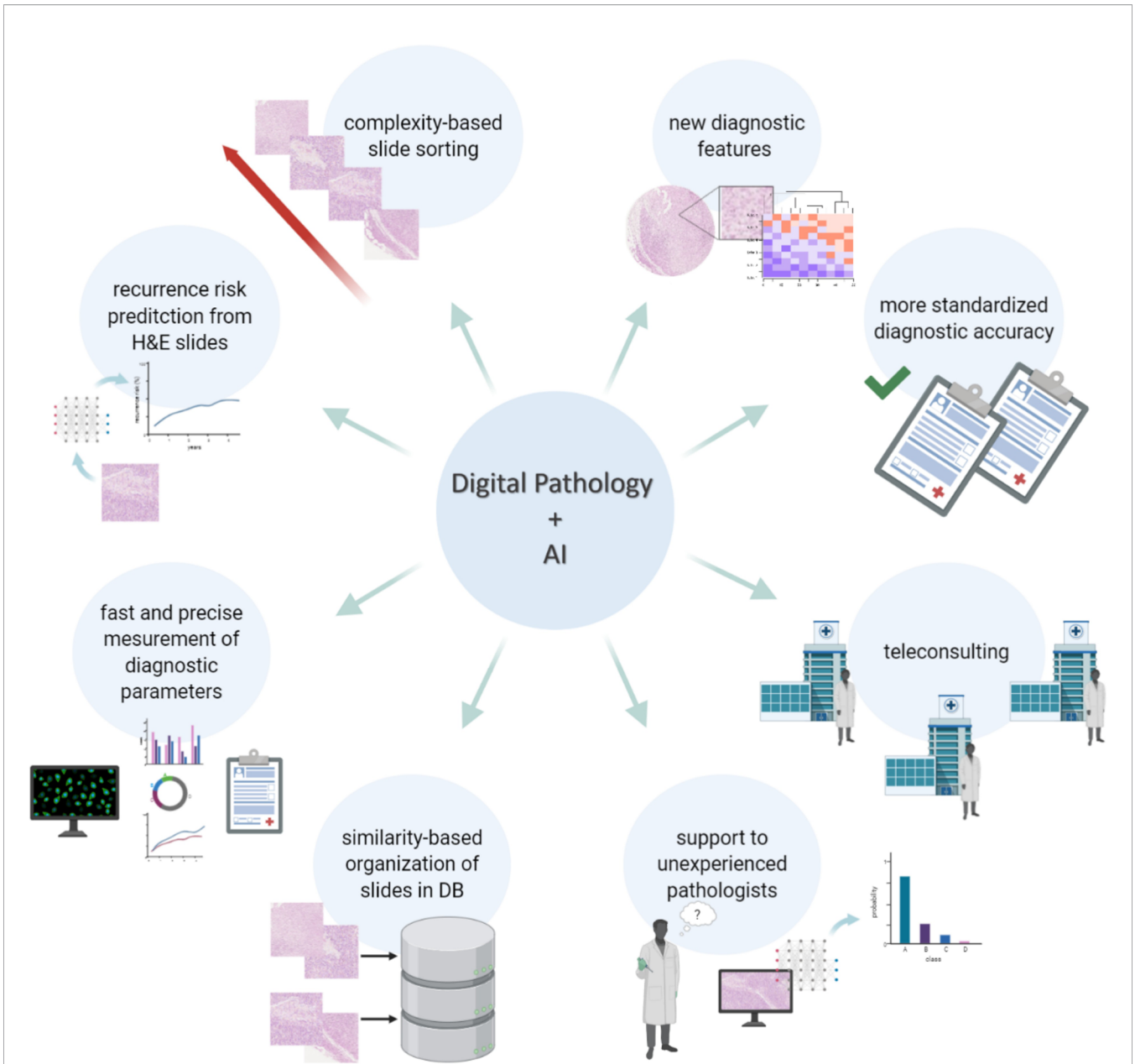

FIGURE 2 | Searching for predictive biomarkers in malignant melanoma with spatial multiplexing techniques: advantages and challenges. Predictive evaluation of malignant melanoma is needed for a more personalized treatment plan, but predictive biomarkers must still be identified. Conventional IHC is a single-plex based method which does not provide information at single-cell level. On the other hand, multiplexed IHC and spatial -omics methods make it possible to extract information from multiple markers at single-cell resolution and to investigate cell-cell interactions. However, despite the great advantages, those techniques have not yet been validated in clinics and it is currently not possible to integrate the information from different -omics on the same section at single-cell level. Moreover, those methods are strictly dependent on computational techniques for the downstream analysis, hence they carry all the challenges related to image analysis.

to tumor cells, the density of intratumoral PD-L1$^+$ cells and LDH expression (AUC = 0.85) to response to therapy (40). Similarly, others have shown that pre-treatment samples obtained from responders to anti-PD1 therapy showed that increased amounts of CD8$^-$, PD-1$^-$ and PD-L1$^+$ cells resided at the invasive tumor margins and within the tumor, with close proximity the ligands PD-1 and PD-L1 (24). In addition, the use of multiplexed immunofluorescence highlighted a potential predictive role for specific cancer-associated fibroblasts (39) and CD103$^+$ tumor-resident CD8$^+$ T cells (29) in melanoma patients treated with anti-PD-1 therapy. Also, the potential contributing role of tumor-associated B-cells has been studied using multiplexed immunofluorescence, showing an association between co-occurrence of tumor associated CD8$^+$ T cells and CD20$^+$ B cells with improved survival, while revealing the formation of tertiary lymphoid structures (TLS) in these CD8$^+$CD20$^+$ tumors

(42) and their potential role in response to immunotherapy (43). Overall, according to a recently published meta-analyses, the extended information that could be extracted using multiplexed IHC/IF appears to be associated with improved relative diagnostic accuracy in predicting clinical response to anti-PD-1 therapy over the other previously mentioned biomarkers (PD-L1 conventional IHC, TMB, GEP) (73).

Strikingly, most of the research trying to map the melanoma TME were done using "low-plex" methods (less than 10 markers on the same section), and yet the majority of them added interesting insights into the anti-melanoma immune response and response to immunotherapy. The reason why even a low-plex approach can be more insightful compared to other molecular methods (e.g. NGS analysis) which often cover even more parameters, could be related to the insights gained within the spatial component. Indeed, the spatial dimension (i.e. understanding the exact position of each cell type within a tissue) could be considered as a biomarker itself. Available analysis methods are now able to generate cell density metrics for specific tissue regions, assess the distance between various cell types, among many more. Such higher-order insights grant the possibility to go beyond mere cytometric analysis of the tissue (i.e. the overall cellular composition of a tissue) and investigate "cellular sociology" in order to make assumptions about their interactions in particular niches. Moreover, already in the early days of single-cell genomics, it was clear that the success of the different single-cell technologies would depend, in part, on the extent to which researchers preserve the states of cells and the original composition of a tissue (74). After all, most of the initial single-cell methods required cells to be dissociated from the tissue, thereby losing all spatial information while potentially affecting the original cell states. To deal with this flaw, the most recent single-cell methods aim at preserving the cells in their original context and state.

Within the available spatial omics methods, we can distinguish spatial proteomics, transcriptomics and genomics (**Figure 2**). Most of the spatial proteomics techniques are antibody based methods that achieve their plexability from either multi-spectral imaging and/or iterative imaging of successive antibody staining cycles combined with fluorophore bleaching/inactivation/cleaving or antibody stripping (75–80). Similarly, spatial transcriptomics enable the in-situ visualization of RNA transcripts within the tissue either by measuring pre-determined targets or even global expression data (81–86). A detailed description and comparison of the different available techniques for spatial -omics, goes beyond the scope of this review.

Several of the abovementioned technologies have been applied to melanoma in an attempt to improve prognostic and predictive performance of potential biomarkers, or as a discovery tool to unravel mechanistic insights in the TME. Accordingly, our group previously used MILAN – an imaging/antibody-based single-cell proteomics method - to functionally study tissue architecture, thereby redefining the TIL infiltrate in primary melanoma into a functional classification with an improved prognostic value as compared to the dogmatic morphological classification (44) and described a higher level of interaction between melanoma cells with active $CD8^+$ and $CD4^+$ T cells in patients responding to anti-PD-1 as compared to the non-responding patients (87). Others have used imaging mass cytometry (IMC) with a 25-antibody panel to identify tumor and immune cell markers in melanoma patients treated with immune checkpoint blockers, revealing significant associations of MHC-I, CSF1R, IRF1, LAG-3, PD-1, MHC-II and beta2-microglobulin expression in tumor tissue with progression-free survival, whereas high levels of TIM-3 and PD-L2 in the stroma also predicted response to immunotherapy (52). Spatial transcriptomics have been used to visualize the distribution of mRNA within the melanoma TME, revealing among others the complex transcriptional spatial landscape and genetic heterogeneity in stage III cutaneous melanoma (32).

The Integration of Multi-Omics Within the Tissue

Most of the methods for spatial omics are limited by their ability to examine only one type of analyte (protein or nucleic acids). One step closer toward a complete understanding of the TME of melanoma and the drivers of response to immunotherapy will require the integration of information retrieved from several -omics approaches, each providing complementary information. The integration of information from different omics technologies and particularly those integrating information from the same section at single-cell level while preserving the spatial context represents the ultimate goal for next-generation pathology. In spite of major progress in the development of methodologies that simultaneously extract various features from the same cell, a genuine, spatially integrated multi-omics approach, enabling the simultaneous analysis of proteome, transcriptome, genome- and epigenome within the spatial coordinates is still not available. Therefore, while the development of such combinatory technologies is ongoing, other approaches are being evaluated, including the computational integration of spatially resolved assays (which typically rely on a predefined, but limited set of features), and an unbiased method, such as single-cell RNA-sequencing (scRNAseq) which requires cells to be removed from the tissue. Another simplified approach consists of performing various spatially resolved omics analyses on serial sections, and integrating the findings in a comprehensive framework. As discussed earlier, the use of multiplex immunofluorescence confirmed the importance of tumor-associated B cells and TLS in metastatic melanoma (42, 43), a finding that was further corroborated by spatial transcriptomics, indicating that T cells in TLS-negative tumors had a dysfunctional molecular phenotype (42) whereas TLS-positive tumors are associated with markers of T cell activation and B cell proliferation (43). Alternatively, combining multiple omics on serial sections can be integrated at the tissue level by making use of vertical registration. For example, digitally superimposing a melan-A classical IHC on 1 section and RNAscope probing for hTERT on the adjacent section, allowed these researchers to show a higher expression of hTERT mRNA in melanoma as compared to benign naevi (41). Yet another approach is to laser-microdissect regions from

a tissue for gene-expression analysis, while being guided by classical IHC staining on the adjacent section. Such approach has been used to compare expression profiles of IHC-positive and IHC-negative areas, thereby improving cell-type purity in the different samples as compared to classical tissue-based transcriptomic data (21). With the development of Spatially-resolved Transcriptomics *via* Epitope Anchoring (SvEA) in pivotal work done by Govek and colleagues, this has recently been made possible (88). In this approach, the transcriptomic data acquired *via* CITE-seq (89) can be mapped to spatially resolved CODEX mIHC data (77), while retaining the single cell spatial resolution by making use of measurements of the same antigens in both methods (88). In spite of the obvious translational potential of this novel approach, it has not yet been applied within the melanoma field. More recently, the GeoMx® DSP (Digital Spatial Profiling) platform has been made commercially available (90). This platform allows protein or RNA quantification within user-defined regions-of-interest (ROI), with the possibility of single-cell resolution ROI selection (The UV laser can be focused as narrow as 10 μm in diameter). This ROI selection is achieved by combining regular, low-plex IF staining together with dozens of primary antibodies or mRNA hybridization probes each covalently attached to indexing oligonucleotides that can be collected for quantification using a UV-photo cleavable linker (91). Using this method, Dikshit and colleagues recently transcriptionally profiled regions with high and low Beta-catenin expression in melanoma, showing a significant correlation with several immune-regulatory targets such as CTLA-4 and PD-1 (49). Similarly, the method was used to show a specific expression profile in fibrotic areas with high macrophage and T cell infiltration in BAP-1 negative uveal melanoma, suggestive of T-cell exhaustion other than PD-1/CTLA-4 engagement, as well as mechanisms of immune exclusion, supporting the clinical observation of immunotherapeutic failure in this subgroup and the need for development of specific treatment approaches (48). Two other studies have used DSP to characterize the tumor expression profile of melanoma patients treated with immune checkpoint blockade in a neoadjuvant setting, showing that baseline immune infiltration was correlated with response to treatment (92, 93). Although offered as an easy applicable method, a detailed understanding of its composition, function and chemistry is advisable to guide experimental design and data interpretation (94).

Finally, AI will have a predominant role in the integration of all the different data types. In the previous section we have discussed how AI has already outperformed pathologists on evaluating morphological features such as mitotic counts (58), Breslow thickness (25) or at detecting lymph node metastases (34, 35) - routine tasks that could significantly enhance the throughput and efficiency of pathologists while ensuring sufficient can be spent on complex cases. However, the strongest ability of AI, and in particular deep learning, is to identify unknown patterns or features that are too complex for pathologists to merely assess by visual eyeballing but which could be of important diagnostic, prognostic, or predictive relevance. This is already true in the case of morphometric features (95). In the case of spatially-resolved, single-cell multi-omics data, the feature space is still significantly larger and the number of hidden associations that could be used as biomarkers is virtually endless. For their translatability to clinical practice however, these complex features require first to be re-engineered to simpler biomarkers or simpler algorithms that identify the specific discriminant features which might be more easily accepted by clinicians (96).

DISCUSSION: NEXT-GENERATION PATHOLOGY AND ITS CHALLENGES

Even though next-generation pathology is becoming gradually more prominent and qualifies as a necessity in research, very few of the previously discussed developments have yet been validated for clinical use. With the increasing importance of understanding the immune contexture and the possible development of panels of prognostic/predictive biomarkers across multiple diseases, we foresee that the implementation of next-generation pathology in clinical practice will be mandatory. However, there are still a lot of hurdles and challenges that need to be overcome before multiplexed IHC and digital pathology will be implementable in clinical practice.

The main difficulty of implementing multiplexed IHC is to overcome the common thinking that it is based on the repetition of multiple conventional IHC assays. Indeed, multiplexed IHC is a complex process and there are various challenges that need to be considered. The first challenge is about choosing the most appropriate method. This choice should consider several factors. First of all, the type of samples to be analyzed: some methods require FFPE materials while others can be performed on frozen samples. In a standard clinical pathology lab, FFPE remains the method of choice to preserve tissue specimen, even though multiple methods (mainly multi-omics) require the availability of frozen materials. The second choice will be to related to the actual staining procedure: this can be achieved either by (i) a cyclic method, in which slides are stained multiple times with low-plex antibody cocktails while between every cycle the signal is removed *via* antibody stripping or bleaching of the fluorophore; or (ii) an all-at-once acquisition, where a cocktail containing all the antibodies of choice are applied on the tissue section in a single step. In the first case the acquisition will be slower, while in the second case the increased speed of acquisition will increase technology costs. For instance, several methods require modified/engineered/conjugated antibodies (e.g. with nucleotide barcodes or metal ions) that are more expensive than conventional clones typically used in routine across clinical pathology labs. On top of this, the instruments that are used to detect the signals are often a factor 2-3 more expensive than conventional autostainers typically used for classical IHC. These machines are generally closed systems that have the advantage to be completely automated, requiring less work by the lab technician being therefore less prone to errors. Nevertheless, these methods may be limited to the acquisition of

regions of interest rather than whole slides; depending on the number of antibodies to be detected the acquisition time could require even hours per square mm. A final parameter to consider on the wet-lab part is the number of samples that should be analyzed simultaneously: while some methods allow the analysis of a single slide at the time, others are compatible with batch processing.

The second big challenge of implementing multiplexed IHC in hospital routine relates to data analysis. At the moment, most of the wet-lab methods are not paired with a system to analyze the data. Importantly, multiplexed IHC can no longer be evaluated through mere visual inspection (as opposed to conventional IHC where it is common practice), but requires specific methods for quantitative, spatially resolved analysis. Therefore, until *ad hoc* software packages will be introduced for specific predictive/prognostic analyses, experts in image analysis and bioinformaticians will remain required for the downstream analysis. In addition, a simple panel of 10 markers will generate 100 digital images when analyzing 10 samples, an amount that will steadily increase when increasing numbers of markers and samples are processed. This is where the hurdles to implement multiplex IHC converge with those of implementing digital pathology.

As described above, digital pathology bears the potential to revolutionize dermatology and dermatopathology. To achieve its implementation, though, multiple challenges have to be overcome, and typically involve hurdles that are cultural, involve validation, available infrastructure and GDPR-related issues. From a cultural point of view, in spite of the advantages listed in the first chapter of this review, pathologists still show some reservations about the use of digital slides for diagnosis, mainly regarding the time needed to evaluate whole digital slides during routine work, with a preference to reserve the digital format for teaching, second opinions and dissemination purposes (31). Second, appropriate validation remains an absolute requirement for any new technique that get implemented for diagnostic purposes. Such validation does not solely happen at the level of a company trying to sell a diagnostic tool, but can also happen directly at a local level, for instance in a pathology department that is willing to introduce a new technique in its workflow. Validation itself will mainly require side-by-side comparisons of manually and digitally interpreted tissue slides (97). Validation is also required for deep learning algorithms, which have the danger to be based on overfitted or miscorrelating data from training sets. In particular, on one side algorithms have to be strictly disease-specific and exclude any other disease that may be encountered during analysis (e.g., algorithms developed for the analysis of melanoma should recognize and revoke the analysis of any other skin tumor). On the other side, since they are extremely dependent on their training, it is important to be aware that if important differences are introduced in time that may artificially change the features of the prospectively collected diagnostic data set, high rates of misclassification can be registered (98). Next to these first two challenges, there are also important infrastructural challenges to be considered that can hamper the implementation of digitization in a clinical institution. A standard microscopy slide, such as the ones routinely used in pathology are typically 75 mm long, 26 mm wide, and approximately 1 mm thick. As the resolution and color depth of digital detectors improve, the size of images that capture these slides keeps on increasing. For a state-of-the-art acquisition instrument with a resolution of 0.44 micrometers/px (20X) and color depth of 16 bit (~65K gray levels), and assuming a 2-dimensional slide with standard dimensions, single images achieve a size of ~20 Gigabytes (Gb). Of course, depending on the size of the scanned area and the type of image compression, whole slide images can range between 0.5 and 4 Gb (96). This is translated to hundreds of Terabytes per year (or even Petabytes when considering a large hospital) that need to be properly acquired, stored, transferred, and processed. Designing and implementing a proper infrastructure for digital pathology that deals with all these tasks is not trivial and key for a successful digital transition. Regarding image acquisition, this is an easily solvable problem, since in the 20 years since the introduction of whole-slide imaging scanners, several of them have been marketed for clinical use in the European Union and in the US (99, 100). Image storage and transfer are instead critical steps and they may require important investments on the side of the institution. There exist different types of solutions for image storage, ranging from local ones such as Direct Attached Storage (DAS), network-based solutions such as Network Attached Storage (NAS), cloud-based solutions (such as Amazon's S3 Glacier storage for example) or external services (regional supercomputer centers). The last two examples require sending data to third parties which could have GDPR issues (see below). In most cases, several of these solutions need to be simultaneously implemented to archive the data depending on different factors, including access frequency (hot/interactive *versus* cold/archival storage) or intended use (101). For image transfer, solutions where data is remotely stored or/and the images are remotely analyzed, the speed in which data is transferred (network bandwidth) becomes a critical factor. If we consider a 10 Gb image and a standard Local Area Network (LAN) with a bandwidth of 100Mbit/s, it will take ~15 minutes to transfer the file. Therefore it is crucial to guarantee an environment with sufficient bandwidth prior to taking the step to digital pathology. Finally, most of the digital image analysis algorithms currently used in clinical practice are limited to traditional image analysis and can be used on ordinary computers with Central Processing Units (CPUs) (96). Deep learning algorithms, on the other hand, are heavily dependent on processing acceleration units such as Graphical Processing Units (GPUs) (102). High-end GPUs are very expensive and therefore centers implementing deep learning in digital pathology might choose for a dedicated workstation/server or even to train/run their algorithms in the cloud or in external supercomputer centers. Lately, the development of Tensor Processing Units (TPUs) are allowing the training of deep neural networks (DNN) 15-30 times faster and 30-80 times more energy efficient than contemporary CPUs or GPUs (103). Additional infrastructural challenges to be considered for implementing deep learning in digital pathology include: the number of users of the

dedicated computers, the flexibility of the system to implement new algorithms or variable case-loads, implementation/running cost of the facility, cyber-security, data maintenance, etc. (96). A practical example of the implementation process of a fully digital workflow at the University Medical Centre in Utrecht can be found in Stathonikos et al. (104).

The last challenge for digital pathology is correlated with the fact that digital images, as well as patient materials, are subject to the regulation on data protection and privacy in the European Union and the European Economic Area on the protection of natural persons with regard to the processing of personal data and on the free movement of such data (General Data Protection Regulation, GDPR) (105). With respect to digital pathology, it contains several basic principles that digital slides containing human samples must comply with. These include: Purpose specification, the valid legal basis for the collection of the data including the goal for which the data is being collected (106); anonymization or pseudo-anonymization, data is only anonymous when it is impossible to track it to natural persons while pseudo-anonymous data requires extra information to map it to natural persons (107, 108); Data minimization, the collected data should be limited to what is strictly necessary for the scope of the project (107) transparency, the registration of the study and the provision of the relevant information to the subject of the study; storage limitation, the collected data should only be kept as long as needed; and security, the stored data should be processed and stored in such way that it avoids or limits the potential for unlawful processing, accidental loss, destruction or damage (107). This includes technical measures such as badge and password-mediated access control, detailed logs monitoring every ongoing process on the system, data encryption, etc. If the data is stored on the cloud or in external sources, a legal contract needs to be written between the collector and the third party which needs to be checked by legal entities (109, 110).

To conclude, the highly requested demand for a better understanding of the TME in melanoma and its use to further improve the clinical response rates to immunotherapy, the fast-moving technological advancements in machine learning and the rise of spatial omics, have pushed dermatopathology into the digital era. Although the use of digital pathology has already proven to be insightful in melanoma, its exploitation to the full potential by combining spatially resolved single-cell data with artificial intelligence for clinical purposes, is still a rather future perspective. However, such an approach possesses the capability to overcome existing limitations and bring us one step closer to personalized medicine. Nonetheless, despite the many advantages, a lot of the imaging-based methods go along with substantial challenges that need to be addressed before its implementation in daily practice will be possible.

AUTHOR CONTRIBUTIONS

YH decided the contents, did the main literature research, wrote all the parts about the omics, reviewed the format and the structure of the paper. AA wrote the part on the dry lab challenges and reviewed the format and the structure of the paper. MA researched the topic on GDPR regulations and reviewed the paper. GM created the images and reviewed the paper. OB reviewed the paper from the oncologist point of view. FS reviewed the paper from the bioengineer point of view. FB decided the contents, structured the flow of the paper, gave the pathology insights, wrote the introduction, the part about AI beyond morphology and the part on the discussion about the wet lab challenges. All authors contributed to the article and approved the submitted version.

FUNDING

AA was supported by the Leuven Kankerinstituut (LKI) and the Opening The Future (OTF) foundation. This work is also supported by the Kom op tegen kanker (KOTK) foundation.

REFERENCES

1. Luikart SD, Kennealey GT, Kirkwood JM. Randomized phase III trial of vinblastine, bleomycin, and cis-dichlorodiammine-platinum versus dacarbazine in malignant melanoma. *J Clin Oncol* (1984) 2(3):164–8. doi: 10.1200/JCO.1984.2.3.164
2. Cancer Genome Atlas Network. Genomic Classification of Cutaneous Melanoma. *Cell* (2015) 161(7):1681–96. doi: 10.1016/j.cell.2015.05.044
3. Chapman PB, Hauschild A, Robert C, Haanen JB, Ascierto P, Larkin J. Improved survival with vemurafenib in melanoma with BRAF V600E mutation. *N Engl J Med* (2011) 364(26):2507–16. doi: 10.1056/NEJMoa1103782
4. Hauschild A, Grob JJ, Demidov LV, Jouary T, Gutzmer R, Millward, et al. Dabrafenib in BRAF-mutated metastatic melanoma: a multicentre, open-label, phase 3 randomised controlled trial. *Lancet* (2012) 380(9839):358–65. doi: 10.1016/S0140-6736(12)60868-X
5. Flaherty KT, Robert C, Hersey P, Nathan P, Garbe C, Milhem M, et al. Improved survival with MEK inhibition in BRAF-mutated melanoma. *N Engl J Med* (2012) 367(2):107–14. doi: 10.1056/NEJMoa1203421
6. Larkin J, Ascierto PA, Dréno B, Atkinson V, Liszkay G, Maio M, et al. Combined vemurafenib and cobimetinib in BRAF-mutated melanoma. *N Engl J Med* (2014) 371(20):1867–76. doi: 10.1056/NEJMoa1408868
7. Robert C, Karaszewska B, Schachter J, Rutkowski P, Mackiewicz A, Stroiakovski D, et al. Improved overall survival in melanoma with combined dabrafenib and trametinib. *N Engl J Med* (2015) 372(1):30–9. doi: 10.1056/NEJMoa1412690
8. Long GV, Stroyakovskiy D, Gogas H, Levchenko E, de Braud F, Larkin J, et al. Combined BRAF and MEK inhibition versus BRAF inhibition alone in melanoma. *N Engl J Med* (2014) 371(20):1877–88. doi: 10.1056/NEJMoa1406037
9. Dummer R, Ascierto PA, Gogas HJ, Arance A, Mandala M, Liszkay G, et al. Encorafenib plus binimetinib versus vemurafenib or encorafenib in patients with BRAF-mutant melanoma (COLUMBUS): a multicentre, open-label, randomised phase 3 trial. *Lancet Oncol* (2018) 19(5):603–15. doi: 10.1016/S1470-2045(18)30142-6
10. Hodi FS, Corless CL, Giobbie-Hurder A, Fletcher JA, Zhu M, Marino-Enriquez A, et al. Imatinib for melanomas harboring mutationally activated or amplified KIT arising on mucosal, acral, and chronically sun-damaged skin. *J Clin Oncol* (2013) 31(26):3182–90. doi: 10.1200/JCO.2012.47.7836
11. Atkins MB, Lotze MT, Dutcher JP, Fisher RI, Weiss G, Margolin K, et al. High-dose recombinant interleukin 2 therapy for patients with metastatic melanoma: analysis of 270 patients treated between 1985 and 1993. *J Clin Oncol* (1999) 17(7):2105–16. doi: 10.1200/JCO.1999.17.7.2105

12. Schwartzentruber DJ, Lawson DH, Richards JM, Conry RM, Miller DM, Treisman J, et al. gp100 peptide vaccine and interleukin-2 in patients with advanced melanoma. *N Engl J Med* (2011) 364(22):2119–27. doi: 10.1056/NEJMoa1012863
13. Smith FO, Downey SG, Klapper JA, Yang JC, Sherry RM, Royal RE, et al. Treatment of metastatic melanoma using interleukin-2 alone or in conjunction with vaccines. *Clin Cancer Res* (2008) 14(17):5610–8. doi: 10.1158/1078-0432.CCR-08-0116
14. Robert C, Thomas L, Bondarenko I, O'Day S, Weber J, Garbe C, et al. Ipilimumab plus dacarbazine for previously untreated metastatic melanoma. *N Engl J Med* (2011) 364(26):2517–26. doi: 10.1056/NEJMoa1104621
15. Robert C, Long GV, Brady B, Dutriaux C, Maio M, Mortier L, et al. Nivolumab in previously untreated melanoma without BRAF mutation. *N Engl J Med* (2015) 372(4):320–30. doi: 10.1056/NEJMoa1412082
16. Robert C, Schachter J, Long GV, Arance A, Grob JJ, Mortier L, et al. KEYNOTE-006 investigators. Pembrolizumab versus Ipilimumab in Advanced Melanoma. *N Engl J Med* (2015) 372(26):2521–32. doi: 10.1056/NEJMoa1503093
17. Larkin J, Chiarion-Sileni V, Gonzalez R, Grob JJ, Cowey CL, Lao CD, et al. Combined Nivolumab and Ipilimumab or Monotherapy in Untreated Melanoma. *N Engl J Med* (2015) 373(1):23–34. doi: 10.1056/NEJMoa1504030
18. Salto-Tellez M, Maxwell P, Hamilton P. Artificial intelligence-the third revolution in pathology. *Histopathology* (2019) 74(3):372–6. doi: 10.1111/his.13760
19. Elder DE, Massi D, Scolyer R, Willemze R. *WHO Classification of Skin Tumours. 4th Edition*. Lyon: IARC (2018).
20. Single-cell biology. *Nature* (2017) 547(7661):19. doi: 10.1038/547019a
21. Makhzami S, Rambow F, Delmas V, Larue L. Efficient gene expression profiling of laser-microdissected melanoma metastases. *Pigment Cell Melanoma Res* (2012) 25(6):783–91. doi: 10.1111/pcmr.12013
22. Bifulco C, Capone M, Feng Z, Madonna G, Simeone E, Curvietto M, et al. MISIPI study: Melanoma ImmunoScore evaluation in patients treated with IPIlimumab. *J Transl Med* (2014) 12(Suppl 1):P11. doi: 10.1186/1479-5876-12-S1-P11
23. Capone M, Madonna G, Sebastiao N, Bird J, Ayala F, Caracò C, et al. Immunoscore: a new possible approach for melanoma classification. *J Immunother Cancer* (2014) 2(Suppl 3):P193. doi: 10.1186/2051-1426-2-S3-P193
24. Tumeh PC, Harview CL, Yearley JH, Shintaku IP, Taylor EJ, Robert L, et al. PD-1 blockade induces responses by inhibiting adaptive immune resistance. *Nature* (2014) 515(7528):568–71. doi: 10.1038/nature13954
25. Xu H, Berendt R, Jha N, Mandal M. Automatic measurement of melanoma depth of invasion in skin histopathological images. *Micron* (2017) 97:56–67. doi: 10.1016/j.micron.2017.03.004
26. Fertig RM, Gaudi S, Cervantes J, Maddy A, Sangueza O, Vu J, et al. Feasibility study in teledermatopathology: An examination of the histopathologic features of mycosis fungoides and spongiotic dermatitis. *J Cutan Pathol* (2017) 44(11):919–24. doi: 10.1111/cup.13018
27. Kent MN, Olsen TG, Feeser TA, Tesno KC, Moad JC, Conroy MP, et al. Diagnostic Accuracy of Virtual Pathology vs Traditional Microscopy in a Large Dermatopathology Study. *JAMA Dermatol* (2017) 153(12):1285–91. doi: 10.1001/jamadermatol.2017.3284
28. Xu H, Lu C, Berendt R, Jha N, Mandal M. Automated analysis and classification of melanocytic tumor on skin whole slide images. *Comput Med Imaging Graph* (2018) 66:124–34. doi: 10.1016/j.compmedimag.2018.01.008
29. Edwards J, Wilmott JS, Madore J, Gide TN, Quek C, Tasker A, et al. CD103+ Tumor-Resident CD8+ T Cells Are Associated with Improved Survival in Immunotherapy-Naïve Melanoma Patients and Expand Significantly During Anti-PD-1 Treatment. *Clin Cancer Res* (2018) 24(13):3036–45. doi: 10.1158/1078-0432.CCR-17-2257
30. Halse H, Colebatch AJ, Petrone P, Henderson MA, Mills JK, Snow H, et al. Multiplex immunohistochemistry accurately defines the immune context of metastatic melanoma. *Sci Rep* (2018) 8(1):11158. doi: 10.1038/s41598-018-28944-3
31. Onega T, Reisch LM, Frederick PD, Geller BM, Nelson HD, Lott JP, et al. Use of Digital Whole Slide Imaging in Dermatopathology. *J Digit Imaging* (2016) 29(2):243–53. doi: 10.1007/s10278-015-9836-y
32. Thrane K, Eriksson H, Maaskola J, Hansson J, Lundeberg J. Spatially Resolved Transcriptomics Enables Dissection of Genetic Heterogeneity in Stage III Cutaneous Malignant Melanoma. *Cancer Res* (2018) 78(20):5970–9. doi: 10.1158/0008-5472.CAN-18-0747
33. Johnson DB, Bordeaux J, Kim JY, Vaupel C, Rimm DL, Ho TH, et al. Quantitative Spatial Profiling of PD-1/PD-L1 Interaction and HLA-DR/IDO-1 Predicts Improved Outcomes of Anti-PD-1 Therapies in Metastatic Melanoma. *Clin Cancer Res* (2018) 24(21):5250–60. doi: 10.1158/1078-0432.CCR-18-0309
34. Alheejawi S, Mandal M, Berendt R, Jha N. Automated Melanoma Staging in Lymph Node Biopsy Image using Deep Learning, *2019 IEEE Canadian Conference of Electrical and Computer Engineering (CCECE)*. Edmonton, AB, Canada (2019). p. 1–4. doi: 10.1109/CCECE.2019.8861878
35. Alheejawi S, Xu H, Berendt R, Jha N, Mandal M. Novel lymph node segmentation and proliferation index measurement for skin melanoma biopsy images. *Comput Med Imaging Graph* (2019) 73:19–29. doi: 10.1016/j.compmedimag.2019.01.006
36. Fu Q, Chen N, Ge C, Li R, Li Z, Zeng B, et al. Prognostic value of tumor-infiltrating lymphocytes in melanoma: a systematic review and meta-analysis. *Oncoimmunology* (2019) 8(7):1593806. doi: 10.1080/2162402X.2019.1593806
37. Wong PF, Wei W, Smithy JW, Acs B, Toki MI, Blenman KRM, et al. Multiplex Quantitative Analysis of Tumor-Infiltrating Lymphocytes and Immunotherapy Outcome in Metastatic Melanoma. *Clin Cancer Res* (2019) 25(8):2442–9. doi: 10.1158/1078-0432.CCR-18-2652
38. Robinson E, Kulkarni PM, Pradhan JS, Gartrell RD, Yang C, Rizk EM, et al. Prediction of distant melanoma recurrence from primary tumor digital H&E images using deep learning. *J Clin Oncol* (2019) 37(15_suppl):9577–7. doi: 10.1200/JCO.2019.37.15_suppl.9577
39. Wong PF, Wei W, Gupta S, Smithy JW, Zelterman D, Kluger HM, et al. Multiplex quantitative analysis of cancer-associated fibroblasts and immunotherapy outcome in metastatic melanoma. *J Immunother Cancer* (2019) 7(1):194. doi: 10.1186/s40425-019-0675-0
40. Gide TN, Silva IP, Quek C, Ahmed T, Menzies AM, Carlino MS, et al. Close proximity of immune and tumor cells underlies response to anti-PD-1 based therapies in metastatic melanoma patients. *Oncoimmunology* (2019) 9(1):1659093. doi: 10.1080/2162402X.2019.1659093
41. Baltzarsen PB, Georgsen JB, Nielsen PS, Steiniche T, Stougaard M. Detection of mRNA of Telomerase Protein in Benign Naevi and Melanomas Using RNAscope. *Appl Immunohistochem Mol Morphol* (2020) 28(1):36–41. doi: 10.1097/PAI.0000000000000690
42. Cabrita R, Lauss M, Sanna A, Donia M, Skaarup Larsen M, Mitra S, et al. Tertiary lymphoid structures improve immunotherapy and survival in melanoma. *Nature* (2020) 577(7791):561–5. doi: 10.1038/s41586-019-1914-8
43. Helmink BA, Reddy SM, Gao J, Zhang S, Basar R, Thakur R, et al. B cells and tertiary lymphoid structures promote immunotherapy response. *Nature* (2020) 577(7791):549–55. doi: 10.1038/s41586-019-1922-8
44. Bosisio FM, Antoranz A, van Herck Y, Bolognesi MM, Marcelis L, Chinello C, et al. Functional heterogeneity of lymphocytic patterns in primary melanoma dissected through single-cell multiplexing. *Elife* (2020) 9:e53008. doi: 10.7554/eLife.53008
45. Ianni JD, Soans RE, Sankarapandian S, Chamarthi RV, Ayyagari D, Olsen TG, et al. Tailored for Real-World: A Whole Slide Image Classification System Validated on Uncurated Multi-Site Data Emulating the Prospective Pathology Workload. *Sci Rep* (2020) 10(1):3217. doi: 10.1038/s41598-020-59985-2
46. Chou M, Illa-Bochaca I, Minxi B, Darvishian F, Johannet P, Moran U, et al. Optimization of an automated tumor-infiltrating lymphocyte algorithm for improved prognostication in primary melanoma. *Mod Pathol* (2021) 34(3):562–71. doi: 10.1038/s41379-020-00686-6
47. Kucharski D, Kleczek P, Jaworek-Korjakowska J, Dyduch G, Gorgon M. Semi-Supervised Nests of Melanocytes Segmentation Method Using Convolutional Autoencoders. *Sensors (Basel)* (2020) 20(6):1546. doi: 10.3390/s20061546
48. Figueiredo CR, Kalirai H, Sacco JJ, Azevedo RA, Duckworth A, Slupsky JR, et al. Loss of BAP1 expression is associated with an immunosuppressive microenvironment in uveal melanoma, with implications for immunotherapy development. *J Pathol* (2020) 250(4):420–39. doi: 10.1002/path.5384
49. Dikshit A, Zollinger A, Merritt C, Nguyen K, McKay-Fleisch J, Anderson C, et al. Molecularly guided highly multiplexed digital spatial analysis reveals differential gene expression profiles in the WNT-β-catenin pathway between

melanoma and prostate tumors. *Cancer Res* (2020) 80(16 Supplement):2707. doi: 10.1158/1538-7445.AM2020-2707
50. Klein S, Mauch C, Brinker K, Noh KW, Knez S, Büttner R, et al. Tumor infiltrating lymphocyte clusters are associated with response to immune checkpoint inhibition in BRAF V600E/K mutated malignant melanomas. *Sci Rep* (2021) 11(1):1834. doi: 10.1038/s41598-021-81330-4
51. Moore MR, Friesner ID, Rizk EM, Fullerton BT, Mondal M, Trager MH, et al. Automated digital TIL analysis (ADTA) adds prognostic value to standard assessment of depth and ulceration in primary melanoma. *Sci Rep* (2021) 11(1):2809. doi: 10.1038/s41598-021-82305-1
52. Martinez-Morilla S, Villarroel-Espindola F, Wong PF, Kluger H, Toki M, Aung TN, et al. (2020). Biomarker discovery in immunotherapy-treated melanoma patients with imaging mass cytometry [abstract], in: *Proceedings of the Annual Meeting of the American Association for Cancer Research 2020*, Philadelphia (PA): AACR, 2020 Apr 27-28 and Jun 22-24, Vol. 80. p. Abstract nr 2001, Cancer Res.
53. Elmore JG, Barnhill RL, Elder DE, Longton GM, Pepe MS, Reisch LM, et al. Pathologists' diagnosis of invasive melanoma and melanocytic proliferations: observer accuracy and reproducibility study. *BMJ* (2017) 357:j2813. doi: 10.1136/bmj.j2813
54. Farmer ER, Gonin R, Hanna MP. Discordance in the histopathologic diagnosis of melanoma and melanocytic nevi between expert pathologists. *Hum Pathol* (1996) 27(6):528–31. doi: 10.1016/s0046-8177(96)90157-4
55. Elder DE, Piepkorn MW, Barnhill RL, Longton GM, Nelson HD, Knezevich SR, et al. Pathologist characteristics associated with accuracy and reproducibility of melanocytic skin lesion interpretation. *J Am Acad Dermatol* (2018) 79(1):52–59.e5. doi: 10.1016/j.jaad.2018.02.070
56. Onega T, Barnhill RL, Piepkorn MW, Longton GM, Elder DE, Weinstock MA, et al. Accuracy of Digital Pathologic Analysis vs Traditional Microscopy in the Interpretation of Melanocytic Lesions. *JAMA Dermatol* (2018) 154 (10):1159–66. doi: 10.1001/jamadermatol.2018.2388
57. Kalra S, Tizhoosh HR, Shah S, Choi C, Damaskinos S, Safarpoor A, et al. Pan-cancer diagnostic consensus through searching archival histopathology images using artificial intelligence. *NPJ Digit Med* (2020) 3:31. doi: 10.1038/s41746-020-0238-2
58. Cireşan DC, Giusti A, Gambardella LM, Schmidhuber J. Mitosis detection in breast cancer histology images with deep neural networks. *Med Image Comput Comput Assist Interv* (2013) 16(Pt 2):411–8. doi: 10.1007/978-3-642-40763-5_51
59. Filosa A, Filosa G. Melanoma Diagnosis: The Importance of Histopathological Report. *Dermatopathol (Basel)* (2018) 5(1):41–3. doi: 10.1159/000486670
60. Larkin J, Chiarion-Sileni V, Gonzalez R, Grob JJ, Rutkowski P, Lao CD, et al. Five-Year Survival with Combined Nivolumab and Ipilimumab in Advanced Melanoma. *N Engl J Med* (2019) 381(16):1535–46. doi: 10.1056/NEJMoa1910836
61. Rotte A. Combination of CTLA-4 and PD-1 blockers for treatment of cancer. *J Exp Clin Cancer Res* (2019) 38(1):255. doi: 10.1186/s13046-019-1259-z
62. Daud AI, Wolchok JD, Robert C, Hwu WJ, Weber JS, Ribas A, et al. Programmed Death-Ligand 1 Expression and Response to the Anti-Programmed Death 1 Antibody Pembrolizumab in Melanoma. *J Clin Oncol* (2016) 34(34):4102–9. doi: 10.1200/JCO.2016.67.2477
63. Morrison C, Pabla S, Conroy JM, Nesline MK, Glenn ST, Dressman D, et al. Predicting response to checkpoint inhibitors in melanoma beyond PD-L1 and mutational burden. *J Immunother Cancer* (2018) 6(1):32. doi: 10.1186/s40425-018-0344-8
64. Hugo W, Zaretsky JM, Sun L, Song C, Moreno BH, Hu-Lieskovan S, et al. Genomic and Transcriptomic Features of Response to Anti-PD-1 Therapy in Metastatic Melanoma. *Cell* (2016) 165(1):35–44. doi: 10.1016/j.cell.2016.02.065
65. Auslander N, Zhang G, Lee JS, Frederick DT, Miao B, Moll T, et al. Robust prediction of response to immune checkpoint blockade therapy in metastatic melanoma. *Nat Med* (2018) 24(10):1545–9. doi: 10.1038/s41591-018-0157-9
66. HistoGeneX. *Histo Highlights* (2016). Available at: https://www.histogenex.com/images/PDFs/Histo-Highlights-July-2016-HistoGeneX-Newsletter.pdf (Accessed November 25, 2020).
67. Høiberg S. *Feature-based registration of sectional images. European patent specification EP2095332B1*. Munchen: Germany: European Patent Office (2009).
68. Visiopharm. *High-quality alignment of serial sections* (2020). Available at: https://visiopharm.com/visiopharm-digital-image-analysis-software-features/tissuealign/ (Accessed November 25, 2020).
69. Shakya R, Nguyen TH, Waterhouse N, Khanna R. Immune contexture analysis in immuno-oncology: applications and challenges of multiplex fluorescent immunohistochemistry. *Clin Transl Immunol* (2020) 9(10): e1183. doi: 10.1002/cti2.1183
70. Galon J, Costes A, Sanchez-Cabo F, Kirilovsky A, Mlecnik B, Lagorce-Pagès C, et al. Type, density, and location of immune cells within human colorectal tumors predict clinical outcome. *Science* (2006) 313(5795):1960–4. doi: 10.1126/science.1129139
71. Galon J, Mlecnik B, Bindea G, Angell HK, Berger A, Lagorce C, et al. Towards the introduction of the 'Immunoscore' in the classification of malignant tumours. *J Pathol* (2014) 232(2):199–209. doi: 10.1002/path.4287
72. Galon J, Fox BA, Bifulco CB, Masucci G, Rau T, Botti, et al. Immunoscore and Immunoprofiling in cancer: an update from the melanoma and immunotherapy bridge 2015. *J Transl Med* (2016) 14:273. doi: 10.1186/s12967-016-1029-z
73. Lu S, Stein JE, Rimm DL, Wang DW, Bell JM, Johnson DB, et al. Comparison of Biomarker Modalities for Predicting Response to PD-1/PD-L1 Checkpoint Blockade: A Systematic Review and Meta-analysis. *JAMA Oncol* (2019) 5(8):1195–204. doi: 10.1001/jamaoncol.2019.1549
74. Giladi A, Amit I. Immunology, one cell at a time. *Nature* (2017) 547 (7661):27–9. doi: 10.1038/547027a
75. Giesen C, Wang HA, Schapiro D, Zivanovic N, Jacobs A, Hattendorf B, et al. Highly multiplexed imaging of tumor tissues with subcellular resolution by mass cytometry. *Nat Methods* (2014) 11(4):417–22. doi: 10.1038/nmeth.2869
76. Angelo M, Bendall SC, Finck R, Hale MB, Hitzman C, Borowsky AD, et al. Multiplexed ion beam imaging of human breast tumors. *Nat Med* (2014) 20 (4):436–42. doi: 10.1038/nm.3488
77. Goltsev Y, Samusik N, Kennedy-Darling J, Bhate S, Hale M, Vazquez G, et al. Deep Profiling of Mouse Splenic Architecture with CODEX Multiplexed Imaging. *Cell* (2018) 174(4):968–981.e15. doi: 10.1016/j.cell.2018.07.010
78. Lin JR, Fallahi-Sichani M, Sorger PK. Highly multiplexed imaging of single cells using a high-throughput cyclic immunofluorescence method. *Nat Commun* (2015) 6:8390. doi: 10.1038/ncomms9390
79. Bolognesi MM, Manzoni M, Scalia CR, Zannella S, Bosisio FM, Faretta M, et al. G. Multiplex Staining by Sequential Immunostaining and Antibody Removal on Routine Tissue Sections. *J Histochem Cytochem* (2017) 65 (8):431–44. doi: 10.1369/0022155417719419
80. De Smet F, Antoranz Martinez A, Bosisio FM. Next-Generation Pathology by Multiplexed Immunohistochemistry. *Trends Biochem Sci* (2020) 20: S0968–0004(20)30245-0. doi: 10.1016/j.tibs.2020.09.009
81. Rodriques SG, Stickels RR, Goeva A, Martin CA, Murray E, Vanderburg CR, et al. Slide-seq: A scalable technology for measuring genome-wide expression at high spatial resolution. *Science* (2019) 363(6434):1463–7. doi: 10.1126/science.aaw1219
82. Wang F, Flanagan J, Su N, Wang LC, Bui S, Nielson A, et al. RNAscope: a novel in situ RNA analysis platform for formalin-fixed, paraffin-embedded tissues. *J Mol Diagn* (2012) 14(1):22–9. doi: 10.1016/j.jmoldx.2011.08.002
83. Nagendran M, Riordan DP, Harbury PB, Desai TJ. Automated cell-type classification in intact tissues by single-cell molecular profiling. *Elife* (2018) 7:e30510. doi: 10.7554/eLife.30510
84. Eng CL, Lawson M, Zhu Q, Dries R, Koulena N, Takei Y, et al. Transcriptome-scale super-resolved imaging in tissues by RNA seqFISH. *Nature* (2019) 568(7751):235–9. doi: 10.1038/s41586-019-1049-y
85. Zollinger DR, Lingle SE, Sorg K, Beechem JM, Merritt CR. GeoMx™ RNA Assay: High Multiplex, Digital, Spatial Analysis of RNA in FFPE Tissue. *Methods Mol Biol* (2020) 2148:331–45. doi: 10.1007/978-1-0716-0623-0_21
86. Lee JH, Daugharthy ER, Scheiman J, Kalhor R, Yang JL, Ferrante TC, et al. Highly multiplexed subcellular RNA sequencing in situ. *Science* (2014) 343 (6177):1360–3. doi: 10.1126/science.1250212

87. Bosisio F, Antoranz A, van Herck Y, Bolognesi M, Lynch S, Rahman A, et al. (2020). High Resolution Multiplexing of Melanoma Microenvironment in Responders/Non-Responders to Checkpoint Therapy, in: *MODERN PATHOLOGY: vol. 33(SUPPL 2), (457-458). Presented at the 109th Annual Meeting of the United-States-and-Canadian-Academy-of-Pathology (USCAP)*, Los Angeles, CA, 29 Feb 2020-05 Mar 2020.
88. Govek KW, Troisi EC, Miao Z, Woodhouse S, Camara PG. Single-Cell Transcriptomic Analysis of mIHC Images via Antigen Mapping. *bioRxiv* (2020), 672501. doi: 10.1101/672501
89. Stoeckius M, Hafemeister C, Stephenson W, Houck-Loomis B, Chattopadhyay PK, Swerdlow H, et al. Simultaneous epitope and transcriptome measurement in single cells. *Nat Methods* (2017) 14(9):865–8. doi: 10.1038/nmeth.4380
90. *GeoMx Digital Spatial Profiling | NanoString Technologies*. Available at: https://www.nanostring.com/products/geomx-digital-spatial-profiler/geomx-dsp, SITE.
91. Merritt CR, Ong GT, Church SE, Barker K, Danaher P, Geiss G, et al. Multiplex digital spatial profiling of proteins and RNA in fixed tissue. *Nat Biotechnol* (2020) 38(5):586–99. doi: 10.1038/s41587-020-0472-9
92. Amaria RN, Reddy SM, Tawbi HA, Davies MA, Ross MI, Glitza IC, et al. Neoadjuvant immune checkpoint blockade in high-risk resectable melanoma. *Nat Med* (2018) 24(11):1649–54. doi: 10.1038/s41591-018-0197-1
93. Blank CU, Rozeman EA, Fanchi LF, Sikorska K, van de Wiel B, Kvistborg P, et al. Neoadjuvant versus adjuvant ipilimumab plus nivolumab in macroscopic stage III melanoma. *Nat Med* (2018) 24(11):1655–61. doi: 10.1038/s41591-018-0198-0
94. Decalf J, Albert ML, Ziai J. New tools for pathology: a user's review of a highly multiplexed method for in situ analysis of protein and RNA expression in tissue. *J Pathol* (2019) 247(5):650–61. doi: 10.1002/path.5223
95. Dong F, Irshad H, Oh EY, Lerwill MF, Brachtel EF, Jones NC, et al. Computational pathology to discriminate benign from malignant intraductal proliferations of the breast. *PloS One* (2014) 9(12):e114885. doi: 10.1371/journal.pone.0114885
96. Abels E, Pantanowitz L, Aeffner F, Zarella MD, van der Laak J, Bui MM, et al. Computational pathology definitions, best practices, and recommendations for regulatory guidance: a white paper from the Digital Pathology Association. *J Pathol* (2019) 249(3):286–94. doi: 10.1002/path.5331
97. Pantanowitz L, Sinard JH, Henricks WH, Fatheree LA, Carter AB, Contis L, et al. Validating whole slide imaging for diagnostic purposes in pathology: guideline from the College of American Pathologists Pathology and Laboratory Quality Center. *Arch Pathol Lab Med* (2013) 137(12):1710–22. doi: 10.5858/arpa.2013-0093-CP
98. Esteva A, Topol E. Can skin cancer diagnosis be transformed by AI? *Lancet* (2019) 394(10211):1795. doi: 10.1016/S0140-6736(19)32726-6
99. Pantanowitz L, Sharma A, Carter AB, Kurc T, Sussman A, Saltz J. Twenty Years of Digital Pathology: An Overview of the Road Travelled, What is on the Horizon, and the Emergence of Vendor-Neutral Archives. *J Pathol Inform* (2018) Nov 219:40. doi: 10.4103/jpi.jpi_69_18
100. Evans AJ, Bauer TW, Bui MM, Cornish TC, Duncan H, Glassy EF, et al. US Food and Drug Administration Approval of Whole Slide Imaging for Primary Diagnosis: A Key Milestone Is Reached and New Questions Are Raised. *Arch Pathol Lab Med* (2018) 142(11):1383–7. doi: 10.5858/arpa.2017-0496-CP
101. Zarella MD, Bowman D, Aeffner F, Farahani N, Xthona A, Absar SF, et al. A Practical Guide to Whole Slide Imaging: A White Paper From the Digital Pathology Association. *Arch Pathol Lab Med* (2019) 143(2):222–34. doi: 10.5858/arpa.2018-0343-RA
102. Tizhoosh HR, Pantanowitz L. Artificial Intelligence and Digital Pathology: Challenges and Opportunities. *J Pathol Inform* (2018) 9:38. doi: 10.4103/jpi.jpi_53_18
103. Jouppi N, Young C, Patil N, Patterson D. Motivation for and Evaluation of the First Tensor Processing Unit. *IEEE Micro* (2018) 38(3):10–9. doi: 10.1109/MM.2018.032271057
104. Stathonikos N, Nguyen TQ, Spoto CP, Verdaasdonk MAM, van Diest PJ. Being fully digital: perspective of a Dutch academic pathology laboratory. *Histopathology* (2019) 75(5):621–35. doi: 10.1111/his.13953
105. *EUR-Lex - 32016R0679 - EN - EUR-Lex*. Available at: https://eur-lex.europa.eu/eli/reg/2016/679/oj.
106. *Art. 89 GDPR – Safeguards and derogations relating to processing for archiving purposes in the public interest, scientific or historical research purposes or statistical purposes | General Data Protection Regulation (GDPR)*. Available at: https://gdpr-info.eu/art-89-gdpr/.
107. Art. 5 GDPR – Principles relating to processing of personal data. In: . *General Data Protection Regulation (GDPR)*. Available at: https://gdpr-info.eu/art-5-gdpr/.
108. Art. 6 GDPR – Lawfulness of processing. In: . *General Data Protection Regulation (GDPR)*. Available at: https://gdpr-info.eu/art-6-gdpr/.
109. Art. 40 GDPR – Codes of conduct. In: . *General Data Protection Regulation (GDPR)*. Available at: https://gdpr-info.eu/art-40-gdpr/.
110. Art. 45 GDPR – Transfers on the basis of an adequacy decision. In: . *General Data Protection Regulation (GDPR)*. Available at: https://gdpr-info.eu/art-45-gdpr/.

Conflict of Interest: The authors declare that the research was conducted in the absence of any commercial or financial relationships that could be construed as a potential conflict of interest.

frontiers in Oncology

ORIGINAL RESEARCH
published: 01 April 2021
doi: 10.3389/fonc.2021.593587

A Nomogram Combining a Four-Gene Biomarker and Clinical Factors for Predicting Survival of Melanoma

*Chuan Zhang[1], Dan Dang[2], Yuqian Wang[3] and Xianling Cong[4]**

[1] Department of Pediatric Surgery, The First Hospital of Jilin University, Changchun, China, [2] Department of Neonatology, The First Hospital of Jilin University, Changchun, China, [3] Scientific Research Center, China-Japan Union Hospital of Jilin University, Changchun, China, [4] Department of Dermatology, China-Japan Union Hospital of Jilin University, Changchun, China

Background: Currently there is no effective prognostic indicator for melanoma, the deadliest skin cancer. Thus, we aimed to develop and validate a nomogram predictive model for predicting survival of melanoma.

Methods: Four hundred forty-nine melanoma cases with RNA sequencing (RNA-seq) data from TCGA were randomly divided into the training set I (n = 224) and validation set I (n = 225), 210 melanoma cases with RNA-seq data from Lund cohort of Lund University (available in GSE65904) were used as an external test set. The prognostic gene biomarker was developed and validated based on the above three sets. The developed gene biomarker combined with clinical characteristics was used as variables to develop and validate a nomogram predictive model based on 379 patients with complete clinical data from TCGA (Among 470 cases, 91 cases with missing clinical data were excluded from the study), which were randomly divided into the training set II (n = 189) and validation set II (n = 190). Area under the curve (AUC), concordance index (C-index), calibration curve, and Kaplan-Meier estimate were used to assess predictive performance of the nomogram model.

Results: Four genes, i.e., *CLEC7A*, *CLEC10A*, *HAPLN3*, and *HCP5* comprise an immune-related prognostic biomarker. The predictive performance of the biomarker was validated using tROC and log-rank test in the training set I (n = 224, 5-year AUC of 0.683), validation set I (n = 225, 5-year AUC of 0.644), and test set I (n = 210, 5-year AUC of 0.645). The biomarker was also significantly associated with improved survival in the training set ($P < 0.01$), validation set ($P < 0.05$), and test set ($P < 0.001$), respectively. In addition, a nomogram combing the four-gene biomarker and six clinical factors for predicting survival in melanoma was developed in the training set II (n = 189), and validated in the validation set II (n = 190), with a concordance index of 0.736 ± 0.041 and an AUC of 0.832 ± 0.071.

OPEN ACCESS

Edited by:
Igor Puzanov,
University at Buffalo, United States

Reviewed by:
Ashley M. Holder,
University of Alabama at Birmingham, United States
Robert Laird Judson-Torres,
The University of Utah, United States

****Correspondence:***
Xianling Cong
congxl@jlu.edu.cn

Specialty section:
This article was submitted to Skin Cancer, a section of the journal Frontiers in Oncology

Received: *11 August 2020*
Accepted: *09 March 2021*
Published: *01 April 2021*

Citation:
Zhang C, Dang D, Wang Y and Cong X (2021) A Nomogram Combining a Four-Gene Biomarker and Clinical Factors for Predicting Survival of Melanoma. Front. Oncol. 11:593587. doi: 10.3389/fonc.2021.593587

Conclusion: We developed and validated a nomogram predictive model combining a four-gene biomarker and six clinical factors for melanoma patients, which could facilitate risk stratification and treatment planning.

Keywords: prognostic biomarker, nomogram, microenvironment, melanoma, immune genes

INTRODUCTION

Cutaneous melanoma is the deadliest type of skin cancer (1, 2), and its morbidity has been on the rise annually, especially in the Caucasian population (3, 4). As melanoma is generally recognized as a highly heterogeneous cancer (5) and immunotherapy remains the preferred treatment for advanced melanoma (6), immune-related biomarkers have been exploited as prognostic signatures of melanoma (7–10). However, the current existing immune-related prognostic biomarkers have their limitations. For instance, some biomarkers contain a relatively large number of genes that reduces their potential applicability to some extent (7, 8), while for others, there is a lack of detailed information regarding the potential mechanism and clinical relevance (8, 9). Therefore, the identification of a comparatively reliable and applicable prognostic biomarker for melanoma in order to guide clinical decision-making is essential.

Considering the advancements in gene sequencing technology, a set of gene databases, such as The Cancer Genome Atlas (TCGA) (11, 12) and Gene Expression Omnibus (GEO) have emerged as popular guide sources. A series of bioinformatics tools, including weighted gene co-expression network analysis (WGCNA) (13), cell-type identification by estimating relative subsets of RNA transcripts (CYBERSORT) (14), gene set enrichment analysis (GSEA) (15, 16), and least absolute shrinkage and selection operator (LASSO), have been used to process such big data. The strategy of using a combination of these databases and bioinformatics tools in scientific practice is supported by the reliability of such approaches (17–21).

To identify an immune-related prognostic biomarker and develop a new nomogram predictive model for melanoma patients, we analyzed the RNA sequencing (RNAseq) data and the corresponding clinical data from TCGA and GEO databases using bioinformatic tools. The findings would show useful prognostic factors and a nomogram for predicting survival in melanoma patients. Researchers, clinicians, and patients would handily forecast the survival probability for each individual patient using this nomogram.

MATERIALS AND METHODS

Data Acquisition

Four hundred seventy-two melanoma cases with RNA sequencing data were download from TCGA, and 449 of them with complete survival data were randomly divided into the training set I (n = 224) and validation set I (n = 225) (**Table S1**). Two hundred fourteen melanoma cases with RNA sequencing data and survival data were obtained from Lund cohort of Lund University (available in GSE65904) (22, 23) and 210 of them with complete survival data were utilized as an external test set (**Table S1**). The above three sets were used to identify and validate a prognostic gene biomarker.

Four hundred seventy melanoma cases with clinical data were obtained from TCGA and 91 cases with missing clinical data were excluded from the study. Of them, 379 met our inclusion criterion that they do not contain any missing data for selected variables including age, gender, overall survival time, survival status, and clinical stage. The 379 cases were subsequently randomly assigned to the training set II (n = 189) and validation set II (n = 190) (**Table S2**), which were used to develop and validate a nomogram predictive model. In developing the nomogram, the four-gene biomarker and clinical characteristics were used as variables.

Immune, stromal, and estimate scores of each patient were available from the ESTIMATE database (**Table S2**) (24). A total of 5,559 human immune genes were downloaded from the InnateDB database (**Table S2**) (25).

WGCNA

WGCNA, a reliable and approved bioinformatics method, was employed to identify immune-related modules. We first removed outlier genes and genes expressed at extremely low levels from the data. Construction of a weighted gene network involves the choice of the soft thresholding power β to which co-expression similarity is raised to calculate adjacency. Based on the criterion of approximate scale-free topology, we chose 14 as the soft threshold. Using the soft threshold, we calculated the adjacency (co-expression similarity) and generated a hierarchical clustering tree. The dynamic tree cut could enable the identification of modules with very similar expression profiles. The modules with highly co-expressed genes were merged. Finally, we correlated modules with external traits (herein i.e. immune score) and identified the most relevant module.

Database for Annotation, Visualization, and Integrated Discovery (DAVID) Online Tool

DAVID (version 6.8) (26) is an online bioinformatics tool that provides a comprehensive set of functional annotation tools for interpreting the biological meaning underlying specific gene sets. Herein, DAVID was used to perform the Kyoto Encyclopedia of Genes and Genomes (KEGG) pathway and Gene Ontology (GO) analysis based on the genes from the most relevant module identified using WGCNA. GO analysis can provide information on functions of genes. KEGG pathway analysis can suggest the

possible involved signaling pathways of a gene set. The brief operation process is as follows. Briefly, the symbols of the genes to be analyzed were uploaded onto the website, and *Homo sapiens* is selected as the species. Next, GO-BP-DIRECT, GO-CC-DIRECT, GO-MF-DIRECT, and KEGG PATHWAY were selected to perform functional annotation. All other parameters were set as default.

Identification and Validation of the Immune-Gene Biomarker

Overlapping genes from the most relevant module from WGCNA, immune genes from the IRIS database, and genes from GSE65904, were then analyzed using the univariate Cox regression analysis and least absolute shrinkage and selection operator (LASSO) regression analysis based on the training set I. The genes obtained from the above analysis were used for developing a prognostic immune-gene biomarker using the multivariate Cox regression analysis based on the training set I.

The prognostic signature can be quantified by calculating risk scores using multivariate Cox regression model. The predictive performance of the immune gene biomarker was assessed using area under the curve (AUC), calibration curve, Kaplan-Meier estimate in the training set I, validation set I, and test set, respectively.

Differentially Expressed Tumor-Infiltrating Immune Cell (TIICs) Analysis

TIICs between different groups were compared based on their abundance in each melanoma sample, which was calculated using CYBERSORT (**Table S2**). CYBERSORT is an *in silico* algorithm that enables the precise estimation of immune cell fractions based on RNAseq profiles of bulk samples (14). The accuracy of CYBERSORT has been demonstrated by immunohistochemistry and flow cytometry. Statistical parameters used include: p-value (t-test) and $\log_2$ fold change (logFC).

GSEA

GSEA was performed using the GSEA software (version 3.0) to detect any differences in the KEGG pathways between the low-risk and high-risk groups. The operating parameters were set as follows: the number of permutations at 1,000, weighted enrichment statistic, metric for ranking genes (Signal2Noise), max size (500), and min size (15).

Nomogram Development and Validation

To investigate the prognostic significance of the immune-gene biomarker in combination with common clinical characteristics, we planned to develop a predictive nomogram combining the immune-gene biomarker and clinical factors for melanoma patients. First, univariate Cox regression was used to screen for clinical characteristics that were significantly correlated with overall survival in the training set II. Second, clinical characteristics with a P value less than 0.05 were used to developed a nomogram using multivariate Cox regression model.

To validate the proposed nomogram, four criteria were utilized to assess prediction performance in the validation set II. First, the cases were grouped according to their predicted risk score, and Kaplan-Meier survival curves and log rank test were used to compare survival differences among the groups. Second, a concordance index (C-index) was calculated to estimate the similarity between the ranking of true survival time and of predicted risk score. The theoretical value of the C-index is between 0 and 1; a C-index larger than 0.5 indicates prediction performance better than random guessing. Third, integrated AUC was calculated. Fourth, calibration curves were plotted to evaluate the consistency between predicted survival probability and actual survival proportion at 4 years. A perfect prediction would result in a 45-degree calibration curve (i.e. the identity line).

Statistical Analyses

All statistical analysis was performed in the R Studio software (version 3.6.1). R packages "WGCNA" (13), "Vennerable" (27), "glmnet" (28, 29), "ggplot2" (30), "survival" (31), "survminer" (32), "survivalROC" (33), "rms" (34), "pROC" (35), "forestplot" (36) were used. Continuous values between the two groups were analyzed using t-tests. Non-parametric comparison between the two groups was performed using the Wilcoxon test. $P < 0.05$ was considered statistically significant.

RESULTS

Study Protocol

The schematic diagram of the study protocol is shown in **Figure 1**.

Identification and Validation of the Immune-Related Module

To identify the immune-related module, the melanoma RNAseq data and the corresponding immune scores for each patient were analyzed using WGCNA. Module Black comprising 809 genes was identified as the strongest immune-related module. From 53,898 genes, we filtered out the outlier genes and genes expressed at extremely low levels to obtain 21,194 candidates for WGCNA. The soft threshold was determined as 14 (**Figures 2A, B**). All the genes were classified into 27 modules. After merging the highly co-expressed modules, 23 modules were eventually obtained (**Figure 2C**). Among them, Module Black was the strongest immune-related module (P = 3e-155, R = 0.89). Intriguingly, Module Black was also significantly associated with stromal and estimate scores in melanoma (**Figure 2D**).

To verify whether the selected module correlated with immunity, 809 genes in Module Black were analyzed using DAVID. As shown in **Figures 2 (E, F)**, the top five relevant pathways in both GO analysis and KEGG pathway were found to be immune-related.

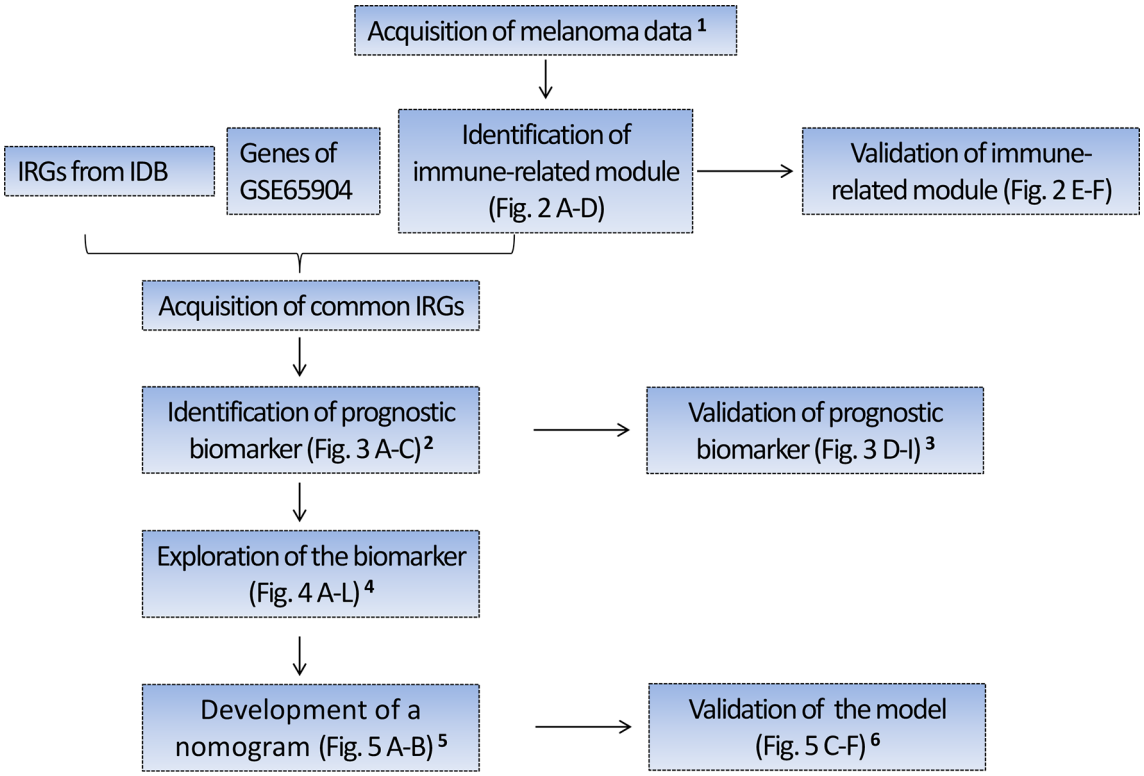

FIGURE 1 | Flow chart depicting the protocol. [1] Four hundred forty-nine melanoma cases with RNA sequencing (RNA-seq) data from TCGA were randomly divided into the training set I (n = 224) and validation set I (n = 225), 210 melanoma cases with RNA-seq data from Lund cohort of Lund University (available in GSE65904) were used as an external test set. The above three sets were used to identify and validate a prognostic gene biomarker. [2] Based on the training set I, we identified a four-gene biomarker from 56 IRGs using the univariate Cox regression analysis and LASSO regression analysis. [3] The predictive performance of the four-gene biomarker was validated in the training set I, validation set I, and an external test set (GSE65904). [4] Exploration of the biomarker includes the association of the four-gene biomarker with the patient's survival, immune score, clinical stage, tissue pathological type, tumor-infiltrating immune cells, and KEGG pathway. [5] Four hundred seventy melanoma cases with clinical data were obtained from TCGA and 91 cases with missing clinical data were excluded from the study. Three hundred seventy-nine cases with complete clinical data were subsequently randomly assigned to the training group II (n = 189) and validation group II (n = 190), which were used to develop and validate the nomogram predictive model. In developing the nomogram, the four-gene biomarker and clinical characteristics were used as variables. [6] The predictive power of nomogram combining the four-gene biomarker and clinical characteristics was assessed in the training set II and validation set II. IRGs, immune-related genes; IDB, the InnateDB database.

Identification and Validation of Prognostic Immune-Gene Biomarker

To select the qualified immune genes for developing an immune-gene biomarker, 56 overlapping genes were obtained by intersecting the 809 genes from Module Black (**Table S2**), 5,559 immune genes from the IRIS database, and 2,786 genes from GSE65904 (**Table S1**). First, we randomly divided 449 melanoma patients with RNA sequencing data and complete survival data from TCGA cohort into the training set I (n = 224) and validation set I (n = 225) (**Table S1**). The selected 56 genes were analyzed as variables using the univariate Cox regression analysis based on the training set I. Twelve genes with a *P* value less than 0.05 (*HLA-DQB1*, *CCR5*, *LCP2*, *CLEC7A*, *IGSF6*, *CLEC10A*, *HAPLN3*, *CEACAM4*, *IL4I1*, *LILRB1*, *FCGR1A*, and *HCP5*) were selected in the univariate Cox regression model (**Figure 3A**).

Then, the 12 genes were further screened using LASSO regression model, and four gene of *CLEC7A*, *CLEC10A*, *HAPLN3*, and *HCP5* were eventually selected to develop a four-gene biomarker using the multivariate Cox regression model (**Figures 3B, C**; detailed computational process is available in **Table S3**).

The proposed four-gene biomarker was validated in the validation set I (n = 225) and an independent testing set (GSE65904, n = 210). The 5-year AUC of the four-gene biomarker was 0.683, 0.644 and 0.645 in the training set, validation set and external test set, respectively (**Figures 3D–F**). Next, we calculated risk score of each patient using the multivariate Cox regression model based on the four-gene biomarker. The survival difference between two groups, which were grouped by the median predicted risk score, was significant (*P* value < 0.05; **Figures 3G–I**).

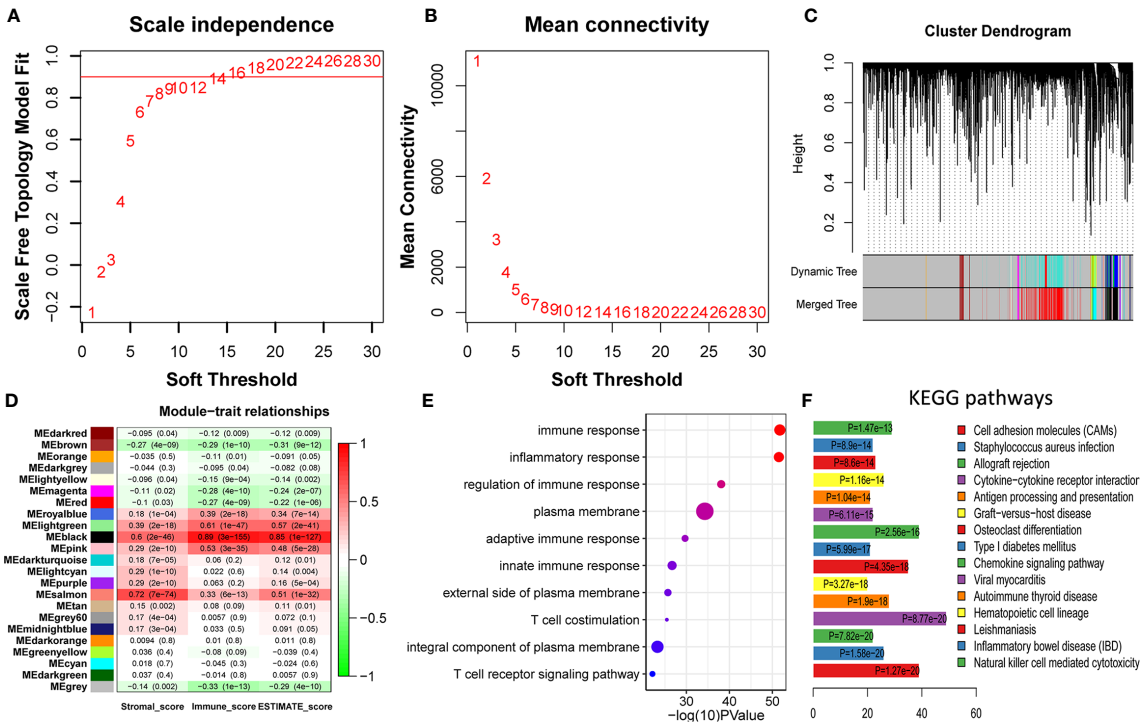

FIGURE 2 | Identification and validation of immune-related modules **(A, B)** Analysis of network topology for various soft-thresholding powers. **(A)** This panel shows the scale-free fit index as a function of the soft-thresholding power. **(B)** This panel displays the mean connectivity as a function of the soft-thresholding power. **(C)** Clustering dendrogram of genes, with dissimilarity based on topological overlap, together with assigned merged module colors and the original module colors. Each color represents a module. **(D)** Module-trait association. Each row represents a module, and each column represents a trait. Each cell contains the corresponding correlation and *P* value. Module Black (MEblack) is the most immune score-related (*P* = 3e-155, *R* = 0.89). **(E)** The top 10 categories are all immune-related in GO enrichment analysis based on genes in Module Black, supporting genes in Module Black are indeed immune-related. **(F)** Most of the top 15 KEGG pathways are also immune-related, underscoring genes of Module Black are related to immunity.

Relationship of Four-Gene Biomarker With Clinical Factors

Since the identified four-gene biomarker manifested prognostic relevance in patients with melanoma, we wondered if four-gene biomarker was significantly correlated with other clinical factors in melanoma. We found that risk score was negatively associated with immune score in melanoma ($P < 0.05$), indicating that the low-risk score was potentially attributed to activated immune function (**Figure 4A**). In addition, we analyzed the relationship between risk score and clinical stages, revealing that there was a significant difference in the risk score between stage I and stage II, as well as between stage II and stage III (**Figure 4B**). The four genes of *CLEC7A*, *CLEC10A*, *HAPLN3*, and *HCP5* were analyzed using log-rank tests with TCGA data, and they all showed significant survival significance ($P < 0.05$; **Figures 4E–H**), implying their protective effects on melanoma.

To explore the association between risk score and TIICs, we divided the TCGA cohort into the low-risk and high-risk groups based on the median risk score and conducted a differentially expressed TIIC analysis between these groups based on the TIIC abundance in each sample. TIIC abundance in each tissue was calculated using CYBERSORT, and the results are shown in **Supplementary Table S3**. The findings revealed that M1 macrophage, $CD4^+$ T cells, $CD8^+$ T cells, and natural killer (NK) cells were the top four upregulated TIICs in the low-risk group (**Figure 4C**), further underscoring activated immune function in this group.

Consistent with the above findings, GSEA also revealed that the top four KEGG pathways in the low-risk group were all immune-related [cytokine-cytokine receptor interaction; cell adhesion molecules (CAMs); systemic lupus erythematosus; the intestinal immune network for IgA production], while the top four pathways in the high-risk group were not immune-related (**Figures 4D, I–L**; **Table S4**).

Development and Validation of a Nomogram

Considering the prognostic significance of the four-gene biomarker, we sought to combine it with nine common clinical factors to better predict survival of melanoma patients. We first conducted a univariate Cox regression analysis to examine the prognostic significance of the four-gene biomarker and nine clinical factors, including age, gender, clinical stage, breshlow depth, clark level, tissue sample type (primary or metastatic melanoma), cancer status (with tumor or tumor-free), immune score, and new tumor event, based on the training set II. Personal

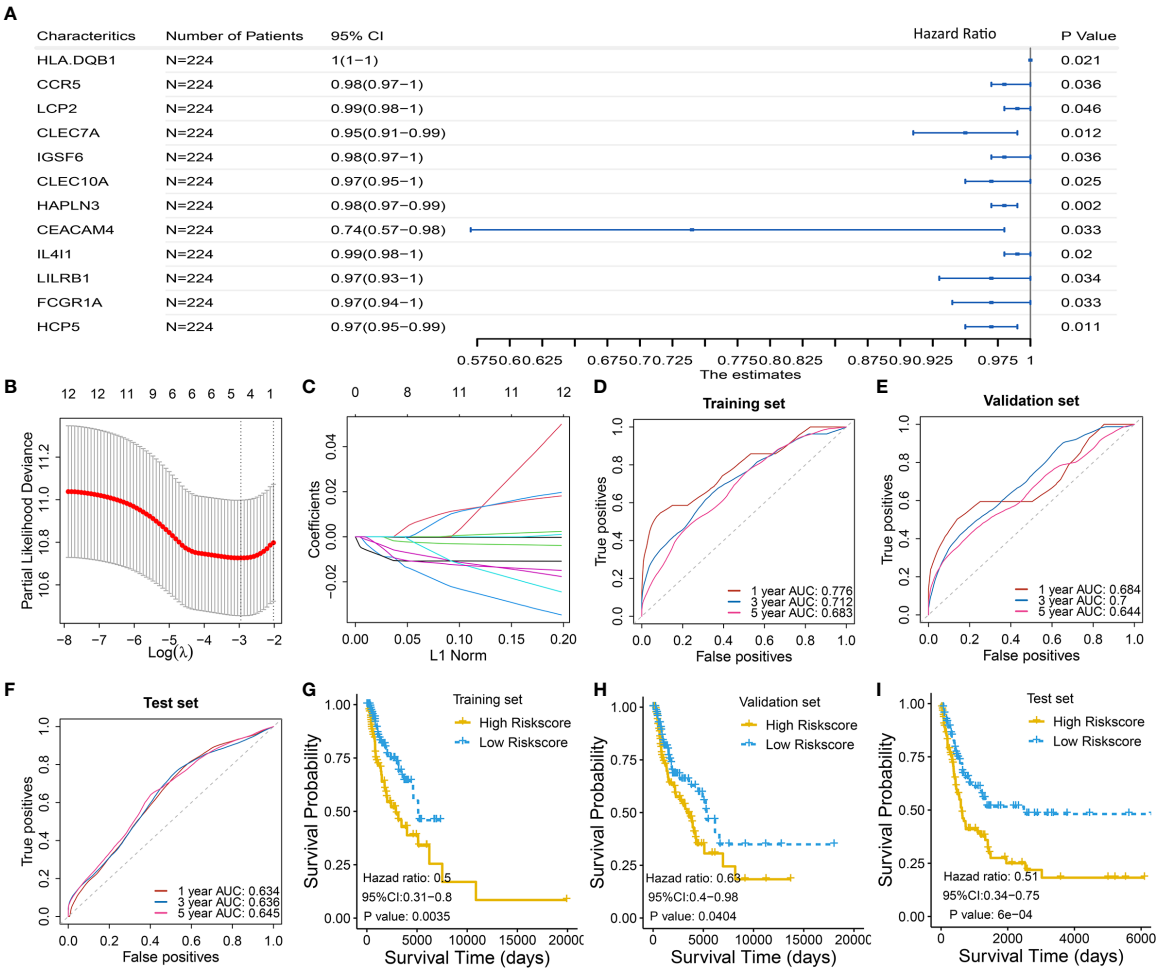

FIGURE 3 | Identification and validation of four-gene biomarker **(A)** Univariate Cox regression were used to screen for genes that were significantly correlated with overall survival in the training set I (n = 224). Twelve genes with *P* value less than 0.05 were significantly associated with overall survival, as shown in the forest plot. **(B–C)** LASSO regression was used to further eliminate redundant genes. The resulting four genes of *CLEC7A*, *CLEC10A*, *HAPLN3*, and *HCP5* were used to develop a four-gene biomarker based on multivariate Cox regression model. **(B)** Tuning parameter (λ) selection in the LASSO model used 10-fold cross-validation *via* minimum criteria. AUC was plotted *versus* log(λ). **(C)** Coefficient profiles of the fractions of 12 immune-related genes. **(D–F)** One-, 3-, and 5-year AUC were calculated for the prognostic four-gene biomarker, showing good predictive performance in the training set I, validation set I, and test set. **(G–I)** Risk scores of melanoma cases were calculated according to multivariate Cox regression model of the four genes, and grouped into low-risk and high-risk group using median risk score as threshold. Low-risk group has a significant longer survival compared to high-risk group, in the training set I, validation set I, and test set.

cancer status (with tumor/tumor-free) is one of the clinical characteristics for melanoma cases from the TCGA cohort (**Figure 5A**). Herein, we defined the personal cancer status of the tumor as cancer status. The results showed that seven factors could be used as effective prognostic characteristics for melanoma, including four-gene biomarker, immune score, age, clinical stage, cancer status, breslow depth, and clark level. Thus, the seven factors were used to developed a nomogram prognostic model based on the training set II (n = 189) (**Figure 5B**).

The proposed nomogram was assessed in the validation set II (n = 190), with a C-index of 0.736 ± 0.041 and an AUC of 0.832 ± 0.071 (**Figure 5C**). A calibration curve at 4 year (**Figure 5D**) also showed high consistency between predicted survival probability and actual survival proportion. The survival difference between two groups, which were grouped by the median predicted risk score, was significant ($P < 0.05$; **Figures 5E, F**). The predicted risk score was calculated by adding up the score of each item using the nomogram depicted in **Figure 5B**.

DISCUSSION

We developed and validated a four-gene biomarker and a nomogram prognostic model combining a four-gene biomarker and six clinical factors for melanoma patients. The four genes (*CLEC7A*, *CLEC10A*, *HAPLN3*, and *HCP5*) were also identified as meaningful anti-tumoral genes in melanoma. Among these, *CLEC7A*, *CLEC10A*, and *HAPLN3* have not yet

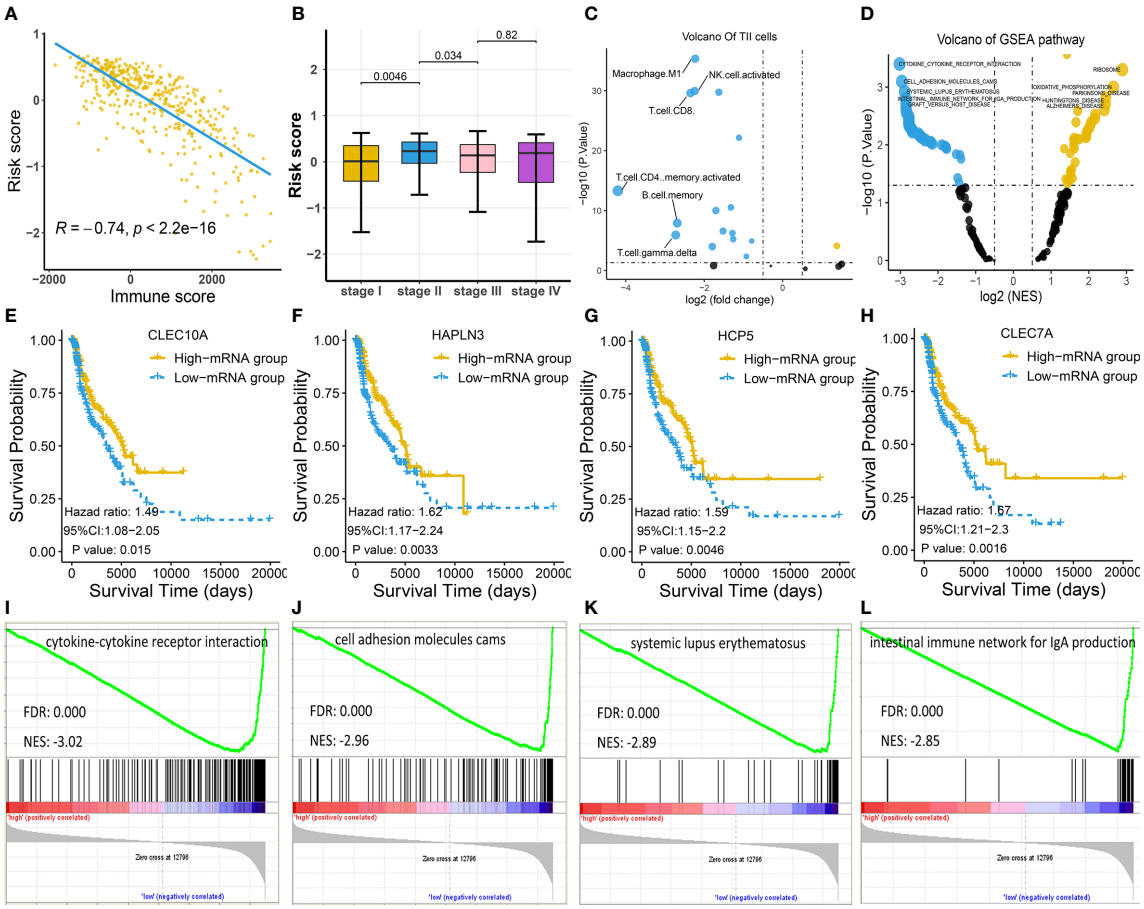

FIGURE 4 | Exploration of the four-gene biomarker **(A–C)** Risk scores of melanoma patients from TCGA cohort were calculated according to the four-gene biomarker, and the association of risk scores with common clinical characteristics were investigated. **(A)** Risk score was negatively correlated with immune score, consistent with low-risk patients who had a prolonged survival in melanoma. **(B)** There was a marked difference in risk score between stage I and stage II, as well as between stage II and stage III, implying qualitative change occurred after stage II. **(C)** The numbers of M1 macrophage, NK, $CD4^+$, and $CD8^+$ T cells were critically elevated in the low-risk group (the blue dot indicates TIICs whose counts are increased in the low-risk group, while the yellow dot indicates TIICs whose counts are increased in the high-risk group). **(D)** KEGG pathway analysis by GSEA displayed significantly differentially enriched pathways between the low-risk and high-risk groups. Each blue dot represents a significantly enriched pathway in the low-risk group, while yellow dot represents that in the high-risk group. **(E–H)** Four genes, *CLEC7A*, *CLEC10A*, *HAPLN3*, and *HCP5*, had a significant relevance with respect to survival; this is indicative of their anti-tumoral roles in melanoma. **(I–L)** The top four pathways in the low-risk group were all immune-related, indicating more active immune function in low-risk group compared to in the high-risk group.

been reported to be correlated with melanoma before. Furthermore, we revealed that the counts of several TIILs (M1 macrophage, NK cells, CD4+ T cells, and CD8+ T cells) were significantly elevated in the low-risk populations. In addition, the number of activated immune pathways was higher in the low-risk populations than that in the high-risk counterparts, which could provide insights for future studies. All these findings may contribute to the development of novel strategies for melanoma treatment and may provide an opportunity to perform in-depth research into the immune underpinning of melanoma.

One of the main findings of this study is the optimized immune-related prognostic biomarker comprising four immune genes (*CLEC7A*, *CLEC10A*, *HAPLN3*, and *HCP5*). The existing prognostic biomarkers usually contained at least 10 genes (37–41), a feature that would substantially reduce their clinical applicability. In contrast, the prognostic immune-related biomarker identified herein comprises only four genes, and is therefore more convenient for clinical application. Meanwhile, the established model herein had been validated in three subsets, i.e., training, validation, and external tests, further supporting its extensive applicability.

Three genes, i.e., *CLEC7A*, *CLEC10A*, and *HAPLN3* have been reported to exhibit prognostic significance with respect to melanoma for the first time, while *HCP5* has been reported to inhibit the development of cutaneous melanoma (42). *CLEC7A* (also known as dectin-1) encodes for a pattern-recognition receptor expressed by myeloid phagocytes (macrophages, dendritic cells, and neutrophils) that can directly drive the antimicrobial activity (43, 44). Although *ClEC7A* activation on macrophages has been reported to induce the development of pancreatic cancer and peri-tumoral immune tolerance (45), there is no evidence regarding the relationship between *CLEC7A* and

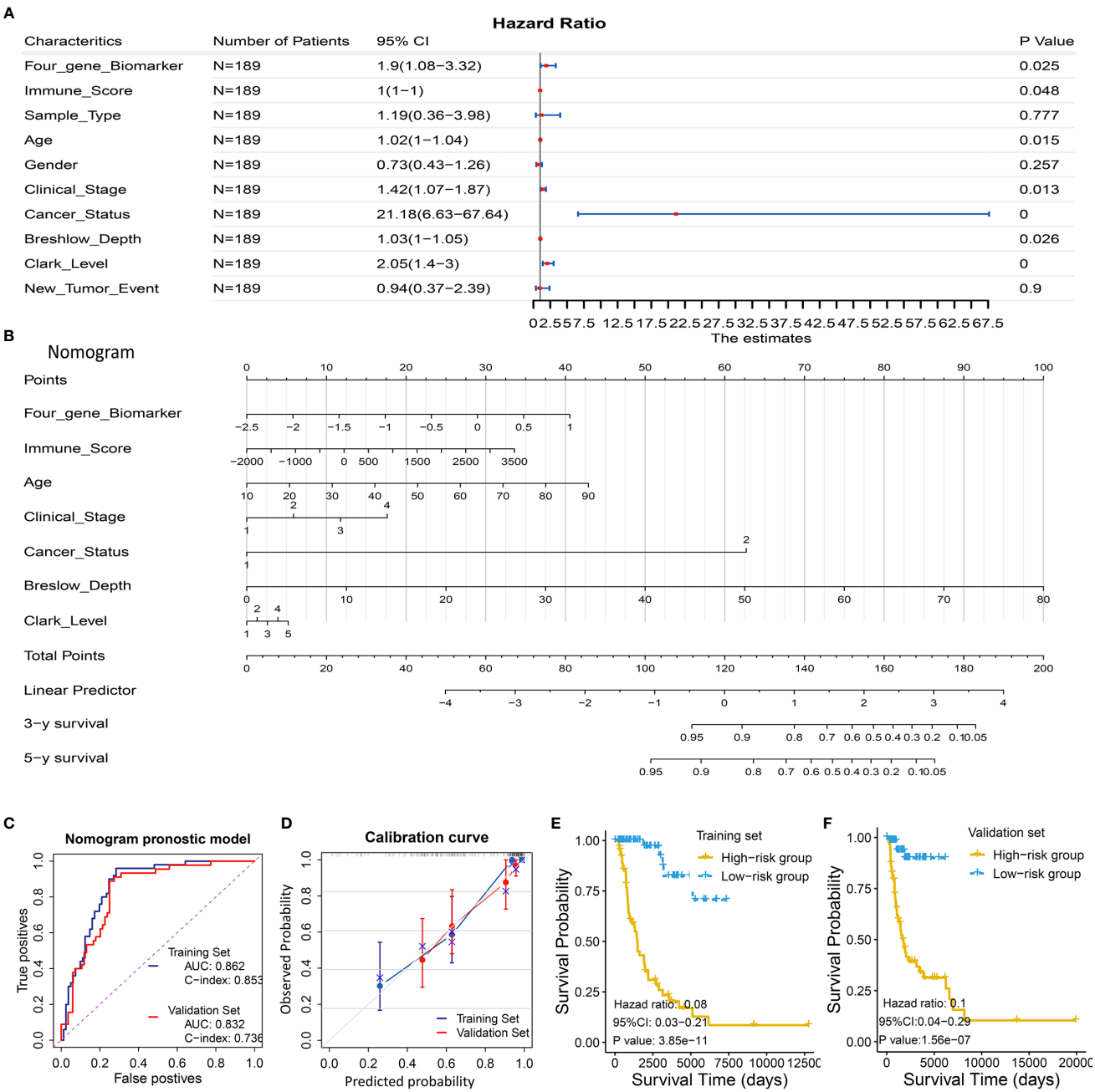

FIGURE 5 | Development and validation of a predictive nomogram for predicting survival probability. **(A, B)** Development of a predictive nomogram combing the four-gene biomarker and clinical factors in melanoma based on the training set II. **(A)** Univariate Cox regression were used to screen for clinical factors that were significantly correlated with overall survival in the training set II (n = 189), as shown in the forest plot. Seven factors including the four-gene biomarker were significantly associated with overall survival. **(B)** A nomogram combing the four-gene biomarker and clinical factors for predicting 3- and 5-year overall survival for melanoma patients. Cancer status represents personal cancer status (with tumor/tumor-free), which is one of the clinical characteristics for melanoma patients. **(C–F)** Four criteria were utilized to assess the predictive performance in the training set II and validation set II. **(C)** AUC and C-index were calculated for the nomogram prognostic models in the training set (n = 189) and validation set (n = 190). AUC of the nomogram was 0.862 ± 0.062 and 0.832 ± 0.071, and C-index was 0.853 ± 0.024 and 0.736 ± 0.041, in the training group and validation group, respectively. **(D)** Calibration curves of nomograms in training set and validation set. X-axis represents predicted probability and Y-axis represents true probability. Each point in the plot represents a subgroup of patients. Error bars represent 95% confidence intervals. 45° represents perfect prediction, and the actual performances of our nomogram are very well. **(E, F)** The resulting nomogram prognostic model was utilized to calculate risk score of cases in the training set and validation set. Low risk score subgroup had a significantly improved survival compared to high risk score (grouped according to median risk score value), in training set and validation set. The findings support the predictive power of the proposed nomogram.

melanoma. We revealed that elevated expression of *CLEC7A* could result in enhanced anti-tumoral immunity and may be correlated with prolonged survival in melanoma. *CLEC7A* could function *via* NK cells and M1 macrophages to suppress metastasis (46), consistent with the increase in the population of NK cells and M1 macrophages in the low-risk group in our study. However, the precise underlying mechanism remains largely unknown. *CLEC10A* was reported to play an important role in immune cell maturation and *CLEC10A* expression is known to correlate with improved survival in breast and ovarian cancers (47–49). Furthermore, *CLEC10A* could suppress HDM-induced Toll-like receptor 4 (TLR4)-mediated inflammatory cytokine production in mice to maintain homeostasis against inflammation. Our results demonstrate that high *CLEC10A* expression was associated with improved melanoma survival and immune scores, indicating its potential role in anti-tumoral immunity. Meanwhile, over-modulated expression of *HAPLN3* was suggested to relate with the initiation of breast cancer (50); however, its function in melanoma is presently unclear. The role of the long non-coding RNA (lncRNA) *HCP5* in cancer remains controversial. Some reports suggest that *HCP5* could induce tumor progression in cases of follicular thyroid carcinoma and lung adenocarcinoma (51–53), while others claim that *HCP5* may suppress the development of cutaneous melanoma by modulating *RARRES3* expression by sponging miR-12 (42). Consistent with previous studies, we observed an association between upregulated *HCP5* expression and improved survival in melanoma and that *HCP5* might boost the anti-tumoral immunity. Nevertheless, further *in vitro* and *in vivo* investigations are warranted to study the role of these four pivotal genes in melanoma and their precise mechanisms of action.

Our study demonstrates that the risk score was significantly associated with the immune score and tumor-infiltrating immune cell abundance, thereby supporting the importance of immune function in melanoma. M1 macrophages are associated with improved prognostic outcomes in melanoma (54–57). NK cells were confirmed to induce macrophage polarization toward the M1 phenotype and suppress tumor growth (58). Similarly, we observed higher immune scores and high abundance of M1 macrophage, CD4+, CD8+, and NK cells in the low-risk population. Further, we revealed the proportion of melanoma-infiltrating immune cells and their association with melanoma prognosis.

Another important finding is the activation of several immune pathways in the low-risk group and its correlation with prolonged survival in melanoma. Cytokine-cytokine receptor interaction pathway was the most significant in the low-risk group; this pathway plays an important role in recovery after infection with the respiratory syncytial virus as well as in colorectal cancer, renal cell carcinoma, and esophageal cancer (59–62).

This study has important implications for the treatment as well as prognosis of melanoma. First, our study provides a new prognostic biomarker and a new nomogram that could aid clinical treatment strategies for melanoma. Second, we revealed several critical immune genes, cells, and pathways that could serve as promising therapeutic targets in melanoma.

This study has a few limitations that warrant further research. First, as the four immune genes exhibit critical significance in melanoma prognoses, further *in vitro* and *in vivo* studies are required to explore their physiological mechanisms of actions. In addition, M1 macrophage, NK, $CD8^+$, and $CD4^+$ T cells are indicated to benefit the survival of melanoma patients, warranting further investigation regarding the precise underlying mechanism. Third, the performance of the four-gene biomarker and similar prediction models was not statistically compared. To clarify this, we searched the PubMed database and observed that the prognostic power of the established model is still acceptable and stable as compared with that of previously established models. The 5-year AUC values of tROC for the present biomarker in training, validation, and testing sets were 0.683, 0.644, and 0.645, respectively, while those of the other models were 0.723, 0.560, and 0.682 (63); 0.648, 0.544, and 0.755 (64); and 0.68,0.65, and 0.63 (65), respectively. However, the nomogram prognostic model combing clinical factors showed a better prediction power, with an AUC value of 0.862 in the training group and 0.832 in the validation set, respectively. The drawback is that the nomogram model was not assessed in an external test set for lacking a data set with some routinely available clinical data including breslow depth, clark level, clinical stage, and survival information.

In conclusion, we successfully constructed and validated a four-gene biomarker and a nomogram prognostic model by investigating data from TCGA and GEO databases using bioinformatic tools. Our study also revealed several favorable relevant immune genes, cells, and pathways in melanoma that could serve as potential therapeutic targets. These findings provide the rationale for further investigation and would aid clinical decision-making in melanoma immunotherapy.

DATA AVAILABILITY STATEMENT

The datasets analyzed during the present study are available in the TCGA repository (https://portal.gdc.cancer.gov/) and GEO database (https://www.ncbi.nlm.nih.gov/geo/query/acc.cgi?acc=GSE65904).

ETHICS STATEMENT

Ethical review and approval were not required for the study on human participants in accordance with the local legislation and institutional requirements. The patients/participants provided their written informed consent to participate in this study. Ethical review and approval were not required for the animal study because all data are available in online database which have obtained ethical review and approval before. Written informed consent was obtained from the individual(s) for the publication

of any potentially identifiable images or data included in this article.

AUTHOR CONTRIBUTIONS

CZ and XC were responsible for the literature review and writing *Introduction* and *Discussion* of the manuscript. DD and YW analyzed the bioinformatics data and wrote *Material and Methods* and *Results* sections of the manuscript. All authors contributed to the article and approved the submitted version.

FUNDING

The present study was funded by two projects: The Scientific Research Foundation of Jilin Province (nos. 20200601010JC and 20190701061GH).

SUPPLEMENTARY MATERIAL

The Supplementary Material for this article can be found online at: https://www.frontiersin.org/articles/10.3389/fonc.2021.593587/full#supplementary-material

REFERENCES

1. Gershenwald JE, Guy GP Jr. Stemming the Rising Incidence of Melanoma: Calling Prevention to Action. *J Natl Cancer Inst* (2016) 108(1):djv381. doi: 10.1093/jnci/djv381
2. Tripp MK, Watson M, Balk SJ, Swetter SM, Gershenwald JE. State of the science on prevention and screening to reduce melanoma incidence and mortality: The time is now. *CA Cancer J Clin* (2016) 66:460–80. doi: 10.3322/caac.21352
3. Rastrelli M, Tropea S, Rossi CR, Alaibac M. Melanoma: epidemiology, risk factors, pathogenesis, diagnosis and classification. *In Vivo* (2014) 28:1005–11.
4. Watts CG, Madronio C, Morton RL, Goumas C, Armstrong BK, Curtin A, et al. Clinical Features Associated With Individuals at Higher Risk of Melanoma: A Population-Based Study. *JAMA Dermatol* (2017) 153:23–9. doi: 10.1001/jamadermatol.2016.3327
5. Yan Y, Leontovich AA, Gerdes MJ, Desai K, Dong J, Sood A, et al. Understanding heterogeneous tumor microenvironment in metastatic melanoma. *PloS One* (2019) 14:e0216485. doi: 10.1371/journal.pone.0216485
6. Rodríguez-Cerdeira C, Carnero Gregorio M, López-Barcenas A, Sánchez-Blanco E, Sánchez-Blanco B, Fabbrocini G, et al. Advances in Immunotherapy for Melanoma: A Comprehensive Review. *Mediators Inflamm* (2017) 2017:3264217. doi: 10.1155/2017/3264217
7. Yang S, Liu T, Nan H, Wang Y, Chen H, Zhang X, et al. Comprehensive analysis of prognostic immune-related genes in the tumor microenvironment of cutaneous melanoma. *J Cell Physiol* (2020) 235:1025–35. doi: 10.1002/jcp.29018
8. Huang R, Mao M, Lu Y, Yu Q, Liao L. A novel immune-related genes prognosis biomarker for melanoma: associated with tumor microenvironment. *Aging (Albany NY)* (2020) 12:6966–80. doi: 10.18632/aging.103054
9. Huang B, Han W, Sheng ZF, Shen GL. Identification of immune-related biomarkers associated with tumorigenesis and prognosis in cutaneous melanoma patients. *Cancer Cell Int* (2020) 20:195. doi: 10.1186/s12935-020-01271-2
10. Neagu M, Constantin C, Tanase C. Immune-related biomarkers for diagnosis/prognosis and therapy monitoring of cutaneous melanoma. *Expert Rev Mol Diagn* (2010) 10:897–919. doi: 10.1586/erm.10.81
11. Grossman RL, Heath AP, Ferretti V, Varmus HE, Lowy DR, Kibbe WA, et al. Toward a Shared Vision for Cancer Genomic Data. *N Engl J Med* (2016) 375:1109–12. doi: 10.1056/NEJMp1607591
12. Weinstein JN, Collisson EA, Mills GB, Shaw KR, Ozenberger BA, Ellrott K, et al. The Cancer Genome Atlas Pan-Cancer analysis project. *Nat Genet* (2013) 45:1113–20. doi: 10.1038/ng.2764
13. Langfelder P, Horvath S. WGCNA: an R package for weighted correlation network analysis. *BMC Bioinf* (2008) 9:559. doi: 10.1186/1471-2105-9-559
14. Newman AM, Steen CB, Liu CL, Gentles AJ, Chaudhuri AA, Scherer F, et al. Determining cell type abundance and expression from bulk tissues with digital cytometry. *Nat Biotechnol* (2019) 37:773–82. doi: 10.1038/s41587-019-0114-2
15. Subramanian A, Tamayo P, Mootha VK, Mukherjee S, Ebert BL, Gillette MA, et al. Gene set enrichment analysis: a knowledge-based approach for interpreting genome-wide expression profiles. *Proc Natl Acad Sci USA* (2005) 102:15545–50. doi: 10.1073/pnas.0506580102
16. Mootha VK, Lindgren CM, Eriksson KF, Subramanian A, Sihag S, Lehar J, et al. PGC-1alpha-responsive genes involved in oxidative phosphorylation are coordinately downregulated in human diabetes. *Nat Genet* (2003) 34:267–73. doi: 10.1038/ng1180
17. Kimball AB, Grant RA, Wang F, Osborne R, Tiesman JP. Beyond the blot: cutting edge tools for genomics, proteomics and metabolomics analyses and previous successes. *Br J Dermatol* (2012) 166(Suppl 2):1–8. doi: 10.1111/j.1365-2133.2012.10859.x
18. Shu L, Liu Y, Li J, Wu X, Li Y, Huang H. Landscape Profiling Analysis of DPP4 in Malignancies: Therapeutic Implication for Tumor Patients With Coronavirus Disease 2019. *Front Oncol* (2021) 11:624899. doi: 10.3389/fonc.2021.624899
19. Man Z, Chen Y, Gao L, Xei G, Li Q, Lu Q, et al. A Prognostic Model Based on RNA Binding Protein Predicts Clinical Outcomes in Hepatocellular Carcinoma Patients. *Front Oncol* (2020) 10:613102. doi: 10.3389/fonc.2020.613102
20. Guan X, Xu ZY, Chen R, Qin JJ, Cheng XD. Identification of an Immune Gene-Associated Prognostic Signature and Its Association With a Poor Prognosis in Gastric Cancer Patients. *Front Oncol* (2020) 10:629909. doi: 10.3389/fonc.2020.629909
21. Jung SY, Papp JC, Sobel EM, Pellegrini M, Yu H, Zhang ZF. Genetically Predicted C-Reactive Protein Associated With Postmenopausal Breast Cancer Risk: Interrelation With Estrogen and Cancer Molecular Subtypes Using Mendelian Randomization. *Front Oncol* (2020) 10:630994. doi: 10.3389/fonc.2020.630994
22. Cirenajwis H, Ekedahl H, Lauss M, Harbst K, Carneiro A, Enoksson J, et al. Molecular stratification of metastatic melanoma using gene expression profiling: Prediction of survival outcome and benefit from molecular targeted therapy. *Oncotarget* (2015) 6:12297–309. doi: 10.18632/oncotarget.3655
23. Cabrita R, Lauss M, Sanna A, Donia M, Skaarup Larsen M, Mitra S, et al. Tertiary lymphoid structures improve immunotherapy and survival in melanoma. *Nature* (2020) 577:561–5. doi: 10.1038/s41586-019-1914-8
24. Yoshihara K, Shahmoradgoli M, Martínez E, Vegesna R, Kim H, Torres-Garcia W, et al. Inferring tumour purity and stromal and immune cell admixture from expression data. *Nat Commun* (2013) 4:2612. doi: 10.1038/ncomms3612
25. Breuer K, Foroushani AK, Laird MR, Chen C, Sribnaia A, Lo R, et al. InnateDB: systems biology of innate immunity and beyond–recent updates and continuing curation. *Nucleic Acids Res* (2013) 41:D1228–33. doi: 10.1093/nar/gks1147
26. Huang da W, Sherman BT, Lempicki RA. Systematic and integrative analysis of large gene lists using DAVID bioinformatics resources. *Nat Protoc* (2009) 4:44–57. doi: 10.1038/nprot.2008.211
27. Swinton J. A package for Venn diagrams in R with the Vennerable package. (2009).
28. Friedman J, Hastie T, Tibshirani R. Regularization Paths for Generalized Linear Models via Coordinate Descent. *J Stat Softw* (2010) 33:1–22. doi: 10.18637/jss.v033.i01
29. Simon N, Friedman J, Hastie T, Tibshirani R. Regularization Paths for Cox's Proportional Hazards Model via Coordinate Descent. *J Stat Softw* (2011) 39:1–13. doi: 10.18637/jss.v039.i05

30. Hadley Wickham WC, Henry L, Pedersen TL, Takahashi K, Wilke C, Woo K, et al. *Dewey Dunnington, ggplot2: Elegant Graphics for Data Analysis*. New York: Springer-Verlag (2016).
31. Grambsch PM, Therneau TM. *Modeling Survival Data: Extending the Cox Model*. New York: Springer (2000).
32. Kosinski M, Kassambara A, Biecek P, Fabian S. *A Package for Drawing Survival Curves using "ggplot2" in R*. (2020).
33. Saha-Chaudhuri P, Heagerty PJ. A Package for Compute time-dependent ROC curve from censored survival data using Kaplan-Meier (KM) or Nearest Neighbor Estimation (NNE) method of Heagerty, Lumley & Pepe in R. (2013).
34. Harrell FEJr. *A Package for Regression Modeling Strategies in R*. (2020).
35. Robin X, Turck N, Hainard A, Tiberti N, Lisacek F, Sanchez JC, et al. pROC: an open-source package for R and S+ to analyze and compare ROC curves. *BMC Bioinf* (2011) 12:77. doi: 10.1186/1471-2105-12-77
36. Max Gordon TL. A Package for Advanced Forest Plot Using 'grid' Graphics in R. (2020).
37. Wu M, Li X, Zhang T, Liu Z, Zhao Y. Identification of a Nine-Gene Signature and Establishment of a Prognostic Nomogram Predicting Overall Survival of Pancreatic Cancer. *Front Oncol* (2019) 9:996. doi: 10.3389/fonc.2019.00996
38. Zhu X, Tian X, Sun T, Yu C, Cao Y, Yan T, et al. GeneExpressScore Signature: a robust prognostic and predictive classifier in gastric cancer. *Mol Oncol* (2018) 12:1871–83. doi: 10.1002/1878-0261.12351
39. Shen S, Wang G, Zhang R, Zhao Y, Yu H, Wei Y, et al. Development and validation of an immune gene-set based Prognostic signature in ovarian cancer. *EBioMedicine* (2019) 40:318–26. doi: 10.1016/j.ebiom.2018.12.054
40. Liu GM, Zeng HD, Zhang CY, Xu JW. Identification of a six-gene signature predicting overall survival for hepatocellular carcinoma. *Cancer Cell Int* (2019) 19:138. doi: 10.1186/s12935-019-0858-2
41. Zhang J, Zhang X, Piao C, Bi J, Zhang Z, Li Z, et al. A long non-coding RNA signature to improve prognostic prediction in clear cell renal cell carcinoma. *Bio Med Pharmacother* (2019) 118:109079. doi: 10.1016/j.biopha.2019.109079
42. Wei X, Gu X, Ma M, Lou C. Long noncoding RNA HCP5 suppresses skin cutaneous melanoma development by regulating RARRES3 gene expression via sponging miR-12. *Onco Targets Ther* (2019) 12:6323–35. doi: 10.2147/OTT.S195796
43. Goodridge HS, Reyes CN, Becker CA, Katsumoto TR, Ma J, Wolf AJ, et al. Activation of the innate immune receptor Dectin-1 upon formation of a 'phagocytic synapse'. *Nature* (2011) 472:471–5. doi: 10.1038/nature10071
44. Kankkunen P, Teirilä L, Rintahaka J, Alenius H, Wolff H, Matikainen S. (1,3)-beta-glucans activate both dectin-1 and NLRP3 inflammasome in human macrophages. *J Immunol* (2010) 184:6335–42. doi: 10.4049/jimmunol.0903019
45. Daley D, Mani VR, Mohan N, Akkad N, Ochi A, Heindel DW, et al. Dectin 1 activation on macrophages by galectin 9 promotes pancreatic carcinoma and peritumoral immune tolerance. *Nat Med* (2017) 23:556–67. doi: 10.1038/nm.4314
46. Mattiola I, Tomay F, De Pizzol M, Silva-Gomes R, Savino B, Gulic T, et al. The macrophage tetraspan MS4A4A enhances dectin-1-dependent NK cell-mediated resistance to metastasis. *Nat Immunol* (2019) 20:1012–22. doi: 10.1038/s41590-019-0417-y
47. Kurze AK, Buhs S, Eggert D, Oliveira-Ferrer L, Müller V, Niendorf A, et al. Immature O-glycans recognized by the macrophage glycoreceptor CLEC10A (MGL) are induced by 4-hydroxy-tamoxifen, oxidative stress and DNA-damage in breast cancer cells. *Cell Commun Signal* (2019) 17:107. doi: 10.1186/s12964-019-0420-9
48. Hoober JK, Eggink LL, Cote R. Stories From the Dendritic Cell Guardhouse. *Front Immunol* (2019) 10:2880. doi: 10.3389/fimmu.2019.02880
49. Kanemaru K, Noguchi E, Tahara-Hanaoka S, Mizuno S, Tateno H, Denda-Nagai K, et al. Clec10a regulates mite-induced dermatitis. *Sci Immunol* (2019) 4(42):eaax6908. doi: 10.1126/sciimmunol.aax6908
50. Kuo SJ, Chien SY, Lin C, Chan SE, Tsai HT, Chen DR. Significant elevation of CLDN16 and HAPLN3 gene expression in human breast cancer. *Oncol Rep* (2010) 24:759–66. doi: 10.3892/or_00000918
51. Liang L, Xu J, Wang M, Xu G, Zhang N, Wang G, et al. LncRNA HCP5 promotes follicular thyroid carcinoma progression via miRNAs sponge. *Cell Death Dis* (2018) 9:372. doi: 10.1038/s41419-018-0382-7
52. Jiang L, Wang R, Fang L, Ge X, Chen L, Zhou M, et al. HCP5 is a SMAD3-responsive long non-coding RNA that promotes lung adenocarcinoma metastasis via miR-203/SNAI axis. *Theranostics* (2019) 9:2460–74. doi: 10.7150/thno.31097
53. Kulski JK. Long Noncoding RNA HCP5, a Hybrid HLA Class I Endogenous Retroviral Gene: Structure, Expression, and Disease Associations. *Cells* (2019) 8(5):480. doi: 10.3390/cells8050480
54. Falleni M, Savi F, Tosi D, Agape E, Cerri A, Moneghini L, et al. M1 and M2 macrophages' clinicopathological significance in cutaneous melanoma. *Melanoma Res* (2017) 27:200–10. doi: 10.1097/CMR.0000000000000352
55. Cao M, Yan H, Han X, Weng L, Wei Q, Sun X, et al. Ginseng-derived nanoparticles alter macrophage polarization to inhibit melanoma growth. *J Immunother Cancer* (2019) 7:326. doi: 10.1186/s40425-019-0817-4
56. Kou Y, Ji L, Wang H, Wang W, Zheng H, Zou J, et al. Connexin 43 upregulation by dioscin inhibits melanoma progression via suppressing malignancy and inducing M1 polarization. *Int J Cancer* (2017) 141:1690–703. doi: 10.1002/ijc.30872
57. Khan Z, Cao DY, Giani JF, Bernstein EA, Veiras LC, Fuchs S, et al. Overexpression of the C-domain of angiotensin-converting enzyme reduces melanoma growth by stimulating M1 macrophage polarization. *J Biol Chem* (2019) 294:4368–80. doi: 10.1074/jbc.RA118.006275
58. Paul S, Chhatar S, Mishra A, Lal G. Natural killer T cell activation increases iNOS(+)CD206(-) M1 macrophage and controls the growth of solid tumor. *J Immunother Cancer* (2019) 7:208. doi: 10.1186/s40425-019-0697-7
59. Qian Z, Zhang Z, Wang Y. T cell receptor signaling pathway and cytokine-cytokine receptor interaction affect the rehabilitation process after respiratory syncytial virus infection. *PeerJ* (2019) 7:e7089. doi: 10.7717/peerj.7089
60. Liu J, Li H, Sun L, Wang Z, Xing C, Yuan Y. Aberrantly methylated-differentially expressed genes and pathways in colorectal cancer. *Cancer Cell Int* (2017) 17:75. doi: 10.1186/s12935-017-0444-4
61. Li F, Guo P, Dong K, Guo P, Wang H, Lv X. Identification of Key Biomarkers and Potential Molecular Mechanisms in Renal Cell Carcinoma by Bioinformatics Analysis. *J Comput Biol* (2019) 26:1278–95. doi: 10.1089/cmb.2019.0145
62. Yamamura K, Baba Y, Nakagawa S, Mima K, Miyake K, Nakamura K, et al. Human Microbiome Fusobacterium Nucleatum in Esophageal Cancer Tissue Is Associated with Prognosis. *Clin Cancer Res* (2016) 22:5574–81. doi: 10.1158/1078-0432.CCR-16-1786
63. Tian M, Yang J, Han J, He J, Liao W. A novel immune checkpoint-related seven-gene signature for predicting prognosis and immunotherapy response in melanoma. *Int Immunopharmacol* (2020) 87:106821. doi: 10.1016/j.intimp.2020.106821
64. Wan Q, Jin L, Su Y, Liu Y, Li C, Wang Z. Development and validation of autophagy-related-gene biomarker and nomogram for predicting the survival of cutaneous melanoma. *IUBMB Life* (2020) 72:1364–78. doi: 10.1002/iub.2258
65. Sheng Y, Tong L, Geyu L. An immune risk score with potential implications in prognosis and immunotherapy of metastatic melanoma. *Int Immunopharmacol* (2020) 88:106921. doi: 10.1016/j.intimp.2020.106921

Conflict of Interest: The authors declare that the research was conducted in the absence of any commercial or financial relationships that could be construed as a potential conflict of interest.

frontiers in Oncology

ORIGINAL RESEARCH
published: 01 April 2021
doi: 10.3389/fonc.2021.582676

Safety and Tolerability of BRAF Inhibitor and BRAF Inhibitor-Based Combination Therapy in Chinese Patients With Advanced Melanoma: A Real World Study

*Xing Liu†, Jing-jing Li†, Ya Ding, Dan-dan Li, Xi-zhi Wen, De-sheng Weng, Jiu-hong Wang, Hang Jiang and Xiao-shi Zhang**

Biotherapy Center, Sun Yat-sen University Cancer Center, Guangzhou, China

The toxicity spectrum between Chinese and Caucasian patients with melanoma who were treated with BRAF inhibitors (BRAFi) may differ. The purpose of the present study was to assess the safety and tolerability of BRAFi and BRAFi-based combination therapies [MEK inhibitors (MEKi) or anti-programmed death-1 (PD-1) antibody] in Chinese patients with *BRAF V600E/K* mutation-positive metastatic melanoma. We also investigated whether treatment-related adverse events (AEs) correlated with the prognosis. This retrospective study collected data from 43 patients with *BRAF V600E/K* mutation-positive metastatic melanoma from a single Chinese cancer center. Of the 43 patients, 12 patients received BRAFi monotherapy, 12 patients received BRAFi+MEKi, and 19 patients received BRAFi combined with the anti-PD-1 antibody. The median follow-up time was 19 months. In the BRAFi group, the most common AEs were rashes, palmoplantar erythrodysesthesia, and arthralgia. Four out of 12 (30%) patients experienced grade 3–4 treatment-related AEs. All grades of AEs in the BRAFi+MEKi group were similar to the BRAFi group, except for higher pyrexia (58.3%) and fewer cutaneous AEs. Three out of 12 (25%) patients experienced grade 3–4 AEs, especially pyrexia (16.7%). In the BRAFi+anti-PD-1 antibody group, AEs were similar to the BRAFi group, except for an increased aminotransferase level (36.8%), increased bilirubin (31.6%), and hypothyroidism (15.8%). Eleven out of 19 (57.9%) patients experienced grade 3–4 AEs and four out of 19 (21%) patients discontinued the therapy due to AEs. Treatment-related hepatotoxicity (trHE), defined as an increase in either alanine aminotransferase (ALT), aspartate transaminase (AST), or bilirubin levels, was the only AE identified as a significant poor-prognosis indicator in this study. The median progression-free survival of patients with trHE (41.9%) was 8 months, whereas it was 18 months for those without trHE [$p = 0.046$, hazard ratio (HR) = 2.116]. Moreover, this association was independent of medication regimens ($p = 0.014$, HR = 2.971). The overall response rate of patients with trHE was significantly lower than those without trHE (44.4 vs. 60.0%, $p = 0.024$), and we observed a similar trend in patients treated with BRAFi, BRAFi+MEKi, and BRAFi+anti-PD-1 antibody. In conclusion, BRAFi and BRAFi-based combination

OPEN ACCESS

Edited by:
Igor Puzanov,
University at Buffalo, United States

Reviewed by:
Simone M. Goldinger,
University of Zurich, Switzerland
Jennifer Yunyan Zhang,
Duke University, United States

***Correspondence:**
Xiao-shi Zhang
zhangxsh@sysucc.org.cn

†These authors share first authorship

Specialty section:
This article was submitted to Skin Cancer, a section of the journal Frontiers in Oncology

Received: *13 July 2020*
Accepted: *12 February 2021*
Published: *01 April 2021*

Citation:
Liu X, Li J-j, Ding Y, Li D-d, Wen X-z, Weng D-s, Wang J-h, Jiang H and Zhang X-s (2021) Safety and Tolerability of BRAF Inhibitor and BRAF Inhibitor-Based Combination Therapy in Chinese Patients With Advanced Melanoma: A Real World Study. Front. Oncol. 11:582676. doi: 10.3389/fonc.2021.582676

therapies were tolerable with reversible AEs in Chinese patients with melanoma. The trHE in patients receiving BRAFi and BRAFi-based regimens might indicate a poor therapy-related prognosis.

Keywords: BRAFV600E/K-positive, advanced melanoma, BRAF inhibitor, BRAF inhibitor-based combination, China

INTRODUCTION

Melanoma is one of the most deadly diseases in China, with an estimated 5-year overall survival (OS) of merely 4.6% (1). *BRAF(V600E/K)* mutation, a component of the mitogen-activated protein kinase (MAPK) pathway, is regarded as a significant oncogene in melanoma. The overall response rate (ORR) of BRAF inhibitor monotherapy has been reported to be as high as 36–53% from clinical trials in Caucasian patients, with a median duration of response of merely 6–8 months (2–4). At present, patients with *BRAF V600*-mutant metastatic melanoma are recommended for combination treatment with BRAF inhibitors (BRAFi) and MEK inhibitors (MEKi), such as dabrafenib+trametinib (D+T), vemurafenib+cobimetinib (V+C), and encorafenib+binimetinib (E+B), because the combination can block the negative feedback loops for the activation of the MAPK pathway and delay the development of drug resistance (5–7).

Clinical characteristics, such as pathology, anatomical origin, and prognoses, differ significantly among different ethnic groups (8). The incidence of cutaneous melanoma is lower in Asian patients than in Caucasians (50–70% vs. 91.2%) (9, 10). Acral cutaneous melanoma has a higher incidence, accounting for up to 58% of all cutaneous melanomas in Asians, compared to Caucasians (1–7%) (11). Furthermore, Guo et al. reported that *BRAF* mutations in Chinese patients with melanoma were more frequent in non-acral cutaneous melanoma (43.3%) than in acral cutaneous melanoma; however, the frequencies reported by Maldona and Cohe in Caucasian non-acral cutaneous melanoma (60%) were still higher (12–14). Only one small study (n = 46) reported the toxicity spectrum of vemurafenib in Chinese patients with melanoma. By comparing data from this study with those from the pivotal BRIM-3 study (15), we found that the toxicity spectrum between Chinese and Caucasian patients with melanoma treated with vemurafenib was different. Chinese patients had a higher incidence of higher blood cholesterol levels (59 vs. <1%), hypertriglyceridemia (22 vs. <1%), total bile acid increase (22 vs. 0%), hyperuricemia (17 vs. <1%), serum bilirubin level increase (54 vs. 9%), leukopenia (22 vs. 0%), proteinuria (24 vs. <1%), and melanocytic nevus (52 vs. 10%). These differences may impact the completion of treatment. For example, an AE of grade 3, corresponding to an increase in serum cholesterol levels, led to an interruption in the treatment of Chinese patients with melanoma (15, 16). In addition, the safety and tolerability of the BRAFi+MEKi combination in Chinese patients with melanoma have not been reported. Therefore, the available data regarding the tolerability and safety of BRAFi and BRAFi+MEKi in Chinese patients are significant, especially from a real-world experience.

Recently, the combination of targeted therapy with immunotherapy was proposed to improve the long-term outcomes of patients. A preclinical study showed that BRAF/MEK-targeted therapies had effects, such as enhancing intratumor T-cell infiltration, increasing tumor antigens, and increasing the expression of programmed death-1 (PD-L1), on the tumor microenvironment, which supported their combination with PD-1/PD-L1 inhibitors (17–19). Ascierto et al. performed a randomized phase 2 trial enrolling 60 Caucasian patients with *BRAF V600*-mutant metastatic melanoma who were treated with a triple-combination therapy, including dabrafenib, trametinib, and pembrolizumab. Although progression-free survival (PFS) of the triple-combination was promising, grade 3–5 adverse events (AEs) occurred in 58.3% of patients and led to treatment discontinuation in 25 patients (41.7%) (20). A similar phenomenon could be observed in two other triple-treatment combinations (21, 22). However, the clinical experience relative to the tolerance of BRAFi, combined with immune-checkpoint inhibitors (ICIs), is still lacking in Chinese patients.

Thus, the purpose of this study was to analyze the safety and tolerability of BRAFi and BRAFi-based combination therapy (MEKi or anti-PD-1 antibody) in Chinese patients with *BRAF V600E/K* mutation-positive metastatic melanoma. Furthermore, we also investigated which treatment-related AE could represent as a predictor of efficacy.

MATERIALS AND METHODS

Patients

A retrospective study of 43 previously treated or untreated advanced melanoma patients attending the Sun Yat-sen University Cancer Center between May 2015 and March 2020 was carried out. All data were extracted from the database containing electronic medical records of the institution. Patients were diagnosed with biopsy-confirmed advanced melanoma, and molecular profiling confirmed the presence of the *BRAF V600E/K* mutation. Only patients with a *BRAF* mutation who were treated with BRAFi (vemurafenib 960 mg, orally twice daily), BRAFi+MEKi [dabrafenib (D) 300 mg orally twice daily; trametinib (T) 2 mg orally once daily], or BRAFi+anti-PD-1 antibody [vemurafenib 960 mg orally twice daily, for 4–6 weeks, combined with pembrolizumab (2 mg/kg, every 3 weeks) once the disease was controlled) were eligible for analysis. Demographic, clinical, and survival data were retrieved from the medical records. All patients who accepted systemic therapy had a performance status of 0–2.

Data Collection and Analysis

The following baseline characteristics were recorded for each patient: age, sex, Eastern Cooperative Oncology Group performance status (PS), disease stage (AJCC 8th edition), the number of disease sites, lactate dehydrogenase (LDH) levels, and the therapeutic regimen. AEs caused by the therapy were defined and graded according to the Common Terminology Criteria for Adverse Events, version 4.

Only *BRAF V600E/K* mutated patients receiving BRAFi, BRAFi+MEKi, or vemurafenib+pembrolizumab were enrolled in this study. The clinical data of all patients enrolled in this study were retrospectively analyzed. Efficacy included the ORR according to RECIST v1.1 criteria and was confirmed by repeat assessment at least 4 weeks after the criteria were first met. Tumor assessments [computed tomography (CT) or magnetic resonance imaging (MRI)] were obtained at screening, after 8–12 weeks (or as clinically indicated), until documented disease progression. PFS was estimated using Kaplan-Meier Statistical analysis. Safety assessments consisted of monitoring and recording of AEs. AEs were graded according to National Cancer Institute Common Terminology Criteria for Adverse Events, version 4.0.

Statistical Analysis

Analysis of the correlation between AEs and PFS was performed. The median follow-up time was analyzed by the Reverse Kaplan-Meier method. Single continuous variables and categorical variables were examined with the Student's *t*-test and the chi-square tests, respectively. The multivariate Cox regression analysis was used to compare the PFS between patients who developed trHE and those who did not, and the analysis was adjusted for the baseline LDH level, medical regimens, and liver metastases. Statistical analyses were performed using the statistical packages SPSS (SPSS for Windows, version 22.0, SPSS Inc., Chicago, IL). All tests were two-tailed. Statistical significance was determined by a p-value < 0.05.

RESULTS

Cohort Characteristics

In this study, 43 metastatic melanoma patients were eligible for analysis. Patients were treated with BRAFi ($n = 12$), BRAFi+MEKi ($n = 12$), and BRAFi+anti-PD-1 antibody ($n = 19$) as follows: vemurafenib ($n = 12$), D+T ($n = 11$) and V+C ($n = 1$), and vemurafenib+anti-PD-1 antibody (pembrolizumab) ($n = 19$). All patients had either a *BRAF V600E* mutation or a *BRAF V600K* mutation.

Baseline demographics and disease characteristics are shown in **Table 1**. Although baseline characteristics of the three groups were essentially the same, patients treated with vemurafenib combined with the anti-PD-1 antibody presented the best baseline values, including the lines of therapy, disease sites, and the LDH level. Most patients started the three regimens in this study as first or second-line (85.9%) therapy, and over half (57.9%) of the patients were treated with BRAFi+anti-PD-1 antibody as the first-line therapy. All patients had normal blood levels of aminotransferases [alanine aminotransferase (ALT) and aspartate transaminase (AST)] and bilirubin before treatment; however, 17 patients experienced hepatic metastasis and one patient was identified as positive for hepatitis B-antigen.

Toxicity Profile of the Three Regimens

The total median follow-up time was 19 months (range, 11–26 months). At the time of data cutoff, 13 patients (30%) continued treatment and 30 patients (70%) had discontinued treatment because of disease progression (BRAFi, $n = 12$; BRAFi+MEKi, $n = 8$; BRAFi+Anti-PD-1 antibody, $n = 6$) or AEs (BRAFi+Anti-PD-1 antibody, $n = 4$). Almost all patients in the three groups experienced at least one AE (**Table 2**). Grade 3 or 4 treatment-related AEs were reported in four of 12 (33%), three of 12 (25%), and 11 of 19 (57.9%) patients in the vemurafenib, BRAFi +MEKi, and vemurafenib+anti-PD-1 antibody groups, respectively.

Similar to the pivotal clinical trials in Caucasian patients (5, 23) compared with the vemurafenib group, the frequencies of cutaneous toxicity [rash (66.7 vs. 83.3%), palmoplantar erythrodysesthesia (16.7 vs. 83.3%), keratoacanthoma (0 vs. 16.7%)], and arthralgia (33.3 vs. 58.3%) were lower in patients in the BRAFi group combined with the MEKi group. This mainly resulted from paradoxical activation of the MAPK pathway due to BRAFi monotherapy (24, 25). Meanwhile, photosensitivity (25.0 vs. 0%) was more common in the vemurafenib group, which is commonly described in patients using vemurafenib (5), and did not occur with dabrafenib or trametinib treatment (26). MEKi-specific AEs included serious pyrexia (16.7%), which was more common in the BRAFi+MEKi group. In both BRAFi and BRAFi+MEKi groups, the most common grade $\geq$3 AEs included rash, pruritus, arthralgia, and increased aminotransferase levels, except for pyrexia (16.7 vs. 0%), which was similar in both groups. In the BRAFi group, four patients (33.3%) modified the dose of vemurafenib to 720 mg twice daily due to grade 3 AEs [arthralgia, $n = 2$; rash, $n = 1$; increased aminotransferase levels (ALT and AST), $n = 1$]. None of the patients discontinued therapy due to AEs. In the BRAFi+MEKi group, no AEs leading to dose modification or treatment discontinuation were reported because most treatment-related AEs were of grades 1–2 and could be alleviated with medications (antiallergic drugs, steroids, or hepatoprotective drugs). Only one patient experienced a grade 3 AE involving increased levels of both ALT and AST and interrupted D+T. The patient received appropriate treatment with hepatoprotective drugs to restore ALT and AST levels (**Supplementary Table 1**).

In the vemurafenib+anti-PD-1 antibody group, grade 3–4 AEs (57.9%) included rash (36.8%), arthralgia (21.1%), pruritus (15.8%), palmoplantar erythrodysesthesia (10.5%), and myalgia (3.8%). These AEs usually were more severe after the addition of an anti-PD-1 antibody. Eight patients experienced grade 3 rash or palmoplantar erythrodysesthesia, which occurred before the addition of anti-PD-1 antibody in one patient and which occurred after the addition of anti-PD-1 antibody in the other seven patients. Musculoskeletal AEs occurred frequently, especially arthralgia (62.8%), which worsened with continued treatment, but could be alleviated by lowering the dose of BRAFi. Pneumonitis was reported in one patient but no action was taken. Signs of altered imaging on CT scans disappeared after 2 weeks. Hypothyroidism and hyperthyroidism were reported in three

TABLE 1 | Clinical characteristics of the study population ($n = 43$).

	BRAFi	BRAFi+MEKi	BRAFi+PD-1 antibody	Total
	***N* = 12**	***N* = 12**	***N* = 19**	***N* = 43**
Sex—no. (%)				
Male	5 (41.7)	6 (50.0)	13 (68.4)	24 (55.8)
Female	7 (58.3)	6 (50.0)	6 (31.6)	19 (44.2)
Median (range) age—years	52 (29–55)	44 (27–63)	49 (33–67)	47 (27–67)
Performance status—no. (%)				
0	1 (8.3)	9 (75.0)	13 (68.4)	23 (53.5)
1	10 (83.3)	2 (16.7)	6 (31.6)	18 (41.9)
2	1 (8.3)	1 (8.3)	0	2 (4.6)
LDH—no. (%)				
<ULN	7 (58.3)	9	14 (73.7)	32 (74.4)
>ULN	5 (41.7)	3 (25.0)	5 (26.3)	11 (25.6)
Disease stage (AJCC#7)—no. (%)				
M1a	2 (16.7)	3 (25.0)	9 (47.4)	14 (32.6)
M1b	3 (25.0)	4 (33.3)	5 (26.3)	12 (27.9)
M1c	6 (50.0)	4 (33.3)	2 (10.5)	12 (27.9)
M1d	1 (8.3)	1 (8.3)	3 (15.8)	5 (11.6)
Disease site—no. (%)				
≤3	4 (33.3)	7 (58.3)	12 (63.2)	23 (53.5)
>3	8 (66.7)	5 (41.7)	7 (36.8)	20 (46.5)
Brain metastases—no. (%)				
Yes	1 (8.3)	1 (8.3)	3 (15.8)	5 (11.7)
No	11 (91.7)	11 (91.7)	16 (84.2)	38 (88.3)
Regime—no. (%)				
Vemurafenib	12 (100.0)	-	-	12 (27.9)
Dabrafenib+trametinib	-	11 (91.7)	-	11 (25.6)
Vemurafenib+cobimetinib	-	1 (8.3)	-	1 (2.3)
Vemurafenib+pembrolizumab	-	-	19 (100)	19 (44.2)
Basic liver function—no. (%)				
Liver metastasis	6 (50.0)	5 (41.7)	5 (26.3)	16 (37.2)
Hepatitis B-antigen–positive.	0	0	1 (5.3)	1 (2.3)
Normal	6 (50.0)	7 (58.3)	13 (68.4)	26 (60.5)
Line of therapy—no. (%)				
1	4 (33.3)	4 (33.3)	11 (57.9)	19 (44.2)
2	6 (50.0)	6 (50.0)	7 (36.8)	19 (44.2)
3	2 (16.7)	1 (8.3)	1 (5.3)	4 (9.3)
4	0	1 (8.3)	0	1 (2.3)

LDH, lactate dehydrogenase; ULN, upper normal limit; BRAFi, BRAF inhibitor; MEKi, MEK inhibitor.

patients and one patient, respectively. Both events were treated with endocrine therapy and those patients ultimately continued with the regimen (vemurafenib+anti-PD-1 antibody). Eighteen patients (94.7%) modified the dose of vemurafenib. Of these, four patients (21.1%) were still unable to tolerate AEs (grade 3 of fatigue: $n = 1$; iritis: $n = 1$; grade 3 rash: $n = 2$) and had finally discontinued the combined regimen. Two patients (10.5%) required a dose reduction of vemurafenib both before (decreased 960–720 mg twice daily) and after (720 mg decreased to 480 mg twice daily) the addition of anti-PD-1 antibody. Before the addition of the anti-PD-1 antibody, five patients (26.3%) required a reduction in the dose of vemurafenib to 480 mg two times daily due to AEs. The remaining 11 patients (57.9%) reduced the dose of vemurafenib after the addition of anti-PD-1 antibody, and four of these 11 patients eventually discontinued the combined therapy. Ten patients modified the vemurafenib dosage to 480 mg two times daily, two patients modified their dosage to 720 mg two times daily, and two patients modified vemurafenib treatment to

TABLE 2 | Adverse events of three regimes.

N (%)	BRAFi *N* = 12		BRAFi+MEKi *N* = 12		BRAFi+PD-1 antibody *N* = 19	
Grade	**Any***	**III-IV**	**Any***	**III-IV**	**Any***	**III-IV**
Any adverse event	12 (100)	4 (33.3)	12 (100)	3 (25.0)	19 (100)	11 (57.9)
Dermatological events						
Rash	10 (83.3)	2 (16.7)	8 (66.7)	1 (8.3)	16 (84.2)	7 (36.8)
Palmo–plantar erythrodysesthesia	10 (83.3)	0	2 (16.7)	0	8 (42.1)	2 (10.5)
Alopecia	7 (58.3)	0	0	0	6 (31.6)	0
Pruritus	6 (50.0)	2 (16.7)	6 (50.0)	1 (8.3)	12 (63.2)	3 (15.8)
Photosensitivity reaction	3 (25.0)	0	0	0	6 (31.6)	0
Keratocanthoma	2 (16.7)	0	0	0	8 (42.1)	0
Musculoskeletal events						
Arthralgia	7 (58.3)	2 (16.7)	4 (33.3)	1 (8.3)	16 (84.2)	4 (21.1)
Myalgia	5 (41.7)	0	3 (23.1)	0	14 (53.8)	1 (3.8)
Gastrointestinal events						
Diarrhea	3 (25.0)	0	1 (8.3)	0	4 (21.1)	0
Nausea	3 (25.0)	0	3 (25.0)	0	3 (15.8)	0
Vomiting	3 (25.0)	0	2 (16.7)	0	3 (15.8)	0
General disorders						
Fatigue	4 (33.3)	0	3 (25.0)	0	9 (47.4)	0
Pyrexia	2 (16.7)	0	7 (58.3)	2 (16.7)	4 (21.1)	1 (5.3)
Headache	1 (8.3)	0	2 (16.7)	0	3 (15.8)	0
Dizziness	1 (8.3)	0	2 (16.7)	0	3 (15.8)	0
Investigations/laboratory examinations						
Increased alanine aminotransferase level	3 (25.0)	1 (8.3)	4 (33.3)	1 (8.3)	7 (36.8)	0
Increased aspartate aminotransferase level	1 (8.3)	1 (8.3)	3 (25.0)	1 (8.3)	4 (21.1)	0
Increased bilirubin	0	0	0	0	6 (31.6)	0
Increased blood creatinine	1 (8.3)	0	3 (25.0)	0	4 (21.1)	0
Hyperglycemia	3 (25.0)	0	6 (50.0)	0	5 (26.3)	0
Pulmonary events						
Cough	0	0	2 (16.7)	0	1 (5.3)	0
Pneumonia	0	0	0	0	1 (5.3)	0
Endocrine dyscrasia						
Hypothyroidism	0	0	0	0	3 (15.8)	0
Hyperthyroidism	0	0	0	0	1 (5.3)	0

Any, any grade; AE, adverse event; ALT, alanine aminotransferase; AST, aspartate aminotransferase; CTC, common toxicity criteria; BRAFi, BRAF inhibitor; MEKi, MEK inhibitor.*

240 mg two times daily. Ten patients required a dose reduction of vemurafenib due to rash or arthralgia. We observed that two patients who received a dose reduction of vemurafenib to 240 mg achieved a complete response (CR) and stable disease (SD), respectively, and both CR and SD were maintained up to the last follow-up, which indicated that the combination of low-dose vemurafenib and anti-PD-1 antibody could also benefit patients. There was no significant difference in the ORR between the three groups with different doses of vemurafenib (ORR: 100% of 720 mg; 70% of 420 mg; 50% of 240 mg). However, it is possible that no significant differences were observed due to sample size limitations.

We defined trHE as the increase of either ALT, AST, or bilirubin in this study. Treatment with hepatoprotective drugs (e.g., polyene phosphatidylcholine, compound glycyrrhizin, and reduced glutathione) could decrease the aminotransferase levels and reduce the bilirubin levels (e.g., ademetionine 1,4-butanedisulfonate). All patients with trHE only presented laboratory abnormalities and had no clinical symptoms. Overall, 18 patients (41.9%) developed trHE (**Supplementary Table 1**). In the BRAFi group, trHE was reported in three patients and one patient experienced a grade 3 increase in both ALT and AST levels. In the BRAFi+MEKi group, trHE was reported in four patients and one patient experienced grade 3 increase of

both ALT and AST levels. Increased bilirubin was not reported in either the BRAFi or BRAFi+MEKi groups. Two patients developed grade 3 trHE (elevated AST and ALT levels), which was successfully resolved by interruption of therapy and treatment with hepatoprotective drugs; the patients subsequently continued their therapy without any trHE relapse. In the BRAFi+anti-PD-1 antibody group, four patients (21.1%) experienced a grade 1 increase in bilirubin levels 1 month after the addition of the anti-PD-1 antibody. However, the levels returned to normal after ∼4 weeks following treatment with ademetionine and polyene phosphatidylcholine. Five patients (26.3%) developed an increase either of ALT or AST levels within 4 weeks after the addition of the anti-PD-1 antibody, which resolved after 0.5–4 weeks with hepatoprotective drugs ($n = 4$) or recovered spontaneously ($n = 1$). Similarly, the two remaining patients (10.5%) showed a concomitant increase of bilirubin and aminotransferases (ALT and AST) 3 weeks after the addition of the anti-PD-1 antibody to the treatment, although they resumed the regime after treatment with hepatoprotective drugs.

In this study, four of 43 patients received a third-line therapy (BRAFi: $n = 2$, BRAFi+MEKi: $n = 1$, vemurafenib+pembrolizumab: $n = 1$), and only one patient (BRAFi+MEKi) received a fourth-line treatment. Nineteen of 43 patients received a second-line therapy (BRAFi: $n = 6$, BRAFi+MEKi: $n = 6$, vemurafenib+pembrolizumab: $n = 7$) (**Table 1**). For patients receiving a second-line treatment or more, their primary therapies included only chemotherapy, such as taxinol combined with cis-platinum complexes (DDP), dacarbazine (DTIC) combined with DDP, or temozolomide (TMZ) combined with paraplatin. The common clinical AEs associated with these chemotherapeutic drugs included short-term toxicity, which were relieved before the start of this study. Similarly, the efficacy of these chemotherapeutic agents could be observed in short term (2–3 months), which is in contrast to similar delayed effects observed with ICIs.

AEs and Clinical Response Analysis

After 22 AEs were screened by the Kaplan-Meier survival analysis, only trHE showed a significant correlation with PFS. Univariate analyses revealed that PS, LDH level, liver metastases, treatment regimens, as well as trHE, were significant prognostic indicators for PFS (**Table 3**). The results of the multivariate analysis indicated that TrHE retained its significance as a predictive factor, whereas PS, LDH levels, liver metastases, and treatment regimens provided no significant prognostic value for PFS (**Table 4**). The median PFS of patients with trHE was 8 months compared with 18 months for the remaining patients [$p = 0.046$, hazard ratio (HR) = 2.116, Cox regression analysis; **Figure 1A**]. Moreover, this association was independent of the baseline LDH level, medication regimens, PS, or the presence of liver metastases ($p = 0.014$, HR = 2.971, Cox regression analysis; **Figure 1B**). The ORR of patients with trHE was significantly lower than in those without trHE (44.4 vs. 60.0%, $p = 0.024$), and we observed a similar trend in patients treated with BRAFi (33.3 vs. 44.4%, $p = 0.110$), BRAFi+MEKi (50 vs. 75%, $p < 0.001$), and BRAFi+anti-PD-1 antibody (45.5 vs. 62.5%, $p = 0.016$) (**Table 5**). In the BRAFi group, 0/3 (0%) patients experienced trHE and achieved a CR to therapy, 1/3 (33.3%) achieved a partial response (PR), and 2/3 (66.7%) had SD as per RECIST v1.1 criteria. In the BRAFi+MEKi group, 1/4 (25%) with trHE achieved a CR, 1/4 (25%) achieved a PR, and 2/4 (50%) had SD. In the group treated with BRAFi+anti-PD-1 antibody, patients developing trHE achieved lower CR than those without trHE (18.1 vs. 50.0%, $p < 0.001$). The PFS of all patients in the two groups, with or without treatment-related hepatotoxicity, are shown in **Figure 2**. According to **Supplementary Table 2**, there were no statistically significant differences in age, initial LDH level, number of diseases, receiving first-line treatment or not, or the presence of liver metastasis between patients experiencing hepatotoxicity and those without hepatotoxicity.

TABLE 3 | Univariate analyses of prognostic factors for PFS in patients with malignant melanoma.

Characteristics	mPFS (month)	Univariate analyses (*P*-value)
Age		0.768
≤45 years	12	
>45 years	9	
Gender		0.627
Men	11	
Female	12	
Performance status		0.001
0	25	
1	6	
2	4	
LDH		0.002
≤ULN	14	
>ULN	5	
Disease sites		0.308
≤3	14	
>3	6	
Liver metastases		0.024
Yes	5	
No	14	
CNS metastases		0.107
Yes	5	
No	12	
Regimen		0.016
BRAFi	5	
BRAFi+MEKi	12	
BRAFi+anti-PD-1 antibody	Not reach	
TrHE		0.046
Yes	8	
No	18	

LDH, lactate dehydrogenase; BRAFi, BRAF inhibitor; MEKi, MEK inhibitor; trHE, treatment-related hepatotoxicity defined as the increase of either ALT, AST or blood bilirubin levels.

DISCUSSION

Targeted therapy with MAPKi regimens has dramatically changed the landscape of treatment of *BRAF*-mutant metastatic

melanoma. Currently, the combination of MAPKi and ICIs may be a potentially effective approach to treat malignant melanoma. However, the toxicity spectrum of these therapies in different ethnic groups may be variable and will impact the treatment efficacy. Therefore, a description of the real-world experience regarding the tolerability and safety of BRAFi and BRAFi-based combinations in Chinese patients is significant.

In this study, patients receiving BRAFi monotherapy (vemurafenib) generally developed a similar pattern of AEs compared with Caucasian patients, and the occurrence of AEs appeared to be proportional to the dose of the drug (27). Compared with a study of vemurafenib treatment in 3,219 Caucasian patients, the Chinese patients in this study experienced higher incidence of aminotransferase level increase (25 vs. 0%) and hyperglycemia (25 vs. 0%). The most common grade 3 or higher AEs were keratoacanthoma (8%) and squamous cell cancer (cuSCC) of the skin (8%) in 3,219 Caucasian patients, which differed from this study (2). In the present study, arthralgia (16.3%) and rash (8.3%) were the most common grade 3 AEs, and all keratoacanthoma were grade 1–2 (16.7%). CuSCC was not observed in this study, and a similar rate as in reported in this study was observed in a phase I/II study of vemurafenib in Japanese patients with melanoma (28). Compared with Caucasian patients, the frequency of AEs (100 vs. 90%) was higher in this study; however, the frequency of grade 3/4 AEs (33 vs. 37%) in this study was lower, and no grade 4 AEs were observed among the patients. Meanwhile, the vemurafenib group of this study reported a higher incidence of liver system-related AEs (aminotransferase level increase) than in Caucasians. Differences between Asian and Caucasian populations might potentially lead to associated differences in the incidence of AEs. Since plasma concentrations of vemurafenib were generally consistent between Asian and Caucasian patients (16), differences in AE could be attributed to differences in culture and lifestyle, such as duration of exposure to sunlight and diet, as well as to differences in genetic susceptibility. Finally, compared with Caucasian patients, Chinese patients demonstrated equivalent or even better tolerance of BRAFi monotherapy.

Most cutaneous side effects, especially rash, pruritus, and palmar-plantar dysesthesia, decreased in the combination therapy group (D+T) compared with the BRAFi monotherapy treatment group in this study. A review evaluating AEs in Caucasians receiving V+C, D+T, and E+B reported that the targeted combination regimen resulted in fewer skin toxicities and more gastrointestinal side effects, particularly vomiting and diarrhea, which were probably caused by the MEKi (29). This was consistent with our observations regarding skin toxicity, but differed from the gastrointestinal AEs observed in this study. Furthermore, compared to Caucasians in the COMBI-V clinical trial, the patients receiving D+T had higher any

TABLE 4 | Multivariate analyses of prognostic factors for PFS.

Prognosticators	*P*-value
Performance status	0.371
LDH	0.107
Liver metastases	0.533
Regimen	0.166
TrHE	0.014

LDH, lactate dehydrogenase; Regimen, including BRAFi, BRAFi+MEKi and BRAFi+anti-PD-1 antibody; trHE, treatment-related hepatotoxicity defined as the increase of either ALT, AST or bilirubin levels.

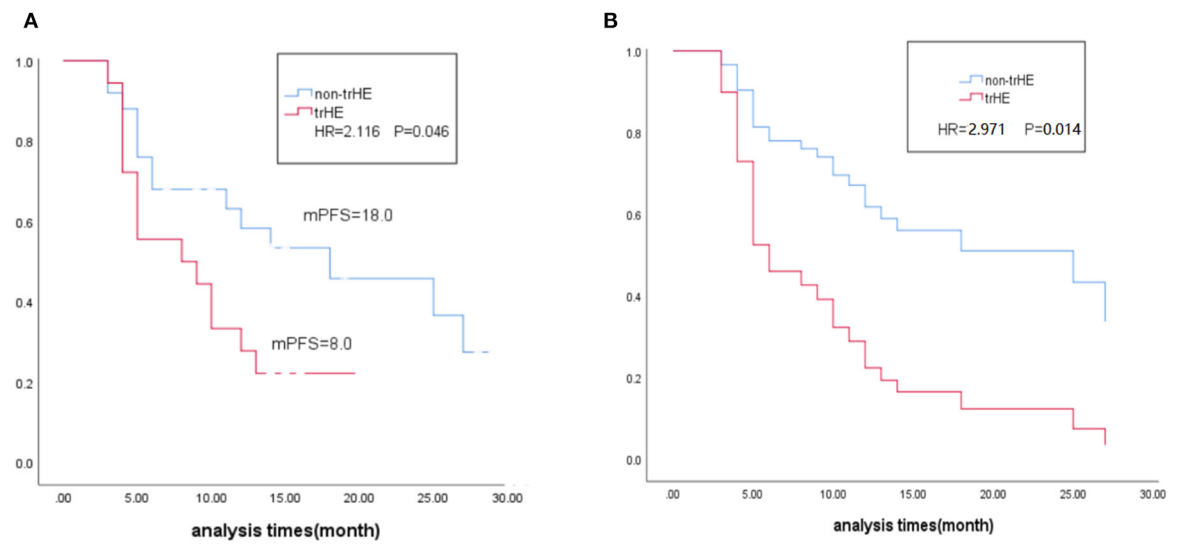

FIGURE 1 | (A) Kaplane-Meier survival estimates in relation to occurrence of trHE. **(B)** Multivariate Cox regression estimates in relation to occurrence of trHE, corrected for baseline LDH level, medication regimens and liver metastases. trHE, treatment-related hepatotoxicity defined as the increase of either ALT, AST, or bilirubin levels; mPES, median progression-free survival; HR, hazard ratio; LDH, lactate dehydrogenase.

TABLE 5 | Efficacy outcomes.

Outcome	trHE	Non-trHE
All	*n* = 18	*n* = 25
Confirmed ORR, *n* (%) [95% CI]	8 (44.4) [19.02–69.87]	15 (60) [39.36–80.64]
CR	3 (16.7)	5 (20)
PR	5 (27.8)	10 (40)
SD	9 (50)	10 (40)
PD	1 (5.6)	0
DCR	17 (94.4)	25 (100)
Median PFS, months (95% CI)	8.0 (0–16.32)	18.0 (4.56–31.43)
BRAFi	*n* = 3	*n* = 9
ORR	1 (33.3)	4(44.4)
CR	0	0
PR	1 (33.3)	4 (44.4)
SD	2 (66.7)	5 (45.6)
DCR	3 (100)	9 (100)
BRAFi+MEKi	*n* = 4	*n* = 8
ORR	2 (50)	6 (75)
CR	1 (25)	1 (12.5)
PR	1 (25)	5 (62.5)
SD	2 (50)	2 (25)
DCR	4 (100)	8 (100)
BRAFi+anti-PD-1 antibody	*n* = 11	*n* = 8
ORR	5 (45.5)	5 (62.5)
CR	2 (18.1)	4 (50)
PR	3 (27.3)	1 (12.5)
SD	5 (45.5)	3 (37.5)
PD	1 (9.1)	0
DCR	9 (90.9)	8 (100)

ORR, overall response rate; CI, confidence interval; CR, complete response; PR, partial response; SD, stable disease; PD, progressive disease; DCR, disease control rate; PFS, progression-free survival.

grade incidence of arthralgia (33.3 vs. 26.6%) and skin toxicity, especially rash (66.7 vs. 24%) and pruritus (50 vs. 10%), but less gastrointestinal AEs, including diarrhea (8.3 vs. 34%), nausea (25 vs. 36%), and vomiting (16.7 vs. 31%) (29, 30). There was little difference in the incidence of pyrexia (any grade) between the BARFi+MEKi group and the COMBI-V group (58 vs. 55%). In the BRAFi+MEKi group, the most common grade 3 AE was pyrexia (16.7%), while it was less frequent (4.6%) in the COMBI-V study. Moreover, grade 3 hypertension (15.8%) was more frequent in the COMBI-V study compared to the Chinese patients included in this study.

Recently, a clinical trial evaluating dabrafenib (300 mg twice daily), trametinib (2 mg once daily), and pembrolizumab (2 mg/kg every 3 weeks) was conducted in 60 patients with *BRAF V600E/K*-mutated metastatic melanoma. It was suggested that this triple-combined therapy might benefit a subset of Caucasian patients with manageable AEs (20). Compared with the triple-drug combination group, the BRAFi+anti-PD-1 antibody group had higher AEs of different grades (100 vs. 98.3%) and lower AEs of grades 3–4 (58 vs. 70%). The most common AEs in our BRAFi+anti-PD-1 antibody group were skin-related toxicities, with an incidence of up to 95%, and included rash (84.2%), pruritus (63.2%), and palmoplantar erythrodysesthesia (42.1%), followed by arthralgia (84.2%), fatigue (47.4%), and increased ALT or AST (26.3%) levels. However, in the triple-combination therapy, pyrexia (80%) was the most frequent AE, followed by rash (41.7%), diarrhea (40%), and nausea (35%). Pyrexia in our BRAFi+anti-PD-1 antibody group was clearly less frequent compared to the triple-combined therapy (any grade: 21 vs. 80%, grade 3: 5 vs. 11.7%), which was probably was due to the absence of MEKi and sequential therapy in our study. Severe treatment-related AEs also differed between the two groups. In this study, the most common grade 3 AEs were rash (36.8%) and arthralgia (15.8%), compared to increased ALT or AST levels (15%) and pyrexia in the triple-combination therapy. In addition, six patients (31.6%) in our group experienced increased bilirubin levels, which were not reported in the triple-drug combination clinical trial. Most severe AEs in the BRAFi+anti-PD-1 antibody group could be alleviated by temporarily interrupting treatment and subsequently reducing the dose of vemurafenib; however, four patients (21%) were still unable to tolerate this treatment. Compared to this study, 25 Caucasians (41.7%) in the triple-combined therapy group discontinued treatment and six of them terminated the therapy due to grade 3–4 increased AST or ALT levels. Compared with the triple-drug combination therapy, hepatotoxicity in the BRAFi+anti-PD-1 antibody group was mostly grade 1–2, which could be alleviated by symptomatic liver protection treatment. The reasons for interrupting the treatment were severe skin or arthralgia toxicity 1 or 2 weeks after starting the therapy. Overall, 94.7% of patients in the BRAFi+anti-PD-1 antibody group underwent dose reduction of vemurafenib, which might have contributed to the reduced incidence of subsequent severe hepatotoxicity.

From the above data, it may be concluded that the tolerance level of the BRAFi +PD-1 antibody regimen by Chinese patients was acceptable. A similar conclusion could be drawn from another phase I triple-drug trial on 15 Caucasians when compared with this study (21).

We defined trHE as an increase of either ALT, AST, or bilirubin. However, distinguishing these laboratory indicators based on either the treatment induced or liver metastasis is discussed below. First, 18 patients had normal ALT, AST, and bilirubin levels before starting treatment with BRAFi or BRAFi-based combinations and did not receive any other medicines that potentially lead to liver injury. Further, trHE was reported after receiving treatment. trHE was relieved after receiving hepatoprotective drugs. Second, four patients had liver metastasis before experiencing trHE, and there was no evidence about the progression of their liver metastasis while experiencing trHE. The remaining patients did not experience any liver metastasis either before or after trHE as determined by imaging studies. In addition, only one patient had a history of hepatitis B, and the DNA load of the hepatitis B virus showed no significant enhancement. Finally, none of the patients experienced a secondary trHE in subsequent treatment. However, these phenomena might have resulted from our small sample size and short observation time.

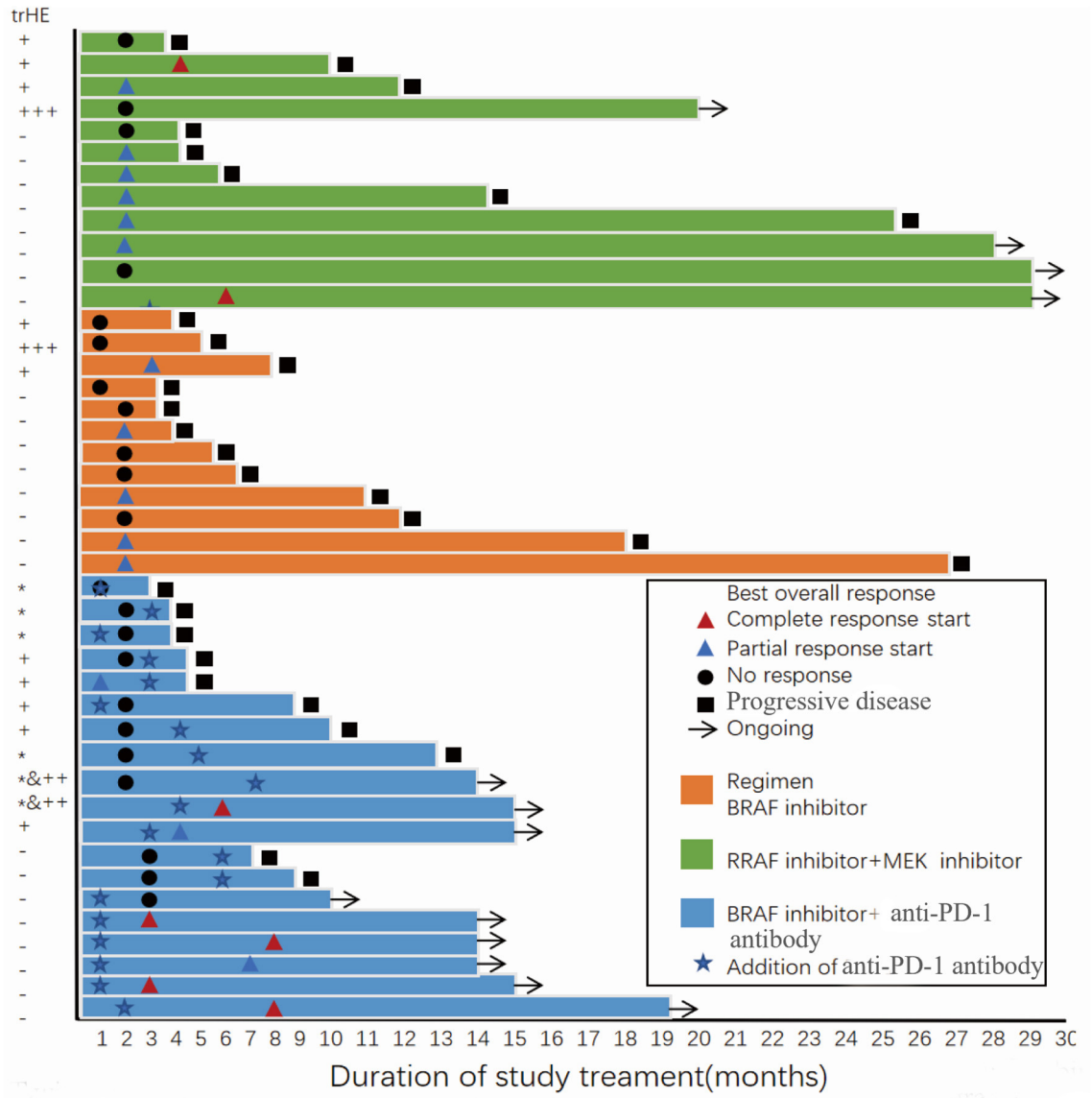

FIGURE 2 | Progression-free survival and best overall response of all patients in the two groups with or without treatment-related hepatotoxicity. trHE, treatment-related hepatotoxicity defined as the increase of either ALT, AST, or bilirubin levels; +, grade 1 increase of either ALT or AST level; + + +, grade 3 increase of either ALT or AST level; *, grade 1 increase of bilirubin; ++&*, concomitant increase of bilirubin (grade 1) and either ALT or AST (grade 2).

Patients experiencing trHE had shorter PFS and lower ORR, which we speculated occurred for the following possible reasons. First, different prognosis may be influenced by the general condition of the patient, staging, liver involvement, basic liver metastasis, and treatment. Further analysis showed that there was no statistical difference between the two groups (with or without trHE) in terms of age, first-line treatment, LDH level, lesion number, and other basic status indicators (**Supplementary Table 2**). Second, glycyrrhizic acid, a hepatoprotective drug and the main ingredient of compound glycyrrhizin glucoside [stronger neo-minophagen C (SNMC)], has anti-inflammatory and anti-allergic effects and exhibits steroidal hormone-like properties (31). Thus, glycyrrhizic acid may be a potential inhibitor of the immune response. In this study, three patients (in each of the three groups) were treated with SNMC for trHE and all of them achieved SD. Due to the limited sample size, it was difficult to determine the positive or negative effect of SNMC. Finally, we questioned the impact of reducing vemurafenib or treatment termination on the prognosis of patients in the trHE group. However, after analysis, in the BRAFi group, we found that only one patient with trHE had received a reduced dose of vemurafenib. The best response of the patient was PR, and his PFS was 6 months, which reached the general PFS observed with BRAFi monotherapy. No other patient had terminated treatment. In the BRAFi+anti-PD-1 antibody group, trHE did not lead to discontinuation. Only one patient

required a dose reduction of vemurafenib due to trHE. He had SD, which was maintained up to the follow-up deadline (PFS = 14 months).

The present study has some limitations, such as treatment selection bias due to the retrospective nature of the study, the single-center analysis, and the small study sample. Essentially, the underlying mechanism of hepatotoxicity induced by BRAFi and BRAFi-based combined regimens and its relationship with treatment outcomes need to be further explored.

In conclusion, in this study, treatment-related AEs in the Chinese population receiving BRAFi and BRAFi-based regimens were generally consistent with those reported in Caucasians, although the occurrence of grade 3 AEs was lower in Chinese patients. The trHE in patients receiving BRAFi and BRAFi-based regimens may indicate a poor treatment-related prognosis.

DATA AVAILABILITY STATEMENT

The original contributions presented in the study are included in the article/**Supplementary Material**, further inquiries can be directed to the corresponding author/s.

ETHICS STATEMENT

The studies involving human participants were reviewed and approved by Ethics Committee of Sun Yat-sen University Cancer Center, Sun Yat-sen University. The patients/participants provided their written informed consent to participate in this study.

AUTHOR CONTRIBUTIONS

X-sZ: study design and concepts. XL, J-jL, D-sW, X-zW, D-dL, YD, J-hW, and HJ: data acquisition. XL and J-jL: quality control of data, algorithms, data analysis, and interpretation. XL: statistical analysis, manuscript preparation, and manuscript editing. All authors read and approved the final manuscript.

FUNDING

This work was supported by the National Natural Science Foundation of China (81772910) and Guangzhou Health and Family Planning Commission Technology Project (20191A1515011263).

SUPPLEMENTARY MATERIAL

The Supplementary Material for this article can be found online at: https://www.frontiersin.org/articles/10.3389/fonc.2021.582676/full#supplementary-material

REFERENCES

1. Chi Z, Li S, Sheng X, Si L, Cui C, Han M, et al. Clinical presentation, histology, and prognoses of malignant melanoma in ethnic Chinese: a study of 522 consecutive cases. *BMC Cancer.* (2011) 11:85. doi: 10.1186/1471-2407-11-85
2. Blank CU, Larkin J, Arance AM, Hauschild A, Queirolo P, Del Vecchio M, et al. Open-label, multicentre safety study of vemurafenib in 3,219 patients with BRAF(V600) mutation-positive metastatic melanoma: 2-year follow-up data and long-term responders' analysis. *Eur J Cancer.* (2017) 79:176–84. doi: 10.1016/j.ejca.2017.04.007
3. Chapman PB, Robert C, Larkin J, Haanen JB, Ribas A, Hogg D, et al. Vemurafenib in patients with BRAFV600 mutation-positive metastatic melanoma: final overall survival results of the randomized BRIM-3 study. *Ann Oncol.* (2017) 28:2581–7. doi: 10.1093/annonc/mdx339
4. Sosman JA, Kim KB, Schuchter L, Gonzalez R, Pavlick AC, Weber JS, et al. Survival in BRAF V600-mutant advanced melanoma treated with vemurafenib. *N Engl J Med.* (2012) 366:707–14. doi: 10.1056/NEJMoa1112302
5. Ascierto PA, McArthur GA, Dreno B, Atkinson V, Liszkay G, Di Giacomo AM, et al. Cobimetinib combined with vemurafenib in advanced BRAF(V600)-mutant melanoma (coBRIM): updated efficacy results from a randomised, double-blind, phase 3 trial. *Lancet Oncol.* (2016) 17:1248–60. doi: 10.1016/S1470-2045(16)30122-X
6. Dummer R, Ascierto PA, Gogas HJ, Arance A, Mandala M, Liszkay G, et al. Encorafenib plus binimetinib vs. vemurafenib or encorafenib in patients with BRAF-mutant melanoma (COLUMBUS): a multicentre, open-label, randomised phase 3 trial. *Lancet Oncol.* (2018) 19:603–15. doi: 10.1016/S1470-2045(18)30142-6
7. Long GV, Eroglu Z, Infante J, Patel S, Daud A, Johnson DB, et al. Long-term outcomes in patients with BRAF V600-mutant metastatic melanoma who received dabrafenib combined with trametinib. *J Clin Oncol.* (2018) 36:667–73. doi: 10.1200/JCO.2017.74.1025
8. Cormier JN, Xing Y, Ding M, Lee JE, Mansfield PF, Gershenwald JE, et al. Ethnic differences among patients with cutaneous melanoma. *Arch Intern Med.* (2006) 166:1907–14. doi: 10.1001/archinte.166.17.1907
9. Sahoo MR, Gowda MS, Kaladagi RM. Primary amelanotic melanoma of the rectum mimicking adenocarcinoma. *Am J Case Rep.* (2013) 14:280–3. doi: 10.12659/AJCR.889089
10. Wang X, Si L, Guo J. Treatment algorithm of metastatic mucosal melanoma. *Chin Clin Oncol.* (2014) 3:38. doi: 10.3978/j.issn.2304-3865.2014.08.04
11. Chang JW, Yeh KY, Wang CH, Yang TS, Chiang HF, Wei FC, et al. Malignant melanoma in Taiwan: a prognostic study of 181 cases. *Melanoma Res.* (2004) 14:537–41. doi: 10.1097/00008390-200412000-00016
12. Cohen Y, Rosenbaum E, Begum S, Goldenberg D, Esche C, Lavie O, et al. Exon 15 BRAF mutations are uncommon in melanomas arising in non-sun-exposed sites. *Clin Cancer Res.* (2004) 10:3444–7. doi: 10.1158/1078-0432.CCR-03-0562
13. Maldonado JL, Fridlyand J, Patel H, Jain AN, Busam K, Kageshita T, et al. Determinants of BRAF mutations in primary melanomas. *J Natl Cancer Inst.* (2003) 95:1878–90. doi: 10.1093/jnci/djg123
14. Zhu YY, Si L, Chi ZH, Cui CL, Sheng XL, Li SM, et al. BRAF mutation in Chinese melanoma patients. *Chin Clin Oncol.* (2009) 14:585–8. doi: 10.3969/j.issn.1009-0460.2009.07.002
15. McArthur GA, Chapman PB, Robert C, Larkin J, Haanen JB, Dummer R, et al. Safety and efficacy of vemurafenib in BRAF(V600E) and BRAF(V600K) mutation-positive melanoma (BRIM-3): extended follow-up of a phase 3, randomised, open-label study. *Lancet Oncol.* (2014) 15:323–32. doi: 10.1016/S1470-2045(14)70012-9
16. Si L, Zhang X, Xu Z, Jiang Q, Bu L, Wang X, et al. Vemurafenib in Chinese patients with BRAF(V600) mutation-positive unresectable or metastatic melanoma: an open-label, multicenter phase I study. *BMC Cancer.* (2018) 18:520. doi: 10.1186/s12885-018-4336-3
17. Deken MA, Gadiot J, Jordanova ES, Lacroix R, van Gool M, Kroon P, et al. Targeting the MAPK and PI3K pathways in combination

with PD1 blockade in melanoma. *Oncoimmunology.* (2016) 5:e1238557. doi: 10.1080/2162402X.2016.1238557
18. Frederick DT, Piris A, Cogdill AP, Cooper ZA, Lezcano C, Ferrone CR, et al. BRAF inhibition is associated with enhanced melanoma antigen expression and a more favorable tumor microenvironment in patients with metastatic melanoma. *Clin Cancer Res.* (2013) 19:1225–31. doi: 10.1158/1078-0432.CCR-12-1630
19. Wilmott JS, Long GV, Howle JR, Haydu LE, Sharma RN, Thompson JF, et al. Selective BRAF inhibitors induce marked T-cell infiltration into human metastatic melanoma. *Clin Cancer Res.* (2012) 18:1386–94. doi: 10.1158/1078-0432.CCR-11-2479
20. Ascierto PA, Ferrucci PF, Fisher R, Del Vecchio M, Atkinson V, Schmidt H, et al. Dabrafenib, trametinib and pembrolizumab or placebo in BRAF-mutant melanoma. *Nat Med.* (2019) 25:941–6. doi: 10.1038/s41591-019-0448-9
21. Ribas A, Lawrence D, Atkinson V, Agarwal S, Miller WH Jr, Carlino MS, et al. Combined BRAF and MEK inhibition with PD-1 blockade immunotherapy in BRAF-mutant melanoma. *Nat Med.* (2019) 25:936–40. doi: 10.1038/s41591-019-0476-5
22. Sullivan RJ, Hamid O, Gonzalez R, Infante JR, Patel MR, Hodi FS, et al. Atezolizumab plus cobimetinib and vemurafenib in BRAF-mutated melanoma patients. *Nat Med.* (2019) 25:929–35. doi: 10.1038/s41591-019-0474-7
23. Robert C, Karaszewska B, Schachter J, Rutkowski P, Mackiewicz A, Stroiakovski D, et al. Improved overall survival in melanoma with combined dabrafenib and trametinib. *N Engl J Med.* (2015) 372:30–9. doi: 10.1056/NEJMoa1412690
24. Lacouture ME, Duvic M, Hauschild A, Prieto VG, Robert C, Schadendorf D, et al. Analysis of dermatologic events in vemurafenib-treated patients with melanoma. *Oncologist.* (2013) 18:314–22. doi: 10.1634/theoncologist.2012-0333
25. Carlos G, Anforth R, Clements A, Menzies AM, Carlino MS, Chou S, et al. Cutaneous toxic effects of BRAF inhibitors alone and in combination with MEK inhibitors for metastatic melanoma. *JAMA Dermatol.* (2015) 151:1103–9. doi: 10.1001/jamadermatol.2015.1745
26. Eigentler TK, Ghoreschi K, Berneburg M, Garbe C. Evaluation of photosensitivity in dabrafenib treated metastatic melanoma patients: results from a phase IIa study. *J Clin Oncol.* (2016) 34(suppl.):e21077. doi: 10.1200/JCO.2016.34.15_suppl.e21077
27. Flaherty KT, Puzanov I, Kim KB, Ribas A, McArthur GA, Sosman JA, et al. Inhibition of mutated, activated BRAF in metastatic melanoma. *N Engl J Med.* (2010) 363:809–19. doi: 10.1056/NEJMoa1002011
28. Yamazaki N, Kiyohara Y, Sugaya N, Uhara H. Phase I/II study of vemurafenib in patients with unresectable or recurrent melanoma with BRAF(V) (600) mutations. *J Dermatol.* (2015) 42:661–6. doi: 10.1111/1346-8138.12873
29. Heinzerling L, Eigentler TK, Fluck M, Hassel JC, Heller-Schenck D, Leipe J, et al. Tolerability of BRAF/MEK inhibitor combinations: adverse event evaluation and management. *ESMO Open.* (2019) 4:e000491. doi: 10.1136/esmoopen-2019-000491
30. Schadendorf D, Long GV, Stroiakovski D, Karaszewska B, Hauschild A, Levchenko E, et al. Three-year pooled analysis of factors associated with clinical outcomes across dabrafenib and trametinib combination therapy phase 3 randomised trials. *Eur J Cancer.* (2017) 82:45–55. doi: 10.1016/j.ejca.2017.05.033
31. Yu ZQ YB, Wang Y, Chen LY, Bi MR, Wang FX, Ma YJ. Protective effect of Stronger Neo-Minophagen C on patients with fulminant liver failure. *Shijie Huaren Xiaohua Zazhi.* (2006) 14:1318-22. doi: 10.3969/j.issn.1009-3079.2006.13.016

Conflict of Interest: The authors declare that the research was conducted in the absence of any commercial or financial relationships that could be construed as a potential conflict of interest.

frontiers in Oncology

ORIGINAL RESEARCH
published: 12 April 2021
doi: 10.3389/fonc.2021.621430

Identification of Hub Genes Associated With Melanoma Development by Comprehensive Bioinformatics Analysis

Jie Jiang, Chong Liu, Guoyong Xu, Tuo Liang, Chaojie Yu, Shian Liao, Zide Zhang, Zhaojun Lu, Zequn Wang, Jiarui Chen, Tianyou Chen, Hao Li and Xinli Zhan *

Spinal Orthopedic Ward, The First Clinical Affiliated Hospital of Guangxi Medical University, Nanning, China

Introduction: This study aimed to identify important genes associated with melanoma to further develop new target gene therapies and analyze their significance concerning prognosis.

Materials and methods: Gene expression data for melanoma and normal tissue were downloaded from three databases. Differentially co-expressed genes were identified by WGCNA and DEGs analysis. These genes were subjected to GO, and KEGG enrichment analysis and construction of the PPI visualized with Cytoscape and screened for the top 10 Hub genes using CytoHubba. We validated the Hub gene's protein levels with an immunohistochemical assay to confirm the accuracy of our analysis.

Results: A total of 435 differentially co-expressed genes were obtained. Survival curves showed that high expression of FOXM1,\ EXO1, KIF20A, TPX2, and CDC20 in melanoma patients with 5 of the top 10 hub genes was associated with reduced overall survival (OS). Immunohistochemistry showed that all five genes were expressed at higher protein levels in melanoma than in paracancerous tissues.

Conclusion: FOXM1, EXO1, KIF20A, TPX2, and CDC20 are prognosis-associated core genes of melanoma, and their high expression correlates with the low prognosis of melanoma patients and can be used as biomarkers for melanoma diagnosis, treatment, and prognosis prediction.

Keywords: melanoma, weighted gene co-expression network analysis, differential expression gene analysis, biomarker, predict prognosis, immunohistochemistry

OPEN ACCESS

Edited by:
Igor Puzanov, University at Buffalo, United States

Reviewed by:
Jennifer Yunyan Zhang, Duke University, United States
Gagan Chhabra, University of Wisconsin-Madison, United States

***Correspondence:**
Xinli Zhan
zhanxinli_215@163.com

Specialty section:
This article was submitted to Skin Cancer, a section of the journal Frontiers in Oncology

Received: *26 October 2020*
Accepted: *19 March 2021*
Published: *12 April 2021*

Citation:
Jiang J, Liu C, Xu G, Liang T, Yu C, Liao S, Zhang Z, Lu Z, Wang Z, Chen J, Chen T, Li H and Zhan X (2021) Identification of Hub Genes Associated With Melanoma Development by Comprehensive Bioinformatics Analysis. Front. Oncol. 11:621430. doi: 10.3389/fonc.2021.621430

INTRODUCTION

Melanoma, a highly malignant tumor originating from melanocytes, most commonly occurs in the skin and can evolve from a congenital benign cell nevus or develop from a dysplastic nevus. According to a 2014 article on the epidemiology of melanoma: men are about 1.5 times more likely to develop melanoma than women; the development of malignant melanoma may be associated with changes in external environmental factors (e.g., UV exposure) (1). In the past few years, the primary means of treating melanoma have included: surgery, medication, and radiation therapy (2). A review of the literature on microsurgery versus extensive local excision for melanoma showed that after controlling for potential confounding variables, patients treated for melanoma with microsurgery were more likely to be alive at five years than those treated for melanoma with extensive local excision (3). Despite the many treatment options for melanoma, patient survival is still limited.

In recent years, with the rapid development of bioinformatics technology, bioinformatics has become increasingly popular for studying the molecular mechanisms of diseases and discovering disease-specific biomarkers that are increasingly being used to diagnose and treat diseases accurately (4–6). Weighted gene co-expression network analysis (WGCNA), one of the bioinformatics analysis methods, describes co-expression patterns between genes in microarray samples, providing new insights for predicting the function of co-expressed genes and the development of diseases (7). Differentially expressed genes(DEGs) are widely used in cancer research and are excellent cancer research methods (8–10). It provides a genomics-based method for discovering changes in gene expression levels between experimental and control groups (11). We could look for potential disease-related biomarkers in genes with significant differences in gene expression. Thus, we have combined the two approaches by combining genes from relevant modules obtained by the WGCNA method with differentially expressed genes to enhance the discrimination of genes that are expected to be candidate markers of disease.

In this study, in order to obtain melanoma hub genes, we analyzed melanoma mRNA expression data downloaded from the UCSC database, GTEx database, and GEO database by WGCNA method and differential expression gene method. We further verified our analysis's accuracy and reliability by GO enrichment analysis, KEGG pathway enrichment analysis, protein-protein functional interaction network (PPI), survival analysis, and immunohistochemistry experiments to validate the results obtained from the analysis.

MATERIALS AND METHODS

Data Download

Gene expression data for melanoma were downloaded from UCSC Xena (http://xena.ucsc.edu/) and the GEO database (https://www.ncbi.nlm.nih.gov/gds/). Furthermore, we downloaded all the data and corresponding clinical information on melanoma from the UCSC Xena database free of charge. Data downloaded from the UCSC Xena database contained 471 melanoma samples; gene expression data for 813 normal skin samples were downloaded from the GTEx database (https://www.gtexportal.org/home/); the number of melanoma cases for which all clinical information was complete was 322. In total, 55,188 genes were included in our acceptance of our subsequent analysis. On the other hand, we downloaded melanoma sample GSE3189 from the GEO database, a dataset containing 45 melanoma samples, 18 nevus samples, and 7 normal skin samples (12). We removed 18 moles from the sample. This dataset was studied using the platform GPL96 [HG-U133A] Affymetrix Human Genome U133A Array. Based on the manufacturer's annotation files, we converted the probe files into gene symbols and removed duplicate probes, all expression data were transformed by log2, and the data were standardized. Eventually, a total of 12,549 genes were included for our subsequent analysis.

Using WGCNA to Identify Key Co-Expression Modules

WGCNA is a framework for establishing and analyzing weighted gene co-expression networks and is a widely used bioinformatics analysis method that uses the interrelationship between two variables to study biological networks. In this study, all statistical analysis operations were performed based on R (x64 version 4.0.2). We used the R package (WGCNA) to construct a gene co-expression network from the gene expression data of melanoma from UCSC Xena and the gene expression data of melanoma data of GSE3189 from the GEO database (7). To construct the scale-free network, we use the R command: softPower =sft$powerEstimate, which commands R to automatically select the optimal power value, which ends up with a soft threshold of 12 for the UCSC Xena database and 5 for the GEO database. We then construct the adjacency matrix by the following formula: a_{ij} = power (S_{ij}, β) = $|S_{ij}|$^β (a_{ij} denotes the adjacency matrix between gene i and gene j; S_{ij} denotes a similarity matrix completed by Pearson correlations for all gene pairs.; β denotes the soft threshold). Subsequently, we calculated the degree of dissimilarity between the nodes and converted the adjacency matrix into a TOM matrix. After that, we identified gene networks/modules using a dynamic shear tree algorithm. We correlated previously computed module features with clinical features to investigate the co-expression network's functional modules further. As a result, the modules that were subsequently selected were closely correlated with clinical features and were selected by us for subsequent analyses. More detailed methods have been elucidated in detail by previous researchers (7).

Identification of Differentially Expressed Genes and Selection of Significantly Expressed Modules

We used the R package (Limma) to perform differentially expressed genes (DEGs) analysis on gene expression data from both databases (13). To identify DEGs between melanoma and normal tissues, we performed the differential analysis of gene

Abbreviations: WGCNA, Weighted gene co-expression network analysis; DEGs, Differentially expressed genes; PPI, protein-protein functional interaction network; GO, Gene Ontology; CC, Cellular component; BP, Biological process; MF, Molecular function; OS, overall survival.

expression matrices from the two databases using the limma package, respectively. Cut off value was set to |logFC|>=1, adjusted P-value<0.05. We then used the R package (pheatmap) to construct heat maps of the DEGs filtered from the two databases; the R package (ggplot2) to plot the DEGs volcanoes. Next, co-expression genes extracted from the co-expression network overlapped with DEGs were used to identify potential prognostic genes. The overlapping portions of genes were used for subsequent analysis using the R package (VeenDiagram) (14)to visualize and plot the genes' overlapping portions into Veen diagrams.

GO Enrichment Analysis and KEGG Pathway Enrichment Analysis of Target Genes

To explore the overlapping parts of Gene Ontology (GO) (15) and KEGG pathway enrichment analysis (16), we used the R package (clusterProfiler, org.Hs.eg.db, enrichplot, ggplot2) (17) for analysis and visualization. The cut off value is set to p-value<0.05. The GO enrichment analysis consists of three main panels, namely Cellular component (CC), Biological process (BP), and Molecular function (MF). KEGG pathway enrichment analysis was mainly enriched in Melanoma, Transcriptional misregulation in cancer.

Construction of Protein-Protein Interaction Networks and Screening of Hub Genes

We used the STRING (https://string-db.org/) (18) online database to construct protein-protein interaction (PPI) networks for overlapping partial genes. Subsequently, the resulting PPI network is imported into Cytoscape (v3.8.0) to visualize the PPI. We used a plugin in Cytoscape (CytoHubba) (19) to find Hub genes in these genes. We used the MCC algorithm, and the top 10 genes obtained to the MCC algorithm were used as the central genes for our study.

The Relationship Between Hub Genes and Prognosis, and Their Expression in Various Subgroups

In this study, to verify Hub genes' reliability, we used information from patients whose clinical information was complete for survival analysis. All patients were divided into two groups based on Hub genes' median expression value, with patients greater than or equal to the median value assigned to the high expression group and patients less than the median value assigned to the low expression group. We plotted the Kaplan-Meier univariate survival analysis of overall survival (OS) using the R package (survival, survminer) for the top 10 hub genes. To further explore the effect of Hub genes on prognosis, we analyzed the relationship between five Hub genes and survival status and survival time using multivariate COX regression and constructed a prognostic model. We calculated the risk value of each patient and included patients with higher than average risk values in the high-risk group and those with lower or equal risk values in the low-risk group, and subsequently plotted Kaplan-Meier curves according to the high-risk and low-risk groups. Subsequently, we analyzed the top 10 Hub genes concerning disease-free survival using the online database GEPIA2 (http://gepia.cancer-pku.cn/). After that, we explored the differential expression of Hub genes in cancer and normal tissues, plotting each Hub genes' expression levels in different subgroups between cancer and normal tissues as a box line graph.

Immunohistochemistry

We used tumor sections and normal skin sections of melanoma patients who underwent surgical treatment at the First Clinical Affiliated Hospital of Guangxi Medical University for immunohistological studies, which were approved by the Ethics Department of the First Clinical Affiliated Hospital of Guangxi Medical University and conformed to the World Medical Association Declaration of Helsinki. We performed immunohistological analysis of six pairs (melanoma and normal skin) of pathological sections for each gene. Immunohistochemical staining of formalin-fixed melanoma tissue samples and paraffin-embedded and paracancerous tissue samples were performed. The FOXM1 and TPX2 antibodies for immunohistochemical staining were purchased from the Abcam; the KIF20A antibody was purchased from the Bioss; the CDC20 antibody was purchased from the Proteintech; the EXO1 antibody was purchased from the Abclonal. After removing paraffin, hydration, and sealing, the specimens were mixed with anti-FOXM1, KIF20A, TPX2, CDC20, and EXO1 and incubated overnight at 4°C (dilution ratios of 1:250, 1:200, 1:4000, 1:300, 1:100, respectively). Finally, in order to calculate the positivity rate of immunohistology images more precisely, we performed statistical analysis of images from immunohistology studies using Image J software. We then performed statistical analysis of the immunohistological positive rate for melanoma and the immunohistological positive rate for normal skin samples using the paired sample mean t-test in IBM SPSS Statistics 25 software. Finally, we use GraphPad Prism 8 to visualize the statistical results.

RESULTS

Construction of Weighted Gene Co-Expression Modules

To identify modules associated with prognosis in patients with melanoma, we performed gene co-expression network analysis of gene expression matrices from the UCSC Xena database and GSE3189 using the WGCNA package. There are six co-expression modules constructed from UCSC Xena database expression data (**Figure 1A**) and seven co-expression modules constructed from GSE3189 (**Figure 2A**), not including the grey module cluster to which it is assigned. We developed a heat map module features' relationship, which was used to assess each co-expression module's relationship with two clinical features (normal and cancer). The two modules' features are shown in **Figure 1B** and **Figure 2B**. From the pictures, we can find that the highest correlation between the magenta module in UCSC Xena and the blue module in GSE3189 and normal organization (magenta module: r=-0.98,

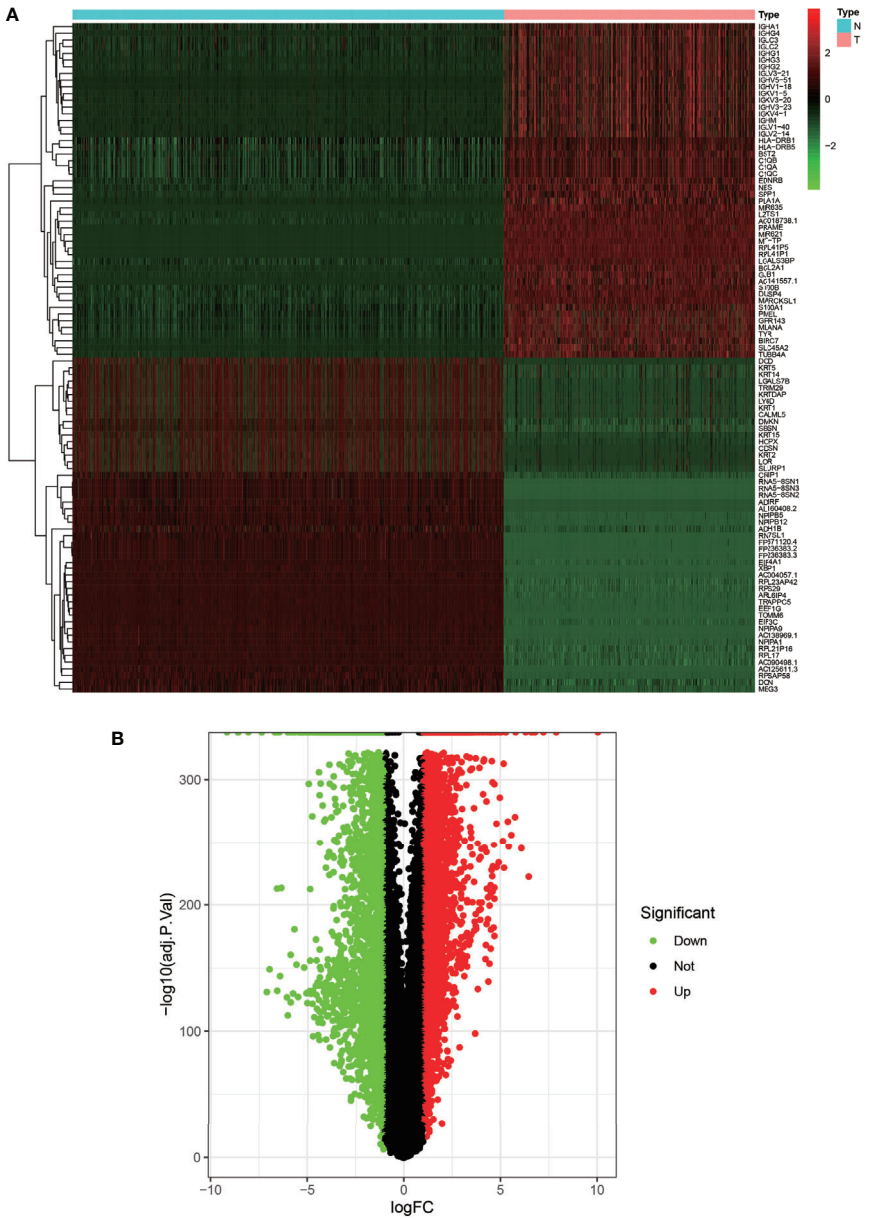

FIGURE 1 | Heat map and volcano map of DEGs from the UCSC Xena database. **(A)** Heat map of the top 50 upregulated and top 50 down-regulated DEGs obtained from the identification. The red part indicates upregulated genes, and the green part indicates down-regulated genes. **(B)** Volcano plot with cut off value set to |logFC|>1,P-value<0.05. Red dots indicate upregulated genes, green dots indicate down-regulated genes, and black represents non-significant genes.

P-value<1e-200; blue module: r=-0.96, P-value<1e-200). Therefore, we extracted the genes from these two modules to further dig deeper into the useful information in them.

Identification of DEGs and Gene Identification With Co-Expression Modules

We set the cut-off value for DEGs as |logFC|>=1, adjusted P-value<0.05, and a total of 6609 DEGs were identified in the UCSC Xena dataset; heat maps and volcanoes of DEGs are shown in **Figure 3**; 6223 DEGs were identified in the GSE3198 dataset; heat maps and volcanoes of differential genes See **Figure 4**. We present the top 100 differentially expressed genes calculated from the GEO database in **Table 1**; the top 100 differentially expressed genes calculated from the UCSC Xena database are presented in **Table 2**. Genes from the magenta module in UCSC Xena and genes from the blue module in GSE3189, as well as DEGs from both databases, yielded a total of 435 overlapping genes extracted for subsequent analysis (**Figure 5**).

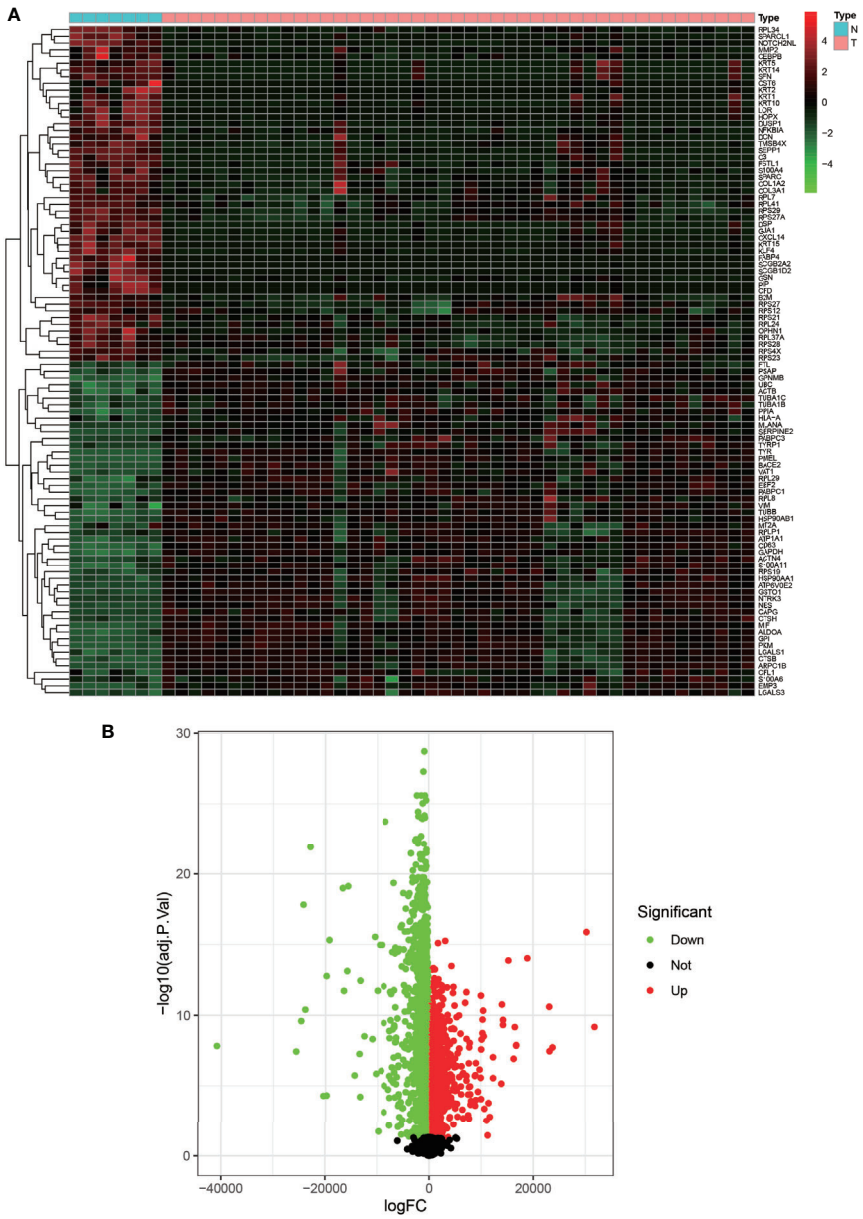

FIGURE 2 | Heat map and volcano map of GSE3189. **(A)** Heat map of the top 50 upregulated and top 50 down-regulated DEGs obtained from the identification. The red part indicates upregulated genes, and the green part indicates down-regulated genes. **(B)** Volcano plot with cut off value set to |logFC|>1,P-value<0.05. Red dots indicate upregulated genes, green dots indicate down-regulated genes, and black represents non-significant genes.

GO Enrichment Analysis of 435 Genes and KEGG Pathway Enrichment Analysis

We performed GO enrichment analysis, and KEGG pathway enrichment analysis further explores the 435 genes' potential functions in the overlapping sections. We learned from the GO enrichment analysis that BP was primarily enriched in neutrophil degranulation and neutrophil activation involved in the immune response. CC was mainly enriched in vacuolar and lysosomal membranes. MF was mainly enriched in histone deacetylase binding and integrin-binding (**Figure 6A**). KEGG pathway enrichment analysis was mainly distributed in the melanoma, Transcriptional misregulation in cancer, and Mismatch repair pathways (**Figure 6B**).

PPI Construction and Hub Gene Identification

We imported 435 genes from the overlapping parts into the STRING online database to obtain the PPI network. Subsequently, the PPI network was imported into Cytoscape software to visualize the PPI (**Figure 7A**) using the MCC

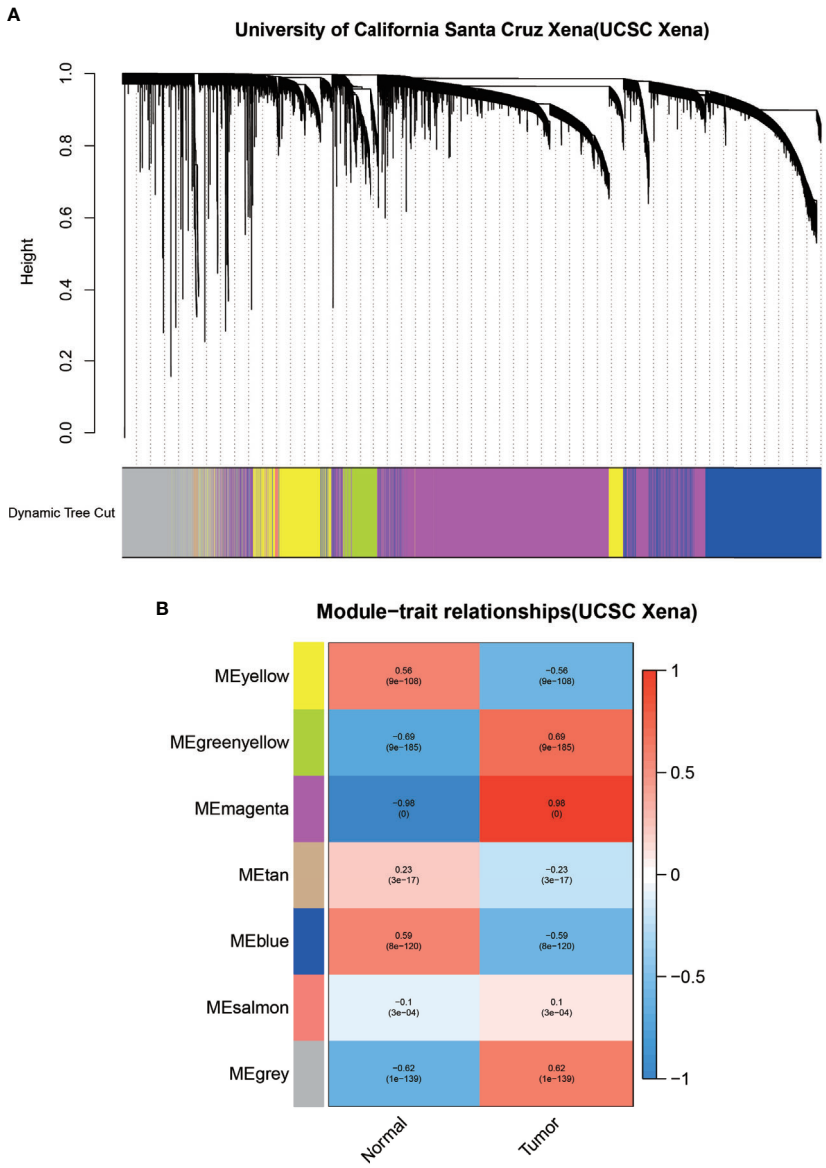

FIGURE 3 | Identification of modules associated with clinical information in the UCSC Xena database. **(A)** Clustered tree diagram of co-expression network modules sorted by gene-level clustering of matrices obtained by Equation 1-TOM. Each color represents a different co-expressed gene. **(B)** Relationship diagram of the features of the modules. Each row corresponds to a color module, and each column corresponds to a clinical feature (normal and cancer). Each cell contains the correlation and P-value of the corresponding module.

algorithm in the CytoHuba plugin to filter the top 10 Hub genes from the PPI network (**Figure 7B**). We ranked the top 10 Hub genes based on their MCC algorithm scores, which were Aurora Kinase B (AURKB), Exonuclease 1 (EXO1), Kinesin Family Member 20A (KIF20A), TPX2 Microtubule Nucleation Factor (TPX2), Assembly Factor For Spindle Microtubules(ASPM), Mitotic Arrest Deficient 2 Like 1 (MAD2L1), Forkhead Box M1(FOXM1), Cell Division Cycle 20(CDC20), Non-SMC Condensin I Complex Subunit H(NCAPH), Baculoviral IAP Repeat Containing 5(BIRC5).

Prognostic Value of Hub Genes and Validation of Protein Expression

We further analyzed the top 10 Hub genes (AURKB, EXO1, KIF20A, TPX2, ASPM, MAD2L1, FOXM1, CDC20, NCAPH, BIRC5) that were screened by the CytoHubba plugin. We analyzed the relationship between the top 10 Hub genes and prognosis separately and plotted univariate survival curves for overall survival using the R package based on the Kaplan-Meier method. Kaplan-Meier analysis showed (**Figure 8**) that 5 of the top 10 Hub genes (FOXM1, EXO1, KIF20A, TPX2, CDC20)

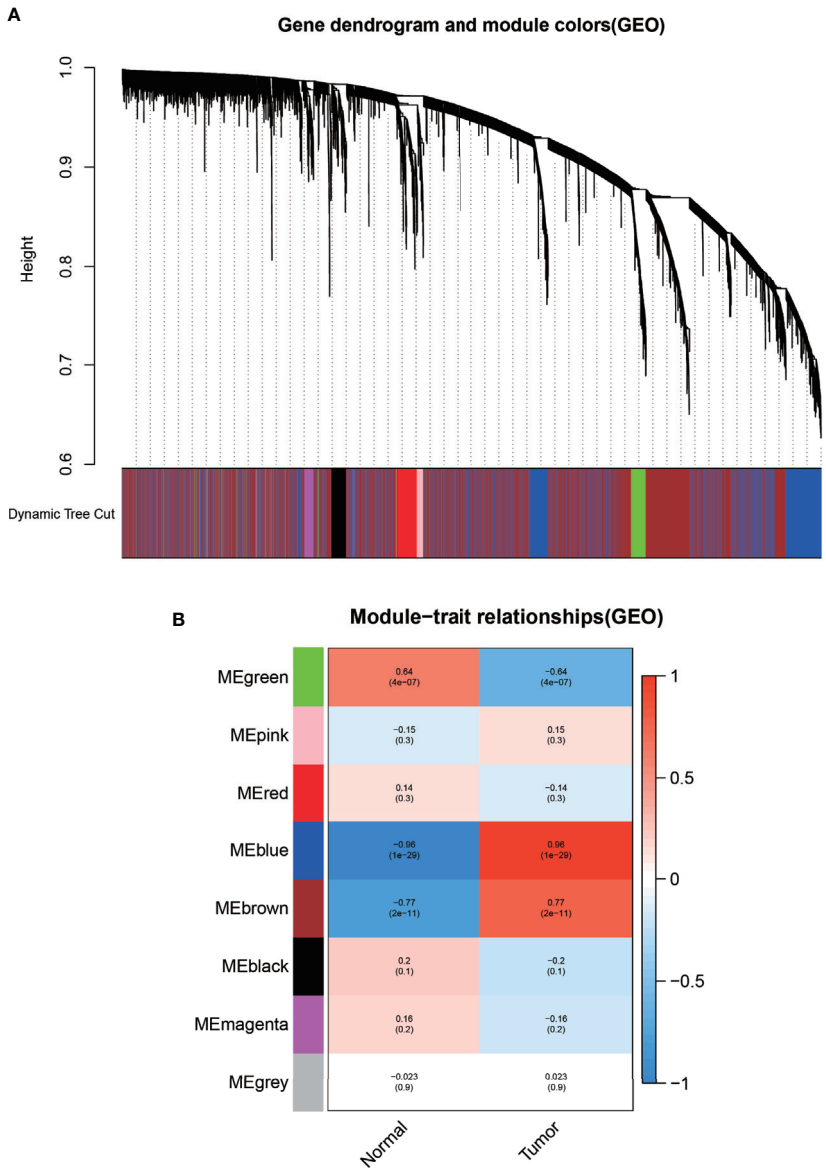

FIGURE 4 | Identification of modules related to clinical information in the GSE3189 database. **(A)** Clustered tree diagram of co-expression network modules sorted by gene-level clustering of matrices obtained by Equation 1-TOM. Each color represents a different co-expressed gene. **(B)** Relationship diagram of the features of the modules. Each row corresponds to a color module, and each column corresponds to a clinical feature (normal and cancer). Each cell contains the correlation and P-value of the corresponding module.

were significantly correlated with prognosis ($p<0.01$), and that the relationship between all five hub genes and the prognosis of melanoma patients was such that high expression of the gene was accompanied by low patient Prognosis. In addition, we analyzed the survival curves of the prognostic models constructed based on these five Hub genes, as shown in **Figure 8K**. The survival rate in the high-risk group was much lower than that in the low-risk group, and the difference was statistically significant (P-value < 0.05). We used the GEPIA2 database to predict disease-free survival for the top 10 Hub genes, and the predictions are shown in **Figure 9**. We divided all patients into two groups according to metastasis and primary status of the tumor. From **Figure 10A**, we found that the mean expression value of ASPM was significantly higher in the metastatic group than in the primary group (P-value<0.001); in **Figure 10B**, we found that the expression value of AURB was significantly higher in the primary group than in the metastatic group (P-value=0.003).

Immunohistochemistry

After a series of laboratory manipulations, we completed specific staining of all pathological tissue sections for labeled antibodies. All immunohistological images were observed

TABLE 1 | Top 100 differentially expressed genes from UCSC Xena database differential expression analysis.

id	logFC	AveExpr	t	P. Value	adj. P. Val	B
HSD11B2	-845.579	176.0964	-29.2765	1.53E-33	1.92E-29	-4.0536
BCAM	-1017.36	323.9158	-26.9444	8.18E-32	5.13E-28	-4.0592
METTL7A	-2269.49	605.8938	-24.4868	7.60E-30	2.55E-26	-4.06674
LMOD1	-734.009	145.4836	-24.383	9.28E-30	2.55E-26	-4.06711
PLLP	-1437.35	434.1048	-24.3356	1.02E-29	2.55E-26	-4.06728
C1orf116	-494.735	91.70493	-23.8478	2.63E-29	5.50E-26	-4.06905
CDC20	389.965	482.6639	4.868726	1.13E-05	5.12E-05	-4.42177
PDZD2	-1159.37	213.1139	-23.5115	5.11E-29	9.16E-26	-4.07034
NFIB	-2039.56	544.4306	-22.7616	2.31E-28	3.63E-25	-4.07338
RAI2	-816.532	222.9485	-22.4094	4.77E-28	6.66E-25	-4.07491
SOD3	-1970.04	667.2363	-22.299	6.00E-28	7.53E-25	-4.0754
CLDN8	-739.437	164.3889	-22.1417	8.33E-28	9.50E-25	-4.07611
EPB41L4B	-1068.95	305.8102	-22.0679	9.72E-28	1.02E-24	-4.07644
TCF7L2	-1366.23	604.587	-22.0259	1.06E-27	1.02E-24	-4.07664
COBL	-1201.85	249.6083	-21.9426	1.26E-27	1.13E-24	-4.07702
NOTCH2NL	-8409.06	2198.169	-21.6906	2.15E-27	1.80E-24	-4.07822
DDAH1	-1470.08	560.094	-20.5529	2.54E-26	2.00E-23	-4.08409
PTPRK	-2420.67	866.2715	-20.3232	4.24E-26	3.13E-23	-4.08537
AKR1C3	-2026.43	340.9329	-20.173	5.94E-26	3.95E-23	-4.08624
BLCAP	-2587.68	2066.668	-20.1707	5.98E-26	3.95E-23	-4.08625
MKL2	-2073.3	890.3276	-19.8971	1.11E-25	6.96E-23	-4.08786
FOXC1	-924.752	352.5952	-19.8629	1.20E-25	7.17E-23	-4.08807
SCGB2A2	-22896.1	3285.843	-19.6068	2.16E-25	1.23E-22	-4.08964
HLF	-432.825	163.8867	-19.397	3.50E-25	1.91E-22	-4.09096
GPRC5C	-452.72	116.5967	-19.1655	6.00E-25	3.14E-22	-4.09247
TPM1	-3431.4	1077.406	-19.1101	6.84E-25	3.43E-22	-4.09284
INHBB	-1629.71	542.9868	-19.015	8.55E-25	4.03E-22	-4.09347
KCNK5	-1100.18	338.3407	-19.0084	8.68E-25	4.03E-22	-4.09352
LPP	-1662.54	1114.69	-18.9759	9.38E-25	4.20E-22	-4.09374
BAG1	-1512.62	963.4278	-18.63	2.13E-24	9.04E-22	-4.09613
BBOX1	-1291.96	255.0336	-18.6242	2.16E-24	9.04E-22	-4.09617
NEBL	-609.949	272.7083	-18.4247	3.49E-24	1.41E-21	-4.0976
SEMA3G	-2467.01	524.8589	-18.2258	5.65E-24	2.21E-21	-4.09907
AOX1	-462.531	149.6399	-18.1128	7.44E-24	2.83E-21	-4.09992
OSR2	-1470.39	407.5353	-17.9596	1.08E-23	4.00E-21	-4.1011
AFF1	-921.029	598.5215	-17.915	1.21E-23	4.30E-21	-4.10145
ANK3	-626.259	224.7039	-17.9063	1.23E-23	4.30E-21	-4.10151
TNS1	-3044.64	867.9854	-17.7824	1.68E-23	5.69E-21	-4.10249
KIF20A	549.666	571.9327	5.727454	5.48E-07	3.36E-06	-4.37847
RNASE4	-1188.56	335.7413	-17.3161	5.38E-23	1.77E-20	-4.10632
KRT23	-1993.11	437.5972	-17.3038	5.55E-23	1.77E-20	-4.10642
TPD52L1	-3095.22	669.0397	-17.297	5.64E-23	1.77E-20	-4.10648
SYBU	-920.434	364.3275	-17.2781	5.92E-23	1.81E-20	-4.10664
ADRB2	-1071.55	319.8041	-17.2099	7.04E-23	2.10E-20	-4.10722
FBXW12	-2471.35	1018.696	-17.0651	1.02E-22	2.97E-20	-4.10848
NXN	-3120.53	896.8017	-16.9564	1.34E-22	3.83E-20	-4.10944
SLK	-1140.23	736.8274	-16.9376	1.41E-22	3.93E-20	-4.10961
NPR1	-306.481	115.5731	-16.9289	1.44E-22	3.93E-20	-4.10969
KLF4	-6760.93	1402.794	-16.8796	1.63E-22	4.36E-20	-4.11013
TACC2	-1660.96	469.7259	-16.6594	2.89E-22	7.53E-20	-4.11214
CFD	-15658.5	2463.293	-16.6522	2.94E-22	7.53E-20	-4.11221
MANSC1	-749.192	222.4662	-16.556	3.78E-22	9.47E-20	-4.11311
SCGB1D2	-16696.7	2299.639	-16.5155	4.20E-22	1.03E-19	-4.11349
CYP4F12	-834.366	226.1397	-16.4526	4.94E-22	1.19E-19	-4.11409
ARHGAP29	-1972.3	562.7853	-16.4261	5.30E-22	1.23E-19	-4.11435
PAPD7	-1521.75	1286.389	-16.426	5.30E-22	1.23E-19	-4.11435
HOXA5	-1120.97	339.1495	-16.1654	1.05E-21	2.34E-19	-4.1169
TPX2	844.8853	941.0447	6.308941	6.73E-08	5.11E-07	-4.35103
AKR1C1	-4886.37	1050.501	-16.1645	1.06E-21	2.34E-19	-4.11691
PGRMC2	-789.323	518.6895	-16.1623	1.06E-21	2.34E-19	-4.11693
DEFB1	-3728.94	773.1849	-16.1416	1.12E-21	2.43E-19	-4.11714
NISCH	-3781.98	2154.822	-16.1158	1.20E-21	2.55E-19	-4.1174
PID1	-660.945	181.8225	-16.0308	1.51E-21	3.15E-19	-4.11826

(Continued)

TABLE 1 | Continued

id	logFC	AveExpr	t	P. Value	adj. P. Val	B
ECHDC2	-2053.82	566.7756	-16.0213	1.54E-21	3.18E-19	-4.11835
ZNF721	-3930.63	1696.277	-15.9616	1.81E-21	3.66E-19	-4.11896
FZD10	-935.976	244.2876	-15.9546	1.84E-21	3.67E-19	-4.11904
FOXM1	407.8747	439.4756	4.447452	4.73E-05	0.000185	-4.44386
MGST2	-1763.19	647.3899	-15.9227	2.01E-21	3.94E-19	-4.11937
CLDN5	-1893.35	403.8225	-15.9111	2.07E-21	4.00E-19	-4.11948
PGF	-1363.34	863.4405	-15.8693	2.32E-21	4.40E-19	-4.11992
MYO5C	-2220.87	777.6688	-15.8323	2.56E-21	4.79E-19	-4.12031
RIOK3	-807.68	826.6529	-15.7848	2.91E-21	5.37E-19	-4.1208
SLIT3	-750.592	281.9049	-15.5706	5.19E-21	9.43E-19	-4.1231
DKFZP586I1420	-1528.75	783.6597	-15.5415	5.61E-21	1.01E-18	-4.12342
IRF6	-2781.83	874.8339	-15.4857	6.54E-21	1.15E-18	-4.12403
KLF2	-2970.81	1606.61	-15.4511	7.18E-21	1.25E-18	-4.12441
CA6	-3085.23	529.0964	-15.4115	8.00E-21	1.38E-18	-4.12485
EMX2	-455.309	100.5197	-15.3847	8.61E-21	1.46E-18	-4.12515
CXCL14	-24233.7	4778.02	-15.3585	9.25E-21	1.55E-18	-4.12544
PPAP2A	-2079.6	1113.894	-15.2372	1.29E-20	2.13E-18	-4.12682
MAST4	-2097.42	497.6463	-15.2144	1.37E-20	2.24E-18	-4.12708
CARD10	-205.013	117.4037	-15.1947	1.45E-20	2.33E-18	-4.12731
LAMA3	-1212.8	241.0786	-15.1253	1.76E-20	2.79E-18	-4.12811
TACSTD2	-4413.24	865.4007	-15.1017	1.88E-20	2.94E-18	-4.12838
LIMS2	-1426.29	640.6591	-15.077	2.01E-20	3.11E-18	-4.12867
FAM117A	-1093.53	570.1012	-15.0156	2.38E-20	3.65E-18	-4.1294
EXO1	205.6559	242.1595	5.043051	6.17E-06	2.97E-05	-4.41276
KRT18	-2757.63	602.0107	-14.9803	2.63E-20	3.97E-18	-4.12981
MYH11	-3199.73	525.7094	-14.9037	3.26E-20	4.86E-18	-4.13073
AZGP1	-2910.91	538.8767	-14.6937	5.87E-20	8.66E-18	-4.13329
KIAA0485	-632.996	214.483	-14.6163	7.30E-20	1.07E-17	-4.13426
PCNXL2	-186.091	153.767	-14.548	8.86E-20	1.28E-17	-4.13512
ATP6V0A4	-650.17	187.6908	-14.4758	1.09E-19	1.55E-17	-4.13604
PPP1CB	-868.475	534.1197	-14.4146	1.29E-19	1.82E-17	-4.13683
VWF	-3563.29	1541.653	-14.3503	1.56E-19	2.17E-17	-4.13767
SLC24A3	-519.411	131.0307	-14.3207	1.69E-19	2.33E-17	-4.13806
CHRDL1	-3642.25	614.9238	-14.3008	1.79E-19	2.44E-17	-4.13832
EFS	-860.828	247.5087	-14.284	1.88E-19	2.54E-17	-4.13854
N4BP2L2	-1182.53	803.6723	-14.2559	2.04E-19	2.72E-17	-4.13891
MAP3K4	-1498.72	670.2975	-14.2228	2.24E-19	2.96E-17	-4.13935

under an inverted microscope and images were collected, and we compared the staining differences between melanoma specimens and paraneoplastic tissue specimens. We performed immunohistological staining analysis on a total of 60 pathological tissue sections of six pairs (melanoma tissue and normal skin tissue) for each gene, and the positive rate of each image was counted using Image J software. After IBM SPSS Statistics 25 paired sample mean t-test, finally, we visualized the statistical results using GraphPad Prism 8. After analysis of 60 immunohistochemical images, we found that these five Hub genes were significantly more abundantly expressed in melanoma than in paraneoplastic tissue. This result also further validates the accuracy and validity of our bioinformatics analysis. We selected from 60 immunohistochemical images the images with the most significant differences between these 5 Hub genes in melanoma and paracancerous tissue in **Figures 11A1–M2**. In addition, we counted the positive rate of immunohistological images of six pairs of pathological tissue sections for each antibody separately, and from **Figures 11P–T** we found that the positive rate of immunohistochemical staining for these five genes in melanoma was significantly higher than that in paraneoplastic tissue, and the difference was statistically significant.

DISCUSSION

Melanoma is associated with many factors, is more common in light-skinned races, and has a family history of occurrence. Although melanoma treatment has improved from before, the prognosis for melanoma patients is low due to the lack of precise molecular markers. Therefore, there is an urgent need to identify better and more accurate biomarkers to utilize in the prognosis, diagnosis, and treatment of melanoma. In our study, we used integrated bioinformatics to analyze a total of 435 critical genes with co-expression trends identified in the UCSC Xena, GTEx database, and the GSE3189 database. These genes were subjected to GO enrichment analysis based on the R package (clusterProfiler), mainly enriched in neutrophil activation involved in immune response, stem cell division, and melanosome. As early as 2011, it was noted that there might be a close relationship between neutrophil activation and cancer (20). Moreover, the relationship between the stem cell division and melanosome and cancer has also been reported in the literature (21, 22). Similarly, these genes were subjected to KEGG pathway enrichment analysis based on the R package (clusterProfiler), and the enrichment results showed that

TABLE 2 | Top 100 differentially expressed genes from GEO database differential expression analysis.

id	logFC	AveExpr	t	P. Value	adj. P. Val	B
TOMM6	-6.70878	4.247851	-441.582	0	0	3210.479
EEF1G	-9.17482	6.273636	-358.094	0	0	2946.723
ARL6IP4	-5.34494	4.568667	-270.314	0	0	2593.078
U2AF1	-4.89304	3.189738	-267.824	0	0	2581.47
KIF20A	2.257505	2.184619	35.43105	2.64E-192	3.28E-191	428.7177
TRAPPC5	-5.2377	3.597862	-265.289	0	0	2569.541
DDX47	-4.1377	3.218522	-263.144	0	0	2559.36
AC026464.4	-4.12231	2.667977	-234.28	0	0	2413.931
AC008894.2	-3.89785	2.492557	-231.702	0	0	2400.115
ZNF410	-3.7731	3.023446	-226.448	0	0	2371.487
AC138969.1	-6.58451	4.261407	-224.402	0	0	2360.166
EIF4A1	-6.5225	5.862644	-219.31	0	0	2331.554
XBP1	-5.49276	3.477893	-217.59	0	0	2321.745
RPS29	-5.7619	8.791745	-217.216	0	0	2319.602
RPL41P1	7.895229	2.907401	210.3463	0	0	2279.615
SARNP	-4.32075	3.616277	-209.23	0	0	2273.003
C17orf49	-4.48374	3.787316	-208.004	0	0	2265.695
AP003108.2	-3.86539	2.574211	-207.004	0	0	2259.706
NPIPA9	-6.47004	4.114255	-205.125	0	0	2248.382
U2AF1L5	-4.59973	2.953342	-204.651	0	0	2245.511
AL445363.3	-3.97251	2.527661	-204.223	0	0	2242.909
PLSCR3	-4.35472	3.215705	-204.113	0	0	2242.24
MT-TP	10.04972	3.69955	203.6833	0	0	2239.626
AC004057.1	-8.07281	5.336825	-200.98	0	0	2223.05
UBE2V1	-3.5256	4.398678	-200.156	0	0	2217.955
EIF3CL	-4.40254	3.018283	-194.219	0	0	2180.647
CHMP4A	-4.13699	4.114164	-192.739	0	0	2171.174
RPL23AP42	-5.9686	6.903515	-192.172	0	0	2167.53
RBM34	-3.73833	3.315043	-189.086	0	0	2147.518
FAM156A	-4.2274	2.753841	-188.932	0	0	2146.508
PSMC1	-3.54821	4.637263	-186.871	0	0	2132.96
AC234031.1	-4.1459	2.626985	-185.406	0	0	2123.242
EIF3C	-5.4449	5.199535	-181.198	0	0	2094.928
NDST2	-3.18778	2.770728	-179.958	0	0	2086.466
RPL41P5	5.796619	2.135216	178.8032	0	0	2078.539
POLR2J3	-4.77323	3.508843	-175.214	0	0	2053.594
NPIPA1	-5.2232	4.152355	-173.431	0	0	2041.021
MIR621	5.055425	1.860197	171.4897	0	0	2027.203
RPL17	-5.68075	7.892466	-170.602	0	0	2020.837
CBWD3	-3.53714	2.282208	-170.004	0	0	2016.528
KLC1	-3.77402	4.474801	-168.533	0	0	2005.876
FOXM1	2.234867	2.87717	39.80523	2.75E-226	4.47E-225	506.9552
AC090498.1	-5.26043	8.372091	-167.292	0	0	1996.823
PSMA6	-3.37821	4.795774	-166.672	0	0	1992.276
OVCA2	-4.03462	2.55463	-165.63	0	0	1984.594
MIA2	-2.42462	2.010625	-163.757	0	0	1970.685
SKP1	-3.17494	6.591382	-163.588	0	0	1969.42
RNASEK	-4.25662	5.849365	-163.016	0	0	1965.143
BBS1	-2.78795	2.33777	-162.105	0	0	1958.295
RPL36A	-4.99421	7.771035	-161.219	0	0	1951.603
FP236383.3	-8.60309	5.458479	-157.818	0	0	1925.6
FP236383.2	-8.60554	5.457578	-157.788	0	0	1925.369
FP671120.4	-8.58582	5.464812	-156.76	0	0	1917.402
ANKHD1	-4.26189	3.413317	-155.416	0	0	1906.921
ACAD11	-3.32657	2.373162	-155.294	0	0	1905.971
CBWD5	-4.00438	2.944129	-152.563	0	0	1884.402
EEF1D	-3.77282	6.967246	-150.509	0	0	1867.955
GTF2IP1	-4.45164	3.217918	-147.968	0	0	1847.323
SLX1A	-3.90342	2.487477	-147.257	0	0	1841.492
AARSD1	-2.72754	3.419285	-146.946	0	0	1838.933
LIMD1-AS1	-2.12395	1.48131	-146.44	0	0	1834.767
MEMO1	-2.96218	2.820104	-146.034	0	0	1831.403
RBM4	-3.22088	4.409497	-145.28	0	0	1825.147

(Continued)

TABLE 2 | Continued

id	logFC	AveExpr	t	P. Value	adj. P. Val	B
TPX2	2.923316	3.337959	48.93582	1.21E-295	3.49E-294	666.6618
CBWD2	-2.6548	2.865867	-144.03	0	0	1814.718
ATRIP	-2.07223	1.378742	-143.514	0	0	1810.388
PSMA2	-3.10176	4.482894	-142.944	0	0	1805.587
CCZ1B	-3.28051	3.403163	-142.938	0	0	1805.538
CMC4	-2.51744	1.594191	-142.923	0	0	1805.411
TEN1	-4.06633	2.761896	-141.258	0	0	1791.289
INO80B-WBP1	-2.89703	1.857204	-141.116	0	0	1790.079
RPL39	-4.41911	8.980427	-141.005	0	0	1789.13
CBWD1	-3.30889	2.794308	-140.982	0	0	1788.929
TOP3B	-3.1789	2.223469	-140.981	0	0	1788.919
RPL21P16	-5.33883	6.932082	-139.741	0	0	1778.293
SNX15	-2.94194	2.13521	-139.636	0	0	1777.391
PDLIM2	-4.65201	4.800814	-139.272	0	0	1774.247
RPS15A	-3.63592	8.609921	-138.656	0	0	1768.919
SERF1B	-3.59774	2.582927	-137.965	0	0	1762.917
NPIPB5	-6.03868	4.198667	-137.514	0	0	1758.987
TREX1	-4.57687	2.897972	-135.122	0	0	1737.954
AC125611.3	-5.4162	3.434745	-134.031	0	0	1728.242
NDUFV2	-3.10642	4.693101	-133.939	0	0	1727.428
NPIPB3	-5.02126	3.613232	-133.427	0	0	1722.841
ARPC4-TTLL3	-3.05658	2.139033	-133.188	0	0	1720.697
ATXN3	-2.43806	2.558439	-132.717	0	0	1716.468
CDC20	2.434468	3.290483	34.57408	1.23E-185	1.45E-184	413.3673
WDR73	-2.31081	2.425118	-132.685	0	0	1716.175
AGAP5	-1.97576	1.318344	-131.963	0	0	1709.66
CCZ1	-3.07563	3.369659	-130.65	0	0	1697.731
NBPF10	-2.28028	1.696457	-129.814	0	0	1690.075
ASB3	-1.85253	1.913987	-128.674	0	0	1679.575
HNRNPCP2	3.389508	2.234573	127.7404	0	0	1670.918
RN7SL1	-5.42918	3.437632	-127.724	0	0	1670.761
OGFOD2	-2.30304	2.232653	-127.586	0	0	1669.478
H3F3A	-3.73636	6.047482	-126.989	0	0	1663.912
SLX1A-SULT1A3	-2.75166	1.760848	-125.534	0	0	1650.232
AC139256.2	-3.3025	2.974018	-125.191	0	0	1646.99
EXO1	1.960164	1.554693	42.1115	4.53E-244	8.56E-243	547.9027

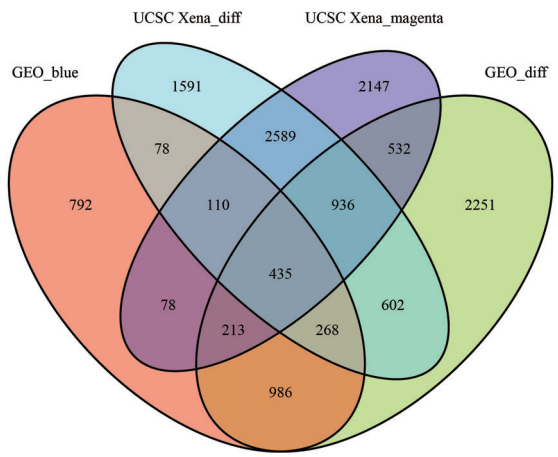

FIGURE 5 | The veen plots between DEGs and co-expression modules. Geo_blue indicates the most significant module identified by WGCNA analysis of GSE3189; UCSC Xena_diff indicates DEGs identified by the UCSC Xena database; UCSC Xena_magenta indicates DEGs identified by WGCNA analysis The most significant modules out; GEO_diff indicates DEGs identified by GSE3189.

these genes were associated with various cancer pathways, including melanoma, endometrial cancer, prostate cancer, etc.; they were also enriched in transcriptional dysregulation pathways in cancer. In humans, dysregulation of genes such as cofactors and chromatin can lead to many diseases (23). These genes are even enriched in the melanoma pathway, suggesting that these genes are strongly associated with melanoma. Besides, we screened for the top 10 hub genes associated with melanoma based on how the MCC score was calculated for the CytoHubba plugin in Cytoscape. We also found that by analyzing the survival of melanoma patients corresponding to high and low expression of these genes, five of the top 10 hub genes were strongly associated with survival, and all showed that high expression of the genes was associated with a low prognosis in melanoma patients. Finally, we performed immunohistochemical analysis using the HPA database and showed that all four genes showed increased expression in melanoma tumor tissues, whereas their expression was not evident in normal tissues.

FOXM1, also known as Forkhead Box M1, is a gene that encodes a protein that is a transcriptional activator involved in cell proliferation. FOXM1 acts downstream of the PI3K-AKT pathway, the Ras-ERK pathway, the JNK/p38MAPK signaling

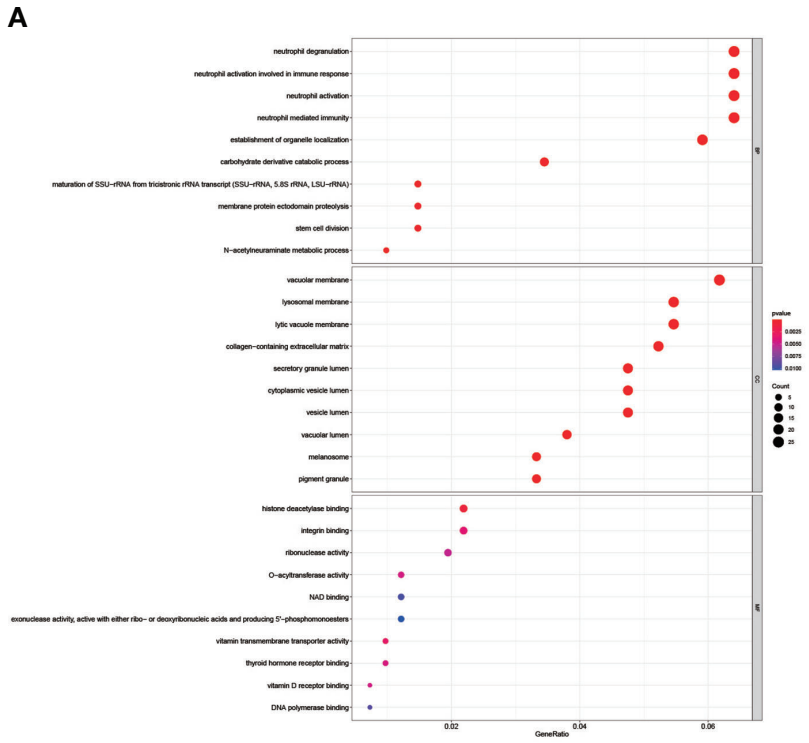

FIGURE 6 | GO enrichment analysis and KEGG pathway enrichment analysis of DEGs. **(A)** shows the GO enrichment analysis of DEGs; **(B)** shows the DEGs' KEGG pathway enrichment analysis.

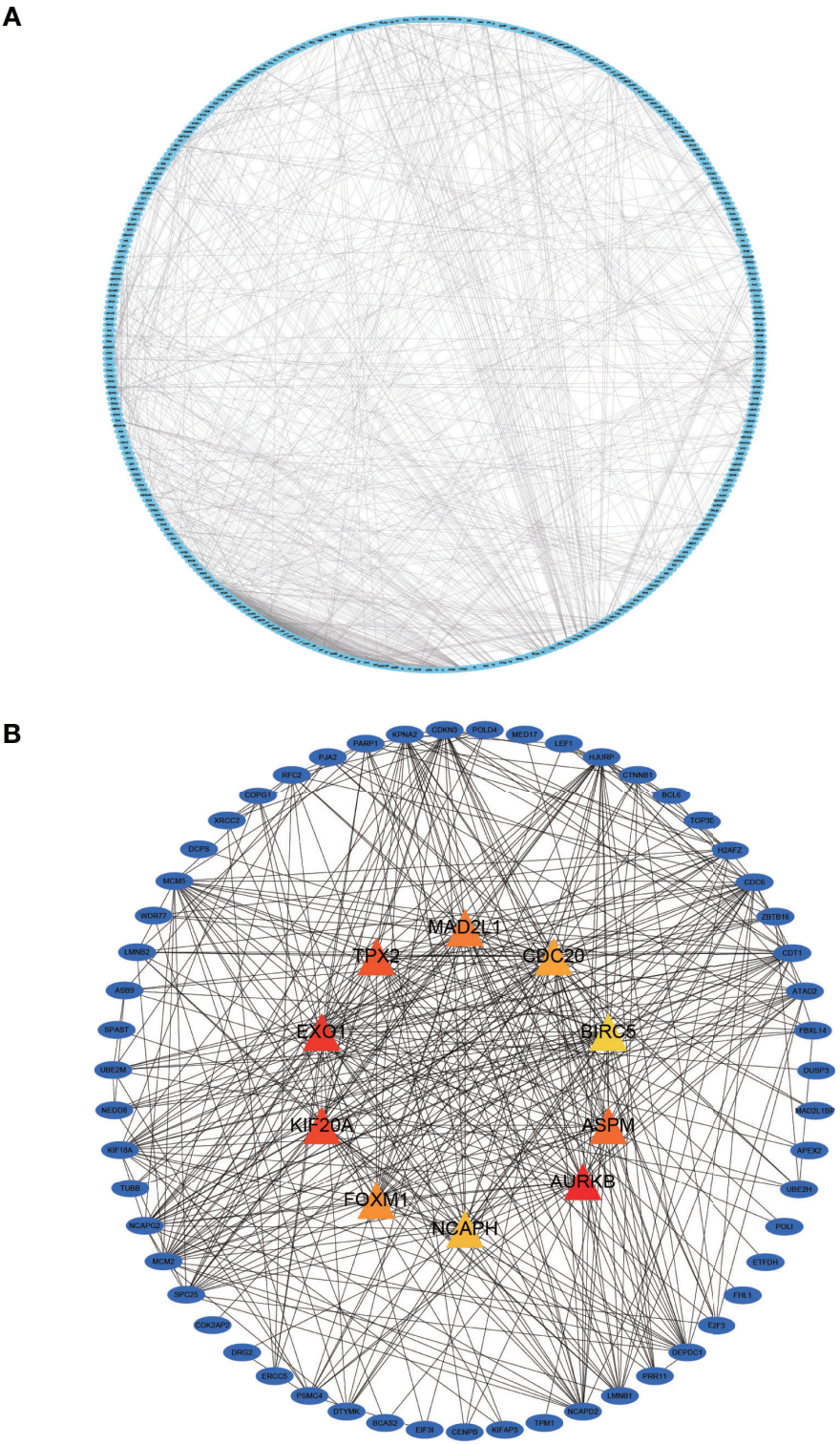

FIGURE 7 | Protein-protein interaction (PPI) network diagram of DEGs and visualization of the Hub gene. **(A)** shows the PPI network diagram derived from the STRING input library; **(B)** shows the Hub gene identified by Cytohubba.

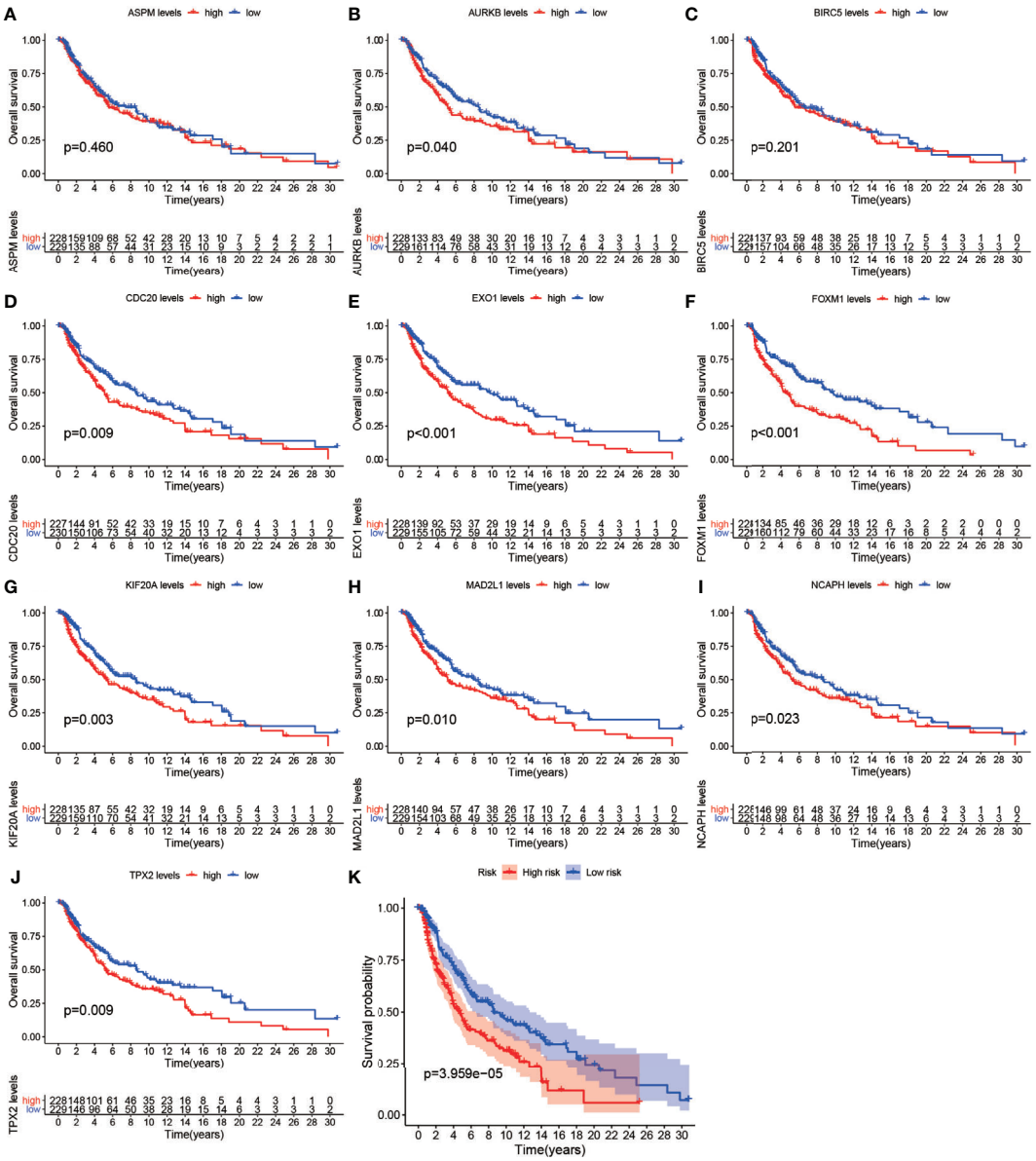

FIGURE 8 | Survival analysis. **(A–J)** shows the survival curves of the first 10 Hub genes. **(K)** shows the survival curves for high-risk and low-risk based on the prognostic model.

cascade and is essential for cell proliferation, differentiation, senescence, DNA damage and repair, and control of the cell cycle (24). It has also been reported that FOXM1 was overexpressed in a variety of human cancers and that the oncogenic potential of this gene is based on its ability to reactivate target genes involved in different stages of cancer development (25). It has been shown that the positive feedback of FOXM1 promotes the growth and invasion of gastric cancer and that FOXM1 promotes gastric cancer progression by interacting with PVT1 (26). FOXM1 has also been reported in non-serious epithelial ovarian carcinoma: FOXM1 was upregulated in all epithelial ovarian cancers (27). It has also been shown that the FOXM1-PSMB4 axis can play a catalytic role in the proliferation and development of cervical cancer (28). More surprisingly, FOXM1 plays a vital role in many other cancers (29–32). In our study, FOXM1 was upregulated in tumor tissues compared to normal tissues, suggesting a significant correlation with melanoma. Previous studies have shown that higher levels of FOXM1 in tumor tissues have been strongly associated with low prognosis in melanoma patients, consistent with our study (33–35). Kinesin Family Member 20A (KIF20A) is also a protein-encoding gene, and what is known

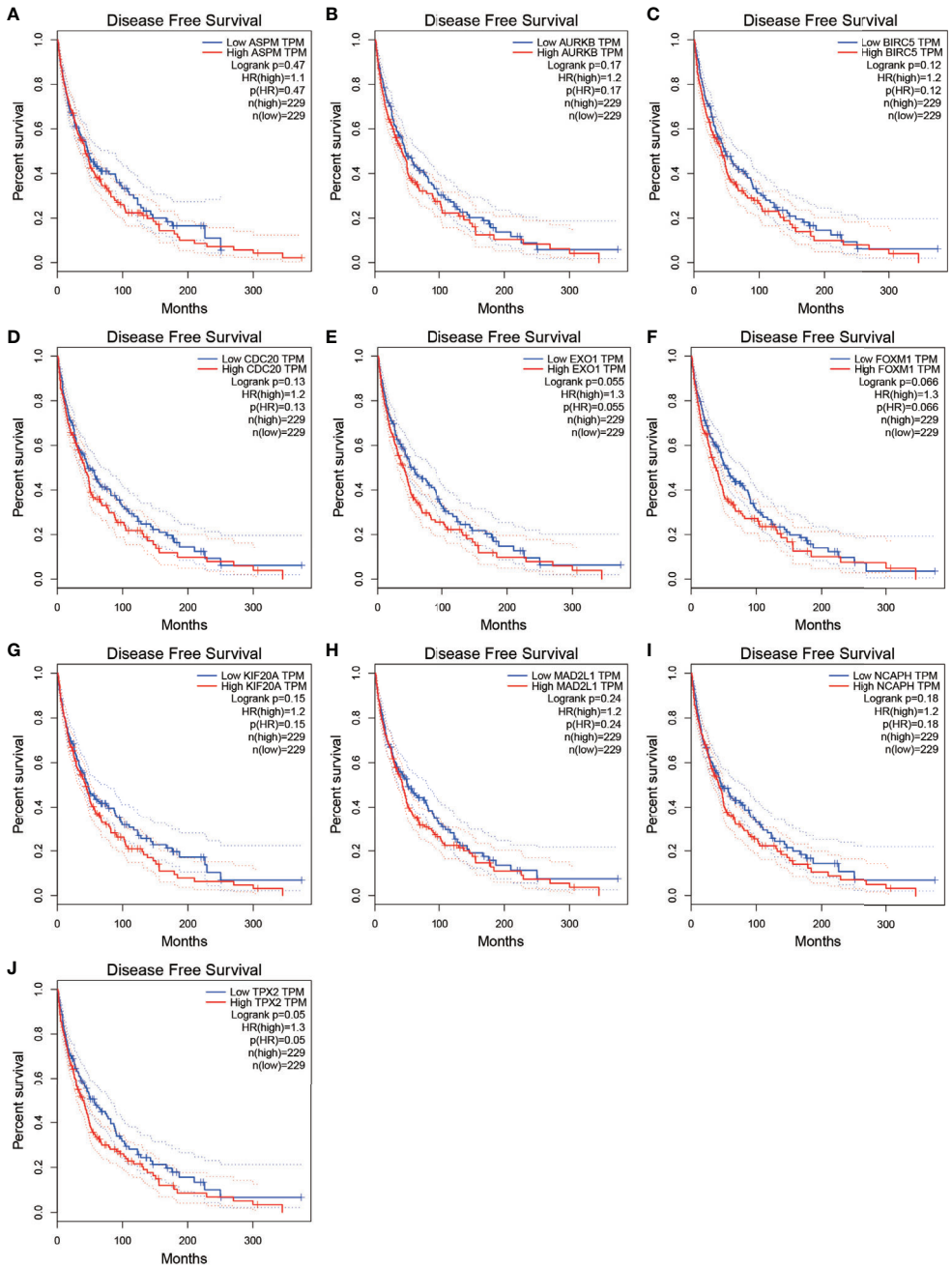

FIGURE 9 | Disease-free survival for the top 10 Hub genes. **(A–J)** show the curves of disease-free survival based on the GEPIA2 database.

about the diseases associated with this gene is mainly familial restriction Familial Isolated Restrictive Cardiomyopathy and Charcot- Marie-Tooth Disease, Type 4C. Research has also been conducted on the role of this gene in cancer. It has been reported that patients with bladder cancer with high expression of KIF20A have poorer tumor stages and that KIF20A promotes metastasis and proliferation of bladder cancer cells (36). Also, it has been shown that skin tumor thickness in KIF20A-positive patients with primary melanoma is significantly greater than skin tumor thickness in patients negative for this gene and that KIF20A-positive patients are more likely to relapse earlier (37). It is well known that while tumor recurrence has a very significant relationship with patient prognosis, this indirectly suggests that KIF20A is associated with survival in melanoma patients, which is consistent with the results of our study. The TPX2 Microtubule Nucleation Factor (TPX2) is a

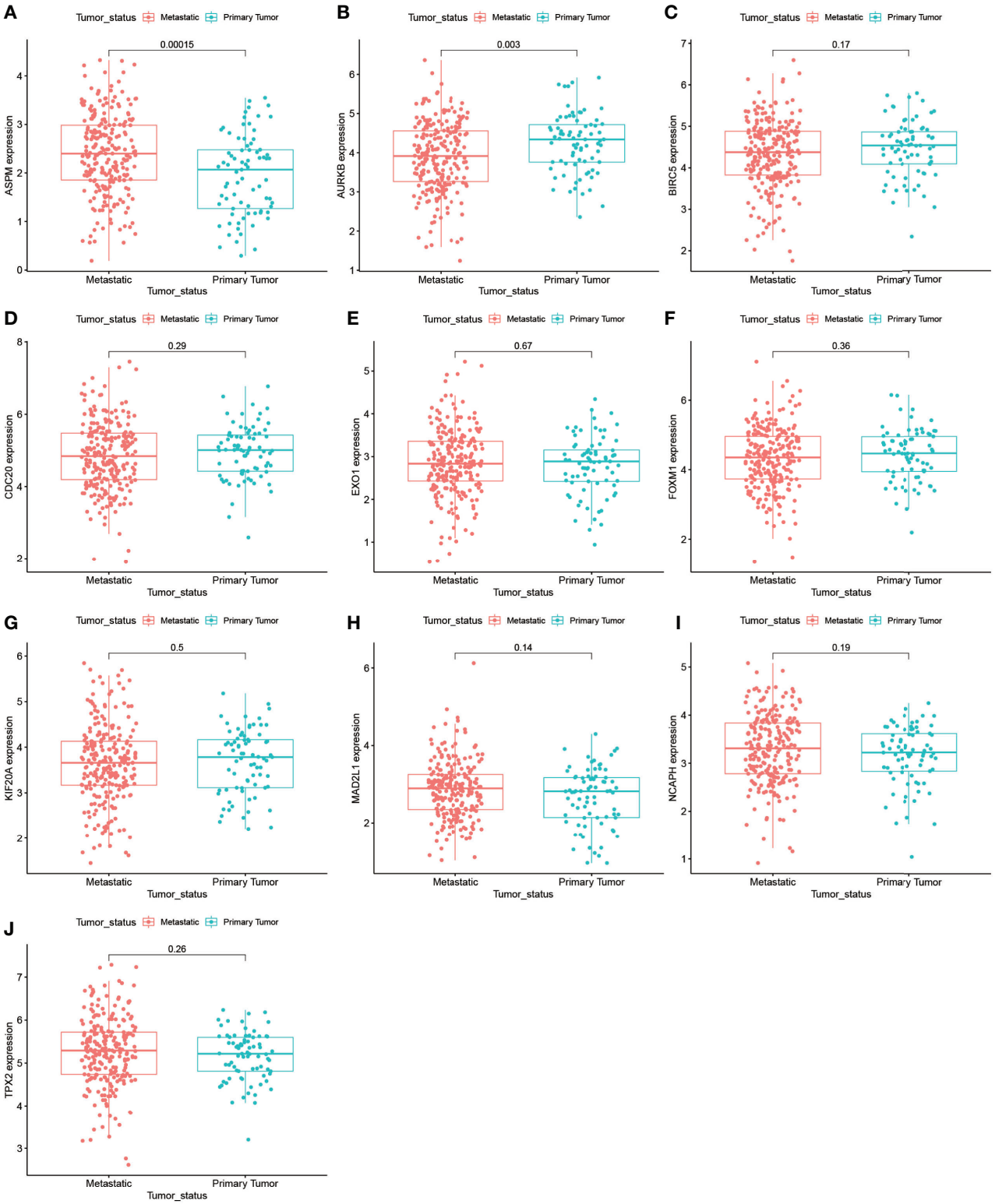

FIGURE 10 | Gene expression of the top 10 Hub genes in the metastasis and primary tumor groups. **(A–J)** demonstrate the differences in gene expression of the top 10 Hub genes in the metastasis-bearing group and in the primary tumor group.

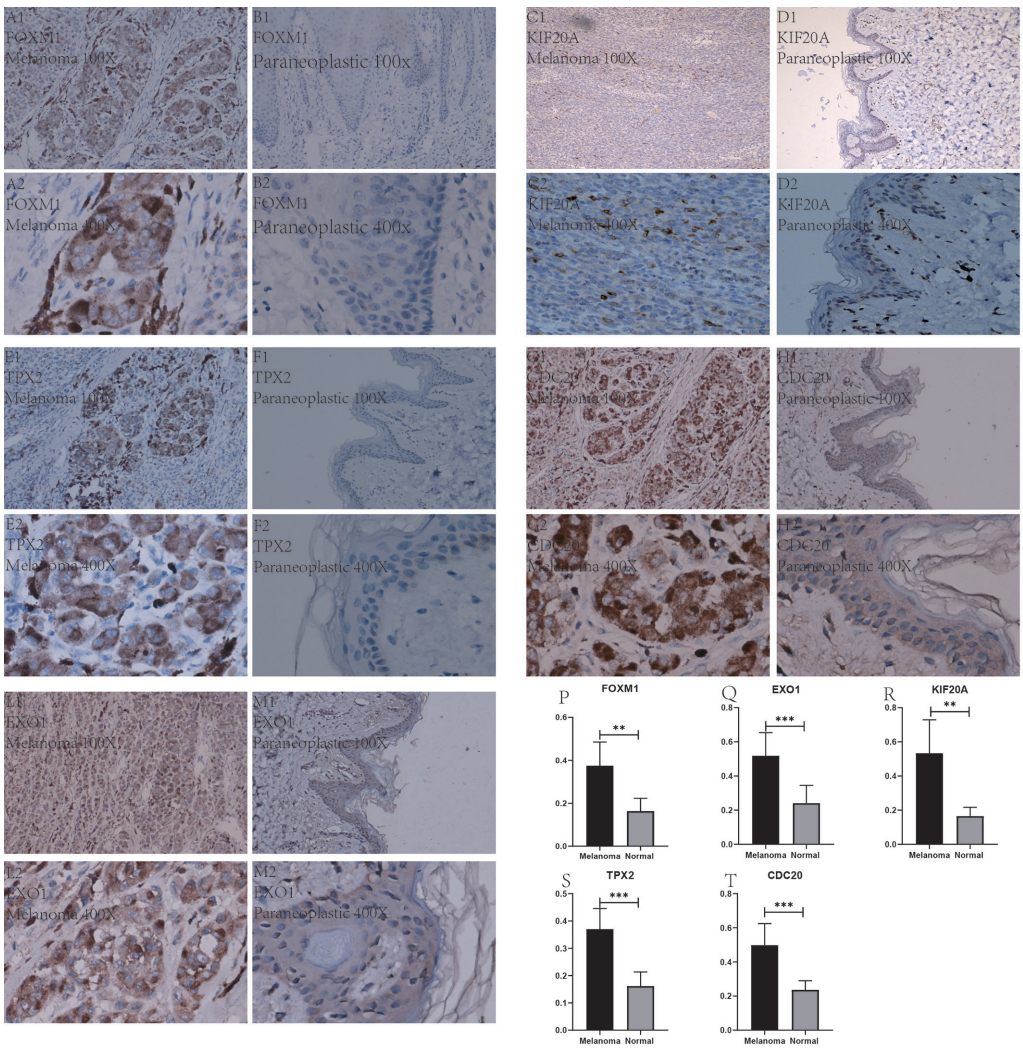

FIGURE 11 | Immunohistochemical plots of the five Hub genes associated with prognosis and statistical analysis of the positivity rate. **(A1–M2)** show the protein expression of each gene in melanoma and in the paracancerous tissue. **(P–T)** shows the statistical analysis of the staining positivity rate for each gene in melanoma and in the paracancerous tissue. **representative P-value < 0.01, ***representative P-value < 0.001.

protein-coding gene. The main diseases known to be associated with the TPX2 gene include Capillary Leak Syndrome and Colorectal Cancer. It has been shown that activation of TPX2 expression increases the invasion and proliferation of cervical cancer, promoting cancer development (38). A study of TPX2 in esophageal cancer showed that the 5-year survival rate of esophageal cancer patients with concomitant high TPX2 expression levels was significantly lower than that of esophageal cancer patients with low TPX2 expression levels (39). Interestingly, in our study, patients with high TPX2 expression of melanoma had a relatively shorter overall survival than patients with low expression. Cell Division Cycle 20 (CDC20) is also a protein-coding gene. The main diseases known to be associated with this gene are Ceroid Lipofuscinosis, Neuronal, 2. Back in 2015, there were reports that CDC20 could be used as a novel cancer treatment modality (40). In hepatocellular carcinoma, the upregulation of CDC20 expression predicted a decline in overall survival and disease-free survival (41). Exonuclease 1 (EXO1) is a protein-coding gene. Diseases associated with EXO1 include Werner's syndrome and Aicardi-Goutieres syndrome. In a recent article on the regulation of bladder cancer cells by phospholipase C-ϵ through EXO1, the authors noted that gene expression of EXO1 was significantly higher in 72 bladder cancer tissue specimens than in 24 adjacent paracancerous tissue samples (42). These five genes have been well-reported in other cancers, and there is not enough evidence to confirm their role in melanoma. In summary, the expression of the five hub genes we studied were all strongly associated with cancer, and in our study, high levels of

expression of these genes were accompanied by shorter survival times for melanoma patients.

Our study combines the WGCNA approach with the DEGs approach through bioinformatics, searching for Hub genes through CytoHubba, a Cytoscape plugin, performing GO enrichment analysis and KEGG pathway analysis of the resulting intersection genes, as well as gene expression of different genes in the metastatic and primary tumor groups, and for the top 10 hub genes Survival analysis and prediction of disease-free survival with the GEPIA database were performed. Finally, the accuracy of our analysis was validated by immunohistochemistry experiments. The protein expression of FOXM1, KIF20A, TPX2, CDC20, and EXO1 was higher in melanoma than in paraneoplastic tissues, consistent with our analysis results. Our study, like others, has limitations regarding the different tumor types. Although we identified potential prognostic genes between melanoma and normal tissue using three different sources of databases with two different bioinformatics analyses, it was less accurate for each of the different subtypes of melanoma patients. Besides, this study should have done more adequate experiments to verify the role of the genes derived from our analysis in melanoma.

In conclusion, by combining the WGCNA analysis method with differentially expressed gene analysis, our study identified the genes FOXM1, KIF20A, TPX2, CDC20, and EXO1 highly correlated with survival melanoma patients and have the potential to serve as a prognostic biomarker in melanoma. Finally, we verified the accuracy and feasibility of our analysis results through immunohistochemistry experiments.

CONCLUSION

FOXM1, KIF20A, TPX2, CDC20, and EXO1 are hub genes of melanoma prognostic, and their high expression is strongly associated with low prognosis in melanoma patients. FOXM1, KIF20A, TPX2, CDC20, and EXO1 could be used as biomarkers for melanoma diagnosis, treatment, and prognosis prediction.

DATA AVAILABILITY STATEMENT

The original contributions presented in the study are included in the article/supplementary material. Further inquiries can be directed to the corresponding author.

ETHICS STATEMENT

The studies involving human participants were reviewed and approved by Ethical Review Committee of the First Clinical Affiliated Hospital of Guangxi Medical University. Written informed consent for participation was not required for this study in accordance with the national legislation and the institutional requirements.

AUTHOR CONTRIBUTIONS

JJ, CL, and XZ designed the study. GX, TL, SL, and CY analyzed the data. ZZ, ZL, ZW, JC, TC, and HL visualized the figures. JJ wrote and revised the manuscript. CL and XZ revised the manuscript. All co-authors participated in the laboratory operations. All authors contributed to the article and approved the submitted version.

FUNDING

This study was supported by the Youth Science Foundation of Guangxi Medical University, Grant/Award Numbers: GXMUYFY201712; Guangxi Young and Middle-aged Teacher's Basic Ability Promoting Project, Grant/Award Number: 2019KY0119; and National Natural Science Foundation of China, Grant/Award Numbers: 81560359, 81860393.

ACKNOWLEDGMENTS

We thank all the people who contributed to this study.

REFERENCES

1. Rastrelli M, Tropea S, Rossi CR, Alaibac M. Melanoma: epidemiology, risk factors, pathogenesis, diagnosis and classification In Vivo. *In Vivo* (2014) 28:1005–11.
2. Pavri SN, Clune J, Ariyan S, Narayan D. Malignant Melanoma: Beyond the Basics. *Plast Reconstr Surg* (2016) 138:330e–40e. doi: 10.1097/PRS.0000000000002367
3. Hanson J, Demer A, Liszewski W, Foman N, Maher I. Improved overall survival of melanoma of the head and neck treated with Mohs micrographic surgery versus wide local excision. *J Am Acad Dermatol* (2020) 82(1):149–55. doi: 10.1016/j.jaad.2019.08.059
4. Best MG, Wesseling P, Wurdinger T. Tumor-Educated Platelets as a Noninvasive Biomarker Source for Cancer Detection and Progression Monitoring. *Cancer Res* (2018) 78:3407–12. doi: 10.1158/0008-5472.CAN-18-0887
5. Chu H-W, Chang K-P, Hsu C-W, Chang IY-F, Liu H-P, Chen Y-T, et al. Identification of Salivary Biomarkers for Oral Cancer Detection with Untargeted and Targeted Quantitative Proteomics Approaches. *Mol Cell Proteomics* (2019) 18:1796–806. doi: 10.1074/mcp.RA119.001530
6. Shan C, Zhang Y, Hao X, Gao J, Chen X, Wang K. Biogenesis, functions and clinical significance of circRNAs in gastric cancer. *Mol Cancer* (2019) 18:136. doi: 10.1186/s12943-019-1069-0
7. Langfelder P, Horvath S. WGCNA: an R package for weighted correlation network analysis. *BMC Bioinf* (2008) 9:559. doi: 10.1186/1471-2105-9-559
8. Unfried JP, Serrano G, Suárez B, Sangro P, Ferretti V, Prior C, et al. Identification of Coding and Long Noncoding RNAs Differentially Expressed in Tumors and Preferentially Expressed in Healthy Tissues. *Cancer Res* (2019) 79(20):5167–80. doi: 10.1158/0008-5472.CAN-19-0400
9. Ma Q, Xu Y, Liao H, et al. Identification and validation of key genes associated with non-small-cell lung cancer. *J Cell Physiol* (2019) 234:22742–52. doi: 10.1002/jcp.28839
10. Grossi E, Raimondi I, Goñi E, González J, Marchese FP, Chapaprieta V, et al. A lncRNA-SWI/SNF complex crosstalk controls transcriptional activation at specific promoter regions. *Nat Commun* (2020) 11(1):936. doi: 10.1038/s41467-020-14623-3

11. San Segundo-Val I, . Sanz-Lozano CS. Introduction to the Gene Expression Analysis Methods. *Mol Biol* (2016) 1434:29–43. doi: 10.1007/978-1-4939-3652-6_3
12. Talantov D, Mazumder A, . Yu JX, Briggs T, Jiang Y, Backus J, et al. Novel genes associated with malignant melanoma but not benign melanocytic lesions. *Clin Cancer Res* (2005) 11:7234–42. doi: 10.1158/1078-0432.CCR-05-0683
13. Ritchie ME, Phipson B, Wu Di, Hu Y, . Law CW, Shi W, et al. limma powers differential expression analyses for RNA-sequencing and microarray studies. *Nucleic Acids Res* (2015) 43:e47. doi: 10.1093/nar/gkv007
14. Chen H, . Boutros PC. VennDiagram: a package for the generation of highly-customizable Venn and Euler diagrams in R BMC. *bioinformatics* (2011) 12:35. doi: 10.1186/1471-2105-12-35
15. Gaudet P, Dessimoz C. Gene Ontology: Pitfalls, Biases, and Remedies. *Methods Mol Biol* (2017) 1446:189–205. doi: 10.1007/978-1-4939-3743-1_14
16. Kanehisa M, Furumichi M, Tanabe M, Sato Y, Morishima K. KEGG: new perspectives on genomes, pathways, diseases and drugs. *Nucleic Acids Res* (2017) 45:D353–D61. doi: 10.1093/nar/gkw1092
17. Yu G, Wang L-G, Han Y, He Q-Y. clusterProfiler: an R package for comparing biological themes among gene clusters. *OMICS* (2012) 16:284–87. doi: 10.1089/omi.2011.0118
18. Szklarczyk D, Morris JH, Cook H, Kuhn M, Wyder S, Simonovic M, et al. The STRING database in 2017: quality-controlled protein-protein association networks, made broadly accessible. *Nucleic Acids Res* (2017) 45:D362–8. doi: 10.1093/nar/gkw937
19. Shannon P, Markiel A, Ozier O, Baliga NS, Wang JT, Ramage D, et al. Cytoscape: a software environment for integrated models of biomolecular interaction networks. *Genome Res* (2003) 13:(11)2498–504. doi: 10.1101/gr.1239303
20. Mantovani A, Cassatella MA, Costantini C, Jaillon S. Neutrophils in the activation and regulation of innate and adaptive immunity. *Nat Rev Immunol* (2011) 11:519–31. doi: 10.1038/nri3024
21. Biton M, Haber AL, Rogel N, Burgin G, Beyaz S, Schnell A, et al. T Helper Cell Cytokines Modulate Intestinal Stem Cell Renewal and Differentiation. *Cell* (2018) 175(5):1307–20 .e22. doi: 10.1016/j.cell.2018.10.008
22. Dror S, Sander L, Schwartz H, Sheinboim D, Barzilai A, Dishon Y, et al. Melanoma miRNA trafficking controls tumour primary niche formation. *Nat Cell Biol* (2016) 18(9):1006–17. doi: 10.1038/ncb3399
23. Lee TI, Young RA. Transcriptional regulation and its misregulation in disease. *Cell* (2013) 152:1237–51. doi: 10.1016/j.cell.2013.02.014
24. Yao S, Fan LY, Lam EW. The FOXO3-FOXM1 axis: A key cancer drug target and a modulator of cancer drug resistance. *Semin Cancer Biol* (2018) 50:77–89. doi: 10.1016/j.semcancer.2017.11.018
25. Gartel AL. FOXM1 in Cancer: Interactions and Vulnerabilities. *Cancer Res* (2017) 77:3135–39. doi: 10.1158/0008-5472.CAN-16-3566
26. Xu MD, Wang Y, Weng W, Wei P, Qi P, Zhang Q, et al. PVT1A Positive Feedback Loop of lncRNA- and FOXM1 Facilitates Gastric Cancer Growth and Invasion. *Clin Cancer Res* (2017) 23:(8)2071–80. doi: 10.1158/1078-0432.CCR-16-0742
27. Tassi RA, Todeschini P, Siegel ER, et al. FOXM1 expression is significantly associated with chemotherapy resistance and adverse prognosis in non-serous epithelial ovarian cancer patients. (2017) 36:63. doi: 10.1186/s13046-017-0536-y
28. Zhou DM, Liu J, Liu F, Luo GW, Li HT, Zhang R, et al. A novel FoxM1-PSMB4 axis contributes to proliferation and progression of cervical cancer. *Biochem Biophys Res Commun* (2020) 521(3):746–52. doi: 10.1016/j.bbrc.2019.10.183
29. Li XY, Wu HY, Mao XF, Jiang LX, Wang YX. USP5 promotes tumorigenesis and progression of pancreatic cancer by stabilizing FoxM1 protein. *Biochem Biophys Res Commun* (2017) 492:48–54. doi: 10.1016/j.bbrc.2017.08.040
30. Cui J, Shi M, Xie D, Wei D, Jia Z, Zheng S, et al. FOXM1 promotes the warburg effect and pancreatic cancer progression via transactivation of LDHA expression. *Clin Cancer Res* (2014) 20(10):2595–606. doi: 10.1158/1078-0432.CCR-13-2407
31. Zhou Z, Chen H, Xie R, Wang H, Li S, Xu Q, et al. Epigenetically modulated FOXM1 suppresses dendritic cell maturation in pancreatic cancer and colon cancer. *Mol Oncol* (2019) 13(4):873–93. doi: 10.1002/1878-0261.12443
32. Arceci A, Bonacci T, Wang X, Stewart K, Damrauer JS, Hoadley KA, et al. FOXM1 Deubiquitination by USP21 Regulates Cell Cycle Progression and Paclitaxel Sensitivity in Basal-like Breast Cancer. *Cell Rep* (2019) 26:3076–86.e6. doi: 10.1016/j.celrep.2019.02.054
33. Puig-Butille JA, Vinyals A, Ferreres JR, Aguilera P, Cabré E, Tell-Martí G, et al. AURKA Overexpression Is Driven by FOXM1 and MAPK/ERK Activation in Melanoma Cells Harboring BRAF or NRAS Mutations: Impact on Melanoma Prognosis and Therapy. *J Invest Dermatol* (2017) 137(6):1297–310. doi: 10.1016/j.jid.2017.01.021
34. Kruiswijk F, Hasenfuss SC, Sivapatham R, Baar MP, Putavet D, Naipal KA, et al. Targeted inhibition of metastatic melanoma through interference with Pin1-FOXM1. *signaling* (2016) 35(17):2166–77. doi: 10.1038/onc.2015.282
35. Kuzu OF, Gowda R, Sharma A, Noory MA, Kardos G, Madhunapantula SV, et al. Identification of WEE1 as a target to make AKT inhibition more effective in melanoma. *Cancer Biol Ther* (2018) 19(1):53–62. doi: 10.1080/15384047.2017.1360446
36. Shen T, Yang L, Zhang Z, Yu J, Dai L, Gao M, et al. KIF20A Affects the Prognosis of Bladder Cancer by Promoting the Proliferation and Metastasis of Bladder Cancer Cells. *Dis Markers* (2019) 2019:4863182. doi: 10.1155/2019/4863182
37. Yamashita J, Fukushima S, Jinnin M, Honda N, Makino K, Sakai K, et al. Kinesin family member 20A is a novel melanoma-associated antigen. *Acta Derm Venereol* (2012) 92(6):593–7. doi: 10.2340/00015555-1416
38. Song T, Xu A, Zhang Z, Gao F, Zhao L, Chen X, et al. CircRNA hsa_circRNA_101996 increases cervical cancer proliferation and invasion through activating TPX2 expression by restraining miR-8075. *J Cell Physiol* (2019) 234:14296–305. doi: 10.1002/jcp.28128
39. Sui C, Song Z, Yu H, Wang HJ. Prognostic significance of TPX2 and NIBP in esophageal cancer;. *Oncol Lett* (2019) 18:4221–29. doi: 10.3892/ol.2019.10747
40. Wang L, Zhang J, Wan L, Zhou X, Wang Z, Wei WJ. Targeting Cdc20 as a novel cancer therapeutic strategy. *Pharmacol Ther* (2015) 151:141–51. doi: 10.1016/j.pharmthera.2015.04.002
41. Zhuang L, Yang Z, Meng ZJ. Upregulation of BUB1B, CCNB1, CDC7, CDC20, and MCM3 in Tumor Tissues Predicted Worse Overall Survival and Disease-Free Survival in Hepatocellular Carcinoma Patients. *BioMed Res Int* (2018) 2018:7897346. doi: 10.1155/2018/7897346
42. Fan J, Zhao Y, Yuan H, Yang J, Li T, He Z, et al. Phospholipase C-ϵ regulates bladder cancer cells via ATM/EXO1. *Am J Cancer Res* (2020) 10:2319–36.

Conflict of Interest: The authors declare that the research was conducted in the absence of any commercial or financial relationships that could be construed as a potential conflict of interest.

frontiers in Oncology

REVIEW
published: 22 April 2021
doi: 10.3389/fonc.2021.608987

MicroRNA Signature in Melanoma: Biomarkers and Therapeutic Targets

Soudeh Ghafouri-Fard[1], *Mahdi Gholipour*[1] *and Mohammad Taheri*[2]*

[1] Department of Medical Genetics, Shahid Beheshti University of Medical Sciences, Tehran, Iran, [2] Urology and Nephrology Research Center, Shahid Beheshti University of Medical Sciences, Tehran, Iran

Melanoma is the utmost fatal kind of skin neoplasms. Molecular changes occurring during the pathogenic processes of initiation and progression of melanoma are diverse and include activating mutations in BRAF and NRAS genes, hyper-activation of PI3K/AKT pathway, inactivation of p53 and alterations in CDK4/CDKN2A axis. Moreover, several miRNAs have been identified to be implicated in the biology of melanoma through modulation of expression of genes being involved in these pathways. In the current review, we provide a summary of the bulk of information about the role of miRNAs in the pathobiology of melanoma, their possible application as biomarkers and their emerging role as therapeutic targets for this kind of skin cancer.

Keywords: miRNA, melanoma, biomarker, expression, polymorphism

OPEN ACCESS

Edited by:
Giuseppe Palmieri,
National Research Council (CNR), Italy

Reviewed by:
Georg Wondrak,
University of Arizona, United States
Eva Hernando,
New York University, United States

***Correspondence:**
Mohammad Taheri
mohammad_823@yahoo.com

Specialty section:
This article was submitted to Skin Cancer, a section of the journal Frontiers in Oncology

Received: *22 September 2020*
Accepted: *30 March 2021*
Published: *22 April 2021*

Citation:
Ghafouri-Fard S, Gholipour M and Taheri M (2021) MicroRNA Signature in Melanoma: Biomarkers and Therapeutic Targets. Front. Oncol. 11:608987. doi: 10.3389/fonc.2021.608987

INTRODUCTION

Arising from unrestrained proliferation of melanocytes, melanoma is the utmost fatal kind of skin neoplasm (1). Though melanoma encompasses less than 5% of all skin cancers, it accounts for most of skin neoplasms mortalities (2). When the cancer is diagnosed in early stages, surgical resection of the tumor is the appropriate therapeutic options for enhancement of survival of patients. Yet, based on the metastatic potential of melanoma, surgery is not satisfactory in advanced stages of melanoma (3). Although the mortality rate of primary melanoma is about 11%, metastatic melanoma has a poor prognosis resulting from inefficiency of conventional therapies (4, 5). Meanwhile, novel therapeutic option might offer efficient methods for these patients. For instance, immunotherapeutic approaches such as administration of Anti-PD1 (nivolumab, pembrolizumab) alone, or the combination of anti-PD1 with anti-cytotoxic T lymphocyte-associated protein 4 (CTLA4) ipilimumab has raised the survival of patients who suffer from advanced stages of melanoma (6).

Targeted therapies, like combinations of BRAF inhibitors (Dabrafenib) and MEK inhibitors (vemurafenib) are also frequently used on BRAFV600E mutant melanomas. Superficial spreading, nodular, lentigo maligna and acral lentiginous melanomas represent the main types of melanoma with the first one being the most frequent type (4). Ultraviolet radiation and melanocytic nevi are two main risk factors for development of this kind of skin cancer (4). Molecular changes occurring during the pathogenic processes of initiation and progression of melanoma are diverse and include activating mutations in BRAF and NRAS genes, hyper-activation of PI3K/AKT pathway, inactivation of p53 and alterations in CDK4/CDKN2A axis (4). In addition, several studies have shown the critical role of microRNAs (miRNAs) both in the initiation and in the progression of melanoma (7). These transcripts have sizes around 22 nucleotides and are generated through a

multi-step process from DNA sequences into primary, precursor and mature miRNAs, respectively. As a general rule, they regulate gene expression through binding with complementary sequences in the 3′ untranslated region (3′ UTR) of mRNAs and subsequently lead to degradation and suppression of translation of the target transcript. Less frequently, they interact with the 5′ UTR, coding or promoter regions (8). Moreover, there are some reports of activation of translation of certain genes by miRNAs in some situations. For instance, let-7 family of miRNAs can induce translation when cell cycle is arrested in spite of their inhibitory effects on translation during cell proliferation (9). Therefore, miRNAs are regarded as important mediators of gene expression. Besides, their presence in extracellular vesicles provides them the opportunity to module communication between various cells (8). In the current paper, we summarize the bulk of information about the role of miRNAs in the pathobiology of melanoma, their possible application as biomarkers and their emerging role as therapeutic targets for this kind of skin cancer.

DYSREGULATED MIRNAS IN MELANOMA

Expression pattern of miRNAs in melanoma cell lines and clinical specimens has been assessed by both high throughput and candidate gene approaches. An example of the former types of studies is the study conducted by Zhang et al. (10). They reported DNA copy number changes in miRNA coding genes in the majority of the assessed melanoma samples. Notably, miRNA copy alterations have been correlated with miRNA expression. Moreover, they reported copy number alterations in genes contributing in the biogenesis or function of miRNAs in tumor samples (10). Through a microarray-based technique, Aksenenko et al. have identified differential expression of 143 miRNAs between melanoma samples and adjacent skin tissues. Among the dysregulated miRNAs has been the up-regulated miRNA hsa-miR-146a-5p which has been predicted to be associated with Toll-like receptor, NF-κB and ErB pathways. Moreover, this miRNA has been shown to target one of the most recurrently mutated genes in melanoma i.e., the NRAS gene (11).

miRNA also affect activity of melanoma-related signaling pathways. **Figure 1** depicts the functional association between two miRNAs and AKT and NF-κB signaling pathways.

Expression profiling of miRNAs in melanocytes and melanoma cells originated from primary or metastatic melanoma cells has provided valuable data about the role of miRNAs in each phase of cancer development. A panel of miRNAs including miR-133a, miR-199b, miR-453, miR-520f, miR-521, and miR-551b has been found consistently up-regulated in the course of cancer development from melanocytes to primary cancerous cell and from primary to metastatic melanomas. On the other hand, miR-190 had the opposite trend during this course. Furthermore, expressions of miR-126, miR-29c, miR-506, miR-507, and miR-520d* have been found to be increased during the early progression of melanoma and have been decreased in the metastatic phase. Two other miRNAs including miR-489 and miR-527 had the opposite pattern of expression (15). Levati et al. have demonstrated up-regulation of miR-17-5p, miR-18a, miR-20a, and miR-92a while down-regulation of miR-146a, miR-146b and miR-155 in most of assessed melanoma cell lines compared with melanocytes (16).

Other studies have reported dysregulation of several other miRNAs in the melanoma samples. Among up-regulated miRNAs are miR-221 and miR-222 which induce malignant features through decreasing expression of c-KIT receptor and p27Kip. Both miRNAs promote epithelial-mesenchymal transition (17, 18). Moreover, expression of miR-210 has been demonstrated to be elevated in several cancer types including melanoma. Its expression has been correlated with metastatic potential of melanoma tumors. Up-regulation of miR-210 in cancer cell lines facilitates evasion from hypoxia-induced cell cycle arrest and partly upturned the hypoxic gene expression profile. This miRNA has been revealed to target a known MYC antagonist namely MNT. Therefore, miR-210 has been shown to modulate the hypoxia response in cancer cells *via* regulating an important transcriptional suppressor of the MYC-MAX axis (19). In an attempt to detect the miRNAs that are regulated by BRAFV600E mutation *via* the ERK pathway, Vitiello et al. have conducted RNA sequencing on A375 cell line and a vemurafenib-resistant clone. Their experiments have led to identification of miR-204 and miR-211 as the utmost over-expressed miRNAs by vemurafenib. In spite of belonging to an identical miRNA family, miR-204 and miR-211 have distinguishing characteristics. miR-204 is regulated by STAT3 and its transcript levels are increased in amelanotic melanoma cells, where it functions as a mediator of anti-migratory effects of vemurafenib by modulating expression of AP1S2. On the contrary, miR-211, as a direct target of MITF, is over-expressed in melanotic melanoma cells. miR-211 regulates expression of EDEM1 and subsequently weakens the destruction of Tyrosinase. Thus, miR-211 is a facilitator of pro-pigmentation function of vemurafenib (20). **Table 1** displays the list of over-expressed miRNAs in melanoma.

Numerous tumor suppressor miRNAs have been down-regulated in melanoma samples. For instance, while miR-34a is constantly detected in normal melanocytes, it is not expressed in uveal melanoma cells. Forced over-expression of this miRNA in uveal melanoma cells remarkably diminishes their growth and migratory abilities. Mechanistically, this miRNA inhibits expression of c-Met protein and decreases the levels of phosphorylated Akt and cell cycle-related proteins (83). Besides, miR-34b, miR-34c, and miR-199a* have been shown to down-regulate MET expression, suppressing the invasive growth features in the melanoma cells (84). Furthermore, expressions of the let-7 miRNAs have been shown to be decreased in primary melanomas compared with benign nevus samples. Forced up-regulation of let-7b in melanoma cells has led to significant decrease in the expression of cyclins D1, D3, and A, and CDK4. The functional interaction between let-7b and

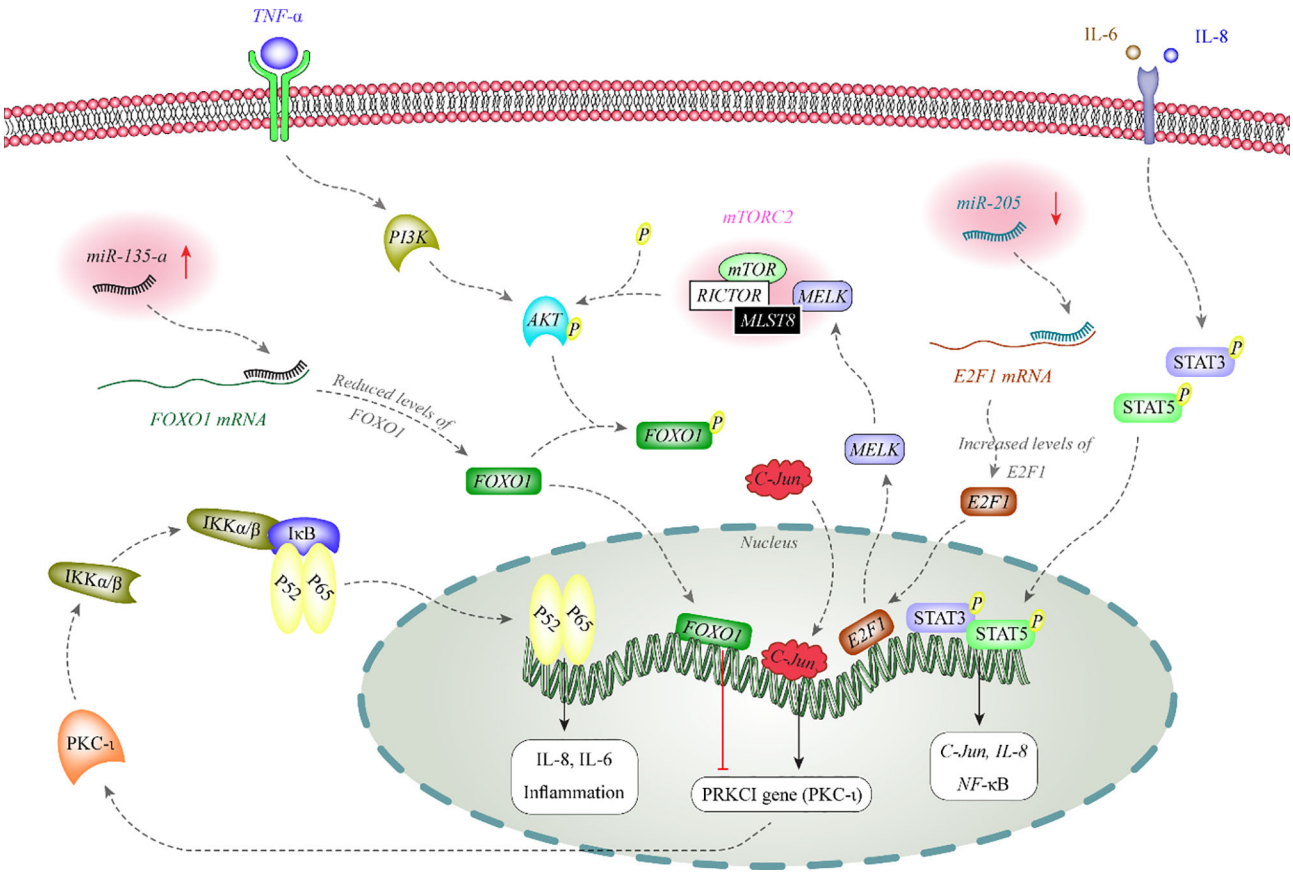

FIGURE 1 | AKT phosphorylates FOXO1 to inhibit its nuclear translocation. FOXO1 has a role in the suppression of expression of PKC-iota in the nucleus. PKC-iota is an inducer of NF-κB which enhances expression of inflammatory genes in the nucleus. Expression of miR-135-a is increased in melanoma. This miRNA binds with the 3' UTR of FOXO1 to decrease its expression (12, 13). On the other hand, miR-205 is decreased in melanoma. This miRNA inhibits expression of E2F1 through binding with its 3' UTR. E2F1 increases expression of MELK. MELK activates mTORC2 through binding with MLST8. mTORC2 has a role in phosphorylation and activation of AKT (14).

cyclin D1 has been verified through *in vitro* experiments (85). The inhibitory effect of let-7a on expression of integrin beta 3 has been verified in another study (86). In addition, functional studies have shown the role of miR-155 in the suppression of proliferation of a number of melanoma cell lines and induction of apoptosis in these cells (16). **Table 2** lists the down-regulated miRNAs in melanoma.

DIAGNOSTIC/PROGNOSTIC MIRNAS IN MELANOMA

Hanniford et al. have introduced a miRNA panel consisting of miR-150-5p, miR-15b-5p, miR-16-5p, and miR-374b-3p whose expression levels could predict the possibility of brain metastasis of melanoma tumors along with clinical stage. Moreover, Kaplan-Meier analysis showed the significance of this miRNA panel in determination of brain-metastasis-free and overall survival of patients with melanoma (273). Stark et al. have assessed expression levels of 17 miRNAs in both melanoma tissues and serum samples of these patients compared with cancer-free individuals. Expression levels of these miRNAs in melanoma samples have been shown to predict stage, recurrence, and survival of patients. Notably, serum expression of a seven-miRNA panel could distinguish melanoma patients from control subjects with 93% sensitivity and more than 82% specificity if at least 4 miRNAs were expressed. Based on the superiority of this miRNA panel above the conventional serological biomarkers for melanoma, it has been suggested as a tool for monitoring disease course in early metastatic melanoma cases to identify relapse after tumor excision or adjuvant therapy (23). Worley et al. have used a high throughput technique to identify the miRNAs whose expression profile could predict the metastatic potential of uveal melanomas. Their approach led to identification of let-7b and miR-199a as the most robust discriminators. Notably, expression profile of six miRNAs could differentiate low and high risk groups with optimal sensitivity and specificity values (274). **Table 3** shows the role of miRNAs in the prediction of prognosis of melanoma using Kaplan-Meier or Cox regression analyses.

TABLE 1 | List of over-expressed miRNAs in melanoma.

microRNA	Samples	Assessed cell lines	Functional analysis	Gene interaction	Signaling pathway	Association with clinical features	Function	Reference
miR-211	SCID mice (SKMEL28 or SK-P8-2 or 501-Mel and 501-Mel-P5-5 cell lines were injected to mice)	SKMEL28, vemurafenib-resistant SKMEL28 and 501-Mel cell lines	Yes	–	PI3K signaling pathway	–	Has oncogenic role. Its deletion attenuates proliferation, invasion and tumorigenicity and inhibits PI3K signaling. Also induces metabolic vulnerability of melanoma cells and sensitizes vemurafenib resistant cells to vemurafenib	(21)
miR-211-5p	NOD/SCID/IL2gR$^{-/-}$ (NSG) mice (A375 cell line was injected to mice)	A375, SK-Mel-103, SK-Mel-28, SK-Mel-147	Yes	NUAK1, SLUG	–	–	Promotes proliferation and induces resistance to vemurafenib and MEK inhibitor trametinib in melanoma cells	(22)
miR-211-5p	86 melanoma tissues, serum samples from 130 healthy controls and 255 melanoma patients	–	No	–	–	Disease stage, survival	A possible diagnostic biomarker	(23)
miR-16	86 melanoma tissues, serum samples from 130 healthy controls and 255 melanoma patients	–	No	–	–	Disease stage	A possible diagnostic biomarker	(23)
miR-204-5p	NOD/SCID/IL2gR$^{-/-}$ (NSG) mice (A375 cell line was injected to mice)	A375, SK-Mel-103, SK-Mel-28, SK-Mel-147	Yes	EFNB2, NUAK1, SLUG	–	–	Promotes proliferation and induces resistance to vemurafenib and MEK inhibitor trametinib in melanoma cells	(22)
miR-378	36 melanoma tissues and paired ANTs, 14 Nude athymic BalB/C mice (A875 cell line was injected to mice)	A875, A375	Yes	FOXN3	Wnt/β-catenin signaling pathway	lymph node metastasis	Induces migration and invasion and activates EMT process in melanoma cells through downregulation of FOXN3 and activation of Wnt/β-catenin pathway	(24)
miR-378a-5p	FFPE tissues specimens of 27 metastatic melanoma and 13 *in situ* melanoma, female mice (M14 cell line was injected to mice)	M14, A375, SBCL1, HUVEC	Yes	STAMBP, HOXD10	–	–	Enhances migration, invasion and angiogenesis ability of melanoma cells	(25)
miR-1908	71 paraffin-embedded melanoma skin lesions, NOD scid, NOD scid gamma, athymic nu/nu, and C57Bl6 mice (MeWo-LM2 cell line was injected to mice)	MeWo-LM2, A375, SK-Mel-2, WM-266-4, HT-144, A2058, HUVECs	Yes	ApoE, DNAJA4	ApoE signaling	shorter metastasis-free survival	Augments invasion, metastasis, metastatic endothelial recruitment (MER) and angiogenesis in melanoma cells through targeting ApoE and DNAJA4	(26)
miR-199a-3p			Yes	ApoE, DNAJA4	ApoE signaling	shorter metastasis-free survival		(26)
miR-199a-5p			Yes	ApoE, DNAJA4	ApoE signaling	shorter metastasis-free survival		(26)
miR-106b	97 primary cutaneous melanoma tissue samples, 17 melanoma metastases, 15 dysplastic nevi	–	No	–	–	Poor prognosis, Breslow thickness, tumor ulceration, advanced clinical stage	May implicate in progression of cutaneous melanoma and can be a potential prognostic biomarker	(27)
miR-106a	–	A375, A2058, HEMn,	Yes	Cx43	–	–	Enhances melanoma cells proliferation *via* suppression of Cx43	(28)

(Continued)

TABLE 1 | Continued

microRNA	Samples	Assessed cell lines	Functional analysis	Gene interaction	Signaling pathway	Association with clinical features	Function	Reference
miR-146a	FFPE tissue specimens of 22 primary melanoma tumors, 18 nevocellular nevi, 13 healthy skin samples, wild type and miR146a-/- C57BL/6 mice (B16.F10 cell line was injected to mice)	B16.F10	Yes	Stat1	–	TNM stage	Negatively regulates immune responses. also affects proliferation, migration and mitochondrial fitness of melanoma cells through regulating STAT1/IFNγ axis	(29)
miR-146a	Mice (A375 cell line was injected to mice)	A375, MA-1, MC-1, MA-2, MC-2, WK-Mel	Yes	LFNG, NUMB, ITGAV, ROCK1	NOTCH/ PTEN/Akt pathway	–	Has dual function. It enhances melanoma cell growth but inhibits metastasis formation (and is poorly expressed in circulating tumor cells)	(30)
miR-146a	10 primary melanoma and nevus tissues from the same patients and 15 primary melanoma tissues and metastases from the same patients	WI-38, IMR-90t, 293T, SKMEL28	Yes	NUMB	Notch signaling pathway	–	Increases proliferative ability and tumorigenecity of melanoma cells through targeting NUMB	(31)
miR-146a	55 melanoma tissues and paired ANTs	A375, WM115, M14, G361, HACAT	Yes	SMAD4	–	TNM stage, lymph node metastasis	Promotes migration and invasion of melanoma cells through targeting SMAD4	(32)
miR-10b	FFPE tissue specimens of 40 primary melanomas that are metastasis-free, 39 primary melanomas with metastasis, 32 metastases	–	No	–	–	Tumor metastasis	Is a potential prognostic biomarker in detection of thicker melanomas that have enhanced risk of metastasis	(33)
miR-10b	–	Mel 505, PMWK, sk-mel-28, sk-mel-24, VMM39, MEL 224, YUHEF, YUROB,	Yes	–	–	–	Its expression positively correlates with B-RafV600E mutation and increases anchorage-independent growth of B-Raf wild-type melanoma cells	(34)
miR-10b	78 melanoma tissues and 30 non-tumor skin samples, nude mice (A375 cell line was injected to mice)	A375, SK-MEL-1, SK-MEL-28, WM451, human primary melanocytes	Yes	ITCH	Wnt/β-catenin signaling pathway	Overall survival	Its knockdown results in ITCH-mediated suppression of proliferation, migration and invasion in melanoma cells.	(35)
miR-21	67 malignant melanoma tissue and 67 normal control skin samples	–	No	PDCD4	–	tumor size, higher Clark classification level, lymph node metastases	Can be a possible biomarker or therapeutic target in melanoma	(36)
miR-21	86 primary cutaneous melanomas tissues, 10 melanoma metastases, 10 dysplastic nevi samples	HTB-67, A375	Yes	–	–	Overall survival, Breslow thickness, advanced clinical stage,	Its silencing suppresses growth and increases apoptosis, chemosensitivity and radiosensitivity of melanoma cells	(37)
miR-21	12 FFPE primary melanoma tissues and 12 melanocytic nevi	WM9, WM35b, WM451, WM793, WM951, WM1205, SKMel23, SKMel113, MV3, MEWO	Yes	Cdc25a	–	Recurrence-free survival, overall survival	Its downregulation promotes apoptosis.	(38)
miR-21	female 01B74 Athymic NCr-nu/nu mice (A375 cell line was injected to mice)	WM1552c, WM793b, MEL 39, A375	Yes	TIMP3	–	–	Increases invasive ability of melanoma cells through targeting TIMP3	(39)

(Continued)

TABLE 1 | Continued

microRNA	Samples	Assessed cell lines	Functional analysis	Gene interaction	Signaling pathway	Association with clinical features	Function	Reference
miR-21	45 melanoma tissues and ANTs	A375	Yes	SPRY1, PDCD4, PTEN	ERK/NF-κB signaling pathway	histological differentiation, TNM stage, lymphatic metastasis	Its inhibition decreases proliferation, migration and invasion and induces apoptosis	(40)
miR-21	BALB/c nude mice (OCM-1 cell line was injected to mice)	OCM-1, M619, MuM-2B	Yes	p53	–	–	Promotes proliferation, migration and invasion of melanoma cells through targeting p53	(41)
miR-21-5p	20 melanoma tissues and paired ANTs	A375, M14	Yes	CDKN2C	–	–	Enhances proliferation and cell cycle G1/S transition in melanoma cells through targeting CDKN2C	(42)
miR-652	26 uveal melanoma tissues and paired ANTs	MUM-2B, MEL270, ARPE-19	Yes	HOXA9	HIF-1alpha signaling	–	Increases proliferation and migration in uveal melanoma cell through promoting HIF-1alpha signaling by suppression of HOXA9	(43)
miR-367	28 uveal melanoma tissues and paired ANTs	M17, M23, MUM-2B, C918, um95	Yes	PTEN	–	–	Enhances proliferation and migration in uveal melanoma cell *via* targeting PTEN	(44)
miR-4286	FFPE specimens of 16 melanoma tissues and 3 melanocytic nevi samples	BRO, SK-MEL-1	Yes	APLN, FPGS, GPR55, HMGA1, RRN3, TP523	–	–	Its inhibition results in decreased proliferation and increased apoptosis.	(45)
miR-367	50 melanoma tissues and 25 benign nevi tissues, 6 Nude mice (A375 cell line was injected to mice)	A375, WM35, SK-MEL-5, SK-MEL-2, HEMa-LP	Yes	PTEN	–	Decreased overall survival, tumor thickness, TNM stage, lymph node involvement, distant metastasis	Elevates proliferation, migration and invasion in cutaneous melanoma cells through targeting PTEN	(46)
miR-638	7 primary melanomas, 9 lymph node metastases, and 8 remote skin metastases	BRO, A-375, HT144, RPM-MC, 1F6, HEM, SK-Mel-147, SK-Mel-28	Yes	TP53INP2	p53 signaling pathway	–	Enhances proliferation and invasion of melanoma cells and prevents apoptosis and autophagy *via* targeting TP53INP2	(47)
miR-338-5p	46 melanoma tissues and 25 normal nevi samples, Nude mice (A375 cell line was injected to mice)	A375, WM35, SK-MEL-5, SK-MEL-2, HEMa-LP	Yes	CD82	AKT pathway	Poor Prognosis, patients survival, tumor stage, metastasis	Promotes proliferation and metastasis *via* targeting CD82	(48)
miR-363-3p	–	A2058, WM793B	Yes	p21	–	–	Promotes stemness of melanoma cells *via* suppression of p21	(49)
miR-15b	128 FFPE tissues of primary melanomas and 11 melanocytic nevi samples	WM9, WM35, WM451, WM793, WM951, WM1205, SKMel23, SKMel113, MV3, MeWo	Yes	–	–	Overall survival	Its knockdown decreases proliferation and induces apoptosis.	(50)
miR-454	25 uveal melanoma tissues and ANTs	OCM-1A, MUM-2C, C918, MUM-2B, D78	Yes	PTEN	–	–	Promotes cell proliferation, colony formation and invasion uveal melanoma cells	(51)

(Continued)

TABLE 1 | Continued

microRNA	Samples	Assessed cell lines	Functional analysis	Gene interaction	Signaling pathway	Association with clinical features	Function	Reference
miR-214	57 primary melanoma tissues, 13 *in situ* melanomas and 18 cutaneous metastases, female CD1 nude mice (A375 or 106 WK-Mel, GR4-Mel, 1300-Mel, SK-Mel-173 and SK-Mel-197 cell lines were injected to mice)	293T, MDA-MB-231, 4T1, A375, 1300-Mel, GR4-Mel, WK-Mel, Dett-Mel, SK-MEL-103, SK-MEL-173, SK-MEL-187, SK-MEL-197, HEMa-LP	Yes	TFAP2C	–	–	Enhances cell movement and metastasis *via* suppression of TFAP2C	(52)
miR-122-5p	Human melanoma tissues and pigmented nevus tissues	293T, SK-MEL-110, A375	Yes	NOP14	–	–	Its inhibition represses proliferation and induces cell cycle arrest at G1 phases through regulation of NOP14	(53)
miR-182	22 primary melanoma tissues, 59 metastatic melanoma tissues and 19 nevi samples, C57BL/6J mice (B16F10 cell line was injected to mice)	SK-MEL-19, SK-MEL-29, SK-MEL-85, SK-MEL-94, SK-MEL-100, SK-MEL-103, SK-MEL-147, SK-MEL-173, SK-MEL-187, SK-MEL-192, SK-MEL-197, 501mel, HEK293T, A375, B16F10, WM35	Yes	FOXO3, MITF-M	–	–	Enhances migration, invasion and metastasis in melanoma cells through suppression of FOXO3 and MITF-M expression	(54)
miR-221	Serum samples from 72 cutaneous malignant melanoma and 54 healthy controls	–	No	–	–	Patient survival, tumor thickness, differentiation, T classification, N classification, metastasis, advanced clinical stage	Can be a potential prognostic biomarker in cutaneous melanoma	(55)
miR-221	–	WM35, WM983A, WM164, 1205Lu	Yes	cKit, p27 (Kip1)	–	–	Promotes proliferation of melanoma cells through targeting cKit and p27. Also its inhibition induces apoptosis	(18)
miR-767	8 melanoma tissues and ANTs	MeWo, MHEM, A375, WM-115, UACC257, WM35, A7, PEM	Yes	CYLD	–	–	Enhances proliferation of melanoma cells through inhibition of CYLD	(56)
miR-135a	20 melanoma tissues and paired ANTs	HEM, sk-mel-1, A375	Yes	FOXO1	AKT signaling pathway	–	Promotes melanoma cells proliferation, tumorigenicity and cell cycle progression *via* targeting FOXO1	(12)
miR-135b	20 melanoma tissues and paired ANTs	A-375	Yes	LATS2	–	–	Its inhibition decreases proliferation and migration and induces apoptosis in melanoma cells	(57)
miR-25	–	A875, MV3, M14, uacc-257, HEM-a	Yes	RBM47	PI3K/Akt/mTOR signaling pathway	–	Promotes proliferation and migration of melanoma cells through targeting RBM47	(58)
miR-25	30 primary melanoma tissues and related non-cancerous skin samples	HEM, MV3, SK-HEP-1, A375	Yes	DKK3	WNT/β-Catenin signaling Pathway	–	Enhances proliferation and invasion in melanoma cells *via* targeting DKK3	(59)
miR-125a	22 melanoma tissue	SK-MEL-239, A375, 451Lu	Yes	BAK1, MLK3	–	–	Promotes BRAF inhibitors resistance through inhibition of intrinsic apoptotic pathway by targeting BAK1 and MLK3	(60)

(Continued)

TABLE 1 | Continued

microRNA	Samples	Assessed cell lines	Functional analysis	Gene interaction	Signaling pathway	Association with clinical features	Function	Reference
miR–106b –5p	18 primary melanoma tissues and 18 benign nevi	SK-MEL-1, A-375, HEM	Yes	PTEN	Akt/ERK signaling pathway	–	Promotes proliferation and progression of melanoma through targeting PTEN and regulation of Akt/ERK pathway	(61)
miR-181b	3 uveal melanoma tissues and 3 normal tissues	SP6.5, VUP, OCM1, 92-1, MUM2b	Yes	CTDSPL	–	–	Promotes cell cycle progression in uveal melanoma cells through targeting CTDSPL	(62)
miR-769	8 melanoma tissues and ANTs	g MHEM, SK-MEL-28, WM-115, UACC257, A375, A7, MeWo, PEM	Yes	GSK3B	–	–	Enhances proliferation of melanoma cells *via* targeting GSK3B and suppression of its expression	(63)
miR–20a	10 uveal melanoma tissues and 10 normal uveal tissues	MUM-2B, MUM-2C, D78	Yes	–	–	–	Promotes proliferation, migration and invasion in uveal melanoma cells	(64)
miR-30d	109 primary melanoma tissues and 17 melanoma metastases	HEK293T, A375, B16F10, WM35, WM98	Yes	GALNT7	–	Overall survival, tumor thickness, tumor stage, shorter time to recurrence	Promotes metastatic capacity of melanoma cells through targeting GALNT7	(65)
miR-30b	109 primary melanoma tissues and 17 melanoma metastases	HEK293T, A375, B16F10, WM35, WM98	Yes	–	–	Overall survival, tumor thickness, tumor stage, shorter time to recurrence	Promotes metastatic capacity of melanoma cells	(65)
miR-224	Primary melanoma tissues and melanoma metastases, athymic NMRI nude mice	SK-Mel-28, SK-Mel-29, SK-Mel-103, SK-Mel-147	Yes	TXNIP	–	–	Increases migration and invasion and induces EMT process through targeting TXNIP	(66)
miR-452	Primary melanoma tissues and melanoma metastases, athymic NMRI nude mice	SK-Mel-28, SK-Mel-29, SK-Mel-103, SK-Mel-147	Yes	TXNIP	–	–	Increases migration and invasion and induces EMT process through targeting TXNIP	(66)
miR-19b	14 melanoma tissues, C57BL/6 mice	293T, A2058, CRL1579, SKMEL28, G361, HNEM	Yes	PITX1	–	–	Regulates proliferation and hTERT expression in melanoma cells through targeting PITX1	(67)
miR-3151	21 RNA samples of melanoma patients	MM A375, Mel-39, MeWo, HEK293, A375	Yes	TP53	–	–	Its knockdown induces TP53-mediated inhibition of proliferation and promotion of apoptosis in melanoma cells	(68)
miR-301a	46 melanoma tissues and 18 benign melanocytic naevi	SK-MEL-1, A-375	Yes	PTEN	Akt and FAK signaling pathways	Poor prognosis, metastasis	Its inhibition suppresses proliferation, colony formation, migration and invasion in melanoma cells through targeting PTEN.	(69)
miR-4262	110 cutaneous melanoma tissues and ANTs	HACAT, HFF, A375, Malme-3M, SK-MEL-2, SK-MEL-5, M14	Yes	KLF6	–	–	Promotes proliferation of melanoma cells through targeting KLF6	(70)
miRNA-106b	Female athymic nude mice (A375 cell line was injected to mice)	A375, Hs294t, SK-Mel28, SK-Mel 119, Mel 1241, Mel 1011, Mel 928, NHEM	Yes	–	–	–	Its downregulation inhibits melanoma cells proliferation and induces cell cycle arrest at G1 phase	(71)

(Continued)

TABLE 1 | Continued

microRNA	Samples	Assessed cell lines	Functional analysis	Gene interaction	Signaling pathway	Association with clinical features	Function	Reference
miR-519d	21 primary melanoma tissues, 19 normal skin and 21 metastatic melanoma samples, C.B-17/Icr-scid mice (A2058 cell line was injected to mice)	A2058, SK-Mel-28, A375, SK-Mel-90, MeWo	Yes	EphA4	ERK1/2 signaling pathway	–	Promotes proliferation, migration and invasion of melanoma cells *via* downregulation of EphA4	(72)
miR-370	41 melanoma tissues and ANTs, BALB/c nude mice (A375 cell line was injected to mice)	SK-MEL-1, A375, HEMn-LP	Yes	PDHB	–	TNM stage	Promotes proliferation, invasion and glycolysis in melanoma cells and induces apoptosis through targeting PDHB	(73)
miR-373	16 melanoma tissues and normal skin samples	A375, WM115, WM75, mela	Yes	SIK1	–	–	Promotes migration of melanoma cells through targeting SIK1	(74)
miR-92a	75 melanoma tissues and paired ANTs	A375.S2, A7, MeWo, RPMI-7951, SK-MEL-5, SK-MEL-24, SKMEL-28, PEM	Yes	–	–	Overall survival, tumor stage, lymph node metastasis, distant metastasis	Its knockdown suppresses proliferation and migration of melanoma cells	(75)
miR-517	62 melanoma tissues and 40 normal skin tissues	HACAT, A375, G-361, OCM-1	Yes	CDKN1C	JNK signaling pathway	–	Its silencing induces oxidative stress injury in melanoma cells through upregulation of CDKN1C and inactivation of JNK signaling pathway	(76)
miR-27a	43 paraffin-embedded melanoma tissues and 22 pigmented nevus samples, female BALB/c nude mice (A375 cell line was injected to mice)	Mel-RM, A375	Yes	SYK	mTOR signaling pathway	TNM staging, lymph node metastasis	Its silencing promotes autophagy and apoptosis in melanoma cells through SYK-mediated modulation of mTOR signaling pathway	(77)
miR-186	8 melanoma tissues and ANTs	A375-S2, SKMEL-28, SKMEL-5, MeWO, RPMI-7951, NHEM	Yes	CYLD	–	–	Enhances proliferation and anchorage-independent growth of melanoma cells *via* downregulation of CYLD	(78)
miR-1246	Tissues from 43 melanoma patients	HEM, A375, A2058	Yes	FOXA2	–	–	promoted cell viability and metastasis in melanoma cells *via* targeting FOXA2	(79)
miR-150	20 melanoma tissues and paired ANTs	M14, A357, WM115, NHEM	Yes	PDCD4	–	–	Its silencing inhibits cell proliferation, migration and invasion and induces apoptosis in melanoma cells.	(80)
miR-520f	10 melanoma and paired ANTs	UACC257, WM-115, A7, MeWo, A375, NHEM, WM-115, PEM	Yes	ITCH	–	–	Promotes proliferation, colony construction and anchorage-independent growth in melanoma cells *via* targeting ITCH	(81)
miR–633	11 melanoma tissues and 10 ANTs	A375, A2058, B16, MEL-RM and M21	Yes	KAI1	–	–	Raises migratory ability and proliferation of melanoma cells *via* targeting KAI1 and reducing KAI1 expression	(82)

Receiver operating characteristic (ROC) curves have been used to assess the diagnostic or prognostic values of miRNAs in melanoma. Based on the area under curve (AUC) values, several miRNAs can be suggested as appropriate biomarkers for this kind of cancer. In the field of miRNA application in melanoma diagnosis, these curves depict the diagnostic capability of expression level of a miRNA as a binary classifier system for detection of melanoma cases as its discrimination threshold is

TABLE 2 | List of under-expressed miRNAs in melanoma.

microRNA	Samples	Assessed cell lines	Functional analysis	Gene interaction	Signaling pathway	Association with clinical features	Function	Reference
miR-429	6 BALB/c-nu mice (A375 cell line was injected to mice)	A-375, 293T	Yes	AKT1	–	–	Represses proliferation and migration of melanoma cells by targeting AKT1	(87)
miR-429-5p	55 melanoma tissues and normal skin tissues	A375, PEM	Yes	LIMK1	–	Tumor thickness, tumor stage	Blocks migration and invasion of melanoma cells through targeting LIMK1	(88)
miRNA-326	23 melanoma tissues and paired ANTs	SK-MEL-28, A375, HT144, A2058, HEMs	Yes	KRAS	AKT and ERK signaling pathways	–	Suppresses cell proliferation and invasion and promotes apoptosis through downregulation of KRAS and inactivating AKT and ERK signaling pathways	(89)
miR-34b	5 uveal melanoma tissues and ANTs	SP6.5	Yes	c-Met	–	–	Its overexpression expression inhibits melanoma cells proliferation and migration and induces cell cycle arrest by targeting c-Met	(90)
miR-34c	5 uveal melanoma tissues and ANTs	SP6.5	Yes	c-Met	–	–	Its overexpression expression inhibits melanoma cells proliferation and migration and induces cell cycle arrest by targeting c-Met.	(90)
miR-34a	–	M17, M23, SP6.5, U-96	Yes	LGR4, MMP2	–	–	Its overexpression decreases migration and invasion of uveal melanoma cells through targeting LGR4 and regulation of EMT process.	(91)
miR-34a	6 *in situ* melanoma tissues, 6 metastatic melanoma tissues, 6 nevi tissue and 18 ANTs	WM35, WM451, A375	Yes	FLOT2	–	–	Its overexpression represses proliferation and metastasis in melanoma cells *via* targeting FLOT2.	(92)
miR-34a	3 uveal melanoma tissues	M17, M21, M23, SP6.5, D78, HEK-293	Yes	c-Met	Akt and ERK1/2 signaling pathways	–	Suppresses proliferation and migration of uveal melanoma cells through downregulation of c-Met	(83)
miR-34a	Fifteen patient-derived primary cultures of melanoma, SCID-NOD mice (HAG cell line was injected to mice)	C8161 (HAG), C81-61 (PAG)	Yes	–	–	–	Suppresses proliferation, invasion and tube formation in melanoma cells	(93)
miR-184	Fifteen patient-derived primary cultures of melanoma, SCID-NOD mice (HAG cell line was injected to mice)	C8161 (HAG), C81-61 (PAG)	Yes	–	–	–	Suppresses proliferation, invasion and tube formation in melanoma cells	(93)
miR-182	Uveal melanoma tissues and normal uveal tissues, Female nude mice (M23 and SP6.5 cell lines were injected to mice)	M23, SP6.5, HEK-293	Yes	MITF, BCL2 and cyclin D2	Akt and ERK1/2 signaling pathways	–	Inhibits cell proliferation, migration and invasion and promotes apoptosis in melanoma cells	(94)
miR-185	Fifteen patient-derived primary cultures of melanoma, SCID-NOD mice (HAG cell line was injected to mice)	C8161 (HAG), C81-61 (PAG)	Yes	–	–	–	Suppresses proliferation, invasion and tube formation in melanoma cells	(93)
miR-185	52 cutaneous melanoma tissues, 41 uveal melanoma	G361, GR-M, OCM-1	Yes	IL-10Rα	–	–	Its ectopic expression decreases proliferation of all	(95)

(Continued)

TABLE 2 | Continued

microRNA	Samples	Assessed cell lines	Functional analysis	Gene interaction	Signaling pathway	Association with clinical features	Function	Reference
	tissues and 35 normal skin specimens						melanoma cell lines through targeting IL-10Rα	
miR-204	Fifteen patient-derived primary cultures of melanoma, SCID-NOD mice (HAG cell line was injected to mice)	C8161 (HAG), C81-61 (PAG)	Yes	–	–	–	Suppresses proliferation, invasion and tube formation in melanoma cells	(93)
miR-365	Skin Cutaneous Melanoma (SKCM) dataset for 470 melanoma samples was downloaded from TCGA	NHEM, A375, A2058, SK-MEL-2, SK-MEL-28	Yes	BCL2, CCND1	–	–	Inhibits cell proliferation, migration and invasion and promotes apoptosis in melanoma cells.	(96)
miR-365	40 melanoma tissues and paired ANTs, female BALB/c nude mice (A375 cell line was injected to mice)	A375, G361, LIBR, HME1	Yes	NRP1	–	lymph node metastasis, clinical stage, overall survival, relapse-free survival	Inhibits melanoma growth and metastasis by targeting NRP1	(97)
miR-485-5p	20 human primary melanoma tissues and paired ANTs	A375, SK-HEP-1, SK-MEL-1, MV3, HPM	Yes	FZD7	wnt signaling pathway	–	Suppresses proliferation and invasion of melanoma cells through targeting FZD7 and consequently inhibition of wnt signaling	(98)
miR-612	89 melanoma tissues and paired ANTs, nude mice (A375 cell line was injected to mice)	SK-MEL-28, SK-MEL-3, A375, HT-144, Hs294T, HEM, HEK293T	Yes	Espin	–	melanoma thickness, lymph node metastasis, poor survival	Its overexpression inhibits melanoma growth, migration and invasion through downregulation of Espin also sensitizes melanoma cells to doxorubicin	(99)
miR-7-5p	20 male NOD.CB17-Prkdcscid Il2rgtm1Wjl/SzJ (NSG) mice (1205Lu cell line was injected to mice)	WM266-4, SK-MEL-2, A2058, 1205Lu	Yes	RelA	NF-κB signaling pathway	–	Inhibits cell proliferation, migration and invasion in melanoma *via* inhibiting RelA and reducing activity of NF-κB signaling	(100)
miR-7-5p	–	WM266-4, A375, A2058	Yes	IRS-2	Akt signaling pathway	–	Inhibits migration and invasion of melanoma cells through targeting IRS-2 and inhibition of Akt signaling	(101)
miR-7	BALB/c nude mice (A375 cell line was injected to mice)	A375, Mel-CV	Yes	EGFR, IGF-1R, CRAF	MAPK and PI3K/AKT signaling pathways	–	Its upregulation reverses BRAF inhibitor resistance in melanoma cells through inhibition of MAPK and PI3K/AKT signaling pathways	(102)
miR-153-3p	20 melanoma tissues and matched ANTs	A375, SK-MEL-28, D78	Yes	SNAI1	–	–	Its overexpression represses proliferation and invasion and induces apoptosis by downregulating SNAI1	(103)
miR-625	30 melanoma tissues and paired ANTs, SPF grade male BALB/c nude mice (A375 cell line was injected to mice)	A375, M14	Yes	SOX2	–	–	Inhibits proliferation, migration and invasion of melanoma cells by targeting SOX2	(104)
miR-23a	30 specific-pathogen-free (SPF) closed colony male ICR mice (B16 cell line was injected to mice)	B16	Yes	SDCBP	MAPK/ERK Signaling Pathway	–	Its overexpression decreases proliferation, migration and invasion and induces cell cycle arrest at G1 phase and apoptosis in melanoma cells *via* suppression of SDCBP	(105)

(Continued)

TABLE 2 | Continued

microRNA	Samples	Assessed cell lines	Functional analysis	Gene interaction	Signaling pathway	Association with clinical features	Function	Reference
							expression and regulation of MAPK/ERK Signaling	
miR-23a	Serum samples from 192 melanoma cases and 51 matched cancer-free controls, tissue specimens from 66 melanoma cases and 22 nevus cases, female BALB/C-Nu nude mice (A2058 cell line was injected to mice)	WM35, WM793, 451LU, A2058, A375	Yes	ATG12	AMPK-RhoA pathway	Patient survival, tumor thickness, ulceration, AJCC stage	Decreases migration and invasion in melanoma cells through targeting ATG12 and regulation of autophagy	(106)
miR-23b	114 primary melanoma tissues and ANTs, Nude mice (A375 and SK-MEL-28 cell lines were injected to mice)	A375, Hs294t, SK-MEL-5, SK-MEL-28, B16F10, nHEM	Yes	NAMPT	NF-κB signaling pathway	Patient survival, Clark level, sentinel-lymph-node positive, AJCC stage	Suppresses cell proliferation and angiogenesis and promotes apoptosis through targeting NAMPT	(107)
miR-23a-3p	117 mucosal melanoma and 12 mucosal nevi, female NOD/SCID mice (HMVII cell line was injected to mice)	GAK, VMRC-MELG, HMVII, HEK293T	Yes	ADCY1	cAMP and MAPK signaling pathways	TNM stage, poor overall survival and disease free survival	Inhibits proliferation, migration and invasion of mucosal melanoma cells through targeting ADCY1 and inhibition of cAMP and MAPK signaling pathways	(108)
miR-15a	24 C57BL/6 mice (B16-F10 cell line was injected to mice)	A375, SK-MEL-28, WM1552C, B16-F10	Yes	CDCA4, AKT3	–	–	Inhibits cell proliferation, migration and invasion and contributes to cell cycle arrest at G1/G0 phase through targeting CDCA4	(109)
miR-15a	52 cutaneous melanoma tissues, 41 uveal melanoma tissues and 35 normal skin specimens	G361, GR-M, OCM-1	Yes	IL-10Rα	–	–	Its ectopic expression decreases proliferation of all melanoma cell lines through targeting IL-10Rα	(95)
miR-143-3p	30 formalin fixed paraffin-embedded (FFPE) primary melanoma lesions and lymph node	NHEM, Sk-Mel-28, A375, WM983A, WM1862	Yes	COX-2	–	–	Represses cell proliferation, migration and invasion and induces apoptosis through targeting COX-2	(110)
miR-143	–	NHEM, WM115, SK-Mel-28, A2058	Yes	–	–	–	Its overexpression inhibits cell proliferation and induces apoptosis in melanoma cells	(111)
miR-708	60 C57BL/6J male mice (B16 cell line was injected to mice)	B16, B16F10, HEK293	Yes	BAMBI	Wnt Signaling Pathway, TGF-β Signaling Pathway	–	Its overexpression decreases proliferation, migration and invasion and induces apoptosis in melanoma cells through targeting BAMBI and activation of TGF-β Pathway and suppression of Wnt pathway	(112)
miR-708	40 clean male Kunming mice (B16 cell line was injected to mice)	B16, A375, WM239, WM451	Yes	LEF1	Wnt signaling pathway	–	Its overexpression expression inhibits proliferation, migration and invasion and induces apoptosis in melanoma cell through targeting LEF1	(113)
miR-216b	30 melanoma tissues and ANTs, NOD-SCID mice (A375 cell line was injected to mice)	HEK-293T, A375, A875, SK-MEL-1, HaCaT	Yes	FOXM1	FOXM1 signaling pathway	–	Decreases proliferation, migration and colony formation ability of melanoma cells by targeting FOXM1	(114)

(Continued)

TABLE 2 | Continued

microRNA	Samples	Assessed cell lines	Functional analysis	Gene interaction	Signaling pathway	Association with clinical features	Function	Reference
miR-216a-5p	86 uveal melanoma tissues, nude mice (A375 cell line was injected to mice)	HEK293T, A375, MUM-2B,	Yes	HK2	–	Patient survival	Suppresses proliferation and dampens glycolysis in melanoma cell *via* targeting HK2	(115)
miR-150-5p	nude mice (A375 cell line was injected to mice)	A375, SK-MEL-2, HEK293T	Yes	SIX1	–	–	Inhibits proliferation, migration and invasion of melanoma cells through SIX1-mediated regulation of glycolysis	(116)
miR-150	51 melanoma tissues and paired ANTs, BALB/c nude mice (A375 cell line was injected to mice)	MeWo, MHEM, A375, WM-115, WM35, PEM	Yes	MYB	–	Patient prognosis	Represses proliferation, migration and invasion of melanoma cells by inhibition of MYB	(117)
miR-150-5p	52 serum samples from stage III and 40 serum samples from stage IV patients, 76 stage III and 10 stage IV FFPE tissue samples	–	No	–	–	Patient survival,	A potential prognostic biomarker	(118)
miR-142-3p	52 serum samples from stage III and 40 serum samples from stage IV patients, 76 stage III and 10 stage IV FFPE tissue samples	–	No	–	–	Patient survival, disease stage	A potential prognostic biomarker	(118)
miR-142-5p	52 serum samples from stage III and 40 serum samples from stage IV patients, 76 stage III and 10 stage IV FFPE tissue samples	–	No	–	–	Patient survival, disease stage	A potential prognostic biomarker	(118)
miR-136	40 male Kunming mice (B16 cell line was injected to mice)	B16, A375, WM239, WM451	Yes	PMEL	Wnt signaling pathway	–	Its overexpression suppresses proliferation, migration, invasion and EMT process and induces apoptosis in melanoma cells by targeting PMEL and inhibition of Wnt signaling pathway	(119)
miR-214	RNA-seq data of 342 melanoma tumors were downloaded from TCGA	MRA2, MRA4, MRA5, MRA6, MRA9	Yes	ANKRD6, CTBP1	–	–	Its overexpression enhances malignant properties of melanoma cells and induces drug resistance in these cells through targeting negative regulators of Wnt signaling.	(120)
miR-125b	48 primary melanoma tissues, 36 lymph nodes metastases and 12 neoplastic skin samples, Female athymic BALB/c nude mice (Mel lm cell line was injected to mice)	NHEM, Mel lm, Mel Ju, Mel Ho, A375	Yes	ITGA9	–	–	Inhibits proliferation, invasion and EMT process in melanoma cells by targeting ITGA9	(121)
miR-125b	68 primary malignant melanoma tissues and 49 lymph node metastases	NHEM, Mel lm, Mel Ju, Melanoma Ho, A375	Yes	MLK3	c-Jun signaling pathway	–	Its overexpression reduces proliferation and invasion of melanoma cell by targeting MLK3/JNK pathway	(122)
miR-125b	5 primary melanoma tissues and 5 melanoma metastases	Mel Juso, Mel lm, Mel Ju, A375, 1205 Lu, HMB2, NHEM	Yes	c-Jun	–	–	Its upregulation reduces proliferation and migration in melanoma cell by targeting c-Jun	(123)

(Continued)

TABLE 2 | Continued

microRNA	Samples	Assessed cell lines	Functional analysis	Gene interaction	Signaling pathway	Association with clinical features	Function	Reference
miR-125b	–	IGR, SK-Mel28, SK-Mel25, SK-Mel5, MelJuso, SM, MeWo	Yes	VDR	vitamin D signaling	–	Influences VDR expression and resistance of melanoma cell lines to 1,25(OH) (2)D (3)	(124)
miR-125b	65 primary melanoma tissues and 67 melanoma metastases	A375, SKMEL-147, 451 Lu	No	–	–	Patient survival, Breslow thickness, ulceration, Mitosis/mm^2, growth phase,	Can be a potential prognostic biomarker	(125)
miR-596	FFPE tissues specimens of 36 melanomas and 22 nevi	A375, SK-Mel-19, A2058, Malme-3M, SK-Mel-12, SK-Mel-2, Malme-3	Yes	MEK1, MCL1, BCL2L1	MAPK/ERK signaling pathway	Poor overall survival	Its overexpression reduces proliferation, migration and invasion and stimulates apoptosis through targeting MEK1, MCL1 and BCL2L1 and regulation of MAPK/ERK and apoptotic pathways	(126)
miR-137	–	A2058, WM793B, HEMa-LP, HEK-293T	Yes	FGF9	–	–	Its enforced expression by Propofol decreases proliferation, migration and invasion in melanoma cells through inhibition of FGF9 expression	(127)
miRNA-29c	30 malignant melanoma tissues and 10 paracancer tissues	A375, SK-MEL-1, SK-MEL-5, HEMa-LP	Yes	CDK6	–	Poor prognosis, TNM stage	Reduces cell proliferation and induces cell cycle arrest at G1 phase through suppressing expression of CDK6	(128)
miR-488-5p	primary melanoma tumors, melanoma metastases, normal skin and nevi	Mel Im, 501mel, NHEM	Yes	DIXDC1	Wnt/β-catenin signaling pathway	–	Has a tumor suppressive role. Its overexpression represses proliferation and migration and induces apoptosis in melanoma cells	(129)
miR-488-3p	20 malignant melanoma tissues and ANTs, 12 male Nu/Nu mice	A375, B16, SK-MEL-28, WM451, HEMn-LP	Yes	PRKDC	–	–	Its ectopic expression sensitizes melanoma cells to cisplatin *via* targeting PRKDC	(130)
miR-675	21 melanoma tissues and ANTs	A375, A2058, HT144, SK-MEL-28, HEM	Yes	MTDH	–	–	Has a tumor suppressive role. Its overexpression inhibits proliferation and invasion in melanoma cells partly by targeting MTDH	(131)
miR-622	Primary tumor and metastatic tumor tissue, male athymic nu/nu mice (Mel Im cell line was injected to mice)	Mel Juso, Mel Ei, Htz19, Mel Im, NHEM	Yes	KRAS	–	Patient survival	Its re-expression suppresses proliferation, migration and clonogenicity in melanoma cells.	(132)
miR-92	Female C57Bl/6 mice (B16-F10 cell line was injected to mice)	B16-F10	Yes	integrin α_V and α_5	TGFβ signaling pathway	–	Implicates in integrin activation of TGFβ in melanoma cancer stem cells that gives rise to immunosuppressive tumor microenvironment and increased tumorigenesis	(133)
miR-4487	86 melanoma samples, serum samples from 130 normal controls and 255	–	No	–	–	Diseases stage, survival	A probable diagnostic biomarker	(23)
miR-4706	melanoma cases	–	No	–	–			(23)

(Continued)

TABLE 2 | Continued

microRNA	Samples	Assessed cell lines	Functional analysis	Gene interaction	Signaling pathway	Association with clinical features	Function	Reference
						Diseases stage, survival		
miR-4731		–	No	–	–	Diseases stage		(23)
miR-509-3p		–	No	–	–	Diseases stage		(23)
miR-509-5p		–	No	–	–	Diseases stage		(23)
miR-203	–	KMeC, LMeC, CMeC-1, A2058, Mewo, HEM	Yes	CREB	–	–	Inhibits melanoma growth and melanosome transport regulating CREB/MITF/RAB27a pathway	(134)
miR-203	8 primary melanoma tissues, 11 metastases and 5 normal skin tissues	A375, A2058, SKMEL13, HT144, SKMEL5	Yes	BMI1	–	Tumor metastasis	Represses melanoma cells invasion and tumor sphere formation by targeting BMI1	(135)
miR-203	148 melanoma tissues and paired ANTs	–	No	–	–	Overall survival, tumor thickness, tumor stage	Can be a potential prognostic factor and a new therapeutic target for the treatment of melanoma	(136)
miR-203	–	A2058, Mewo, HEMa-LP	Yes	kif5b	–	–	Its exogenous expression suppresses melanoma cells growth and regulates melanosomes transport and tyrosinase expression through targeting kif5b	(137)
miR-203	–	Mewo, A2058, HEM	Yes	E2F3a, E2F3b, ZBP-89	–	–	Induces cell cycle arrest and senescence in melanoma cells *via* targeting E2F3	(138)
miR-203	24 melanoma tissues and paired ANTs	A375, HaCaT,	Yes	versican	–	–	Inhibits migration of melanoma cells through targeting versican	(139)
miR-17-3p	28 uveal melanoma tissues and 12 control samples, 30 male BALB/c nude mice (OCM-1A cell line was injected to mice)	OCM-1A, MUM-2C, C918, MUM-2B, UMs	Yes	PVT1, MDM2	p53 signaling pathway	–	Its overexpression inhibits proliferation, migration and invasion and promotes apoptosis through PVT1/miR-17-3p/MDM2 axis	(140)
miR-137	30 primary melanoma tissues and paired ANTs	A375, SK-MEL-1, SK-MEL-5, HEMa-LP, HEMn-LP	Yes	GLS	–	Poor survival, TMN stage	Has a tumor suppressive role. It inhibits proliferation and glutamine catabolism in melanoma cells *via* targeting glutaminase	(141)
miR-137	–	M17, M23, SP6.5, um95, HEK-293	Yes	MITF, CDK6	–	–	Its ectopic expression inhibits uveal melanoma cells proliferation and induces cell cycle arrest at G1 phase through downregulation of MITF and CDK6	(142)
miR-137	–	Ma-Mel-79b, Ma-Mel-86b	Yes	GLO1	–	–	Its overexpression suppresses proliferation of melanoma cells by targeting GLO1	(143)
miR-137	*miR-137* expression data of 450 melanoma patients was obtained from TCGA	WM1650, ME1402, MM200, WM1158	Yes	TBX3	–	Patient survival	Inhibits melanoma cell migration and anchorage independent growth by targeting TBX3	(144)
miR-137	30 melanoma tissues and 10 normal skin tissues, BALB/c female mice (A375	A2058, A375, A875, SKMEL5, TE353-SK, Hacat	Yes	AURKA	–	–	Decreases proliferation and colony formation ability of melanoma cells through targeting AURKA	(145)

(Continued)

TABLE 2 | Continued

microRNA	Samples	Assessed cell lines	Functional analysis	Gene interaction	Signaling pathway	Association with clinical features	Function	Reference
	cell line was injected to mice)							
miR-137	97 melanoma tissues and paired ANTs	–	No	–	–	Patient survival, TNM stage, ulcer, occurrence site	Its low expression is associated with poor prognosis in melanoma patients.	(146)
miR-137	–	Ma-Mel-12, MaMel-20, Ma-Mel-37b, Ma-Mel-57, Ma-Mel-73a, Ma-Mel-79b, MaMel-86b, SK-Mel-2, SK-Mel5	Yes	PAK2	–	–	Suppresses proliferation of melanoma cells *via* inhibiting PAK2	(147)
miR-137	–	WM278, A375, HEK293	Yes	CtBP1	–	–	Suppresses EMT process and induces apoptosis in melanoma cells through targeting CtBP1	(148)
miR-137	–	melanoma cell lines established from metastasis of 33 patients with stage III or IV melanoma	Yes	c-Met, YB1, EZH2, MITF	–	Patient survival	Inhibits cell proliferation, migration and invasion and induces apoptosis in melanoma cells *via* targeting c-Met, YB1, EZH2 and MITF	(149)
miR-137	15 melanoma tissues and 15 normal pigmented nevus samples	HaCaT, SK-MEL-1, A375, WM451	Yes	PIK3R3	–	–	Represses migration and invasion of melanoma cells *via* targeting PIK3R3	(150)
miR–30a –5p	22 malignant melanoma tissues and ANTs, BALB/c nude mice (A375 cell line was injected to mice)	A375, SK-HEP-1, SK-MEL-1, MV3, HPM	Yes	SOX4	–	–	Inhibits melanoma cells proliferation, migration and invasion *via* targeting SOX4	(151)
miR-218	10 primary melanoma tissues, 10 lymph node metastases and 10 benign nevi samples	A375, SK-MEL-2	Yes	CIP2A, BMI1			Inhibits proliferation, migration and invasion in melanoma cells by targeting CIP2A, BMI1	(152)
miR-605	male BALB/c nude mice (Mel-RM and SK-Mel-28 were injected to mice)	HEMn-MP, SK-MEL-31, ME4405, WM1321, Me1007, Mel-RM, SK-MEL-2, SK-MEL-103, WM1366, Mel-RMU, WM278, A375, MM200, SK-Mel-28	Yes	INPP4B	–	–	Inhibits proliferation and growth of melanoma cells through suppression of INPP4B and consequently INPP4B-mediated negative regulation of SGK3	(153)
miR-24–1 –5p	77 malignant melanoma tissues and paired ANTs	A375	Yes	UBD	JNK signaling pathway		Its overexpression gives rise to promotion of autophagy and apoptosis in melanoma cells *via* targeting UBD and activation of JNK signaling pathway	(154)
miR-205-5p	6 melanoma tissues and 6 skin nevus samples	HaCaT, A431, A375, A2058 and SK-MEL-2	Yes	TNFAIP8	–	–	Enhances apoptosis rate and sensitizes melanoma cells to vemurafenib through targeting TNFAIP8	(155)
miR-205-5p	32 primary cutaneous melanoma tissues and 8 metastatic samples	–	No	–	–	Distant metastasis	Can be a potential biomarker of distant metastases	(156)
miR-145-5p *miR-203-3p*	32 primary cutaneous melanoma tissues and 8 metastatic samples	–	No	–	–	Breslow thickness, high Clark level, ulceration, mitotic rate	Can be potential markers of aggressiveness in melanoma	(156)
miR-205	10 primary melanoma tissues, 10 metastatic melanoma tissues and 10	WM35, WM793, WM115A, 1205Lu, 293T	Yes	–	–	–	Its enforced expression reduces migration, motility	(157)

(Continued)

TABLE 2 | Continued

microRNA	Samples	Assessed cell lines	Functional analysis	Gene interaction	Signaling pathway	Association with clinical features	Function	Reference
	benign nevi samples, 16 male athymic nu/nu mice (WM115A cell line was injected to mice)						and proliferation of melanoma cells	
miR-205	20 primary melanoma tissues, 27 metastatic melanoma tissues and 20 benign nevi	WM3211, DO4, WM278, 1205-Lu, C8161.9, Normal human melanocytes	Yes	E2F1, E2F5	AKT signaling pathway	–	Its overexpression suppresses proliferation and colony formation and induces apoptosis in melanoma cell *via* targeting E2F1	(14)
miR-205	65 primary melanoma tissues and 67 melanoma metastases	A375, SKMEL-147, 451 Lu	No	ZEB1	–	Patient survival, Breslow thickness, ulceration, Mitosis/$mm^{2,}$ growth phase, Histological type	Influences invasive ability of melanoma cells and can be a potential prognostic biomarker	(125)
miR-205	5 high-invasive uveal melanoma tissues, 5 low-invasive uveal melanoma tissues and 5 healthy controls	OCM-1A, C918, 293T	Yes	NRP1	–	–	Its overexpression represses proliferation and invasion of melanoma cells *via* targeting NRP1	(158)
miR-145-5p	83 melanoma samples and paired ANTs, 30 male BALB/c nude mice (CHL-1, WMM917, or SK-mel-28 cell lines were injected to mice)	HEK293T, SK-mel-28, CHL-1, VMM917, NHEM	Yes	NRAS	MAPK and PI3K/AKT signaling pathways	Tumor thickness, NRAS mutation, tumor stage	Its high expression inhibit proliferation, migration and invasion and promotes apoptosis in VMM917 and CHL-1 melanoma cells through targeting NRAS	(159)
miR-145-5p	55 melanoma samples and paired ANTs, 10 female athymic BALB/c nude mice (A375 cell line was injected to mice)	A375, WM35, VMM5A, M14, A875, HMCB, 293T	Yes	TLR4	NF-κB signaling pathway	–	Suppresses proliferation, migration and invasion of melanoma cell *via* targeting TLR4	(160)
miR-145-5p	12 uveal melanoma tissues and 12 normal uveal tissues	OCM-1, MUM- 2B	Yes	N-RAS, VEGF	–	–	Inhibits tumor growth, angiogenesis and invasion of uveal melanoma cells through targeting N-RAS and VEGF	(161)
miR-195	341 matched mRNA-Seq and miRNA-Seq tumor samples, along with one normal sample for each data set were obtained from TCGA	SK-MEL-5, SK-MEL-19, SK-MEL-37, SK-MEL-147, UACC-62, WM35, WM793B, WM1366, WM1552C, WM1617, Lox10, MZ2Mel, HaCat, NGM	Yes	PHB1	–	–	Its upregulation results in decreased cell proliferation and high cytotoxic effects of cisplatin and temozolomide on melanoma cells	(162)
miR-211	Male BALB/c nude mice (SK-MEL-28 cell line was injected)	A375, SK-MEL-28	Yes	–	–	Poor prognosis, tumor thickness, AJCC stage	Its upregulation sensitizes melanoma cells to cisplatin and increases cisplatin anticancer effect	(163)
miR-211	–	A375, WM1552C, HEM-l	Yes	PDK4	–	–	Acts as a metabolic switch and sensitizes melanoma cells to hypoxia through targeting PDK4	(164)
miR-211	6 primary melanoma tissues and 24 melanoma metastases	HEM-l, A375, G361, LOX-IMV1, HT-144, RPMI-7951, SK-MEL2,	Yes	KCNMA1	–	–	Its overexpression reduces growth and invasion of melanoma cells *via* targeting KCNMA1	(165)

(Continued)

TABLE 2 | Continued

microRNA	Samples	Assessed cell lines	Functional analysis	Gene interaction	Signaling pathway	Association with clinical features	Function	Reference
		SK-MEL28, WM793B, WM1552C,						
miR-211	–	HM, WM115, A375, SK-MEL-1	Yes	RAB22A	–	–	Regulates EMT process through targeting RAB22A	(166)
miR-211	–	HMV-I, HMV-II, G-361, SK-MEL-28, NHEM-L, NHEM-M, NHEM-D, MM-EP, MM-RU, MM-WK, HEK-293	Yes	PRAME	–	–	Regulates PRAME expression in melanoma cells its overexpression cause reduction in PRAME expression	(167)
miR-211	–	61 melanoma cell lines (some of them include: A2–A15, D4–D25, ME1007, ME1402, ME4405, ME10538, Mel-FH, Mel-RM, Mel-RMU, MM470, MM537, MM629)	Yes	BRN2	–	–	Changes invasion capacity of melanoma cells through targeting BRN2	(168)
miR-211	miRNA expression was derived for eleven melanoma cell lines and matched to samples obtained from GEO	WM3526, WM3682, 451LU	Yes	NUAK1	–	–	Its upregulation inhibits invasion and restores adhesion through targeting NUAK1	(169)
miR-211	52 cutaneous melanoma tissues, 41 uveal melanoma tissues and 35 normal skin specimens	G361, GR-M, OCM-1	Yes	IL-10Rα	–	–	Its ectopic expression decreases proliferation of all melanoma cell lines through targeting IL-10Rα	(95)
miR-211	–	A375M, UACC62, HeLa	Yes	IGF2R, TGFBR2, NFAT5	–	–	Its overexpression inhibits migration and invasion of invasive melanoma cells	(170)
miR-181a	10 melanoma tissues and paired ANTs	WM266-4, A2058	Yes	Bcl-2	–	–	Is upregulated by Piceatannol treatment and contributes to anticancer role of piceatannol through targeting Bcl-2	(171)
miR-181	17 matched melanoma tissues before and after resistance of patients to BRAF inhibitors	A375, M14	Yes	TFAM	–	Patient survival	Its overexpression impedes melanoma growth and alleviates resistance to dabrafenib through targeting TFAM	(172)
miR-375	24 melanoma tissues, normal skin and nevi samples	HEM-l, HEK, WM793B, WM278, WM1552C	Yes	–	–	–	Its ectopic expression suppresses proliferation invasion, and cell motility and induces changes in cell shape in melanoma cells	(173)
miR-328	–	HEM, SK-MEL-1, A375	Yes	TGFB2	–	–	Its overexpression represses proliferation and induces cell cycle arrest at G1 phase	(174)
miR-4633-5p	56 Primary human sinonasal mucosal melanoma tissues	A375, M435S	Yes	–	Akt pathway	Metastasis	Inhibits cell growth, invasion and secretion of MMP2 in melanoma	(175)
miR-455	20 melanoma tissues and paired ANTs	SKMEL1, A375, HT144, A2058, HEK293T	Yes	IGF–1R	–	–	Suppresses proliferation and invasion in melanoma cells *via* targeting IGF1R	(176)
miR-145	5 high-invasive uveal melanoma tissues, 5 low-invasive uveal melanoma tissues and 5 healthy controls	OCM-1A, C918, 293T	Yes	NRP1	–	–	Represses proliferation and invasion of melanoma cells *via* targeting NRP1	(158)
miR-145	33 oral canine malignant melanoma tissues and 11	KMeC, LMeC, CMeC-1,	Yes	c-MYC, FASCIN1	–	–	Inhibits proliferation and migration in melanoma cells	(177)

(Continued)

TABLE 2 | Continued

microRNA	Samples	Assessed cell lines	Functional analysis	Gene interaction	Signaling pathway	Association with clinical features	Function	Reference
	canine normal oral mucosa tissues,	CMeC-2, A2058, Mewo, HEM					through suppression of c-MYC and FASCIN1	
miR-145	11 uveal melanoma tissues and 12 normal controls	MUM-2B, OCM-1	Yes	IRS-1	–	–	Inhibits cell proliferation through blocking G1/S transition and induces apoptosis in uveal melanoma cells *via* targeting IRS-1	(178)
miR-145	–	BLM, FM3P, WM793	Yes	–	–	–	Its overexpression inhibits migration and invasion in metastatic melanoma cells	(179)
miR-219-5p	42 melanoma tissues and 20 nevi tissues, 6 nude mice (A375 cell line was injected to mice)	A375, WM35, SK-MEL-5, SK-MEL-2, HEMa-LP	Yes	Bcl-2		Overall survival, TNM stage, distant metastasis	Reduces proliferation, migration and invasion and promotes apoptosis in melanoma cells by targeting Bcl-2	(180)
miR-31	9 primary melanoma tissues, 71 metastatic melanoma and 2 dysplastic nevi	SK-Mel5, SK-Mel28, MM603	Yes	SRC, MET, NIK, RAB27a	–	–	Has tumor suppressive role and its ectopic expression inhibits migration and invasion in melanoma cells	(181)
miR-31	Fifteen patient-derived primary cultures of melanoma, SCID-NOD mice (HAG cell line was injected to mice)	C8161 (HAG), C81-61 (PAG)	Yes	–	–	–	Suppresses proliferation, invasion and tube formation in melanoma cells	(93)
miR-124a	6 primary uveal melanoma and paired ANTs, Female nude mice (M23 and SP6.5 cell lines were injected to mice)	M17, M21, M23, SP6.5, HEK-293, um95	Yes	CDK4, CDK6, cyclin D2, EZH2	–	–	Has a tumor suppressive role and represses proliferation, migration and invasion in uveal melanoma cells	(182)
miR-124	107 melanoma tissues and paired ANTs	HEM, SK-MEL-1, A375	Yes	RLIP76	–	TNM stage	Suppresses melanoma cells proliferation and invasion and induces apoptosis by targeting RLIP76	(183)
miR-124	68 melanoma tissues and paired ANTs	B16, A375, HACAT	Yes	Versican	–	Tumor thickness, clinical stage, lymph node involvement	Inhibits proliferation, migration and invasion of melanoma cells through targeting Versican	(184)
miR-206	serum samples from 60 melanoma patients and 30 healthy controls	–	No	–	–	Poor prognosis, response to treatment, clinical stage	May be implicated in melanoma progression an can be a potential prognostic factor	(185)
miR-206	36 melanoma tissues and 16 Healthy control tissues	A375, MALME-3M, RPMI7951, SKMEL-2, SK-MEL-5, NHEM-Ad-Adult	Yes	CDK4, Cyclin D1, Cyclin C	–	–	Reduces proliferation, migration and invasion and induces cell cycle arrest at G1 phase in melanoma cells	(186)
miR-186	–	SK-MEL-1, G-361, A375, A875, HEMn-LP	Yes	–	–	–	Inhibits proliferation, migration and invasion in melanoma cells	(187)
miR-26b	59 melanoma tissues and ANTs	HEK293, B16F10, B16F0, A375, HMCB, Hs695T	Yes	TRAF5	MAPK pathway	–	Reduces cell growth and induces apoptosis in melanoma cells by targeting TRAF5	(188)
miR-196a	3 primary melanoma tissues and 5 melanoma metastases	Mel Ei, Mel Wei, Mel Juso, Mel Im, Mel Ju, HMB2, SkMel 3, SkMel 28, NHEM	Yes	HOX-C8	–	–	Decreases invasion in melanoma cells through suppression of HOX-C8 expression	(189)
miR-196a	–	Mel Ei, Mel Wei, Mel Ho, Mel Juso, Mel Ju,	Yes	HOX-B7	–	–	Regulates migration of melanoma cells through	(190)

(Continued)

TABLE 2 | Continued

microRNA	Samples	Assessed cell lines	Functional analysis	Gene interaction	Signaling pathway	Association with clinical features	Function	Reference
		SkMel 28, SkMel 3, NHEM					influencing miR-196a/HOX-B7/Ets-1/bFGF/BMP4 axis	
miR-193b	FFPE specimens of 8 benign nevi, and 8 metastatic melanomas	Malme-3M, SKMEL-28, SKMEL-5	Yes	CCND1	–	–	Suppresses proliferation and cell cycle arrest at G1 phase in melanoma cells through downregulation of CCND1	(191)
miR-193b	FFPE tissue specimens of 8 benign nevi, 8 metastatic melanoma and 15 primary melanoma tissues	Malme-3M, MeWo, SK-MEL-2, SK-MEL-28	Yes	Mcl-1	–	–	Sensitizes melanoma cells to ABT-737 and regulates expression of Mcl-1	(192)
miR-200c	10 primary melanoma tissues, 10 metastatic melanomas and 10 benign nevi samples, male athymic nu/nu mice (WM115A cell line was injected to mice)	WM35, WM793, WM115A, WM3523A, 1205Lu, 293T	Yes	BMI-1	–	–	Inhibits proliferation, migration and metastasis of melanoma cells *via* suppression of BMI-1 expression	(193)
miR-200c	65 primary melanoma tissues and 67 melanoma metastases	A375, SKMEL-147, 451 Lu	No	–	–	Patient survival, Breslow thickness, ulceration, Mitosis/$mm^{2,}$ growth phase, location, histological type	Can be potential prognostic biomarker	(125)
miR-200a	Paraffin-embedded archival tissue specimens of 7 primary melanoma, 33 lymph node metastasis, 25 distant organ metastasis and 10 benign nevi	MELANO, MEL 2183, COLO 829	Yes	CDK6	–	–	Inhibits proliferation and induces cell cycle arrest in melanoma cells through targeting CDK6	(194)
miR-200a	46 melanoma tissues and paired ANTs	A375, SK-HEP-1, WM35, SK-MEL-28	Yes	GOLM1	PI3K/Akt signaling pathway	Overall survival, tumor thickness, TNM stage	Inhibits proliferation, migration and invasion of melanoma cells *via* targeting GOLM1 and regulation of PI3K/Akt signaling pathway	(195)
miR-155	25 uveal melanoma tissues and ANTs	OCM-1A, MUM-2C, C918, MUM-2B, D78	Yes	NDFIP1	–	–	Enhances proliferation and invasion of uveal melanoma cells *via* targeting	(196)
miR-155	–	SK-Mel-28, WM-266-4, GL-Me, 397-Mel, CH-Mel, DR-Mel, SN-Mel,	Yes	SKI	–	–	Inhibits melanoma cells proliferation through targeting SKI	(197)
miR-155	–	CG-Mel, CH-Mel, CL-Mel, CN-Mel, CR-Mel, CT-Mel, DR-Mel, GL-Mel, GR-Mel, MR-Mel, M14, PNM-Mel, PNP-Mel, SK-Mel-28, SN-Mel, WM-266-4, 397-Mel, normal melanocytes	Yes	–	–	–	Its ectopic expression represses proliferation and induces apoptosis in melanoma cells	(16)
miR-155	60 melanoma tissues and paired ANTs	A375, SKMEL-28, A2058, HEM	Yes	CBL	–	tumor thickness, TNM stage, lymph node metastasis	Suppresses proliferation, migration and invasion of melanoma cells *via* targeting CBL	(198)
miR-18b	92 primary melanoma tissues and 48 benign nevi samples, 20 nude mice	1205-Lu, DO4, WM3211, WM278	Yes	MDM2	p53 signaling pathway	Overall survival	Reduces proliferation, migration and invasion and induces apoptosis in	(199)

(Continued)

TABLE 2 | Continued

microRNA	Samples	Assessed cell lines	Functional analysis	Gene interaction	Signaling pathway	Association with clinical features	Function	Reference
	(1205-Lu cell line was injected to mice)						melanoma cell through downregulation of MDM2	
miR-18b	68 melanoma tissues and paired ANTs, 6 male BALB/C-nu/nu nude mice (B16 cell line was injected to mice)	HEK293 cells, MM B16, A375, HACAT	Yes	HIF-1α	–	tumor thickness, tumor stage	Inhibits glycolysis and cell proliferation and induces cell cycles arrest in melanoma cells through targeting HIF-1α	(200)
miR-26a	–	SK-MEL-28, HT-144, HEK293, HEMNLP, HEMNLP2, WM278, WM852c, 1205Lu, A375, RPMI7951	Yes	SODD	–	–	Decreases cell viability and induces apoptosis in melanoma cells through targeting SODD.	(201)
miR-26a	–	A2058, A375, SK-MEL-5, SK-MEL-28	Yes	Lin28B, Zcchc11	–	–	Increases microRNA synthesis by targeting Lin28B and Zcchc11 to inhibit tumor growth and metastasis	(202)
miR-26a	male C57BL/6 mice (B16-F10 cell line was injected to mice)	WM1552C, SKMEL-28, B16-F10	Yes	MITF	–	–	Inhibits proliferation and invasion of melanoma cells *via* targeting MITF	(203)
miR-9	10 primary melanoma tissues and 10 metastases	WM35, WM793, WM115A, 1205Lu, 293T	Yes	NF-κB1	NF-κB1-Snail1 signaling pathway	–	Reduces proliferation and migration of melanoma cells through regulation of NF-κB1-Snail1 pathway.	(204)
miR-9	24 melanoma tissues and 14 benign nevi samples	WM852, WM1791C, WM8, FO-1, WM983A, WM793, Daju, WM209	Yes	RYBP	–	–	Suppresses proliferation migration and invasion in melanoma cells through targeting RYBP	(205)
miR-9	–	MUM-2B, C918, MUM-2C, OCM-1A	Yes	NF-κB1	NF-κB1 signaling pathway	–	Suppresses migration and invasion of uveal melanoma cells *via* targeting cells NF-κB1 and downregulation of the NF-κB1 signaling pathway	(206)
miR-9	73 melanoma tissues and paired ANTs, Male BALB/C-nu/nu nude mice (A375 cell line was injected to mice)	HACAT, G361, B16, A375, HME1	Yes	NRP1	–	tumor stage, lymph node metastasis	Decreases melanoma cells proliferation, migration and invasion of through targeting NRP1.	(207)
miR-9	24 primary melanoma tissues and paired ANTs	B16, A375, G361, HME1, HACAT, HEK293	Yes	SIRT1	–	–	Inhibits proliferation and migration of melanoma cells partly through targeting SIRT1	(208)
let-7b	10 primary melanoma tissues and 10 benign melanocytic nevi	SK-Mel-147, G361	Yes	cyclin D1, cyclin D3, cyclin A, Cdk-4	–	–	Suppresses progression of cell cycle and anchorage-independent growth in melanoma	(85)
let-7b	16 melanoma tissues and 8 normal tissues	s SK-mel-28, A375, A2058, HaCaT	Yes	UHRF1	–	–	Suppresses proliferation of melanoma cell by targeting UHRF1	(209)
let-7b	–	OCM1, OM431	Yes	cyclin D1	–	–	Sensitizes radioresistance uveal melanoma cells to radiotherapy by targeting cyclin D1	(210)
let-7b	106 mucosal melanoma tissues, mucosal nevi Female NOD/SCID (HMVII cell line was injected to mice)	HMVII, GAK, 293T	Yes	MTDH, CALU	–	Patient survival, ECOG score	Suppresses melanoma cells proliferation, migration, invasion and induces apoptosis through targeting MTDH and CALU	(211)
let-7c	106 mucosal melanoma tissues, mucosal nevi Female NOD/SCID (HMVII	HMVII, GAK, 293T	Yes	MTDH, CALU	–	Patient survival, ECOG score	Suppresses melanoma cells proliferation, migration, invasion and induces	(211)

(Continued)

TABLE 2 | Continued

microRNA	Samples	Assessed cell lines	Functional analysis	Gene interaction	Signaling pathway	Association with clinical features	Function	Reference
	cell line was injected to mice)						apoptosis through targeting MTDH and CALU	
let-7a	–	Mel Im, Mel Wei, Mel Juso, Mel Ei, Mel Ho, Mel Ju, HMB2, SK-Mel 28	Yes	integrin β3	–	–	Its overexpression decreases invasive ability of melanoma cells through downregulation of integrin β3	(86)
miR-330-3p	77 melanoma tissues and 38 Normal skin tissues,	SK-MEL-2, UACC903	Yes	TPX2	–	–	Suppresses proliferation of melanoma cells through negative regulation of TPX2	(212)
miR-330-5p	26 primary melanoma tissues and 26 matched non-tumor tissues	HEMn-LP, A375, A875	Yes	TYR, PDIA3	–	–	Represses proliferation, migration and invasion of melanoma cells *via* suppression of TYR and PDIA3 expression	(213)
miR-183	30 melanoma tissues and 14 normal skin samples, female BALB/c mice (SK-MEL-1 cell line was injected to mice)	A375, C32, EDMEL3, G361, HBL, WM1115, SK-MEL-1, M14, MV3, A875, M21, Hermes1, Hermes4, Hacat, TE353.SK, HEK293T	Yes	ITGB1	ITGB1 signaling pathway	Poor prognosis, advanced pathological stage	Suppresses proliferation of melanoma cells through targeting ITGB1	(214)
miR-144	5 uveal melanoma tissues and 5 uveal normal tissues	MUM-2B, C918, MUM-2C, OCM-1A, D78	Yes	c-Met	–	–	Inhibit proliferation and migration in uveal melanoma cells *via* targeting c-Met	(215)
miR-144	26 uveal melanoma tissues and normal choroid samples	MEL270, OMM2.5, UPMM3, UPMM2	Yes	ADAM10, c-Met	–	–	Suppresses proliferation, migration and cell cycle progression in melanoma cells through targeting ADAM10 and c-Met	(216)
miR-122	26 uveal melanoma tissues and normal choroid samples	MEL270, OMM2.5, UPMM3, UPMM2	Yes	ADAM10, c-Met	–	–	Suppresses proliferation, migration and cell cycle progression in melanoma cells through targeting ADAM10 and c-Met	(216)
miR-107	15 primary melanoma tissues, 15 melanoma metastases and 15 nevi samples	SK-MEL-1, A375, G-361, SK0MEL-3, SH-4, SK-MEL-24	Yes	POU3F2	–	late stage	Decreases proliferation, migration and invasion in melanoma cells	(217)
miR-296-3p	18 choroidal malignant melanoma tissues and 6 normal choroidal tissues	C918,	Yes	MMP–2, MMP–9	–	–	Suppresses proliferation, migration and invasion and stimulates apoptosis	(218)
miR-542-3p	24 melanoma tissues and 12 non-neoplastic skin tissues, C57BL/6J mice (B16F10 cell line was injected to mice)	A375, SK-MEL-19, SK-MEL-28, WM451, B16F10	Yes	PIM1	–	–	Inhibits migration, invasion and EMT process in melanoma cells *via* targeting PIM1	(219)
miR-625-5p	Primary melanoma tissues and normal tissues	A2085, A375, A875, Mel-RM, M14, M21, WM35, HFE	Yes	PKM2	–	TNM stage, tumor size, poor differentiation	Inhibits melanoma cells proliferation and glycolysis and sensitizes these cell to BRAF inhibitor *via* targeting PKM2	(220)
miR-339-3p	NSG mice (A375 cell line was injected to mice)	A375, WM266.4, WM115	Yes	MCL1	–	–	Reduces invasive ability and metastasis in melanoma cells through targeting MCL1	(221)
miR-590-5p	female athymic Balb/C nude mice (A2058 cell line was injected to mice)	A2058, A375, HEMa-LP, 293, HM	Yes	YAP1	–	–	Reduces proliferation and induces apoptosis in melanoma cells *via* downregulation of YAP1	(222)
miR-768-3p	–	MM200, Mel-CV, IgR3, Mel-RMu, Sk-Mel-28, Me1007, Mel-JD, Mel-	Yes	eIF4E	–	–	Suppresses cell proliferation and survival and reduces nascent protein synthesis in	(223)

(Continued)

TABLE 2 | Continued

microRNA	Samples	Assessed cell lines	Functional analysis	Gene interaction	Signaling pathway	Association with clinical features	Function	Reference
		FH, Me4405, Mel-RM, HEMn-MP, HEMn-DP					melanoma cells through targeting eIF4E	
miR-451a.1	105 melanoma tissues and 101 normal skin tissues	A2058, A375P, C32, A375SM, WM983A, WM278, WM35, WM1552C	Yes	CAB39	–	–	Inhibits migration and invasion of melanoma cells (this effect is not mediated by CAB39)	(224)
miR-32	Genetically engineered mice (Mice carrying an HGF/SF transgene) (A375P cell line was injected to mice)	WM3928, A375P, YUGEN8	Yes	MCL-1	MAPK pathway	–	Decreases tumorigenicity and induces apoptosis in melanoma cells *via* targeting MCL-1	(225)
miR-493	52 melanoma tissues and paired ANTs	PEM, SK-MEL-28, WM-115, UACC257, A375, A7, MeWo, NHEM	Yes	IRS4	–	–	Suppresses proliferation and cell cycle progression in melanoma cells through targeting IRS4	(226)
miR-382	211 primary melanoma tissues, NOD/Shi-scid/IL-2Rγ^{null} (NOG, Taconic) mice (451Lu cell line was injected to mice)	501MEL, 451Lu, WM1361a, SK-MEL-147, SK-MEL-173, SK-MEL-28	Yes	CTTN, RAC1, ARPC2	–	Tumor thickness, recurrence-free survival	Inhibits tumor metastasis, invasion and matrix degradation through targeting CTTN, RAC1 and ARPC2	(227)
miR-516b	211 primary melanoma tissues, NOD/Shi-scid/IL-2Rγ^{null} (NOG, Taconic) mice (451Lu cell line was injected to mice)	501MEL, 451Lu, WM1361a, SK-MEL-147, SK-MEL-173, SK-MEL-28	Yes	–	–	Tumor thickness	Suppresses tumor growth and metastasis	(227)
miR-194	60 melanoma tissues and paired ANTs	A375, A875	Yes	GEF-H1	–	TNM stages	Inhibits proliferation and metastasis of melanoma cells through suppression of GEF-H1/RhoA pathway	(228)
miR-194	24 melanoma tissues and paired ANTs,	SK-Mel2,	Yes	–	PI3K/AKT/FoxO3a and p53/p21 signaling pathways	Patient survival	Inhibits cell proliferation and induces apoptosis through regulation of PI3K/AKT/FoxO3a and p53/p21 signaling pathways	(229)
miR-128	14 primary cutaneous melanoma tissues and ANTs	A375,	Yes	CCL18	–	–	Inhibits migration and colony formation ability and promotes apoptosis in melanoma cells through targeting CL18	(230)
miR-1280	37 melanoma tissues and 24 benign nevi samples	A375, Mamel66a, Mamel103b, 1205-Lu, C8161.9	Yes	Src	–	–	Suppresses proliferation, cell cycle progression and invasion and promotes apoptosis in melanoma cells *via* targeting Src	(231)
miR-573	11 melanoma tissues and paired ANTs, BABL/c nude mice (A375, SK-MEL-2 cell lines were injected to mice)	A375, SK-MEL-2	Yes	MCAM	–	–	Suppresses proliferation and invasion of melanoma cells *via* targeting MCAM	(232)
miR-33a-5p	29 melanoma tissues and ANTs, nude mice (SKMEL-28 cell line was injected to mice)	SKMEL-28, A375, WM35, SKMEL-1, PIG1	Yes	SNAI2	PI3K/AKT/mTOR signaling pathway	Lymph node metastasis, tumor size, STM stage	Suppresses proliferation, migration and invasion and induces apoptosis in melanoma cell through targeting SNAI2	(233)
miR-33a-5p	20 melanoma and match nevus tissues	A375, WM35, WM451, SK-MEL-1, HM	Yes	–	–	–	Reduces proliferation and promotes radiosensitivity by suppressing glycolysis in melanoma cells	(234)
miR-33a	Male BALB/C-nu/nu mice (A375 cell line was injected to mice)	WM35, WM451, A375, SK-MEL-1, HM	Yes	HIF-1α	–	–	Inhibits proliferation, invasion and metastasis in melanoma cells *via* targeting HIF-1α	(235)

(Continued)

TABLE 2 | Continued

microRNA	Samples	Assessed cell lines	Functional analysis	Gene interaction	Signaling pathway	Association with clinical features	Function	Reference
miR-33a	–	SK-MEL-1, WM-115, PEMI, PEM2	Yes	PCTAIRE1	–	–	Suppresses proliferation and colony formation ability of melanoma cells through targeting PCTAIRE1	(236)
miR-33b	–	WM35, WM451, SK-MEL-1, HM, HEK293	Yes	HIF-1α	–	–	Suppresses melanoma cells proliferation and glycolysis through targeting HIF-1α	(237)
miR-98	20 melanoma tissues and 20 normal nevi, 80 male mice (B16-F1 cell line was injected to mice)	B16-F1	Yes	IL-6	–	Patient survival, tumor stage	Suppresses migration and metastasis of melanoma cell through miR-98-IL-6-negative feedback loop	(238)
miR-425	Melanoma tissues and normal tissues	A375, SK-MEL-28, UACC257, WM-115, NHEM	Yes	IGF-1	PI3K-Akt signaling pathway	–	Suppresses proliferation and metastasis of melanoma cell *via* targeting IGF-1 and inhibition of PI3K-Akt signaling pathway	(239)
miR-337	40 melanoma tissues and paired ANTs	HEK293, A375, A875	Yes	STAT3	–	Patient prognosis	Suppresses growth and metastasis in melanoma cells *via* targeting STAT3	(240)
miR-637	61 melanoma tissues and ANTs	A375, SK-MEL-28, Mel-RM, HaCaT	Yes	P-REX2a	PTEN/AKT signaling pathway	lymph node metastasis, TNM stage	Inhibits proliferation and G1-S transition in melanoma cells through targeting P-REX2a	(241)
miR-329	36 paraffin-embedded melanoma tissues and 10 pigmented nevi samples	PEM, WM-115, A375, A7, UACC257	Yes	HMGB2	β-catenin signaling pathway	–	Suppresses proliferation, migration and invasion and promotes apoptosis in melanoma cell through negative regulation of HMGB2	(242)
miR-579-3p	FFPE samples from 9 stage III/IV melanomas, 10 stage I/II melanomas, 4 dysplastic nevi, 10 melanocytic nevi and 4 patients before and after BRAF inhibitor treatment	M14, LOX IMVI, COLO 38, MALME-3M, SKMEL5, WM115, WM266, M229, HEK-293	Yes	BRAF, MDM2	–	–	Inhibits growth and migration of melanoma cells, induces apoptosis and impairs drug resistance in melanoma	(243)
miR-101	–	HEK293T, NHEM, 29 melanoma cell lines established from metastases of melanoma patients	Yes	MITF, EZH2		Patient survival	Suppresses proliferation, migration and invasion of melanoma cells through targeting MITF and EZH2	(244)
miR-664	9 melanoma and 2 BMN tissues, 10 Nude mice (A375 cell line was injected to mice)	A375.S2, A7, MeWo, RPMI-7951, SK-MEL-5, SK-MEL-24, SK-MEL-28, PEM	Yes	PLP2	–	Patient survival	Decreases proliferation and tumorigenicity of melanoma cells through targeting PLP2	(245)
miR-29a	–	HACAT, HFF, A375, Malme-3M, SK-MEL-2, SK-MEL-5, M14	Yes	Bmi1	Wnt/β-catenin and NF-κB signaling pathways	–	Suppresses cell growth, migration and invasion in melanoma cells and induces apoptosis by targeting Bmi1	(246)
miR-524-5p	male NOD/SCID mice (SK-Mel-19 cell line was injected to mice)	HEK293, Malme-3M, Malme-3, A375, SK-Mel-19	Yes	BRAF, ERK2	MAPK/ERK signaling pathway	–	Inhibits proliferation and migration of melanoma cells through targeting BRAF and ERK2 and inhibition of MAPK/ERK signaling pathway	(247)
miR-138	Whole blood samples from 5 melanoma patients and 6 healthy controls	A2058	Yes	–	PI3K/AKT/mTOR signaling pathway	Patient survival	Suppresses cell proliferation and induces apoptosis in melanoma cells *via* inhibition	(248)

(Continued)

TABLE 2 | Continued

microRNA	Samples	Assessed cell lines	Functional analysis	Gene interaction	Signaling pathway	Association with clinical features	Function	Reference
							of PI3K/AKT/mTOR signaling pathway	
miR-138	–	WM451, HM	Yes	HIF-1α	–	–	Inhibits melanoma cells proliferation, invasion and glycolysis through targeting HIF-1α	(249)
miR-138	16 melanoma tissues and 16 precancerous tissues, female mice (WM35 and A375 cell lines were injected to mice)	WM35, A375, HEK293	Yes	HIF1α	–	–	Inhibits proliferation, migration and invasion and promotes apoptosis in melanoma cells through targeting HIF1α	(250)
miR-126	108 primary cutaneous melanoma tissues, 18 melanoma metastases and 16 dysplastic nevi samples	–	No	–	–	Patient survival, Breslow thickness, tumor ulceration, tumor stage	Can be an independent prognostic factor for overall survival	(251)
*miR-126&126**	adult athymic nude mice (A375M and Me665/1 cell lines were injected to mice)	A375M, A375, Me665/1, NHEM, Me1007, Mel501, WM983A, Me1402/R, Me665/2, GR-mel, ST-mel,	Yes	ADAM9, MMP7	–	–	Decrease proliferation, invasion and chemotaxis of melanoma cells through targeting ADAM9 and MMP7	(252)
miR-377	FFPE tissues samples of 6 primary cutaneous melanoma and 13 benign nevi	mel33B1, mel-14PA, mel-15AY, mel-526, mel-624, NHEM	Yes	E2F3, MAP3K7	MAP3K7/ NF-kB signaling pathway	–	Decreases proliferative ability and colony-forming capability in melanoma cells	(253)
miR-139-5p	82 malignant melanoma tissues and 30 benign skin disease tissues from healthy controls	PIG1, A375, SK-MEL-1, SKMEL-2, SK-MEL-5, SK-MEL-28	Yes	IGF1R	PI3K/AKT signaling pathway	–	Inhibits cell proliferation, migration and invasion and promotes apoptosis through targeting IGF1R	(254)
miR-342	27 melanoma tissues and paired ANTs	HEM, A375, A2058, SK-MEL-28, HT144	Yes	ZEB1	–	–	Inhibits proliferation and invasion of melanoma cells through targeting ZEB1	(255)
miR-127	40 melanoma tissues and paired ANTs, male BALB/c nude mice (WM35 cell line was injected to mice)	WM35, SK-MEL-5, SK-MEL-2, A375, HeMa-Lp	Yes	DLK1	–	Overall survival, tumor thickness, tumor stage	Suppresses cell proliferation and induces apoptosis through downregulation of DLK1	(256)
miR-22	48 melanoma tissues and paired ANTs, nude mice (A375 cell line was injected to mice)	HEM, A375, SK-MEL-1, WM35, SK-MEL-28	Yes	FMNL2	Wnt/β-Catenin Signaling Pathway	Overall survival, tumor thickness, TNM stage	Suppresses proliferation, migration and invasion of melanoma cells through targeting FMNL2	(257)
miR-3065-5p	12 primary melanoma and 9 benign melanocytic tumors	BRO, SK-MEL1	Yes	HIPK1, ITGA1	–	–	Induces cell cycle arrest at G1 phases and inhibits migration of melanoma cells	(258)
miR-204-5p	12 primary melanoma and 9 benign melanocytic tumors	BRO, SK-MEL1	Yes	–	–	–	Decreases proliferation, invasion and colony formation ability of melanoma cells	(258)
miR-204-5p	30 melanoma tissues and 20 benign nevi tissues, 10 immunodeficient female nude mice (A375 cell line was injected to mice)	A375, WM35, SK-MEL-5, SK-MEL-2	Yes	MMP9, BCL2	–	Overall survival	Inhibits proliferation, migration and invasion and induces apoptosis in melanoma cells through targeting MMP9 and BCL2	(259)
miR-610	105 melanoma tissues and ANTs, female BALB/c mice (A375 and MV3 were injected to mice)	SK-MEL-1, A375, SK-MEL-28, MV3, B16-F1, HPM	Yes	LRP6	–	Patient survival, tumor stage, tumor thickness	Represses cell proliferation, cell cycle progression and induces apoptosis in melanoma cells by targeting LRP6	(260)

(Continued)

TABLE 2 | Continued

microRNA	Samples	Assessed cell lines	Functional analysis	Gene interaction	Signaling pathway	Association with clinical features	Function	Reference
miR-3662	80 melanoma tissues and paired ANTs, BALB/c nude mice (A375 and OCM-1A cell lines were injected to mice)	A375, OCM-1A	Yes	ZEB1	–	–	Inhibits invasion and EMT process in melanoma cell *via* targeting ZEB1	(261)
miR-331	22 melanoma tissues and paired ANTs	HEM, A375, A2058, HT144, SK-MEL-1, SK-MEL-28	Yes	AEG-1	PTEN/AKT signaling pathway	–	Suppresses proliferation and invasion of melanoma cells through targeting AEG-1	(262)
miR-149-5p	Melanoma tissues and ANTs	A2058, A375, HSC-1, SK-37, SKMLE-1, WM451, HaCaT	Yes	LRIG2	–	–	Reduces proliferation, colony formation and induces apoptosis in melanoma cells through targeting LRIG2	(263)
miR-338-3p	60 melanoma tissues and paired ANTs,	A375, G361	Yes	MACC1	–	clinical stage, lymph node metastasis	Inhibits proliferation, migration and invasion in melanoma cells through targeting MACC1	(264)
miR-4458	–	A375, A2058, SK-MEL-28, SK-MEL-2, HEMa-LP	Yes	PBX3	–	–	Represses proliferation, migration and induces apoptosis in melanoma cells *via* targeting PBX3	(265)
miR-489-3p	nude mice (A375 cell line was injected to mice)	A375, SK-MEL-2	Yes	SIX1	–	–	Inhibits proliferation, migration and invasion of melanoma cells and regulates glycolysis through targeting SIX1	(266)
miR-431	113 melanoma tissues and paired ANTs	A875, HBL, 1205Lu, A375, SK-MEL-1, HEMa-LP, CHL-1	Yes	NOTCH2	–	Overall survival, tumor stage, ulceration	Suppresses cell proliferation, migration and invasion and induces apoptosis in melanoma cells through targeting NOTCH2	(267)
miR-134	18 melanoma tissues and paired ANTs	BT549, MB-231, MB-486, MCF7, SK-BR-3, 293T	Yes	CTHCR1	–	–	Decreases proliferation, migration, invasion and induces cell cycle arrest and apoptosis in melanoma cells through downregulation of CTHCR1	(268)
miR-224-5p	30 uveal melanoma tissues and paired ANTs	OCM-1A, HEK 293T	Yes	PIK3R3, AKT3	–	–	Suppresses proliferation, migration and invasion of melanoma cells *via* targeting PIK3R3 and AKT3	(269)
miR-140-5p	25 melanoma tissues and paired ANTs, 20 adult athymic nude mice (SK-MEL-1 cell line was injected to mice)	A375, A875, SK-MEL-5, SK-MEL-1, SK-MEL-28, HEMa-LP, HaCaT	Yes	SOX4	Wnt/β-catenin and NF-κB signaling pathways	clinical stage	Its overexpression inhibits proliferation and invasion of melanoma cells by targeting SOX4 and inactivation of Wnt/β-catenin and NF-κB signaling pathways	(270)
miR-140-3p	25 melanoma tissues and paired ANTs, 30 male BALB/c nude mice (M229, A375 and M14 cell lines were injected to mice)	M14, MALME-3M, M229, WM226, A375, SKMEL5, LOX IMVI, HPM	Yes	ABHD2	JNK and AKT/ p70S6K Signaling Pathway	Overall survival	Blocks proliferation, migration and invasion and induces apoptosis in melanoma cell through targeting ABHD2	(271)
miR-135b	27 melanoma tissues and 27 normal skin tissues	A375, PEM	Yes	RBX1	–	–	Suppresses proliferation, migration and invasion of melanoma cells through targeting RBX1	(272)

changed. In other words, these curves are generated by plotting the true positive rate against the false positive rate at different threshold points. Notably, serum expression levels of several miRNAs have high sensitivity and specificity values for differentiating between melanoma patients and healthy subjects or between metastatic and non-metastatic melanomas. **Tables 4**, **5** list the miRNAs whose application as diagnostic or prognostic markers has been evaluated using ROC curve analysis, respectively.

TABLE 3 | Role of melanoma in prediction of prognosis of melanoma (DMFS, distant metastasis free survival; OS, overall survival; DFS, disease-free survival; RFS, relapse-free survival; MSS, melanoma specific survival).

microRNA	Sample number	Kaplan-Meier analysis	Univariate cox regression	Multivariate cox regression	Reference
miR-10b	79 primary melanoma tissues and 32 metastases	–	Is a potential prognostic biomarker associated with metastasis	Can be an independent potential prognostic factor	(33)
miR-10b	78 melanoma tissues and 30 non-tumor skin samples	Its high expression is associated with poor OS in melanoma patients.	–	–	(35)
miR-10b	Blood samples from 85 melanoma patients and 30 healthy volunteers	Its high serum levels is associated with short DFS and OS.	–	Its serum level is an independent prognostic factor for OS and CFS in melanoma patients.	(275)
miR-30d	109 primary melanoma tissues and 17 melanoma metastases	Its high expression is associated with poor OS.	–	Its expression pattern is an independent prognostic factor for melanoma mortality.	(65)
miR-30b	109 primary melanoma tissues and 17 melanoma metastases	Its high expression is associated with poor OS.	–	–	(65)
miR-92a	75 melanoma tissues and paired ANTs	Its high expression is associated with poor OS.	–	–	(75)
miR-596	36 melanomas samples and 22 nevi	Its low expression was associated with significantly shorter OS.	–	–	(126)
miRNA-29c	30 malignant melanoma tissues and 10 paracancer tissues	Its low expression associated with poor prognosis.	–	–	(128)
miR-365	40 melanoma tissues and paired ANTs	Its low expression associated with shorter OS and RFS.	–	–	(97)
miR-137	30 primary melanoma tissues and paired ANTs	Its low expression associated with poor survival.	–	Can be an independent risk factor of OS	(141)
miR-137	97 melanoma tissues and paired ANTs	Its low expression is associated shorter OS in melanoma patients.	–	Its expression is an independent prognostic marker of OS in melanoma patients.	(146)
miR-142-3p *miR-142-5p*	66 stage III FFPE tissues	Their low expression associated with poor survival.	–	–	(118)
miR-21	86 primary cutaneous melanomas tissues, 10 melanoma metastases, 10 dysplastic nevi samples	Its high expression associated with shorter 5-year DFS and shorter 5-year OS.	–	Its expression pattern can be an independent prognostic factor for overall survival in melanoma patients.	(37)
miR-21	12 FFPE primary melanoma tissues and 12 melanocytic nevi	Its high expression is associated with poor RFS and OS.	–	–	(38)
miR-181	17 matched melanoma tissues before and after resistance of patients to BRAF inhibitors	Its low expression is correlated with low progression free survival (PFS) and OS	–	–	(172)
miR-4633-5p	56 Primary human sinonasal mucosal melanoma tissues	–	Its expression pattern can be a prognostic factor in identifying metastatic sinonasal mucosal melanoma.	It can be an independent prognostic factor for metastasis.	(175)
miR-191	32 lymph node metastases	Its low expression associated with poor melanoma-specific survival.	–	–	(276)
miR-193b	32 lymph node metastases	Its high associated with poor melanoma-specific survival.	–	–	(276)
hsa-miR-211-5p *hsa-miR-514a-3p* *hsa-miR-508-3p* *hsa-miR-509-3-5p* *hsa-miR-513c-5p*	UM dataset of miRNA expression profiles was obtained from the UCSC Xena Browser	Their high expression were associated with poor OS.	–	–	(277)

(Continued)

TABLE 3 | Continued

microRNA	Sample number	Kaplan-Meier analysis	Univariate cox regression	Multivariate cox regression	Reference
hsa-miR-513a-5p hsa-let-7b-5p hsa-miR-452-5p hsa-miR-224-5p hsa-miR-592 hsa-let-7b-3p hsa-miR-199a-5p		Their low expressions were associated with poor OS.	–	–	(277)
Six miRNAs signature: mir-15 mir-342-3p mir-455-3p mir-145 mir-155 mir-497	59 metastatic and primary melanoma, Congenital nevi	This signature can estimate post-recurrence survival.	–	This miRNA signature is an independent predictor of post-recurrence survival in metastatic melanoma.	(278)
miR-338-5p	46 melanoma tissues and 25 normal nevi samples	Its high expression is associated with decreased OS.	Its expression correlates to patient survival	It can be an independent prognostic factor for OS.	(48)
miR-203	148 melanoma tissues and paired ANTs	Its low expression is associated with poor OS.	–	It can be an independent prognostic marker for melanoma patients.	(136)
miR-29c	149 melanoma tissues with AJCC stage I–IV	Its low expression is associated with poor DFS and OS in stage III melanoma patients.	Its expression correlates to DFS and OS	Its expression is significantly correlated to OS but not DFS.	(279)
miR-206	serum samples from 60 melanoma patients and 30 healthy controls	Its low serum levels is associated with poor DFS and OS.	–	Its serum level is independent prognostic factors for DFS and OS.	(185)
miR-18b	92 primary melanoma tissues and 48 benign nevi samples	Its low expression is associated with shorter OS.	–	–	(199)
miR-15b	128 FFPE tissues of primary melanomas and 11 melanocytic nevi samples	Its high expression is associated with RFS and OS.	–	Its expression pattern can be an independent prognostic factor for DFS and OS.	(50)
miR-183	30 melanoma tissues and 14 normal skin samples	Its low expression is associated with poor OS.	–	–	(214)
miR-23a	Serum samples from 192 melanoma patients and 51 matched cancer-free controls	Its low serum level is associated with poor OS.	Its serum level is predictor of patients OS.	Its serum level is an independent prognostic biomarker for OS.	(106)
miR-23b	114 primary melanoma tissues and ANTs	Its low expression is associated with short 3-year survival in melanoma patients.	–	–	(107)
miR-216a-5p	86 uveal melanoma tissues	Its low expression is associated with poor DFS and OS.	–	–	(115)
miR-221	Serum samples from 72 cutaneous malignant melanoma and 54 healthy controls	Its high expression is associated with poor RFS and OS.	–	Its expression can be an independent predictor of DFS and OS	(55)
miR-205	319 melanoma tissue samples	Its low expression is associated with short MMS in melanoma patients.	Its expression can be a predictor of MMS	Its expression pattern can be an independent prognostic marker for MMS	(280)
miR-205	65 primary melanoma tissues and 67 melanoma metastases	Its low expression is associated with shorter DMFS and MSS.	–	Its expression pattern can be an independent prognostic factor of MMS	(125)

(Continued)

TABLE 3 | Continued

microRNA	Sample number	Kaplan-Meier analysis	Univariate cox regression	Multivariate cox regression	Reference
miR-200c	65 primary melanoma tissues and 67 melanoma metastases	Its low expression is associated with shorter DMFS and MSS.	–	Its expression pattern can be an independent prognostic factor of survival	(125)
miR-200a	46 melanoma tissues and paired ANTs	Its low expression is associated with poor OS.	–	–	(195)
miR-125	65 primary melanoma tissues and 67 melanoma metastases	Its low expression is associated with shorter DMFS and MSS.	–	Its expression pattern can be an independent prognostic factor of survival	(125)
miR-150	51 melanoma tissues and paired ANTs	Its low expression is associated with short RFS and OS.	–	–	(117)
let-7b	106 mucosal melanoma tissues, mucosal nevi samples	Its low expression is associated with poor DFS.	Its expression level correlates with DFS in melanoma patients	Its expression pattern is an independent prognostic marker for DFS	(211)
let-7c	106 mucosal melanoma tissues, mucosal nevi samples	Its low expression is associated with poor DFS.	Its expression level correlates with DFS in melanoma patients	Its expression pattern is an independent prognostic marker for DFS	(211)
miR-126	108 primary cutaneous melanoma tissues, 18 melanoma metastases and 16 dysplastic nevi samples	Its low expression is associated with poor OS in melanoma patients	–	Can be an independent prognostic factor for overall survival	(251)
miR-127	40 melanoma tissues and paired ANTs	Its low expression is associated with short OS	–	–	(256)
miR-22	48 melanoma tissues and paired ANTs	Its low expression is associated with shorter OS	–	–	(257)
miR-610	105 melanoma tissues and ANTs	Its low expression is associated with short 5-year survival	–	–	(260)
miR-431	113 melanoma tissues and paired ANTs	Its low expression is associated with poor OS in melanoma patients	Can be a potential prognostic marker for melanoma patients	Can be an independent prognostic factor for melanoma patients	(267)
miR-140-3p	25 melanoma tissues and paired ANTs	Its low is associated with poor OS	Its expression pattern correlates with OS in melanoma patients	Its expression pattern is an independent prognostic factor for OS in melanoma patients	(271)
miR-125b	29 FFPE melanoma specimens and 16 intradermal nevus specimens	Its low expression is associated with short OS	–	Its expression level can be an independent prognostic marker for OS	(281)

IMPLICATIONS OF MIRNAS IN THE TREATMENT OF MELANOMA

miRNAs are implicated in the therapeutic effects of several anti-cancer agents. For instance, Genistein, the isoflavone extracted from soybean, has been shown to suppress proliferation of human uveal melanoma cells possibly through modulating expression of miR-27a and its target gene ZBTB10 (291).

miRNAs are also involved in conferring resistance to immunotherapeutic modalities. For instance, expression of miR-222 has been shown to be higher in melanoma samples obtained from patients who did not respond to ipilimumab compared with those benefitting from this option (292). Mechanistically, the ADAR1/miR-222/ICAM1 axis has been reported to be involved in this process (292). Other miRNAs such as miR-488-3p, miR-195 and miR-211 participate in the regulation of response to the chemotherapeutic agent cisplatin (130, 162, 163)

Application of miRNAs in the therapeutic settings is limited by target specificity issues (293). However, some miRNAs are currently being tested in some diseases. Among these therapeutic modalities are miR-122/miravirsen and miR-92/MRG 110 which have been manufactured by Roche/Santaris and Regulus Therapeutics, respectively (293).

ASSOCIATION BETWEEN POLYMORPHISMS WITHIN MIRNAS AND RISK OF MELANOMA

Theoretically, polymorphisms with miRNA coding genes can alter their expression or function. Although such polymorphisms are predicted to influence the risk of different cancers such as melanoma, this field has not been vastly explored. Few studies have assessed association between a certain polymorphism within miR-146a namely the rs2910164 G/C and melanoma risk. In spite of the proposed role for allele C of this polymorphism in conferring risk of melanoma (294, 295), cell line studies have shown that G allele confers high proliferative capacity to melanoma cells (296). **Table 6** summarizes the results of these studies.

TABLE 4 | Application of miRNAs as diagnostic tools in melanoma.

microRNA	Expression pattern	Sample	Diagnostic biomarker	ROC curve analysis			Reference
				Sensitivity	Specificity	Area under the ROC curves (AUC)	
miR-16 miR-211-5p miR-4487 miR-4706 miR-4731 miR-509-3p miR-509-5p	Upregulated Upregulated Downregulated Downregulated Downregulated Downregulated	Serum samples	Diagnostic (diagnosis of presence of melanoma)	93%	≥ 82%	–	(23)
miR-211-5p	Downregulated	Tissue samples	Diagnostic (invasive melanoma)	–	–	0.933	(282)
		Tissue samples	Diagnostic (melanoma in situ)	–	–	0.933	
		Tissue samples	Diagnostic (dysplastic nevi)	–	–	0.951	
miR-211	Downregulated	Tissue samples	Diagnostic (discriminating melanomas from nevi)	90%	86.2%	0.862	(283)
miR-532-5p miR-106b	- -	Serum exosomes	Diagnostic (distinguishing melanoma patients from healthy individuals)	–	–	0.936	(284)
miR-15b-5p	Upregulated	Plasma samples	Diagnostic (diagnosis of cutaneous melanoma)	90.0%	–	0.80	(285)
miR-150-5p	Upregulated	Plasma samples	Diagnostic (diagnosis of cutaneous melanoma)	96.7%	–	0.94	
miR-149-3p	Upregulated	Plasma samples	Diagnostic (diagnosis of cutaneous melanoma)	93.3%	–	0.95	
miR-193a-3p	Downregulated	Plasma samples	Diagnostic (diagnosis of cutaneous melanoma)	76.7	–	0.84	
miR-524-5p	Downregulated	Plasma samples	Diagnostic (diagnosis of cutaneous melanoma)	90.0%	–	0.80	
miR-149-3p miR-150-5p miR-193a-3p	Upregulated Upregulated Downregulated	Plasma samples	Diagnostic (diagnosis of cutaneous melanoma)	94.8%	–	0.97	
hsa-miR-186 hsa-let-7d hsa-miR-18a hsa-miR-145 hsa-miR-99a hsa-miR-664 hsa-miR-501-5p hsa-miR-378 hsa-miR-29c hsa-miR-1280 hsa-miR-365 hsa-miR-1249 hsa-miR-	Upregulated Upregulated Upregulated Upregulated Upregulated Upregulated Upregulated Upregulated - Upregulated Upregulated Upregulated Upregulated - Downregulated	Blood samples (expression of miRNAs in blood cells)	Diagnostic	98.9%	95%	97.4%	(286)

(Continued)

TABLE 4 | Continued

microRNA	Expression pattern	Sample	Diagnostic biomarker	ROC curve analysis			Reference
				Sensitivity	Specificity	Area under the ROC curves (AUC)	
328 hsa-miR-422a hsa-miR-30 d hsa-miR-17							
miR-125b	Downregulated	Tissue samples	Diagnostic biomarker (diagnosis of melanoma)	–	–	0.880	(281)
miR-211	Downregulated	Serum samples	Diagnostic biomarker (distinguish metastatic from uveal melanoma localized one)	–	–	0.96	(287)
miR-16 miR-145 miR-146a miR-204 miR-211 miR-363-3p	Downregulated Downregulated Downregulated Downregulated Downregulated Downregulated	Serum samples	Diagnostic biomarker (identifying uveal melanoma)	93%	100%	–	
miR-10b	Upregulated	Serum samples	Diagnostic biomarker (distinguishing melanoma patients from controls)	–	–	0.841	(275)

DISCUSSION

Dysregulation of miRNAs in melanoma samples and cell line have been reported by several studies. The functional consequences of such dysregulation on cell behavior have also been appraised. However, the underlying mechanism of such dysregulation is not clarified completely. Copy number variations in miRNA-coding genes or genes associated with the biogenesis or function of miRNAs may be responsible for the observed dysregulation of miRNAs in melanoma and other types of cancers (10). Moreover, the role of epigenetic factors in this process should not be ignored. For instance, CpG methylation of the miR-34a promoter has been suggested as an underlying mechanism for down-regulation of this miRNA in primary melanoma samples and melanoma cell lines (297). Another possible mediators of miRNA dysregulation in the melanoma are melanoma-inducing transcription factors such as MITF whose role in the expression of a number of miRNAs has been verified (298). As several miRNAs are implicated in the modulation of skin response to ultraviolet radiation (299), this environmental carcinogen might also affect expression of miRNAs which are involved in the melanomagenesis.

Mechanistically, several melanoma-associated miRNAs function upstream or downstream of known oncogenes in melanoma. For instance, miR-137 and miR-182 are among miRNAs that target MITF oncogene (54, 300). Moreover, expressions of several miRNAs such as a number of let-7 family members, miR-221/222, miR-17-92 and miR-106-363 clusters, miR-29, miR-146a, miR-148b, and miR-125b have been shown to be modulated by MITF (298). Moreover, several miRNAs such as miR-7, miR-23a and miR-596 have functional interactions with MAPK/ERK and PI3K/PTEN/Akt signaling pathways in the context of melanoma. A number of miRNAs such as miR-378, miR-10b, miR-25, miR-485-5p, miR-708, miR-136, miR-488-5p, miR-29a, miR-22 and miR-140-5p have interactions with Wnt/β-catenin pathway. Finally, miR-21, miR-7-5p, miR-23b, miR-145-5p, miR-9, miR-29a, miR-377 and miR-140-5p interacts with NF-κB signaling in the context of melanoma development. Thus, a number of miRNAs provide functional links between cancer-related pathways in this context.

miRNAs have functions both in the paternal cell in which they are produced as well as in the adjoining cells. These transcripts can modulate characteristics of adjacent melanoma cells or directly affect tumor niche by modifying extracellular matrix and function of resident cells in this environment including fibroblasts and endothelial or immune cells. This activity of miRNAs potentiates them as contributors of melanoma metastatic potential through affecting intravasation of cancer cells into vessels, viability of tumor cells in the circulation, their leakage in the target tissues, and establishment of the pre-metastatic milieu in remote organs (301).

Several miRNAs have been shown to differentiate melanoma patients from healthy subjects or distinguish between metastatic and non-metastatic melanoma patients. The prognostic assays founded on miRNAs signature can enhance the efficacy of conventional staging systems in predicting patients' prognosis and their management in the clinical settings in the terms of choosing adjuvant therapies or clinical trial enrolment. Therefore, these miRNAs are potential biomarkers for this kind of skin cancer.

Numerous miRNAs have been dysregulated in tumor samples or peripheral blood of patients with melanoma. Such dysregulation can be used as biomarker for early detection of melanoma or follow-up of patients after initial treatments to uncover any possible tumor recurrence. Blood-based biomarkers are expected to substitute invasive methods of cancer diagnosis

TABLE 5 | Prognostic role of miRNAs in melanoma as identified by ROC curve analysis.

microRNA	Expression pattern	Sample	Prognostic biomarker	ROC curve analysis			Reference
				Sensitivity	Specificity	Area under the ROC curves (AUC)	
miR-150-5p	Downregulated	Serum samples	Prognostic (discrimination of survival in stage IV)	–	–	0.69	(118)
		Tissue samples	Prognostic (discrimination of stage)	–	–	0.733	
miR-142-3p	Downregulated	Serum samples	Prognostic (discrimination of stage IV from stage III)	–	–	0.69	
		Tissue samples	Prognostic (discrimination of stage)	–	–	0.797	
miR-142-5p	Downregulated	Tissue samples	Prognostic (discrimination of stage)	–	–	0.733	
miR-150-5p Downregulated miR-142-3p Downregulated miR-142-5p	Downregulated	Tissue samples	Prognostic (discrimination of stage)	–	–	0.838	
miR-4633-5p	Downregulated	Tissue samples	Prognostic (identifying metastatic sinonasal mucosal melanoma)	87.5%	100%	0.88	(175)
miR-1246 miR-185	Upregulated Upregulated	Plasma samples	Prognostic (identifying metastatic melanoma)	90.5%	89.1%	–	(288)
miR-9 miR-145 miR-150 miR-155 miR-205	Upregulated - - - -	Serum samples	Prognostic (distinguishing metastatic melanoma)	–	–	0.77	(289)
miR-532-5p	-	Serum exosomes	Prognostic (distinguishing patients with and without metastasis)	–	–	0.818	(284)
miR-106b		Serum exosomes	Prognostic (discriminates stage I–II patients from stage III–IV patients)	–	–	0.820	
miR-23a	Downregulated	Serum samples	Prognostic (distinguishing primary melanoma from metastatic one)	76.0%	75.3%	0.797	(106)
miR-195 miR-224 miR-365a miR-365b miR-452 miR-4709 miR-7702 miR-513c miR-873	- - - - - - - - -	Tissue samples	Prognostic biomarker (for OS)	–	–	0.858	(290)
let-7b	Downregulated	Tissue samples	Prognostic biomarker (for DFS)	–	–	0.634	(211)
let-7c	Downregulated	Tissue samples	Prognostic biomarker (for DFS)	–	–	0.647	
miR-10b	Upregulated	Serum samples	Prognostic biomarker (advanced stage vs early stage)	–	–	0.785	(275)

in future. Based on the heterogeneous pattern of miRNAs expression in tumor samples and the varied expressions among affected individuals, multi-miRNA panels are more promising in the diagnostic approaches compared with individual miRNAs.

Finally, miRNAs might be implicated in the anti-cancer effects of a number of therapeutic agents including both chemical and herbal medicines. Evidence for supporting this idea has come from several studies including a study which revealed the role of miR-27a in mediating the anti-proliferative effects of Genistein in human uveal melanoma cells (291). Moreover, the observed up-regulation of miR-222 in melanoma samples obtained from patients who did not respond to ipilimumab compared with those benefitting from this option (292) implies its contribution in resistance to this agent. Therefore, miRNAs are promising targets for modulation of response of melanoma cells to a wide range of therapeutic options.

PERSPECTIVES AND FUTURE DIRECTIONS

Assessment of expression pattern of miRNAs in cohorts of melanoma patients from different ethnicities and uncovering

TABLE 6 | Summary of studies which assessed association between miRNA polymorphisms and risk of melanoma.

microRNA	SNP	Genotyping method	Samples	Association with melanoma	Functional experiments	Reference
miR-146a	rs2910164G>C	–	Blood samples from 224 patients and 264 healthy controls	Allele C was associated with risk of melanoma in males and has allelic dosage effect (CC homozygotes has greater risk)	–	(294)
miR-146a and RNASEL polymorphisms interaction	rs2910164 G/C (in miR-146a) rs486907 A/G (in RNASEL)	PCR-RFLP	Blood samples from 304 sporadic melanoma patients and 314 control individuals	Men carrying allelic combination miR-146a rs2910164 C and RNASEL rs486907 A have highest risk of melanoma	–	(295)
miR-146a	rs2910164 G/C	PCR-RFLP	Skin samples from 50 melanoma patients and 107 controls, 8 blood samples from patients	GC genotype was significantly increased in the patients compared with the controls	G allele confers high proliferative capacity to melanoma cell lines and GC cell lines have more invasive and migratory ability than CC cell lines	(296)

their association with genetic polymorphisms would facilitate design of prognostic/diagnostic panels. The relationship between aberrant miRNA profile and response to therapeutic regimens should be unraveled. Such kinds of approaches pave the way for design of personalized methods of treatment of melanoma. Therapeutic targeting of miRNAs can influence melanoma course and enhance sensitivity to both conventional therapies and immunotherapeutic approaches. Yet, safety and bioavailability issues remained to be solved before implementation of these techniques in the clinical settings.

AUTHOR CONTRIBUTIONS

SG-F and MT wrote the draft and revised it. MG collected the tables and designed it. All authors contributed to the article and approved the submitted version.

REFERENCES

1. Linos E, Swetter SM, Cockburn MG, Colditz GA, Clarke CA. Increasing Burden of Melanoma in the United States. *J Invest Dermatol* (2009) 129 (7):1666–74. doi: 10.1038/jid.2008.423
2. Noone A, Howlader N, Krapcho M, Miller D, Brest A, Yu M, et al. *SEER Cancer Statistics Review, 1975-2015* Vol. 4. Bethesda, MD: National Cancer Institute (2018).
3. Erdei E, Torres SM. A New Understanding in the Epidemiology of Melanoma. *Expert Rev Anticancer Ther* (2010) 10(11):1811–23. doi: 10.1586/era.10.170
4. Liu Y, Sheikh MS. Melanoma: Molecular Pathogenesis and Therapeutic Management. *Mol Cell Pharmacol* (2014) 6(3):228.
5. Safa A, Gholipour M, Dinger ME, Taheri M, Ghafouri-Fard S. The Critical Roles of LncRNAs in the Pathogenesis of Melanoma. *Exp Mol Pathol* (2020) 117:104558. doi: 10.1016/j.yexmp.2020.104558
6. Gellrich FF, Schmitz M, Beissert S, Meier F. Anti-PD-1 and Novel Combinations in the Treatment of Melanoma—an Update. *J Clin Med* (2020) 9(1):223. doi: 10.3390/jcm9010223
7. Howell PM, Li X, Riker AI, Xi Y. MicroRNA in Melanoma. *Ochsner J* (2010) 10(2):83–92.
8. O'Brien J, Hayder H, Zayed Y, Peng C. Overview of MicroRNA Biogenesis, Mechanisms of Actions, and Circulation. *Front Endocrinol* (2018) 9:402. doi: 10.3389/fendo.2018.00402
9. Vasudevan S, Steitz JA. AU-rich-element-mediated Upregulation of Translation by FXR1 and Argonaute 2. *Cell* (2007) 128(6):1105–18. doi: 10.1016/j.cell.2007.01.038
10. Zhang L, Huang J, Yang N, Greshock J, Megraw MS, Giannakakis A, et al. MicroRNAs Exhibit High Frequency Genomic Alterations in Human Cancer. *Proc Natl Acad Sci* (2006) 103(24):9136–41. doi: 10.1073/pnas.0508889103
11. Aksenenko M, Palkina N, Komina A, Tashireva L, Ruksha T. Differences in MicroRNA Expression Between Melanoma and Healthy Adjacent Skin. *BMC Dermatol* (2019) 19(1):1–9. doi: 10.1186/s12895-018-0081-1
12. Ren J-W, Li Z-J, Tu C. MiR-135 Post-Transcriptionally Regulates FOXO1 Expression and Promotes Cell Proliferation in Human Malignant Melanoma Cells. *Int J Clin Exp Pathol* (2015) 8(6):6356.
13. Ratnayake WS, Apostolatos CA, Breedy S, Apostolatos AH, Acevedo-Duncan M. FOXO1 Regulates Oncogenic PKC-ι Expression in Melanoma Inversely to c-Jun in an Autocrine Manner Via IL-17E and ICAM-1 Activation. *World Acad Sci J* (2019) 1(1):25–38. doi: 10.3892/wasj.2018.1
14. Dar AA, Majid S, de Semir D, Nosrati M, Bezrookove V, Kashani-Sabet M. MiRNA-205 Suppresses Melanoma Cell Proliferation and Induces Senescence Via Regulation of E2F1 Protein. *J Biol Chem* (2011) 286 (19):16606–14. doi: 10.1074/jbc.M111.227611
15. Mueller DW, Rehli M, Bosserhoff AK. MiRNA Expression Profiling in Melanocytes and Melanoma Cell Lines Reveals MiRNAs Associated With Formation and Progression of Malignant Melanoma. *J Invest Dermatol* (2009) 129(7):1740–51. doi: 10.1038/jid.2008.452
16. Levati L, Alvino E, Pagani E, Arcelli D, Caporaso P, Bondanza S, et al. Altered Expression of Selected MicroRNAs in Melanoma: Antiproliferative and Proapoptotic Activity of Mirna-155. *Int J Oncol* (2009) 35(2):393–400. doi: 10.3892/ijo_00000352
17. Felicetti F, Errico MC, Segnalini P, Mattia G, Carè A. MicroRNA-221 and-222 Pathway Controls Melanoma Progression. *Expert Rev Anticancer Ther* (2008) 8(11):1759–65. doi: 10.1586/14737140.8.11.1759
18. Igoucheva O, Alexeev V. MicroRNA-dependent Regulation of cKit in Cutaneous Melanoma. *Biochem Biophys Res Commun* (2009) 379(3):790–4. doi: 10.1016/j.bbrc.2008.12.152
19. Zhang Z, Sun H, Dai H, Walsh R, Imakura M, Schelter J, et al. MicroRNA miR-210 Modulates Cellular Response to Hypoxia Through the MYC Antagonist MNT. *Cell Cycle* (2009) 8(17):2756–68. doi: 10.4161/cc.8.17.9387
20. Vitiello M, Tuccoli A, D'Aurizio R, Sarti S, Giannecchini L, Lubrano S, et al. Context-Dependent miR-204 and miR-211 Affect the Biological Properties of Amelanotic and Melanotic Melanoma Cells. *Oncotarget* (2017) 8 (15):25395. doi: 10.18632/oncotarget.15915
21. Sahoo A, Sahoo SK, Joshi P, Lee B, Perera RJ. MicroRNA-211 Loss Promotes Metabolic Vulnerability and BRAF Inhibitor Sensitivity in Melanoma. *J Invest Dermatol* (2019) 139(1):167–76. doi: 10.1016/j.jid.2018.06.189
22. Díaz-Martínez M, Benito-Jardón L, Alonso L, Koetz-Ploch L, Hernando E, Teixidó J. miR-204-5p and miR-211-5p Contribute to BRAF Inhibitor Resistance in Melanoma. *Cancer Res* (2018) 78(4):1017–30. doi: 10.1158/0008-5472.CAN-17-1318

23. Stark MS, Klein K, Weide B, Haydu LE, Pflugfelder A, Tang YH, et al. The Prognostic and Predictive Value of Melanoma-Related MicroRNAs Using Tissue and Serum: A MicroRNA Expression Analysis. *EBioMedicine* (2015) 2(7):671–80. doi: 10.1016/j.ebiom.2015.05.011
24. Sun M, Ma X, Tu C, Wang X, Qu J, Wang S, et al. MicroRNA-378 Regulates Epithelial–Mesenchymal Transition and Metastasis of Melanoma by Inhibiting FOXN3 Expression Through the Wnt/β-Catenin Pathway. *Cell Biol Int* (2019) 43(10):1113–24. doi: 10.1002/cbin.11027
25. Tupone MG, D'Aguanno S, Di Martile M, Valentini E, Desideri M, Trisciuoglio D, et al. MicroRNA-378a-5p is a Novel Positive Regulator of Melanoma Progression. *Oncogenesis* (2020) 9(2):1–13. doi: 10.1038/s41389-020-0203-6
26. Pencheva N, Tran H, Buss C, Huh D, Drobnjak M, Busam K, et al. Convergent Multi-MiRNA Targeting of Apoe Drives LRP1/LRP8-dependent Melanoma Metastasis and Angiogenesis. *Cell* (2012) 151 (5):1068–82. doi: 10.1016/j.cell.2012.10.028
27. Lin N, Zhou Y, Lian X, Tu Y. Expression of MicroRNA-106b and Its Clinical Significance in Cutaneous Melanoma. *Genet Mol Res* (2015) 14(4):16379–85. doi: 10.4238/2015.December.9.6
28. Wang J, Li H, Zhang J, Zhang C, Hou X. Suppression of Connexin 43 Expression by miR-106a Promotes Melanoma Cell Proliferation. *Eur Rev Med Pharmacol Sci* (2019) 23(3):965–71. doi: 10.26355/eurrev_201902_16983
29. Mastroianni J, Stickel N, Andrlova H, Hanke K, Melchinger W, Duquesne S, et al. miR-146a Controls Immune Response in the Melanoma Microenvironment. *Cancer Res* (2019) 79(1):183–95. doi: 10.1158/0008-5472.CAN-18-1397
30. Raimo M, Orso F, Grassi E, Cimino D, Penna E, De Pittà C, et al. miR-146a Exerts Differential Effects on Melanoma Growth and Metastatization. *Mol Cancer Res* (2016) 14(6):548–62. doi: 10.1158/1541-7786.MCR-15-0425-T
31. Forloni M, Dogra SK, Dong Y, Conte D, Ou J, Zhu LJ, et al. miR-146a Promotes the Initiation and Progression of Melanoma by Activating Notch Signaling. *Elife* (2014) 3:e01460. doi: 10.7554/eLife.01460
32. Pu W, Shang Y, Shao Q, Yuan X. miR-146a Promotes Cell Migration and Invasion in Melanoma by Directly Targeting SMAD4. *Oncol Lett* (2018) 15 (5):7111–7. doi: 10.3892/ol.2018.8172
33. Saldanha G, Elshaw S, Sachs P, Alharbi H, Shah P, Jothi A, et al. MicroRNA-10b is a Prognostic Biomarker for Melanoma. *Modern Pathol* (2016) 29 (2):112–21. doi: 10.1038/modpathol.2015.149
34. Datar I, Kalpana G, Choi J, Basuroy T, Trumbly R, Chaitanya Arudra SK, et al. Critical Role of miR-10b in B-RafV600E Dependent Anchorage Independent Growth and Invasion of Melanoma Cells. *PloS One* (2019) 14(4):e0204387. doi: 10.1371/journal.pone.0204387
35. Wang S, Wu Y, Xu Y, Tang X. miR-10b Promoted Melanoma Progression Through Wnt/β-Catenin Pathway by Repressing ITCH Expression. *Gene* (2019) 710:39–47. doi: 10.1016/j.gene.2019.05.043
36. Jiao J, Fan Y, Zhang Y. Expression and Clinicopathological Significance of MicroRNA-21 and Programmed Cell Death 4 in Malignant Melanoma. *J Int Med Res* (2015) 43(5):672–8. doi: 10.1177/0300060515583707
37. Jiang L, Lv X, Li J, Li J, Li X, Li W, et al. The Status of MicroRNA-21 Expression and Its Clinical Significance in Human Cutaneous Malignant Melanoma. *Acta Histochem* (2012) 114(6):582–8. doi: 10.1016/j.acthis.2011.11.001
38. Satzger I, Mattern A, Kuettler U, Weinspach D, Niebuhr M, Kapp A, et al. Micro RNA-21 is Upregulated in Malignant Melanoma and Influences Apoptosis of Melanocytic Cells. *Exp Dermatol* (2012) 21(7):509–14. doi: 10.1111/j.1600-0625.2012.01510.x
39. Del Campo SEM, Latchana N, Levine KM, Grignol VP, Fairchild ET, Jaime-Ramirez AC, et al. MiR-21 Enhances Melanoma Invasiveness Via Inhibition of Tissue Inhibitor of Metalloproteinases 3 Expression: in Vivo Effects of MiR-21 Inhibitor. *PloS One* (2015) 10(1):e0115919. doi: 10.1371/journal.pone.0115919
40. Mao XH, Chen M, Wang Y, Cui PG, Liu SB, Xu ZY. MicroRNA-21 Regulates the ERK/NF-κb Signaling Pathway to Affect the Proliferation, Migration, and Apoptosis of Human Melanoma A375 Cells by Targeting SPRY1, PDCD4, and PTEN. *Mol Carcinogen* (2017) 56(3):886–94. doi: 10.1002/mc.22542
41. Wang Y-C, Yang X, Wei W-B, Xu X-L. Role of MicroRNA-21 in Uveal Melanoma Cell Invasion and Metastasis by Regulating p53 and Its Downstream Protein. *Int J Ophthalmol* (2018) 11(8):1258. doi: 10.18240/ijo.2018.08.03
42. Yang Z, Liao B, Xiang X, Ke S. miR-21-5p Promotes Cell Proliferation and G1/s Transition in Melanoma by Targeting CDKN2C. *FEBS Open Bio* (2020) 10(5):752–60. doi: 10.1002/2211-5463.12819
43. Xia Z, Yang C, Yang X, Wu S, Feng Z, Qu L, et al. MiR-652 Promotes Proliferation and Migration of Uveal Melanoma Cells by Targeting HOXA9. *Med Sci Monit* (2019) 25:8722. doi: 10.12659/MSM.917099
44. Ling J, Lu P, Zhang Y, Jiang S, Zhang Z. miR-367 Promotes Uveal Melanoma Cell Proliferation and Migration by Regulating PTEN. *Genet Mol Res* (2017) 16(3). doi: 10.4238/gmr16039067
45. Komina A, Palkina N, Aksenenko M, Tsyrenzhapova S, Ruksha T. Antiproliferative and Pro-Apoptotic Effects of MiR-4286 Inhibition in Melanoma Cells. *PloS One* (2016) 11(12):e0168229. doi: 10.1371/journal.pone.0168229
46. Long J, Luo J, Yin X. miR−367 Enhances the Proliferation and Invasion of Cutaneous Malignant Melanoma by Regulating Phosphatase and Tensin Homolog Expression. *Mol Med Rep* (2018) 17(5):6526–32. doi: 10.3892/mmr.2018.8663
47. Bhattacharya A, Schmitz U, Raatz Y, Schönherr M, Kottek T, Schauer M, et al. miR-638 Promotes Melanoma Metastasis and Protects Melanoma Cells From Apoptosis and Autophagy. *Oncotarget* (2015) 6(5):2966. doi: 10.18632/oncotarget.3070
48. Long J, Luo J, Yin X. MiR-338-5p Promotes the Growth and Metastasis of Malignant Melanoma Cells Via Targeting CD82. *Biomed Pharmacother* (2018) 102:1195–202. doi: 10.1016/j.biopha.2018.03.075
49. Hao T, Li C, Ding X, Xing X. MicroRNA-363-3p/p21 (Cip1/Waf1) Axis is Regulated by HIF-2α in Mediating Stemness of Melanoma Cells. *Neoplasma* (2019) 66(3):427–36. doi: 10.4149/neo_2018_180828N655
50. Satzger I, Mattern A, Kuettler U, Weinspach D, Voelker B, Kapp A, et al. MicroRNA-15b Represents an Independent Prognostic Parameter and is Correlated With Tumor Cell Proliferation and Apoptosis in Malignant Melanoma. *Int J Cancer* (2010) 126(11):2553–62. doi: 10.1002/ijc.24960
51. Sun L, Wang Q, Gao X, Shi D, Mi S, Han Q. MicroRNA-454 Functions as an Oncogene by Regulating PTEN in Uveal Melanoma. *FEBS Lett* (2015) 589 (19):2791–6. doi: 10.1016/j.febslet.2015.08.007
52. Penna E, Orso F, Cimino D, Tenaglia E, Lembo A, Quaglino E, et al. MicroRNA-214 Contributes to Melanoma Tumour Progression Through Suppression of TFAP2C. *EMBO J* (2011) 30(10):1990–2007. doi: 10.1038/emboj.2011.102
53. Li J, Zhao R, Fang R, Wang J. miR-122-5p Inhibits the Proliferation of Melanoma Cells by Targeting NOP14. *J South Med Univ* (2018) 38 (11):1360–5. doi: 10.12122/j.issn.1673-4254.2018.11.14
54. Segura MF, Hanniford D, Menendez S, Reavie L, Zou X, Alvarez-Diaz S, et al. Aberrant miR-182 Expression Promotes Melanoma Metastasis by Repressing FOXO3 and Microphthalmia-Associated Transcription Factor. *Proc Natl Acad Sci* (2009) 106(6):1814–9. doi: 10.1073/pnas.0808263106
55. Li P, He Q-Y, Luo C-Q, Qian L-Y. Circulating miR-221 Expression Level and Prognosis of Cutaneous Malignant Melanoma. *Med Sci Monit* (2014) 20:2472. doi: 10.12659/MSM.891327
56. Zhang K, Guo L. MiR-767 Promoted Cell Proliferation in Human Melanoma by Suppressing CYLD Expression. *Gene* (2018) 641:272–8. doi: 10.1016/j.gene.2017.10.055
57. Hu Y, Wang Q, Zhu X-H. MiR-135b is a Novel Oncogenic Factor in Cutaneous Melanoma by Targeting LATS2. *Melanoma Res* (2019) 29 (2):119–25. doi: 10.1097/CMR.0000000000000524
58. Jiang Q-Q, Liu W-B. miR-25 Promotes Melanoma Progression by Regulating RNA Binding Motif Protein 47. *Médecine/Sciences* (2018) 34:59–65. doi: 10.1051/medsci/201834f111
59. Huo J, Zhang Y, Li R, Wang Y, Wu J, Zhang D. Upregulated MicroRNA-25 Mediates the Migration of Melanoma Cells by Targeting DKK3 Through the WNT/β-Catenin Pathway. *Int J Mol Sci* (2016) 17(11):1124. doi: 10.3390/ijms17111124
60. Koetz-Ploch L, Hanniford D, Dolgalev I, Sokolova E, Zhong J, Díaz-Martínez M, et al. Micro RNA-125a Promotes Resistance to BRAF

Inhibitors Through Suppression of the Intrinsic Apoptotic Pathway. *Pigment Cell Melanoma Res* (2017) 30(3):328–38. doi: 10.1111/pcmr.12578
61. Chen X-E, Chen P, Chen S-S, Ma T, Shi G, Zhou Y, et al. miR–106b–5p Promotes Cell Cycle Progression of Malignant Melanoma by Targeting PTEN. *Oncol Rep* (2018) 39(1):331–7. doi: 10.3892/or.2017.6099
62. Zhang L, He X, Li F, Pan H, Huang X, Wen X, et al. The miR-181 Family Promotes Cell Cycle by Targeting CTDSPL, a Phosphatase-Like Tumor Suppressor in Uveal Melanoma. *J Exp Clin Cancer Res* (2018) 37(1):1–13. doi: 10.1186/s13046-018-0679-5
63. Qiu H-J, Lu X-H, Yang S-S, Weng C-Y, Zhang E-K, Chen F-C. MiR-769 Promoted Cell Proliferation in Human Melanoma by Suppressing GSK3B Expression. *Biomed Pharmacother* (2016) 82:117–23. doi: 10.1016/j.biopha.2016.04.052
64. Zhou J, Jiang J, Wang S, Xia X. Oncogenic Role of MicroRNA–20a in Human Uveal Melanoma. *Mol Med Rep* (2016) 14(2):1560–6. doi: 10.3892/mmr.2016.5433
65. Gaziel-Sovran A, Segura MF, Di Micco R, Collins MK, Hanniford D, de Miera EV-S, et al. miR-30b/30d Regulation of GalNAc Transferases Enhances Invasion and Immunosuppression During Metastasis. *Cancer Cell* (2011) 20(1):104–18. doi: 10.1016/j.ccr.2011.05.027
66. Knoll S, Fürst K, Kowtharapu B, Schmitz U, Marquardt S, Wolkenhauer O, et al. E2F1 Induces miR-224/452 Expression to Drive EMT Through TXNIP Downregulation. *EMBO Rep* (2014) 15(12):1315–29. doi: 10.15252/embr.201439392
67. Ohira T, Naohiro S, Nakayama Y, Osaki M, Okada F, Oshimura M, et al. miR-19b Regulates HTERT MRNA Expression Through Targeting PITX1 MRNA in Melanoma Cells. *Sci Rep* (2015) 5(1):1–9. doi: 10.1038/srep08201
68. Lankenau MA, Patel R, Liyanarachchi S, Maharry SE, Hoag KW, Duggan M, et al. MicroRNA-3151 Inactivates TP53 in BRAF-mutated Human Malignancies. *Proc Natl Acad Sci* (2015) 112(49):E6744–E51. doi: 10.1073/pnas.1520390112
69. Cui L, Li Y, Lv X, Li J, Wang X, Lei Z, et al. Expression of MicroRNA-301a and Its Functional Roles in Malignant Melanoma. *Cell Physiol Biochem* (2016) 40(1–2):230–44. doi: 10.1159/000452540
70. Zhang D, Li Z, Zhang Y, Tu C, Huo J, Liu Y. miR-4262 Promotes the Proliferation of Human Cutaneous Malignant Melanoma Cells Through KLF6-mediated EGFR Inactivation and p21 Upregulation. *Oncol Rep* (2016) 36(6):3657–63. doi: 10.3892/or.2016.5190
71. Prasad R, Katiyar SK. Down-Regulation of MiRNA-106b Inhibits Growth of Melanoma Cells by Promoting G1-Phase Cell Cycle Arrest and Reactivation of P21/WAF1/Cip1 Protein. *Oncotarget* (2014) 5(21):10636. doi: 10.18632/oncotarget.2527
72. Hua K-T, Hong J-B, Sheen Y-S, Huang H-Y, Huang Y-L, Chen J-S, et al. miR-519d Promotes Melanoma Progression by Downregulating Epha4. *Cancer Res* (2018) 78(1):216–29. doi: 10.1158/0008-5472.CAN-17-1933
73. Wei S, Ma W. MiR-370 Functions as Oncogene in Melanoma by Direct Targeting Pyruvate Dehydrogenase B. *Biomed Pharmacother* (2017) 90:278–86. doi: 10.1016/j.biopha.2017.03.068
74. Bai X, Yang M, Xu Y. MicroRNA–373 Promotes Cell Migration Via Targeting Salt–Inducible Kinase 1 Expression in Melanoma. *Exp Ther Med* (2018) 16(6):4759–64. doi: 10.3892/etm.2018.6784
75. Sun H, Yang G, Wang S, Zhang Y, Ding J, Zhang X. MicroRNA-92a Regulates the Development of Cutaneous Malignant Melanoma by Mediating FOXP1. *Eur Rev Med Pharmacol Sci* (2019) 23(20):8991–9. doi: 10.26355/eurrev_201910_19299
76. Yang C, Yan Z, Hu F, Wei W, Sun Z, Xu W. Silencing of MicroRNA-517a Induces Oxidative Stress Injury in Melanoma Cells Via Inactivation of the JNK Signaling Pathway by Upregulating CDKN1C. *Cancer Cell Int* (2020) 20(1):32. doi: 10.1186/s12935-019-1064-y
77. Tang H, Xu X, Xiao W, Liao Y, Xiao X, Li L, et al. Silencing of MicroRNA-27a Facilitates Autophagy and Apoptosis of Melanoma Cells Through the Activation of the SYK-dependent MTOR Signaling Pathway. *J Cell Biochem* (2019) 120(8):13262–74. doi: 10.1002/jcb.28600
78. Qiu H, Yuan S, Lu X. miR–186 Suppressed CYLD Expression and Promoted Cell Proliferation in Human Melanoma. *Oncol Lett* (2016) 12(4):2301–6. doi: 10.3892/ol.2016.5002
79. Yu Y, Yu F, Sun P. MicroRNA-1246 Promotes Melanoma Progression Through Targeting Foxa2. *OncoTargets Ther* (2020) 13:1245. doi: 10.2147/OTT.S234276
80. Wan J, Yang J, Huang Y, Deng L. MicroRNA–150 Inhibitors Enhance Cell Apoptosis of Melanoma by Targeting PDCD4. *Oncol Lett* (2018) 15(2):1475–82. doi: 10.3892/ol.2017.7445
81. Sun M-X, An Q, Chen L-M, Guo L. MIR-520f Regulated Itch Expression and Promoted Cell Proliferation in Human Melanoma Cells. *Dose-Response* (2020) 18(2):1559325820918450. doi: 10.1177/1559325820918450
82. Wang Z, Liu Y. MicroRNA–633 Enhances Melanoma Cell Proliferation and Migration by Suppressing KAI1. *Oncol Lett* (2021) 21(2):1–. doi: 10.3892/ol.2020.12349
83. Yan D, Zhou X, Chen X, Hu D-N, Da Dong X, Wang J, et al. MicroRNA-34a Inhibits Uveal Melanoma Cell Proliferation and Migration Through Downregulation of C-Met. *Invest Ophthalmol Visual Sci* (2009) 50(4):1559–65. doi: 10.1167/iovs.08-2681
84. Migliore C, Petrelli A, Ghiso E, Corso S, Capparuccia L, Eramo A, et al. MicroRNAs Impair MET-mediated Invasive Growth. *Cancer Res* (2008) 68(24):10128–36. doi: 10.1158/0008-5472.CAN-08-2148
85. Schultz J, Lorenz P, Gross G, Ibrahim S, Kunz M. MicroRNA let-7b Targets Important Cell Cycle Molecules in Malignant Melanoma Cells and Interferes With Anchorage-Independent Growth. *Cell Res* (2008) 18(5):549–57. doi: 10.1038/cr.2008.45
86. Müller D, Bosserhoff A-K. Integrin β 3 Expression is Regulated by let-7a MiRNA in Malignant Melanoma. *Oncogene* (2008) 27(52):6698–706. doi: 10.1038/onc.2008.282
87. Huang D, Wang F, Wu W, Lian C, Liu E. MicroRNA-429 Inhibits Cancer Cell Proliferation and Migration by Targeting the AKT1 in Melanoma. *Cancer Biomark* (2019) 26(1):63–8. doi: 10.3233/CBM-190289
88. Sheng H, Guo Y, Cao D, Li X, Zhao Y, Ding H, et al. MiR-429-5p Attenuates the Migration and Invasion of Malignant Melanoma by Targeting LIMK1. *Eur Rev Med Pharmacol Sci* (2020) 24(5):2625–31. doi: 10.26355/eurrev_202003_20531
89. Kang K, Zhang J, Zhang X, Chen Z. MicroRNA-326 Inhibits Melanoma Progression by Targeting KRAS and Suppressing the AKT and ERK Signalling Pathways. *Oncol Rep* (2018) 39(1):401–10. doi: 10.3892/or.2017.6074
90. Dong F, Lou D. MicroRNA-34b/c Suppresses Uveal Melanoma Cell Proliferation and Migration Through Multiple Targets. *Mol Vis* (2012) 18:537.
91. Hou Q, Han S, Yang L, Chen S, Chen J, Ma N, et al. The Interplay of MicroRNA-34a, LGR4, EMT-associated Factors, and MMP2 in Regulating Uveal Melanoma Cells. *Invest Ophthalmol Visual Sci* (2019) 60(13):4503–10. doi: 10.1167/iovs.18-26477
92. Liu R, Xie H, Luo C, Chen Z, Zhou X, Xia K, et al. Identification of FLOT2 as a Novel Target for MicroRNA-34a in Melanoma. *J Cancer Res Clin Oncol* (2015) 141(6):993–1006. doi: 10.1007/s00432-014-1874-1
93. Greenberg E, Hershkovitz L, Itzhaki O, Hajdu S, Nemlich Y, Ortenberg R, et al. Regulation of Cancer Aggressive Features in Melanoma Cells by Micrornas. *PloS One* (2011) 6(4):e18936. doi: 10.1371/journal.pone.0018936
94. Yan D, Da Dong X, Chen X, Yao S, Wang L, Wang J, et al. Role of MicroRNA-182 in Posterior Uveal Melanoma: Regulation of Tumor Development Through MITF, BCL2 and Cyclin D2. *PloS One* (2012) 7(7):e40967. doi: 10.1371/journal.pone.0040967
95. Venza I, Visalli M, Beninati C, Benfatto S, Teti D, Venza M. Il-10rα Expression is Post-Transcriptionally Regulated by miR-15a, miR-185, and miR-211 in Melanoma. *BMC Med Genomics* (2015) 8(1):1–9. doi: 10.1186/s12920-015-0156-3
96. Zhu Y, Wen X, Zhao P. MicroRNA-365 Inhibits Cell Growth and Promotes Apoptosis in Melanoma by Targeting BCL2 and Cyclin D1 (CCND1). *Med Sci Monit* (2018) 24:3679. doi: 10.12659/MSM.909633
97. Bai J, Zhang Z, Li X, Liu H. MicroRNA-365 Inhibits Growth, Invasion and Metastasis of Malignant Melanoma by Targeting NRP1 Expression. *Cancer Biomark* (2015) 15(5):599–608. doi: 10.3233/CBM-150500
98. Wu J, Li J, Ren J, Zhang D. MicroRNA-485-5p Represses Melanoma Cell Invasion and Proliferation by Suppressing Frizzled7. *Biomed Pharmacother* (2017) 90:303–10. doi: 10.1016/j.biopha.2017.03.064
99. Zhu Y, H-l Z, Wang Q-Y, Chen M-J, Liu L-B. Overexpression of MicroRNA-612 Restrains the Growth, Invasion, and Tumorigenesis of Melanoma Cells by Targeting Espin. *Molec Cells* (2018) 41(2):119. doi: 10.14348/molcells.2018.2235

100. Giles KM, Brown RA, Ganda C, Podgorny MJ, Candy PA, Wintle LC, et al. MicroRNA-7-5p Inhibits Melanoma Cell Proliferation and Metastasis by Suppressing Rela/NF-κb. *Oncotarget* (2016) 7(22):31663. doi: 10.18632/oncotarget.9421
101. Giles KM, Brown RA, Epis MR, Kalinowski FC, Leedman PJ. MiRNA-7-5p Inhibits Melanoma Cell Migration and Invasion. *Biochem Biophys Res Commun* (2013) 430(2):706–10. doi: 10.1016/j.bbrc.2012.11.086
102. Sun X, Li J, Sun Y, Zhang Y, Dong L, Shen C, et al. miR-7 Reverses the Resistance to BRAFi in Melanoma by Targeting EGFR/IGF-1R/CRAF and Inhibiting the MAPK and PI3K/AKT Signaling Pathways. *Oncotarget* (2016) 7(33):53558. doi: 10.18632/oncotarget.10669
103. Zeng HF, Yan S, Wu SF. MicroRNA-153-3p Suppress Cell Proliferation and Invasion by Targeting SNAI1 in Melanoma. *Biochem Biophys Res Commun* (2017) 487(1):140–5. doi: 10.1016/j.bbrc.2017.04.032
104. Fang W, Fan Y, Fa Z, Xu J, Yu H, Li P, et al. MicroRNA-625 Inhibits Tumorigenicity by Suppressing Proliferation, Migration and Invasion in Malignant Melanoma. *Oncotarget* (2017) 8(8):13253. doi: 10.18632/oncotarget.14710
105. Lu S, Xu Q. MicroRNA-23a Inhibits Melanoma Cell Proliferation, Migration, and Invasion in Mice Through a Negative Feedback Regulation of Sdcbp and the MAPK/ERK Signaling Pathway. *IUBMB Life* (2019) 71(5):587–600. doi: 10.1002/iub.1979
106. Guo W, Wang H, Yang Y, Guo S, Zhang W, Liu Y, et al. Down-Regulated miR-23a Contributes to the Metastasis of Cutaneous Melanoma by Promoting Autophagy. *Theranostics* (2017) 7(8):2231. doi: 10.7150/thno.18835
107. Lv R, Yu J, Sun Q. Anti-Angiogenic Role of MicroRNA-23b in Melanoma by Disturbing NF-κb Signaling Pathway Via Targeted Inhibition of NAMPT. *Future Oncol* (2020) 16(10):541–458. doi: 10.2217/fon-2019-0699
108. Ma M, Dai J, Tang H, Xu T, Yu S, Si L, et al. MicroRNA-23a-3p Inhibits Mucosal Melanoma Growth and Progression Through Targeting Adenylate Cyclase 1 and Attenuating CAMP and MAPK Pathways. *Theranostics* (2019) 9(4):945. doi: 10.7150/thno.30516
109. Alderman C, Sehlaoui A, Xiao Z, Yang Y. MicroRNA-15a Inhibits the Growth and Invasiveness of Malignant Melanoma and Directly Targets on CDCA4 Gene. *Tumor Biol* (2016) 37(10):13941–50. doi: 10.1007/s13277-016-5271-z
110. Panza E, Ercolano G, De Cicco P, Armogida C, Scognamiglio G, Botti G, et al. MicroRNA-143-3p Inhibits Growth and Invasiveness of Melanoma Cells by Targeting Cyclooxygenase-2 and Inversely Correlates With Malignant Melanoma Progression. *Biochem Pharmacol* (2018) 156:52–9. doi: 10.1016/j.bcp.2018.08.008
111. Nabipoorashrafi SA, Shomali N, Sadat-Hatamnezhad L, Mahami-Oskouei M, Mahmoudi J, Sandoghchian Shotorbani B, et al. miR-143 Acts as an Inhibitor of Migration and Proliferation as Well as an Inducer of Apoptosis in Melanoma Cancer Cells in Vitro. *IUBMB Life* (2020) 72(9):2034–44. doi: 10.1002/iub.2345
112. Lu H-J, Yan J, Jin P-Y, Zheng G-H, Zhang H-L, Bai M, et al. Mechanism of MicroRNA-708 Targeting BAMBI in Cell Proliferation, Migration, and Apoptosis in Mice With Melanoma Via the Wnt and TGF-β Signaling Pathways. *Technol Cancer Res Treat* (2018) 17:1533034618756784. doi: 10.1177/1533034618756784
113. Song X-F, Wang Q-H, Huo R. Effects of MicroRNA-708 on Epithelial-Mesenchymal Transition, Cell Proliferation and Apoptosis in Melanoma Cells by Targeting LEF1 Through the Wnt Signaling Pathway. *Pathol Oncol Res* (2019) 25(1):377–89. doi: 10.1007/s12253-017-0334-z
114. Sun M, Wang X, Tu C, Wang S, Qu J, Xiao S. MicroRNA-216b Inhibits Cell Proliferation and Migration in Human Melanoma by Targeting FOXM1 in Vitro and in Vivo. *Cell Biol Int* (2017) 41(12):1272–82. doi: 10.1002/cbin.10754
115. Liu Y, Huo Y, Wang D, Tai Y, Li J, Pang D, et al. MiR-216a-5p/Hexokinase 2 Axis Regulates Uveal Melanoma Growth Through Modulation of Warburg Effect. *Biochem Biophys Res Commun* (2018) 501(4):885–92. doi: 10.1016/j.bbrc.2018.05.069
116. Yang X, Zhao H, Yang J, Ma Y, Liu Z, Li C, et al. MiR-150-5p Regulates Melanoma Proliferation, Invasion and Metastasis Via SIX1-mediated Warburg Effect. *Biochem Biophys Res Commun* (2019) 515(1):85–91. doi: 10.1016/j.bbrc.2019.05.111
117. Sun X, Zhang C, Cao Y, Liu E. miR-150 Suppresses Tumor Growth in Melanoma Through Downregulation of MYB. *Oncol Res* (2019) 27(3):317. doi: 10.3727/096504018X15228863026239
118. Tembe V, Schramm SJ, Stark MS, Patrick E, Jayaswal V, Tang YH, et al. MicroRNA and MRNA Expression Profiling in Metastatic Melanoma Reveal Associations With BRAF Mutation and Patient Prognosis. *Pigment Cell Melanoma Res* (2015) 28(3):254–66. doi: 10.1111/pcmr.12343
119. Wang J-J, Li Z-F, Li X-J, Han Z, Zhang L, Liu Z-J. Effects of MicroRNA-136 on Melanoma Cell Proliferation, Apoptosis, and Epithelial–Mesenchymal Transition by Targetting PMEL Through the Wnt Signaling Pathway. *Biosci Rep* (2017) 37(5):BSR20170743. doi: 10.1042/BSR20170743
120. Prabhakar K, Rodríguez CI, Jayanthy AS, Mikheil DM, Bhasker AI, Perera RJ, et al. Role of miR-214 in Regulation of β-Catenin and the Malignant Phenotype of Melanoma. *Mol Carcinogen* (2019) 58(11):1974–84. doi: 10.1002/mc.23089
121. Zhang J, Na S, Liu C, Pan S, Cai J, Qiu J. MicroRNA-125b Suppresses the Epithelial–Mesenchymal Transition and Cell Invasion by Targeting ITGA9 in Melanoma. *Tumor Biol* (2016) 37(5):5941–9. doi: 10.1007/s13277-015-4409-8
122. Zhang J, Lu L, Xiong Y, Qin W, Zhang Y, Qian Y, et al. MLK 3 Promotes Melanoma Proliferation and Invasion and is a Target of Micro RNA-125b. *Clin Exp Dermatol* (2014) 39(3):376–84. doi: 10.1111/ced.12286
123. Kappelmann M, Kuphal S, Meister G, Vardimon L, Bosserhoff A. MicroRNA miR-125b Controls Melanoma Progression by Direct Regulation of c-Jun Protein Expression. *Oncogene* (2013) 32(24):2984–91. doi: 10.1038/onc.2012.307
124. Essa S, Denzer N, Mahlknecht U, Klein R, Collnot E, Tilgen W, et al. VDR MicroRNA Expression and Epigenetic Silencing of Vitamin D Signaling in Melanoma Cells. *J Steroid Biochem Mol Biol* (2010) 121(1–2):110–3. doi: 10.1016/j.jsbmb.2010.02.003
125. Sánchez-Sendra B, Martinez-Ciarpaglini C, González-Muñoz JF, Murgui A, Terrádez L, Monteagudo C. Downregulation of Intratumoral Expression of miR-205, miR-200c and miR-125b in Primary Human Cutaneous Melanomas Predicts Shorter Survival. *Sci Rep* (2018) 8(1):1–14. doi: 10.1038/s41598-018-35317-3
126. Liu S-M, Lin C-H, Lu J, Lin I-Y, Tsai M-S, Chen M-H, et al. miR-596 Modulates Melanoma Growth by Regulating Cell Survival and Death. *J Invest Dermatol* (2018) 138(4):911–21. doi: 10.1016/j.jid.2017.11.016
127. Yu H, Ma M, Wang X, Zhou Z, Li R, Guo Q. Propofol Suppresses Proliferation, Invasion, and Migration of Human Melanoma Cells Via Regulating MicroRNA-137 and Fibroblast Growth Factor 9. *J Cell Physiol* (2019) 234(12):23279–88. doi: 10.1002/jcp.28896
128. Yang H, Shen C. MicroRNA-29c Induces G1 Arrest of Melanoma by Targeting CDK6. *J BUON* (2019) 24:819–25.
129. Arnold J, Engelmann JC, Schneider N, Bosserhoff AK, Kuphal S. miR-488-5p and Its Role in Melanoma. *Exp Mol Pathol* (2020) 112:104348. doi: 10.1016/j.yexmp.2019.104348
130. Li N, Ma Y, Ma L, Guan Y, Ma L, Yang D. MicroRNA-488-3p Sensitizes Malignant Melanoma Cells to Cisplatin by Targeting PRKDC. *Cell Biol Int* (2017) 41(6):622–9. doi: 10.1002/cbin.10765
131. Liu K, Jin J, Rong K, Zhuo L, Li P. MicroRNA−675 Inhibits Cell Proliferation and Invasion in Melanoma by Directly Targeting Metadherin. *Mol Med Rep* (2018) 17(2):3372–9. doi: 10.3892/mmr.2017.8264
132. Dietrich P, Kuphal S, Spruss T, Hellerbrand C, Bosserhoff AK. Micro RNA-622 is a Novel Mediator of Tumorigenicity in Melanoma by Targeting Kirsten Rat Sarcoma. *Pigment Cell Melanoma Res* (2018) 31(5):614–29. doi: 10.1111/pcmr.12698
133. Shidal C, Singh NP, Nagarkatti P, Nagarkatti M. MicroRNA-92 Expression in CD133+ Melanoma Stem Cells Regulates Immunosuppression in the Tumor Microenvironment Via Integrin-Dependent Activation of Tgfβ. *Cancer Res* (2019) 79(14):3622–35. doi: 10.1158/0008-5472.CAN-18-2659
134. Noguchi S, Kumazaki M, Mori T, Baba K, Okuda M, Mizuno T, et al. Analysis of MicroRNA-203 Function in CREB/MITF/RAB27a Pathway: Comparison Between Canine and Human Melanoma Cells. *Vet Comp Oncol* (2016) 14(4):384–94. doi: 10.1111/vco.12118
135. Chang X, Sun Y, Han S, Zhu W, Zhang H, Lian S. MiR-203 Inhibits Melanoma Invasive and Proliferative Abilities by Targeting the Polycomb Group Gene BMI1. *Biochem Biophys Res Commun* (2015) 456(1):361–6. doi: 10.1016/j.bbrc.2014.11.087
136. Wang K, Zhang Z-W. Expression of miR-203 is Decreased and Associated With the Prognosis of Melanoma Patients. *Int J Clin Exp Pathol* (2015) 8(10):13249.

137. Noguchi S, Kumazaki M, Yasui Y, Mori T, Yamada N, Akao Y. MicroRNA-203 Regulates Melanosome Transport and Tyrosinase Expression in Melanoma Cells by Targeting Kinesin Superfamily Protein 5b. *J Invest Dermatol* (2014) 134(2):461–9. doi: 10.1038/jid.2013.310
138. Noguchi S, Mori T, Otsuka Y, Yamada N, Yasui Y, Iwasaki J, et al. Anti-Oncogenic MicroRNA-203 Induces Senescence by Targeting E2F3 Protein in Human Melanoma Cells. *J Biol Chem* (2012) 287(15):11769–77. doi: 10.1074/jbc.M111.325027
139. Bu P, Yang P. MicroRNA−203 Inhibits Malignant Melanoma Cell Migration by Targeting Versican. *Exp Ther Med* (2014) 8(1):309–15. doi: 10.3892/etm.2014.1708
140. Wu S, Chen H, Han N, Zhang C, Yan H. Long Noncoding RNA PVT1 Silencing Prevents the Development of Uveal Melanoma by Impairing MicroRNA-17-3p–Dependent MDM2 Upregulation. *Invest Ophthalmol Visual Sci* (2019) 60(14):4904–14. doi: 10.1167/iovs.19-27704
141. Luan W, Zhou Z, Zhu Y, Xia Y, Wang J, Xu B. miR-137 Inhibits Glutamine Catabolism and Growth of Malignant Melanoma by Targeting Glutaminase. *Biochem Biophys Res Commun* (2018) 495(1):46–52. doi: 10.1016/j.bbrc.2017.10.152
142. Chen X, Wang J, Shen H, Lu J, Li C, Hu D-N, et al. Epigenetics, MicroRNAs, and Carcinogenesis: Functional Role of MicroRNA-137 in Uveal Melanoma. *Invest Ophthalmol Visual Sci* (2011) 52(3):1193–9. doi: 10.1167/iovs.10-5272
143. Lv N, Hao S, Luo C, Abukiwan A, Hao Y, Gai F, et al. miR-137 Inhibits Melanoma Cell Proliferation Through Downregulation of GLO1. *Sci China Life Sci* (2018) 61(5):541–9. doi: 10.1007/s11427-017-9138-9
144. Peres J, Kwesi-Maliepaard EM, Rambow F, Larue L, Prince S. The Tumour Suppressor, miR-137, Inhibits Malignant Melanoma Migration by Targetting the TBX3 Transcription Factor. *Cancer Lett* (2017) 405:111–9. doi: 10.1016/j.canlet.2017.07.018
145. Chang X, Zhang H, Lian S, Zhu W. miR-137 Suppresses Tumor Growth of Malignant Melanoma by Targeting Aurora Kinase a. *Biochem Biophys Res Commun* (2016) 475(3):251–6. doi: 10.1016/j.bbrc.2016.05.090
146. Li N. Low Expression of Mir-137 Predicts Poor Prognosis in Cutaneous Melanoma Patients. *Med Sci Monit* (2016) 22:140. doi: 10.12659/MSM.895207
147. Hao S, Luo C, Abukiwan A, Wang G, He J, Huang L, et al. miR-137 Inhibits Proliferation of Melanoma Cells by Targeting PAK 2. *Exp Dermatol* (2015) 24(12):947–52. doi: 10.1111/exd.12812
148. Deng Y, Deng H, Bi F, Liu J, Bemis LT, Norris D, et al. MicroRNA-137 Targets Carboxyl-Terminal Binding Protein 1 in Melanoma Cell Lines. *Int J Biol Sci* (2011) 7(1):133. doi: 10.7150/ijbs.7.133
149. Luo C, Tetteh PW, Merz PR, Dickes E, Abukiwan A, Hotz-Wagenblatt A, et al. miR-137 Inhibits the Invasion of Melanoma Cells Through Downregulation of Multiple Oncogenic Target Genes. *J Invest Dermatol* (2013) 133(3):768–75. doi: 10.1038/jid.2012.357
150. Qi J, Ww W, Chen W, Lu WY, Shang AQ. Mechanism of miR-137 Regulating Migration and Invasion of Melanoma Cells by Targeting PIK3R3 Gene. *J Cell Biochem* (2019) 120(5):8393–400. doi: 10.1002/jcb.28124
151. Liu E, Sun X, Li J, Zhang C. miR−30a−5p Inhibits the Proliferation, Migration and Invasion of Melanoma Cells by Targeting SOX4. *Mol Med Rep* (2018) 18(2):2492–8. doi: 10.3892/mmr.2018.9166
152. Wei Y, Du Y, Chen X, Li P, Wang Y, Zang W, et al. Expression Patterns of MicroRNA-218 and Its Potential Functions by Targeting CIP2A and BMI1 Genes in Melanoma. *Tumor Biol* (2014) 35(8):8007–15. doi: 10.1007/s13277-014-2079-6
153. Chen L, Cao Y, Rong D, Wang Y, Cao Y. MicroRNA-605 Functions as a Tumor Suppressor by Targeting INPP4B in Melanoma. *Oncol Rep* (2017) 38(2):1276–86. doi: 10.3892/or.2017.5740
154. Xiao Y, Diao Q, Liang Y, Peng Y, Zeng K. MicroRNA−24−1−5p Promotes Malignant Melanoma Cell Autophagy and Apoptosis Via Regulating Ubiquitin D. *Mol Med Rep* (2017) 16(6):8448–54. doi: 10.3892/mmr.2017.7614
155. Ge X, Niture S, Lin M, Cagle P, Li PA, Kumar D. MicroRNA-205-5p Inhibits Skin Cancer Cell Proliferation and Increase Drug Sensitivity by Targeting TNFAIP8. *Sci Rep* (2021) 11(1):1–14. doi: 10.1038/s41598-021-85097-6
156. Valentini V, Zelli V, Gaggiano E, Silvestri V, Rizzolo P, Bucalo A, et al. MiRNAs as Potential Prognostic Biomarkers for Metastasis in Thin and Thick Primary Cutaneous Melanomas. *Anticancer Res* (2019) 39(8):4085–93. doi: 10.21873/anticanres.13566
157. Liu S, Tetzlaff MT, Liu A, Liegl-Atzwanger B, Guo J, Xu X. Loss of MicroRNA-205 Expression is Associated With Melanoma Progression. *Lab Invest* (2012) 92(7):1084–96. doi: 10.1038/labinvest.2012.62
158. Li Y, Luo J-T, Liu Y-M, Wei W-B. MiRNA-145/miRNA-205 Inhibits Proliferation and Invasion of Uveal Melanoma Cells by Targeting NPR1/CDC42. *Int J Ophthalmol* (2020) 13(5):718. doi: 10.18240/ijo.2020.05.04
159. Liu S, Gao G, Yan D, Chen X, Yao X, Guo S, et al. Effects of miR-145-5p Through NRAS on the Cell Proliferation, Apoptosis, Migration, and Invasion in Melanoma by Inhibiting MAPK and PI 3K/AKT Pathways. *Cancer Med* (2017) 6(4):819–33. doi: 10.1002/cam4.1030
160. Jin C, Wang A, Liu L, Wang G, Li G, Han Z. miR-145-5p Inhibits Tumor Occurrence and Metastasis Through the NF-κb Signaling Pathway by Targeting TLR4 in Malignant Melanoma. *J Cell Biochem* (2019) 120(7):11115–26. doi: 10.1002/jcb.28388
161. Yang J-Y, Li Y, Wang Q, Zhou W-J, Yan Y-N, Wei W-B. MicroRNA-145 Suppresses Uveal Melanoma Angiogenesis and Growth by Targeting Neuroblastoma RAS Viral Oncogene Homolog and Vascular Endothelial Growth Factor. *Chin Med J* (2020) 133(16):1922. doi: 10.1097/CM9.0000000000000875
162. Cirilo PDR, de Sousa Andrade LN, Corrêa BRS, Qiao M, Furuya TK, Chammas R, et al. MicroRNA-195 Acts as an Anti-Proliferative MiRNA in Human Melanoma Cells by Targeting Prohibitin 1. *BMC Cancer* (2017) 17(1):1–12. doi: 10.1186/s12885-017-3721-7
163. Li N, Liu Y, Pang H, Lee D, Zhou Y, Xiao Z. Methylation-Mediated Silencing of MicroRNA-211 Decreases the Sensitivity of Melanoma Cells to Cisplatin. *Med Sci Monit* (2019) 25:1590. doi: 10.12659/MSM.911862
164. Mazar J, Qi F, Lee B, Marchica J, Govindarajan S, Shelley J, et al. MicroRNA 211 Functions as a Metabolic Switch in Human Melanoma Cells. *Mol Cell Biol* (2016) 36(7):1090–108. doi: 10.1128/MCB.00762-15
165. Mazar J, DeYoung K, Khaitan D, Meister E, Almodovar A, Goydos J, et al. The Regulation of MiRNA-211 Expression and Its Role in Melanoma Cell Invasiveness. *PloS One* (2010) 5(11):e13779. doi: 10.1371/journal.pone.0013779
166. Yu H, Yang W. MiR-211 is Epigenetically Regulated by DNMT1 Mediated Methylation and Inhibits EMT of Melanoma Cells by Targeting RAB22A. *Biochem Biophys Res Commun* (2016) 476(4):400–5. doi: 10.1016/j.bbrc.2016.05.133
167. Sakurai E, Maesawa C, Shibazaki M, Yasuhira S, Oikawa H, Sato M, et al. Downregulation of MicroRNA-211 is Involved in Expression of Preferentially Expressed Antigen of Melanoma in Melanoma Cells. *Int J Oncol* (2011) 39(3):665–72. doi: 10.3892/ijo.2011.1084
168. Boyle GM, Woods SL, Bonazzi VF, Stark MS, Hacker E, Aoude LG, et al. Melanoma Cell Invasiveness is Regulated by miR-211 Suppression of the BRN2 Transcription Factor. *Pigment Cell Melanoma Res* (2011) 24(3):525–37. doi: 10.1111/j.1755-148X.2011.00849.x
169. Bell RE, Khaled M, Netanely D, Schubert S, Golan T, Buxbaum A, et al. Transcription Factor/MicroRNA Axis Blocks Melanoma Invasion Program by miR-211 Targeting NUAK1. *J Invest Dermatol* (2014) 134(2):441–51. doi: 10.1038/jid.2013.340
170. Levy C, Khaled M, Iliopoulos D, Janas MM, Schubert S, Pinner S, et al. Intronic miR-211 Assumes the Tumor Suppressive Function of Its Host Gene in Melanoma. *Mol Cell* (2010) 40(5):841–9. doi: 10.1016/j.molcel.2010.11.020
171. Du M, Zhang Z, Gao T. Piceatannol Induced Apoptosis Through Up-Regulation of MicroRNA-181a in Melanoma Cells. *Biol Res* (2017) 50. doi: 10.1186/s40659-017-0141-8
172. Barbato A, Iuliano A, Volpe M, D'Alterio R, Brillante S, Massa F, et al. Integrated Genomics Identifies Mir-181/TFAM Pathway as a Critical Driver of Drug Resistance in Melanoma. *Int J Mol Sci* (2021) 22(4):1801. doi: 10.3390/ijms22041801
173. Mazar J, DeBlasio D, Govindarajan SS, Zhang S, Perera RJ. Epigenetic Regulation of MicroRNA-375 and Its Role in Melanoma Development in Humans. *FEBS Lett* (2011) 585(15):2467–76. doi: 10.1016/j.febslet.2011.06.025
174. Li J-R, Wang J-Q, Gong Q, Fang R-H, Guo Y-L. MicroRNA-328 Inhibits Proliferation of Human Melanoma Cells by Targeting TGFB2. *Asian Pac J Cancer Prev* (2015) 16(4):1575–9. doi: 10.7314/APJCP.2015.16.4.1575

175. Zou B, Zhu W, Liu H, Wang S, Zhu H. Identification and Functional Evaluation of miR-4633-5p as a Biomarker and Tumor Suppressor in Metastatic Melanoma. *Cell Physiol Biochem* (2018) 49(4):1364–79. doi: 10.1159/000493414
176. Wang H, Yu L, Shan X. Expression Levels of MicroRNA−455 and Its Potential Functions by Targeting IGF−1R in Melanoma. *Mol Med Rep* (2017) 15(6):3852–8. doi: 10.3892/mmr.2017.6468
177. Noguchi S, Mori T, Hoshino Y, Yamada N, Nakagawa T, Sasaki N, et al. Comparative Study of Anti-Oncogenic MicroRNA-145 in Canine and Human Malignant Melanoma. *J Vet Med Sci* (2011) 74(1):1108090601. doi: 10.1292/jvms.11-0264
178. Yang L, Qiming H, Xuehui S, Xiang J, Li S, Xiaolin X, et al. MicroRNA 145 May Play an Important Role in Uveal Melanoma Cell Growth by Potentially Targeting Insulin Receptor Substrate-1. *Chin Med J* (2014) 127(8):1410–6. doi: 10.3760/cma.j.issn.0366-6999.20133206
179. Dynoodt P, Speeckaert R, De Wever O, Chevolet I, Brochez L, Lambert J, et al. miR-145 Overexpression Suppresses the Migration and Invasion of Metastatic Melanoma Cells. *Int J Oncol* (2013) 42(4):1443–51. doi: 10.3892/ijo.2013.1823
180. Long J, Menggen Q, Wuren Q, Shi Q, Pi X. MiR-219-5p Inhibits the Growth and Metastasis of Malignant Melanoma by Targeting BCL-2. *BioMed Res Int* (2017) 2017(9032502):7. doi: 10.1155/2017/9032502
181. Asangani IA, Harms PW, Dodson L, Pandhi M, Kunju LP, Maher CA, et al. Genetic and Epigenetic Loss of MicroRNA-31 Leads to Feed-Forward Expression of EZH2 in Melanoma. *Oncotarget* (2012) 3(9):1011. doi: 10.18632/oncotarget.622
182. Chen X, He D, Da Dong X, Dong F, Wang J, Wang L, et al. MicroRNA-124a is Epigenetically Regulated and Acts as a Tumor Suppressor by Controlling Multiple Targets in Uveal Melanoma. *Invest Ophthalmol Visual Sci* (2013) 54 (3):2248–56. doi: 10.1167/iovs.12-10977
183. Zhang D, Han Y, Xu L. Upregulation of miR-124 by Physcion 8-O-β-Glucopyranoside Inhibits Proliferation and Invasion of Malignant Melanoma Cells Via Repressing RLIP76. *Biomed Pharmacother* (2016) 84:166–76. doi: 10.1016/j.biopha.2016.09.022
184. Yang P, Bu P, Li C. miR−124 Inhibits Proliferation, Migration and Invasion of Malignant Melanoma Cells Via Targeting Versican. *Exp Ther Med* (2017) 14(4):3555–62. doi: 10.3892/etm.2017.4998
185. Tian R, Liu T, Qiao L, Gao M, Li J. Decreased Serum MicroRNA-206 Level Predicts Unfavorable Prognosis in Patients With Melanoma. *Int J Clin Exp Pathol* (2015) 8(3):3097.
186. Georgantas RWII, Streicher K, Luo X, Greenlees L, Zhu W, Liu Z, et al. Micro RNA-206 Induces G 1 Arrest in Melanoma by Inhibition of CDK 4 and C Yclin D. *Pigment Cell Melanoma Res* (2014) 27(2):275–86. doi: 10.1111/pcmr.12200
187. Su B-B, Zhou S-W, Gan C-B, Zhang X-N. MiR-186 Inhibits Cell Proliferation and Invasion in Human Cutaneous Malignant Melanoma. *J Cancer Res Ther* (2018) 14(8):60. doi: 10.4103/0973-1482.157340
188. Li M, Long C, Yang G, Luo Y, Du H. MiR-26b Inhibits Melanoma Cell Proliferation and Enhances Apoptosis by Suppressing TRAF5-mediated MAPK Activation. *Biochem Biophys Res Commun* (2016) 471(3):361–7. doi: 10.1016/j.bbrc.2016.02.021
189. Mueller DW, Bosserhoff AK. MicroRNA miR-196a Controls Melanoma-Associated Genes by Regulating HOX-C8 Expression. *Int J Cancer* (2011) 129(5):1064–74. doi: 10.1002/ijc.25768
190. Braig S, Mueller DW, Rothhammer T, Bosserhoff A-K. MicroRNA miR-196a is a Central Regulator of HOX-B7 and BMP4 Expression in Malignant Melanoma. *Cell Mol Life Sci* (2010) 67(20):3535–48. doi: 10.1007/s00018-010-0394-7
191. Chen J, Feilotter HE, Paré GC, Zhang X, Pemberton JG, Garady C, et al. MicroRNA-193b Represses Cell Proliferation and Regulates Cyclin D1 in Melanoma. *Am J Pathol* (2010) 176(5):2520–9. doi: 10.2353/ajpath.2010.091061
192. Chen J, Zhang X, Lentz C, Abi-Daoud M, Paré GC, Yang X, et al. miR-193b Regulates Mcl-1 in Melanoma. *Am J Pathol* (2011) 179(5):2162–8. doi: 10.1016/j.ajpath.2011.07.010
193. Liu S, Tetzlaff MT, Cui R, Xu X. miR-200c Inhibits Melanoma Progression and Drug Resistance Through Down-Regulation of BMI-1. *Am J Pathol* (2012) 181(5):1823–35. doi: 10.1016/j.ajpath.2012.07.009
194. Bustos MA, Ono S, Marzese DM, Oyama T, Iida Y, Cheung G, et al. MiR-200a Regulates CDK4/6 Inhibitor Effect by Targeting CDK6 in Metastatic Melanoma. *J Invest Dermatol* (2017) 137(9):1955–64. doi: 10.1016/j.jid.2017.03.039
195. Chen W, Xu Y, Zhang X. Targeting GOLM1 by MicroRNA-200a in Melanoma Suppresses Cell Proliferation, Invasion and Migration Via Regulating PI3K/Akt Signaling Pathway and Epithelial-Mesenchymal Transition. *Eur Rev Med Pharmacol Sci* (2019) 23(16):6997–7007. doi: 10.26355/eurrev_201908_18740
196. Peng J, Liu H, Liu C. MiR-155 Promotes Uveal Melanoma Cell Proliferation and Invasion by Regulating NDFIP1 Expression. *Technol Cancer Res Treat* (2017) 16(6):1160–7. doi: 10.1177/1533034617737923
197. Levati L, Pagani E, Romani S, Castiglia D, Piccinni E, Covaciu C, et al. MicroRNA-155 Targets the SKI Gene in Human Melanoma Cell Lines. *Pigment Cell Melanoma Res* (2011) 24(3):538–50. doi: 10.1111/j.1755-148X.2011.00857.x
198. Li H, Song J, Chen H, Wang Q, Meng L, Li Y. MiR-155 Inhibits Proliferation, Invasion and Migration of Melanoma Via Targeting CBL. *Eur Rev Med Pharmacol Sci* (2019) 23(21):9525–34. doi: 10.26355/eurrev_201911_19447
199. Dar AA, Majid S, Rittsteuer C, de Semir D, Bezrookove V, Tong S, et al. The Role of miR-18b in MDM2-p53 Pathway Signaling and Melanoma Progression. *J Natl Cancer Inst* (2013) 105(6):433–42. doi: 10.1093/jnci/djt003
200. Chen Y, Zhang Z, Luo C, Chen Z, Zhou J. MicroRNA-18b Inhibits the Growth of Malignant Melanoma Via Inhibition of HIF-1α-Mediated Glycolysis. *Oncol Rep* (2016) 36(1):471–9. doi: 10.3892/or.2016.4824
201. Reuland SN, Smith SM, Bemis LT, Goldstein NB, Almeida AR, Partyka KA, et al. MicroRNA-26a is Strongly Downregulated in Melanoma and Induces Cell Death Through Repression of Silencer of Death Domains (SODD). *J Invest Dermatol* (2013) 133(5):1286–93. doi: 10.1038/jid.2012.400
202. Fu X, Meng Z, Liang W, Tian Y, Wang X, Han W, et al. miR-26a Enhances MiRNA Biogenesis by Targeting Lin28B and Zcchc11 to Suppress Tumor Growth and Metastasis. *Oncogene* (2014) 33(34):4296–306. doi: 10.1038/onc.2013.385
203. Qian H, Yang C, Yang Y. MicroRNA-26a Inhibits the Growth and Invasiveness of Malignant Melanoma and Directly Targets on MITF Gene. *Cell Death Discovery* (2017) 3(1):1–9. doi: 10.1038/cddiscovery.2017.28
204. Liu S, Kumar SM, Lu H, Liu A, Yang R, Pushparajan A, et al. MicroRNA-9 Up-Regulates E-Cadherin Through Inhibition of NF-κb1–Snail1 Pathway in Melanoma. *J Pathol* (2012) 226(1):61–72. doi: 10.1002/path.2964
205. Zhao G, Li Q, Wang A, Jiao J. YY1 Regulates Melanoma Tumorigenesis Through a miR-9~ RYBP Axis. *J Exp Clin Cancer Res* (2015) 34(1):1–11. doi: 10.1186/s13046-015-0177-y
206. Liu N, Sun Q, Chen J, Li J, Zeng Y, Zhai S, et al. MicroRNA-9 Suppresses Uveal Melanoma Cell Migration and Invasion Through the NF-κb1 Pathway. *Oncol Rep* (2012) 28(3):961–8. doi: 10.3892/or.2012.1905
207. Xu D, Chen X, He Q, Luo C. MicroRNA-9 Suppresses the Growth, Migration, and Invasion of Malignant Melanoma Cells Via Targeting NRP1. *OncoTargets Ther* (2016) 9:7047. doi: 10.2147/OTT.S107235
208. Bu P, Luo C, He Q, Yang P, Li X, Xu D. MicroRNA-9 Inhibits the Proliferation and Migration of Malignant Melanoma Cells Via Targeting Sirituin 1. *Exp Ther Med* (2017) 14(2):931–8. doi: 10.3892/etm.2017.4595
209. Lu N-H, Wei C-Y, Qi F-Z, Gu J-Y. Hsa-let-7b Suppresses Cell Proliferation by Targeting UHRF1 in Melanoma. *Cancer Invest* (2020) 38(1):52–60. doi: 10.1080/07357907.2019.1709482
210. Zhou Y, Zhang L, Fan J, Jia R, Song X, Xu X, et al. Let-7b Overexpression Leads to Increased Radiosensitivity of Uveal Melanoma Cells. *Melanoma Res* (2015) 25(2):119–26. doi: 10.1097/CMR.0000000000000140
211. Tang H, Ma M, Dai J, Cui C, Si L, Sheng X, et al. miR-let-7b and miR-let-7c Suppress Tumourigenesis of Human Mucosal Melanoma and Enhance the Sensitivity to Chemotherapy. *J Exp Clin Cancer Res* (2019) 38(1):1–14. doi: 10.1186/s13046-019-1190-3
212. Yao Y, Zuo J, Wei Y. Targeting of TRX2 by miR-330-3p in Melanoma Inhibits Proliferation. *Biomed Pharmacother* (2018) 107:1020–9. doi: 10.1016/j.biopha.2018.08.058
213. Su B-B, Zhou S-W, Gan C-B, Zhang X-N. MiR-330-5p Regulates Tyrosinase and PDIA3 Expression and Suppresses Cell Proliferation and Invasion in

Cutaneous Malignant Melanoma. *J Surg Res* (2016) 203(2):434–40. doi: 10.1016/j.jss.2016.03.021
214. Sun Y, Cheng H, Wang G, Yu G, Zhang D, Wang Y, et al. Deregulation of miR-183 Promotes Melanoma Development Via LncRNA MALAT1 Regulation and ITGB1 Signal Activation. *Oncotarget* (2017) 8(2):3509. doi: 10.18632/oncotarget.13862
215. Sun L, Bian G, Meng Z, Dang G, Shi D, Mi S. MiR-144 Inhibits Uveal Melanoma Cell Proliferation and Invasion by Regulating c-Met Expression. *PloS One* (2015) 10(5):e0124428. doi: 10.1371/journal.pone.0124428
216. Amaro A, Croce M, Ferrini S, Barisione G, Gualco M, Perri P, et al. Potential Onco-Suppressive Role of miR122 and miR144 in Uveal Melanoma Through ADAM10 and C-Met Inhibition. *Cancers* (2020) 12(6):1468. doi: 10.3390/cancers12061468
217. Zhao G, Wei Z, Guo Y. MicroRNA-107 is a Novel Tumor Suppressor Targeting POU3F2 in Melanoma. *Biol Res* (2020) 53(1):1–10. doi: 10.1186/s40659-020-00278-3
218. Wang X, Hu Y, Cui J, Zhou Y, Chen L. Coordinated Targeting of MMP-2/MMP-9 by Mir-296-3p/FOXCUT Exerts Tumor-Suppressing Effects in Choroidal Malignant Melanoma. *Mol Cell Biochem* (2018) 445(1):25–33. doi: 10.1007/s11010-017-3248-x
219. Rang Z, Yang G, Y-w W, Cui F. miR-542-3p Suppresses Invasion and Metastasis by Targeting the Proto-Oncogene Serine/Threonine Protein Kinase, PIM1, in Melanoma. *Biochem Biophys Res Commun* (2016) 474(2):315–20. doi: 10.1016/j.bbrc.2016.04.093
220. Zhang H, Feng C, Zhang M, Zeng A, Si L, Yu N, et al. Mir-625-5p/PKM2 Negatively Regulates Melanoma Glycolysis State. *J Cell Biochem* (2019) 120(3):2964–72. doi: 10.1002/jcb.26917
221. Weber CE, Luo C, Hotz-Wagenblatt A, Gardyan A, Kordaß T, Holland-Letz T, et al. miR-339-3p is a Tumor Suppressor in Melanoma. *Cancer Res* (2016) 76(12):3562–71. doi: 10.1158/0008-5472.CAN-15-2932
222. Mou K, Ding M, Han D, Zhou Y, Mu X, Liu W, et al. miR−590−5p Inhibits Tumor Growth in Malignant Melanoma by Suppressing YAP1 Expression. *Oncol Rep* (2018) 40(4):2056–66. doi: 10.3892/or.2018.6633
223. Jiang C, Croft A, Tseng H, Guo S, Jin L, Hersey P, et al. Repression of MicroRNA-768-3p by MEK/ERK Signalling Contributes to Enhanced MRNA Translation in Human Melanoma. *Oncogene* (2014) 33(20):2577–88. doi: 10.1038/onc.2013.237
224. Babapoor S, Fleming E, Wu R, Dadras SS. A Novel miR-451a isomiR, Associated With Amelanotypic Phenotype, Acts as a Tumor Suppressor in Melanoma by Retarding Cell Migration and Invasion. *PloS One* (2014) 9(9):e107502. doi: 10.1371/journal.pone.0107502
225. Mishra PJ, Mishra PJ, Merlino G. Integrated Genomics Identifies Mir-32/MCL-1 Pathway as a Critical Driver of Melanomagenesis: Implications for miR-replacement and Combination Therapy. *PloS One* (2016) 11(11):e0165102. doi: 10.1371/journal.pone.0165102
226. Cui A, Jin Z, Gao Z, Jin M, Zhu L, Li L, et al. Downregulation of miR-493 Promoted Melanoma Proliferation by Suppressing IRS4 Expression. *Tumor Biol* (2017) 39(5):1010428317701640. doi: 10.1177/1010428317701640
227. Hanniford D, Segura MF, Zhong J, Philips E, Jirau-Serrano X, Darvishian F, et al. Identification of Metastasis-Suppressive MicroRNAs in Primary Melanoma. *J Natl Cancer Inst* (2015) 107(3):dju494. doi: 10.1093/jnci/dju494
228. Guo B, Hui Q, Zhang Y, Chang P, Tao K. miR-194 is a Negative Regulator of GEF-H1 Pathway in Melanoma. *Oncol Rep* (2016) 36(4):2412–20. doi: 10.3892/or.2016.5020
229. Bai M, Zhang M, Long F, Yu N, Zeng A, Zhao R. Circulating MicroRNA-194 Regulates Human Melanoma Cells Via PI3K/AKT/FoxO3a and p53/p21 Signaling Pathway. *Oncol Rep* (2017) 37(5):2702–10. doi: 10.3892/or.2017.5537
230. Song H, Tao Y, Ni N, Zhou X, Xiong J, Zeng X, et al. miR-128 Targets the CC Chemokine Ligand 18 Gene (CCL18) in Cutaneous Malignant Melanoma Progression. *J Dermatol Sci* (2018) 91(3):317–24. doi: 10.1016/j.jdermsci.2018.06.011
231. Sun V, Zhou WB, Nosrati M, Majid S, Thummala S, De Semir D, et al. Antitumor Activity of miR-1280 in Melanoma by Regulation of Src. *Mol Ther* (2015) 23(1):71–8. doi: 10.1038/mt.2014.176
232. Wang H-F, Chen H, Ma M-W, Wang J-A, Tang T-T, Ni L-S, et al. miR-573 Regulates Melanoma Progression by Targeting the Melanoma Cell Adhesion Molecule. *Oncol Rep* (2013) 30(1):520–6. doi: 10.3892/or.2013.2451
233. Zhang Z, Yang N. MiR-33a-5p Inhibits the Growth and Metastasis of Melanoma Cells by Targeting SNAI2. *Neoplasma* (2020) 67(4):813–24. doi: 10.4149/neo_2020_190823N811
234. Cao K, Li J, Chen J, Qian L, Wang A, Chen X, et al. MicroRNA-33a-5p Increases Radiosensitivity by Inhibiting Glycolysis in Melanoma. *Oncotarget* (2017) 8(48):83660. doi: 10.18632/oncotarget.19014
235. Zhou J, Xu D, Xie H, Tang J, Liu R, Li J, et al. miR-33a Functions as a Tumor Suppressor in Melanoma by Targeting HIF-1α. *Cancer Biol Ther* (2015) 16(6):846–55. doi: 10.1080/15384047.2015.1030545
236. Tian F, Wei H, Tian H, Qiu Y, Xu J. miR-33a is Downregulated in Melanoma Cells and Modulates Cell Proliferation by Targeting PCTAIRE1. *Oncol Lett* (2016) 11(4):2741–6. doi: 10.3892/ol.2016.4321
237. Zhao Y, Wu C, Li L. MicroRNA−33b Inhibits Cell Proliferation and Glycolysis by Targeting Hypoxia−Inducible Factor−1α in Malignant Melanoma. *Exp Ther Med* (2017) 14(2):1299–306. doi: 10.3892/etm.2017.4702
238. Li F, Li X-J, Qiao L, Shi F, Liu W, Li Y, et al. miR-98 Suppresses Melanoma Metastasis Through a Negative Feedback Loop With Its Target Gene IL-6. *Exp Mol Med* (2014) 46(10):e116–e. doi: 10.1038/emm.2014.63
239. Liu P, Hu Y, Ma L, Du M, Xia L, Hu Z. miR-425 Inhibits Melanoma Metastasis Through Repression of PI3K-Akt Pathway by Targeting IGF-1. *Biomed Pharmacother* (2015) 75:51–7. doi: 10.1016/j.biopha.2015.08.010
240. Xiao W, Yao E, Zheng W, Tian F, Tian L. miR-337 Can be a Key Negative Regulator in Melanoma. *Cancer Biol Ther* (2017) 18(6):392–9. doi: 10.1080/15384047.2017.1323581
241. Zhang J, Liu W-L, Zhang L, Ge R, He F, Gao T-Y, et al. MiR-637 Suppresses Melanoma Progression Through Directly Targeting P-REX2a and Inhibiting PTEN/AKT Signaling Pathway. *Cell Mol Biol* (2018) 64(11):50–7. doi: 10.14715/cmb/2018.64.11.10
242. Mo Y, Fang RH, Wu J, Si Y, Jia SQ, Li Q, et al. MicroRNA-329 Upregulation Impairs the HMGB2/β-Catenin Pathway and Regulates Cell Biological Behaviors in Melanoma. *J Cell Physiol* (2019) 234(12):23518–27. doi: 10.1002/jcp.28920
243. Fattore L, Mancini R, Acunzo M, Romano G, Laganà A, Pisanu ME, et al. miR-579-3p Controls Melanoma Progression and Resistance to Target Therapy. *Proc Natl Acad Sci* (2016) 113(34):E5005–13. doi: 10.1073/pnas.1607753113
244. Luo C, Merz PR, Chen Y, Dickes E, Pscherer A, Schadendorf D, et al. MiR-101 Inhibits Melanoma Cell Invasion and Proliferation by Targeting MITF and EZH2. *Cancer Lett* (2013) 341(2):240–7. doi: 10.1016/j.canlet.2013.08.021
245. Ding Z, Jian S, Peng X, Liu Y, Wang J, Zheng L, et al. Loss of MiR-664 Expression Enhances Cutaneous Malignant Melanoma Proliferation by Upregulating PLP2. *Medicine* (2015) 94(33):e1327. doi: 10.1097/MD.0000000000001327
246. Xiong Y, Liu L, Qiu Y, Liu L. MicroRNA-29a Inhibits Growth, Migration and Invasion of Melanoma A375 Cells in Vitro by Directly Targeting BMI1. *Cell Physiol Biochem* (2018) 50(1):385–97. doi: 10.1159/000494015
247. Liu S-M, Lu J, Lee H-C, Chung F-H, Ma N. miR-524-5p Suppresses the Growth of Oncogenic BRAF Melanoma by Targeting BRAF and ERK2. *Oncotarget* (2014) 5(19):9444. doi: 10.18632/oncotarget.2452
248. Meng F, Zhang Y, Li X, Wang J, Wang Z. Clinical Significance of miR-138 in Patients With Malignant Melanoma Through Targeting of PDK1 in the PI3K/AKT Autophagy Signaling Pathway. *Oncol Rep* (2017) 38(3):1655–62. doi: 10.3892/or.2017.5838
249. Chen Y, Cao K, Wang S, Chen J, He B, He G, et al. MicroRNA-138 Suppresses Proliferation, Invasion and Glycolysis in Malignant Melanoma Cells by Targeting HIF-1α. *Exp Ther Med* (2016) 11(6):2513–8. doi: 10.3892/etm.2016.3220
250. Qiu H, Chen F, Chen M. MicroRNA-138 Negatively Regulates the Hypoxia-Inducible Factor 1α to Suppress Melanoma Growth and Metastasis. *Biol Open* (2019) 8(8). doi: 10.1242/bio.042937
251. Lin N, Zhou Y, Lian X, Tu Y. Down-Regulation of Tissue MicroRNA-126 was Associated With Poor Prognosis in Patients With Cutaneous Melanoma. *Int J Clin Exp Med* (2015) 8(3):4297.
252. Felli N, Felicetti F, Lustri AM, Errico MC, Bottero L, Cannistraci A, et al. miR-126&126* Restored Expressions Play a Tumor Suppressor Role by Directly Regulating ADAM9 and MMP7 in Melanoma. *PloS One* (2013) 8(2):e56824. doi: 10.1371/journal.pone.0056824

253. Zehavi L, Schayek H, Jacob-Hirsch J, Sidi Y, Leibowitz-Amit R, Avni D. MiR-377 Targets E2F3 and Alters the NF-kB Signaling Pathway Through MAP3K7 in Malignant Melanoma. *Mol Cancer* (2015) 14(1):1–16. doi: 10.1186/s12943-015-0338-9
254. Yang C, Xia Z, Zhu L, Li Y, Zheng Z, Liang J, et al. MicroRNA-139-5p Modulates the Growth and Metastasis of Malignant Melanoma Cells Via the PI3K/AKT Signaling Pathway by Binding to IGF1R. *Cell Cycle* (2019) 18 (24):3513–24. doi: 10.1080/15384101.2019.1690881
255. Shi Q, He Q, Wei J. MicroRNA-342 Prohibits Proliferation and Invasion of Melanoma Cells by Directly Targeting Zinc-Finger E-Box-Binding Homeobox 1. *Oncol Res* (2018) 26(9):1447. doi: 10.3727/096504018X15193823766141
256. Tian P, Tao L, Wang Y, Han X. MicroRNA-127 Inhibits the Progression of Melanoma by Downregulating Delta-Like Homologue 1. *BioMed Res Int* (2020) 2020(8523465):10. doi: 10.1155/2020/8523465
257. Shi L, Huo J, Chen S, Xue J, Gao W, Li X, et al. MicroRNA-22 Targets FMNL2 to Inhibit Melanoma Progression Via the Regulation of the Wnt/β-Catenin Signaling Pathway and Epithelial-Mesenchymal Transition. *Eur Rev Med Pharmacol Sci* (2019) 23(12):5332–42. doi: 10.26355/eurrev_201906_18200
258. Palkina N, Komina A, Aksenenko M, Moshev A, Savchenko A, Ruksha T. miR–204–5p and miR–3065–5p Exert Antitumor Effects on Melanoma Cells. *Oncol Lett* (2018) 15(6):8269–80. doi: 10.3892/ol.2018.8443
259. Luan W, Qian Y, Ni X, Bu X, Xia Y, Wang J, et al. miR-204-5p Acts as a Tumor Suppressor by Targeting Matrix Metalloproteinases-9 and B-Cell Lymphoma-2 in Malignant Melanoma. *OncoTargets Ther* (2017) 10:1237. doi: 10.2147/OTT.S128819
260. Zhang G, Ai D, Yang X, Ji S, Wang Z, Feng S. MicroRNA-610 Inhibits Tumor Growth of Melanoma by Targeting LRP6. *Oncotarget* (2017) 8 (57):97361. doi: 10.18632/oncotarget.22125
261. Zhu L, Liu Z, Dong R, Wang X, Zhang M, Guo X, et al. MicroRNA-3662 Targets ZEB1 and Attenuates the Invasion of the Highly Aggressive Melanoma Cell Line A375. *Cancer Manage Res* (2019) 11:5845. doi: 10.2147/CMAR.S200540
262. Chen L, Ma G, Cao X, An X, Liu X. MicroRNA-331 Inhibits Proliferation and Invasion of Melanoma Cells by Targeting Astrocyte-Elevated gene-1. *Oncol Res* (2018) 26(9):1429. doi: 10.3727/096504018X15186047251584
263. Chen W, Zhang J, Xu H, Dai J, Zhang X. The Negative Regulation of miR-149-5p in Melanoma Cell Survival and Apoptosis by Targeting LRIG2. *Am J Trans Res* (2017) 9(9):4331.
264. Zhang C, Li H, Wang J, Zhang J, Hou X. MicroRNA–338–3p Suppresses Cell Proliferation, Migration and Invasion in Human Malignant Melanoma by Targeting MACC1. *Exp Ther Med* (2019) 18(2):997–1004. doi: 10.3892/etm.2019.7644
265. Zhou H, Rao Y, Sun Q, Liu Y, Zhou X, Chen Y, et al. MiR-4458/human Antigen R (HuR) Modulates PBX3 MRNA Stability in Melanoma Tumorigenesis. *Arch Dermatol Res* (2020) 312:665–73. doi: 10.1007/s00403-020-02051-8
266. Yang X, Zhu X, Yan Z, Li C, Zhao H, Ma L, et al. Mir-489-3p/SIX1 Axis Regulates Melanoma Proliferation and Glycolytic Potential. *Mol Ther-Oncolyt* (2020) 16:30–40. doi: 10.1016/j.omto.2019.11.001
267. Sun Y, Li X, Wang H, Wu J. MiR-431 is a Prognostic Marker and Suppresses Cell Growth, Migration and Invasion by Targeting NOTCH2 in Melanoma. *Eur Rev Med Pharmacol Sci* (2019) 23(9):3876–84. doi: 10.26355/eurrev_201905_17815
268. Li Y, Fu Y, Gao Y, Li H, Ma L, Shu C, et al. MicroRNA-134 Inhibits Melanoma Growth and Metastasis by Negatively Regulating Collagen Triple Helix Repeat Containing-1 (CTHRC1). *Int J Clin Exp Pathol* (2018) 11 (9):4319.
269. Li J, Liu X, Li C, Wang W. miR-224-5p Inhibits Proliferation, Migration, and Invasion by Targeting PIK3R3/AKT3 in Uveal Melanoma. *J Cell Biochem* (2019) 120(8):12412–21. doi: 10.1002/jcb.28507
270. Zhao G, Yin Y, Zhao B. miR-140-5p is Negatively Correlated With Proliferation, Invasion, and Tumorigenesis in Malignant Melanoma by Targeting SOX4 Via the Wnt/β-Catenin and NF-κb Cascades. *J Cell Physiol* (2020) 235(3):2161–70. doi: 10.1002/jcp.29122
271. He Y, Yang Y, Liao Y, Xu J, Liu L, Li C, et al. miR-140-3p Inhibits Cutaneous Melanoma Progression by Disrupting AKT/p70S6K and JNK Pathways Through ABHD2. *Mol Ther-Oncolyt* (2020) 17:83–93. doi: 10.1016/j.omto.2020.03.009
272. Zhang X, Xin Z. MiR-135b-5p Inhibits the Progression of Malignant Melanoma Cells by Targeting RBX1. *Eur Rev Med Pharmacol Sci* (2020) 24(3):1309–15. doi: 10.21203/rs.3.rs-16546/v3
273. Hanniford D, Zhong J, Koetz L, Gaziel-Sovran A, Lackaye DJ, Shang S, et al. A MiRNA-based Signature Detected in Primary Melanoma Tissue Predicts Development of Brain Metastasis. *Clin Cancer Res* (2015) 21(21):4903–12. doi: 10.1158/1078-0432.CCR-14-2566
274. Worley LA, Long MD, Onken MD, Harbour JW. Micro-RNAs Associated With Metastasis in Uveal Melanoma Identified by Multiplexed Microarray Profiling. *Melanoma Res* (2008) 18(3):184–90. doi: 10.1097/CMR.0b013e3282feeac6
275. Bai M, Zhang H, Si L, Yu N, Zeng A, Zhao R. Upregulation of Serum miR-10b is Associated With Poor Prognosis in Patients With Melanoma. *J Cancer* (2017) 8(13):2487. doi: 10.7150/jca.18824
276. Caramuta S, Egyházi S, Rodolfo M, Witten D, Hansson J, Larsson C, et al. MicroRNA Expression Profiles Associated With Mutational Status and Survival in Malignant Melanoma. *J Invest Dermatol* (2010) 130(8):2062–70. doi: 10.1038/jid.2010.63
277. Falzone L, Romano GL, Salemi R, Bucolo C, Tomasello B, Lupo G, et al. Prognostic Significance of Deregulated MicroRNAs in Uveal Melanomas. *Mol Med Rep* (2019) 19(4):2599–610. doi: 10.3892/mmr.2019.9949
278. Segura MF, Belitskaya-Lévy I, Rose AE, Zakrzewski J, Gaziel A, Hanniford D, et al. Melanoma MicroRNA Signature Predicts Post-Recurrence Survival. *Clin Cancer Res* (2010) 16(5):1577–86. doi: 10.1158/1078-0432.CCR-09-2721
279. Nguyen T, Kuo C, Nicholl MB, Sim M-S, Turner RR, Morton DL, et al. Downregulation of MicroRNA-29c is Associated With Hypermethylation of Tumor-Related Genes and Disease Outcome in Cutaneous Melanoma. *Epigenetics* (2011) 6(3):388–94. doi: 10.4161/epi.6.3.14056
280. Hanna JA, Hahn L, Agarwal S, Rimm DL. In Situ Measurement of miR-205 in Malignant Melanoma Tissue Supports Its Role as a Tumor Suppressor Microrna. *Lab Invest* (2012) 92(10):1390–7. doi: 10.1038/labinvest.2012.119
281. Yan J, Jiang Q, Lu H, Na S, Long S, Xin Y, et al. Association Between MicroRNA–125b Expression in Formalin–Fixed Paraffin–Embedded Tumor Tissues and Prognosis in Patients With Melanoma. *Oncol Lett* (2019) 18(2):1856–62. doi: 10.3892/ol.2019.10506
282. Kozubek J, Ma Z, Fleming E, Duggan T, Wu R, Shin D-G, et al. In-Depth Characterization of MicroRNA Transcriptome in Melanoma. *PloS One* (2013) 8(9):e72699. doi: 10.1371/journal.pone.0072699
283. Babapoor S, Horwich M, Wu R, Levinson S, Gandhi M, Makkar H, et al. MicroRNA in Situ Hybridization for miR-211 Detection as an Ancillary Test in Melanoma Diagnosis. *Modern Pathol* (2016) 29(5):461–75. doi: 10.1038/modpathol.2016.44
284. Tengda L, Shuping L, Mingli G, Jie G, Yun L, Weiwei Z, et al. Serum Exosomal MicroRNAs as Potent Circulating Biomarkers for Melanoma. *Melanoma Res* (2018) 28(4):295–303. doi: 10.1097/CMR.0000000000000450
285. Fogli S, Polini B, Carpi S, Pardini B, Naccarati A, Dubbini N, et al. Identification of Plasma MicroRNAs as New Potential Biomarkers With High Diagnostic Power in Human Cutaneous Melanoma. *Tumor Biol* (2017) 39(5):1010428317701646. doi: 10.1177/1010428317701646
286. Leidinger P, Keller A, Borries A, Reichrath J, Rass K, Jager SU, et al. High-Throughput MiRNA Profiling of Human Melanoma Blood Samples. *BMC Cancer* (2010) 10(1):1–11. doi: 10.1186/1471-2407-10-262
287. Stark MS, Gray ES, Isaacs T, Chen FK, Millward M, McEvoy A, et al. A Panel of Circulating MicroRNAs Detects Uveal Melanoma With High Precision. *Trans Vision Sci Technol* (2019) 8(6):12–. doi: 10.1167/tvst.8.6.12
288. Armand-Labit V, Meyer N, Casanova A, Bonnabau H, Platzer V, Tournier E, et al. Identification of a Circulating MicroRNA Profile as a Biomarker of Metastatic Cutaneous Melanoma. *Acta Dermato-Venereolog* (2016) 96 (1):29–34. doi: 10.2340/00015555-2156
289. Shiiyama R, Fukushima S, Jinnin M, Yamashita J, Miyashita A, Nakahara S, et al. Sensitive Detection of Melanoma Metastasis Using Circulating MicroRNA Expression Profiles. *Melanoma Res* (2013) 23(5):366–72. doi: 10.1097/CMR.0b013e328363e485
290. Xin X, Zhang Y, Ling F, Wang L, Sheng X, Qin L, et al. Identification of a Nine-MiRNA Signature for the Prognosis of Uveal Melanoma. *Exp Eye Res* (2019) 180:242–9. doi: 10.1016/j.exer.2019.01.004

291. Sun Q, Cong R, Yan H, Gu H, Zeng Y, Liu N, et al. Genistein Inhibits Growth of Human Uveal Melanoma Cells and Affects MicroRNA-27a and Target Gene Expression. *Oncol Rep* (2009) 22(3):563–7. doi: 10.3892/or_00000472
292. Galore-Haskel G, Nemlich Y, Greenberg E, Ashkenazi S, Hakim M, Itzhaki O, et al. A Novel Immune Resistance Mechanism of Melanoma Cells Controlled by the ADAR1 Enzyme. *Oncotarget* (2015) 6(30):28999. doi: 10.18632/oncotarget.4905
293. Varrone F, Caputo E. The MiRNAs Role in Melanoma and in Its Resistance to Therapy. *Int J Mol Sci* (2020) 21(3):878. doi: 10.3390/ijms21030878
294. Gomez-Lira M, Ferronato S, Orlandi E, Dal Molin A, Malerba G, Frigerio S, et al. Association of Micro RNA 146a Polymorphism rs2910164 and the Risk of Melanoma in an Italian Population. *Exp Dermatol* (2015) 24(10):794–5. doi: 10.1111/exd.12778
295. Sangalli A, Orlandi E, Poli A, Maurichi A, Santinami M, Nicolis M, et al. Sex-Specific Effect of RNASEL rs486907 and miR-146a rs2910164 Polymorphisms' Interaction as a Susceptibility Factor for Melanoma Skin Cancer. *Melanoma Res* (2017) 27(4):309–14. doi: 10.1097/CMR.0000000000000360
296. Yamashita J, Iwakiri T, Fukushima S, Jinnin M, Miyashita A, Hamasaki T, et al. The rs2910164 G> C Polymorphism in MicroRNA-146a is Associated With the Incidence of Malignant Melanoma. *Melanoma Res* (2013) 23 (1):13–20. doi: 10.1097/CMR.0b013e32835c5b30
297. Lodygin D, Tarasov V, Epanchintsev A, Berking C, Knyazeva T, Körner H, et al. Inactivation of miR-34a by Aberrant CpG Methylation in Multiple Types of Cancer. *Cell Cycle* (2008) 7(16):2591–600. doi: 10.4161/cc.7.16.6533
298. Ozsolak F, Poling LL, Wang Z, Liu H, Liu XS, Roeder RG, et al. Chromatin Structure Analyses Identify MiRNA Promoters. *Genes Dev* (2008) 22 (22):3172–83. doi: 10.1101/gad.1706508
299. Syed D N, Imran Khan M, Shabbir M, Mukhtar H. MicroRNAs in Skin Response to UV Radiation. *Curr Drug Targets* (2013) 14(10):1128–34. doi: 10.2174/13894501113149990184
300. Bemis LT, Chen R, Amato CM, Classen EH, Robinson SE, Coffey DG, et al. MicroRNA-137 Targets Microphthalmia-Associated Transcription Factor in Melanoma Cell Lines. *Cancer Res* (2008) 68(5):1362–8. doi: 10.1158/0008-5472.CAN-07-2912
301. Gajos-Michniewicz A, Czyz M. Role of MiRNAs in Melanoma Metastasis. *Cancers* (2019) 11(3):326. doi: 10.3390/cancers11030326

Conflict of Interest: The authors declare that the research was conducted in the absence of any commercial or financial relationships that could be construed as a potential conflict of interest.

frontiers in Oncology

ORIGINAL RESEARCH
published: 28 May 2021
doi: 10.3389/fonc.2021.615963

Identification of Genes Related to Immune Infiltration in the Tumor Microenvironment of Cutaneous Melanoma

Rujia Qin[1†], *Wen Peng*[1†], *Xuemin Wang*[1], *Chunyan Li*[1], *Yan Xi*[1], *Zhaoming Zhong*[1,2*] *and Chuanzheng Sun*[1*]

[1] Department of Head and Neck Surgery Section II, The Third Affiliated Hospital of Kunming Medical University, Yunnan Cancer Hospital, Kunming, China, [2] Department of Medical Oncology, The First Affiliated Hospital of Kunming Medical University, Kunming, China

OPEN ACCESS

Edited by:
Giuseppe Palmieri,
National Research Council (CNR), Italy

Reviewed by:
Susanna Dolci,
University of Rome Tor Vergata, Italy
Chuanliang Cui,
Peking University Cancer Hospital, China

***Correspondence:**
Zhaoming Zhong
zhongzhm@126.com
Chuanzheng Sun
scz008@126.com

[†]These authors have contributed equally to this work

Specialty section:
This article was submitted to Skin Cancer, a section of the journal Frontiers in Oncology

Received: 10 October 2020
Accepted: 28 April 2021
Published: 28 May 2021

Citation:
Qin R, Peng W, Wang X, Li C, Xi Y, Zhong Z and Sun C (2021) Identification of Genes Related to Immune Infiltration in the Tumor Microenvironment of Cutaneous Melanoma. Front. Oncol. 11:615963. doi: 10.3389/fonc.2021.615963

Cutaneous melanoma (CM) is the leading cause of skin cancer deaths and is typically diagnosed at an advanced stage, resulting in a poor prognosis. The tumor microenvironment (TME) plays a significant role in tumorigenesis and CM progression, but the dynamic regulation of immune and stromal components is not yet fully understood. In the present study, we quantified the ratio between immune and stromal components and the proportion of tumor-infiltrating immune cells (TICs), based on the ESTIMATE and CIBERSORT computational methods, in 471 cases of skin CM (SKCM) obtained from The Cancer Genome Atlas (TCGA) database. Differentially expressed genes (DEGs) were analyzed by univariate Cox regression analysis, least absolute shrinkage, and selection operator (LASSO) regression analysis, and multivariate Cox regression analysis to identify prognosis-related genes. The developed prognosis model contains ten genes, which are all vital for patient prognosis. The areas under the curve (AUC) values for the developed prognostic model at 1, 3, 5, and 10 years were 0.832, 0.831, 0.880, and 0.857 in the training dataset, respectively. The GSE54467 dataset was used as a validation set to determine the predictive ability of the prognostic signature. Protein–protein interaction (PPI) analysis and weighted gene co-expression network analysis (WGCNA) were used to verify "real" hub genes closely related to the TME. These hub genes were verified for differential expression by immunohistochemistry (IHC) analyses. In conclusion, this study might provide potential diagnostic and prognostic biomarkers for CM.

Keywords: cutaneous melanoma, tumor microenvironment, ESTIMATE, CIBERSORT, protein–protein interaction, weighted gene co-expression network analysis, tumor- infiltrating immune cells, prognosis

INTRODUCTION

Cutaneous melanoma (CM), a highly aggressive malignancy, represents approximately 2% of skin cancers and approximately 75% of skin cancer deaths due to rapid progression and metastasis (1). Surgical resection is the optimal treatment option for most early stage melanomas, but limited effective late-stage therapies exist, and only a small proportion of late-stage patients respond to single or combined therapies, limiting patient survival (2). Additional exploration of CM carcinogenesis and treatment remains urgently necessary.

Recently, increasing evidence indicates that the tumor microenvironment (TME) is involved in tumor development. Interactions between cancer cells, stromal cells, and tumor-infiltrating immune cells (TICs) are critical for malignant cancer progression, including the promotion of replicative immortality, invasion, metastasis, and immune surveillance evasion. The TME influences clinical outcomes and contains potential targets for therapeutic modulation (3). Several studies have reported that TICs represent a promising TME index for evaluating therapeutic efficacy (4). TIC components and their activation states are vital parameters that affect patient prognosis and tumor characteristics. Anti-cytotoxic T-lymphocyte antigen 4 (CTLA-4) therapy can activate T cells and induce programmed-death ligand 1(PD-L1) expression in tumor cells and TICs. In many cancers, including CM, $CD8^+$ T cell activation can prolong patients' survival times (5). A study indicated that increased $CD8^+$ T cell trafficking contributes to anti-programmed-death 1 (PD-1)/CTLA-4 therapeutic efficacy against melanoma metastasis and may represent an effective immunotherapy strategy (6). Neutrophils also play a context-dependent role in melanoma and can actively switch to an anti-tumor mode (7). These studies suggested that crosstalk between cancer cells and the TME plays an indispensable part in CM development, which has made the accurate delineation of the dynamic regulatory effects of immune and stromal components on the TME challenging.

In the present study, the proportions of immune and stromal components and the TIC ratio were quantified based on the ESTIMATE and CIBERSORT computational methods in skin CM (SKCM) samples obtained from The Cancer Genome Atlas (TCGA) database. Differentially expressed genes (DEGs) were identified in the high-ImmuneScore and high-StromalScore groups compared with the corresponding low-score groups. We utilized patient survival information obtained from TCGA to perform univariate Cox regression, least absolute shrinkage and selection operator (LASSO) regression, and multivariate Cox regression analyses to verify prognosis-related genes. The 79 SKCM samples from the GSE54467 dataset were used as a validation set to verify the predictive ability of the prognostic model. Additionally, we defined a protein–protein interaction (PPI) network based on the identified DEGs to verify hub genes. DEGs in the TCGA database were also examined by weighted gene co-expression network analysis (WGCNA) to identify hub genes related to the ImmuneScore and StromalScore of SKCM. Genes identified in both networks were identified as "real" hub genes critical to the TME. These "real" hub genes were verified by examining differential expression using immunohistochemistry (IHC) analyses. These results provided a better understanding of the underlying biological mechanisms of immune-related genes and may improve SKCM prognosis.

MATERIALS AND METHODS

Data Collection and Data Processing

The RNA sequencing (RNA-seq) data of 471 SKCM samples were downloaded from TCGA (https://portal.gdc.cancer.gov/). Corresponding clinical information was obtained from the UCSC Xena database (http://xena.ucsc.edu/). We used the fragments per kilobase of transcript per million mapped reads (FPKM) method to standardize the data (8). To ensure that significantly expressed genes were evaluated, genes with average expression values <0.1 were excluded from each case. P-values of DEGs were identified using a Wilcox test. Genes with fold change (FC) >1 (high- and low-score groups) and false discovery rate (FDR) <0.05 after $\log_2$ transformation were regarded as DEGs.

To increase robustness, RNA-seq data and clinical information from an independent cohort of 79 tumor samples were obtained from the GSE54467 dataset (https://www.ncbi.nlm.nih.gov/geo/query/acc.cgi?acc=GSE54467) as a validation set. Processed expression data were $\log_2$ transformed before further analysis. When multiple probes corresponded to the same gene, the average of all probes was used. Data normalization and background adjustments were conducted using the "limma" R package.

A total of 80 samples were collected from CM patients who underwent surgical resection at the Third Affiliated Hospital of Kunming Medical University from January 2013 to December 2016. CM and adjacent normal tissues were obtained as formalin-fixed paraffin-embedded (FFPE) samples. The study was approved by the Ethics Committee of the Third Affiliated Hospital of Kunming Medical University. The clinical materials and outcome data were reviewed after approval was obtained from the institutional review board.

Generation of the ImmuneScore, StromalScore, and ESTIMATEScore

The proportions of immune-stromal TME components were quantified for each patient using the ESTIMATE R package. The algorithm includes the ImmuneScore, StromalScore, and ESTIMATEScore, which positively correlate with proportions of immune components, stromal components, and both, respectively, with higher scores indicating increased proportions in the TME (9).

Functional Enrichment Analysis

The Gene Ontology (GO) analysis consists of biological processes (BPs), cellular components (CCs), and molecular functions (MFs) (10). The Kyoto Encyclopedia of Genes and Genomes (KEGG) database is used for the functional annotation, systematic analysis, and visualization of gene functions (11). GO functional annotations and KEGG enrichment analyses were used to understand the potential biological significance of genes using the clusterProfiler package in R. We listed the top 10 terms in every category, limited to those terms with both p- and q-values <0.05.

Risk Score System Establishment

Patients' clinical information was downloaded from the UCSC Xena database. After removing samples without survival data, 454 samples remained for follow-up survival analysis. We randomly divided the samples into training (227 samples) and test (227 samples) groups to ensure the generalizability of the prognostic signature. Univariate Cox proportional hazards regression analysis was performed on the training cohort, with

P <0.01 designated as significant, and significant variables were integrated into the LASSO regression analysis (12). To produce the minimum cross-validation error, LASSO regression analysis was used to generate a generalized linear model with 10-fold cross-validation (13). A multivariate Cox proportional hazard regression model, based on the two-step method, was generated to verify key genes involved in the prognostic model. Ten immune-related genes and their corresponding coefficients were used to generate the prognosis model for SKCM. The risk score for each patient was calculated as follows:

$$Riskscore = \exp r_{gene1} * \beta_{gene1} + \exp r_{gene2} * \beta_{gene2} + \exp r_{gene3} * \beta_{gene3} \ldots\ldots\ldots \exp r_{genen} * \beta_{genen}$$

where expr represents the selected gene expression level, and β represents the regression coefficients of the multivariate Cox regression model (14). A risk score was calculated for each sample included in this study. Patients were stratified into high- and low-risk groups, according to the median risk value.

CIBERSORT Estimation

The relative proportions of 22 immune cell types were calculated in each SKCM sample based on the expression file, as assessed by CIBERSORT (15). TIC abundance profiles for all tumor samples were estimated using CIBERSORT. Only the 260 tumor samples with P <0.05 in the CIBERSORT analysis were considered eligible for subsequent analyses.

PPI Network Construction and Module Analysis

A PPI network can identify hub genes and gene modules according to the level of interaction. The Search Tool for The Retrieval of Interaction Genes (STRING, https://string-db.org/) is an online tool for analyzing consensus genes and constructing PPI networks (16). DEGs were submitted to the STRING database to evaluate PPI information, and nodes with interaction scores >0.95 were selected for PPI network construction. The PPI network was visualized using Cytoscape 3.7.0 software. The top 30 genes, according to the number of nodes, were designated hub genes in the PPI analysis. The biological significance of gene modules was visualized with the plug-in Molecular Complex Detection (MCODE) in Cytoscape to identify the most significant module (17).

Co-expression Network Construction of DEGs

The WGCNA package in R was used to generate a co-expression network of DEGs. Pearson's correlation analysis was conducted as a similarity measure for all pair-wise genes. The power function $Amn = |Cmn|^{\beta}$ (Cmn = Pearson's correlation between gene m and gene n; Amn = adjacency between gene m and gene n) allowed for the construction of a weighted adjacency matrix. The soft threshold power (β) of the correlation matrix was used to emphasize strong correlations between genes and penalize weak correlations. A β value was selected to construct a co-expression network, and the adjacency was transformed into a topological overlap matrix (TOM) to measure the network connectivity of genes (18). To identify genes with expression profiles similar to the gene modules, we used average linkage hierarchical clustering based on TOM dissimilarity measurements, and the minimum number of genes per module was set to the default of 20 (19). Dissimilarities among the module eigengenes (MEs) in the module dendrogram were calculated, and similar modules were merged.

Identification of Significant Modules and Functional Annotation

Correlations between clinical information and modules were determined using two methods. MEs were used as the principal component for each gene module. Gene significance (GS) scores were calculated to determine correlations among gene expression in the module, defined as the $\log_{10}$ transformation of the P-value (GS = logP) for each gene. Module significance (MS) was defined as the average GS in a specific module, representing the correlation between the module and scores. In general, modules with the largest MS values were considered those associated with the scores. To explore the functions of the modules, GO and KEGG enrichment analyses were used to identify the underlying biological significance of module genes. Only terms with both p- and q-values <0.05 were included.

Finding "Real" Hub Gene and Verification

In this study, we selected two important modules in the co-expression network, and hub genes were defined as those with high module membership (MM), as measured by Pearson's correlation analysis (weighted correlation 0.8). The hub genes in the module had the highest correlation with the scores (weighted correlation 0.5). A PPI network with a combined interaction score of >0.95 was constructed. The top 30 genes, ordered by the number of nodes, were selected as hub genes in the PPI analysis. Hub genes identified in both the co-expression and PPI networks were regarded as "real" hub genes for subsequent analysis.

First, the GEPIA database (http://gepia.cancer-pku.cn) and the Human Protein Atlas (HPA; http://www.proteinatlas.org/) were used to validate the expression of "real" hub genes between tumor and normal skin tissues in SKCM (20). Then, the differential expression of "real" hub genes was verified in 80 human CM tissues and adjacent tissues analyzed by IHC. In addition, we investigated four genes reported as key targets for immune checkpoint inhibitors: PD-1 and its ligand PD-L1, indoleamine 2,3-dioxygenase 1 (IDO1), and CTLA-4 in cancer (21–23). To determine the possible roles of our "real" hub genes in immune checkpoint blockade (ICB) treatment, we analyzed the correlation between these immune checkpoint inhibitors and our hub genes. The Tumor Immune Estimation Resource (TIMER) (https://cistrome.shinyapps.io/timer/) algorithm was used to explore the correlation between "real" hub genes and immune cell infiltration in SKCM patients (24). All statistical analyses were performed using R software (version 3.6.3). Differences were considered significant at P <0.05.

IHC

Paraffin-embedded tumor samples and adjacent samples from CM patients were collected, fixed with 10% formalin buffer, dehydrated, and sectioned. IHC staining was performed using rabbit anti-VAV1 antibody (1:100), rabbit anti-ITGB2 antibody (1:200), and rabbit anti-HLA-DRA antibody (1:200). Semiquantitative expression levels were used to determine the extent and intensity of stained tumor cells. The staining intensity was divided into four levels: blank = 0, yellow = 1, dark yellow = 2, and brown = 3. The frequency of positive cells was divided into five levels: 0–5% = 0, 6–25% = 1, 26–50% = 2, 51–75% = 3, and 76–100% = 4. The immune response score was calculated as the stain intensity score multiplied by the frequency of positive cells. All slides were independently evaluated by two pathologists blinded to the patient's identity and clinical diagnosis.

RESULTS

Scores Correlate With Survival and Are Clinically Relevant in SKCM Patients

In the present study, we systematically analyzed the critical roles and prognostic value of genes related to immune infiltration in SKCM. **Figure 1** shows the overall study design. Correlations between immune and stromal cell proportions and survival rates were determined by grouping melanoma patients into high- and low-score groups, according to the median value of 471 SKCM patients. Kaplan–Meier survival curves were conducted for the ImmuneScore, StromalScore, and ESTIMATEScore. As shown in **Figure 2A**, high-ImmuneScore patients had better survival than low-ImmuneScore patients. Although no significant correlation was found between the StromalScore and overall survival (OS) (**Figure 2B**), the OS was significantly higher among high-ESTIMATEScore patients than low-ESTIMATEScore patients (**Figure 2C**). These results indicated that the proportions of immune components were significant prognosis indicators for SKCM patients.

To clarify the correlation between scores and clinical features, we analyzed the clinical features of SKCM patients from the UCSC Xena database. Older patients had significantly lower scores than younger patients (**Figure 2D**; P = 0.009 and P = 0.001, respectively). Women had higher ImmuneScores and StromalScores than men although not significantly different (**Figure 2E**; P = 0.071 and P = 0.340, respectively). Advanced-stage cases generally had higher scores than early stage cases (**Figure 2F**; P = 0.066 and P = 0.007, respectively), and metastatic tumors had higher scores than primary tumors (**Figure 2G**; P < 0.001). Patients without ulcerations or with lower Breslow depths had higher immune and stromal scores (**Figures 2H, I**). These results indicated that the TME, especially TICs, may play indispensable roles in SKCM progression, although further exploration remains necessary.

Identification of DEGs Shared by the ImmuneScore and StromalScore

To clarify changes in gene expression levels among immune and stromal components in the TME, we compared high- and low-score samples to identify DEGs. The results indicated that 927 genes were upregulated, and 280 genes were downregulated by comparing the high-score group *vs.* the low-score group for the ImmuneScore. Similarly, 1,093 genes were upregulated, and 207 genes were downregulated by comparing the high-score group *vs.* the low-score group for the StromalScore (**Figures 3A, B**).

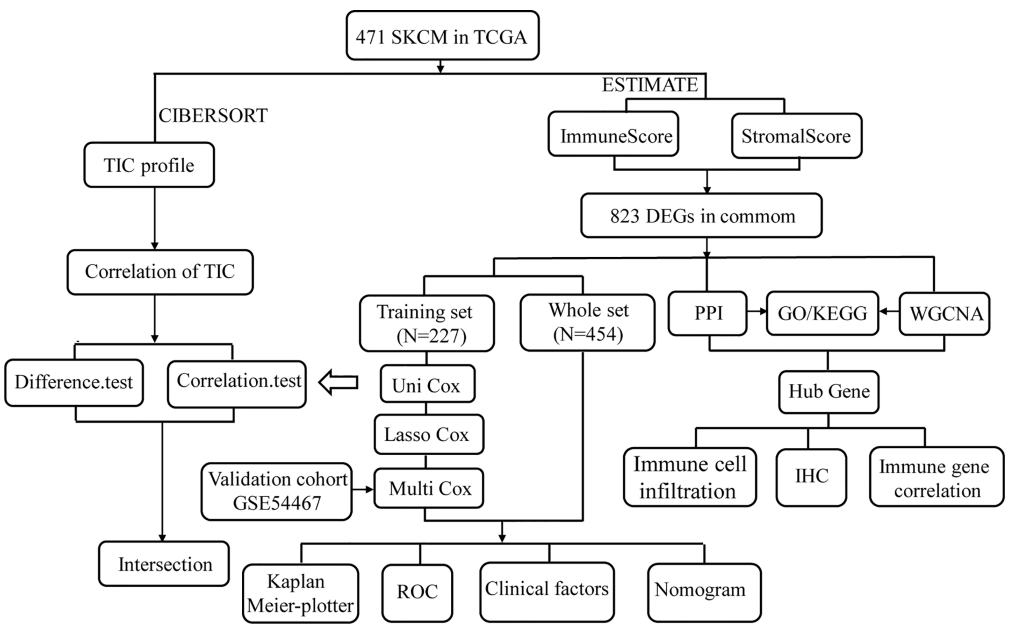

FIGURE 1 | Analysis workflow of this study.

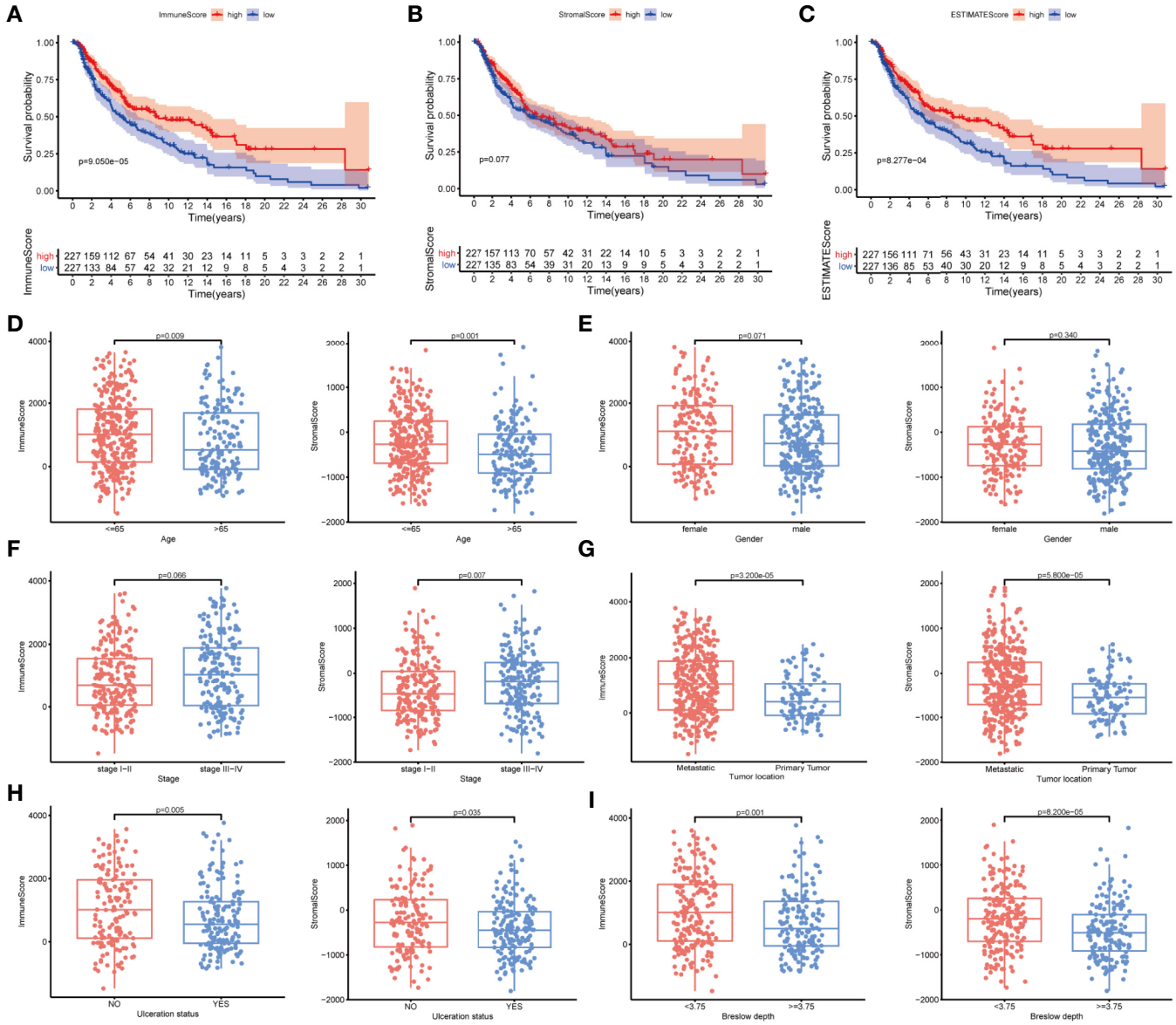

FIGURE 2 | The correlation between scores with clinicopathological features in cutaneous melanoma (CM). **(A–C)** Kaplan–Meier survival analysis identified skin CM (SKCM) patients in the high- or low-ImmuneScore, -StromalScore, and -ESTIMATEScore groups by comparison with the median scores for each analysis. **(D–I)** Correlation between the ImmuneScore and StromalScore and age, sex, tumor node metastasis (TNM) stage, tumor location, ulceration status, and Breslow depth.

The identified intersection genes included 749 upregulated and 74 downregulated genes in both the high-ImmuneScore and high-StromalScore groups compared with the low-score groups, as displayed in the Venn diagram (**Figures 3C, D**). The functions of these 823 genes were predicted, and GO analysis was performed, which showed that these genes were primarily associated with immune-related GO terms, such as leukocyte cell–cell adhesion and leukocyte proliferation (**Figure 3E**). The genes were highly enriched in cell adhesion molecules, cytokine–cytokine receptor interactions, and hematopoietic cell lineages, according to KEGG analysis (**Figure 3F**). The gene enrichment analysis indicated that these genes were primarily associated with immune-related pathway activation, suggesting that immune factors play an indispensable role in the TME of SKCM patients.

Prognosis-Related Model Construction and Analysis

Among the intersecting DEGs, 436 genes were significantly correlated with prognosis by univariate Cox regression analysis (**Supplementary Table 1**). The genes with the highest potential prognostic significance were identified by LASSO regression analysis. Following 10-fold cross-validation, 20 genes remained (**Figures 3G, H**). A multivariate Cox proportional hazards model was generated to build an immune-related prognostic signature based on the LASSO regression analysis (**Figure 3I**). Ten genes (nuclear receptor subfamily 1 group H member 3, *NR1H3*; interleukin 18 receptor accessory protein, *IL18RAP*; *CD40*; glycine receptor alpha 2, *GLRA2*; tumor necrosis factor (TNF) alpha-induced protein 2, *TNFAIP2*; *C4B*; epididymal sperm

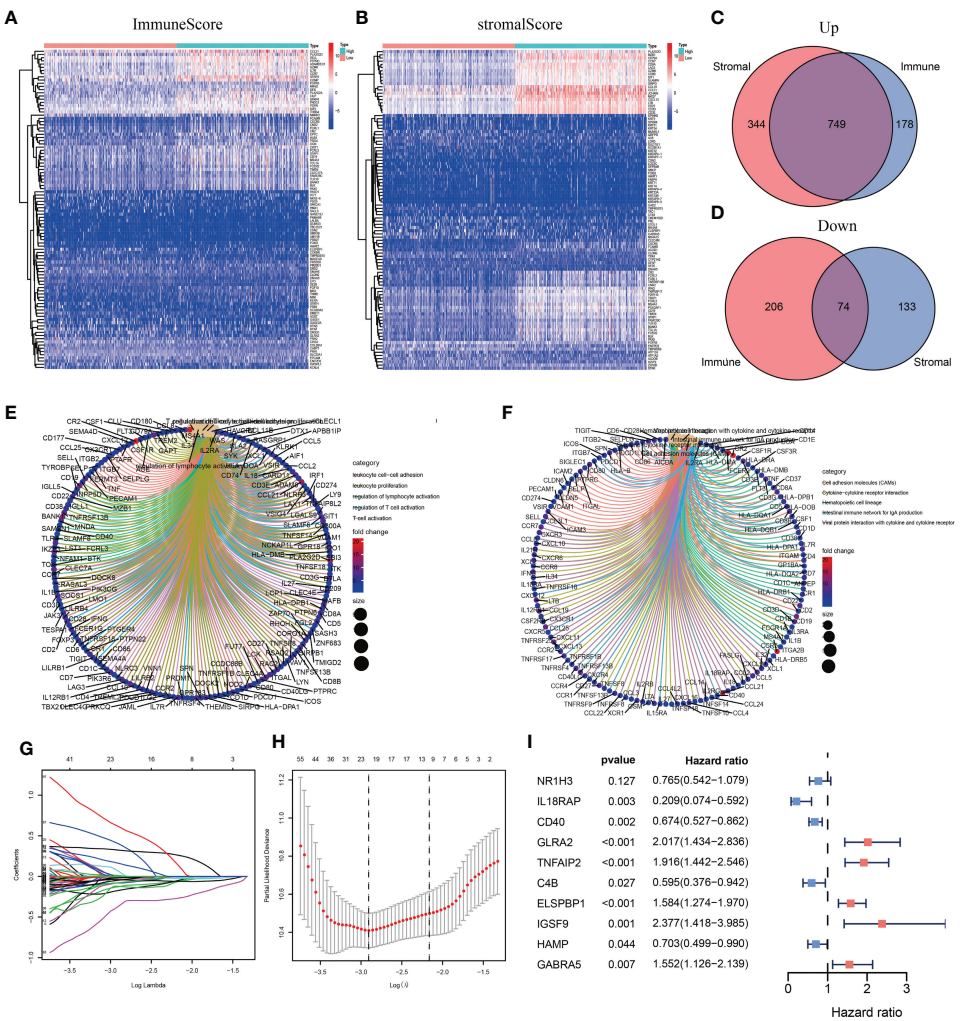

FIGURE 3 | Heatmaps, Venn diagrams, and enrichment analysis of differentially expressed genes (DEGs) and the construction of the prognostic classifier. **(A, B)** Heatmap for DEGs generated by comparing the high-score group *vs.* the low-score group for the ImmuneScore and StromalScore. **(C, D)** Venn diagrams showing common upregulated and downregulated DEGs shared by the ImmuneScore and StromalScore analyses. **(E, F)** Gene Ontology (GO) and Kyoto Encyclopedia of Genes and Genomes (KEGG) enrichment analyses for 823 DEGs. **(G, H)** The number of included factors was determined by LASSO analysis. **(I)** A forest plot showing the hazard ratios (HRs) and P-values from the multivariate Cox regression.

binding protein 1, *ELSPBP1*; immunoglobulin superfamily member 9, *IGSF9*; hepcidin antimicrobial peptide, *HAMP*; and gamma-aminobutyric acid type A receptor subunit alpha5, *GABRA5*) were identified by the multivariate Cox proportional hazards regression analysis and were used to generate a prognostic signature by calculating a risk score, as follows:

$$Riskscore = (-0.2685 \times NR1H3) + (-1.5631 \times IL18RAP) + (-0.3943 \times CD40) + (0.7016 \times GLRA2) + (0.6504 \times TNFAIP2) + (-0.5186 \times C4B) + (0.4602 \times ELSPBP1) + (0.8657 \times IGSF9) + (-0.3526 \times HAMP) + (0.4398 \times GABRA5)$$

We divided patients into low- and high-risk groups based on the median risk score of the training group. The risk score distribution was ranked according to the risk score values shown in the training cohort, the external validation cohort, and the whole cohort. Patients with a high-risk score had higher mortality than patients with a low-risk score (**Figure 4A**). Consistent with these results, the Kaplan–Meier curves suggested that patients in the low-risk group had higher survival than those in the high-risk group (**Figure 4B**; all $P < 0.01$). The results showed that the risk scores obtained using the ten-gene prognostic signature predicted survival at 1, 3, 5, and 10 years, with respective AUC values of 0.832, 0.831, 0.880, and 0.857 in the training cohort, 0.636, 0.678, 0.740, and 0.709 in the GSE54467 validation cohort, and 0.736, 0.711, 0.732, and 0.712 in the whole cohort, respectively (**Figure 4C**). These results indicated the high sensitivity and accuracy of the ten-gene prognostic signature in CM.

We evaluated the independent prognostic value of our ten-gene model (**Figure 5A**). The risk score was analyzed in combination with age, sex, tumor node metastasis (TNM) stage, tumor location, ulceration status, and Breslow depth, which are closely related to patient survival. Multivariate Cox regression analysis indicated that the ten-gene model is a robust and independent prognostic factor in the whole cohort ($P < 0.001$, **Figure 5B**). Although only age, sex, and TNM stage data were available for GSE54467, we also tested the validation dataset, which demonstrated consistent results (**Supplementary Figures 1A, B**). The correlation between our prognostic signature and clinical SKCM characteristics was evaluated for the whole cohort (**Figure 5C**). The results indicated that our

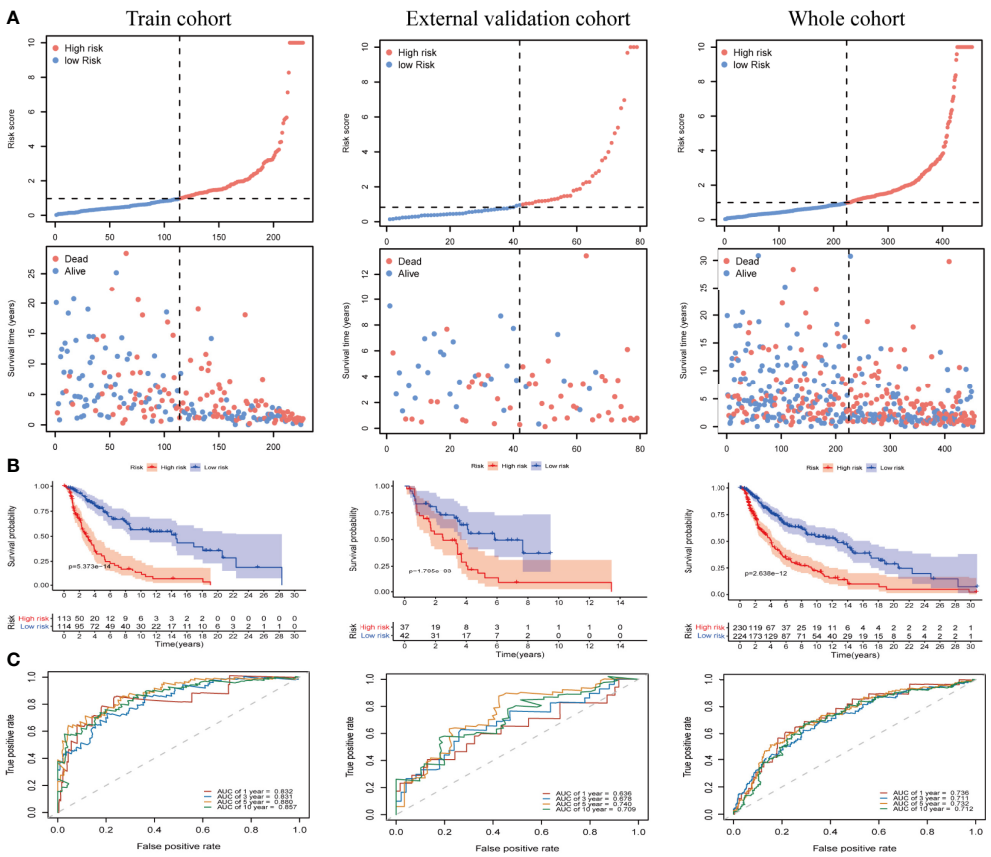

FIGURE 4 | Risk score analyses for the developed immune-related prognostic signature in the training cohort, the external validation cohort, and the whole cohort. **(A)** Patients were ranked by risk score values and the corresponding survival status. **(B)** Kaplan–Meier curves for the immune-related signature. **(C)** Receiver operator characteristic (ROC) curves for survival as predicted by the risk score.

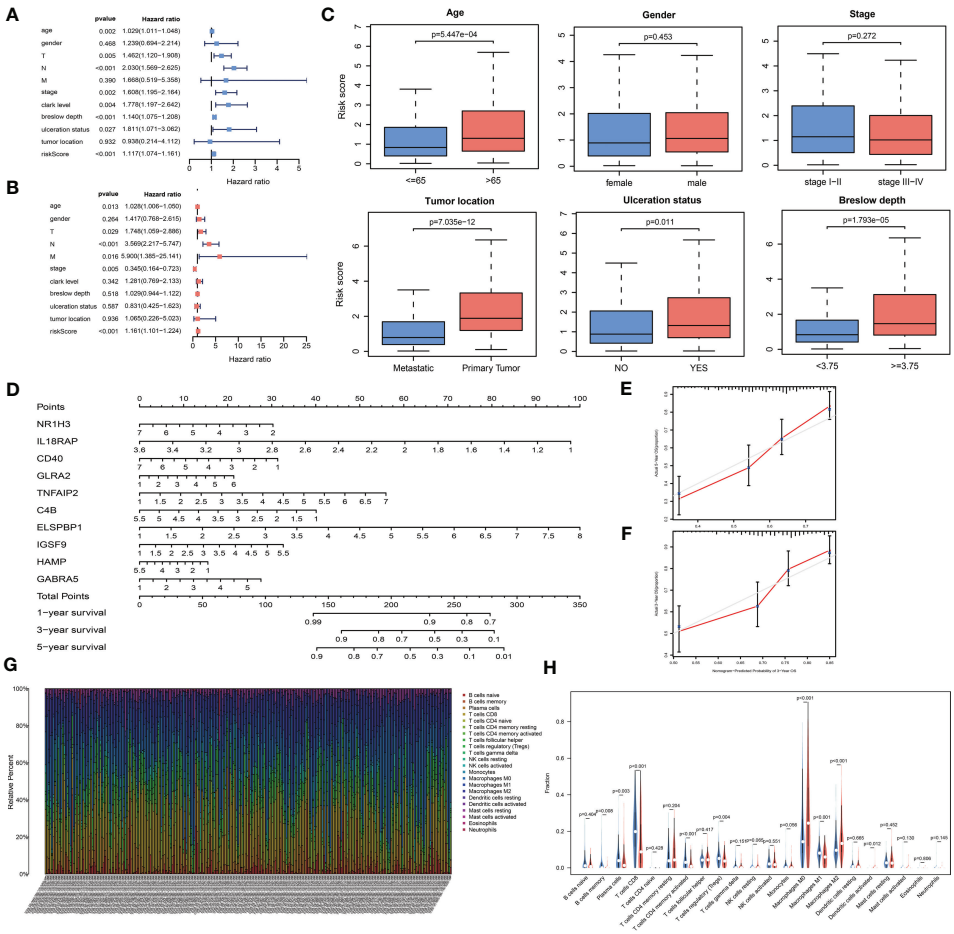

FIGURE 5 | The analysis of the prognosis-related model. **(A, B)** Univariable and multivariable analyses based on the risk group and other clinical features in the TCGA cohort. **(C)** Box plots displaying the correlation between different clinical features and the risk score. **(D)** Nomogram showing the overall survival (OS) for 1, 3, and 5 years in the TCGA cohort. **(E, F)** Calibration plots of the nomogram for predicting OS at 3 and 5 years. **(G)** Bar plot showing the ratios of 22 tumor-infiltrating immune cells (TIC) types in skin cutaneous melanoma (SKCM) patients. **(H)** Violin plot showing the proportions of 22 types of TICs in SKCM patients with low- or high- risk scores relative to the median risk score.

prognostic model was not associated with sex or TNM stage but was significantly correlated with age ($P < 0.001$), tumor location ($P < 0.001$), ulceration status ($P = 0.011$), and Breslow depth ($P < 0.001$) in CM, suggesting that the genes in our prognostic model may play essential roles in CM progression.

To build a quantitative model for survival probability prediction in SKCM, we used the ten-gene marker to develop a nomogram plot for estimating the survival probability after 1, 3, and 5 years in the TCGA cohort (**Figure 5D**). The nomogram performance was visualized intuitively by drawing calibration plots, which indicated that the prediction results were consistent with the observed results (**Figures 5E, F**).

Correlation Between Risk Score and TIC Proportions

The TIC subsets in the TME were quantified according to the CIBERSORT algorithm to determine correlations with the risk score. The abundances of 22 immune cell types in SKCM patients were obtained (**Figure 5G**). Nine TIC types were associated with low- and high-risk groups (**Figure 5H**, **Supplementary Figures 1C, D**), including three TIC types positively correlated with the risk score: M0 macrophages, M2 macrophages, and activated dendritic cells. Memory B cells, plasma cells, $CD8^+$ T cells, CD4-activated memory T cells, regulatory T cells (Tregs), and M1 macrophages were negatively correlated with the risk score. These results demonstrated that the risk score might serve as an immune activity indicator.

PPI Network Analysis of DEGs

To determine the hub genes and relevant gene modules involved in SKCM, we built a PPI network for the DEGs using Cytoscape software based on data obtained from the STRING database. The network consisted of 282 nodes and 746 edges (**Figure 6A**). The

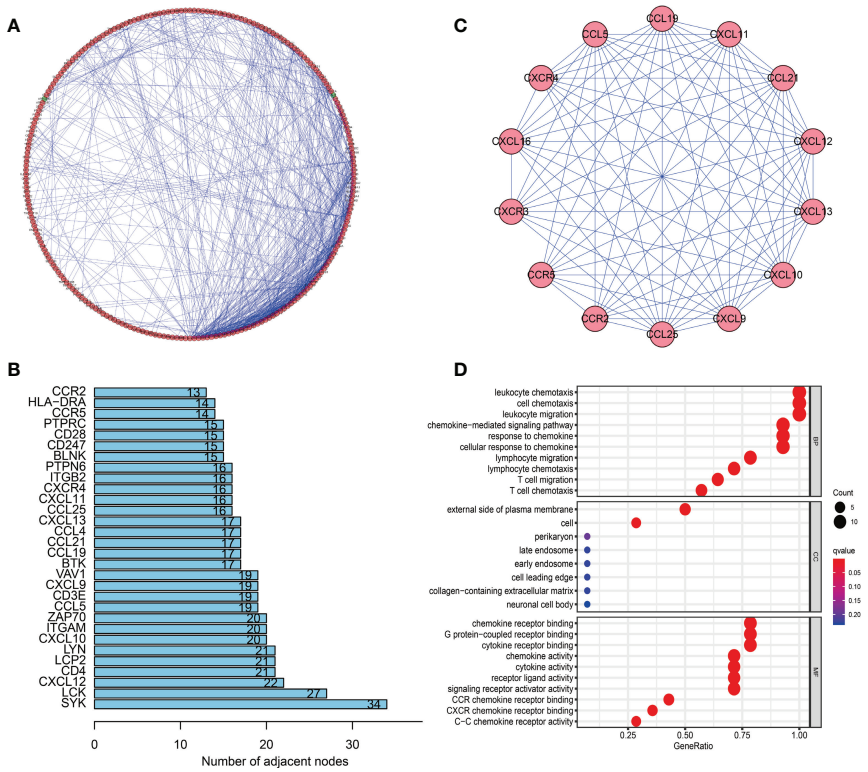

FIGURE 6 | Protein–protein interaction (PPI) network and module analysis. **(A)** PPI network of differentially expressed genes (DEGs). **(B)** The top 30 genes were ranked by the number of nodes. **(C)** PPI network of the top significant module. **(D)** Gene ontology (GO) analysis of the top significant module in the PPI analysis.

top 30 genes according to the number of nodes were displayed in a bar plot (**Figure 6B**). The top significant module was identified by the plug-in MCODE in Cytoscape (**Figure 6C**). Functional and pathway enrichment analyses of the DEGs in the top module were performed. The GO analysis showed that DEGs in the top module were involved in the leukocyte chemotaxis and cell chemotaxis in BPs. The CC analysis indicated genes enriched on the external side of the plasma membrane. The MF analysis showed genes enriched in G protein-coupled receptor binding and chemokine receptor binding (**Figure 6D**). KEGG analysis revealed DEGs principally involved in the chemokine signaling pathway (**Supplementary Figure 2A**).

WGCNA of DEGs

In this study, 471 scored SKCM samples were used for co-expression analysis. The soft-thresholding power was set to 5 to generate a scale-free network (**Figures 7A, B**). A total of eight modules were verified based on the SKCM scores (**Figure 7C**). Module-trait correlation analyses showed the turquoise and blue modules with the highest score associations (**Figure 7D**). GO (**Figures 7E, F**) and KEGG (**Supplementary Figures 2B, C**) enrichment analyses indicated that the turquoise module was principally concentrated in T cell activation, regulation of lymphocyte activation, and regulation of T cell activation, whereas the blue module was associated with T cell activation, leukocyte proliferation, and neutrophil degranulation. The genes in the blue and turquoise modules were pivotal for immune cell infiltration.

Hub Genes Related to TICs in SKCM

We identified 15 genes closely related to immune function in the turquoise module and 32 genes in the blue module as candidate hub genes (**Figures 7G, H**). The shared genes between the top 30 PPI nodes and the turquoise and blue modules were identified. Vav guanine nucleotide exchange factor 1 (*VAV1*) in turquoise, integrin subunit beta 2 (*ITGB2*) and major histocompatibility complex, class II, DR alpha (*HLA-DRA*) in blue were identified as candidates for further analysis and validation (**Figures 7I, J**). These genes were defined as "real" hub genes associated with TICs in SKCM.

To identify the roles played by "real" hub genes in SKCM, we first used the GEPIA and the HPA database to compare "real" hub gene expression between CM and normal skin tissues. The results showed that the three hub genes were significantly upregulated in tumor tissues compared with normal skin (**Figure 8A**, **Supplementary Figures 3A–C**). Then, we performed IHC analyses to determine and compare the expression levels of hub genes in 80 human CM and adjacent

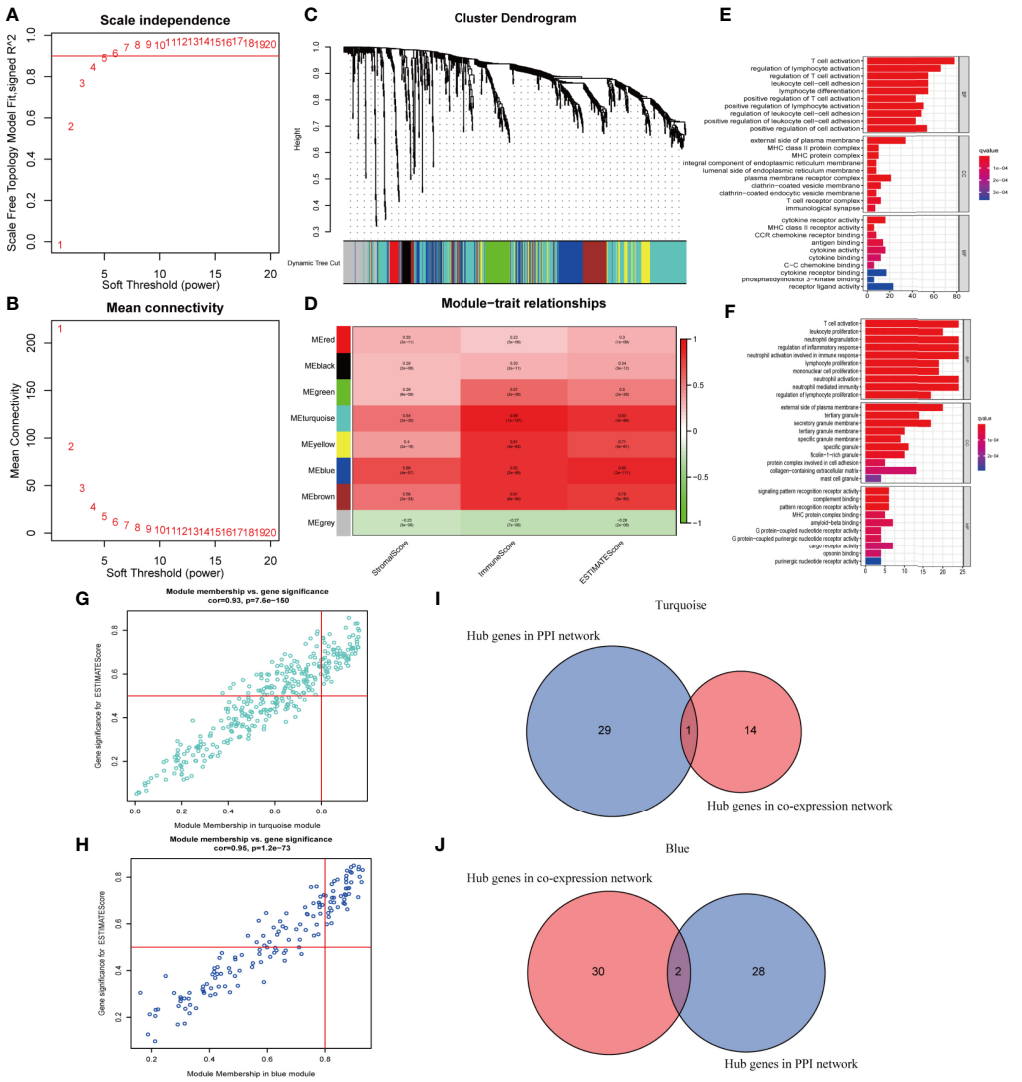

FIGURE 7 | Modules related to skin cutaneous melanoma (SKCM) scores and hub gene detection. **(A, B)** Analysis of the scale-free fit index and the mean connectivity for various soft-thresholding powers. **(C)** Dendrogram of all differentially expressed genes (DEGs) clustered based on a dissimilarity measure. **(D)** A heatmap showing the correlation between the gene modules and scores. **(E, F)** Gene ontology (GO) analyses of the turquoise and blue modules. **(G, H)** Scatter plot of the module eigengenes (MEs) in the turquoise and blue modules. **(I, J)** Identification of "real" hub genes in the protein–protein interaction (PPI) network and the co-expression network in the turquoise and blue modules.

tissues. Representative images of IHC staining for the hub genes are shown in **Figure 8B**. According to IHC staining results, we measured the expression of hub genes in 80 CM and adjacent tissues. The results indicated that the expression of the three hub genes significantly higher in tumor tissues than in adjacent tissues (**Figure 8C**). To understand the functions of "real" hub genes, we investigated the correlations between hub genes and immune infiltration using the TIMER database. There was a positive correlation between hub gene expression and the immune cell infiltration in SKCM (**Figures 9A–C**). The expression of immune checkpoint genes may be associated with the therapeutic efficacy of immune checkpoint inhibitors (25). ICB tumor immunotherapy has advanced in recent years, including for CM (22, 26). We evaluated the association between four key ICB targets and the "real" hub genes: PD-1, PD-L1, CTLA-4, and IDO1 (21–23). We found that *VAV1* was positively related to PD-1 ($r = 0.73$; $P < 0.001$), PD-L1 ($r = 0.35$; $P < 0.001$), CTLA4 ($r = 0.23$; $P < 0.001$), and IDO1 ($r = 0.41$; $P < 0.001$) (**Figure 9D**). Similar results were obtained for *ITGB2* and *HLA-DRA* (**Figures 9E, F**), suggesting that these hub genes may play significant roles in the responses to ICB immunotherapy in SKCM. These results indicated that these three genes play significant roles in immune infiltration processes in SKCM patients and may represent potential therapeutic targets.

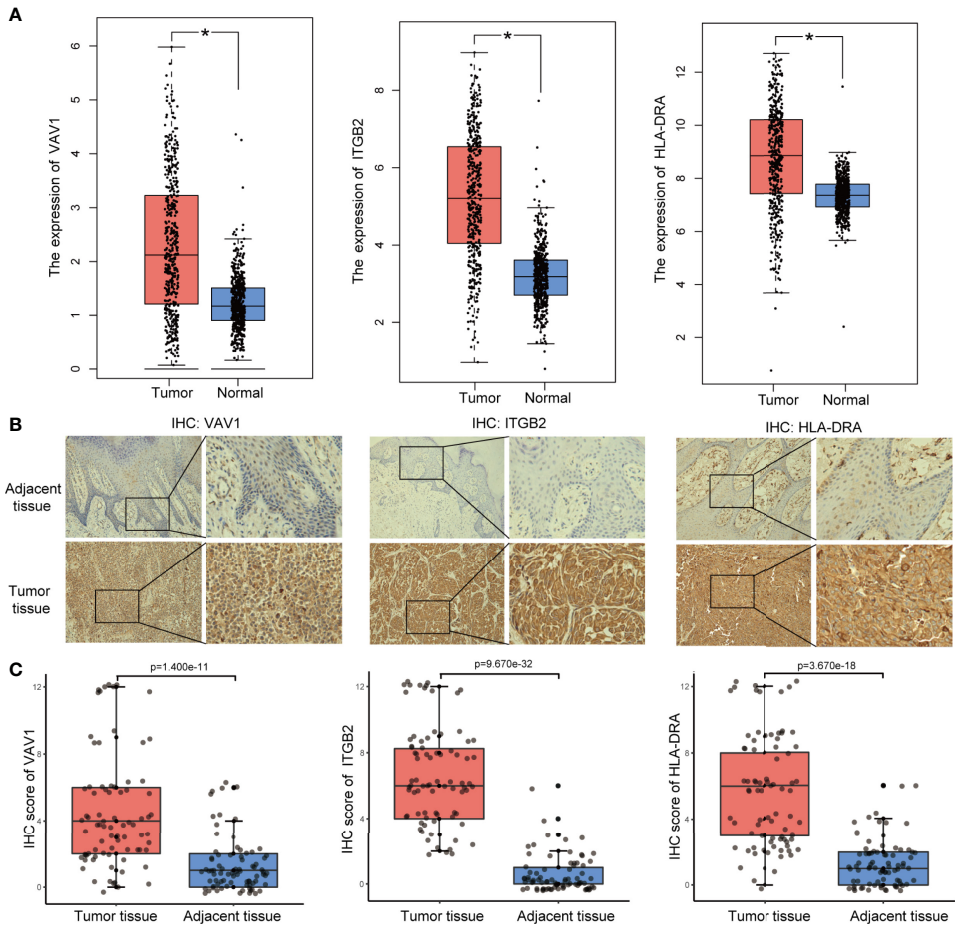

FIGURE 8 | Validation of "real" hub genes. **(A)** Hub gene expression in CM and normal skin tissues, based on the GEPIA database. **(B)** Examples of immunohistochemistry (IHC) staining for hub genes in CM tissues and corresponding adjacent tissues. **(C)** The expression of hub genes in 80 human CM tissues and adjacent tissues analyzed by IHC.

DISCUSSION

The CM incidence and mortality have increased recently, which is a public issue that attracts worldwide attention. Despite many studies on SKCM, early diagnosis, treatment, and prognosis remain poor. Investigating the potential molecular biological mechanisms underlying SKCM progression and development is important. Recently, many advanced therapeutic options have been developed for melanoma patients, improving disease-free rates and OS. However, limitations persist, including low sustained response rates, drug toxicity, low tolerance, high cost, and patient responses are heterogeneous (27). The rapid development of high-throughput sequencing technology facilitates the detection of abnormal gene expression during tumor progression, providing effective targets for diagnosis and treatment. A lack of reliable biomarkers exists to monitor therapeutic efficacy. Therefore, we attempted to identify genes that affect patient prognosis by investigating the TME.

Increasing evidence suggests the TME is a vital modulator of tumor progression, and the identification of potential therapeutic targets associated with TME remodeling can promote the TME transformation from tumor-supportive to tumor-suppressive. Transcriptome analysis of SKCM data from the TCGA and Gene Expression Omnibus (GEO) databases demonstrated that the proportions of immune and stromal components in the TME had important influences on SKCM progression. Our results emphasized the importance of interactions between tumor and immune cells, providing new insights into SKCM immunotherapy. Despite recent achievements in ICB-based tumor immunotherapy for advanced SKCM patients (28, 29), fewer than one-third of patients treated with ICB achieve good therapeutic effects. Immune checkpoint gene expression cannot accurately predict ICB treatment efficacy. Therefore, biomarkers capable of predicting the ICB immunotherapy response are essential (30).

In this study, we generated an immune-related prognostic model to predict the patient survival rate, which consisted of ten genes: *NR1H3*, *IL18RAP*, *CD40*, *GLRA2*, *TNFAIP2*, *C4B*, *ELSPBP1*, *IGSF9*, *HAMP*, and *GABRA5*. Some genes in the model have previously been associated with the formation and

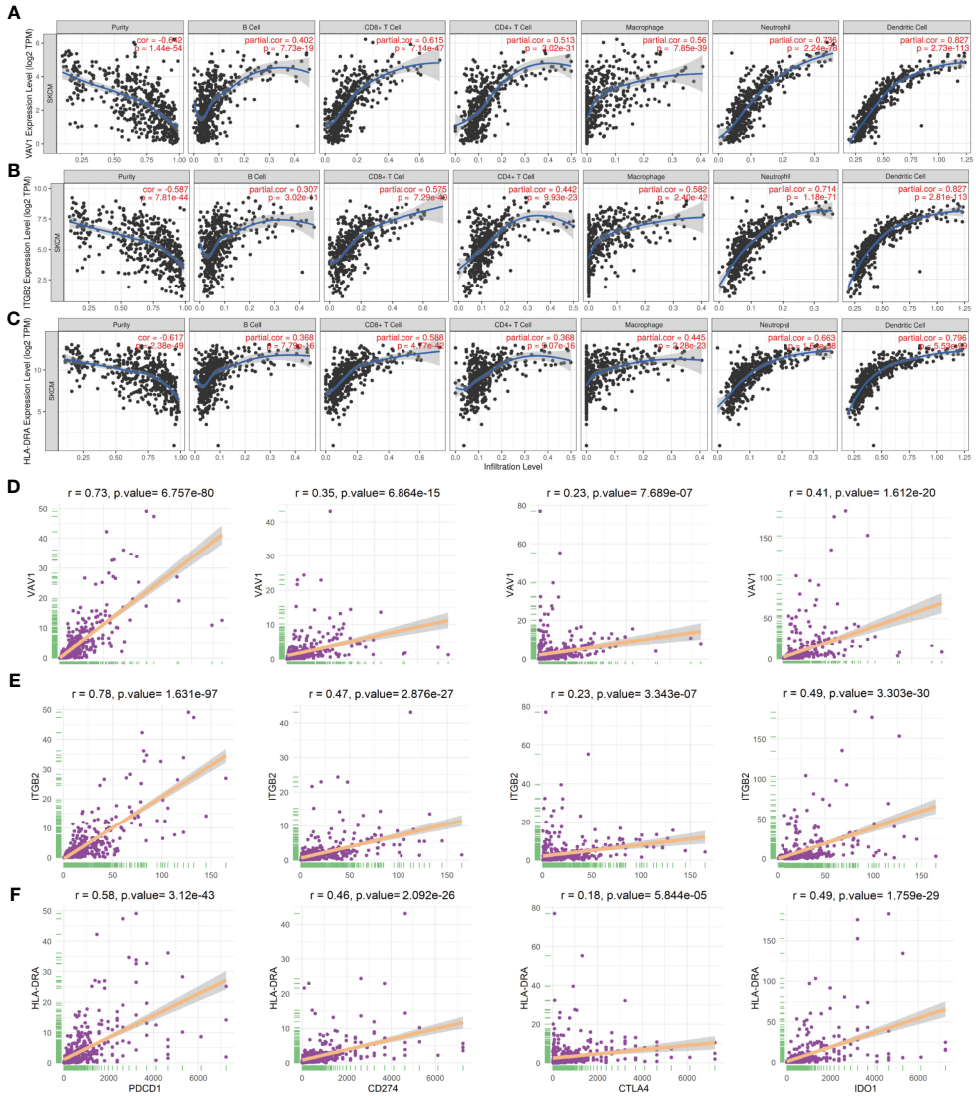

FIGURE 9 | "Real" hub genes were related to immune infiltration processes. **(A–C)** Correlation between immune cell abundance and hub gene expression. "Purity" represents the purity of the tumor cells in the sample. **(D–F)** The correlation between hub genes and the immune checkpoint inhibitor targets PD-1, PD-L1, CTLA-4, and IDO1.

regulation of the TME. For example, *NR1H3* belongs to the NR1 subfamily of nuclear receptors, which are vital regulators of macrophage function and transcription processes during inflammation (31). Related studies have demonstrated that *NR1H3* can impair the anti-tumor response by inhibiting the CCR7 expression on dendritic cells, suggesting a novel mechanism for immune escape (32). In addition, the *NR1H3*-mediated promotion of the epithelial-mesenchymal transition (EMT) and migration of tumor cells has been reported in several cancers (33, 34). *IL18RAP* also modulates the TME and impacts cancer progression through proinflammatory functions. *ILI8RAP* is an accessory subunit of the heterodimeric interleukin 18 (IL18) receptor (35). CD40 is a member of the TNF receptor superfamily (36). In mouse melanoma, tumor endothelial cells upregulate *IDO1* in response to the increased secretion of interferon (IFN)γ by CD40-stimulated immunotherapy, revealing a new immunosuppressive feedback mechanism (37). Immunotherapy success in CM depends on the activation of functional T cells in the tumor. Singh et al. showed that locally focused ultrasound (FUS) heating combined with *in situ* anti-CD40 agonist antibody improved T cells and macrophage function, promoting effective melanoma immunotherapy (38). *TNFAIP2* expression can be induced by TNFα. The abnormal expression of *TNFAIP2* has been identified in various malignant tumors, involved in unlimited proliferation, angiogenesis, and migration, including urothelial cancer, esophageal squamous cell carcinoma, and nasopharyngeal carcinoma (39–42). Although some biological functions of these ten genes have not previously

been reported in SKCM, their roles in progression and tumor immunity require further study. We indicate that the ten-gene prognosis model can be used as an indicator of the SKCM immunotherapy response.

By combining the PPI and WGCNA, three genes were verified as "real" hub genes associated with the TME in SKCM. Based on correlations between genes, we construct a WGCNA network, and a PPI network was generated based on available literature. The combination of the WGCNA and PPI methods appears to be suitable for hub gene identification. Several studies have indicated the abnormal expression of hub genes in various malignant tumors, which may represent important prognostic biomarkers. *VAV1* is a member of the *VAV* gene family and is vital for hematopoiesis, which plays an indispensable role in T cell and B cell activation (43). Related studies have indicated that IDO can inhibit the T cell response and promote immune tolerance by downregulating *VAV1* expression and inhibiting the *VAV1*/Rac cascade reaction (44). *ITGB2* encodes integrin beta chain, a cell surface protein involved in cell adhesion and cell surface-mediated signal transduction. *ITGB2* plays a significant role in the immune response, and *ITGB2* deficiency causes leukocyte adhesion defects (45, 46). A prospective study revealed that high *ITGB2* expression in cancer-associated fibroblasts promoted tumor proliferation in oral squamous cell carcinoma through NADH oxidation in the mitochondrial oxidative phosphorylation system (47). Another study showed that *ITGB2* downregulated Treg cells levels and inhibited renal carcinoma development (48). *HLA-DRA* is an HLA class II alpha chain paralog that plays a vital role in the immune system and responses by presenting peptides. *HLA-DRA* is highly expressed in bladder cancer tissues than corresponding adjacent tissues and indicates poor progression-free survival (49). In kidney renal clear cell carcinoma, *HLA-DRA* serves as a reliable biomarker and may play a vital role in cancer immunotherapy (50). A recent clinical trial showed that *HLA-DRA* predicted the advanced melanoma immune response to tremelimumab, which blocks CTLA-4 (51).

However, this study has some limitations. First, there is no detailed clinical data on the treatment of patients in TCGA and GEO databases, although other clinical factors available from the databases have been included. Second, analysis based on transcriptomics can represent only certain aspects of the immune microenvironment but not the overall process of change. In addition, further experimental studies are needed to elucidate the potential mechanism of the prognostic model and hub genes in the occurrence and development of CM.

CONCLUSION

We successfully constructed a prediction model with good accuracy. Differences in OS between high- and low-risk groups were associated with immune cell infiltration and the complex regulation of multiple signaling pathways. By combining the PPI and WGCNA network analyses, "real" hub genes closely related to the TME were identified. Our study provides additional supplementary insights for analyzing the pathogenesis and response to immunotherapy of CM.

DATA AVAILABILITY STATEMENT

Publicly available datasets were analyzed in this study. The datasets generated for this study can be found here: The Cancer Genome Atlas (TCGA) (https://portal.gdc.cancer.gov/) and Gene Expression Omnibus (GEO) datasets (https://www.ncbi.nlm.nih.gov/geo/query/acc.cgi?acc=GSE54467).

ETHICS STATEMENT

The study involving human participants was reviewed and approved by the Third Affiliated Hospital of Kunming Medical University. The patients/participants provided their written informed consent to participate in this study.

AUTHOR CONTRIBUTIONS

RQ and WP were responsible for the study design, data acquisition, and analysis and were major contributors to writing the manuscript. XW, CL, and YX helped to perform the data analysis. CS and ZZ were responsible for the integrity of the entire study and manuscript review. All authors contributed to the article and approved the submitted version.

FUNDING

This work was supported by grants from the National Natural Science Foundation of China (81560470, 81773127 and 81960543), Special Funds for Innovation Team of Basic and Clinical Research of Head and neck Tumor in Yunnan Province; Special Funds for High-Level Medical Leaders in Yunnan Province (L–2017025), and Yunnan Province Basic Research Program (2018FE001-058/246, 2019FE001-075 and 202001 AY070001-024).

ACKNOWLEDGMENTS

We thank the TCGA and GEO databases for the availability of the data.

SUPPLEMENTARY MATERIAL

The Supplementary Material for this article can be found online at: https://www.frontiersin.org/articles/10.3389/fonc.2021.615963/full#supplementary-material

REFERENCES

1. Tracey EH, Vij A. Updates in Melanoma. *Dermatologic Clinics* (2019) 37 (1):73–82. doi: 10.1016/j.det.2018.08.003
2. Schadendorf D, van Akkooi ACJ, Berking C, Griewank KG, Gutzmer R, Hauschild A, et al. Melanoma. *Lancet (London England)* (2018) 392 (10151):971–84. doi: 10.1016/s0140-6736(18)31559-9
3. Margolis N, Markovits E, Markel G. Reprogramming Lymphocytes for the Treatment of Melanoma: From Biology to Therapy. *Adv Drug Delivery Rev* (2019) 141:104–24. doi: 10.1016/j.addr.2019.06.005
4. Gajewski TF, Schreiber H, Fu YX. Innate and Adaptive Immune Cells in the Tumor Microenvironment. *Nat Immunol* (2013) 14(10):1014–22. doi: 10.1038/ni.2703
5. Fridman WH, Pagès F, Sautès-Fridman C, Galon J. The Immune Contexture in Human Tumours: Impact on Clinical Outcome. *Nat Rev Cancer* (2012) 12 (4):298–306. doi: 10.1038/nrc3245
6. Taggart D, Andreou T, Scott KJ, Williams J, Rippaus N, Brownlie RJ, et al. Anti-PD-1/Anti-CTLA-4 Efficacy in Melanoma Brain Metastases Depends on Extracranial Disease and Augmentation of CD8(+) T Cell Trafficking. *Proc Natl Acad Sci United States America* (2018) 115(7):E1540–e9. doi: 10.1073/pnas.1714089115
7. Forsthuber A, Lipp K, Andersen L, Ebersberger S, Graña C, Ellmeier W, et al. CXCL5 as Regulator of Neutrophil Function In Cutaneous Melanoma. *J Invest Dermatol* (2019) 139(1):186–94. doi: 10.1016/j.jid.2018.07.006
8. Song K, Li L, Zhang G. Bias and Correction in RNA-Seq Data for Marine Species. *Marine Biotechnol (New York NY)* (2017) 19(5):541–50. doi: 10.1007/s10126-017-9773-5
9. Yoshihara K, Shahmoradgoli M, Martínez E, Vegesna R, Kim H, Torres-Garcia W, et al. Inferring Tumour Purity and Stromal and Immune Cell Admixture From Expression Data. *Nat Commun* (2013) 4:2612. doi: 10.1038/ncomms3612
10. Harris MA, Clark J, Ireland A, Lomax J, Ashburner M, Foulger R, et al. The Gene Ontology (GO) Database and Informatics Resource. *Nucleic Acids Res* (2004) 32(Database issue):D258–61. doi: 10.1093/nar/gkh036
11. Kanehisa M, Goto S. KEGG: Kyoto Encyclopedia of Genes and Genomes. *Nucleic Acids Res* (2000) 28(1):27–30. doi: 10.1093/nar/28.1.27
12. Lunn M, McNeil D. Applying Cox Regression to Competing Risks. *Biometrics* (1995) 51(2):524–32. doi: 10.2307/2532940
13. Shahraki HR, Salehi A, Zare N. Survival Prognostic Factors of Male Breast Cancer in Southern Iran: A LASSO-Cox Regression Approach. *Asian Pac J Cancer Prev APJCP* (2015) 16(15):6773–7. doi: 10.7314/apjcp.2015.16.15.6773
14. Huang R, Liao X, Li Q. Identification and Validation of Potential Prognostic Gene Biomarkers for Predicting Survival in Patients With Acute Myeloid Leukemia. *OncoTargets Ther* (2017) 10:5243–54. doi: 10.2147/ott.S147717
15. Newman AM, Liu CL, Green MR, Gentles AJ, Feng W, Xu Y, et al. Robust Enumeration of Cell Subsets From Tissue Expression Profiles. *Nat Methods* (2015) 12(5):453–7. doi: 10.1038/nmeth.3337
16. Szklarczyk D, Gable AL, Lyon D, Junge A, Wyder S, Huerta-Cepas J, et al. STRING V11: Protein-Protein Association Networks With Increased Coverage, Supporting Functional Discovery in Genome-Wide Experimental Datasets. *Nucleic Acids Res* (2019) 47(D1):D607–d13. doi: 10.1093/nar/gky1131
17. Bader GD, Hogue CW. An Automated Method for Finding Molecular Complexes in Large Protein Interaction Networks. *BMC Bioinf* (2003) 4:2. doi: 10.1186/1471-2105-4-2
18. Botía JA, Vandrovcova J, Forabosco P, Guelfi S, D'Sa K, Hardy J, et al. An Additional K-Means Clustering Step Improves the Biological Features of WGCNA Gene Co-Expression Networks. *BMC Syst Biol* (2017) 11(1):47. doi: 10.1186/s12918-017-0420-6
19. Rahmani B, Zimmermann MT, Grill DE, Kennedy RB, Oberg AL, White BC, et al. Recursive Indirect-Paths Modularity (RIP-M) for Detecting Community Structure in RNA-Seq Co-Expression Networks. *Front Genet* (2016) 7:80. doi: 10.3389/fgene.2016.00080
20. Uhlén M, Fagerberg L, Hallström BM, Lindskog C, Oksvold P, Mardinoglu A, et al. Proteomics. Tissue-Based Map of the Human Proteome. *Sci (New York NY)* (6220) 2015) 347:1260419. doi: 10.1126/science.1260419
21. Kim JE, Patel MA, Mangraviti A, Kim ES, Theodros D, Velarde E, et al. Combination Therapy With Anti-PD-1, Anti-TIM-3, and Focal Radiation Results in Regression of Murine Gliomas. *Clin Cancer Res an Off J Am Assoc Cancer Res* (2017) 23(1):124–36. doi: 10.1158/1078-0432.Ccr-15-1535
22. Nishino M, Ramaiya NH, Hatabu H, Hodi FS. Monitoring Immune-Checkpoint Blockade: Response Evaluation and Biomarker Development. *Nat Rev Clin Oncol* (2017) 14(11):655–68. doi: 10.1038/nrclinonc.2017.88
23. Zhai L, Ladomersky E, Lenzen A, Nguyen B, Patel R, Lauing KL, et al. IDO1 in Cancer: A Gemini of Immune Checkpoints. *Cell Mol Immunol* (2018) 15 (5):447–57. doi: 10.1038/cmi.2017.143
24. Li T, Fan J, Wang B, Traugh N, Chen Q, Liu JS, et al. TIMER: A Web Server for Comprehensive Analysis of Tumor-Infiltrating Immune Cells. *Cancer Res* (2017) 77(21):e108–e10. doi: 10.1158/0008-5472.Can-17-0307
25. Goodman A, Patel SP, Kurzrock R. PD-1-PD-L1 Immune-Checkpoint Blockade in B-Cell Lymphomas. *Nat Rev Clin Oncol* (2017) 14(4):203–20. doi: 10.1038/nrclinonc.2016.168
26. Champiat S, Lambotte O, Barreau E, Belkhir R, Berdelou A, Carbonnel F, et al. Management of Immune Checkpoint Blockade Dysimmune Toxicities: A Collaborative Position Paper. *Ann Oncol Off J Eur Soc Med Oncol* (2016) 27 (4):559–74. doi: 10.1093/annonc/mdv623
27. Pelster MS, Amaria RN. Combined Targeted Therapy and Immunotherapy in Melanoma: A Review of the Impact on the Tumor Microenvironment and Outcomes of Early Clinical Trials. *Ther Adv Med Oncol* (2019) 11:1758835919830826. doi: 10.1177/1758835919830826
28. Babacan NA, Eroglu Z. Treatment Options for Advanced Melanoma After Anti-PD-1 Therapy. *Curr Oncol Rep* (2020) 22(4):38. doi: 10.1007/s11912-020-0894-z
29. Valpione S, Campana LG. Immunotherapy for Advanced Melanoma: Future Directions. *Immunotherapy* (2016) 8(2):199–209. doi: 10.2217/imt.15.111
30. Mushtaq MU, Papadas A, Pagenkopf A, Flietner E, Morrow Z, Chaudhary SG, et al. Tumor Matrix Remodeling and Novel Immunotherapies: The Promise of Matrix-Derived Immune Biomarkers. *J Immunother Cancer* (2018) 6(1):65. doi: 10.1186/s40425-018-0376-0
31. Kim HA, Baek WY, Han MH, Jung JY, Suh CH. The Liver X Receptor is Upregulated in Monocyte-Derived Macrophages and Modulates Inflammatory Cytokines Based on Lxrα Polymorphism. *Mediators Inflamm* (2019) 2019:6217548. doi: 10.1155/2019/6217548
32. Youlin K, Weiyang H, Simin L, Xin G. Prostaglandin E(2) Inhibits Prostate Cancer Progression by Countervailing Tumor Microenvironment-Induced Impairment of Dendritic Cell Migration Through Lxrα/CCR7 Pathway. *J Immunol Res* (2018) 2018:5808962. doi: 10.1155/2018/5808962
33. Wang K, Xu T, Ruan H, Xiao H, Liu J, Song Z, et al. Lxrα Promotes Cell Metastasis by Regulating the NLRP3 Inflammasome in Renal Cell Carcinoma. *Cell Death Dis* (2019) 10(3):159. doi: 10.1038/s41419-019-1345-3
34. Ji L, Zhang B, Zhao G. Liver X Receptor α (Lxrα) Promoted Invasion and EMT of Gastric Cancer Cells by Regulation of NF-κb Activity. *Hum Cell* (2017) 30(2):124–32. doi: 10.1007/s13577-016-0157-3
35. Lin GW, Xu C, Chen K, Huang HQ, Chen J, Song B, et al. Genetic Risk of Extranodal Natural Killer T-Cell Lymphoma: A Genome-Wide Association Study in Multiple Populations. *Lancet Oncol* (2020) 21(2):306–16. doi: 10.1016/s1470-2045(19)30799-5
36. Vonderheide RH. CD40 Agonist Antibodies in Cancer Immunotherapy. *Annu Rev Med* (2020) 71:47–58. doi: 10.1146/annurev-med-062518-045435
37. Georganaki M, Ramachandran M, Tuit S, Núñez NG, Karampatzakis A, Fotaki G, et al. Tumor Endothelial Cell Up-Regulation of IDO1 is an Immunosuppressive Feed-Back Mechanism That Reduces the Response to CD40-Stimulating Immunotherapy. *Oncoimmunology* (2020) 9(1):1730538. doi: 10.1080/2162402x.2020.1730538
38. Singh MP, Sethuraman SN, Ritchey J, Fiering S, Guha C, Malayer J, et al. In-Situ Vaccination Using Focused Ultrasound Heating and Anti-CD-40 Agonistic Antibody Enhances T-Cell Mediated Local and Abscopal Effects in Murine Melanoma. *Int J Hyperthermia Off J Eur Soc Hyperthermic Oncol North Am Hyperthermia Group* (2019) 36(sup1):64–73. doi: 10.1080/02656736.2019.1663280
39. Jia L, Shi Y, Wen Y, Li W, Feng J, Chen C. The Roles of TNFAIP2 in Cancers and Infectious Diseases. *J Cell Mol Med* (2018) 22(11):5188–95. doi: 10.1111/jcmm.13822
40. Niwa N, Tanaka N, Hongo H, Miyazaki Y, Takamatsu K, Mizuno R, et al. TNFAIP2 Expression Induces Epithelial-to-Mesenchymal Transition and Confers Platinum Resistance in Urothelial Cancer Cells. *Lab Invest J Tech Methods Pathol* (2019) 99(11):1702–13. doi: 10.1038/s41374-019-0285-y
41. Xie Y, Wang B. Downregulation of TNFAIP2 Suppresses Proliferation and Metastasis in Esophageal Squamous Cell Carcinoma Through Activation of

the Wnt/β-Catenin Signaling Pathway. *Oncol Rep* (2017) 37(5):2920–8. doi: 10.3892/or.2017.5557
42. Chen LC, Chen CC, Liang Y, Tsang NM, Chang YS, Hsueh C. A Novel Role for TNFAIP2: Its Correlation With Invasion and Metastasis in Nasopharyngeal Carcinoma. *Mod Pathol an Off J United States Can Acad Pathol Inc* (2011) 24(2):175–84. doi: 10.1038/modpathol.2010.193
43. Barreira M, Rodríguez-Fdez S, Bustelo XR. New Insights Into the Vav1 Activation Cycle in Lymphocytes. *Cell Signalling* (2018) 45:132–44. doi: 10.1016/j.cellsig.2018.01.026
44. Li R, Li H, Sun Q, Liu L, Zhang C, Ren X. Indoleamine 2,3-Dioxygenase Regulates T Cell Activity Through Vav1/Rac Pathway. *Mol Immunol* (2017) 81:102–7. doi: 10.1016/j.molimm.2016.11.018
45. Zhang Y, Yang X, He X, Liu H, Guo P, Liu X, et al. A Novel Mutation of the ITGB2 Gene in a Chinese Zhuang Minority Patient With Leukocyte Adhesion Deficiency Type 1 and Glucose-6-Phosphate Dehydrogenase Deficiency. *Gene* (2019) 715:144027. doi: 10.1016/j.gene.2019.144027
46. Sule G, Kelley WJ, Gockman K, Yalavarthi S, Vreede AP, Banka AL, et al. Increased Adhesive Potential of Antiphospholipid Syndrome Neutrophils Mediated by β2 Integrin Mac-1. *Arthritis Rheumatol (Hoboken NJ)* (2020) 72(1):114–24. doi: 10.1002/art.41057
47. Zhang X, Dong Y, Zhao M, Ding L, Yang X, Jing Y, et al. ITGB2-Mediated Metabolic Switch in Cafs Promotes OSCC Proliferation by Oxidation of NADH in Mitochondrial Oxidative Phosphorylation System. *Theranostics* (2020) 10(26):12044–59. doi: 10.7150/thno.47901
48. Fu JH, Zhou CC, Mu HQ, Nan CJ, Li S, Lu DQ. CD18 Inhibits Progression of Kidney Cancer by Down-Regulating Treg Cell Levels. *Eur Rev Med Pharmacol Sci* (2019) 23(7):2750–5. doi: 10.26355/eurrev_201904_17548
49. Piao XM, Kang HW, Jeong P, Byun YJ, Lee HY, Kim K, et al. A Prognostic Immune Predictor, HLA-DRA, Plays Diverse Roles in Non-Muscle Invasive and Muscle Invasive Bladder Cancer. *Urol Oncol* (2021) 39(4):237. doi: 10.1016/j.urolonc.2020.11.017
50. Chu G, Jiao W, Yang X, Liang Y, Li Z, Niu H. C3, C3AR1, HLA-DRA, and HLA-E as Potential Prognostic Biomarkers for Renal Clear Cell Carcinoma. *Trans Androl Urol* (2020) 9(6):2640–56. doi: 10.21037/tau-20-699
51. Friedlander P, Wassmann K, Christenfeld AM, Fisher D, Kyi C, Kirkwood JM, et al. Whole-Blood RNA Transcript-Based Models Can Predict Clinical Response in Two Large Independent Clinical Studies of Patients With Advanced Melanoma Treated With the Checkpoint Inhibitor, Tremelimumab. *J Immunother Cancer* (2017) 5(1):67. doi: 10.1186/s40425-017-0272-z

Conflict of Interest: The authors declare that the research was conducted in the absence of any commercial or financial relationships that could be construed as a potential conflict of interest.

frontiers in Oncology

REVIEW
published: 28 May 2021
doi: 10.3389/fonc.2021.635488

Cutaneous Melanoma Classification: The Importance of High-Throughput Genomic Technologies

Cristian Scatena[1], *Daniela Murtas*[2] *and Sara Tomei*[3]*

[1] Division of Pathology, Department of Translational Research and New Technologies in Medicine and Surgery, University of Pisa, Pisa, Italy, [2] Department of Biomedical Sciences, Section of Cytomorphology, University of Cagliari, Cagliari, Italy, [3] Omics Core, Integrated Genomics Services, Research Department, Sidra Medicine, Doha, Qatar

Cutaneous melanoma is an aggressive tumor responsible for 90% of mortality related to skin cancer. In the recent years, the discovery of driving mutations in melanoma has led to better treatment approaches. The last decade has seen a genomic revolution in the field of cancer. Such genomic revolution has led to the production of an unprecedented mole of data. High-throughput genomic technologies have facilitated the genomic, transcriptomic and epigenomic profiling of several cancers, including melanoma. Nevertheless, there are a number of newer genomic technologies that have not yet been employed in large studies. In this article we describe the current classification of cutaneous melanoma, we review the current knowledge of the main genetic alterations of cutaneous melanoma and their related impact on targeted therapies, and we describe the most recent high-throughput genomic technologies, highlighting their advantages and disadvantages. We hope that the current review will also help scientists to identify the most suitable technology to address melanoma-related relevant questions. The translation of this knowledge and all actual advancements into the clinical practice will be helpful in better defining the different molecular subsets of melanoma patients and provide new tools to address relevant questions on disease management. Genomic technologies might indeed allow to better predict the biological - and, subsequently, clinical - behavior for each subset of melanoma patients as well as to even identify all molecular changes in tumor cell populations during disease evolution toward a real achievement of a personalized medicine.

Keywords: melanoma, genomics, next-generation sequencing, DNA, mutations

OPEN ACCESS

Edited by:
Giuseppe Palmieri,
National Research Council (CNR), Italy

Reviewed by:
Panagiotis Paliogiannis,
Azienda Ospedaliero Universitaria Sassari, Italy
Camelia Quek,
Melanoma Institute Australia, Australia
Filippo Fraggetta,
Cannizzaro Hospital, Italy

***Correspondence:**
Sara Tomei
stomei@sidra.org

Specialty section:
This article was submitted to Skin Cancer, a section of the journal Frontiers in Oncology

Received: *30 November 2020*
Accepted: *30 March 2021*
Published: *28 May 2021*

Citation:
Scatena C, Murtas D and Tomei S (2021) Cutaneous Melanoma Classification: The Importance of High-Throughput Genomic Technologies. Front. Oncol. 11:635488. doi: 10.3389/fonc.2021.635488

INTRODUCTION ON CUTANEOUS MELANOMA

Cutaneous melanoma represents an aggressive tumor with a continuous increase in incidence, although mortality rates have begun to decline thanks to promising new targeted treatments (1). The incidence of cutaneous melanoma is increasing in white populations worldwide, in particular if people receive excessive sun exposure (2–4). In the United States the incidence is 20-30 cases per 100,000 inhabitants, while in Australia it is particularly high, with a rate of 50-60 cases per 100,000

inhabitants. In Europe, instead, the incidence is <10-25 cases per 100,000 inhabitants (5), but it has been predicted to increase in the next decades (6).

Factors that increase the risk for melanoma include: *i)* fair skin, that easily burns in the sun; *ii)* the presence of numerous common naevi, large congenital naevi or atypical (dysplastic) naevi, commonly genetically determined (7, 8); *iii)* exposure to UV irradiation, in particular high and intermittent sun exposure (9); *iv)* genetic susceptibility, as inherited variants of melanocortin-1 receptor (MC1R); *v)* a family history of melanoma.

As for most tumors, also cutaneous melanoma is traditionally classified into primary and metastatic; primary melanoma is further divided into: i) melanoma *in situ*, when the atypical melanocytes are limited to the epidermis; ii) invasive melanoma, if it conquers the dermis. Invasive melanoma is historically classified according to clinical and histopathological characteristics into four major histological subtypes: *i)* superficial spreading melanoma (SSM), which accounts for 41% of cases; *ii)* nodular melanoma (NM), accounting for 16% of cases; *iii)* lentigo maligna melanoma (LMM), accounting for 2.7% - 14% of cases; and *iv)* acral melanoma (AM), accounting for 1% - 5%, with acral lentiginous melanoma (ALM) that represents its most common subtype (**Figure 1**). For the latter subtype, higher rates are reported in Asian and African American population (10, 11). In details:

i. *In situ*/SSM appears as a pigmented macule with irregular contours that may progressively evolve into a papule or plaque, so far as invasion occurs; histologically, melanoma *in situ* is defined as the presence of a pagetoid spread of malignant melanocytes throughout the epidermis; instead, invasive SSM presents as a proliferation of atypical melanocytes in the superficial dermis.
ii. NM appears as an exophytic/nodular, brown-to-black, often eroded tumor, characterized by a vertical growth phase. The epidermal lateral component, when present, is observed within three rete ridges, at the maximum.
iii. LMM represents the invasive progression of melanoma *in situ*/lentigo maligna and is mainly located on the sun damaged surfaces, as the face of elderly people (12). Histologically, lentigo maligna is described as a lentiginous proliferation of atypical spindle melanocytes along the base of the epidermis, without invading the dermis; instead, LMM has at least single cell infiltration into the papillary dermis. Actinic damage and dermal elastosis are typically present in the surrounding skin.
iv. To conclude, AM is a slow-growing macule/plaque or nodule localized on the extremities (subungual or palmoplantar/volar skin) with poorly circumscribed pigmentation. The most frequent histological subtype is ALM, followed by NM and SSM. A proliferation of atypical spindle (often pigmented) melanocytes at the base of the epidermis constitutes ALM. Rarely AM manifests as a large amelanotic nodule that easily can be misdiagnosed as a benign condition.

Rare histological subtypes of cutaneous melanoma are: *v)* desmoplastic melanoma (DM) (1% - 4% of cases) (13); and *vi)* amelanotic melanoma (14).

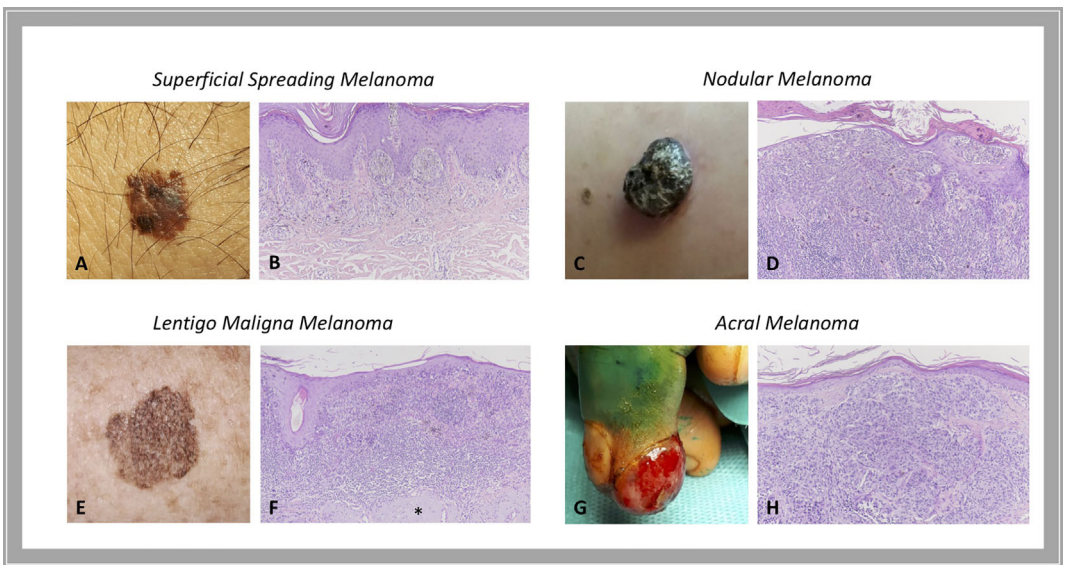

FIGURE 1 | Histological subtypes of melanoma: clinical-pathological correlations. Superficial spreading melanoma is a pigmented macule with irregular contours **(A)** that, when invasion occurs, presents as a proliferation of atypical melanocytes in the papillary dermis **(B)**. Nodular melanoma is a brown-to-black exophytic tumor **(C)** characterized by a predominant vertical growth phase, with pigmented epithelioid or spindle atypical melanocytes that invade the reticular dermis **(D)**. Lentigo maligna melanoma presents as a large, pigmented macule with irregular contours on sun damaged skin **(E)** that is described histologically as a lentiginous proliferation of atypical spindle melanocytes at the dermo-epidermal junction with invasion into the papillary dermis; actinic damage and dermal elastosis (*) are typically present in the surrounding skin **(F)**. Acral melanoma may be an amelanotic nodule localized on the extremities **(G)** characterized by a proliferation of atypical, not pigmented, spindle melanocytes throughout the dermis **(H)**. Courtesy of Dermatology Unit, Department of Clinical and Experimental Medicine, University of Pisa.

Curiously, in the current staging system for cutaneous melanoma (American Joint Committee on Cancer – AJCC, 8th edition, 2017) histological subtypes are not mentioned as prognostic factors (15). Instead, important markers of worse prognosis include: i) vertical tumor thickness (Breslow's depth); ii) ulceration; iii) number of mitosis/mm^2 (no longer used for sub-classification); iv) deepness of invasion (Clark's level); v) tumor infiltrating lymphocytes (TILs); vi) lymphovascular invasion; and vii) neurotropism. Also, older age, the male sex and the localization to head and neck or trunk are associated to a poorer outcome (16, 17). However, the identification of genetic alterations in specific subtypes of cutaneous melanoma has made histological classification regain prominence (18). Indeed, in the latest WHO classification of skin tumors (4th edition, 2018), melanoma is classified according to the association with sun-exposure and genomic features. Melanomas that arise in sun-exposed skin include: i) melanoma in skin with a low degree of cumulative sun damage (low-CSD melanoma), mostly SSM; ii) melanoma in chronically sun-exposed skin, mostly LMM and desmoplastic melanoma. NM may belong to both categories. Instead, Spitz melanoma, melanoma developed in congenital or blue naevus, acral melanoma, melanoma arising in blue naevus, mucosal melanoma (oral, genital or sinonasal), uveal melanoma, nevoid and some nodular melanomas arise in sun-sheltered sites (11).

Instead, metastatic melanoma is defined as a melanoma that has spread to other sites of the body. Melanoma may metastasize locally through the lymphatic system (as satellite, in-transit, or regional nodal metastases) or systemically through the hematic route to distant skin/subcutaneous tissue or lymph nodes, lung, liver or brain (19).

CURRENT KNOWLEDGE OF GENETIC ALTERATIONS IN CUTANEOUS MELANOMA

The initiation and progression of cutaneous melanoma are finely driven by specific genomic alterations (20, 21). Although hundreds of genes can be found mutated in a single case of cutaneous melanoma, only some mutations are true "drivers" of the tumor, either as gain-of-function (GOF)/activating or loss-of-function (LOF)/deleterious mutations. Melanoma may display mutations in known oncogenes that then result overactive in melanoma cells, granting uncontrolled tumor growth. Mutations may also occur in tumor suppressor genes that control cell growth; when mutated, those genes lose their function. Their inactivation may thus result in the activation of downstream growth pathways, allowing unchecked tumor growth (22–24).

In the last decades, the driving alterations leading to cutaneous melanoma have been largely catalogued, comprising both activating and deleterious mutations, and including single nucleotide variants (SNVs, somatic and germline mutations) and copy number variations (CNVs). Somatic mutations are genetic alterations occurring in single cells of somatic tissues. When mutated, such cells undergo uncontrolled division and can be causative of melanoma. Germline mutations are less common and occur within melanoma-predisposing genes in the germ line, thus they can be passed on from one generation to the next, leading to the so-called hereditary or familial melanomas (25).

The current knowledge on genetic alterations is catalogued and continuously updated in databases such as The Skin Cutaneous Melanoma catalogue in The Cancer Genome Atlas (TCGA), Pan-Cancer Atlas data set (available at: https://cancergenome.nih.gov), the cBioPortal for Cancer Genomics (available at: www.cbioportal.org), OncoKB, ClinVar, "1000 Genomes" project, and Cancer Hotspots (available at: www.cancerhotspots.org) (26, 27), as described later in this review.

Activating mutations occur in oncogenes. The two most frequent alterations, commonly mutually exclusive both in cell lines and tumors, have been described in the kinase domain of B-Raf Proto-Oncogene, Serine/Threonine Kinase (*BRAF*), encoded by exons 11 and 15, and in exons 2, 3 and 4 of Neuroblastoma RAS Viral Oncogene Homolog *(NRAS)* gene, with a frequency of 50-70% and 15-30%, respectively (20, 21, 27–31).

BRAF encodes for a serine/threonine protein kinase of the Rapidly Accelerated Fibrosarcoma (RAF) family, which transfers growth signals to the cells, playing a pivotal role in activating the mitogen-activated protein kinase/extracellular signal-regulated kinase (MAPK/ERK) signaling pathway and influencing cell cycle, differentiation, and apoptosis. More than 90% of *BRAF* gene mutations occur at codon 600 of exon 15, within the activation segment of the kinase, by substitution of a single nucleotide (GTG to GAG), which results in a single amino acid substitution from valine (V) to glutamic acid (E) (BRAF-V600E). The BRAF^{V600E} mutation has been described to confer a 400-fold increased activity to the protein (20, 31). Another prevalent *BRAF* mutation at the same residue, accounting for 10-30% of all BRAF^{V600}-mutated melanomas, is V600K mutation (BRAF-V600K) in which the valine residue (V) is replaced by a lysine (K) through a two nucleotides substitution (GTG to AAG) (32). A small proportion, about 1-5% of melanoma patients, harbor mutations at codon K601 in exon 15 of the *BRAF* gene (BRAF-K601E), the third most common type of *BRAF* mutation, resulting in a single amino acid change from lysine (K) to glutamic acid (E) (33–35). *BRAF* mutation and expression have also been shown to affect the immunological phenotype of melanoma. By functional interpretation analysis of 6296 genes differentially expressed between BRAF-mutant samples with high or low BRAF mRNA expression, Interleukin 2 (IL-2) and Janus Kinase/Signal Transducers and Activators of Transcription (JAK/STAT) signaling emerged among the deregulated pathways, supporting the immunoregulatory role of BRAF in melanoma (21).

NRAS oncogene is a member of the superfamily of p21 GTPases, which have intrinsic GTPase activity, playing as a molecular switch for the transmission of regulatory cell signals. These proteins participate in the activation of the MAPK/Phosphoinositide-3-Kinase (MAPK/PI3K) pathway, during cell proliferation, differentiation, and survival.

Although *NRAS* mutations associated with malignant transformation have been predominantly detected in codons 12, 13 (exon 2), and 61 (exon 3), the most common *NRAS* gene mutation in cutaneous melanoma occurs at position 61, where glutamine (Q) is substituted by arginine (R), lysine (K), or leucine (L) (NRAS-Q61R/K/L). *NRAS* mutations lead to the reduction of the intrinsic GTPase activity of NRAS and its constitutive activation, with consequent growth factor-independent melanocyte proliferation and ultimately melanomagenesis (20, 30, 31, 36).

Additionally, high-frequency activating mutations have been identified in Ras-related C3 Botulinum Toxin Substrate 1 (*RAC1*), Mast/Stem Cell Growth Factor Receptor Kit (*KIT*), Telomerase Reverse Transcriptase (*TERT*) promoter region (*TERT*prom), Mitogen-Activated Protein Kinase Kinase 1 and 2 (*MAP2K1* and *MAP2K2*), G Protein Subunit Alpha Q (*GNAQ*), G-Protein Subunit α11 (*GNA11*), Isocitrate Dehydrogenase 1 (*IDH1*), Erb-b2 Receptor Tyrosine Kinase 2/4 (ERBB2/4), Kirsten Rat Sarcoma Viral Oncogene Homolog, GTPase (*KRAS*), and Splicing Factor 3b Subunit 1 (*SF3B1*) genes (24, 27, 37–42).

A recurrent activating mutation in *RAC1*, a RAS-related member of the Rho GTPases subfamily, has been identified in 9.2% of sun-exposed melanomas. This C>T transition (CCT to TCT) results in a proline (P) to serine (S) amino acid substitution and it has been described as consistent with a molecular signature associated with UV radiation damage. The RAC1 P29S mutation is more frequent in melanomas BRAF and NRAS wild-type and occurs early in tumorigenesis. Activated mutant RAC1 shows enhanced binding activity towards RAC1 downstream effectors and its expression leads to increased melanocyte proliferation, altered cell migration, and activated MAPK signaling (38, 43, 44).

The tyrosine-protein kinase Kit acts as a cell surface receptor regulating proliferation and survival, by activating the MAPK, PI3K, and JAK/STAT pathways. *KIT* (C-KIT/CD117) gene mutations show heterogeneous distribution through the gene and they have been detected in hot-spots at exon 9 (c459/465/471/483), 11 (c551/559/576), 13 (c642), and 17 (c816), accounting for 5-15% of mutations of diagnosed melanomas. In light of the relatively high mutation rate of *KIT* in cutaneous melanoma and since *BRAF*, *KIT*, and *NRAS* mutations appear to be mutually exclusive, the screening of *KIT* mutations, at least in exons 9/11/13, is suggested in BRAF/NRAS double-wild-type melanoma patients (31, 34, 45, 46).

The *TERT* gene encodes the catalytic subunit of telomerase, responsible for the maintenance of chromosomal telomere length, thus sustaining cell survival. Mutations in the *TERT*prom lead to a 2-fold to 4-fold increase in the transcription of *TERT*, along with enhanced telomerase activity, and are often found in $BRAF^{V600}$ and NRAS-mutant melanomas, where the combined alterations cooperate in boosting cancer progression and aggressiveness. The two most recurrent, mutually exclusive, *TERT*prom mutations are cysteine (C) to threonine (T) mutations located at position 228 (C228T) and 250 (C250T) (34, 37, 47).

Deleterious mutations in tumor suppressor genes most frequently affect Neurofibromin 1 (*NF1*), Phosphatase and Tensin Homolog (*PTEN*), Tumor Protein 53 *(TP53)*, RAS P21 Protein Activator 2 (*RASA2)*, Protein Phosphatase 6 Catalytic Subunit (*PPP6C*), and genes encoding SWItch/Sucrose Non-Fermentable (SWI/SNF) subunits, most commonly AT-Rich Interaction Domain 2 (*ARID2*) (23, 27, 48).

NF1 is a tumor suppressor protein that plays a pivotal role in the control of cell growth by negatively regulating Rat Sarcoma (RAS) proteins. The GTPase-activating protein (GAP)-related domain of NF1 is known to convert the active RAS-guanosine triphosphate (RAS-GTP) to the inactive RAS-guanosine diphosphate (RAS-GDP), thereby inhibiting downstream RAS signaling (49). The *NF1* gene is mutated in 10–15% of melanoma cases. By large-scale targeted sequencing, whole-exome sequencing (WES), and whole-genome sequencing (WGS), *NF1* has been established as one of the key drivers of melanoma. Most *NF1* mutations cause a loss-of-function of this tumor suppressor gene, with about 80% of patients having a nonsense mutation, an insertion, or a deletion that leads to a truncated protein. *NF1* loss−of−function induces the hyperactivation of NRAS protein and thus, the activation of MAPK and PI3K signaling pathways (50). These *NF1* mutations are more common in melanomas occurring on chronically sun-exposed skin or in older patients, in melanomas with higher mutation burden, wild-type for *BRAF* and *NRAS*, and in the desmoplastic melanoma subtype (28, 49, 51).

PTEN is a well characterized tumor suppressor gene that encodes for the PTEN protein, a key negative regulator of the PI3K signaling pathway and an effector of apoptosis through Protein Kinase B/AKT Serine/Threonine Kinase (PKB/AKT). Somatic *PTEN* alterations have been identified in 14% of cases in the TCGA melanoma cohort, comprising both mutations and focal deletions. *PTEN* mutations frequently coexist with *BRAF* mutations, but not with *NRAS* ones. Reportedly, *PTEN* loss in melanoma is a frequent event, occurring in about 30% of primary tumors, with an even higher frequency in melanoma cell lines (47, 52). The loss of functional PTEN leads to reduced apoptosis along with increased mitogen signaling and cell survival, thus promoting tumor progression (53). Moreover, PTEN loss can influence the immune microenvironment in terms of a poor T- and B-cell tumor infiltration, sustaining immune evasion (54). T cell-based immunotherapy approaches have shown promising results in melanoma (55, 56). Yet, some patients do not respond to these therapeutic approaches. The loss of PTEN has been reported to be a molecular determinant that might explain immune resistance due to its inhibition of the T cell trafficking into tumors (57).

The *TP53* gene is considered the "guardian of the genome" due to its pleiotropic function in protecting cells from genotoxic damages, acting as tumor suppressor and transcriptional activator/repressor of several downstream genes controlling cell-cycle progression, DNA repair, and also triggering apoptosis (58, 59). *TP53* mutations have been reported in about 15% of TCGA cases, they are mostly ultraviolet (UV)

radiation-induced, and lead to tumor initiation and progression. In melanoma, p53 wild-type form may get inactivated by a variety of mechanisms, including inactivation of p14 which in turn causes overexpression of the Mouse Double Minute 2 (*MDM2)* proto-oncogene (48, 60). *TP53* is mutated in melanomas harboring any of the major subsets of *BRAF*, *NRAS*, or *NF1* mutations. Conversely, in triple-wild-type tumors, there is a prevalent amplification of *MDM2*, a key regulator of p53 protein that ubiquitinates p53, leading to its degradation (50). Loss-of-function of mutated *TP53* causes a critical dysregulation of diverse apoptotic pathways, supervised by p53, including Caspase3, Fas Cell Surface Death Receptor (FAS), and cytotoxic T-cell (CTL)-mediated apoptosis. Moreover, inactivity of mutant *TP53* decreases the surface level of the major histocompatibility complex (MHC)-peptide complex, resulting in downregulated immune surveillance (61). **Figure 2** illustrates the main molecular pathways involved in melanomagenesis.

Specific classes of cutaneous melanoma have been associated to specific genetic alterations. In particular: i) low-CSD melanoma (located on the trunk or extremities and belonging to the superficial spreading or nodular histological subtypes) carries *BRAF* mutations; ii) melanoma in chronically sun-exposed skin (located in the head and neck region) carries *NRAS* and/or other *RAS* mutations; iii) non sun-related melanomas (located on acral sites or mucosae) carry *C-KIT* mutations or amplifications (62).

Moreover, *BRAF*-mutated melanomas are more common in younger patients (63) whereas NRAS mutations are encountered in older patients and in the nodular histological subtype (64). On the other hand, most AM do not display mutations in *BRAF* or *NRAS* but bear *C-KIT* alterations (SNVs or amplifications) in 3-36% of cases (65) (**Figure 3**).

The genomic profiling of cutaneous melanoma represents a great tool to improve the management of patients with such an aggressive disease since it carries the potential to increase prognostic accuracy and to promote the development and optimize the use of molecular targeted therapies (66). The identification of genomic alterations through genomic analysis (such as DNA sequencing) is expected to promote the tuning of novel, fast and easy-to-use tests for patients' stratifications (67).

About 90% of melanomas are primary tumors without metastatic dissemination. For such diseases the tumor-specific 10-year-survival is about 75-95%. Interestingly, the relationship between survival and tumor driven mutational status has been extensively investigated: *BRAF*-mutated melanoma has been associated with a shorter survival in patients with both metastatic (68, 69) and early-stage disease (70, 71); moreover, for patients with metastatic *BRAF*-mutated melanoma receiving BRAF inhibitors, a worse prognosis has been also associated with alterations in the thrombophilic status, such as high D-dimer levels at baseline (72, 73). *NRAS* mutations did not display any effect on the survival if measured in the primary tumor (74, 75); instead, if measured in the metastases, *NRAS* mutations were associated with improved survival (76, 77). On the other hand, in *NRAS*-mutated melanoma data on survival result conflicting: some studies report no difference in patients' survival (74, 75), whereas in one study *NRAS* mutations were associated with improved survival in metastatic disease (78, 79).

According to the TCGA Pan-Cancer Atlas data set, 65% of melanomas that have *BRAF*, *NRAS*, *NF1*, or *KIT* as driver mutation co-occur with mutations in at least one other

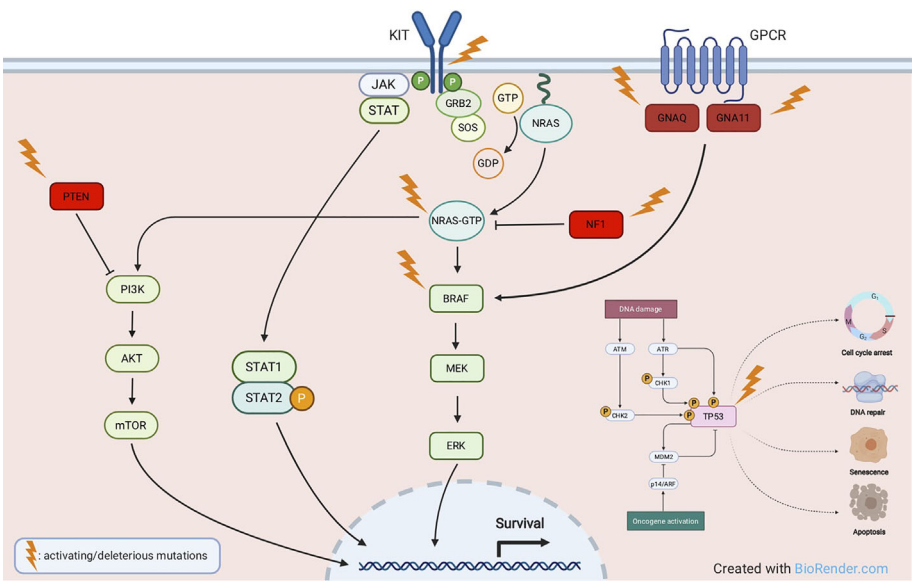

FIGURE 2 | Main molecular pathways involved in melanomagenesis. Activating mutations are commonly detected in oncogenes like *KIT, NRAS, BRAF, GNAQ, GNA11*, whereas deleterious mutations most frequently affect tumor suppressor genes like *NF1, PTEN* and *TP53*.

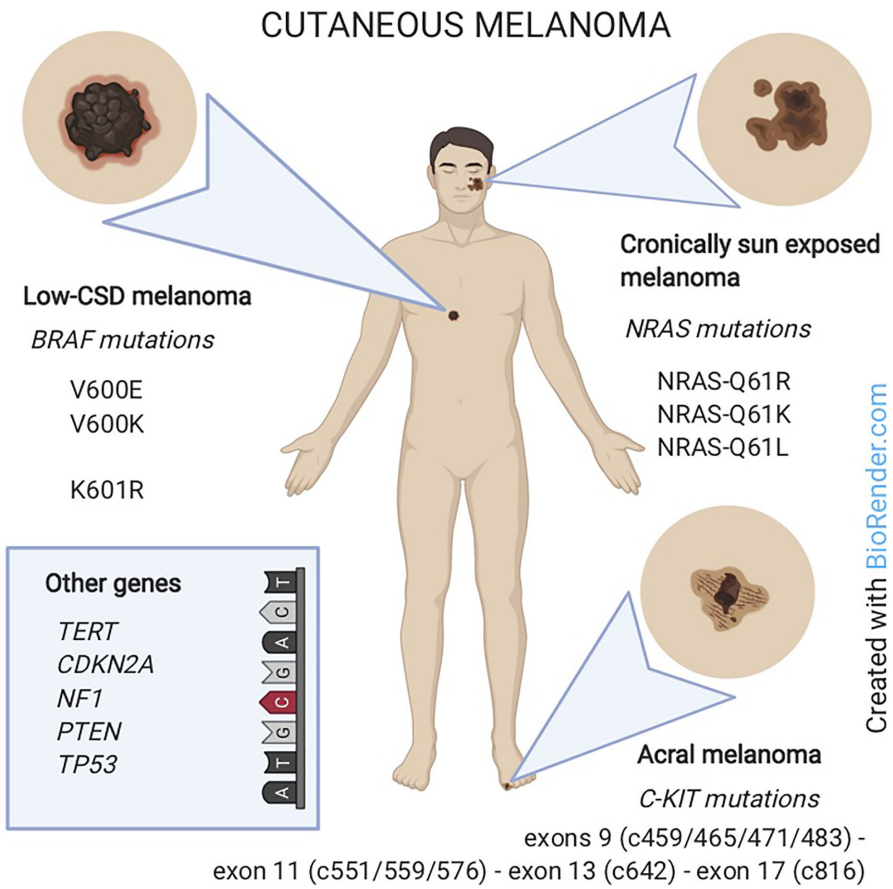

FIGURE 3 | Melanoma classification according to the association with sun-exposure and genomic features. Low-CSD melanoma (mainly on the trunk) carries *BRAF* mutations. Melanoma in chronically sun-exposed skin (in the head and neck region) carries *NRAS* mutations. Non-sun-related melanomas (on acral sites) carry C-KIT mutations. In rare cases, other genes as *TERT*, *CDKN2A*, *NF1*, *PTEN* or *TP53* are involved.

pathway, most frequently affecting *PTEN*, Cyclin-Dependent Kinase Inhibitor 2A (*CDKN2A*), and *TP53* (27, 50).

Regarding somatic CNVs assessment, deletions have been identified most frequently in the tumor suppressors PTEN, *PPP6C*, and *CDKN2A* genes, while amplifications occur repeatedly in *KIT*, Epidermal Growth Factor Receptor *(EGFR)*, and Cyclin-Dependent Kinase 4 (*CDK4*) oncogenes. CNVs influence particularly the CDK4 pathway, as also suggested by the fact that *CDKN2A* deletion or *CDK4* amplification result in CDK4 pathway activation. This pathway results altered in more than 40% of metastatic melanoma patients, including the majority of those with *NRAS*-mutant tumors (27). In a recent study, Melanocyte Inducing Transcription Factor (*MITF*) and *EGFR* genes have shown the highest frequency of genomic amplification, with a lower rate in primary melanomas as compared to metastatic melanomas, considering both tumor tissues and cell lines (80).

The diagnosis of primary melanoma is not always straightforward, especially when histologic features of the lesion overlap with those of various precursor lesions. Moreover, occasionally, melanomas can either lose their antigenicity to melanocytic markers or even show aberrant expression of non-melanocytic markers. The diagnostic uncertainty can thus lead to significant therapeutic implications (81). For this reason, the mutational testing could contribute to a more accurate diagnosis (82, 83).

Large-scale sequencing projects cataloguing mutations in cutaneous melanoma have been carried out mostly on advanced melanomas, overlooking the time of occurrence of genetic changes during tumor progression. Cutaneous melanomas often arise from distinctive precursor lesions such as melanocytic naevi, intermediate lesions, or melanoma *in situ*. By next generation sequencing (NGS) and targeted sequencing techniques, with a panel of cancer-relevant genes, Shain et al. (84) have recently proposed an "evolution/progression model" uncovering the sequence of pathogenic mutations occurring from precursor to malignant melanocytic lesions, trying to define a genetic signature for each stage of the neoplastic progression. As melanoma progresses, the pattern of genetic changes leads to genetically distinct subpopulations, that account for tumor heterogeneity.

Early lesions show the $BRAF^{V600E}$ mutation as the only apparent pathogenic mutation, implying that $BRAF^{V600E}$ may

occur early in naevi as a putative driving alteration. Lesions classified as intermediate by histopathological characteristics and melanomas *in situ* harbor a broader spectrum of oncogenic alterations, including $BRAF^{V600K}$ or $BRAF^{K601E}$, *NRAS*, *GNAQ* or *GNA11*, and *TERT*prom mutations, showing genetic differences between benign and malignant neoplasms. Copy-number alterations are common in descendant neoplasms. Loss of *CDKN2A*, as well as mutations in *ARID2* gene, emerge exclusively in invasive melanomas. Finally, *PTEN* and *TP53* alterations increase exclusively in advanced melanomas, implying that these mutations may occur later and contribute significantly to tumor progression. It seems thus clear that the tumor mutation burden increases from benign through intermediate lesions to melanoma (84).

Among melanocytic diseases, Spitz tumors include Spitz nevus, atypical Spitz tumor (AST) and Spitz melanoma (or Malignant Spitz Tumor, MST), a challenging diagnostic group. The genetic characterization of these lesions and the identification of novel molecular markers are useful to improve the differential diagnosis of such diseases, the prediction of their biological behavior, and the achievement of efficient personalized treatments. The mutations driving the growth of benign Spitz naevi, considered initiating alterations, include Harvey Rat Sarcoma Viral Oncogene Homolog (*HRAS)* mutations, most frequently Q61K/R in exon 3, $BRAF^{V600E}$, as well as larger genomic rearrangements involving the Anaplastic Lymphoma Receptor Tyrosine Kinase (*ALK*), Neurotrophic Receptor Tyrosine Kinase 1 (*NTRK1*), Ret Proto-Oncogene (*RET*), ROS Proto-Oncogene 1, Receptor Tyrosine Kinase (*ROS1*), Met receptor tyrosine kinases (*MET RTK*s), and *BRAF* genes. The pathogenesis of AST mostly derives from mutations leading to *CDKN2A* and *TP53* loss-of-function. Further genomic alterations, most frequently occurring within *PTEN* and *ARID2A* genes, as well as in the *TERT* promoter region, result in disease progression towards high-grade malignant Spitz melanoma (85, 86). A summary of the main genetic alterations in melanoma is provided in **Table 1**.

In addition to genetic variations, increasing evidence supports the involvement of epigenetic modifications, such as gene silencing by non-coding RNAs, in melanoma pathogenesis. Up- and down-regulation of microRNAs (miRNAs) can modulate the expression of target genes governing key signaling pathways responsible for melanoma progression (48, 87, 88).

Although there is still limited data on miRNA expression profiles in melanoma, techniques such as quantitative *in situ* hybridization (qISH) for fluorescent detection of candidate miRNAs, qRT-PCR, *SplintR-qPCR*, and miRNA microarray, have been employed to uncover differential miRNA expression levels in melanomas, in comparison to normal melanocytes and benign melanocytic lesions, as well as between primary and metastatic melanomas (89–91).

The deregulated expression of miRNAs leads to dysregulation of key signaling pathways controlling tumor cell proliferation, cell-to-cell interactions, epithelial-to-mesenchymal transition (EMT) (89, 92, 93), stemness potential (88, 92), as well as senescence (59) and programmed cell death (87, 94), influencing the progression and metastatic process of melanoma. Tumor-suppressor miRNAs, including let-7a/b, miR-23b, -34a/b/c, -132, -137, -191, -192, -194, -200c, -205, -211, -375, -455, -602, -454-3p, -509, and -582, are under-expressed in tumor tissues and melanoma cell lines, while oncogenic miRNAs (oncomiRs) result over-expressed and include miR-10b, -17, -19, -21, -107, -126, -146a, -155, -193b, -214, -221/222, -365, -373, -506–514 cluster, -520c, and -801 (59, 88, 89, 92, 95–97). In primary melanomas, the downregulated expression of several miRNAs, such as miR-125b, -182, -200c, -203, -205, and -211 has been shown, along with increased levels of miR-10b, -221/222 (90, 91). In metastatic specimens, a miRNA expression profile has been proposed consisting of miR-145, -150, -155, -342-3p, -455-3p, and -497, considered predictors of post-recurrence survival (59). The analysis of miRNA expression profile from melanoma lymph node metastases has identified a unique signature consisting of the downregulation of miR-191, combined with the upregulation of miR-193a/b, -338, -365, and let-7, those being predictors of short-term survival in melanoma patients (59).

Melanospheres express high levels of miR-10b, -21, -182-5p, -191-5p, -373, -378d, -520c, -542-3p, -1301, -1915-3p, -3934, -4767, which feasibly control their stemness and metastatic potential (88, 92, 98).

Frequent dysregulation of miRNA expression has been reported in association with the mutational status. Bandarchi and colleagues (96) found that a low expression of miR-193a, -338, and -565 was associated with *BRAF* missense mutations, while a low expression of miR-663 was associated with *NRAS* mutations. However, they did not observe any specific differentially expressed miRNAs between *BRAF*- and *NRAS*-mutated melanomas. Oncogenic BRAF/mitogen-activated protein kinase kinases (MKK)/ERK signaling in melanoma cells modulates a network of miRNAs, by means of downregulation (let-7i, miR-22, -34a/b, -125a, -132, -211) or upregulation (miR-17-5p, -20a, -92b, -106a/b, -221/222) of miRNA expression (99).

High *KIT* gene expression in $BRAF^{V600K}$-mutated melanomas has been reported, concurrent with the significant downregulation of KIT-targeting miRNAs, including miR-222. This suggests that *KIT* and miR-222 might cooperate, by growth and pro-survival signals, toward clinical aggressiveness (32).

MITF expression seems to be regulated by miR-26a, -101, -137, -148, -182, -211, -218, -340, and -542-3p. On the other hand, *MITF* transcription factor/oncoprotein modulates miR-146a, -221/222 cluster, and -363 expression levels (59, 100).

FAMILIAL CUTANEOUS MELANOMA

The susceptibility to melanoma is commonly observed in people carrying common variants in lower risk susceptibility genes; however, 5-10% of cases develop in melanoma-prone families, with at least two cases in the same family (101), probably carrying mutations in high penetrance susceptibility

TABLE 1 | Summary of the main molecular alterations in cutaneous melanoma described in this review.

Main Alterations	Locus	Mutation	Frequency (%)	Pathway	Function
SOMATIC ACTIVATING MUTATIONS					
BRAF	7q34	V600E; V600K; K601E	50-70	MAPK signaling	Cell proliferation and survival
NRAS	1p13.2	Q61R/K/L	15-30	MAPK/PI3K signaling	Cell proliferation, differentiation and survival
RAC1	7p22.1	P29S	~9	MAPK signaling	Cell proliferation and migration
KIT	4q12	L576P; K642E	5-15	MAPK/PI3K and JAK/STAT signaling	Cell proliferation and survival
TERTprom	5p15.33	C228T; C250T	14	Telomerase activity	Cell survival
MAP2K1/MAP2K2	15q22.31/ 19p13.3	E203K/E207K	~8	MAPK signaling	Cell proliferation
GNAQ/11	9q21.2/ 9P13.3	Q209L	rare	MAPK signaling	Cell proliferation
IDH1	2q33.3	R132C/S	~5	Metabolism of isocitrate	Cell proliferation and impaired differentiation
ERBB2/4	17q21/2q34	L755C; L755S; V777L; P780S; L785F; S341L, R393W	1/19	Tyrosine kinases signaling	Cell proliferation and survival
KRAS	12p12.1	G12V; G12D	~2	GTPase activity	Cell proliferation and survival
SF3B1	2q33.1	R625C; R625H	33	Alternative splicing	Tumorigenesis
SOMATIC LOSS-OF-FUNCTION MUTATIONS					
NF1	17q11.2	C1318T; C3049T; G3497A; C3826T; A4256G; A4267G; C5242T; C5260T; C5380T; T5795C; C5839T (chromosomal aberrations, deletions, insertions, duplications)	10-15	MAPK/PI3K signaling	Cell proliferation, differentiation and survival
PTEN	10q23	A499G; C112T; T416G; G380A; T1032G (deletions, insertions)	14	PI3K signaling	Apoptosis, cell survival and immune evasion
TP53	17p13.1	Several UV-induced	15	Caspase3, FAS and CTL mediated apoptotic pathways	Cell-cycle progression, DNA repair and apoptosis
RASA2	3q23	R310*; S400F	~5	RAS signaling	Cell proliferation and migration
GERMLINE LOSS-OF-FUNCTION MUTATIONS					
CDKN2A	9p21	G101W; E69G	20-40	RB pathway	Apoptosis and cell survival
CDK4	12q14.1	R24H; R24C	NA	G1/S phase cell cycle checkpoint	Cell-cycle progression

**mutation introducing a codon stop that gives rise to a truncated protein.*

genes (102, 103). From an epidemiological perspective, familial melanoma differs from sporadic melanoma for:

i. an **earlier age** at diagnosis (104–107)

ii. a greater proportion of **sunburns**. We could hypothesize that familial cases may have an intrinsic cutaneous reactivity, deriving from some genetic characteristics, such as MC1R or DNA repair capacity (108, 109). However, the high number

of sunburns in familial cases demonstrates the absence of carefulness towards the primary prevention

iii. a higher **number of naevi**, 'great naevi' in particular or atypical naevi, especially if on the trunk or the lower limb (110–113). We may hypothesize that the higher number of great or atypical melanocytic naevi depends on sunburns or that it is an independent factor due to genetic pressure, i.e. *CDKN2A* mutation or polymorphisms on chromosome 9 and 22 (114)

iv. a **more frequent** association of **melanoma on naevus**. Melanomas arise from pre-existent naevi in about 20–30% cases (115). This finding may be the consequence of the presence of a higher number of melanocytic naevi and sunburns in the familial melanoma group, as previously hypothesized

v. a greater proportion of multiple primary melanomas (MPMs), in a synchronous or metachronous manner (116)

On the other hand, familial melanoma does not differ from sporadic melanoma with regard to the main histopathological prognostic factors such as Clark's level and Breslow's thickness (110). Moreover, in the familial melanomas the diagnostic anticipation is believed to be genetic in nature and not to be due to a better or frequent skin self/medical examination (attributable to increased awareness of the risk). Indeed, *CDKN2A* mutation may represent a biological pressure responsible for the earlier onset of the disease. In particular, germline mutations convey pro-tumorigenic features and often affect the high-risk susceptibility genes *CDKN2A* and, less commonly, *CDK4*, associated with familial melanoma, where the phenotype of *CDKN2A* or *CDK4*-mutated families is indistinguishable (27, 80, 117).

The *CDKN2A* gene is the major high-penetrance familial melanoma predisposition gene, with germline mutations identified in 20%-40% of melanoma families (118). Similarly, *CDKN2A* mutations have been reported associated to MPMs in Italian patients, being more frequent in MPM cases with a positive family history (119).

The tumor suppressor *CDKN2A* is located at the 9p21 locus and encodes 2 different proteins, p16INK4A (p16) and p14ARF (p14), which promote the cell cycle arrest in G1 phase by inhibiting RB protein phosphorylation through CDK4 and act through the p53 pathway inducing cell cycle arrest or favoring apoptosis, respectively (118, 120, 121). Mutations in *CDKN2A* produce an imbalance between functional p16 and Cyclin D1, causing abnormal cell growth. Several recurrent mutations in *CDKN2A* have been described as founder mutations. As an example, glycine (G) to tryptophan (W) mutation at codon 101 (G101W) is considered highly oncogenic since it leads to an impaired interaction with Cyclin Dependent Kinase 4/6 (CDK4/CDK6). Also, the glutamic acid (E) to glycine (G) mutation at codon 69 (E69G) has been reported to be deleterious (27). Variants in *CDKN2A* and other intronic mutations have also been described to predispose to melanoma (122).

The *CDK4* oncogene is the second identified high-penetrance familial melanoma predisposition gene, playing a pivotal role in the G1/S phase cell cycle checkpoint. *CDK4* pathogenetic mutations often arise in codon 24 of exon 2, a critical site for the tumor suppressor protein p16 binding. When *CDK4* is mutated, p16 cannot inhibit the CDK4 kinase activity, resulting in increased phosphorylation of the Retinoblastoma Protein (RB) bound to members of the E2F family of transcription factors, with consequent increased E2F release. E2F activates the transcription of pro-S phase cell cycle genes, promoting G1/S phase transition (118).

In families without mutations in *CDKN2A* and *CDK4* genes, the use of NGS methodologies has allowed the identification of rare germline mutations in a few novel melanoma susceptibility genes, namely BRCA1 Associated Protein 1 *(BAP1), TERT*, Protection of Telomeres 1 (*POT1*), ACD Shelterin Complex Subunit and Telomerase Recruitment Factor (*ACD*), TERF2 Interacting Protein (*TERF2IP*) (high risk genes) and *MC1R, MITF* (low to moderate risk genes).

By investigating a melanoma-prone family by linkage analysis and high-throughput sequencing, disease-segregating germline mutations have been identified in the *TERT* gene, causing up to 2-fold increase in its transcription (123). Telomere maintenance has been uncovered as a crucial pathway in melanoma predisposition. *POT1*, *ACD*, and *TERF2IP* are members of the Shelterin protein complex, crucial for the safeguard of telomeres, and have been also described to be mutated in familial melanoma patients (118, 121).

A summary of the main somatic and germline alterations in melanoma is provided in **Table 1**.

GENOMIC TECHNOLOGIES

Over the past decades there have been major advances in our understanding of the human genome, mostly due to the rapid development of genomic technologies that allow the interrogation of hundred-thousand loci and/or provide single base pair resolution. The common denominator of these technologies is the capacity to produce a large amount of data in a number of samples assessed, hence the definition of "high-throughput" technologies. In the biomedical context, the application of high-throughput genomic technologies can be used to identify biological markers (biomarkers) to understand disease course and/or predict treatment response or patient survival (124). Biomarkers can be broadly classified into three categories: diagnostic (for the assessment of presence/absence of disease); predictive (how a patient responds to a treatment) and prognostic (how long a patient survives after intervention) (124). Biomarkers can be assessed at different levels, namely: genome, epigenome and transcriptome. At the DNA (genome) level, high-throughput technologies can be applied to detect Single Nucleotide Variants (SNVs), indels, Structural Variants (SVs), CNVs and fusion genes (125). DNA-sequencing techniques include whole-genome sequencing (WGS, to detect alterations in coding and non-coding regions of the genome), whole-exome sequencing (WES, limited to coding regions) and targeted sequencing (focusing on specific regions of the genome when

prior information is available). At the epigenomic level, high-throughput technologies are applied to detect chemical modifications of the DNA which regulate gene expression; both microarray and sequencing technologies can be used to detect and quantify DNA methylation status; chromatin immunoprecipitation sequencing (ChIP-Seq) can be implemented to characterize transcription factor binding sites and patterns of histone modifications (126, 127). At the transcriptome level, high-throughput technologies are applied to study RNA species with mRNA being the most commonly studied form of RNA (128–130).

It is now becoming clear that no two cancers are exactly the same. This concept is leading to the development of individual-specific therapeutic approaches, based on the identification and quantification of specific genomic features (131).

Until now, most of the medical treatments have been the result of the "one-size-fits-all" approach. However, while some treatments can result very effective in some patients, some other patients might not benefit to the same extent or might even have adverse effects from a given therapy. Personalized medicine aims at understanding individual differences in people's genetic and environmental backgrounds and at giving medical professionals the tools they need to develop tailored and most efficient therapeutic strategies.

It has now been accepted that the integration of the personalized medicine approach into the oncology field may lead to improvement in cancer treatments, especially considering the interindividual variability (131).

With the completion of the Human Genome Project in 2003, scientists have started acquiring the tools to read and interpret individual genetic codes. Since then, technologies have significantly improved. We describe below examples of high-throughput genomic technologies that can be applied to the oncology field. A summary of those technologies is provided in **Table 2**.

NEXT-GENERATION SEQUENCING TECHNOLOGIES

The last decade has witnessed a rapid increase in the number of next-generation sequencing (NGS) technologies implemented, with entire genome sequencing producing gigabases of reads on a daily basis (124, 132–134). The application of NGS technologies is currently providing a more comprehensive understanding of the mutational landscape of cancer and as a consequence, a better understanding of its pathogenesis (20, 21, 135–137).

NGS technologies generally require the conversion of the nucleic acid materials derived from biological specimens into a form that is suitable for sequencing, this step is called "library preparation" and represents perhaps the most challenging step with biological and bioinformatic implications (124, 138). Library preparation is generally characterized by an amplification step by polymerase chain reaction (PCR) (138, 139). This step is particularly prone to bias introduction (138). Although several PCR-free methods are currently available, they are not free of

TABLE 2 | Summary of the advantages and disadvantages of the genomic technologies described in this review.

Technology	Examples	Description	Advantages	Disadvantages
Short-read sequencing	Illumina	Cyclic reversible termination	Cost-effective, overall higher sequence fidelity, supported by several analysis tools	Not able to resolve structural variants, phase alleles and provide coverage for respective regions; GC bias
	SOLiD – Life Technologies	Sequencing by ligation		
	Ion Torrent	Ion semiconductor sequencing		
	Roche/454	Pyrosequencing	First commercial NGS platform; read length up to 1 kb	Inaccuracy in homopolymer sequencing, high error rate, low yield, high cost per bp. Operation has shut down in 2013
Long-read sequencing	Pacific Biosciences	Single Molecule, Real-Time Sequencing	Generate reads in excess of 10 kb; perform *de novo* assembly; mapping certainty; transcript isoform identification; detection of structural variants; direct detection of epigenetic modifications	Lower accuracy per read; bioinformatic challenges including limited pipelines available, coverage biases, overall high error rates
	Oxford Nanopore	Nanopore Sequencing		
Single-cell platforms	Fluidigm C1	Microfluidics-based	Allow the analysis of individual cells; can identify clonal cell subpopulations	Nucleic acid amplification necessary
	Chromium 10X Genomics	Droplet-based		
	BD Rhapsody	Microwell-based		
Spatial genomics	Visium 10X Genomics	Positionally capturing mRNAs from thin tissue sections onto an oligonucleotide array	Resolve genomic information of individual cells within the spatial context of their native tissue	Relatively new
	Nanostring GeoMx DSP	Standard immunofluorescence combined to optical barcoding quantification		
Optical Mapping	Bionano Genomics	High-resolution imaging of long DNA molecules	Resolve complex regions of the genome up to hundreds kbp in length; allow genome finishing	No single bp resolution; specific protocols required for the extraction of DNA of high molecular weight

flaws (138, 139). Library preparation methods are of paramount importance when only a small amount of starting material is available and clinical samples cannot be collected again. During the library preparation step, adaptors are ligated to fragmented DNA and then amplified before sequencing. Amplified templates can be generated in solution or on a solid support by covalently attached oligo. On the solid support of the Illumina platform for instance, fragmented adapter-ligated DNA molecules are bound to these primers and amplified through a series of amplifications to generate identical sequences that provide template for the sequencing reaction. Upon library preparation, the sequencing step is performed.

There are different approaches for high-throughput sequencing, according to the genomic platform employed, each of which uses bespoke protocols. Below, we list the most common high-throughput genomic sequencing technologies and provide some examples of their application in the context of melanoma.

The first NGS platform was launched in 2005, and several other methodologies have followed, as reviewed in detail in other reports (132–134, 140). Their major feature is the ability to generate thousands/millions sequence reads at the same time (133, 141).

Illumina is perhaps the most commonly used genomic technology in the research and healthcare settings; the technology employs the so-called flow cell, a solid surface on which adapters are covalently attached; the flow cells adapters are complementary to the library adapters. Illumina uses the principle of cyclic reversible termination where nucleotides chemically modified are used as terminators of the sequencing reaction. In the Illumina sequencing workflow, all four nucleotides are added to each cycle and each of the four nucleotides carries an identifying fluorescent label. Once the right nucleotide gets incorporated, the unincorporated nucleotides are washed away, and the flow cell gets imaged; the fluorescent groups are then chemically cleaved and the 3'-OH groups deblocked to allow the next cycle to occur.

In early 2017, Illumina released the NovaSeq series which exceeded existing sequencing performance metrics and allows multiple applications in the same run (142) ("NovaSeq 6000 System - Illumina: https://www.illumina.com/systems/sequencing-platforms/novaseq.html") (142).

Studies employing WES and WGS on the Illumina platform have recently improved the characterization of somatic mutations in melanoma and demonstrated that melanoma displays one of the highest rates of somatic mutations as compared to other types of cancers, which makes it challenging to distinguish driver from passenger mutations (24, 143–145). The highest mutation frequency in cutaneous melanoma is explained by the exposure to ultraviolet (UV) radiation, a well-documented carcinogen (143). It was also reported that cutaneous melanoma is particularly prone to cytidine to thymidine transition (C>T). Such alteration is specific of a UV-light induced mutational signature (146).

Another mode of sequencing is represented by the one applied by Life Technologies with the SOLiD (Sequencing by Oligonucleotide Ligation and Detection) NGS system. The chemistry employs a sequencing by ligation method and a template preparation based on the creation of clonal bead populations. DNA fragments are amplified clonally on beads, placed on the solid-phase of a flow cell. In the sequencing by ligation approach, a mix of differently labeled nucleotide probes are flushed into the flow cell. When the correct probe is incorporated, it gets ligated into the primer on the solid-phase; the unincorporated nucleotides are washed away and the fluorescence gets recorded. The fluorescent dye is then removed and the next sequencing cycle commences (147).

A completely different approach to NGS relies on the detection of hydrogen ions released after nucleotide incorporation. This approach was employed by Ion Torrent in 2010, later purchased by Life Technologies and subsequently by Thermo Fisher Scientific. The chips employed in this technology are designed to detect pH changes that occur as the sequencing reaction progresses (148). In a recent study, Manca and colleagues have employed the Ion Torrent PGM (Personal Genome Machine) System to evaluate the mutational concordance between primary and metastatic melanoma (83). The authors showed a high level of concordance in the mutational patterns registered in the primary and metastatic samples, especially with regards to the pathogenic mutations in driver genes (83).

In pyrosequencing such as the sequencing employed by Roche/454, a labeled nucleotide is detected when an inorganic pyrophosphate from the incorporated nucleotide releases a signal following enzymatic transformation (140). Library preparation is performed by random fragmentation of genomic DNA and an emulsion-based PCR. The PCR is employed to clonally amplify template DNA in single droplet-encapsulated reaction beads that contain oligonucleotide probes with complementary sequence to the adaptor binding the DNA fragments. The emulsion PCR beads are attached on a solid surface. The addition of nucleotides complementary to the template strand leads to the production of a chemiluminescent signal recorded by the instrument CCD camera. A specialized software then analyzes the position of the beads and the light flashes with each type of nucleotides that are incorporated into the synthesized DNA (149). The Roche/454 sequencing was the first NGS technology to sequence a complete human genome. The technology has been employed in the diagnostic setting for *BRAF* mutational assessment (150–153). However, the inaccuracy of the technology in homopolymer sequencing, the high error rate, low yield and high cost per bp have largely limited its application. In fact, Roche has shut down the 454-sequencing operation in 2013 as the technology became noncompetitive.

The technologies described above are employed to sequence short reads. Short-read sequencing technologies are cost-effective, accurate and supported by many analysis tools (154). Nevertheless, short reads make it more difficult to reconstruct the original genomic map. Short-read sequencing technologies have additional inherent limitations, including GC bias, difficulties in mapping repetitive elements of the genome, difficulties in discriminating paralogues sequences and in allele-phasing (155).

Newer technologies include Pacific Biosciences (PacBio) and Oxford Nanopore Technologies (ONT), both platforms being employed for the so called "long-read sequencing". While short-read sequencing technologies produce reads of up to 600 bases, long-read sequencing technologies produce reads in excess of 10 kb (154, 156). Those long-read sequencing technologies have considerable advantages, including longer read lengths, the direct detection of epigenetic modifications, the capability to resolve repetitive elements, to allow the characterization of full-length transcriptomes and to allow variant phasing (155, 157, 158). Long-reads also carry more information about structural variation as compared to short-reads. Long-read sequencing is already considered the gold standard for some applications, as for instance the HLA (Human Leukocyte Antigen) typing for tissue transplants. The long-read sequencing technologies are expected to open up new avenues for melanoma characterization and development of targeted therapeutic strategies.

The technology employed by PacBio interrogates a single molecule of DNA in real time. The technology is characterized by the absence of PCR amplification and by the real-time acquisition of the signal. PacBio launched the Sequel II system in 2019 which by employing the High Fidelity (Hi-Fi) sequencing mode allows for high fidelity reads and a superior call rate when compared to other technologies, as demonstrated by the recent Precision FDA Truth Challenge V2 that evaluated different technologies for variant calling in human genomes and demonstrated a higher performance of the PacBio HiFi technology as compared to Illumina and ONT (159) ("PrecisionFDA Truth Challenge V2: Calling Variants from Short and Long Reads in Difficult-to-Map Regions: https://precision.fda.gov/challenges/10/view/results") (159). The Single Molecule Real-Time (SMRT) Sequencing employed by PacBio can also be used to detect methylation changes in the genome. The technology relies on the kinetics of polymerase incorporation of individual nucleotides, allowing the direct detection of these modified cytosines (160, 161). The PacBio system was the first to be launched as "third-generation sequencing". Sequencing occurs into the so-called "zero mode waveguides" (ZMW), that are single pockets where DNA and polymerase bind to and where the signal is detected by the incorporation of phosphate-labeled nucleotides to the well (162). In the latest Sequel II system, the SMRT cells used for sequencing contain 8M ZMW which represents an improvement of the data output as compared to the previous SMRT cells that contain 1M ZMW.

In ONT sequencing single-stranded DNA molecules are driven into nanopores; when each nucleotide of the DNA strands partially obstructs the nanopore, an alteration of the electrical property is recorded and analyzed (163, 164). Since the technology uses unmodified DNA, the major advantage consists into yielding results very quickly from minimal starting quantities. The first prototype of the platform consisted in the MinION that was launched in the market in 2014 (147).

Despite the technical advantages of long-read sequencing technologies, their application in the field of cancer has been very limited. Cavalier and colleagues (165) employed SMRT sequencing for the detection of tyrosine kinase inhibitors (TKI) resistance mutations down to a level of 1% in chronic myeloid leukemia (CML) patients. Additionally, they were able to phase co-existing mutations, providing new information about the clonal distribution of resistance mutations in BCR-ABL1. Other two studies have applied long-read sequencing for the detection of multiple *TP53* mutations distributed in different alleles in acute myeloblastic leukemia (AML) and myelodysplastic syndrome (MDS) and for phasing of somatic mosaicism mutations in GJB2 in a patient with keratitis-ichthyosis-deafness syndrome, respectively (166, 167). Despite the examples above and to the best of our knowledge, the long-read sequencing technologies have not yet been applied to the field of cutaneous melanoma. They could offer many advantages especially with regards to the study of SV, insertions, deletions, duplications, inversions or translocations. SV unfortunately have been neglected from a proper characterization in cutaneous melanoma despite being an important source of diversity between genomes and despite being proved to be relevant in human health (154, 168, 169).

Other advantages of long read-sequencing technologies rely in the possibility to sequence full length transcripts and identify novel splicing isoforms (155, 170) as well as detect base modifications (156). As an example, in SMRT sequencing, base modifications are inferred from the delay between fluorescent pulses, referred to as interpulse duration (IPD) (171). SMRT sequencing allows the detection of 6mA, 4mC, 5mC, and 5hmC DNA modifications, although at different sensitivity (171). In nanopore sequencing, modified RNA or DNA bases affect the flow of the current through the pore differently than non-modified bases, resulting in signal shifts (172).

While the implementation of long-read sequencing technologies on large scale projects is limited by the cost and community expertise, we expect this to change rapidly. We believe that the application of these newer technologies will make it possible to resolve complex regions of the genome and to characterize the epigenome landscape and the full-length transcriptome of cutaneous melanoma. Additionally, the integration of the data produced by short- and long-reads technologies will produce more complete and contiguous genomes, which will open exciting avenues in genomics as well as facilitate the further understanding of the molecular mechanisms underlying melanoma onset and progression. NGS technologies will also provide a useful tool for the development of therapeutic strategies tailored to the genetic makeup of individual cutaneous melanomas.

Another important technology worth to note is represented by single-cell sequencing, which is a powerful approach to explore the organization and function of the tumor microenvironment. Cutaneous melanoma is characterized by tumor heterogeneity, which represents a relevant obstacle for its treatment. The bulk sequencing techniques cannot identify rare clonal subpopulations that might be responsible of tumor aggressiveness or resistance to therapy. The application of single-cell sequencing technologies allows the analysis of DNA sequences, epigenetic markers and gene expression patterns in

individual cells (173). Single-cell sequencing technology encompasses the following steps: i. isolation of single cells; ii. isolation and amplification of genetic material; iii. sequencing of the genetic material and data analysis (174). The capture of individual cells can be pursued through micromanipulation, fluorescence-activated cell sorting (FACS), magnetic-activated cell sorting (MACS) and microfluidics (173, 175). Such approaches require cells or nuclei to be in suspension, thus they cannot always maintain the spatial context in tissues. Laser capture microdissection (LCM) bypasses this limitation and can also be used to isolate rare cells. When comparing single-cell DNA sequencing to single-cell RNA sequencing, the first method has been proven more challenging than the latter one (173). DNA amplification is necessary when performing single-cell DNA sequencing. DNA amplification methods mainly include the degenerative oligonucleotide PCR (DOP-PCR), which provides uniform amplification but a low coverage and the multiple displacement amplification (MDA), that uses polymerase strand displacement activity and can lead to a high genome coverage but with a non-uniform amplification. Several alternative methods have been refined to decrease allelic drop-out and false positive rate (176). Those methods include: Nuc-seq, which sorts nuclei in G2/M phase; the multiple annealing and looping-based amplification cycle (MALBAC), which uses quasi-linear preamplification coupled with strand displacement active polymerase; and the micro-well displacement amplification system (MIDAS), that employs small reaction volumes and eliminates non-uniform amplification (177). Once amplified, DNA is provided as substrate for library construction for NGS. So far, Illumina seems to be the most employed platform due to low cost per base at high throughput.

To sequence the transcriptome of a single-cell, RNA undergoes to a whole transcriptome amplification (WTA) step. Initial WTA methods engaged the T7 RNA polymerase for amplifying cDNA linearly though *in vitro* transcription (IVT) (178). Further methods included oligo d(T) primers attached to adaptor sequences for the reverse transcription step and amplification of polyadenylated mRNA by PCR (179). However, these methods are not free of flaws as they display 3' mRNA bias. To overcome such bias, the SMART-Seq method has been introduced, which amplifies only full-length mRNA transcripts using a reverse transcriptase from the Moloney Murine Leukemia Virus (MMLV), with template-switching and terminal transferase activity (173, 180). The SMART-Seq2 method was further developed and led to an improved detection, coverage and accuracy as compared to SMART-Seq method (181). Additional protocols are also available for transcriptome analysis and include single-cell tagged reverse transcription (STRT), cell expression by linear amplification and sequencing (CEL-seq), CEL-seq2, QuartzSeq, droplet-based RNA-seq, and massively parallel RNA single-cell sequencing (MARS-seq) (173, 182–185). Currently, there exist many commercial platforms for modern-approaches of single-cell sequencing. The Fluidigm C1 is a microfluidics-based system that captures individual cells through integrated fluidic circuits (186). However, the employment of such platform has been limited due to the low throughput and the cell size bias because of its determined size range of the capture site for a given chip (187). The Chromium system from 10X Genomics is a droplet-based platform displaying high sensitivity, high accuracy, low technical noise and high cost (173). Drop-Seq, which is also a droplet-based platform, represents a more cost-efficient solution as compared to the Chromium system. The BD Rhapsody system for single-cell analysis is a microwell-based platform that is used for targeted RNA sequencing, thus more useful when aiming at detecting rare information (188). Additional platforms for single-cell analysis have been described elsewhere (188).

Single-cell sequencing has been employed in melanoma. An interesting study has recently investigated the role of heterogenous spheroids in the stromal niche of cutaneous melanoma by single-cell RNA sequencing (189). The authors identified molecules that could play a role in the control of the interaction between melanoma cells and cancer-associated fibroblasts. Another important study applied single-cell RNA sequencing to assess the transcriptomes of single cells cultured from patients' biopsies with different BRAF and NRAS mutational profiles. The authors were able to identify sub-populations of cells defined by transcriptional modules involved in proliferation, oxidative phosphorylation, pigmentation and cellular stroma (190). We expect that with the advancement of the genomic technologies, more groups will employ single-cell sequencing to shed light on the molecular mechanisms underlying cutaneous melanoma pathogenesis and responsiveness to therapy.

SPATIAL GENOMICS

The combination of state-of-the-art genomic technologies to high-resolution microscopy has led to the establishment of the so-called spatial genomics, an innovative technology that aims at resolving genomic information of individual cells within the spatial context of their native tissue. The general methodology overlays genomic data on a tissue section to provide spatial context (191). The two major players in the spatial genomic field are represented by the Visium technology from 10X Genomics (192), and the Nanostring GeoMx Digital Spatial Profiler (DSP) (193). The 10X Genomics Visium technology captures mRNA molecules from thin tissue sections initially imaged histologically onto an oligonucleotide array. cDNA is then synthesized from the captured mRNA and used for library preparation. Libraries are finally sequenced, and the data processed to identify transcripts and measure their expression. The Nanostring GeoMx DSP platform provides morphological context with high-plex protein or gene expression profiling. Individual slides are first fluorescently stained to allow the GeoMx platform to capture images with morphological context. The technology relies on the use of photocleavable oligonucleotide tags that are attached to antibodies through a light-sensitive linker. The high-plex oligos then get separated from the antibodies or RNA in the region of interest through UV light. Finally, the photocleaved oligos are retrieved from the surface of the tissue and processed

for quantitative analysis. The Nanostring GeoMx platform has been applied to carry high-plex characterization of B- and T-cells in melanoma tumors (194). The study revealed that tertiary lymphoid structures play a crucial role in melanoma immune microenvironment through conferring different T-cell phenotypes, thus suggesting that the formation of tertiary lymphoid structures should be investigated to foster responses to cancer immunotherapy (194).

The application of spatial transcriptomics for the study of cutaneous melanoma has also revealed a complex transcriptional landscape of lymph node metastases in a spatial context (195).

The 10X Genomics Visium technology has been applied to skin squamous cells carcinoma (196). The authors identified multiple cells responsible for immunosuppressive functions in dendritic cells, exhausted T cells and Tregs, refining local tumor structures. Spatial genomics offers a great potential to uncover the mechanisms that govern cell interaction in the tumor microenvironment (197) and we expect this field to expand significantly along with advancement of genomic technologies.

OPTICAL MAPPING TECHNOLOGY

Genomic SVs have been well established to be associated with cancer. Genomic SVs arise from the genome instability created during cancer onset and progression (198). Nevertheless, SV analysis of cancer genomes has been severely limited to date by technical shortcomings. Traditionally, SVs have been detected by microarray (limited to imbalanced copy number variation (CNV) with a short dynamic range, low resolution, and relative readouts), next-generation sequencing (NGS) (primarily CNV, some balanced events but too short to span most repeats) and karyotyping and fluorescence *in situ* hybridization (FISH) (both are very low resolution). The optical mapping technology from Bionano Genomics is able to interrogate genome structural differences of hundreds of kilobase pairs and span interspersed and even long tandem repeats making it ideally suitable for elucidating the structure and copy number of complex regions of the genome, such as complex pseudogene and paralogous gene families. The platform does not produce single base pair resolution as it uses an optical mapping technique. Long molecules of DNA are first isolated using Bionano specific extraction methods (DNA >100kbp), the DNA is labeled at specific motifs through labeling enzymes and linearized through nanochannels for visualization. The Bionano technology can identify megabases-long CNVs as well as long-range translocation and other rearrangements ("Bionano Genomics: https://bionanogenomics.com") (199). An interesting study from Xu and colleagues applied optical mapping technology to study leukemia SVs. The authors identified new SVs in leukemia samples and underscored that the missed knowledge of SVs in cancer samples might hamper advancement in the development of diagnostic and therapeutic strategies (200). By combining WGS to optical mapping, they were able to recover twice as many SVs as revealed by WGS alone. Additionally, they were able to pinpoint variants that likely arose as somatic alterations.

To the best of our knowledge, the optical mapping technology has not yet been used for the investigation of SVs in cutaneous melanoma and its application may lead to useful insights for cutaneous melanoma characterization and to a better clinical management.

INTERNATIONAL EFFORTS

The increase of whole genome sequencing and transcriptome sequencing data following the implementation of NGS technologies offered the possibility to perform meta-analysis studies aiming at identifying patterns of genomic alterations across different tumor types (201). Several consortia were established with the aim to federate a large amount of sequencing data of cancer genomes.

The International Cancer Genome Consortium (ICGC) was first established in 2007 to study the genomes of ~25,000 primary untreated cancers as part of the "25K Initiative" (202) ("The International Cancer Genome Consortium: https://icgc.org") (202). In a later phase, the ICGC launched the Pan Cancer Analysis of Whole Genomes (PCAWG), also known as the Pan-Cancer Project. A technical working group was assembled to develop the informatic pipelines by aggregating the raw data from different groups that studied individual tumor types and by aligning the sequences to the human genome. This made it possible to generate a set of high-quality somatic mutation calls for the downstream analyses (201–203). ICGC has also planned another initiative, named "The ARGO (Accelerate Research in Genomic Oncology) Project" aiming at using clinical questions and patient clinical data to drive the interrogation of cancer genomes. The ARGO Project is expected to provide a unique resource of multi-omics data for cancer patients undergoing clinical trials in order to facilitate the discovery of new therapeutic strategies. As of October, 2020 the ICGC repository includes two skin cancer and one melanoma projects (**Supplementary Figure 1**).

The "Catalogue Of Somatic Mutations In Cancer" (COSMIC) represents an additional resource to explore the impact of somatic mutations in cancer. The COSMIC database was launched in 2004 with data from just four genes (204). The resource continued to expand rapidly and by 2005 it included 529 genes from more than hundred thousand tumors (204). A new version of the resource has been launched on August 27, 2020 and it includes 1,459,483 samples. It encompasses a curated update on spliceosomes and also the launch of a new product, "The Cancer Mutation Census (CSM)" (205) ("COSMIC, The Catalogue Of Somatic Mutations In Cancer: https://cancer.sanger.ac.uk/cosmic") (205).

The Cancer Genome Atlas (TCGA) represents another initiative empowering cancer genome data analysis to facilitate our understanding of the molecular mechanisms underlying cancer development. The project began in 2006 when it was launched as a three years pilot project with a conjunct

investment from the National Cancer Institute (NCI) and the National Human Genome Research Institute (NHGRI) (206) ["The Cancer Genome Atlas (TCGA): https://www.cancer.gov/about-nci/organization/ccg/research/structural-genomics/tcga"] (206). The project has characterized over 20,000 primary cancer and matched normal samples encompassing 33 cancer types (206) ["The Cancer Genome Atlas (TCGA): https://www.cancer.gov/about-nci/organization/ccg/research/structural-genomics/tcga"] (206). The TCGA has generated petabytes of genomic, epigenomic, transcriptomic and proteomic data; such data is publicly available and has already led to improvements in the diagnosis, treatment and prevention of cancers. The TGCA repository includes data from 470 characterized cases of cutaneous melanoma, of which 331 samples have been employed in an integrative analysis that included WGS, WES and RNA-sequencing. Such integrative analysis aimed at establishing a framework for the cutaneous melanoma classification into four subtypes that can help clinicians in making decisions for targeted therapies (207). Those four subtypes included: i. the BRAF subtype which accounts for the majority of cutaneous melanomas (~52%) and it is characterized by the presence of a mutation on the *BRAF* gene; ii. the RAS subtype defined by the presence of mutations on the *RAS* gene, accounting for ~28% of cutaneous melanomas; iii. the NF1 subtype characterized by the presence of mutation on *NF1* gene and accounting for ~14% of cutaneous melanomas; iv. the Triple Wild-Type subtype, a more heterogenous subgroup characterized by the absence of mutations on *BRAF*, *RAS* and *NF1* genes. The study reported some interesting findings, including that the patients in the BRAF subtype were younger than the patients in the other groups, while the opposite was observed for patients in the NF1 group. The Triple Wild-Type subtype showed a significant higher number of copy-number segments and displayed more focal amplifications including known oncogenes as compared to the other groups. The same study also showed that a subset of each of the genomic classes of cutaneous melanoma expressed markers indicative of immune infiltration that were associated with improved survival and could carry clinical relevance for immunotherapy treatments (207).

Another useful tool for Cancer Genomics is cBioPortal which provides visualization, analysis and download of large-scale cancer genomics data sets (208) ("cBioPortal: https://www.cbioportal.org") (208). The Portal was initially developed at Memorial Sloan Kettering Cancer Center (MSK) and the cBioPortal software is now available under an open-source license *via* GitHub. The maintenance of the software is performed by a multi-institutional team that includes MSK, the Dana Farber Cancer Institute, the Princess Margaret Cancer Centre in Toronto, the Children's Hospital of Philadelphia, The Hyve in the Netherlands and Bilkent University in Ankara, Turkey (208) ("cBioPortal: https://www.cbioportal.org") (208). The advantage of cBioPortal relies on the user-friendly interface, an example of the data retrieved from cBioPortal is displayed in **Supplementary Figure 2**. The interface shows graphs from 471 patients.

Another important consortium worth of mentioning is the GenoMEL, the Melanoma Genetics Consortium, that represents a non-profit consortium launched in 1997 that includes research groups worldwide and it is focused on the study of genetics in familial melanoma ("GenoMEL, the Melanoma Genetics Consortium: https://genomel.org/research/programme-and-aims/") (209).

Additionally, a unique collaboration of multidisciplinary experts from the European Dermatology Forum (EDF), the European Association of Dermato-Oncology (EADO), and the European Organization of Research and Treatment of Cancer (EORTC) was formed to make recommendations on cutaneous melanoma diagnosis and treatment, based on systematic literature reviews and the experts' experience (5).

The combined efforts of international consortia described above has the potential to provide new insights into the genetic makeup of cutaneous melanoma as well as identifying novel molecular defects that can improve our understanding of cutaneous melanoma pathogenesis.

HOW GENOMIC TECHNOLOGIES ARE MOVING TOWARD PERSONALIZED MEDICINE

Cutaneous melanoma, especially in metastatic stage, represents a challenging clinical situation with a steady need for effective treatment options. The past and current findings on the mutational profile of cutaneous melanoma are opening new doors to understand how this tumor initiates, progresses and metastasizes and are leading to a new orientation for antitumor therapy, referred as targeted therapy, which offers the opportunity for various treatment options that can be used in combination with other treatment modalities, i.e., surgical resection, chemotherapy, radiotherapy, and immunotherapy.

The dramatic importance of molecular biology-based strategies used for the detection of driving mutations in melanoma oncogenes resides in defining targetable alterations and making them "druggable", thus enabling meaningful advances in personalized medicine (210–212).

Since the first step to an efficient therapy is to identify which patients will derive most benefit from given treatments, a growing number of translational studies is now focused on the identification of biomarkers useful in the selection of patients eligible for specific treatments (213, 214). The critical role of MAPK/ERK signaling pathway in melanoma has been used for the development of targeted treatments. Since the activation of MAPK/ERK signaling is often due to mutations in the *BRAF* and *NRAS* genes, mutation testing for these genes has become a standard procedure to guide the oncologist's therapeutic choice and predict the course of therapy (215–217). For instance, only patients with a $BRAF^{V600E}$-mutated melanoma are expected to benefit from targeted therapies with BRAF/mitogen-activated protein kinase (MEK) inhibitors, while patients with a $BRAF^{K601E}$-positive melanoma respond only to a minority of those drugs, such as trametinib (33). Moreover, recent studies

have indicated that $BRAF^{V600E}$ detection through circulating tumor DNA prior to treatment is predictive of response to BRAF/MEK inhibitors (218). Recently, there have been major advancements in the treatment of cutaneous melanoma, due to the introduction of targeted therapies, including for example vemurafenib and dabrafenib (BRAF kinase inhibitors) and trametinib and cobimetinib (MEK inhibitors) (219–221).

As another example, the preclinical observation that CDK4/6 inhibition can attenuate *NRAS* oncogenic signaling when combined with MEK inhibition has led to an undergoing clinical investigation of the synergistic inhibition of CDK4/6 (PD-0332991) and MEK1/2 (selumetinib) in NRAS-mutant melanomas (29).

Despite the advances in the development of novel antitumor approaches, resistance to targeted therapy is a noteworthy issue in the management of melanoma patients, being driven by multiple mechanisms. High genomic instability and heterogeneity can promote primary (*de novo*) or acquired resistance (occurring in tumors previously responsive to the same treatment) (222, 223). A lack of treatment response and poorer progression-free survival have been observed in patients with BRAFV600-mutated metastatic melanoma, treated by MAPK inhibitors, and with coexisting genetic alterations, such as the *TERT*prom c-146C>T mutation, which can affect the MAPK pathway blockade (37). Other mechanisms responsible for MAPK reactivation and sustained ERK signaling include alterations in *MEK* and *NF1* genes. Additionally, the overexpression of the RAF isoform, Raf-1 Proto-Oncogene, Serine/Threonine Kinase (*CRAF*), can induce resistance to BRAF inhibitors by MEK activation or by paradoxical transactivation of RAF dimers, promoting ERK signaling (224, 225). Similarly, poor response to BRAF inhibitors in patients with BRAF-mutant melanoma has been correlated to concurrent loss-of-function mutations in the *PTEN* gene, which can lead to the reactivation of the PI3K/AKT pathway (226). MAPK and PI3K/AKT pathways have also been reported to get reactivated by the expression of miR-204-5p and miR-211-5p in response to short-term treatment with BRAF inhibitors (224).

Co-targeting signaling effectors downstream of driver oncogenes represents an actionable strategy to overcome resistance to BRAF inhibitors. MEK is a downstream effector of BRAF. The combination of targeted therapy with BRAF/MEK inhibitors is being applied routinely in the clinic, significantly improving the response rates of patients with BRAF-mutant metastatic melanoma (227–229). The combination of BRAF and/or MEK inhibitors with immune checkpoint inhibitors is a further option in clinical practice. Since the activation of the Programmed Cell Death Protein 1 (PD-1)/Programmed Death-Ligand 1/2 (PDL-1/2) axis is often exploited by tumor cells to escape immune-mediated death, the use of anti-PD-1 or anti-PDL-1 monoclonal antibodies, in combination with BRAF/MEK inhibitors, has been proven to improve therapeutic response and progression-free survival of cutaneous melanoma patients (223, 230, 231). Recently, it has also been suggested that *TP53* mutation leads to downregulated FAS levels, which impede the induction of apoptosis, limiting the response to immune checkpoint inhibitors, such as anti-cytotoxic T-lymphocyte antigen-4 (CTLA-4), thus serving as a negative predictor of response to therapy (61, 231). *PTEN* silencing in BRAF-mutant melanoma cell lines has been associated to a decreased ability of T-cells to kill the tumors (57).

Our understanding on tumor biology is now allowing testing patients for a broader number of genes at the same time (232). NGS technologies are able to identify genetic aberrations, including rearrangements, CNVs, insertion, and deletions, that have been previously neglected from the clinical testing. NGS-based multigene panels offer a targeted method to assess several genes simultaneously (233). These tests have also the capability to identify specific actionable driver mutations and help in understanding the underlying mechanisms of drug resistance to point out patients more likely to respond to a given therapy. An interesting study from Diefenbach and colleagues has proposed a melanoma NGS multigene panel for the analysis of circulating tumor DNA (234). The panel included 123 amplicons in 30 genes encompassing targetable mutations as well as alterations associated with resistance to treatment. Such panel represented an improvement to the UltraSEEK Melanoma Panel from Agena Bioscience, which can detect 55 clinically relevant variants across 13 genes (235). Another example of melanoma multigene NGS panel is represented by the VarMap NGS panel which includes 8 genes frequently mutated in melanoma and employs the NuProbe's PCR based quantitative Blocker Displacement Amplification (qBDA) technology (236) to allow detection of variants at low frequency. Other NGS-based panel for melanoma include the OnkoSight panel (237), the NeoTYPE panel (238) and the SureSeq myPanel (239) among others.

NGS has also been applied to identify potentially actionable DNA alterations that could explain resistance to targeted therapy. An interesting study has identified resistance-related mutations in BRAF positive patients that initially achieved partial or complete response to BRAF inhibitors but whose melanoma later progressed (240).

While the value of NGS for the identification of driver/actionable mutations in cutaneous melanoma is being recognized, scientists have started appreciating also the role of melanoma high mutational load attributed to UV mutagenesis (38). Cutaneous melanoma has been shown to exhibit a high tumor mutational burden (TMB), defined as the total number of somatic mutations per million bases, as compared to other tumors (146, 241). The high TMB has been attributed to C>T transitions induced by UV light and makes cutaneous melanoma highly immunogenic (242), thus most suitable for immunotherapy. In fact, the TMB in melanoma has been shown to associate to immune infiltration, response to immunotherapy and prognosis (241).

As genomic technologies continue to evolve, we might see a switch from a targeted approach to a genome-wide approach to study melanoma. A refined molecular classification of cutaneous melanomas by high-throughput genomic technologies has the potential to lead toward a more rational approach to therapy, including patient stratification in subgroups that are genetically more homogeneous and likely to differ in clinical variables,

including the pattern of metastasis, disease outcome, clinical response to therapy, thus aiming at personalized treatment approaches (227, 243).

The improved genomic characterization of cutaneous melanoma represents a critical asset with diagnostic and prognostic implications, helping the dermatopathologists in the challenging classification of melanocytic lesions as benign, intermediate, or malignant (48, 84). Defining a mutational signature of driver mutations can also help in identifying those lesions more likely to progress toward high grade melanoma (81).

As a matter of fact, in the era of targeted therapies, molecular subtyping of melanoma is replacing the traditional clinicopathological classification. As an example, based on exome and genome sequencing studies, the TCGA Network has classified cutaneous melanoma into four distinct molecular subtypes: BRAF-mutant, NRAS-mutant, NF1-mutant, and BRAF/NRAS/NF1 wild-type (triple-wild-type group), as described above.

Knowing the tumor genetic signature would be helpful also in the retrospective analysis of clinical trials' data (243).

Finally, gene mutational status analysis could be also helpful as predictor of response to immunotherapy, a novel approach that has revolutionized the management of metastatic melanoma (51, 244, 245).

CONCLUSION

The application of high-throughput technologies holds the promise of personalized medicine, refining the current classification of cutaneous melanoma and allowing the employment of sequencing tests that can guide patient management decisions. Personalized medicine also aims at avoiding the use of potentially harmful treatment strategies, like chemotherapy for instance, by establishing where those treatments are not beneficial for given patients (246).

While the employment of genetic testing in the clinical management of cutaneous melanoma is very well documented (215, 247–250), the application of genomic profiling through high-throughput technologies in the treatment of melanoma is still in its infancy.

NGS technologies are not limitations free. In fact, when applied alone, they cannot capture the entire complexity of melanoma biology. Additionally, not all the newly released genomic technologies have been applied to the study of melanoma. The cost of sequencing technologies is also an important limitation. We expect that with the advancement in sequencing technologies and with the drop in prices, the field of cutaneous melanoma will benefit from new discoveries and these technologies will allow an improved treatment of cutaneous melanoma patients.

We hope that this review provides an up-to-date overview of genomic technologies in the context of melanoma classification and eventually facilitates the application of personalized medicine.

AUTHOR CONTRIBUTIONS

This work was conceived and planned by ST. The original draft preparation and writing were made by CS, DM, and ST. All authors contributed to the article and approved the submitted version.

SUPPLEMENTARY MATERIAL

The Supplementary Material for this article can be found online at: https://www.frontiersin.org/articles/10.3389/fonc.2021.635488/full#supplementary-material

REFERENCES

1. Siegel RL, Miller KD, Jemal A. Cancer Statistics, 2020. *CA Cancer J Clin* (2020) 70(1):7–30. doi: 10.3322/caac.21590
2. Ferlay J, Steliarova-Foucher E, Lortet-Tieulent J, Rosso S, Coebergh JW, Comber H, et al. Cancer Incidence and Mortality Patterns in Europe: Estimates for 40 Countries in 2012. *Eur J Cancer* (2013) 49(6):1374–403. doi: 10.1016/j.ejca.2012.12.027
3. Leiter U, Garbe C. Epidemiology of Melanoma and Nonmelanoma Skin Cancer–the Role of Sunlight. *Adv Exp Med Biol* (2008) 624:89–103. doi: 10.1007/978-0-387-77574-6_8
4. Garbe C, Leiter U. Melanoma Epidemiology and Trends. *Clin Dermatol* (2009) 27(1):3–9. doi: 10.1016/j.clindermatol.2008.09.001
5. Garbe C, Amaral T, Peris K, Hauschild A, Arenberger P, Bastholt L, et al. European Consensus-Based Interdisciplinary Guideline for Melanoma. Part 1: Diagnostics - Update 2019. *Eur J Cancer* (2020) 126:141–58. doi: 10.1016/j.ejca.2019.11.014
6. Whiteman DC, Green AC, Olsen CM. The Growing Burden of Invasive Melanoma: Projections of Incidence Rates and Numbers of New Cases in Six Susceptible Populations Through 2031. *J Invest Dermatol* (2016) 136 (6):1161–71. doi: 10.1016/j.jid.2016.01.035
7. Bauer J, Garbe C. Acquired Melanocytic Nevi as Risk Factor for Melanoma Development. A Comprehensive Review of Epidemiological Data. *Pigment Cell Res* (2003) 16(3):297–306. doi: 10.1034/j.1600-0749.2003.00047.x
8. Garbe C, Buttner P, Weiss J, Soyer HP, Stocker U, Kruger S, et al. Associated Factors in the Prevalence of More Than 50 Common Melanocytic Nevi, Atypical Melanocytic Nevi, and Actinic Lentigines: Multicenter Case-Control Study of the Central Malignant Melanoma Registry of the German Dermatological Society. *J Invest Dermatol* (1994) 102(5):700–5. doi: 10.1111/1523-1747.ep12374298
9. Curtin JA, Fridlyand J, Kageshita T, Patel HN, Busam KJ, Kutzner H, et al. Distinct Sets of Genetic Alterations in Melanoma. *N Engl J Med* (2005) 353 (20):2135–47. doi: 10.1056/NEJMoa050092
10. Clark WH Jr, From L, Bernardino EA, Mihm MC. The Histogenesis and Biologic Behavior of Primary Human Malignant Melanomas of the Skin. *Cancer Res* (1969) 29(3):705–27.
11. Elder DE, Barnhill RL, Bastian BC, Cook MG, de la Fouchardiere A, Gerami P. *Melanocytic Tumour Classification and the Pathway Concept of Melanoma Pathogenesis. WHO Classification of Skin Tumors. 4th ed.* France: International Agency for Research on Cancer (IARC) (2018). p. 66–71.
12. Shain AH, Bastian BC. From Melanocytes to Melanomas. *Nat Rev Cancer* (2016) 16(6):345–58. doi: 10.1038/nrc.2016.37
13. Scolyer RA, Barnhill RL, Bastian BC, Busam KJ, McCarthy SW. *smoplastic Melanoma. WHO Classification of Skin Tumours, 4th ed.* France: International Agency for Research on Cancer (IARC) (2018). p. 105–7.
14. Gong HZ, Zheng HY, Li J. Amelanotic Melanoma. *Melanoma Res* (2019) 29 (3):221–30. doi: 10.1097/CMR.0000000000000571
15. Gershenwald JE, Scolyer RA, Hess KR, Sondak VK, Long GV, Ross MI, et al. Melanoma Staging: Evidence-based Changes in the American Joint Committee on Cancer Eighth Edition Cancer Staging Manual. *CA Cancer J Clin* (2017) 67(6):472–92. doi: 10.3322/caac.21409

16. Green AC, Baade P, Coory M, Aitken JF, Smithers M. Population-Based 20-Year Survival Among People Diagnosed With Thin Melanomas in Queensland, Australia. *J Clin Oncol* (2012) 30(13):1462–7. doi: 10.1200/JCO.2011.38.8561
17. Joosse A, Collette S, Suciu S, Nijsten T, Lejeune F, Kleeberg UR, et al. Superior Outcome of Women With Stage I/II Cutaneous Melanoma: Pooled Analysis of Four European Organisation for Research and Treatment of Cancer Phase III Trials. *J Clin Oncol* (2012) 30(18):2240–7. doi: 10.1200/JCO.2011.38.0584
18. Greenwald HS, Friedman EB, Osman I. Superficial Spreading and Nodular Melanoma are Distinct Biological Entities: A Challenge to the Linear Progression Model. *Melanoma Res* (2012) 22(1):1–8. doi: 10.1097/CMR.0b013e32834e6aa0
19. Tas F. Metastatic Behavior in Melanoma: Timing, Pattern, Survival, and Influencing Factors. *J Oncol* (2012) 2012:647684. doi: 10.1155/2012/647684
20. Al Hashmi M, Sastry KS, Silcock L, Chouchane L, Mattei V, James N, et al. Differential Responsiveness to BRAF Inhibitors of Melanoma Cell Lines BRAF V600E-Mutated. *J Transl Med* (2020) 18(1):192. doi: 10.1186/s12967-020-02350-8
21. Tomei S, Bedognetti D, De Giorgi V, Sommariva M, Civini S, Reinboth J, et al. The Immune-Related Role of BRAF in Melanoma. *Mol Oncol* (2015) 9(1):93–104. doi: 10.1016/j.molonc.2014.07.014
22. Ding L, Kim M, Kanchi KL, Dees ND, Lu C, Griffith M, et al. Clonal Architectures and Driver Mutations in Metastatic Melanomas. *PloS One* (2014) 9(11):e111153. doi: 10.1371/journal.pone.0111153
23. Arafeh R, Qutob N, Emmanuel R, Keren-Paz A, Madore J, Elkahloun A, et al. Recurrent Inactivating RASA2 Mutations in Melanoma. *Nat Genet* (2015) 47(12):1408–10. doi: 10.1038/ng.3427
24. Hayward NK, Wilmott JS, Waddell N, Johansson PA, Field MA, Nones K, et al. Whole-Genome Landscapes of Major Melanoma Subtypes. *Nature* (2017) 545(7653):175–80. doi: 10.1038/nature22071
25. Bruno W, Martinuzzi C, Dalmasso B, Andreotti V, Pastorino L, Cabiddu F, et al. Correction: Combining Molecular and Immunohistochemical Analyses of Key Drivers in Primary Melanomas: Interplay Between Germline and Somatic Variations. *Oncotarget* (2018) 9(47):28798. doi: 10.18632/oncotarget.25684
26. Guan J, Gupta R, Filipp FV. Cancer Systems Biology of TCGA SKCM: Efficient Detection of Genomic Drivers in Melanoma. *Sci Rep* (2015) 5:7857. doi: 10.1038/srep07857
27. Appenzeller S, Gesierich A, Thiem A, Hufnagel A, Jessen C, Kneitz H, et al. The Identification of Patient-Specific Mutations Reveals Dual Pathway Activation in Most Patients With Melanoma and Activated Receptor Tyrosine Kinases in BRAF/NRAS Wild-Type Melanomas. *Cancer* (2019) 125(4):586–600. doi: 10.1002/cncr.31843
28. Leonardi GC, Falzone L, Salemi R, Zanghi A, Spandidos DA, McCubrey JA, et al. Cutaneous Melanoma: From Pathogenesis to Therapy (Review). *Int J Oncol* (2018) 52(4):1071–80. doi: 10.3892/ijo.2018.4287
29. Hayes TK, Luo F, Cohen O, Goodale AB, Lee Y, Pantel S, et al. A Functional Landscape of Resistance to MEK1/2 and CDK4/6 Inhibition in NRAS-Mutant Melanoma. *Cancer Res* (2019) 79(9):2352–66. doi: 10.1158/0008-5472.CAN-18-2711
30. Yin C, Zhu B, Zhang T, Liu T, Chen S, Liu Y, et al. Pharmacological Targeting of STK19 Inhibits Oncogenic Nras-Driven Melanomagenesis. *Cell* (2019) 176(5):1113–27.e16. doi: 10.1016/j.cell.2019.01.002
31. Gutierrez-Castaneda LD, Nova JA, Tovar-Parra JD. Frequency of Mutations in BRAF, NRAS, and KIT in Different Populations and Histological Subtypes of Melanoma: A Systemic Review. *Melanoma Res* (2020) 30(1):62–70. doi: 10.1097/CMR.0000000000000628
32. Li Y, Umbach DM, Li L. Putative Genomic Characteristics of BRAF V600K Versus V600E Cutaneous Melanoma. *Melanoma Res* (2017) 27(6):527–35. doi: 10.1097/CMR.0000000000000388
33. Marconcini R, Galli L, Antonuzzo A, Bursi S, Roncella C, Fontanini G, et al. Metastatic BRAF K601E-Mutated Melanoma Reaches Complete Response to MEK Inhibitor Trametinib Administered for Over 36 Months. *Exp Hematol Oncol* (2017) 6:6. doi: 10.1186/s40164-017-0067-4
34. Bai X, Kong Y, Chi Z, Sheng X, Cui C, Wang X, et al. Mapk Pathway and TERT Promoter Gene Mutation Pattern and Its Prognostic Value in Melanoma Patients: A Retrospective Study of 2,793 Cases. *Clin Cancer Res* (2017) 23(20):6120–7. doi: 10.1158/1078-0432.CCR-17-0980
35. Consoli F, Barbieri G, Picciolini M, Medicina D, Bugatti M, Tovazzi V, et al. A Rare Complex BRAF Mutation Involving Codon V600 and K601 in Primary Cutaneous Melanoma: Case Report. *Front Oncol* (2020) 10:1056. doi: 10.3389/fonc.2020.01056
36. Burd CE, Liu W, Huynh MV, Waqas MA, Gillahan JE, Clark KS, et al. Mutation-Specific RAS Oncogenicity Explains NRAS Codon 61 Selection in Melanoma. *Cancer Discovery* (2014) 4(12):1418–29. doi: 10.1158/2159-8290.CD-14-0729
37. Del Bianco P, Stagni C, Giunco S, Fabozzi A, Elefanti L, Pellegrini S, et al. Tert Promoter Mutations Differently Correlate With the Clinical Outcome of MAPK Inhibitor-Treated Melanoma Patients. *Cancers (Basel)* (2020) 12(4):946. doi: 10.3390/cancers12040946
38. Hodis E, Watson IR, Kryukov GV, Arold ST, Imielinski M, Theurillat JP, et al. A Landscape of Driver Mutations in Melanoma. *Cell* (2012) 150(2):251–63. doi: 10.1016/j.cell.2012.06.024
39. Livingstone E, Zaremba A, Horn S, Ugurel S, Casalini B, Schlaak M, et al. GNAQ and GNA11 Mutant Nonuveal Melanoma: A Subtype Distinct From Both Cutaneous and Uveal Melanoma. *Br J Dermatol* (2020) 183(5):928–39. doi: 10.1111/bjd.18947
40. Gottesdiener LS, O'Connor S, Busam KJ, Won H, Solit DB, Hyman DM, et al. Rates of ERBB2 Alterations Across Melanoma Subtypes and a Complete Response to Trastuzumab Emtansine in an ERBB2-Amplified Acral Melanoma. *Clin Cancer Res* (2018) 24(23):5815–9. doi: 10.1158/1078-0432.CCR-18-1397
41. Lau C, Killian KJ, Samuels Y, Rudloff U. ERBB4 Mutation Analysis: Emerging Molecular Target for Melanoma Treatment. *Methods Mol Biol* (2014) 1102:461–80. doi: 10.1007/978-1-62703-727-3_24
42. Vanni I, Tanda ET, Dalmasso B, Pastorino L, Andreotti V, Bruno W, et al. Non-BRAF Mutant Melanoma: Molecular Features and Therapeutical Implications. *Front Mol Biosci* (2020) 7:172. doi: 10.3389/fmolb.2020.00172
43. Krauthammer M, Kong Y, Ha BH, Evans P, Bacchiocchi A, McCusker JP, et al. Exome Sequencing Identifies Recurrent Somatic RAC1 Mutations in Melanoma. *Nat Genet* (2012) 44(9):1006–14. doi: 10.1038/ng.2359
44. De P, Aske JC, Dey N. Rac1 Takes the Lead in Solid Tumors. *Cells* (2019) 8(5):382. doi: 10.3390/cells8050382
45. Tetu P, Delyon J, Andre J, Reger de Moura C, Sabbah M, Ghanem GE, et al. Fgf2 Induces Resistance to Nilotinib Through MAPK Pathway Activation in KIT Mutated Melanoma. *Cancers (Basel)* (2020) 12(5):1062. doi: 10.3390/cancers12051062
46. Doma V, Barbai T, Beleaua MA, Kovalszky I, Raso E, Timar J, et al. And Pattern of Melanoma in Central Europe. *Pathol Oncol Res* (2020) 26(1):17–22. doi: 10.1007/s12253-019-00788-w
47. Reddy BY, Miller DM, Tsao H. Somatic Driver Mutations in Melanoma. *Cancer* (2017) 123(S11):2104–17. doi: 10.1002/cncr.30593
48. Palmieri G, Colombino M, Casula M, Manca A, Mandala M, Cossu A, et al. Molecular Pathways in Melanomagenesis: What We Learned From Next-Generation Sequencing Approaches. *Curr Oncol Rep* (2018) 20(11):86. doi: 10.1007/s11912-018-0733-7
49. Kiuru M, Busam KJ. The NF1 Gene in Tumor Syndromes and Melanoma. *Lab Invest* (2017) 97(2):146–57. doi: 10.1038/labinvest.2016.142
50. Davis EJ, Johnson DB, Sosman JA, Chandra S. Melanoma: What do All the Mutations Mean? *Cancer* (2018) 124(17):3490–9. doi: 10.1002/cncr.31345
51. Ascierto PA, Agarwala SS, Botti G, Budillon A, Davies MA, Dummer R, et al. Perspectives in Melanoma: Meeting Report From the Melanoma Bridge (November 29th-1 December 1st, 2018, Naples, Italy). *J Transl Med* (2019) 17(1):234. doi: 10.1186/s12967-019-1979-z
52. Haluska FG, Tsao H, Wu H, Haluska FS, Lazar A, Goel V. Genetic Alterations in Signaling Pathways in Melanoma. *Clin Cancer Res* (2006) 12(7 Pt 2):2301s–7s. doi: 10.1158/1078-0432.CCR-05-2518
53. Stahl JM, Cheung M, Sharma A, Trivedi NR, Shanmugam S, Robertson GP. Loss of PTEN Promotes Tumor Development in Malignant Melanoma. *Cancer Res* (2003) 63(11):2881–90.
54. Cabrita R, Mitra S, Sanna A, Ekedahl H, Lovgren K, Olsson H, et al. The Role of PTEN Loss in Immune Escape, Melanoma Prognosis and Therapy Response. *Cancers (Basel)* (2020) 12(3):742. doi: 10.3390/cancers12030742

55. Radvanyi LG, Bernatchez C, Zhang M, Fox PS, Miller P, Chacon J, et al. Specific Lymphocyte Subsets Predict Response to Adoptive Cell Therapy Using Expanded Autologous Tumor-Infiltrating Lymphocytes in Metastatic Melanoma Patients. *Clin Cancer Res* (2012) 18(24):6758–70. doi: 10.1158/1078-0432.CCR-12-1177
56. Larkin J, Chiarion-Sileni V, Gonzalez R, Grob JJ, Cowey CL, Lao CD, et al. Combined Nivolumab and Ipilimumab or Monotherapy in Untreated Melanoma. *N Engl J Med* (2015) 373(1):23–34. doi: 10.1056/NEJMoa1504030
57. Peng W, Chen JQ, Liu C, Malu S, Creasy C, Tetzlaff MT, et al. Loss of PTEN Promotes Resistance to T Cell-Mediated Immunotherapy. *Cancer Discovery* (2016) 6(2):202–16. doi: 10.1158/2159-8290.CD-15-0283
58. Richetta AG, Valentini V, Marraffa F, Paolino G, Rizzolo P, Silvestri V, et al. Metastases Risk in Thin Cutaneous Melanoma: Prognostic Value of Clinical-Pathologic Characteristics and Mutation Profile. *Oncotarget* (2018) 9 (63):32173–81. doi: 10.18632/oncotarget.25864
59. Francisco G, Ramos Cirilo PD, Toledo Gonçalves F, Tortelli Junior TC, Chammas R. Melanoma Genetics: From Susceptibility to Progression. *Melanoma - From Early Detection to Treatment: Intech Open Sci* (2013). doi: 10.5772/54143
60. Krayem M, Sabbah M, Najem A, Wouters A, Lardon F, Simon S, et al. The Benefit of Reactivating p53 Under MAPK Inhibition on the Efficacy of Radiotherapy in Melanoma. *Cancers (Basel)* (2019) 11(8):1093. doi: 10.3390/cancers11081093
61. Xiao W, Du N, Huang T, Guo J, Mo X, Yuan T, et al. Tp53 Mutation as Potential Negative Predictor for Response of Anti-CTLA-4 Therapy in Metastatic Melanoma. *EBioMedicine* (2018) 32:119–24. doi: 10.1016/j.ebiom.2018.05.019
62. Rabbie R, Ferguson P, Molina-Aguilar C, Adams DJ, Robles-Espinoza CD. Melanoma Subtypes: Genomic Profiles, Prognostic Molecular Markers and Therapeutic Possibilities. *J Pathol* (2019) 247(5):539–51. doi: 10.1002/path.5213
63. Bauer J, Buttner P, Murali R, Okamoto I, Kolaitis NA, Landi MT, et al. BRAF Mutations in Cutaneous Melanoma are Independently Associated With Age, Anatomic Site of the Primary Tumor, and the Degree of Solar Elastosis At the Primary Tumor Site. *Pigment Cell Melanoma Res* (2011) 24(2):345–51. doi: 10.1111/j.1755-148X.2011.00837.x
64. Devitt B, Liu W, Salemi R, Wolfe R, Kelly J, Tzen CY, et al. Clinical Outcome and Pathological Features Associated With NRAS Mutation in Cutaneous Melanoma. *Pigment Cell Melanoma Res* (2011) 24(4):666–72. doi: 10.1111/j.1755-148X.2011.00873.x
65. Curtin JA, Busam K, Pinkel D, Bastian BC. Somatic Activation of KIT in Distinct Subtypes of Melanoma. *J Clin Oncol* (2006) 24(26):4340–6. doi: 10.1200/JCO.2006.06.2984
66. Yang K, Oak ASW, Slominski RM, Brozyna AA, Slominski AT. Current Molecular Markers of Melanoma and Treatment Targets. *Int J Mol Sci* (2020) 21(10):3535. doi: 10.3390/ijms21103535
67. Massi D, Simi L, Sensi E, Baroni G, Xue G, Scatena C, et al. Immunohistochemistry is Highly Sensitive and Specific for the Detection of NRASQ61R Mutation in Melanoma. *Mod Pathol* (2015) 28(4):487–97. doi: 10.1038/modpathol.2014.137
68. Long GV, Menzies AM, Nagrial AM, Haydu LE, Hamilton AL, Mann GJ, et al. Prognostic and Clinicopathologic Associations of Oncogenic BRAF in Metastatic Melanoma. *J Clin Oncol* (2011) 29(10):1239–46. doi: 10.1200/JCO.2010.32.4327
69. Ribas A, Flaherty KT. BRAF Targeted Therapy Changes the Treatment Paradigm in Melanoma. *Nat Rev Clin Oncol* (2011) 8(7):426–33. doi: 10.1038/nrclinonc.2011.69
70. Mar VJ, Liu W, Devitt B, Wong SQ, Dobrovic A, McArthur GA, et al. The Role of BRAF Mutations in Primary Melanoma Growth Rate and Survival. *Br J Dermatol* (2015) 173(1):76–82. doi: 10.1111/bjd.13756
71. Nagore E, Requena C, Traves V, Guillen C, Hayward NK, Whiteman DC, et al. Prognostic Value of BRAF Mutations in Localized Cutaneous Melanoma. *J Am Acad Dermatol* (2014) 70(5):858–62.e1-2. doi: 10.1016/j.jaad.2013.10.064
72. Falanga A, Marchetti M, Massi D, Merelli B, Verzeroli C, Russo L, et al. Thrombophilic Status may Predict Prognosis in Patients With Metastatic BRAFV600-Mutated Melanoma Who Are Receiving BRAF Inhibitors. *J Am Acad Dermatol* (2016) 74(6):1254–6.e4. doi: 10.1016/j.jaad.2015.11.006
73. Scatena C, Franceschi S, Franzini M, Sanguinetti C, Romiti N, Caponi L, et al. Dabrafenib and Trametinib Prolong Coagulation Through the Inhibition of Tissue Factor in BRAF(v600e) Mutated Melanoma Cells In Vitro. *Cancer Cell Int* (2019) 19:223. doi: 10.1186/s12935-019-0938-3
74. Akslen LA, Angelini S, Straume O, Bachmann IM, Molven A, Hemminki K, et al. BRAF and NRAS Mutations Are Frequent in Nodular Melanoma But are Not Associated With Tumor Cell Proliferation or Patient Survival. *J Invest Dermatol* (2005) 125(2):312–7. doi: 10.1111/j.0022-202X.2005.23788.x
75. Ellerhorst JA, Greene VR, Ekmekcioglu S, Warneke CL, Johnson MM, Cooke CP, et al. Clinical Correlates of NRAS and BRAF Mutations in Primary Human Melanoma. *Clin Cancer Res* (2011) 17(2):229–35. doi: 10.1158/1078-0432.CCR-10-2276
76. Omholt K, Platz A, Kanter L, Ringborg U, Hansson J. NRAS and BRAF Mutations Arise Early During Melanoma Pathogenesis and Are Preserved Throughout Tumor Progression. *Clin Cancer Res* (2003) 9(17):6483–8.
77. Platz A, Egyhazi S, Ringborg U, Hansson J. Human Cutaneous Melanoma; a Review of NRAS and BRAF Mutation Frequencies in Relation to Histogenetic Subclass and Body Site. *Mol Oncol* (2008) 1(4):395–405. doi: 10.1016/j.molonc.2007.12.003
78. Ugurel S, Thirumaran RK, Bloethner S, Gast A, Sucker A, Mueller-Berghaus J, et al. B-RAF and N-RAS Mutations are Preserved During Short Time In Vitro Propagation and Differentially Impact Prognosis. *PloS One* (2007) 2 (2):e236. doi: 10.1371/journal.pone.0000236
79. Carlino MS, Haydu LE, Kakavand H, Menzies AM, Hamilton AL, Yu B, et al. Correlation of BRAF and NRAS Mutation Status With Outcome, Site of Distant Metastasis and Response to Chemotherapy in Metastatic Melanoma. *Br J Cancer* (2014) 111(2):292–9. doi: 10.1038/bjc.2014.287
80. Sini MC, Doneddu V, Paliogiannis P, Casula M, Colombino M, Manca A, et al. Genetic Alterations in Main Candidate Genes During Melanoma Progression. *Oncotarget* (2018) 9(9):8531–41. doi: 10.18632/oncotarget.23989
81. Alrabadi N, Gibson N, Curless K, Cheng L, Kuhar M, Chen S, et al. Detection of Driver Mutations in BRAF can Aid in Diagnosis and Early Treatment of Dedifferentiated Metastatic Melanoma. *Mod Pathol* (2019) 32(3):330–7. doi: 10.1038/s41379-018-0161-0
82. Hertz DL, McLeod HL. Integrated Patient and Tumor Genetic Testing for Individualized Cancer Therapy. *Clin Pharmacol Ther* (2016) 99(2):143–6. doi: 10.1002/cpt.294
83. Manca A, Paliogiannis P, Colombino M, Casula M, Lissia A, Botti G, et al. Mutational Concordance Between Primary and Metastatic Melanoma: A Next-Generation Sequencing Approach. *J Transl Med* (2019) 17(1):289. doi: 10.1186/s12967-019-2039-4
84. Shain AH, Yeh I, Kovalyshyn I, Sriharan A, Talevich E, Gagnon A, et al. The Genetic Evolution of Melanoma From Precursor Lesions. *N Engl J Med* (2015) 373(20):1926–36. doi: 10.1056/NEJMoa1502583
85. Wiesner T, Kutzner H, Cerroni L, Mihm MC Jr, Busam KJ, Murali R. Genomic Aberrations in Spitzoid Melanocytic Tumours and Their Implications for Diagnosis, Prognosis and Therapy. *Pathology* (2016) 48 (2):113–31. doi: 10.1016/j.pathol.2015.12.007
86. Dimonitsas E, Liakea A, Sakellariou S, Thymara I, Giannopoulos A, Stratigos A, et al. An Update on Molecular Alterations in Melanocytic Tumors With Emphasis on Spitzoid Lesions. *Ann Transl Med* (2018) 6(12):249. doi: 10.21037/atm.2018.05.23
87. Fattore L, Costantini S, Malpicci D, Ruggiero CF, Ascierto PA, Croce CM, et al. MicroRNAs in Melanoma Development and Resistance to Target Therapy. *Oncotarget* (2017) 8(13):22262–78. doi: 10.18632/oncotarget.14763
88. Diana A, Gaido G, Murtas D. Microrna Signature in Human Normal and Tumoral Neural Stem Cells. *Int J Mol Sci* (2019) 20(17):4123. doi: 10.3390/ijms20174123
89. Xu Y, Brenn T, Brown ER, Doherty V, Melton DW. Differential Expression of microRNAs During Melanoma Progression: miR-200c, miR-205 and miR-211 are Downregulated in Melanoma and Act as Tumour Suppressors. *Br J Cancer* (2012) 106(3):553–61. doi: 10.1038/bjc.2011.568
90. Gajos-Michniewicz A, Czyz M. Role of miRNAs in Melanoma Metastasis. *Cancers (Basel)* (2019) 11(3):326. doi: 10.3390/cancers11030326
91. Neagu M, Constantin C, Cretoiu SM, Zurac S. miRNAs in the Diagnosis and Prognosis of Skin Cancer. *Front Cell Dev Biol* (2020) 8:71. doi: 10.3389/fcell.2020.00071

92. Fomeshi MR, Ebrahimi M, Mowla SJ, Khosravani P, Firouzi J, Khayatzadeh H. Evaluation of the Expressions Pattern of miR-10b, 21, 200c, 373 and 520c to Find the Correlation Between Epithelial-to-Mesenchymal Transition and Melanoma Stem Cell Potential in Isolated Cancer Stem Cells. *Cell Mol Biol Lett* (2015) 20(3):448–65. doi: 10.1515/cmble-2015-0025
93. Romano G, Kwong LN. Mirnas, Melanoma and Microenvironment: An Intricate Network. *Int J Mol Sci* (2017) 18(11):2354. doi: 10.3390/ijms18112354
94. Komina A, Palkina N, Aksenenko M, Tsyrenzhapova S, Ruksha T. Antiproliferative and Pro-Apoptotic Effects of MiR-4286 Inhibition in Melanoma Cells. *PloS One* (2016) 11(12):e0168229. doi: 10.1371/journal.pone.0168229
95. Segura MF, Belitskaya-Levy I, Rose AE, Zakrzewski J, Gaziel A, Hanniford D, et al. Melanoma MicroRNA Signature Predicts Post-Recurrence Survival. *Clin Cancer Res* (2010) 16(5):1577–86. doi: 10.1158/1078-0432.CCR-09-2721
96. Bandarchi B, Jabbari CA, Vedadi A, Navab R. Molecular Biology of Normal Melanocytes and Melanoma Cells. *J Clin Pathol* (2013) 66(8):644–8. doi: 10.1136/jclinpath-2013-201471
97. Babapoor S, Horwich M, Wu R, Levinson S, Gandhi M, Makkar H, et al. microRNA in Situ Hybridization for miR-211 Detection as an Ancillary Test in Melanoma Diagnosis. *Mod Pathol* (2016) 29(5):461–75. doi: 10.1038/modpathol.2016.44
98. Wozniak M, Sztiller-Sikorska M, Czyz M. Expression of miRNAs as Important Element of Melanoma Cell Plasticity in Response to Microenvironmental Stimuli. *Anticancer Res* (2015) 35(5):2747–58.
99. Couts KL, Anderson EM, Gross MM, Sullivan K, Ahn NG. Oncogenic B-Raf Signaling in Melanoma Cells Controls a Network of microRNAs With Combinatorial Functions. *Oncogene* (2013) 32(15):1959–70. doi: 10.1038/onc.2012.209
100. Varrone F, Caputo E. The Mirnas Role in Melanoma and in Its Resistance to Therapy. *Int J Mol Sci* (2020) 21(3):878. doi: 10.3390/ijms21030878
101. Gandini S, Sera F, Cattaruzza MS, Pasquini P, Zanetti R, Masini C, et al. Meta-Analysis of Risk Factors for Cutaneous Melanoma: III. Family History, Actinic Damage and Phenotypic Factors. *Eur J Cancer* (2005) 41(14):2040–59. doi: 10.1016/j.ejca.2005.03.034
102. Bishop JN, Harland M, Randerson-Moor J, Bishop DT. Management of Familial Melanoma. *Lancet Oncol* (2007) 8(1):46–54. doi: 10.1016/S1470-2045(06)71010-5
103. de Snoo FA, Kroon MW, Bergman W, ter Huurne JA, Houwing-Duistermaat JJ, van Mourik L, et al. From Sporadic Atypical Nevi to Familial Melanoma: Risk Analysis for Melanoma in Sporadic Atypical Nevus Patients. *J Am Acad Dermatol* (2007) 56(5):748–52. doi: 10.1016/j.jaad.2007.01.010
104. Han JS, Kim YG, Kim S, Lee MC, Lee JS, Kim SH. Bone Scintigraphy in Acute Renal Failure With Severe Loin Pain and Patchy Renal Vasoconstriction. *Nephron* (1991) 59(2):254–60. doi: 10.1159/000186561
105. Chiarugi A, Nardini P, Borgognoni L, Brandani P, Crocetti E, Carli P. Clinico-Pathological Characteristics of Familial Melanoma in a Mediterranean Population. *Melanoma Res* (2008) 18(5):367–9. doi: 10.1097/CMR.0b013e32830d833b
106. Florell SR, Boucher KM, Garibotti G, Astle J, Kerber R, Mineau G, et al. Population-Based Analysis of Prognostic Factors and Survival in Familial Melanoma. *J Clin Oncol* (2005) 23(28):7168–77. doi: 10.1200/JCO.2005.11.999
107. Kopf AW, Hellman LJ, Rogers GS, Gross DF, Rigel DS, Friedman RJ, et al. Familial Malignant Melanoma. *JAMA* (1986) 256(14):1915–9. doi: 10.1001/jama.256.14.1915
108. Landi MT, Baccarelli A, Tarone RE, Pesatori A, Tucker MA, Hedayati M, et al. DNA Repair, Dysplastic Nevi, and Sunlight Sensitivity in the Development of Cutaneous Malignant Melanoma. *J Natl Cancer Inst* (2002) 94(2):94–101. doi: 10.1093/jnci/94.2.94
109. Raimondi S, Sera F, Gandini S, Iodice S, Caini S, Maisonneuve P, et al. MC1R Variants, Melanoma and Red Hair Color Phenotype: A Meta-Analysis. *Int J Cancer* (2008) 122(12):2753–60. doi: 10.1002/ijc.23396
110. Chiarugi A, Nardini P, Crocetti E, Carli P, De Giorgi V, Borgognoni L, et al. Familial and Sporadic Melanoma: Different Clinical and Histopathological Features in the Italian Population - a Multicentre Epidemiological Study - by GIPMe (Italian Multidisciplinary Group on Melanoma). *J Eur Acad Dermatol Venereol* (2012) 26(2):194–9. doi: 10.1111/j.1468-3083.2011.04035.x
111. Nagore E, Botella-Estrada R, Garcia-Casado Z, Requena C, Serra-Guillen C, Llombart B, et al. Comparison Between Familial and Sporadic Cutaneous Melanoma in Valencia, Spain. *J Eur Acad Dermatol Venereol* (2008) 22(8):931–6. doi: 10.1111/j.1468-3083.2008.02682.x
112. Lucchina LC, Barnhill RL, Duke DM, Sober AJ. Familial Cutaneous Melanoma. *Melanoma Res* (1995) 5(6):413–8. doi: 10.1097/00008390-199512000-00004
113. Barnhill RL, Roush GC, Titus-Ernstoff L, Ernstoff MS, Duray PH, Kirkwood JM. Comparison of Nonfamilial and Familial Melanoma. *Dermatology* (1992) 184(1):2–7. doi: 10.1159/000247489
114. Newton-Bishop JA, Chang YM, Iles MM, Taylor JC, Bakker B, Chan M, et al. Melanocytic Nevi, Nevus Genes, and Melanoma Risk in a Large Case-Control Study in the United Kingdom. *Cancer Epidemiol Biomarkers Prev* (2010) 19(8):2043–54. doi: 10.1158/1055-9965.EPI-10-0233
115. Massi D, Carli P, Franchi A, Santucci M. Naevus-Associated Melanomas: Cause or Chance? *Melanoma Res* (1999) 9(1):85–91. doi: 10.1097/00008390-199902000-00011
116. Ferrone CR, Ben Porat L, Panageas KS, Berwick M, Halpern AC, Patel A, et al. Clinicopathological Features of and Risk Factors for Multiple Primary Melanomas. *JAMA* (2005) 294(13):1647–54. doi: 10.1001/jama.294.13.1647
117. Puntervoll HE, Yang XR, Vetti HH, Bachmann IM, Avril MF, Benfodda M, et al. Melanoma Prone Families With CDK4 Germline Mutation: Phenotypic Profile and Associations With MC1R Variants. *J Med Genet* (2013) 50(4):264–70. doi: 10.1136/jmedgenet-2012-101455
118. Rossi M, Pellegrini C, Cardelli L, Ciciarelli V, Di Nardo L, Fargnoli MC. Familial Melanoma: Diagnostic and Management Implications. *Dermatol Pract Concept* (2019) 9(1):10–6. doi: 10.5826/dpc.0901a03
119. Casula M, Paliogiannis P, Ayala F, De Giorgi V, Stanganelli I, Mandala M, et al. Germline and Somatic Mutations in Patients With Multiple Primary Melanomas: A Next Generation Sequencing Study. *BMC Cancer* (2019) 19(1):772. doi: 10.1186/s12885-019-5984-7
120. Goldstein AM, Chan M, Harland M, Hayward NK, Demenais F, Bishop DT, et al. Features Associated With Germline CDKN2A Mutations: A GenoMEL Study of Melanoma-Prone Families From Three Continents. *J Med Genet* (2007) 44(2):99–106. doi: 10.1136/jmg.2006.043802
121. Potrony M, Badenas C, Aguilera P, Puig-Butille JA, Carrera C, Malvehy J, et al. Update in Genetic Susceptibility in Melanoma. *Ann Transl Med* (2015) 3(15):210. doi: 10.3978/j.issn.2305-5839.2015.08.11
122. Huber J, Ramos ES. The P48T Germline Mutation and Polymorphism in the CDKN2A Gene of Patients With Melanoma. *Braz J Med Biol Res* (2006) 39(2):237–41. doi: 10.1590/S0100-879X2006000200010
123. Horn S, Figl A, Rachakonda PS, Fischer C, Sucker A, Gast A, et al. TERT Promoter Mutations in Familial and Sporadic Melanoma. *Science* (2013) 339(6122):959–61. doi: 10.1126/science.1230062
124. Lightbody G, Haberland V, Browne F, Taggart L, Zheng H, Parkes E, et al. Review of Applications of High-Throughput Sequencing in Personalized Medicine: Barriers and Facilitators of Future Progress in Research and Clinical Application. *Brief Bioinform* (2019) 20(5):1795–811. doi: 10.1093/bib/bby051
125. Haraksingh RR, Snyder MP. Impacts of Variation in the Human Genome on Gene Regulation. *J Mol Biol* (2013) 425(21):3970–7. doi: 10.1016/j.jmb.2013.07.015
126. Consortium EP. An Integrated Encyclopedia of DNA Elements in the Human Genome. *Nature* (2012) 489(7414):57–74. doi: 10.1038/nature11247
127. Consortium EP, Birney E, Stamatoyannopoulos JA, Dutta A, Guigo R, Gingeras TR, et al. Identification and Analysis of Functional Elements in 1% of the Human Genome by the ENCODE Pilot Project. *Nature* (2007) 447(7146):799–816. doi: 10.1038/nature05874
128. Lappalainen T, Sammeth M, Friedlander MR, t Hoen PA, Monlong J, Rivas MA, et al. Transcriptome and Genome Sequencing Uncovers Functional Variation in Humans. *Nature* (2013) 501(7468):506–11. doi: 10.1038/nature12531
129. Jiang Z, Zhou X, Li R, Michal JJ, Zhang S, Dodson MV, et al. Whole Transcriptome Analysis With Sequencing: Methods, Challenges and Potential Solutions. *Cell Mol Life Sci* (2015) 72(18):3425–39. doi: 10.1007/s00018-015-1934-y

130. Stark R, Grzelak M, Hadfield J. RNA Sequencing: The Teenage Years. *Nat Rev Genet* (2019) 20(11):631–56. doi: 10.1038/s41576-019-0150-2
131. Krzyszczyk P, Acevedo A, Davidoff EJ, Timmins LM, Marrero-Berrios I, Patel M, et al. The Growing Role of Precision and Personalized Medicine for Cancer Treatment. *Technol (Singap World Sci)* (2018) 6(3-4):79–100. doi: 10.1142/S2339547818300020
132. Mardis ER. Next-Generation DNA Sequencing Methods. *Annu Rev Genomics Hum Genet* (2008) 9:387–402. doi: 10.1146/annurev.genom.9.081307.164359
133. Haimovich AD. Methods, Challenges, and Promise of Next-Generation Sequencing in Cancer Biology. *Yale J Biol Med* (2011) 84(4):439–46.
134. Metzker ML. Sequencing Technologies - the Next Generation. *Nat Rev Genet* (2010) 11(1):31–46. doi: 10.1038/nrg2626
135. Le Gallo M, Lozy F, Bell DW. Next-Generation Sequencing. *Adv Exp Med Biol* (2017) 943:119–48. doi: 10.1007/978-3-319-43139-0_5
136. Kawazoe A, Shitara K. Next-Generation Sequencing and Biomarkers for Gastric Cancer: What is the Future? *Ther Adv Med Oncol* (2019) 11:1758835919848189. doi: 10.1177/1758835919848189
137. Lionetti M, Neri A. Utilizing Next-Generation Sequencing in the Management of Multiple Myeloma. *Expert Rev Mol Diagn* (2017) 17(7):653–63. doi: 10.1080/14737159.2017.1332996
138. van Dijk EL, Jaszczyszyn Y, Thermes C. Library Preparation Methods for Next-Generation Sequencing: Tone Down the Bias. *Exp Cell Res* (2014) 322(1):12–20. doi: 10.1016/j.yexcr.2014.01.008
139. Feng K, Costa J, Edwards JS. Next-Generation Sequencing Library Construction on a Surface. *BMC Genomics* (2018) 19(1):416. doi: 10.1186/s12864-018-4797-4
140. Kunz M, Dannemann M, Kelso J. High-Throughput Sequencing of the Melanoma Genome. *Exp Dermatol* (2013) 22(1):10–7. doi: 10.1111/exd.12054
141. Kircher M, Kelso J. High-Throughput DNA Sequencing–Concepts and Limitations. *Bioessays* (2010) 32(6):524–36. doi: 10.1002/bies.200900181
142. NovaSeq 6000 System - Illumina. Available at: https://www.illumina.com/systems/sequencing-platforms/novaseq.html.
143. Lawrence MS, Stojanov P, Polak P, Kryukov GV, Cibulskis K, Sivachenko A, et al. Mutational Heterogeneity in Cancer and the Search for New Cancer-Associated Genes. *Nature* (2013) 499(7457):214–8. doi: 10.1038/nature12213
144. Pleasance ED, Cheetham RK, Stephens PJ, McBride DJ, Humphray SJ, Greenman CD, et al. A Comprehensive Catalogue of Somatic Mutations From a Human Cancer Genome. *Nature* (2010) 463(7278):191–6. doi: 10.1038/nature08658
145. Greenman C, Stephens P, Smith R, Dalgliesh GL, Hunter C, Bignell G, et al. Patterns of Somatic Mutation in Human Cancer Genomes. *Nature* (2007) 446(7132):153–8. doi: 10.1038/nature05610
146. Alexandrov LB, Nik-Zainal S, Wedge DC, Aparicio SA, Behjati S, Biankin AV, et al. Signatures of Mutational Processes in Human Cancer. *Nature* (2013) 500(7463):415–21. doi: 10.1038/nature12477
147. Garrido-Cardenas JA, Garcia-Maroto F, Alvarez-Bermejo JA, Manzano-Agugliaro F. Dna Sequencing Sensors: An Overview. *Sensors (Basel)* (2017) 17(3):588. doi: 10.3390/s17030588
148. Merriman B, Ion Torrent R, Team D, Rothberg JM. Progress in Ion Torrent Semiconductor Chip Based Sequencing. *Electrophoresis* (2012) 33(23):3397–417. doi: 10.1002/elps.201200424
149. Margulies M, Egholm M, Altman WE, Attiya S, Bader JS, Bemben LA, et al. Genome Sequencing in Microfabricated High-Density Picolitre Reactors. *Nature* (2005) 437(7057):376–80. doi: 10.1038/nature03959
150. Curry JL, Torres-Cabala CA, Tetzlaff MT, Bowman C, Prieto VG. Molecular Platforms Utilized to Detect BRAF V600E Mutation in Melanoma. *Semin Cutan Med Surg* (2012) 31(4):267–73. doi: 10.1016/j.sder.2012.07.007
151. Halait H, Demartin K, Shah S, Soviero S, Langland R, Cheng S, et al. Analytical Performance of a Real-Time PCR-Based Assay for V600 Mutations in the BRAF Gene, Used as the Companion Diagnostic Test for the Novel BRAF Inhibitor Vemurafenib in Metastatic Melanoma. *Diagn Mol Pathol* (2012) 21(1):1–8. doi: 10.1097/PDM.0b013e31823b216f
152. Anderson S, Bloom KJ, Vallera DU, Rueschoff J, Meldrum C, Schilling R, et al. Multisite Analytic Performance Studies of a Real-Time Polymerase Chain Reaction Assay for the Detection of BRAF V600E Mutations in Formalin-Fixed, Paraffin-Embedded Tissue Specimens of Malignant Melanoma. *Arch Pathol Lab Med* (2012) 136(11):1385–91. doi: 10.5858/arpa.2011-0505-OA
153. Lopez-Rios F, Angulo B, Gomez B, Mair D, Martinez R, Conde E, et al. Comparison of Testing Methods for the Detection of BRAF V600E Mutations in Malignant Melanoma: Pre-Approval Validation Study of the Companion Diagnostic Test for Vemurafenib. *PloS One* (2013) 8(1):e53733. doi: 10.1371/journal.pone.0053733
154. Amarasinghe SL, Su S, Dong X, Zappia L, Ritchie ME, Gouil Q. Opportunities and Challenges in Long-Read Sequencing Data Analysis. *Genome Biol* (2020) 21(1):30. doi: 10.1186/s13059-020-1935-5
155. Ardui S, Ameur A, Vermeesch JR, Hestand MS. Single Molecule Real-Time (SMRT) Sequencing Comes of Age: Applications and Utilities for Medical Diagnostics. *Nucleic Acids Res* (2018) 46(5):2159–68. doi: 10.1093/nar/gky066
156. Pollard MO, Gurdasani D, Mentzer AJ, Porter T, Sandhu MS. Long Reads: Their Purpose and Place. *Hum Mol Genet* (2018) 27(R2):R234–R41. doi: 10.1093/hmg/ddy177
157. Flusberg BA, Webster DR, Lee JH, Travers KJ, Olivares EC, Clark TA, et al. Direct Detection of DNA Methylation During Single-Molecule, Real-Time Sequencing. *Nat Methods* (2010) 7(6):461–5. doi: 10.1038/nmeth.1459
158. Jain M, Olsen HE, Paten B, Akeson M. The Oxford Nanopore MinION: Delivery of Nanopore Sequencing to the Genomics Community. *Genome Biol* (2016) 17(1):239. doi: 10.1186/s13059-016-1122-x
159. *Precisionfda Truth Challenge V2: Calling Variants From Short and Long Reads in Difficult-to-Map Regions*. Available at: https://precision.fda.gov/challenges/10/view/results.
160. Song CX, Clark TA, Lu XY, Kislyuk A, Dai Q, Turner SW, et al. Sensitive and Specific Single-Molecule Sequencing of 5-Hydroxymethylcytosine. *Nat Methods* (2011) 9(1):75–7. doi: 10.1038/nmeth.1779
161. Head SR, Komori HK, LaMere SA, Whisenant T, Van Nieuwerburgh F, Salomon DR, et al. Library Construction for Next-Generation Sequencing: Overviews and Challenges. *Biotechniques* (2014) 56(2):61–4, 6, 8, passim. doi: 10.2144/000114133
162. Levene MJ, Korlach J, Turner SW, Foquet M, Craighead HG, Webb WW. Zero-Mode Waveguides for Single-Molecule Analysis At High Concentrations. *Science* (2003) 299(5607):682–6. doi: 10.1126/science.1079700
163. Eisenstein M. Oxford Nanopore Announcement Sets Sequencing Sector Abuzz. *Nat Biotechnol* (2012) 30(4):295–6. doi: 10.1038/nbt0412-295
164. Branton D, Deamer DW, Marziali A, Bayley H, Benner SA, Butler T, et al. The Potential and Challenges of Nanopore Sequencing. *Nat Biotechnol* (2008) 26(10):1146–53. doi: 10.1038/nbt.1495
165. Cavelier L, Ameur A, Haggqvist S, Hoijer I, Cahill N, Olsson-Stromberg U, et al. Clonal Distribution of BCR-ABL1 Mutations and Splice Isoforms by Single-Molecule Long-Read RNA Sequencing. *BMC Cancer* (2015) 15:45. doi: 10.1186/s12885-015-1046-y
166. Lode L, Ameur A, Coste T, Menard A, Richebourg S, Gaillard JB, et al. Single-Molecule DNA Sequencing of Acute Myeloid Leukemia and Myelodysplastic Syndromes With Multiple TP53 Alterations. *Haematologica* (2018) 103(1):e13–e6. doi: 10.3324/haematol.2017.176719
167. Gudmundsson S, Wilbe M, Ekvall S, Ameur A, Cahill N, Alexandrov LB, et al. Revertant Mosaicism Repairs Skin Lesions in a Patient With Keratitis-Ichthyosis-Deafness Syndrome by Second-Site Mutations in Connexin 26. *Hum Mol Genet* (2017) 26(6):1070–7. doi: 10.1093/hmg/ddx017
168. Ho SS, Urban AE, Mills RE. Structural Variation in the Sequencing Era. *Nat Rev Genet* (2020) 21(3):171–89. doi: 10.1038/s41576-019-0180-9
169. Chaisson MJ, Huddleston J, Dennis MY, Sudmant PH, Malig M, Hormozdiari F, et al. Resolving the Complexity of the Human Genome Using Single-Molecule Sequencing. *Nature* (2015) 517(7536):608–11. doi: 10.1038/nature13907
170. Bayega A, Wang YC, Oikonomopoulos S, Djambazian H, Fahiminiya S, Ragoussis J. Transcript Profiling Using Long-Read Sequencing Technologies. *Methods Mol Biol* (2018) 1783:121–47. doi: 10.1007/978-1-4939-7834-2_6
171. Boulias K, Greer EL. Detection of DNA Methylation in Genomic DNA by UHPLC-MS/MS. *Methods Mol Biol* (2021) 2198:79–90. doi: 10.1007/978-1-0716-0876-0_7
172. Liu Q, Georgieva DC, Egli D, Wang K. NanoMod: A Computational Tool to Detect DNA Modifications Using Nanopore Long-Read Sequencing Data. *BMC Genomics* (2019) 20(Suppl 1):78. doi: 10.1186/s12864-018-5372-8

173. Wang Y, Navin NE. Advances and Applications of Single-Cell Sequencing Technologies. *Mol Cell* (2015) 58(4):598–609. doi: 10.1016/j.molcel.2015.05.005
174. Ye B, Gao Q, Zeng Z, Stary CM, Jian Z, Xiong X, et al. Single-Cell Sequencing Technology in Oncology: Applications for Clinical Therapies and Research. *Anal Cell Pathol (Amst)* (2016) 2016:9369240. doi: 10.1155/2016/9369240
175. Hu P, Zhang W, Xin H, Deng G. Single Cell Isolation and Analysis. *Front Cell Dev Biol* (2016) 4:116. doi: 10.3389/fcell.2016.00116
176. Wang Y, Waters J, Leung ML, Unruh A, Roh W, Shi X, et al. Clonal Evolution in Breast Cancer Revealed by Single Nucleus Genome Sequencing. *Nature* (2014) 512(7513):155–60. doi: 10.1038/nature13600
177. Grun D, van Oudenaarden A. Design and Analysis of Single-Cell Sequencing Experiments. *Cell* (2015) 163(4):799–810. doi: 10.1016/j.cell.2015.10.039
178. Van Gelder RN, von Zastrow ME, Yool A, Dement WC, Barchas JD, Eberwine JH. Amplified RNA Synthesized From Limited Quantities of Heterogeneous Cdna. *Proc Natl Acad Sci USA* (1990) 87(5):1663–7. doi: 10.1073/pnas.87.5.1663
179. Tang F, Barbacioru C, Wang Y, Nordman E, Lee C, Xu N, et al. mRNA-Seq Whole-Transcriptome Analysis of a Single Cell. *Nat Methods* (2009) 6 (5):377–82. doi: 10.1038/nmeth.1315
180. Ramskold D, Luo S, Wang YC, Li R, Deng Q, Faridani OR, et al. Full-Length mRNA-Seq From Single-Cell Levels of RNA and Individual Circulating Tumor Cells. *Nat Biotechnol* (2012) 30(8):777–82. doi: 10.1038/nbt.2282
181. Picelli S, Bjorklund AK, Faridani OR, Sagasser S, Winberg G, Sandberg R. Smart-Seq2 for Sensitive Full-Length Transcriptome Profiling in Single Cells. *Nat Methods* (2013) 10(11):1096–8. doi: 10.1038/nmeth.2639
182. Hashimshony T, Wagner F, Sher N, Yanai I. Cel-Seq: Single-Cell RNA-Seq by Multiplexed Linear Amplification. *Cell Rep* (2012) 2(3):666–73. doi: 10.1016/j.celrep.2012.08.003
183. Jaitin DA, Kenigsberg E, Keren-Shaul H, Elefant N, Paul F, Zaretsky I, et al. Massively Parallel Single-Cell RNA-seq for Marker-Free Decomposition of Tissues Into Cell Types. *Science* (2014) 343(6172):776–9. doi: 10.1126/science.1247651
184. Zhang X, Li T, Liu F, Chen Y, Yao J, Li Z, et al. Comparative Analysis of Droplet-Based Ultra-High-Throughput Single-Cell Rna-Seq Systems. *Mol Cell* (2019) 73(1):130–42.e5. doi: 10.1016/j.molcel.2018.10.020
185. Ziegenhain C, Vieth B, Parekh S, Reinius B, Guillaumet-Adkins A, Smets M, et al. Comparative Analysis of Single-Cell Rna Sequencing Methods. *Mol Cell* (2017) 65(4):631–43 e4. doi: 10.1016/j.molcel.2017.01.023
186. Xin Y, Kim J, Ni M, Wei Y, Okamoto H, Lee J, et al. Use of the Fluidigm C1 Platform for RNA Sequencing of Single Mouse Pancreatic Islet Cells. *Proc Natl Acad Sci USA* (2016) 113(12):3293–8. doi: 10.1073/pnas.1602306113
187. Kolodziejczyk AA, Kim JK, Svensson V, Marioni JC, Teichmann SA. The Technology and Biology of Single-Cell RNA Sequencing. *Mol Cell* (2015) 58 (4):610–20. doi: 10.1016/j.molcel.2015.04.005
188. Valihrach L, Androvic P, Kubista M. Platforms for Single-Cell Collection and Analysis. *Int J Mol Sci* (2018) 19(3):807. doi: 10.3390/ijms19030807
189. Novotny J, Strnadova K, Dvorankova B, Kocourkova S, Jaksa R, Dundr P, et al. Single-Cell RNA Sequencing Unravels Heterogeneity of the Stromal Niche in Cutaneous Melanoma Heterogeneous Spheroids. *Cancers (Basel)* (2020) 12(11):3324. doi: 10.3390/cancers12113324
190. Gerber T, Willscher E, Loeffler-Wirth H, Hopp L, Schadendorf D, Schartl M, et al. Mapping Heterogeneity in Patient-Derived Melanoma Cultures by Single-Cell RNA-Seq. *Oncotarget* (2017) 8(1):846–62. doi: 10.18632/oncotarget.13666
191. Larsson L, Frisen J, Lundeberg J. Spatially Resolved Transcriptomics Adds a New Dimension to Genomics. *Nat Methods* (2021) 18(1):15–8. doi: 10.1038/s41592-020-01038-7
192. Bergenstrahle J, Larsson L, Lundeberg J. Seamless Integration of Image and Molecular Analysis for Spatial Transcriptomics Workflows. *BMC Genomics* (2020) 21(1):482. doi: 10.1186/s12864-020-06832-3
193. Zollinger DR, Lingle SE, Sorg K, Beechem JM, Merritt CR. Geomx RNA Assay: High Multiplex, Digital, Spatial Analysis of RNA in FFPE Tissue. *Methods Mol Biol* (2020) 2148:331–45. doi: 10.1007/978-1-0716-0623-0_21
194. Cabrita R, Lauss M, Sanna A, Donia M, Skaarup Larsen M, Mitra S, et al. Tertiary Lymphoid Structures Improve Immunotherapy and Survival in Melanoma. *Nature* (2020) 577(7791):561–5. doi: 10.1038/s41586-019-1914-8
195. Thrane K, Eriksson H, Maaskola J, Hansson J, Lundeberg J. Spatially Resolved Transcriptomics Enables Dissection of Genetic Heterogeneity in Stage Iii Cutaneous Malignant Melanoma. *Cancer Res* (2018) 78(20):5970–9. doi: 10.1158/0008-5472.CAN-18-0747
196. Ji AL, Rubin AJ, Thrane K, Jiang S, Reynolds DL, Meyers RM, et al. Multimodal Analysis of Composition and Spatial Architecture in Human Squamous Cell Carcinoma. *Cell* (2020) 182(6):1661–2. doi: 10.1016/j.cell.2020.08.043
197. Maniatis S, Petrescu J, Phatnani H. Spatially Resolved Transcriptomics and its Applications in Cancer. *Curr Opin Genet Dev* (2021) 66:70–7. doi: 10.1016/j.gde.2020.12.002
198. Abdel-Rahman WM. Genomic Instability and Carcinogenesis: An Update. *Curr Genomics* (2008) 9(8):535–41. doi: 10.2174/138920208786847926
199. *Bionano Genomics*. Available at: https://bionanogenomics.com.
200. Xu J, Song F, Schleicher E, Pool C, Bann D, Hennessy M, et al. An Integrated Framework for Genome Analysis Reveals Numerous Previously Unrecognizable Structural Variants in Leukemia Patients' Samples. *bioRxiv* (2019). doi: 10.1101/563270
201. Consortium ITP-CAoWG. Pan-Cancer Analysis of Whole Genomes. *Nature* (2020) 578(7793):82–93. doi: 10.1038/s41586-020-1969-6
202. The International Cancer Genome Consortium. Available at: https://icgc.org.
203. Zhang J, Baran J, Cros A, Guberman JM, Haider S, Hsu J, et al. International Cancer Genome Consortium Data Portal–a One-Stop Shop for Cancer Genomics Data. *Database (Oxford)* (2011) 2011:bar026. doi: 10.1093/database/bar026
204. Bamford S, Dawson E, Forbes S, Clements J, Pettett R, Dogan A, et al. The COSMIC (Catalogue of Somatic Mutations in Cancer) Database and Website. *Br J Cancer* (2004) 91(2):355–8. doi: 10.1038/sj.bjc.6601894
205. COSMIC and The Catalogue Of Somatic Mutations In Cancer. Available at: https://cancer.sanger.ac.uk/cosmic.
206. The Cancer Genome Atlas (TCGA). Available at: https://www.cancer.gov/about-nci/organization/ccg/research/structural-genomics/tcga.
207. Cancer Genome Atlas N. Genomic Classification of Cutaneous Melanoma. *Cell* (2015) 161(7):1681–96. doi: 10.1016/j.cell.2015.05.044
208. cBioPortal. Available at: https://www.cbioportal.org.
209. GenoMEL, the Melanoma Genetics Consortium. Available at: https://genomel.org/research/programme-and-aims/.
210. Siroy AE, Boland GM, Milton DR, Roszik J, Frankian S, Malke J, et al. Beyond BRAF(V600): Clinical Mutation Panel Testing by Next-Generation Sequencing in Advanced Melanoma. *J Invest Dermatol* (2015) 135(2):508–15. doi: 10.1038/jid.2014.366
211. Ponti G, Manfredini M, Greco S, Pellacani G, Depenni R, Tomasi A, et al. Braf, NRAS and C-KIT Advanced Melanoma: Clinico-Pathological Features, Targeted-Therapy Strategies and Survival. *Anticancer Res* (2017) 37 (12):7043–8. doi: 10.21873/anticanres.12175
212. Griewank KG, Scolyer RA, Thompson JF, Flaherty KT, Schadendorf D, Murali R. Genetic Alterations and Personalized Medicine in Melanoma: Progress and Future Prospects. *J Natl Cancer Inst* (2014) 106(2):djt435. doi: 10.1093/jnci/djt435
213. Ho AW, Tsao H. Targeted Therapies in Melanoma: Translational Research At Its Finest. *J Invest Dermatol* (2015) 135(8):1929–33. doi: 10.1038/jid.2015.14
214. Malicherova B, Burjanivova T, Minarikova E, Kasubova I, Pecova T, Bobrovska M, et al. Detection of Driver Mutations in FFPE Samples From Patients With Verified Malignant Melanoma. *Neoplasma* (2019) 66(1):33–8. doi: 10.4149/neo_2018_180115N31
215. Cheng L, Lopez-Beltran A, Massari F, MacLennan GT, Montironi R. Molecular Testing for BRAF Mutations to Inform Melanoma Treatment Decisions: A Move Toward Precision Medicine. *Mod Pathol* (2018) 31 (1):24–38. doi: 10.1038/modpathol.2017.104
216. Lokhandwala PM, Tseng LH, Rodriguez E, Zheng G, Pallavajjalla A, Gocke CD, et al. Clinical Mutational Profiling and Categorization of BRAF Mutations in Melanomas Using Next Generation Sequencing. *BMC Cancer* (2019) 19(1):665. doi: 10.1186/s12885-019-5864-1
217. Colomer R, Mondejar R, Romero-Laorden N, Alfranca A, Sanchez-Madrid F, Quintela-Fandino M. When Should We Order a Next Generation Sequencing Test in a Patient With Cancer? *E Clin Med* (2020) 25:100487. doi: 10.1016/j.eclinm.2020.100487
218. Salemi R, Falzone L, Madonna G, Polesel J, Cina D, Mallardo D, et al. MMP-9 as a Candidate Marker of Response to BRAF Inhibitors in Melanoma Patients With Braf(V600e) Mutation Detected in Circulating-Free DNA. *Front Pharmacol* (2018) 9:856. doi: 10.3389/fphar.2018.00856

219. Chapman PB, Hauschild A, Robert C, Haanen JB, Ascierto P, Larkin J, et al. Improved Survival With Vemurafenib in Melanoma With BRAF V600E Mutation. *N Engl J Med* (2011) 364(26):2507–16. doi: 10.1056/NEJMoa1103782
220. Sosman JA, Kim KB, Schuchter L, Gonzalez R, Pavlick AC, Weber JS, et al. Survival in BRAF V600-Mutant Advanced Melanoma Treated With Vemurafenib. *N Engl J Med* (2012) 366(8):707–14. doi: 10.1056/NEJMoa1112302
221. Tomei S, Wang E, Delogu LG, Marincola FM, Bedognetti D. Non-BRAF-Targeted Therapy, Immunotherapy, and Combination Therapy for Melanoma. *Expert Opin Biol Ther* (2014) 14(5):663–86. doi: 10.1517/14712598.2014.890586
222. Merlino G, Herlyn M, Fisher DE, Bastian BC, Flaherty KT, Davies MA, et al. The State of Melanoma: Challenges and Opportunities. *Pigment Cell Melanoma Res* (2016) 29(4):404–16. doi: 10.1111/pcmr.12475
223. Falcone I, Conciatori F, Bazzichetto C, Ferretti G, Cognetti F, Ciuffreda L, et al. Tumor Microenvironment: Implications in Melanoma Resistance to Targeted Therapy and Immunotherapy. *Cancers (Basel)* (2020) 12(10):2870. doi: 10.3390/cancers12102870
224. Kozar I, Margue C, Rothengatter S, Haan C, Kreis S. Many Ways to Resistance: How Melanoma Cells Evade Targeted Therapies. *Biochim Biophys Acta Rev Cancer* (2019) 1871(2):313–22. doi: 10.1016/j.bbcan.2019.02.002
225. Santini CC, Longden J, Schoof EM, Simpson CD, Jeschke GR, Creixell P, et al. Global View of the RAF-MEK-ERK Module and its Immediate Downstream Effectors. *Sci Rep* (2019) 9(1):10865. doi: 10.1038/s41598-019-47245-x
226. Catalanotti F, Cheng DT, Shoushtari AN, Johnson DB, Panageas KS, Momtaz P, et al. Pten Loss-of-Function Alterations Are Associated With Intrinsic Resistance to BRAF Inhibitors in Metastatic Melanoma. *JCO Precis Oncol* (2017) 1. doi: 10.1200/PO.16.00054
227. Vanni I, Tanda ET, Spagnolo F, Andreotti V, Bruno W, Ghiorzo P. The Current State of Molecular Testing in the BRAF-Mutated Melanoma Landscape. *Front Mol Biosci* (2020) 7:113. doi: 10.3389/fmolb.2020.00113
228. Greco A, Safi D, Swami U, Ginader T, Milhem M, Zakharia Y. Efficacy and Adverse Events in Metastatic Melanoma Patients Treated With Combination Braf Plus Mek Inhibitors Versus BRAF Inhibitors: A Systematic Review. *Cancers (Basel)* (2019) 11(12):1950. doi: 10.3390/cancers11121950
229. Tanda ET, Vanni I, Boutros A, Andreotti V, Bruno W, Ghiorzo P, et al. Current State of Target Treatment in BRAF Mutated Melanoma. *Front Mol Biosci* (2020) 7:154. doi: 10.3389/fmolb.2020.00154
230. Wong DJ, Ribas A. Targeted Therapy for Melanoma. *Cancer Treat Res* (2016) 167:251–62. doi: 10.1007/978-3-319-22539-5_10
231. Huynh S, Mortier L, Dutriaux C, Maubec E, Boileau M, Dereure O, et al. Combined Therapy With Anti-PD1 and BRAF and/or MEK Inhibitor for Advanced Melanoma: A Multicenter Cohort Study. *Cancers (Basel)* (2020) 12(6):1666. doi: 10.3390/cancers12061666
232. Andre F, Mardis E, Salm M, Soria JC, Siu LL, Swanton C. Prioritizing Targets for Precision Cancer Medicine. *Ann Oncol* (2014) 25(12):2295–303. doi: 10.1093/annonc/mdu478
233. Kelly PA. Next Generation Sequencing and Multi-Gene Panel Testing: Implications for the Oncology Nurse. *Semin Oncol Nurs* (2017) 33(2):208–18. doi: 10.1016/j.soncn.2017.02.007
234. Diefenbach RJ, Lee JH, Menzies AM, Carlino MS, Long GV, Saw RPM, et al. Design and Testing of a Custom Melanoma Next Generation Sequencing Panel for Analysis of Circulating Tumor Dna. *Cancers (Basel)* (2020) 12(8):2228. doi: 10.3390/cancers12082228
235. Kiniwa Y, Nakamura K, Mikoshiba A, Akiyama Y, Morimoto A, Okuyama R. Diversity of Circulating Tumor Cells in Peripheral Blood: Detection of Heterogeneous BRAF Mutations in a Patient With Advanced Melanoma by Single-Cell Analysis. *J Dermatol Sci* (2018) 90(2):211–3. doi: 10.1016/j.jdermsci.2018.01.011
236. Lai W, Xiao M, Yang H, Li L, Fan C, Pei H. Circularized Blocker-Displacement Amplification for Multiplex Detection of Rare DNA Variants. *Chem Commun (Camb)* (2020) 56(82):12331–4. doi: 10.1039/D0CC05283C
237. OnkoSight. Available at: https://www.genpathdiagnostics.com/hcp/oncology/onkosight-next-generation-sequencing/.
238. NeoTYPE. Available at: https://neogenomics.com/test-menu/neotype-melanoma-profile.
239. SureSeq. Available at: https://www.ogt.com/products/1629_sureseq_mypanel_ngs_custom_melanoma_cancer_panel.
240. Wheler J, Yelensky R, Falchook G, Kim KB, Hwu P, Tsimberidou AM, et al. Next Generation Sequencing of Exceptional Responders With BRAF-mutant Melanoma: Implications for Sensitivity and Resistance. *BMC Cancer* (2015) 15:61. doi: 10.1186/s12885-015-1029-z
241. Kang K, Xie F, Mao J, Bai Y, Wang X. Significance of Tumor Mutation Burden in Immune Infiltration and Prognosis in Cutaneous Melanoma. *Front Oncol* (2020) 10:573141. doi: 10.3389/fonc.2020.573141
242. Ko JS. The Immunology of Melanoma. *Clin Lab Med* (2017) 37(3):449–71. doi: 10.1016/j.cll.2017.06.001
243. Viros A, Fridlyand J, Bauer J, Lasithiotakis K, Garbe C, Pinkel D, et al. Improving Melanoma Classification by Integrating Genetic and Morphologic Features. *PloS Med* (2008) 5(6):e120. doi: 10.1371/journal.pmed.0050120
244. Emens LA, Ascierto PA, Darcy PK, Demaria S, Eggermont AMM, Redmond WL, et al. Cancer Immunotherapy: Opportunities and Challenges in the Rapidly Evolving Clinical Landscape. *Eur J Cancer* (2017) 81:116–29. doi: 10.1016/j.ejca.2017.01.035
245. Herzberg B, Fisher DE. Metastatic Melanoma and Immunotherapy. *Clin Immunol* (2016) 172:105–10. doi: 10.1016/j.clim.2016.07.006
246. Collymore DC, Kobilis SL, Lundquist TG, McGivney WT, Pezalla EJ, Poage W. Genomic Testing in Oncology to Improve Clinical Outcomes While Optimizing Utilization: The Evolution of Diagnostic Testing. *Am J Manag Care* (2016) 22(2 Suppl):s20–5.
247. Rashid OM, Zager JS. Genetic Testing in the Multidisciplinary Management of Melanoma. *Surg Oncol Clin N Am* (2015) 24(4):779–93. doi: 10.1016/j.soc.2015.06.003
248. Woodman SE, Lazar AJ, Aldape KD, Davies MA. New Strategies in Melanoma: Molecular Testing in Advanced Disease. *Clin Cancer Res* (2012) 18(5):1195–200. doi: 10.1158/1078-0432.CCR-11-2317
249. Davies H, Bignell GR, Cox C, Stephens P, Edkins S, Clegg S, et al. Mutations of the BRAF Gene in Human Cancer. *Nature* (2002) 417(6892):949–54. doi: 10.1038/nature00766
250. Palmieri G, Capone M, Ascierto ML, Gentilcore G, Stroncek DF, Casula M, et al. Main Roads to Melanoma. *J Transl Med* (2009) 7:86. doi: 10.1186/1479-5876-7-86

Conflict of Interest: The authors declare that the research was conducted in the absence of any commercial or financial relationships that could be construed as a potential conflict of interest.

GLOSSARY

ACD	ACD Shelterin Complex Subunit and Telomerase Recruitment Factor
AKT	AKT Serine/Threonine Kinase
ALK	Anaplastic Lymphoma Receptor Tyrosine Kinase
ALM	acral lentiginous melanoma
AM	acral melanoma
AML	Acute Myeloblastic Leukemia
ARF	Alternate Reading Frame
ARGO	Accelerate Research in Genomic Oncology
ARID2	AT-rich interaction domain 2
AST	atypical Spitz tumor
ATM	Ataxia telangiectasia mutated
ATR	ataxia telangiectasia and Rad3-related
BAP1	BRCA1 Associated Protein 1
BRAF	B-Raf Proto-Oncogene Serine/Threonine Kinase
CDK4/6	Cyclin-Dependent Kinase 4/6CDKN2A: Cyclin-Dependent Kinase Inhibitor 2A
ChiP-Seq	Chromatin Immunoprecipitation Sequencing
CHK	Checkpoint kinase
CML	Chronic Myeloid Leukemia
CNV	Copy Number Variation
COSMIC	Catalogue of Somatic Mutations in Cancer
CRAF	Raf-1 Proto-Oncogene Serine/Threonine Kinase
CSD	cumulative sun damage
CSM	Cancer Mutation Census
CTL	Cytotoxic T-Cell
CTLA-4	Cytotoxic T-Lymphocyte Antigen-4
DOP-PCR	degenerative oligonucleotide PCR
DSP	Digital Spatial Profiler
EADO	European Association of Dermato-Oncology
EDF	European Dermatology Forum
EGFR	Epidermal Growth Factor Receptor
EMT	epithelial-to-mesenchymal transition
EORTC	European Organization of Research and Treatment of Cancer
ERBB2/4	Erb-b2 Receptor Tyrosine Kinase 2/4
ERK	Extracellular Signal-Regulated Kinase
FACS	Fluorescence-Activated Cell Sorting
FAS	Fas Cell Surface Death Receptor
FDA	Food and Drug Administration
FISH	Fluorescence In Situ Hybridization
GAP	GTPase-Activating Protein
GDP	Guanosine Diphosphate
GenoMEL	Melanoma Genetics Consortium
GNA11	G-Protein Subunit α11
GNAQ	G Protein Subunit Alpha Q
GOF	gain-of-function
GPCR	G protein-coupled receptors
GRB2	Growth factor receptor-bound protein 2
GTP	Guanosine Triphosphate
Hi-Fi	High Fidelity
HLA	Human Leukocyte Antigen
HRAS	Harvey Rat Sarcoma Viral Oncogene Homolog
IDH1	Isocitrate Dehydrogenase 1
ICGC	International Cancer Genome Consortium
IL-2	Interleukin 2
IPD	Interpulse Duration
IVT	in vitro transcription
JAK	Janus Kinase
KIT	Mast/Stem Cell Growth Factor Receptor Kit
KRAS	Kirsten Rat Sarcoma Viral Oncogene Homolog
LCM	Laser Capture Microdissection
LMM	Lentigo Maligna Melanoma
LOF	Loss-of-Function
MACS	Magnetic-Activated Cell Sorting
MALBAC	Multiple Annealing and Looping-Based Amplification Cycles
MAPK	Mitogen-Activated Protein Kinase
MAP2K1/2	Mitogen-Activated Protein Kinase Kinase ½
MC1R	Melanocortin-1 Receptor
MDA	multiple displacement amplification
MDM2	Mouse Double Minute 2
MDS	Myelodysplastic Syndrome
MEK	mitogen-activated protein kinase kinase
MET RTK	Met Receptor Tyrosine Kinase
MHC	Major Histocompatibility Complex
MIDAS	Micro-well Displacement Amplification System
MITF	Melanocyte Inducing Transcription Factor
MKK	Mitogen-Activated Protein Kinase Kinases
MMLV	Moloney Murine Leukemia Virus
MPM	multiple primary melanoma
MSK	Memorial Sloan Kettering
MST	malignant Spitz tumor
mTOR	mammalian target of rapamycin
NCI	National Cancer Institute
NF1	Neurofibromin 1
NGS	Next-Generation Sequencing
NHGRI	National Human Genome Research Institute
NM	nodular melanoma
NRAS	Neuroblastoma RAS Viral Oncogene Homolog
NTRK1	Neurotrophic Receptor Tyrosine Kinase 1
ONT	Oxford Nanopore Technologies
PCAWG	Pan Cancer Analysis of Whole Genomes
PCR	Polymerase Chain Reaction
PGM	Personal Genome Machine
PI3K	Phosphoinositide-3-Kinase
PKB	Protein Kinase B
POT1	Protection of Telomeres 1
PPP6C	Protein Phosphatase 6 Catalytic Subunit
PTEN	Phosphatase and Tensin Homolog
qBDA	quantitative Blocker Displacement Amplification
qISH	quantitative in situ hybridization
RAC1	Ras-related C3 Botulinum Toxin Substrate 1
RAF	Rapidly Accelerated Fibrosarcoma
RASA2	RAS P21 Protein Activator 2
RB	Retinoblastoma Protein
RET	Ret Proto-Oncogene
ROS1	ROS Proto-Oncogene 1, Receptor Tyrosine Kinase
SF3B1	Splicing Factor 3b Subunit 1
SMRT	Single Molecule Real-Time
SNF	Sucrose Non-Fermentable
SNP	Single Nucleotide Polymorphism
SNV	Single Nucleotide VariantSOLiD Sequencing by Oligonucleotide Ligation and Detection
SOS	Salt Overly Sensitive
SSM	superficial spreading melanoma
STAT	Signal Transducers and Activators of Transcription
STRT	single-cell tagged reverse transcription
SV	Structural Variations
SWI	SWItch
TCGA	The Cancer Genome Atlas
TERF2IP	TERF2 Interacting Protein
TERT	Telomerase Reverse Transcriptase
TERTprom	TERT promoter region
TKI	Tyrosine Kinase Inhibitor
TMB	Tumor Mutational Burden
TP53	Tumor Protein 53
UV	Ultraviolet
WGS	Whole Genome Sequencing
WES	Whole Exome Sequencing
ZMW	Zero Mode Waveguides

frontiers in Oncology

REVIEW
published: 10 June 2021
doi: 10.3389/fonc.2021.670726

Therapeutic Advancements Across Clinical Stages in Melanoma, With a Focus on Targeted Immunotherapy

Claudia Trojaniello[1], *Jason J. Luke*[2] *and Paolo A. Ascierto*[1]*

[1] Unit of Melanoma, Cancer Immunotherapy and Development Therapeutics, Istituto Nazionale Tumori IRCCS Fondazione G. Pascale, Napoli, Italy, [2] Cancer Immunotherapeutics Center, University of Pittsburgh Medical Center and Hillman Cancer Center, Pittsburgh, PA, United States

Melanoma is the most fatal skin cancer. In the early stages, it can be safely treated with surgery alone. However, since 2011, there has been an important revolution in the treatment of melanoma with new effective treatments. Targeted therapy and immunotherapy with checkpoint inhibitors have changed the history of this disease. To date, more than half of advanced melanoma patients are alive at 5 years; despite this breakthrough, approximately half of the patients still do not respond to treatment. For these reasons, new therapeutic strategies are required to expand the number of patients who can benefit from immunotherapy or combination with targeted therapy. Current research aims at preventing primary and acquired resistance, which are both responsible for treatment failure in about 50% of patients. This could increase the effectiveness of available drugs and allow for the evaluation of new combinations and new targets. The main pathways and molecules under study are the IDO inhibitor, TLR9 agonist, STING, LAG-3, TIM-3, HDAC inhibitors, pegylated IL-2 (NKTR-214), GITR, and adenosine pathway inhibitors, among others (there are currently about 3000 trials that are evaluating immunotherapeutic combinations in different tumors). Other promising strategies are cancer vaccines and oncolytic viruses. Another approach is to isolate and remove immune cells (DCs, T cells, and NK cells) from the patient's blood or tumor infiltrates, add specific gene fragments, expand them in culture with growth factors, and re-inoculate into the same patient. TILs, TCR gene transfer, and CAR-T therapy follow this approach. In this article, we give an overview over the current status of melanoma therapies, the clinical rationale for choosing treatments, and the new immunotherapy approaches.

Keywords: immunotherapy, advanced melanoma, immune system, target therapy, immune checkpoint inhibitor (ICI)

OPEN ACCESS

Edited by:
Marcus O. Butler,
University Health Network, Canada

Reviewed by:
Inna Smalley,
Moffitt Cancer Center, United States
Ioana Cosgarea,
Newcastle University, United Kingdom

***Correspondence:**
Paolo A. Asciertof
p.ascierto@istitutotumori.na.it

Specialty section:
This article was submitted to Skin Cancer, a section of the journal Frontiers in Oncology

Received: *22 February 2021*
Accepted: *10 May 2021*
Published: *10 June 2021*

Citation:
Trojaniello C, Luke JJ and Ascierto PA (2021) Therapeutic Advancements Across Clinical Stages in Melanoma, With a Focus on Targeted Immunotherapy. Front. Oncol. 11:670726. doi: 10.3389/fonc.2021.670726

INTRODUCTION

In recent years, we have witnessed a revolution in treatment and, consequently, a marked improvement in the overall survival (OS) of patients with metastatic melanoma. Before 2011, treatment with chemotherapy had been the standard of care for melanoma patients; the median survival of patients who were diagnosed with advanced melanoma was 6–9 months, with only 25%

alive at 1 year and <10% alive at 5 years (1). Since 2011, with the approval of several agents for the treatment of advanced melanoma, the likelihood of survival for patients with advanced disease has increased. The therapeutic armamentarium in melanoma now comprises immune checkpoint inhibitors (ICIs) and targeted therapy in the adjuvant and metastatic settings, and these agents are also being investigated in the pre-surgical setting. Tumor cells are able to evade immune surveillance in some ways, including the activation of immune checkpoint pathways that suppress the antitumor immune response, and overexpress the ligand for PD-1 (programmed cell ligand PD-1 or PD-L1), which facilitates the escape from the immune system (2).

Antibodies, such as nivolumab or pembrolizumab (anti-PD-1), can reinstitute an intra-tumoral immune response by targeting PD-1, interrupting the co-inhibitors' signature pathways and inducing the immune response against cancer cells (3). The MAPK signaling pathway also plays a pivotal role in the advancement of melanoma (4, 5). Its activation triggers a signal cascade, which leads to the inactivation of MAPK, including RAS (HRAS, NRAS, and KRAS), RAF serine/threonine kinases (ARAF, BRAF, and CRAF), MEK, and ERK. Important cellular activities such as differentiation, proliferation, survival, migration, and angiogenesis are regulated by these kinases. If signaling through this pathway is dysregulated, unconstrained cell growth and cell transformation can occur (6). The activation of *BRAF* mutations can be found in both skin (50%) and mucosal melanomas (10–20%) (7) and can cause constitutive activation of *BRAF* and downstream MAPK signaling (8). It has been demonstrated that patients affected by *BRAF*V600 mutation-positive unresectable or metastatic melanoma can be treated with the MEK inhibitors trametinib, cobimetinib, and binimetinib, and the BRAF inhibitors dabrafenib, vemurafenib, and encorafenib. *BRAF*-resistant melanomas usually determine a reactivation of the MAPK signaling pathway (9). This pathway can be used by the tumor as an "escape route" from the BRAF inhibitor; therefore, the addition of a MEK inhibitor allows to delay the development of resistance. Therapies that combine MEK and BRAF inhibitors have demonstrated to be more effective and to reduce the toxicity resulting from monotherapy with BRAF inhibitors. However, there is still large room for improvement in the treatment of metastatic melanoma by addressing two of its major problems: resistance and treatment-related adverse events (TrAEs). TrAEs, which are frequent in combination therapy, lead to treatment discontinuation in approximately 15% of patients and dose modifications or interruptions in approximately 50% of patients (10), while resistance is developed by 80% of patients within the first 3 years of therapy.

Some preclinical and clinical studies are ongoing, focusing on new combination treatments and new targets, with the aim to improve the outcome of patients with melanoma. At present, there are approximately 2250 active trials testing more than 295 targets. Here, we comprehensively present current approaches for the treatment of metastatic melanoma in adjuvant, neoadjuvant, and metastatic settings.

ADJUVANT TREATMENT

Stage III

Current State of Care

The treatment of choice for early-stage cutaneous melanoma is surgical excision, and, in most cases, it can be curative. However, some patients will ultimately relapse with metastatic or locally advanced disease. Clinical outcomes in patients with stage IIIB, C, and D have historically been poor, with a metastasis-specific survival (MSS) at 5 years of 83%, 69%, and 32%, respectively (11). Around 80% of relapses in resected stage III melanoma occurred within the first 2 years (12).

These differences have implications both in the clinical decision-making and in the design and analysis of clinical trials on adjuvant therapy.

At present, adjuvant treatment is indicated in patients at high risk of recurrence in patients with stage IIIB, C, and D or stage A with sentinel lymph node tumor deposits >1 mm.

Until 2012, IFN-α-2b was the only drug to demonstrate efficacy as adjuvant therapy in melanoma (11, 13). At present, IFN can only be considered in cases of stage IIB/C ulcerated melanoma, for which new-generation adjuvant therapies are not available, even if some clinical trials are ongoing.

Over the past years, some randomized studies in the adjuvant setting have been conducted to evaluate the activity of drugs that are already approved for metastatic disease (**Table 1**). Lymph node dissection has been included as the inclusion criteria in most adjuvant therapy trials; nevertheless, a lot of patients do not receive complete lymph node dissection anymore since the results of MSLT-2 (18). Moreover, the staging system for melanoma from the American Joint Committee on Cancer (AJCC) changed from the 7th to the 8th edition in January

TABLE 1 | Update on the latest results of adjuvant clinical trials.

	EORTC 18071 (14)	COMBI – AD (15)	CheckMate 238 (16)	KEYNOTE 054 (17)
Stage	IIIA (>1 mm)/B/C	IIIA (>1 mm)/B/C	IIIB/C/resected IV	IIIA (>1 mm)/B/C
Treatment arm	Ipilimumab	Dabrafenib + trametinib	Nivolumab	Pembrolizumab
Control arm	Placebo	Placebo	Ipilimumab	Placebo
Update	7 years	5 years	4 years	3 years
RFS	39.2%	52%	51.7%	63.7%
OS	60%	65%	77.9%	NR
DMFS	44.5%	65%	59%	65%
trAEs G3–4	54.1%	31%	14.4%	7.7%

2018 (12). The first adjuvant therapy study was the EORTC 18071, a randomized phase III trial that compared ipilimumab at a dosage of 10 mg/kg for 4 doses, then every 2 months for up to 3 years and placebo in patients with stage III (IIIA >1 mm lymph node metastasis, IIIB, IIIC) (19). This clinical trial showed a benefit of ipilimumab in terms of relapse-free survival (RFS), OS, and distant metastasis-free survival (DMFS) (14). However, this benefit was associated with a grade (G)3/4 adverse events (AE) rate of 54.1%, including a treatment-related mortality rate of 1% (n=5) for patients who received ipilimumab therapy (deaths from colitis, myocarditis, and Guillain-Barré syndrome) (19). Based on these data, ipilimumab was approved in 2015 by the US Food and Drug Administration (FDA) for the adjuvant treatment of melanoma, at a dosage of 10 mg/kg. In Europe, this treatment has never been approved. Currently, the use of ipilimumab in the adjuvant setting has been replaced by anti-PD-1 or BRAF-directed therapies.

The COMBI-AD is a randomized, phase III trial comparing 12 months of adjuvant therapy with both the BRAF and the MEK inhibitors dabrafenib and trametinib, respectively, versus placebo in patients with resected, *BRAF*V600-mutant, stage III melanoma (14). At a minimum study follow-up of 60 months, the trial showed a benefit of targeted therapy in terms of RFS and DMFS (20). Based on these results, the combination was approved by the FDA in April 2018, followed by the EMA for the adjuvant treatment of patients with resected BRAFV600-mutant stage III melanoma.

A phase III clinical trial, the CheckMate 238, has compared nivolumab at a dosage of 3 mg/kg every 2 weeks for 1 year in patients with completely resected stage IIIB/C or IV with ipilimumab at a dosage of 10 mg/kg every 3 weeks (Q3W) for 4 doses and every 12 weeks thereafter for 1 year in the adjuvant setting (21). At a median follow-up of 51.1 months (16), the 4-year RFS was better in the nivolumab arm, while OS at 4 years was similar in both treatment groups (77.9 and 76.6%, respectively). Median OS (mOS) was not reached in both arms. However, 49% of ipilimumab-treated patients received subsequent therapy compared with 41% of those in the nivolumab group. TrAEs of G3/4 were reported in only 14.4% of patients in the nivolumab arm versus 45.9% of those in the ipilimumab arm, with discontinuation due to immune-related adverse events (IrAEs) in 9.7% and 42.6%, respectively (21). Two treatment-related deaths in the ipilimumab group were reported: marrow aplasia in one patient and colitis in one patient.

Based on this study, in December 2017, the FDA and then in July 2018, the EMA approved the use of nivolumab in the adjuvant melanoma setting in all stage III and IV resected patients. Similar RFS results were recently reported in phase III clinical trial KEYNOTE 054 (22) in which patients with stage III melanoma were randomized to treatment with pembrolizumab at a dosage of 200 mg Q3W or placebo. The 3-year RFS and 3–5-year DMFS were higher in the pembrolizumab group (17, 23). IrAEs of G3–4 occurred in 7.7% of patients in the pembrolizumab group and in 0.6% in the placebo group, and, in any case, the occurrence of an irAE was significantly associated with a longer RFS in the pembrolizumab arm (17). There was one pembrolizumab-related death (myositis) (22).

Based on this study, pembrolizumab was approved, first by the EMA in October 2018, then by the FDA in February 2019 for the adjuvant treatment of stage III melanoma patients.

Emerging Strategies

CA209-915 is a phase III, randomized clinical trial studying the effectiveness of adjuvant immunotherapy after complete resection of stage IIIB/C/D or IV melanoma, according to the AJCC 8th edition; drugs involved are nivolumab combined with ipilimumab versus ipilimumab or nivolumab monotherapy. Study enrollment has been completed, but full results have not yet been released. In November 2019, results for only one of the co-primary endpoints were announced. Data showed that the combination did not lead to any improvement in RFS in the all-comer (intent-to-treat) population (24). Previously, in November 2019, the supporting company reported that the combination did not result in a PFS improvement compared with nivolumab alone when used in the adjuvant setting for patients with resected stage IIB/C/D or stage IV melanoma and whose tumors expressed PD-L1 <1%, thus failing to achieve the co-primary endpoint of the trial (25).

IMMUNED is a randomized, double-blind phase II trial, evaluating adjuvant nivolumab plus ipilimumab versus nivolumab versus placebo in patients with resected stage IV melanoma. The primary endpoint was RFS. At a median follow-up of 28.4 months, the median RFS in the placebo group was 6.4 months and 12.4 months in the nivolumab group, whereas it was not reached in the combination group. In the nivolumab plus ipilimumab group, RFS at 2 years was 14% in the placebo group; versus 42% in the nivolumab group and 70% in the combination group. G3–4 TrAEs were reported in 27% of patients in the nivolumab group and in 71% of patients enrolled in the combination group (26).

In another phase IIb trial, patients with resected stage III/IV melanoma were randomized to receive tumor lysate, particle-loaded, dendritic cell (TLPLDC) vaccine versus placebo. By ITT analysis, 36-month OS was 76.2% versus 70.3% in placebo arm (HR: 0.72, p=0.437) and 36-month disease-free survival (DFS) was 35.6% *vs* 27.1% (HR: 0.95, p=0.84). By per-treatment analysis, 36-month DFS was 57.5% in TLPLDC arm versus 35% in the placebo group (HR: 0.50, p=0.025); this effect was more evident in resected stage IV patients, with a 36-month DFS of 60.9% versus 0% (HR: 0.12, p=0.001) (27). A phase III trial will evaluate the improvement of a TLPLDC vaccine as adjuvant treatment for resected stage IV melanoma, in combination with anti-PD-1 versus anti-PD-1 alone.

The SWOG 1404 is a phase III randomized study in stage IIIA (N2)/B/C or resectable IV melanoma in which patients will receive high-dose IFN or pembrolizumab (28). The primary endpoints are RFS and OS.

The CA045-022 is an ongoing phase III randomized, open-label trial, which compares patients with stage III or resected IV receiving adjuvant treatment with bempegaldesleuskin (NKTR-214), a PEGylated interleukin-2 (IL-2), in combination with nivolumab versus those on nivolumab alone (NCT04410445).

Stage II

The Current State of Care

After excellent results were obtained with adjuvant treatment in patients with stage III melanoma, and the subsequent approval of nivolumab, pembrolizumab, and dabrafenib in combination with trametinib, attention has now shifted to stage II melanoma patients.

Patients affected by stage II melanoma are divided into two groups (low and high risk) according to the risk of relapse (**Table 2**) (29). Patients at low risk of recurrence (tumor ≤4 mm in thickness without ulceration or ≤2 mm in thickness with ulceration, stage IIA), have a high probability to be cured only by surgery. However, the 5-year MSS in stage IIC is 82%, which is comparable to the 83% of stage IIIB; patients with stage IIIA disease have a better prognosis than those with stage IIC disease.

In countries without access to clinical trials, adjuvant (PEG)-IFN-α-2b treatment is an option for patients with ulcerated melanomas without palpable nodes (stage IIB/C) or stage III (30).

Emerging Strategies

The KEYNOTE-716 is one of the largest clinical trials currently ongoing. It is a phase III, randomized trial evaluating 1 year of pembrolizumab Q3W versus placebo in patients with stage IIB/C melanoma according to the AJCC 8th edition. The primary endpoint is RFS, and crossover from placebo or re-challenge of pembrolizumab is allowed (NCT03553836).

CA209-76K is a phase III, randomized, double-blind study of nivolumab versus placebo for 12 months after complete resection of stage IIB/C melanoma. In the event of disease recurrence, participants will have the option to receive on-study open-label nivolumab treatment (NCT04099251).

So far, the only trial, in development, evaluating adjuvant sequential treatment with BRAF (encorafenib) and MEK (binimetinib) inhibitors followed by anti-PD-1 versus anti-PD-1 alone versus placebo in melanoma stage IIA/B/C patients is the EORTC 1902.

NEOADJUVANT THERAPY

Current State of Care

At present, no neoadjuvant treatment is approved for patients with melanoma.

The ESMO Consensus Conference positively evaluated the data on neoadjuvant therapy for resectable stage III melanoma, although they did not justify the indication at the moment. However, if any agents would become available and associated with improved survival, it should be considered prior to surgical resection. When the disease is technically resectable but in-transit and/or bulky nodal, and surgery could be associated with major morbidity, neoadjuvant strategies should be considered even outside the context of a clinical trial (31).

Emerging strategies Preclinical studies suggested that neoadjuvant ICI treatment, compared with adjuvant treatment, is associated with antigen-specific T-cell responses. The primary site of the tumor can be used as a spring of antigens for the spread and activation of tumor-specific T cells and to control micro-metastases (32); however, optimal regimens have not been defined (33).

Intravenous Treatment

A study presented at the 2019 ASCO Annual Meeting and conducted in institutions participating in the International Neoadjuvant Melanoma Consortium pooled data from six neoadjuvant systemic therapy trials (anti-PD-1 in 133 patients and BRAF/MEK target therapy in 55 patients). It demonstrated how patients treated with neoadjuvant systemic therapy (nivolumab, either as monotherapy or in addition with ipilimumab, pembrolizumab, or dabrefenib plus trametinib) had better chances to be relapse-free when achieving pathologic complete response (pCR) compared with those who did not achieve it. pCR was achieved in 41% of patients (38% treated with immunotherapy and 47% with targeted therapy). Immunotherapy was more effective than targeted therapy at 12 months; 83% of the patients who received it remained relapse-free compared with just 65% of those who underwent targeted therapy. Patients with pCR showed an improved RFS compared to those without pCR. Moreover, 100% of the patients with pCR who were treated with immunotherapy were relapse-free versus just 72% of those without pCR ($p<0.001$). Targeted therapy at 12 months showed a relapse-free rate of 88% in pCR patients and 43% in patients without pCR (34).

Some clinical trials evaluated the role of neoadjuvant treatment in patients with melanoma:

The OpACIN trial was the first to evaluate neoadjuvant treatment in patients with melanoma (35). This was a randomized phase 1b trial, in high-risk stage III melanoma patients, which compared neoadjuvant nivolumab plus ipilimumab followed by nivolumab and ipilimumab after regional lymph node dissection versus adjuvant ipilimumab plus nivolumab. In both arms, 90% of patients experienced G3/4 trAEs.

At the 4-year follow-up, all of the AEs have recovered to grade ≤1 except endocrine toxicities requiring hormone replacement therapy, and no new G3–4 AEs were observed (36).

TABLE 2 | Low- and high-risk stage II melanoma (29).

	Low risk (stage IIA)	High risk (stage IIB/C)
Thickness	≤2 mm + ulceration ≤4 mm without ulceration	>2 mm + ulceration >4 mm (regardless ulceration)
Lymph node involvement	No	No
Melanoma-specific survival at 5 years (19)	94%	85% \ 82%
Melanoma-specific survival at 10 years (19)	88%	82% \ 75%

Pathologic response (pR) was achieved in 78% of patients in the neoadjuvant arm, with three pCRs, three near pCRs (≤10% viable tumor cells), and one patient achieving a pathological PR (partial response) (pPR ≤50% viable tumor cells). After a mean follow-up of 36 months for OpACIN, only one out of 71 patients (1.4%) relapsed on neoadjuvant therapy with pathological response (pR) (37). After a median follow up of 48 months, none of the seven patients with a confirmed pPR in the neoadjuvant arm have relapsed. The estimated 4-year RFS rate for the neoadjuvant arm was 60% and 60% for the adjuvant arm, and the 4-year OS was 90% and 70%, respectively (36). The OpACIN trial is the first to show how neoadjuvant combination is superior to adjuvant immunotherapy. Furthermore, this trial suggested that pR can function as a surrogate marker for RFS.

Another phase II trial (38) of neoadjuvant treatment enrolled 23 patients with high-risk stage III or oligometastatic stage IV melanoma in two arms: neoadjuvant with four courses of nivolumab versus three courses of ipilimumab in combination with nivolumab, followed by surgical resection and subsequently by adjuvant nivolumab for 6 months. Combination treatment showed high response rates (overall response rate [ORR]: 73%, pCR 45%) but a high rate of grade 3 trAEs (73%). Treatment with nivolumab monotherapy showed moderate responses (ORR 25%, pCR 25%) with a low incidence of grade 3 toxicity (8%), without grade 4 or 5 trAEs. At a median follow-up of 15.6 months, 11/11 of the patients receiving dual checkpoint blockade were still alive. Due to disease progression in 17% of patients in the monotherapy arm and a high rate of grade 3 trAES, the study was stopped early. The combination of ipilimumab with nivolumab resulted in a trend to improved survival outcomes (PFS, DMFS, OS) compared with nivolumab monotherapy, although significance was not reached (38).

OpACIN-neo is a phase II, open-label, randomized trial in high-risk stage III melanoma. In this trial, 86 patients were randomized to one of three neoadjuvant dosing schedules (arm A: 2 × ipilimumab 3 mg/kg + nivolumab 1 mg/kg Q3W; arm B: 2 × ipilimumab 1 mg/kg + nivolumab 3 mg/kg Q3W; and arm C: 2 × ipilimumab 3 mg/kg Q3W followed immediately by 2 × nivolumab 3 mg/kg Q2W for 6 weeks prior to surgery, without adjuvant therapy (39). The primary endpoints were both the proportion of patients with grade 3/4 IrAEs within the first 12 weeks and the rate of patients achieving a radiological objective response and pR at 6 weeks. Arm C was closed early due to high-grade G3/4 AEs. At 24-month follow-up, of the 81 patients alive, 68% still showed irAEs but only 3% experienced ≥grade 3 irAEs (40). Radiologic objective response and pR were reported in 63% and 80% in group A, in 57% and 77% in group B and in 35% and 65% in group C, respectively. OpACIN-neo identified that the treatment regimen in group B, two cycles of ipilimumab 1 mg/kg plus nivolumab 3 mg/kg once Q3W intravenously, can be considered as the most suitable dosing and schedule, associated with the lowest grade G3/4 toxicities and a similar pR rate compared with the other two dosing regimens.

Estimated 24-month RFS was 84% for all patients (95% CI: 76–92%); 90% for arm A (95% CI: 80–100%), 78% for arm B (95% CI: 63–96%) and 83% for arm C (95% CI: 70–100%), thus confirming the high pR rates achieved with combination in neoadjuvant setting (41).

"Nadina study" is a yet-to-start, randomized, international phase III trial, which will evaluate two courses of neo-adjuvant 'low-dose' ipilimumab (1 mg/kg) + nivolumab (3 mg/kg) followed by surgery and then 1 year of anti-PD-1 adjuvant systemic therapy. The PRADO study was an extension cohort of the OpACIN-neo study, which aims to further evaluate the pR rate and toxicity of combination treatment of nivolumab and ipilimumab in the neoadjuvant setting for two cycles and to save patients from surgery on the basis of pR (42). In this study, all patients did receive excision of the index node. Patients that achieved major pR (MpR) in the largest lymph node metastasis, did not undergo lymph node dissection while patients with pPR or with no pathologic response underwent lymph node dissection followed by nivolumab or target adjuvant therapy of 52 weeks. pCR was achieved in 50% of patients, near pCR in 11%, and pPR in 10%. The ORR was 71%. This meant that a complete therapeutic lymph node dissection was needed by just 40 out of 99 patients, thus reducing surgical morbidity. Longer follow-up is necessary to fully evaluate safety and RFS in patients without lymph node dissection (43).

At the ESMO 2020 were reported health-related quality of life data showing that patients with MpR following neoadjuvant immunotherapy who have reduced the extent of surgery have a significantly better health-related quality of life scores (44).

Oral Treatment

Dabrafenib and trametinib were evaluated in the neoadjuvant setting in a single-center, open-label, randomized, phase II trial on 21 patients with surgically resectable clinical stage III or oligometastatic IV melanoma with *BRAF*V600E/K mutations (45). Patients were randomized to receive the neoadjuvant/adjuvant treatment or the standard surgery ± adjuvant therapy. Patients assigned to the targeted therapy arm received 8 weeks of neoadjuvant dabrafenib and trametinib followed by surgery and then adjuvant dabrafenib and trametinib for up to 44 weeks.

An interim safety analysis showed how treatment with neoadjuvant dabrafenib plus adjuvant trametinib allowed longer event-free survival compared with the standard approach; the trial was thus stopped early. The study is now continuing as a single-arm study of neoadjuvant plus adjuvant dabrafenib and trametinib. Event-free survival, the primary endpoint of the trial, was 19.7 months for neoadjuvant plus adjuvant dabrafenib and trametinib, versus 2.9 months for standard care (HR: 0.016, 95% CI: 0.00012–0.14; p<0.0001), without any G4 AEs in either arm.

NeoCombi was a single-arm, open-label, single-center, phase II trial, which enrolled patients who were affected by stage IIIB/C, *BRAF* V600-mutated melanoma and receiving dabrafenib plus trametinib for 12 weeks of neoadjuvant therapy before surgery, followed by 40 weeks of adjuvant therapy (46). The primary endpoints were the rate of patients achieving a pCR and the proportion of patients achieving a response at week 12. At a median follow-up of 27 months, 86% achieved a RECIST (Response Evaluation Criteria in Solid Tumors) response (46%

CR and 40% PR), 14% achieved a stable disease without progression in any patients. After surgery, all patients achieved a pR (49% pCR and 51% non-complete pR). A 2-year RFS in patients with a complete pR was achieved in 63.3% versus 24.4% of patients with a non-complete pR. Serious trAEs occurred in 17% of patients and 29% of patients developed G3–4 AEs (most common were pyrexia and syncope), without treatment-related deaths.

Intratumoral Treatment

The oncolytic virus Talimogen laherparepvec (T-VEC) consists of a genetically modified herpes simplex virus (HSV-1) able to preferentially thrive in neoplastic cells: it enhances antigen loading of MHC class I molecules and promotes the expression of granulocyte–macrophage colony-stimulating factor (GM-CSF), increasing tumor antigen presentation by dendritic cells.

The administration of T-VEC prior to surgery was associated with improved RFS and OS compared with surgery alone in patients with resectable advanced melanoma, according to results of a multicenter, open-label, phase II trial (47). In this study, patients with high-risk stage IIIB-IV M1a resectable melanoma were randomly assigned to immediate surgery or intralesional T-VEC followed by surgery. Among the patients in the T-VEC arm, 22.8% had a pCR. Investigator-assessed clinical response in the T-VEC arm was 13.2%. The disease control rate (DCR) was 40.8%. The most common trAEs were flu-like symptoms; G3 AEs in the T-VEC group consisted of two cases of cellulitis and one case each of anembryonic gestation, cholecystitis, device occlusion, influenza, and wound infection [49]. The 3-year OS rate in T-VEC arm was 83.2% versus 71.6% for surgery alone (HR: 0.54, 80% CI: 0.36–0.83; p=0.061). The 3-year RFS rate was 46.5% with T-VEC plus surgery compared with 31% with surgery alone (HR: 0.67; 80% CI: 0.51–0.88, p=0.043). Median OS at 3 years was not reached in both arms (48).

The Neo-C-Nivo is a phase II study that evaluates the effects of neoadjuvant intra-tumoral CMP-001 in combination with nivolumab in patients with stage IIIB/C/D treatment-naïve melanoma, deemed surgically resectable, with an accessible tumor for biopsy and CMP-001 injection (49). CMP-001 is a type A CpG packaged with a virus-like particle that activates tumor-associated plasmacytoid dendritic cells *via* TLR9 inducing type I IFN and anti-tumor CD8+ T cells (50). The primary endpoint was the MpR and incidence of dose-limiting toxicities, while RFS, OS, and radiographic response were the secondary endpoints. At the final analysis presented at SITC 2020, no dose-limiting toxicities or G4/5 trAEs were observed; the most frequent G3 AE was hypertension (9.7%) followed by arthralgia in 3.2%, colitis in 3.2%, hypophosphatemia in 3.2%, and injection site infection in 3.2% of patients. Radiographic responses were seen in 43%, while 30% had stable disease (SD) and 27% had progressive disease (PD). pCR was achieved in 50% and pMR in 10% with a pR of 70%. Responders had evidence of activated CD8+ T cells peripherally and TIM-3 upregulation was evidenced on CD8+ T cells in non-responders. The RFS at 1 year was 90% in all pathological responders, with a median RFS not reached in pathological responders versus 5 months in non-pathological responders (51).

TREATMENT OF STAGE III/IV NON-RESECTABLE MELANOMA

Current State of Care

The treatment of patients with metastatic or unresectable melanoma has greatly evolved in the last decade, thanks to the development of ICIs and MAPK molecular targeted therapy directed towards the oncogenic BRAF and MEK signaling pathways (**Tables 3** and **4**).

Immunotherapy

The first immunotherapeutic agent approved in metastatic melanoma was ipilimumab, in 2011 (52), based on a randomized phase III (52) clinical trial "MDX010-020" in which patients with metastatic melanoma, pretreated, were randomly assigned to receive ipilimumab, gp100 (peptide vaccine), or ipilimumab in combination with gp100. OS was significantly longer with ipilimumab alone or in combination with gp100 (10.1 months) compared with gp100 alone (6.4 months; HR: 0.68, p<0.001).

In 2014, the results of the randomized phase III trial KEYNOTE 006 (56), which evaluated patients with advanced melanoma receiving pembrolizumab (10 mg/kg Q2W Q3W) or ipilimumab (3 mg/kg Q3W for 4 total doses), accounted for the FDA approval of pembrolizumab (53).

In 2015, nivolumab was approved in untreated patients with metastatic melanoma, based on the results of CheckMate 066 (57), a randomized double-blinded phase III study that evaluated treatment with nivolumab versus dacarbazine in patients with advanced *BRAF* wild-type melanoma in the first-line setting (54).

TABLE 3 | Last results of KEYNOTE 006, CheckMate 066 and CheckMate 067 trial.

	KEYNOTE 006 (53)	CheckMate 066 (54)	CheckMate 067 (55)
Treatment arm	**Pembrolizumab**	**Nivolumab**	**Nivolumab + ipilimumab**
Last update	5 years	5 years	5 years
mPFS	8.4	5.1	11.5
PFS	NR	28%	36%
mOS	32.7	37.3	NR (more than 60)
OS	38.7%	39%	52%
ORR	42%	42%	58%
trAEs G3–4	17%	15%	59%

TABLE 4 | Last results of Combi-D, Combi-V, CoBRIM, Columbus and Imspire 150 trial.

	Combi-D (62)	Combi-V (62)	coBRIM (66)	Columbus (67)	Imspire 150 (68)
Treatment arm	Dabrafenib + trametinib	Dabrafenib + trametinib	Vemurafenib + Cobimetinib	Encorafenib + binimetinib	Vemurafenib + Cobimetinib + Atezolizumab
Control arm	Dabrafenib	Vemurafenib	Vemurafenib	Encorafenib Vemurafenib	Vemurafenib + cobimetinib
Last update	5 years	5 years	5 years	4 years	2 years
mPFS	11.1	11.1	12.6	14.9	15.1
PFS	17%	20%	14%	26%	43.5%
mOS	25.9	25.9	22.5	33.6	28.8
OS	32%	36%	31%	39%	76.7% (2 years)
ORR	68%	68%	68%	64%	66.3%
trAEs G3–4	54%	62%	60%	68%	79%

In 2016, the combination of nivolumab plus ipilimumab in untreated patients with *BRAF* V600 wild-type and *BRAF* V600 mutation-positive metastatic melanoma was approved following the results of the randomized double-blind phase III study CheckMate 067 (55), which compared the combination regimen versus nivolumab or ipilimumab in monotherapy in the first-line treatment of patients with advanced melanoma.

In patients with unresectable cutaneous, subcutaneous, or nodal melanoma, T-VEC was approved in 2015 by the FDA, based on the OPTiM phase III randomized trial (58). In this study, patients with stage IIIB or IV melanoma were randomly assigned to intralesional T-VEC or GM-CSF administered subcutaneously at 125 μg/mq daily for 14 days in 28-day cycles. At a median follow-up of 49 months, mOS was 23.3 months with TVEC and 18.9 months with GM-CSF (p=0.051), in the ITT population estimated OS probability at 5 years was 33% versus not evaluable, durable response rate (DRR) was 19.0 versus 1.4%; ORR was 31.5 versus 6.4%, respectively. In T-VEC patients, the median time to CR was 8.6 months; median CR duration was not reached (59). The subanalysis of the OPTiM trial comparing stage IV M1b or M1c patients with metastases to visceral or lung sites and patients with melanoma at stage IIIB/IV M1a, revealed as DRR of 5% versus 25%, ORR of 9% versus 41%, and CR rates of 4% versus 17%, respectively (60). Therefore, it seems that only stage IIIB–IV M1a disease may be addressed with TVEC monotherapy, likely due to its activity against dermal satellite or in transit metastases and its high degree of control locoregional disease; in stage M1b or M1c systemic effects, which normally require combination approaches, are limited.

Targeted Therapy

At present, there are three combination regimens approved.

The combination of dabrafenib plus trametinib was the first BRAF–MEK combination approved for metastatic melanoma, in 2015, based on the two phase III clinical trials, COMBI-v (61, 62) and COMBI-d (63), comparing the combination with vemurafenib or dabrafenib monotherapies, respectively. The randomized, phase III co-BRIM trial compared the combination of vemurafenib and cobimetinib versus vemurafenib monotherapy (64). In 2015, the FDA approved this combination to treat patients with metastatic melanoma (64, 65). COLUMBUS was a phase III, randomized trial addressing the combination of encorafenib and binimetinib versus vemurafenib (66, 67), thus gaining the approval from the FDA in 2018.

In terms of efficacy, the approved BRAFi/MEKi combinations are overall comparable; response rates range from 60 to 70% and 18-month PFS rates range from 30 to 40% (63, 64, 69) with distinct toxicity profiles.

On the basis of the findings from IMspire150, in 2020, the FDA approved the PD-L1 inhibitor atezolizumab in combination with cobimetinib and vemurafenib for the treatment of patients with advanced melanoma with *BRAF* V600 mutations. The trial was a double-blind, multicenter, placebo-controlled randomized phase III study that enrolled patients with unresectable locally advanced melanoma or previously untreated *BRAF* V600 mutation-positive metastatic melanoma (68).

Emerging Strategies

Alternative Dosing of Ipilimumab + Anti-PD-1

A remarkably interesting phase II study evaluated the need for more than two doses of nivolumab plus ipilimumab followed by maintenance nivolumab, in patients with unresectable stage III/IV melanoma, with the aim to evaluate whether decreasing the dose of the combination would reduce toxicity achieving the same outcome than that of the standard approach (70). Patients were treated with two doses of nivolumab (1 mg/kg) plus ipilimumab (3 mg/kg) followed by a CT scan at week 6; if tumor burden growth was >4%, patients received two further doses of nivolumab plus ipilimumab; if otherwise, patients underwent maintenance nivolumab therapy. Results showed that 68% of patients had tumor shrinkage or no growth at week 6 with two doses of the combination. None of the patients who had PD (32% of patients) at week 6 moved on the response at week 12, showing that efficacy and toxicities with the combination appear to be driven by the first two doses of treatment; however, it is still unclear which patients are at increased likelihood of benefitting from fewer doses. Furthermore, no difference in toxicity was disclosed, with emerging toxicity deemed as probably related to early combination dosages (70).

The CheckMate 511 trial, evaluating two different dosages (ipilimumab 3 mg/kg and nivolumab 1 mg/kg or ipilimumab 1 mg/kg and nivolumab 3 mg/kg) of the nivolumab plus ipilimumab combination, showed similar results. The primary aim of the study was to determine if ipilimumab 1 mg/kg was better tolerated than the 3 mg/kg dosage. Remarkably, the lower dose of ipilimumab combined with 3 mg/kg of nivolumab was associated with a more favorable tolerability profile than the

higher dose (G3/5 toxicity of 34% in the ipilimumab 1 mg/kg arm *vs* 48% in the ipilimumab 3 mg/kg arm; p=0.006). The two regimens did not appear to differ in secondary efficacy endpoints. The ipilimumab 3 mg/kg arm had a slightly numerically higher objective response rate than the ipilimumab 1 mg/kg arm (50.6% *vs* 45.6%), but median PFS and 12-month OS were perfectly comparable in the two arms (71).

In a retrospective study, Da Silva et al. showed that patients resistant to PD-1 monotherapy treated with combination (ipilimumab plus anti-PD-1) had a RR of 31% versus ipilimumab alone 12% (p<0.01), with a PFS and OS at 1 year 27% and 57%, respectively, versus 13% and 38% (p<0.01) (72). OS at 18 months was 53% versus 25%, and mOS was 20.4 versus 8.8 months, respectively. In *BRAF* wild-type patients, RR was higher with combinations versus ipilimumab alone (38% *vs* 9%, p<0.01), while RR was similar, 19% versus 24% in *BRAF*-mutated patients, respectively. AEs ≥3 was similar with combination therapy (30%) or monotherapy (34%, p=0.48) and were not associated with response (72).

In a phase II trial, combination therapy with low-dose ipilimumab with pembrolizumab demonstrates marked antitumor activity in patients with melanoma following PD on a PD-1 antibody. Patients received pembrolizumab 200 mg intravenously Q3W plus ipilimumab 1 mg/kg Q3W for 4 doses. Pembrolizumab was continued in monotherapy for up to 2 years. The primary endpoint, RR, was 31%. Median PFS was 5.0 months (95% CI: 2.8–8.3) and median OS was 24.7 months (95% CI: 15.2–undetermined). Grade 3–4 trAEs were reported in 15 (27%) of 70 patients enrolled in the study, the most common being diarrhea, rash, and transaminase elevation (73).

Loco-Regional Treatment

Talimoneg laherparepvec (T-VEC), an oncolytic virus, was evaluated in patients with advanced melanoma in a phase II study in combination with ipilimumab versus ipilimumab alone. A total of 38 patients (39%) in the combination arm and 18 patients (18%) in the ipilimumab arm had an odds ratio (OR: 2.9; 95% CI: 1.5–5.5; p=0.002). Responses comprise both injected and visceral lesions; specifically, the latter decreased in 52% of patients in the combination arm and 23% of patients in the ipilimumab arm. More common AEs included fatigue, chills, and diarrhea. The incidence of G ≥3 AEs was 45% and 35%, respectively (74). At the interim analysis at 4 years (n=198), median follow-up was 48.3 months for combination and 35.7 months for ipilimumab alone. DRR improved for combination versus monotherapy (33.7% *vs* 13.0%; OR: 3.4; 95% C: 1.7–7.0; p=0.001). Median PFS was 13.5 months with combination and 6.4 months with ipilimumab alone (HR: 0.81; 95% Cl: 0.57–1.15; p=0.23). Median OS was not reached for combination and was 50.1 months for ipilimumab (HR: 0.82; 95% CI: 0.54–1.25; p=0.36). In a subgroup analysis, patients without the *BRAF* V600 mutation receiving the combination therapy showed improved DRR and PFS (DRR: 33.9% *vs* 5.0%; median PFS: 18.0 *vs* 4.5 months); DRR in *BRAF* V600 mutation-positive patients were similar between arms (34.3% *vs* 26.5%; mPFS: 4.2 months *vs* 6.4 months). No additional safety signals were observed in follow-up (75).

In the Masterkey 265 phase Ib trial, T-VEC was evaluated in combination with pembrolizumab in patients with unresectable stage IIIB/IVM1c melanoma (76). The CR rate was 43%. In total, 12/13 responders (92.3%) were still in response, including all nine patients with a CR. Kaplan–Meier estimates of 4-year PFS and OS rates were 55.9% and 71.4%, respectively. Patients who achieved a CR or PR had better OS (p=0.0056) compared with those who did not respond. Median OS was not reached for responders and was 24.4 months for non-responders (77).

Tilsotolimod (IMO 2125), a synthetic Toll-like receptor 9 agonist (TLR9) oligonucleotide, changes the tumor microenvironment by acting on dendritic cells and macrophages and is being evaluated in multiple solid tumors. Type 1 IFN responses induced by local drugs determine in both injected and non-injected lesions an increased downstream T-cell activation and proliferation and antigen presentation (78). ILLUMINATE-204 is a phase I/II trial in patients with advanced melanoma refractory to anti-PD-1 therapy of intratumoral tilsotolimod in combination with ipilimumab (79). In 49 patients with anti-PD-1 refractory melanoma and evaluable for efficacy, investigators reported ORR of 22% with 71% DCR, mOS was 21 months, the median duration of response (mDOR) was 11.4 months. Tumor reduction was observed in both injected and noninjected tumors. trAEs of G3/4 were reported in 48% of patients, the most common serious trAEs were autoimmune hepatitis, hyponatremia, and hypophysitis (80).

In a phase III trial, ILLUMINATE 301, tilsotolimod at a dosage of 8 mg in combination with ipilimumab was well tolerated and showed durable and substantial clinical benefit (NCT02644967).

SD-101, a TLR-9 agonist, was assessed in a phase Ib/II study, at multiple doses injected in a single tumor in combination with pembrolizumab in patients with advanced melanoma naïve to anti-PD-1 treatment (81). This combination showed promising response rates compared with those expected with pembrolizumab alone. Frequently observed G ≥3 trAEs were myalgia 9%, headache 9%, fatigue 9%, chills 7%, and malaise 5% (81). ORR in the 2 mg group was 71% (95% CI: 57–82; CR: 13%) and in the 8 mg group was 49% (95% CI: 33–65; CR: 7%) with responses in both injected and non-injected lesions, including visceral. PFS was higher in the 2 mg group with median PFS in 2 mg not reached, in the 8 mg arm PFS was 10.4 months. The 6-month PFS and OS rates were 81% and 98% in the 2 mg arm and 60% and 92% in the 8 mg arm, respectively (81).

Findings from a phase Ib trial studying the intratumoral TLR9 antagonist CMP-001 were presented at SITC 2019. This agent pushes tumor-associated plasmacytoid dendritic cells to produce interferon and has been shown to produce durable responses when administrated in combination with pembrolizumab for patients with PD-1-resistant metastatic melanoma (82). The best ORR in patients treated with pembrolizumab and CMP-001 was 23.5%, while CMP-001 alone resulted in a lower ORR of 11.5%. Intratumoral CMP-001 was well-tolerated and provided both local and distant responses in patients with advanced melanoma reporting disease progression on prior PD-1 blockade. CMP-001 monotherapy induced systemic tumor regression in some patients, but the duration of response was substantially increased by the addition of pembrolizumab (83).

Electroporated plasmid IL-12 (TAVO or tavokinogene telseplasmid) is a novel immuno-modulating intratumoral therapy, which delivers IL-12 into the tumor microenvironment; it has been shown to synergize with anti-PD-1 antibodies in patients progressed to anti-PD-1. Although the IL-12/IFN-γ axis is usually not active in advanced melanoma, intratumoral electroporation of pIL-12 can recover this axis, favoring anti-PD-1 immunotherapy activity in patients unresponsive to anti-PD-1 treatment (84, 85).

KEYNOTE 695 is a phase II trial evaluating the combination of plasmid IL-12 (TAVO) with pembrolizumab in patients with advanced melanoma refractory to PD-1 treatment. Results showed that the combination is associated with an ORR of 30% (95% CI: 18.0–43.6%), with 6% of patients achieving a CR. In patients with M1c/M1d disease, the ORR was slightly higher (35.3%). Patients who had previously received treatment with ipilimumab showed the highest ORR with the treatment (40%). The median DOR was 12.2 months (95% CI: 5.6–not evaluable). The most common trAEs were fatigue (26.8%), procedural pain (23.2%), diarrhea (19.6%), nausea (10.7%), and rash (10.7%). Three patients had grade 3 toxicities: cellulitis, enteritis, and Lichen planus (86).

PVSRIPO is a novel immunotherapy consisting of a non-neurovirulent poliovirus chimera that activates innate immunity that is injected directly into tumors. The recombinant oncolytic poliovirus is designed to infect antigen-presenting cells, such as macrophages and dendritic cells that express CD155. The poliovirus receptor is often expressed on malignant cells of solid neoplasia, as well as in myeloid and endothelial cells. This strategy was evaluated in a phase I trial in patients with unresectable melanoma progressed after PD-1 and BRAF/MEK therapy (if *BRAF* mutated). Two of four (50%) patients with in-transit disease had pCR. At a median follow-up of 12 months, 50% (6/12) patients remained progression free. All AEs were of G1/2 severity, with pruritis (50.0%) and erythema (33.3%) being the most common trAEs. Around 33% of patients achieved a response (87).

Triplet Therapy

Combinations of immunotherapy and targeted therapy in the treatment of metastatic melanoma suggest even greater benefits in survival than the two approaches alone. Data show that patients who receive the triplet of anti PD-L1 plus MEK inhibitor and BRAF inhibitor have a greater number of T cells in the tumor environment (BRAF inhibitors can increase the ability of T cells, triggered by immunotherapy, to penetrate the tumor) (88). Indeed, targeted therapies could help prevent the spread of cancer, while immunotherapy stimulates the immune system to attack cancer cells.

The phase I/II KEYNOTE-022 (89) trial addressed the safety and efficacy of dabrafenib and trametinib in combination with pembrolizumab in untreated patients with unresectable or metastatic *BRAF*-mutated melanoma. It could not meet its primary endpoint of improved median PFS, although a trend to a longer PFS with pembrolizumab (median PFS 16.0 months compared to 10.3 months with placebo) was reported. An updated analysis of KEYNOTE 022 at 24-month follow-up showed the triplet potential as a treatment option for patients with *BRAF*-mutant advanced melanoma (90). 24-month PFS rates were 41% with pembrolizumab versus 16.3% with placebo; mOS was not reached with pembrolizumab versus 26.3 months with placebo (HR: 0.64; 95% CI: 0.38–1.06). OS rates at 24 months were 63.3% *versus* 51.7%, respectively (HR: 0.64). mDOR was 25.1 months in the pembrolizumab group *versus* 12.1 months in the placebo group. G3–5 AEs occurred in 58.3% of the pembrolizumab group *versus* 25% of the placebo group. The most common G3–5 trAEs were pyrexia (10.0% *versus* 3.3%), increased aspartate aminotransferase (6.7% versus 3.3%), and increased γ-glutamyl transferase (6.7% *versus* 5.0%) (90).

TRIdent is a phase II trial of nivolumab in combination with dabrafenib and trametinib in patients with metastatic melanoma with *BRAF* mutations, refractory to ICI therapy, and in patients with asymptomatic brain metastasis (91). Of the 27 patients, after a median follow-up of 18 months, ORR was 92% (3 CR, 12%), median PFS was 8.5 months, and mDOR was 5.8 months. Around 78% of patients experienced G3–4 trAEs (92).

IMspire170 is a phase III, multicenter, open-label, randomized study, which evaluated cobimetinib plus atezolizumab compared with pembrolizumab in treatment-naive patients with advanced *BRAF*V600 wild-type melanoma (NCT03273153). In the primary analysis, with a median follow-up of 7 months, the combination treatment did not significantly improve the primary endpoint of median PFS compared with pembrolizumab (5.5 versus 5.7 months). ORR was 26% with cobimetinib plus atezolizumab versus 32% with pembrolizumab; DCR was 46% versus 44%. mOS was not reached in either arm (HR: 1.06; 95% CI: 0.69–1.61). Grade ≥3 AEs occurred in 67% versus 33% of patients; AEs lead to discontinuation of all treatments in 12% versus 6% (93).

COMBI-I is a randomized, double-blind, placebo-controlled, phase III study comparing the combination of anti-PD-1 spartalizumab (PDR001) in combination with dabrafenib and trametinib versus the combination of placebo with dabrafenib and trametinib, in previously untreated patients with unresectable or metastatic *BRAF*V600 mutation-positive melanoma (94). This trial failed to meet the primary endpoint of investigator-assessed PFS according to an update on the phase III COMBI-i trial (95).

Emerging Pathways

Anti-LAG-3

Another immune checkpoint is the lymphocyte activation gene 3 (*LAG3*). It is a marker of T-cell exhaustion and negatively regulates their functions.

Initial efficacy of anti-LAG-3 antibody in combination with nivolumab in melanoma patients who progressed on or after prior treatment with anti-PD-1/PD-L1 was reported in a phase I/II trial, showing ORR of 16% and DCR of 45% (96). CA224-047 is a randomized phase II/III trial studying previously untreated metastatic or unresectable melanoma the effects of relatlimab (anti-LAG-3) in combination with nivolumab versus nivolumab alone (NCT03470922). ORR is the primary endpoint for the phase II component, while PFS is the primary endpoint for phase III. Other endpoints include OS, DOR, DCR, safety, and tolerability. The results are not yet available (97).

A first-in-human phase I dose-finding study is evaluating the antibody MK-4280 directed against LAG-3 both in combination with pembrolizumab and as monotherapy for advanced solid tumors (98).

IMP321 (eftilagimod alpha) may lead to stronger antitumor CD8 T-cell responses compared to pembrolizumab monotherapy thanks to the activation of the dendritic cell network and the subsequent T-cell recruitment at the tumor site. This is due to the fact that IMP321 is a LAG-3Ig fusion protein, and, as an MHC class-II agonist, it activates antigen-presenting cell and CD8 T cells. The TACTI-mel study is evaluating the use of eftilagimod alpha. In this multicenter, open-label, dose-escalation, phase I study there was an increase in activated CD8 and CD4 T-cell counts. ORR was observed in 33% of patients refractory PD-1 and in 50% of anti-PD-1-naive patients. The main AE was for reactions at the injection site and there were no reports of dose-limiting toxicities (99).

HDAC-Inhibitors

The immune system can be modulated by an increase of antigen expression on neoplastic cells and suppression of regulatory cells such as myeloid-derived suppressor cells and regulatory T cells. HDAC inhibitors can act on these two mechanisms and thus contrast resistance to checkpoint inhibition (100).

Entinostat (ENT) is an oral class I-selective histone deacetylase inhibitor. In the tumor microenvironment, it leads to the downregulation of immunosuppressive cell types showing synergy with anti-PD-1 inhibition in preclinical models (101). Encore-601 is an open-label phase Ib/II study evaluating ENT in combination with pembrolizumab in patients with recurrent or metastatic melanoma who progressed on or after anti-PD-1 therapy. Of the 53 evaluable patients, nine had a PR and one had a CR, with an ORR of 19% (95% CI: 9–32%). Median PFS was 4.2 months. At data cutoff, the mDOR was 12.5 months. The most common G3–4 AEs included neutropenia, fatigue, and hyponatremia (102).

Tucidinostat (HBI-8000) was evaluated in a phase Ib/II study in combination with nivolumab in patients with unresectable or advanced melanoma who were anti PD-1-naïve. The most common trAEs included fatigue, diarrhea, abdominal pain, and lymphopenia. The most frequent G ≥3 AEs were hypophosphatemia, neutropenia, thrombocytopenia and lymphopenia. ORR was 74% among 31 patients (four CR and 19 PR), with five SD and three PD. The median time to response was 1.9 months (103).

TIGIT

T-cell suppression, production, and activation, as well as tumor cell immune evasion and the inhibition of antiviral immune responses, can be regulated by immunomodulatory receptors, such as TIGIT (104). The anti-TIGIT antibody MK-7684 was studied in a multicenter phase I trial in combination with pembrolizumab. It was used in 34 patients with advanced solid tumors for whom standard treatment options had failed. The ORR was 19%, and the DCR was 47%. AEs occurred in 53% of monotherapy and 65% of combination therapy (105).

Multikinase Inhibitor

Lenvatinib (LEN) is a multikinase inhibitor of VEGFR 1–3, FGFR 1–4, PDGFRα, RET, and KIT. In preclinical studies, LEN increased infiltration of CD8+ T-cell, decreased tumor-associated macrophage populations, and improved inhibitor activity of PD-1 (106). In a multicenter phase Ib/II trial, LEN was evaluated in combination with pembrolizumab. ORR was 47.6% (95% CI: 25.7–70.2). mDOR was 12.5 months, mPFS was 7.6 months, PFS rate at 12 months was 38.3%. G3 trAEs occurred in 62% of patients, with no fatal trAEs. Most common any-grade trAEs were fatigue (52%), decreased appetite (48%), diarrhea (48%), hypertension (48%), dysphonia (43%), and nausea (43%) (107).

LEAP-004 is a phase III, single-arm, study in which patients with unresectable stage III/IV melanoma who progressed on anti-PD-1 treatments, received pembrolizumab plus lenvatinib. At a median follow-up of 12 months, the ORR was 21.4%, and 43.7% of patients achieved SD. In patients previously treated with anti-CTLA-4 plus anti-PD-1/PD-L1, the ORR was 31%. The mDOR was 6.3 months, with 72.6% of patients still responding at 6 months. mPFS was 4.2 months, and at 9 months the PFS rate was 26.2%. mOS was 13.9 months, with 65.4% of patients alive at 9 months. G ≥3 was reported in 44.7%, moving to treatment discontinuation in 7.8%. The most common AEs were hypertension (56.3%), diarrhea (35.9%), nausea (34.0%), and hypothyroidism (33.0%) (108).

IDO

Indoleamine 2,3 dioxygenase-1 (IDO) is an enzyme that when overexpressed in the tumor microenvironment makes it immunosuppressive. There are some preclinical data showing that inhibition of IDO leads to a more immunogenic tumor microenvironment (109, 110).

Inhibition of the IDO-1 enzyme can be achieved with a specific and potent oral inhibitor, such as epacadostat (111), which is being evaluated in combination with ant-PD-1 in multiple tumors type. The open-label phase I/II trial (ECHO-202/KEYNOTE-037) studying epacadostat plus pembrolizumab in patients with advanced melanoma showed promising anti-tumor activity. A total of 64 patients were enrolled in this trial. The ORR was 56% (CR: 14%), and the DCR was 71%. mPFS was 12.4 months, and 18-month PFS was 49%. Among treatment-naïve patients with advanced disease treated with 100 mg of epacadostat, ORR was 58% (CR 8%), and the DCR was 74%. Epacadostat plus pembrolizumab showed a favorable safety profile, with a 20% incidence of related G3/4 toxicity (112). Similarly, in the open-label phase I/II ECHO-204 study of patients with advanced solid tumors, epacadostat plus nivolumab was well tolerated and showed promising activity. In the 30 patients with advanced melanoma not previously treated, eight patients were treated with epacadostat 100 mg and 22 with 300 mg. In the first group, ORR was 75% and DCR was 100%. Preliminary DCR in the group treated with epacadostat 300 mg was 64% (113). After a median follow-up of 417 days, ORR was 62% and DCR was 78%. In treatment-naive patients, ORR was 65% and DCR was 80%; PFS at 6 and 12 months was 77% and 63%, respectively (median not reached); and the OS at 12 months was 92% (median not reached). More frequently reported grade ≥3 trAEs were present in 48% in patients treated with high dose (300 mg) versus 13% in

patients treated with low dose (100mg), the most common G ≥3 were rash and ALT increase. Eight patients in the arm treated with 300 mg discontinued treatment due to trAEs. There were no AE-related deaths (114).

The phase III ECHO/KEYNOTE-252 evaluated epacadostat plus pembrolizumab versus permbolizumab alone. However, no improvement in PFS and OS in unresectable stage III/IV melanoma was reported and the study was stopped after the second interim analysis with a median follow-up of 12.4 months. mPFS was 4.7 months in the combination group versus 4.9 months in the pembrolizumab group (HR: 1.00, p=0.52). mOS was not reached in either group. No differences in outcome were observed regarding to PD-L1, IDO1, or *BRAF* mutation status (115).

Pegylated IL-2

A CD122-preferential IL-2 pathway agonist, such as mempegaldesleukin (BemPEG; NKTR-214), is able to increase T-cell clonality, PD-1 expression, and tumor-infiltrating lymphocytes (116). Furthermore, adding BemPEG to nivolumab can convert baseline tumors from PD-L1 negative to PD-L1 positive (117).

In the PIVOT-02 phase I/II trial, patients with previously untreated metastatic melanoma were treated with the combination of BemPEG plus nivolumab (118). At a median follow-up of 18.6 months, the ORR was 53% (CR 34%). At a median follow-up of 29 months, mPFS for the entire cohort of 30.9 months (95% CI: 5.3–not estimable), and OS was not reached (119). Responses were not dependent upon PD-L1 expression at baseline. On-treatment biomarkers (CD8+ and eosinophils) predicted response to the combination, well before radiographic evidence. The most common G1/2 trAEs were flu-like symptoms (80.5%), rash (70.7%), fatigue (65.9%), pruritus (48.8%), nausea (46.3%), arthralgia (43.9%), decreased appetite (36.6%), and myalgia (36.6%). Registrational phase III trials evaluating BemPEG plus nivolumab are enrolling subjects in first-line metastatic melanoma treatment (CA045-001; NCT03635983).

New Engineered CTLA-4 Antibodies

MGD019 is a bispecific, Fc-bearing (IgG4) DART (dual-affinity re-targeting antibody) molecule that blocks PD-1 and CTLA-4 and shows higher activity on dual PD-1/CTLA-4-expressing cells. T-cell responses *in vitro* can be improved by MGD019 to levels reached by a combination of nivolumab and ipilimumab. This drug was evaluated in a phase I trial in patients with advanced solid tumors, demonstrating an acceptable safety profile and encouraging early evidence of anti-tumor activity. trAEs occurred in 78.8% of patients, most commonly fatigue, nausea, arthralgia, pruritus, and rash (120).

Ipilimumab non-fucosylate (NF) and ipilimumab–probody are two engineered CTLA-4 derivatives being evaluated plus nivolumab versus nivolumab alone in phase I/II trial in advanced solid cancers (NCT03994601 and NCT03369223).

STING Pathway

The Sting pathway has been recognized as a major stimulator of dendritic cells (121). A phase I dose-escalation and dose-expansion clinical trial in patients with advanced, metastatic treatment-refractory solid tumors was designed to evaluate the safety, tolerability, and clinical activity of the novel stimulator of IFN genes (STING) pathway ADU-S100. The most common trAEs were pyrexia, injection site pain, diarrhea, and headache. The combination of ADU-S100 and spartalizumab demonstrated antitumor activity in anti-PD-1-naïve triple-negative breast cancer and in melanoma formerly treated with immunotherapy; among the 25 melanoma patients radiologically evaluable for efficacy, two previously immunotherapy-treated melanoma patients achieved PR (NCT0317293). Following administration, a rise in systemic cytokines including MCP-1, IFN-β, and IL-6 were observed. This indicates target engagement of ADU-S100 and activation of the STING pathway. In a subset of patients, a rise in CD8+ T cells in injected tumors was observed in on-treatment tumor biopsies (122).

T-Cell Therapy

T-cell therapies, such as tumor-infiltrating lymphocyte (TIL) therapy, T-cell receptor (TCR) therapy, and CAR T-cell therapy, which have shown preliminary signals of activity, are ready to have an important impact in metastatic melanoma.

TIL. The TIL therapy being studied in an investigational immunotherapy study is named lifileucel (LN-144). The adoptive cell transfer therapy used in this study involves patients receiving a lymphocyte depleting preconditioning regimen, prior to infusion of autologous TIL, followed by the administration of IL-2. C-144-01 is a multicenter phase II study that evaluated the efficacy and safety of lifileucel in patients with metastatic melanoma who received at least one prior systemic therapy including an ICI and a BRAF inhibitor (if *BRAF* mutated). There were four cohorts in the study in which patients received different forms TIL therapy. In cohort 4, which received second-generation cryopreserved TILs, at a median follow-up of 5.3 months, the ORR observed was 32.4%. The DCR was 72.1% (123). Findings from cohort 4 were consistent with those reported in cohort 2, which received cryopreserved TILs. The investigator-assessed ORR for cohort 2 was 36.4% after a median follow-up of 18.7 months, the DCR was 80.3%, and responses occurred regardless of the location of the resected tumor (124). The most common any-grade AEs observed were thrombocytopenia (89.4%), chills (80.3%), and anemia (68.2%). The most common G3/4 AEs were thrombocytopenia (81.8%), anemia (56.1%) and febrile neutropenia (54.5%). Lifileucel is likely to be approved by the FDA and will likely become part of standard practice in the future.

TCR. A different approach in cancer treatment is the use of therapies exploiting genetically modified T-cells, such as T-cell receptor–engineered T-cell therapy and chimeric antigen receptor T-cell therapy, melanoma antigen recognized by T cells (MART-1), tyrosinase, and glycoprotein (gp100), as well as most antigens, are primarily found in normal melanocytes and melanomas (125, 126).

The melanoma antigene gp100 can be targeted with the first-in-class bispecific fusion protein tebentafusp; this happens through a high-affinity T-cell receptor (TCR) binding domain

and an anti-CD3 T-cell engaging domain, redirecting T cells to kill tumor cells that express gp100. It is being evaluated in a phase I/II trial in metastatic melanoma. Tebentafusp was generally well-tolerated and active in both patients with metastatic uveal melanoma and patients with metastatic cutaneous melanoma. Patients in both cohorts achieved a 1-year OS rate of 65%. Cytokine measurements during treatment were consistent with the induction of markers related with IFN-γ pathway in the tumor and periphery (127). A high-affinity MART-1-specific TCR for TCR gene therapy in metastatic melanoma was evaluated in a phase I trial in patients with metastatic melanoma (128).

A phase II trial of lymphodepleting chemotherapy followed by autologous TILs ± dendritic cells vaccine and high-dose IL-2 for patients with metastatic melanoma is ongoing (129). Patients were randomized to receive TIL alone or TIL plus dendritic cells pulsed with MART-1 peptide. In this trial, also patients with brain metastasis were included (56%). Treatments were well tolerated with no G5 AEs. There were no toxicities conferred by the dendritic cell vaccination. The ORR was 63% (5/8) in TIL + dendritic cell arm (one CR, four PR) and 40% (4/10) in TIL arm alone (one CR, three PR; P=0.64). There was no difference in survival between the arms. The median PFS was 3.6 months in the TIL arm and 7.2 months in the TIL+ dendritic cell arm, while the median OS was 4.1 years in the TIL arm and 2 years in the TIL + dendritic cell arm (130).

CONCLUSION

Metastatic melanoma has long been recognized as an immunologically affected tumor refractory to cytotoxic chemotherapy. With better characterization and understanding of the complex pathophysiology of the melanoma, the past decade has seen the progress of multiple therapies: checkpoint inhibitors and targeted therapy radically changed the prognosis of melanoma. These agents transformed the treatment of metastatic melanoma, demonstrating efficacy in a significant percentage of patients. However, what we have learned over the years is that not all patients can achieve the same benefit; in fact, if 50% of patients can be considered to be cured, there are always 50% who continue to not respond to the treatments available or develop resistance leading to tumor progression. Novel strategies are needed to further advance the standard of care, the immediate challenge is therefore to try to understand the resistance mechanisms, both primary and secondary, which prevents about 50% of patients from benefiting from these treatments, in order to increase the effectiveness of the drugs available by evaluating innovative approaches with the combination of different molecules. Novel targeted agents, particularly targeted immunotherapy, have shown great promise. The impressive results seen for targeted immunotherapy, as well as their potential use in combination regimens due to a tolerable side-effect profile, suggest many promising new paths for advancing the standard of care in refractory melanoma. The main pathways and molecules under study are investigated in this review: IDO inhibitor, TLR9 agonist, STING, oncolytic viruses, LAG-3, HDAC inhibitors, pegylated IL-2 (there are currently about 3000 trials that are evaluating immunotherapeutic combinations in different tumors). An additional emerging and very promising immune treatment is the adoptive T-cell therapy, which consists of TILs, engineered TCR therapy, and CAR-T. The goal of these treatments is to improve the cytotoxicity of cytotoxic T cells, to enhance tumor regression. TILs therapy requires the isolation of tumor-infiltrating lymphocytes from the tumors, expansion by IL-2 treatment, and reinfused into the patients with additional IL-2 treatment. TIL therapy in metastatic melanoma patients showed ORR ≥50%, with 22% of complete remission (131, 132). In the next few years, the possibility of treating melanoma patients at an early stage (i.e., in an adjuvant and neoadjuvant context) with the presence of new combinations in patients who are refractory to first-line therapies in the metastatic setting, may increase the percentage of patients who can be cured.

AUTHOR CONTRIBUTIONS

CT, JL, and PA wrote and approved the manuscript. All authors contributed to the article and approved the submitted version.

FUNDING

JL acknowledges the Department of Defense Career Development Award (W81XWH-17-1-0265), the Sy Holzer Endowed Immunotherapy Research Award, and the Hillman Fellowship for Innovative Cancer Research.

ACKNOWLEDGMENTS

Editorial assistance was provided by Aashni Shah (Polistudium SRL, Milan, Italy). This assistance was supported by internal funds.

REFERENCES

1. Bhatia S, Tykodi SS, Thompson JA. Treatment of Metastatic Melanoma: An Overview. *Oncol (Williston Park)* (2009) 23(6):488–96.
2. Fattore L, Mancini R, Ciliberto G. Cancer Stem Cells and the Slow Cycling Phenotype: How to Cut the Gordian Knot Driving Resistance to Therapy in Melanoma. *Cancers (Basel)* (2020) 12(11):3368. doi: 10.3390/cancers12113368
3. Sharma P, Allison JP. The Future of Immune Checkpoint Therapy. *Science* (2015) 348:56–61. doi: 10.1126/science.aaa8172
4. Chang F, Steelman LS, Shelton JG, Lee JT, Navolanic PM, Blalock WL, et al. Regulation of Cell Cycle Progression and Apoptosis by the Ras/Raf/MEK/ERK Pathway (Review). *Int J Oncol* (2003) 22:469–80. doi: 10.3892/ijo.22.3.469
5. Schulze A, Nicke B, Warne PH, Tomlinson S, Downward J. The Transcriptional Response to Raf Activation is Almost Completely

Dependent on Mitogen-Activated Protein Kinase Kinase Activity and Shows a Major Autocrine Component. *Mol Biol Cell* (2004) 15:3450–63. doi: 10.1091/mbc.e03-11-0807
6. Scholl FA, Dumesic PA, Khavari PA. Effects of Active MEK1 Expression In Vivo. *Cancer Lett* (2005) 230:1–5. doi: 10.1016/j.canlet.2004.12.013
7. Sullivan R, LoRusso P, Boerner S, Dummer R. Achievements and Challenges of Molecular Targeted Therapy in Melanoma. *Am Soc Clin Oncol Educ Book* (2015) 177–86. doi: 10.14694/EdBook_AM.2015.35.177
8. Spagnolo F, Ghiorzo P, Queirolo P. Overcoming Resistance to BRAF Inhibition in BRAF-mutated Metastatic Melanoma. *Oncotarget* (2014) 5 (21):10206–21. doi: 10.18632/oncotarget.2602
9. Sun C, Wang L, Huang S, Heynen GJ, Prahallad A, Robert C, et al. Reversible and Adaptive Resistance to BRAF(V600E) Inhibition in Melanoma. *Nature* (2014) 508:118–22. doi: 10.1038/nature13121
10. Long GV, Eroglu Z, Infante J, Patel S, Daud A, Johnson DB, et al. Long-Term Outcomes in Patients With BRAF V600-Mutant Metastatic Melanoma Who Received Dabrafenib Combined With Trametinib. *J Clin Oncol* (2018) 36:667–73. doi: 10.1200/JCO.2017.74.1025
11. Mocellin S, Pasquali S, Rossi CR, Nitti D. Interferon Alpha Adjuvant Therapy in Patients With High-Risk Melanoma: A Systematic Review and Meta-Analysis. *J Natl Cancer Inst* (2010) 102:493–501. doi: 10.1093/jnci/djq009
12. Gershenwald JE, Scolyer RA, Hess KR, Sondak VK, Long GV, Ross MI, et al. Melanoma Staging: Evidence-Based Changes in the American Joint Committee on Cancer Eighth Edition Cancer Staging Manual. *CA Cancer J Clin* (2017) 67:472–92. doi: 10.3322/caac.21409
13. Mocellin S, Lens MB, Pasquali S, Pilati P, Chiarion-Sileni V. Interpheron Alfa for the Adjuvant Treatment of Cutaneous Melanoma. *Cochrane Database Syst Rev* (2013) 6, CD008955. doi: 10.1002/14651858.CD008955.pub2
14. Eggermont AMM, Chiarion-Sileni V, Grob JJ, Dummer R, Wolchik JD, Schmidt H, et al. Ipilimumab Versus Placebo After Complete Resection of Stage III Melanoma. *ASCO Annu Meeting. J Clin Oncol* (2019) 37 (15_suppl):2512. doi: 10.1200/JCO.2019.37.15_suppl.2512
15. Long GV, Hauschild A, Santinami M, Atkinson V, Mandalà M, Chiarion-Sileni V, et al. Adjuvant Dabrafenib Plus Trametinib in Stage III BRAF-Mutated Melanoma. *N Eng J Med* (2017) 377:1813–23. doi: 10.1056/NEJMoa1708539
16. Ascierto PA, Del Vecchio M, Mandalà M, Gogas H, Arance AM, Dalle S, et al. Adjuvant Nivolumab Versus Ipilimumab in Resected Stage IIIB–C and Stage IV Melanoma (CheckMate 238): 4-Year Results From a Multicentre, Double-Blind, Randomised, Controlled, Phase 3 Trial. *Lancet Oncol* (2020) 21(11):1465–77. doi: 10.1016/S1470-2045(20)30494-0
17. Eggermont AMM, Kicinski M, Blank CU, Mandala M, Long GV, Atkinson V, et al. Association Between Immune-Related Adverse Events and Recurrence-Free Survival Among Patients With Stage III Melanoma Randomized to Receive Pembrolizumab or Placebo: A Secondary Analysis of a Randomized Clinical Trial. *JAMA Oncol* (2020) 6(4):519–27. doi: 10.1001/jamaoncol.2019.5570
18. Faries MB, Thompson JF, Cochran AJ, Andtbacka RH, Mozzillo N, Zager JS, et al. Completion Dissection or Observation for Sentinel-Node Metastasis in Melanoma. *N Engl J Med* (2017) 376:2211–22. doi: 10.1056/NEJMoa1613210
19. Eggermont AMM, Chiarion-Sileni V, Grob JJ, Dummer R, Wolchik JD, Schmidt H, et al. Ipilimumab Versus Placebo After Complete Resection of Stage III Melanoma: Initial Efficacy and Safety Results From the EORTC 18071 Phase III Trial. *J Clin Oncol* (2014) 32:LBA9008–LBA9008. doi: 10.1200/jco.2014.32.18_suppl.lba9008
20. Dummer R, Hauschild A, Santinami M, Atkinson V, Mandalà M, Kirkwood JM, et al. Five-Year Analysis of Adjuvant Dabrafenib Plus Trametinib in Stage III Melanoma. *N Engl J Med* (2020) 383:1139–48. doi: 10.1056/NEJMoa2005493
21. Weber J, Mandala M, Del Vecchio M, Gogas HJ, Arance AM, Cowey CL, et al. Adjuvant Nivolumab Versus Ipilimumab in Resected Stage III or IV Melanoma. *N Engl J Med* (2017) 377:1824–35. doi: 10.1056/NEJMoa1709030
22. Eggermont AMM, Blank CU, Mandala M, Long GV, Atkinson V, Dalle S, et al. Adjuvant Pembrolizumab Versus Placebo in Resected Stage III Melanoma. *N Engl J Med* (2018) 378(19):1789–801. doi: 10.1056/NEJMoa1802357
23. Eggermont AMM, Blank CU, Mandala M, Long GV, Dalle S, Haydon AM, et al. Pembrolizumab Versus Placebo After Complete Resection of High Risk Stage III Melanoma: Final Results Regarding Distant Metastasis-Free Survival Results From the EORTC 1325-MG/Keynote 054 Double-Blinded Phase 3 Trial. *Ann Oncol* (2020) 31(suppl_4):S1142–215. doi: 10.1016/j.annonc.2020.08.2276
24. Bristol Myers Squibb Announces Update on CheckMate -915 Evaluating Opdivo (Nivolumab) Plus Yervoy (Ipilimumab) Versus Opdivo in Resected High-Risk Melanoma Patients. *News release Bristol Myers Squibb* (2020).
25. Bristol-Myers Squibb Announces Update on CheckMate -915 for Opdivo (Nivolumab) Plus Yervoy (Ipilimumab) Versus Opdivo Alone in Patients With Resected High-Risk Melanoma and PD-L1 <1%. *News Release Bristol-Myers Squibb* (2019).
26. Zimmer L, Livingstone E, Hassel JC, Fluck M, Eigentler T, Loquai C, et al. Adjuvant Nivolumab Plus Ipilimumab or Nivolumab Monotherapy Versus Placebo in Patients With Resected Stage IV Melanoma With No Evidence of Disease (IMMUNED): A Randomised, Double-Blind, Placebo-Controlled, Phase 2 Trial. *Lancet* (2020) 395:1558–68. doi: 10.1016/S0140-6736(20)30417-7
27. Adams L, Chick R, Clifton G, Vreeland T, McCarthy O, O'Shea A, et al. Final Analysis of a Prospective, Randomized, Double-Blind, Placebo-Controlled Phase IIB Trial of Tumor Lysate, Particle-Loaded, Dendritic Cell Vaccine in Stage III/IV Melanoma: 36-Months Analysis. *J Immunother Cancer* (2020) 8 (Suppl 3):A1–A959. doi: 10.1136/jitc-2020-SITC2020.0300
28. Grossmann KF, Othus M, Tarhini AA, Patel SP, Moon J, Sondak VK, et al. Swog S1404: A Phase III Randomized Trial Comparing Standard of Care Adjuvant Therapy to Pembrolizumab in Patients With High Risk Resected Melanoma. *J Clin Oncol* (2016) 34(15_suppl). doi: 10.1200/JCO.2016.34.15_suppl.e21032
29. Yushak M, Mehnert J, Luke J, Poklepovic A. Approaches to High-Risk Resected Stage II and III Melanoma. *Soc Clin Oncol Educ Book* (2019) 39: e207–11. doi: 10.1200/EDBK_239283
30. Eggermont AMM, Rutkowski P, Dutriaux C, Hofman-Wellenhof R, Dziewulski P, Marples M, et al. Adjuvant Therapy With Pegylated interferon-alfa2b vs Observation in Stage II B/C Patients With Ulcerated Primary: Results of the European Organisation for Research and Treatment of Cancer 18081 Randomised Trial. *Eur J Cancer* (2020) 133:94–103. doi: 10.1016/j.ejca.2020.04.015
31. Michielin O, van Akkooi A, Lorigan P, Ascierto PA, Dummer R, Robert C, et al. ESMO Consensus Conference Recommendations on the Management of Locoregional Melanoma: Under the Auspices of the ESMO Guidelines Committee. *Ann Oncol* (2020) 31(11)1449–61. doi: 10.1016/j.annonc.2020.07.005
32. Forde PM, Chaft JE, Smith KN, Anagnostou V, Cottrell TR, Hellmann MD, et al. Neoadjuvant PD-1 Blockade in Resectable Lung Cancer. *N Engl J Med* (2018) 378(21):1976–86. doi: 10.1056/NEJMoa1716078
33. Liu J, Blake SJ, Yong MC, Harjunpää H, Ngiow SF, Takeda K, et al. Improved Efficacy of Neoadjuvant Compared to Adjuvant Immunotherapy to Eradicate Metastatic Disease. *Cancer Discovery* (2016) 6:1382–99. doi: 10.1158/2159-8290.CD-16-0577
34. Menzies AM, Amaria RN, Rozeman EA, Huang AC, Tetzlaff MT, van de Wiel BA, et al. Pathological response and survival with neoadjuvant therapy in melanoma: a pooled analysis from the International Neoadjuvant Melanoma Consortium (INMC) Pathological response and survival with neoadjuvant therapy in melanoma: a pooled analysis from the International Neoadjuvant Melanoma Consortium (INMC). *Nat Med* (2021) 27(2):301–9. doi: 10.1038/s41591-020-01188-3
35. Blank CU, Rozeman EA, Fanchi LF, Sikorska K, van de Wiel B, Kvistborg P, et al. Neoadjuvant Versus Adjuvant Ipilimumab Plus Nivolumab in Macroscopic Stage III Melanoma. *Nat Med* (2018) 24:1665–1. doi: 10.1038/s41591-018-0198-0
36. Versluis JM, Reijers ILM, Rozeman EA, Sikorska K, van Houdt WJ, van Thienen JV, et al. 1097 P 4-Year Relapse-Free Survival (RFS), Overall Survival (OS) and Long-Term Toxicity of (Neo-Adjuvant Ipilimumab (IPI) Plus Nivolumab (NIVO) in Macroscopic Stage III Melanoma - OpACIN Trial. *Ann Oncol* (2020) 31: (4):S742–3. doi: 10.1016/j.annonc.2020.08.1221

37. Blank CU, Versluis JM, Rozeman EA, Menzies AM, Reijers IL, Krijgsman O, et al. 36-Months and 18-Months Relapse-Free Survival After (Neo)Adjuvant Ipilimumab Plus Nivolumab in Macroscopic Stage III Melanoma Patients—Update of the OpACIN and OPACIN-neo Trials. *AACR Virtual Annu Meeting* (2020) 80(16 Supplement). doi: 10.1158/1538-7445.AM2020-3412
38. Amaria RN, Reddy SM, Tawbi HA, Davies MA, Ross MI, Glitza IC, et al. Neoadjuvant Immune Checkpoint Blockade in High-Risk Resectable Melanoma. *Nat Med* (2018) 24(11):1649–54. doi: 10.1038/s41591-018-0197-1
39. Rozeman EA, Menzies AM, van Akkooi ACJ, Adhikari C, Bierman C, van de Wiel BA, et al. Identification of the Optimal Combination Dosing Schedule of Neoadjuvant Ipilimumab Plus Nivolumab in Macroscopic Stage III Melanoma (OpACIN-neo): A Multicentre, Phase 2, Randomised, Controlled Trial. *Lancet Oncol* (2019) 20:948–60. doi: 10.1016/S1470-2045(19)30151-2
40. Rozeman EA, Reijers ILM, Hoefsmit EP, Sikorska K, Krijgsman O, Van De Wiel BA, et al. Twenty-Four Months RFS and Updated Toxicity Data From Opacin-Neo: A Study to Identify the Optimal Dosing Schedule of Neoadjuvant Ipilimumab (IPI) and Nivolumab (NIVO) in Stage III Melanoma. *J Clin Oncol* (2020) 38(15_suppl):10015–5. doi: 10.1200/JCO.2020.38.15_suppl.10015
41. Versluis JM, Rozeman EA, Menzies AM, Reijers ILM, Krijgsman O, Hoefsmit EP, et al. Update of the Opacin and Opacin-Neo Trials: 36-Months and 24-Months Relapse-Free Suvival After (Neo) Adjuvant Ipilimumab Plus Nivolumab in Macroscopic Stage III Melanoma Patients. *J Immunother Cancer* (2020) 8(Suppl 2):A1–A67. doi: 10.1136/jitc-2020-ITOC7.3
42. Tetzlaff MT, Messina JL, Stein JE, Xu X, Amaria RN, Blank CU, et al. Pathological Assessment of Resection Specimens After Neoadjuvant Therapy for Metastatic Melanoma. *Ann Oncol* (2018) 29:1861–8. doi: 10.1093/annonc/mdy226
43. Blank CU, Reijers ILM, Penningto T, Verskuis JM, Saw RPM, Rozeman EA, et al. First Safety and Efficacy Results of PRADO: A Phase II Study of Personalized Response-Driven Surgery and Adjuvant Therapy After Neoadjuvant Ipilimumab (IPI) and Nivolumab (NIVO) in Resectable Stage III Melanoma. *J Clin Oncol* (2020) 38(15_suppl):10002–2. doi: 10.1200/JCO.2020.38.15_suppl.10002
44. Van Den Heuvel NMJ, Reijers ILM, Versluis JM, Rozeman EA, Jóźwiak K, Blommers KH, et al. Health-Related Quality of Life in Stage III Melanoma Patients Treated With Neoadjuvant Ipilimumab and Nivolumab Followed by Index Lymph Node Excision Only Versus Therapeutic Lymph Node Dissection: 24-Week Results of the PRADO Trial. *Ann Oncol* (2020) 31 (suppl 4):S737. doi: 10.1016/j.annonc.2020.08.1209
45. Amaria RN, Prieto PA, Tetzlaff MT, Reuben A, Andrews MC, Ross MI, et al. Neoadjuvant Plus Adjuvant Dabrafenib and Trametinib Versus Standard of Care in Patients With High-Risk, Surgically Resectable Melanoma: A Single-Centre, Open-Label, Randomised, Phase 2 Trial. *Lancet Oncol* (2018) 19 (2):181–93. doi: 10.1016/S1470-2045(18)30015-9
46. Long GV, Saw RPM, Lo S, Nieweg OE, Shannon KF, Gonzalez M, et al. Neoadjuvant Dabrafenib Combined With Trametinib for Resectable, Stage IIIB–C, BRAFV600 Mutation-Positive Melanoma (NeoCombi): A Single-Arm, Open-Label, Single-Centre, Phase 2 Trial. *Lancet Oncol* (2019) 20 (7):961–71. doi: 10.1016/S1470-2045(19)30331-6
47. Dummer R, Gyorki D, Hyngstrom J, Berger A, Conry R, Demidov L, et al. *Improved Recurrence-Free Survival (RFS) From a Randomized Phase 2 Study of Neoadjuvant (Neo) Talimogene Laherparepvec (T-VEC) Plus Surgery (Surg) vs Surg for Resectable Stage IIIB-IVM1a Melanoma (MEL). Presented At: The 16th International Congress of the Society for Melanoma Research*. Salt Lake City, UT, USA (2019).
48. Dummer R, Gyorki D, Hyngstrom J, Berger A, Conry R, Demidov L, et al. 3-Year Results of the Phase 2 Randomized Trial for Talimogene Laherparepvec (T-VEC) Neoadjuvant Treatment Plus Surgery vs Surgery in Patients With Resectable Stage IIIB-IVM1a Melanoma. *J Immunother Cancer* (2020) 8. doi: 10.1136/jitc-2020-SITC2020.0432
49. Davar D, Karunamurthy A, Hartman D, DeBlasio R, Chauvin J-MJM, Ding Q, et al. Phase II Trial of Neoadjuvant Nivolumab (Nivo) and Intra-Tumoral (it) CMP-001 in High-Risk Resectable Melanoma (Neo-C-Nivo): Preliminary Results. Presented At SITC 2019. *J ImmunoTher Cancer* (2020) 8. doi: 10.1136/jitc-2020-SITC2020.0303
50. Lemke-Miltner CD, Blackwell SE, Yin C, Krug AE, Morris AJ, Krieg AM, et al. Antibody Opsonization of a TLR9 Agonist–Containing Virus-Like Particle Enhances in Situ Immunization. *J Immunol* (2020) 204(5):1386–94. doi: 10.4049/jimmunol.1900742
51. Davar D, Karunamurthy A, Hartman D, DeBlasio R, Chauvin J-MJM, Ding Q, et al. Phase II Trial of Neoadjuvant Nivolumab (Nivo) and Intra-Tumoral (it) CMP-001 in High-Risk Resectable Melanoma (Neo-C-Nivo): Final Results. *J Immunother Cancer* (2020) 8. doi: 10.1136/jitc-2020-SITC2020.0303
52. Hodi FS, O'Day SJ, McDermott DF, Weber RW, Sosman JA, Haanen JB, et al. Improved Survival With Ipilimumab in Patients With Metastatic Melanoma. *N Engl J Med* (2010) 363:711–23. doi: 10.1056/NEJMoa1003466
53. Robert C, Ribas A, Schachter J, Arance A, Grob JJ, Mortier L, et al. Pembrolizumab Versus Ipilimumab in Advanced Melanoma (KEYNOTE-006): Post-Hoc 5-Year Results From an Open-Label, Multicenter, Randomized, Controlled, Phase 3 Study. *Lancet Oncol* (2019) 20(9):1239–51. doi: 10.1016/S1470-2045(19)30388-2
54. Robert C, Long GV, Brady B, Dutriaux C, Di Giacomo AM, Mortier L, et al. *Five-Year Survival Outcomes in Patients With BRAF Wild-Type Advanced Melanoma Who Received Nivolumab Monotherapy in the Phase 3 CheckMate 066 Study. Presented At the 16th International Congress of the Society for Melanoma Research*. Salt Lake City, UT, USA (2019).
55. Larkin J, Chiarion-Sileni V, Gonzalez R, Grob JJ, Cowey CL, Lao CD, et al. Combined Nivolumab and Ipilimumab or Monotherapy in Untreated Melanoma. *N Engl J Med* (2015) 373(1):23–34. doi: 10.1056/NEJMoa1504030
56. Robert C, Schachter J, Long GV, Arance A, Grob JJ, Mortier L, et al. Pembrolizumab Versus Ipilimumab in Advanced Melanoma. *N Engl J Med* (2015) 372:2521–32. doi: 10.1056/NEJMoa1503093
57. Robert C, Long GV, Brady B, Dutriaux C, Maio M, Mortier L, et al. Nivolumab in Previously Untreated Melanoma Without BRAF Mutation. *N Engl J Med* (2015) 372(4):320–30. doi: 10.1056/NEJMoa1412082
58. Bommareddy PK, Patel A, Hossain S, Kaufman HL. Talimogene Laherparepvec (T-VEC) and Other Oncolytic Viruses for Treatment of Melanoma. *Am J Clin Dermatol* (2017) 18(1):1–15. doi: 10.1007/s40257-016-0238-9
59. Andtbacka RHI, Collichio F, Harrington KJ, Middleton MR, Downey G, Öhrling K, et al. Final Analyses of OPTiM: A Randomized Phase III Trial of Talimogene Laherparepvec Versus Granulocyte-Macrophage Colony Stimulating Factor in Unresectable Stage III– IV Melanoma. L. *J Immunother Cancer* (2019) 7:145. doi: 10.1186/s40425-019-0623-z
60. Harrington KJ, Andtbacka RH, Collichio F, Downey G, Chen L, Szabo Z, et al. Efficacy and Safety of Talimogene Laherparepvec Versus Granulocyte-Macrophage Colony-Stimulating Factor in Patients With Stage IIIB/C and IVM1a Melanoma: Subanalysis of the Phase III Optim Trial. *Onco Targets Ther* (2016) 9:7081–93. doi: 10.2147/OTT.S115245
61. Robert C, Karaszewska B, Schachter J, Rutkowski P, Mackiewicz A, Stroiakovski D, et al. Improved Overall Survival in Melanoma With Combined Dabrafenib and Trametinib. *N Engl J Med* (2015) 372:30–9. doi: 10.1056/NEJMoa1412690
62. Robert C, Grob JJ, Stroyakovskiy D, Karaszewska B, Hauschild A, Levchenko E, et al. Five-Year Outcomes With Dabrafenib Plus Trametinib in Metastatic Melanoma. *N Engl J Med* (2019) 381:626–36. doi: 10.1056/NEJMoa1904059
63. Long GV, Stroyakovskiy D, Gogas H, Levchenko E, de Braud F, Larkin J, et al. Dabrafenib and Trametinib Versus Dabrafenib and Placebo for Val600 BRAF-Mutant Melanoma: A Multicentre, Double-Blind, Phase 3 Randomised Controlled Trial. *Lancet* (2015) 386:444–51. doi: 10.1016/S0140-6736(15)60898-4
64. Larkin J, Ascierto PA, Dréno B, Atkinson V, Liszkay G, Maio M, et al. Combined Vemurafenib and Cobimetinib in BRAF-mutated Melanoma. *N Engl J Med* (2014) 371:1867–76. doi: 10.1056/NEJMoa1408868
65. McArthur GA, Dréno B, Larkin J, et al. *5-Year Survival Update of Cobimetinib Plus Vemurafenib BRAF V600 Mutation-Positive Advanced Melanoma: Final Analysis of the coBRIM Study. Presented At: The 16th International Congress of the Society for Melanoma Research*. Salt Lake City, UT, USA (2019).

66. Dummer R, Ascierto PA, Gogas HJ, Arance A, Mandala M, Liszkay G, et al. Encorafenib Plus Binimetinib Versus Vemurafenib or Encorafenib in Patients With BRAF-mutant Melanoma (COLUMBUS): A Multicentre, Open-Label, Randomised Phase 3 Trial. *Lancet Oncol* (2018) 19:603–15. doi: 10.1016/S1470-2045(18)30142-6
67. Ascierto PA, Dummer R, Gogas HJ, Flaherty KT, Arance A, Mandala M, et al. Update on Tolerability and Overall Survival in COLUMBUS: Landmark Analysis of a Randomised Phase 3 Trial of Encorafenib Plus Binimetinib vs Vemurafenib or Encorafenib in Patients With BRAF V600-Mutant Melanoma. *Eur J Cancer* (2020) 126:33–44. doi: 10.1016/j.ejca.2019.11.016
68. Gutzmer R, Stroyakovskiy D, Gogas H, Robert C, Lewis K, Protsenko S, et al. Atezolizumab, Vemurafenib, and Cobimetinib as First-Line Treatment for Unresectable Advanced BRAFV600 Mutation Positive Melanoma (Imspire150): Primary Analysis of the Randomised, Double-Blind, Placebo-Controlled, Phase 3 Trial. *Lancet* (2020) 395(10240):1835–44. doi: 10.1016/S0140-6736(20)30934-X
69. Dummer R, Ascierto PA, Gogas HJ, Arance A, Mandala M, Liszkay G, et al. Overall Survival in Patients With BRAF-mutant Melanoma Receiving Encorafenib Plus Binimetinib Versus Vemurafenib or Encorafenib (COLUMBUS): A Multicentre, Open-Label, Randomised, Phase 3 Trial. *Lancet Oncol* (2018) 19(10):1315–27. doi: 10.1016/S1470-2045(18)30497-2
70. Postow MA, Goldman DA, Shoushtari AN, Warner AB, Callahan MK, Momtaz P, et al. A Phase II Study to Evaluate the Need for > Two Doses of Nivolumab + Ipilimumab Combination (Combo) Immunotherapy. *J Clin Oncol* (2020) 38(15_suppl):10003–3. doi: 10.1200/JCO.2020.38.15_suppl.10003
71. Lebbé C, Meyer N, Mortier L, Marquez-Rodas I, Robert C, Rutkowski P, et al. Evaluation of Two Dosing Regimens for Nivolumab in Combination With Ipilimumab in Patients With Advanced Melanoma: Results From the Phase IIIb/IV CheckMate 511 Trial. *J Clin Oncol* (2019) 37(11):867–75. doi: 10.1200/JCO.18.01998
72. Da Silva IP, Ahmed T, Lo S, Reijers ILM, Weppler A, Warner AB, et al. Ipilimumab (IPI) Alone or in Combination With anti-PD-1 (IPI+PD1) in Patients (Pts) With Metastatic Melanoma (MM) Resistant to PD1 Monotherapy. *J Clin Oncol* (2019) 38(15_suppl):10005–5. doi: 10.1200/JCO.2020.38.15_suppl.10005
73. Olson D, Luke JJ, Poklepovic AS, Bajaj M, Higgs E, Carll TC, et al. Significant Antitumor Activity for Low-Dose Ipilimumab (IPI) With Pembrolizumab (PEMBRO) Immediately Following Progression on PD1 Ab in Melanoma (MEL) in a Phase II Trial. Presented At: The 2020 ASCO Annual Meeting; may 29-31, 2020. Abstract 10004. *J Clin Oncol* 38(15_suppl):10004. doi: 10.1200/JCO.2020.38.15_suppl.10004
74. Chesney J, Puzanov I, Collichio F, Singh P, Milhem MM, Glaspy J, et al. Randomized, Open-Label Phase II Study Evaluating the Efficacy and Safety of Talimogene Laherparepvec in Combination With Ipilimumab Versus Ipilimumab Alone in Patients With Advanced, Unresectable Melanoma. *J Clin Oncol* (2018) 36(17):1658–67. doi: 10.1200/JCO.2017.73.7379
75. Puzanov I, Chesney J, Collichio F, Singh P, Milhem M, Glaspy J, et al. Talimogene Laherparepvec (T-VEC) in Combination With Ipilimumab (IPI) Versus IPI Alone for Advanced Melanoma: 4-Year Interim Analysis of a Randomized, Open-Label, Phase 2 Trial. *J Immunother Cancer* (2020) 8. doi: 10.1136/jitc-2020-SITC2020.0433
76. Long G, Dummer R, Andtbacka RH. Follow-Up Analysis of MASTERKEY-265 Phase 1b (ph1b) Trial of Talimogene Laherparepvec (T-VEC) in Combination (Combo) With Pembrolizumab (Pembro) in Patients (Pts) With Unresectable Stage IIIB–IVM1c Melanoma (MEL). *Pigment Cell Melanoma Res* (2019) 32:133–4. doi: 10.1136/jitc-2020-SITC2020.0429
77. Long G, Dummer R, Johnson D, Michielin O, Martin-Algarra S, Treichel S, et al. Long-Term Analysis of MASTERKEY-265 Phase IB Trial of Talimogene Laherparepved (T-VEC) Plus Pembrolizumab in Patients With Unresectable Stage IIIB-IVM1C Melanoma. *J Immunother Cancer* (2020) 8(Suppl 3):A337–655. doi: 10.1136/jitc-2020-SITC2020.0429
78. Haymaker C, Uemura M, Hwu W-J, Murthy R, James M, Bhatta A, et al. TLR9 Agonist Harnesses Innate Immunity to Drive Tumor-Infiltrating T Cell Expansion in Distant Lesions in a Phase 1/2 Study of Intratumoral IMO-2125+ipilimumab in anti-PD1 Refractory Melanoma Patients. *J Immunother Cancer* (2017) 5(Suppl 2):018.
79. Diab A, Haymaker C, Uemura M, Murthy R, James M, Geib J, et al. A Phase 1/2 Trial of Intratumoral (I.T.) IMO-2125 (IMO) in Combination With Checkpoint Inhibitors (CPI) in PD-(L)1-refractory Melanoma. *Ann Oncol* (2017) 28(suppl_5):v403–27. doi: 10.1093/annonc/mdx376.052
80. Haymaker C, Andtbacka RHI, Johnson DB, Shaheen MF, Rahimian S, Chunduru S, et al. 1083mo - Final Results From ILLUMINATE-204, a Phase I/II Trial of Intratumoral Tilsotolimod in Combination With Ipilimumab in PD-1 Inhibitor Refractory Advanced Melanoma. *Ann Oncol* (2020) 31(suppl_4):S672–710. doi: 10.1016/annonc/annonc280
81. Milhem MM, Long GV, Hoimes CJ, Amin A, Lao CD, Conry RM, et al. Phase 1b/2, Open Label, Multicenter, Study of the Combination of SD-101 and Pembrolizumab in Patients With Advanced Melanoma Who are Naïve to anti-PD-1 Therapy. *J Clin Oncol* (2019) 37(15_suppl):9534–4. doi: 10.1200/JCO.2019.37.15_suppl.9534
82. Milhem M, Zakharia Y, Davar D, Buchbinder E, Medina T, Daud A, et al. Durable Responses in Anti PD-1 Refractor Melanoma Following Intratumoral Injection of Toll-like Receptor 9 (TLR9) Agonist CMP-001, in Combination With Pembrolizumab. *J Immunother Cancer* (2020) 8. doi: 10.1136/LBA2019.4
83. Milhem M, Zakharia Y, Davar D, Buchbinder E, Medina E, Daud A, et al. Intratumoral Injection of CMP-001, a Toll-Like Receptor (TLR-9) Agonist, in Combination With Pembrolizumab Reversed Programmed Death Receptor 1 (PD-1) Blockade Resistance in Advanced Melanoma. *J Immunother Cancer* (2020) 8(Suppl 3):A1–A959. doi: 10.1136/jitc-2020-SITC2020.0304
84. Algazi A, Bhatia S, Agarwala S, Molina M, Lewis K, Faries M, et al. Intratumoral Delivery of Tavokinogene Telseplasmid Yields Systemic Immune Responses in Metastatic Melanoma Patients. *Ann Oncol* (2020) 31(4):532–40. doi: 10.1016/j.annonc.2019.12.008
85. Algazi AP, Twitty CG, Tsai KK, Atkinson V, Shaheen M, Thomas S, et al. Phase II Trial of IL-12 Plasmid Transfection and PD-1 Blockade in Immunologically Quiescent Melanoma. *Clin Cancer Res* (2020) 26 (12):2827–37. doi: 10.1158/1078-0432.CCR-19-2217
86. Fernandez-Penas P, Carlino MS, Tsai KK, et al. *Durable Responses and Immune Activation With Intratumoral Electroporation of pIL-12 Plus Pembrolizumab in Actively Progressing anti-PD-1 Refractory Advanced Melanoma: KEYNOTE 695 Interim Data. Presented At: 2020 SITC Annual Meeting; November 10-15, 2020; Virtual. Abstract 799.*
87. Beasley GM, Farrow NE, Landa K, Selim MA, Jung S-H, Bigner DD, et al. A Phase I Trial of Intratumoral PVSRIPO in Patients With Unresectable Treatment Refractory Melanoma. Presented At: 2020 SITC Annual Meeting; November 9-14, 2020; Virtual. Abstract 302. *J Immunother Cancer* (2021) 9:e002203. doi: 10.1136/jitc-2020-002203
88. Ribas A, Hersey P, Middleton MR, Gogas H, Flaherty KT, Sondak VK, et al. New Challenges in Endpoints for Drug Development in Advanced Melanoma. *Clin Cancer Res* (2012) 18(2):336–41. doi: 10.1158/1078-0432.CCR-11-2323
89. Ribas A, Hodi FS, Lawrence D, Atkinson V, Agarwal S, Carlino MS, et al. Keynote-022 Update: Phase 1 Study of First-Line Pembrolizumab (Pembro) Plus Dabrafenib (D) and Trametinib (T) for BRAF Mutant Advanced Melanoma. *Ann Oncol* (2017) 28:V430. doi: 10.1093/annonc/mdx377.003
90. Ferrucci PF, Di Giacomo AM, Del Vecchio M, Atkinson V, Schmidt H, Schachter J, et al. Keynote-022 Part 3: A Randomized, Double-Blind, Phase 2 Study of Pembrolizumab, Dabrafenib, and Trametinib in BRAF-mutant Melanoma. *J Immunother Cancer* (2020) 8:e001806. doi: 10.1136/jitc-2020-001806
91. Tawbi HAH, Amaria RN, Glitza IC, Milton D, Hwu WJ, Patel SP, et al. Safety and Preliminary Activity Data From a Single Center Phase II Study of Triplet Combination of Nivolumab (N) With Dabrafenib (D) and Trametinib (T) [Trident] in Patients (Pts) With BRAF-mutated Metastatic Melanoma (MM). *J Clin Oncol* (2018) 36:9560–0. doi: 10.1200/JCO.2018.36.15_suppl.9560
92. Burton EM, Amaria RN, Glitza IC, Shephard M, Diab A, Milton D, et al. Safety and Efficacy of TRiplet Combination of Nivolumab With Dabrafenib and Trametinib [TrideNT] in Patients With BRAF-mutated Metastatic Melanoma: A Single Center Phase II Study. *Ann Oncol* (2019) 30 (suppl_5):v533–63. doi: 10.1093/annonc/mdz255

93. Arance AM, Gogas H, Dreno B, Flaherty KT, Demidov L, Stroyakovskiy D, et al. Combination Treatment With Cobimetinib (C) and Atezolizumab (a) vs Pembrolizumab (P) in Previously Untreated Patients (Pts) With BRAFV600 Wild Type (Wt) Advanced Melanoma: Primary Analysis From the Phase 3 IMspire170 Trial. *Ann Oncol* (2019) 30(suppl_5):v851–934. doi: 10.1093/annonc/mdz394.066
94. Dummer R, Fernández AMA, Hansson J, Larkin JMG, Long GV, Gasal E, et al. Preliminary Findings From Part 1 of COMBI-i: A Phase III Study of Anti–PD-1 Antibody PDR001 Combined With Dabrafenib (D) and Trametinib (T) in Previously Untreated Patients (Pts) With Advanced BRAF V600-Mutant Melanoma. *J Clin Oncol* (2018) 36:189–9. doi: 10.1200/JCO.2018.36.5_suppl.189
95. Nathan PD, Dummer R, Long GV, Ascierto PA, Tawbi H, Robert C, et al. Spartalizumab Plus Dabrafenib and Trametinib (Sparta-DabTram) in Patients (Pts) With Previously Untreated BRAF V600–Mutant Unresectable or Metastatic Melanoma: Results From the Randomized Part 3 of the Phase Iii COMBI-i Trial. *Ann Oncol* (2020) 31(suppl_4):S1142–215. doi: 10.1016/j.annonc.2020.08.2273
96. Ascierto PA, Melero I, Bhatia S, Bobo P, Sanborn RE, Lipson EJ, et al. Initial Efficacy of Anti-Lymphocyte Activation Gene-3 (Anti–LAG-3; BMS-986016) in Combination With Nivolumab (Nivo) in Pts With Melanoma (MEL) Previously Treated With Anti–PD-1/PD-L1 Therapy. *J Clin Oncol* (2017) 35(15_suppl):9520–0. doi: 10.1200/JCO.2017.35.15_suppl.9520
97. Lipson EJ, Long GV, Tawbi H, Schadendorf D, Atkinson, Maurer M, et al. Ca224-047: A Randomized, Double-Blind, Phase 2/3 Study of Relatlimab (anti-LAG-3) in Combination With Nivolumab (anti-PD-1) Versus Nivolumab Alone in Previously Untreated Metastatic or Unresectable Melanoma. *Ann Oncol* (2018) 29(suppl_8):viii442–viii466. doi: 10.1093/annonc/mdy289.058
98. Lakhani N, Bauer TM, Abraham AK, Luddy J, Palcza J, Chartash E, et al. *The Anti–LAG-3 Antibody MK-4280 as Monotherapy and in Combination With Pembrolizumab for Advanced Solid Tumors: First-in-Human Phase 1 Dose-Finding Study. 2018 SITC Annual Meeting. Abstract O26. Presented November 9, 2018.*
99. Atkinson V, Khattak A, Haydon A, Eastgate M, Roy A, Prithviraj P, et al. Eftilagimod Alpha, a Soluble Lymphocyte Activation Gene-3 (LAG-3) Protein Plus Pembrolizumab in Patients With Metastatic Melanoma. *J Immunother Cancer* (2020) 8:e001681. doi: 10.1136/jitc-2020-001681
100. Marks PA, Jiang X. Histone Deacetylase Inhibitors in Programmed Cell Death and Cancer Therapy. *Cell Cycle* (2005) 4:549–51. doi: 10.4161/cc.4.4.1564
101. Cao K, Wang G, Li W, Zhang L, Wang R, Huang Y, et al. Histone Deacetylase Inhibitors Prevent Activation-Induced Cell Death and Promote Anti-Tumor Immunity. *Oncogene* (2015) 34(49):5960–70. doi: 10.1038/onc.2015.46
102. Sullivan RJ, Moschos SJ, Johnson ML, Opyrchal M, Ordentlich P, Brouwer S, et al. *Efficacy and Safety of Entinostat (ENT) and Pembrolizumab (PEMBRO) in Patients With Melanoma Previously Treated With anti-PD-1 Therapy. Presented At: 2019 AACR Annual Meeting; March 29-April 3.* Atlanta, GA (2019) 79(13 Supplement). p. CT072. doi: 10.1158/1538-7445.AM2019-CT072
103. Khushalani NI, Brohl AS, Markowitz J, Bazhenova L, Daniels GA, Yeckes-Rodin H, et al. Significant Anti-Tumor Activity of HBI-8000, a Class I Histone Deacetylase Inhibitor (Hdaci) in Combination With Nivolumab (NIVO) in anti-PD1 Therapy-Naïve Advanced Melanoma (TN-Mel). *J Immunother Cancer* (2020) 8. doi: 10.1136/jitc-2020-SITC2020.0797
104. Yu X, Harden K, Gonzalez LC, Francesco M, Chiang E, Irving B, et al. The Surface Protein TIGIT Suppresses T Cell Activation by Promoting the Generation of Mature Immunoregulatory Dendritic Cells. *Nat Immunol* (2009) 10:48–57. doi: 10.1038/ni.1674
105. Golan T, Bauer TM, Jimeno A, Perets R, Niu J, Lee JJ. Phase 1 Dose-Finding Study of the anti-TIGIT Antibody MK-7684 as Monotherapy and in Combination With Pembrolizumab in Patients With Advanced Solid Tumors. 2018 SITC Annual Meeting. Abstract O25. Presented November 9. (2018) Available at: https://sitc.sitcancer.org/2018/abstracts/titles/?category=Combination+Therapy.
106. Glen H, Mason S, Patel H, Macleod K, Brunton VG. E7080, a Multi-Targeted Tyrosine Kinase Inhibitor Suppresses Tumor Cell Migration and Invasion. *BMC Cancer* (2011) 11:309. doi: 10.1186/1471-2407-11-309
107. Taylor MH, Vogelzang NJ, Cohn AL, Stepan D, Shumaker RC, Dutcus CE, et al. Phase Ib/II Trial of Lenvatinib Plus Pembrolizumab in Advanced Melanoma. *J Clin Oncol* (2019) 37(8_suppl):15. doi: 10.1200/JCO.2019.37.8_suppl.15
108. Arance Fernandez AM, O'Day SJ, de la Cruz Merino L, Petrella T, Jamal R, Ny L, et al. Lenvatinib Plus Pembrolizumab for Advanced Melanoma That Progressed on a PD-1 or PD-L1 Inhibitor: Initial Results of LEAP-004. *Ann Oncol* (2020) 31(suppl_4):S1142–215. doi: 10.1016/annonc/annonc325
109. Muller AJ, DuHadaway JB, Donover PS, Sutanto-Ward E, Prendergast GC. Inhibition of Indoleamine 2,3-Dioxygenase, an Immunoregulatory Target of the Cancer Suppression Gene Bin1, Potentiates Cancer Chemotherapy. *Nat Med* (2005) 11:312–9. doi: 10.1038/nm1196
110. Spranger S, Koblish HK, Horton B, Scherle PA, Newton R, Gajewski TF. Mechanism of Tumor Rejection With Doublets of CTLA-4, Pd-1/Pd-L1, or IDO Blockade Involves Restored IL-2 Production and Proliferation of CD8 (+) T Cells Directly Within the Tumor Microenvironment. *J Immunother Cancer* (2014) 2:3. doi: 10.1186/2051-1426-2-3
111. Liu X, Shin N, Koblish HK, Yang G, Wang Q, Wang K, et al. Selective Inhibition of IDO1 Effectively Regulates Mediators of Anti Tumor Immunity. *Blood* (2010) 115:3520–30. doi: 10.1182/blood-2009-09-246124
112. Hamid O, Gajewski TF, Frankel AE, Bauer TM, Olszanski AJ, Luke JJ, et al. Epacadostat Plus Pembrolizumab in Patients With Advanced Melanoma: Phase 1 and 2 Efficacy and Safety Results From ECHO-202/KEYNOTE-037. *Ann Oncol* (2017) 28428(suppl 5):abstr 12140. doi: 10.1093/annonc/mdx377.001
113. Perez RP, Riese MJ, Lewis KD, Lewis KD, Saleh MN, Daud A, et al. Epacadostat Plus Nivolumab in Patients With Advanced Solid Tumors: Preliminary Phase I/II Results of ECHO-204. *J Clin Oncol* (2017) 3003(15 suppl):3003. doi: 10.1200/JCO.2017.35.15_suppl.3003
114. Daud A, Saleh MN, Hu J, Bleeker JS, Riese MJ, Meier R, et al. Epacadostat Plus Nivolumab for Advanced Melanoma: Updated Phase 2 Results of the ECHO-204 Study. *J Clin Oncol* (2018) 36(15_suppl):9511–1. doi: 10.1200/JCO.2018.36.15_suppl.9511
115. Long GV, Dummer R, Hamid O, Gajewski TF, Caglevic C, Dalle S, et al. Epacadostat Plus Pembrolizumab Versus Placebo Plus Pembrolizumab in Patients With Unresectable or Metastatic Melanoma (ECHO-301/KEYNOTE-252): A Phase 3, Randomised, Double-Blind Study. *Lancet Oncol* (2019) 20(8):1083–97. doi: 10.1016/S1470-2045(19)30274-8
116. Charych D, Khalili S, Dixit V, Kirk P, Chang T, Langowski J, et al. Modeling the Receptor Pharmacology, Pharmacokinetics, and Pharmacodynamics of NKTR-214, a Kinetically-Controlled Interleukin-2 (IL2) Receptor Agonist for Cancer Immunotherapy. *PloS One* (2017) 12:e0179431. doi: 10.1371/journal.pone.0179431
117. Diab A, Tykodi S, Curti B, Cho D, Wong M, Puzanov I, et al. *Immune Monitoring After NKTR-214 Plus Nivolumab (PIVOT-02) in Previously Untreated Patients With Metastatic Stage IV Melanoma. Oral Presentation At SITC.* Washington, DC, United States (2018). p. O4.
118. Diab A, Puzanov I, Maio M, Curti B, Bilen M, Lewis K, et al. Clinical Activity of BEMPEG Plus NIVO in Previously Untreated Patients With Metastatic Melanoma: Updated Results From the Phase 1/2 PIVOT-02 Study. *J Transl Med* (2020) 18(Suppl 1):50.
119. Diab A, Tykodi SS, Daniels GA, Maio M, Curti B, Lewis K, et al. Progression-Free Survival and Biomarker Correlates of Response With BEMPEG Plus NIVO in Previously Untreated Patients With Metastatic Melanoma: Results From the PIVOT-02 Study. Presented At: Society for Immunotherapy of Cancer 35th Anniversary Annual Meeting & Preconference Programs (Sitc 2020); November 11-14, 2020. Abstract 420. *J Immunother Cancer* (2020) 8 (Suppl 3):A656–959. doi: 10.1136/jitc-2020-SITC2020.0420
120. Sharma M, Sanborn RE, Cote GM, Bendell JC, Kaul S, Chen F, et al. First-in-Human, Open-Label, Dose Escalation Study of MGD019, an Investigational Bispecific PD-1 X CTLA-4 DART® Molecule in Patients With Advanced Solid Tumours. *Ann Oncol* (2020) 31(suppl_4):S645–71. doi: 10.1016/j.annonc.2020.08.1140
121. Vatner RE, Janssen EM. Sting, DCs and the Link Between Innate and Adaptive Tumor Immunity. *Mol Immunol* (2019) 110:13–23. doi: 10.1016/j.molimm.2017.12.001
122. Bernstam-Meric F, Sandhu SK, Hamid O, Spreafico A, Kasper S, Dummer R, et al. Phase Ib Study of MIW815 (Adu-S100) in Combination With Spartalizumab (PDR001) in Patients (Pts) With Advanced/Metastatic Solid Tumors or Lymphomas. *J Clin Oncol* (2019) 37(15_suppl):2507–7. doi: 10.1200/JCO.2019.37.15_suppl.2507

123. *Iovance Reports Pivotal Cohort 4 Data for Tumor Infiltrating Lymphocyte (TIL) Therapy Lifileucel From C-144-01 Clinical Study in Advanced Melanoma. News Release. Iovance Biotherapeutics, Inc*. Available at: https://www.globenewswire.com/news-release/2020/05/27/2039716/0/en/Iovance-Reports-Pivotal-Cohort-4-Data-for-Tumor-Infiltrating-Lymphocyte-TIL-Therapy-Lifileucel-from-C-144-01-Clinical-Study-in-Advanced-Melanoma.html (Accessed June 1, 2020).
124. Sarniak A, Khushalani NI, Chesney JA, Lewis KD, Medina TM, HM K, et al. Long-Term Follow Up of Lifileucel (LN-144) Cryopreserved Autologous Tumor Infiltrating Lymphocyte Therapy in Patients With Advanced Melanoma Progressed on Multiple Prior Therapies. *J Clin Oncol* (2020) 38 (suppl):10006. doi: 10.1200/JCO.2020.38.15_suppl.10006
125. Kawakami Y, Eliyahu S, Sakaguchi K, Robbins PF, Rivoltini L, Yannelli JR, et al. Identification of the Immunodominant Peptides of the MART-1 Human Melanoma Antigen Recognized by the Majority of HLA-A2-restricted Tumor Infiltrating Lymphocytes. *J Exp Med* (1994) 180(1):1–6. doi: 10.1084/jem.180.1.347
126. Salgaller ML, Afshar A, Marincola FM, Rivoltini L, Kawakami Y, Rosenberg SA. Recognition of Multiple Epitopes in the Human Melanoma Antigen gp100 by Peripheral Blood Lymphocytes Stimulated In Vitro With Synthetic Peptides. *Cancer Res* (1995) 55(21):4972–9.
127. Middleton MR, McAlpine C, Woodcock VK, Corrie P, Infante JR, Steven NM, et al. Tebentafusp, A Tcr/Anti-CD3 Bispecific Fusion Protein Targeting gp100, Potently Activated Antitumor Immune Responses in Patients With Metastatic Melanoma. *Clin Cancer Res* (2020) 26:5869–78. doi: 10.1158/1078-0432.CCR-20-1247
128. Rohaan MW, Gomez-Eerland R, Geukes Foppen MH, van Zon M, de Boer R, Bakker NAM, et al. Results of a Phase I Trial With MART-1 T Cell Receptor Modified T Cells in Patients With Metastatic Melanoma. *Abstract Immunother Cancer* (2019) 30(Suppl 5):V481–482. doi: 10.1093/annonc/mdz253.010
129. Nguyen LT, Saibil SD, Sotov V, Le MX, Khoja L, Ghazarian D, et al. Phase II Clinical Trial of Adoptive Cell Therapy for Patients With Metastatic Melanoma With Autologous Tumor-Infiltrating Lymphocytes and Low-Dose Interleukin-2. *Cancer Immunol Immunother* (2019) 68(5):773–85. doi: 10.1007/s00262-019-02307-x
130. Saberian C, Amaria RN, Haymaker C, Forget MA, Bassett RL, Glitza IC, et al. Phase II Trial of Lymphodepletion Plus Adoptive Cell Transfer With or Without Dendritic Cell Vaccination in Patients With Metastatic Melanoma. *J Immunother Cancer* (2020) 8(Suppl 3):A337–655. doi: 10.1136/jitc-2020-SITC2020.0311
131. Rosenberg SA, Yang JC, Sherry RM, Kammula US, Hughes MS, Phan GQ, et al. Durable Complete Responses in Heavily Pretreated Patients With Metastatic Melanoma Using T-cell Transfer Immunotherapy. *Clin Cancer Res* (2011) 17:4550–7. doi: 10.1158/1078-0432.CCR-11-0116
132. Besser MJ, Shapira-Frommer R, Treves AJ, Zippel D, Itzhaki O, Hershkovitz L, et al. Clinical Responses in a Phase II Study Using Adoptive Transfer of Short-Term Cultured Tumor Infiltration Lymphocytes in Metastatic Melanoma Patients. *Clin Cancer Res* (2010) 16:2646–55. doi: 10.1158/1078-0432.CCR-10-0041

Conflict of Interest: PA has/had a consultant/advisory role for Bristol Myers Squibb, Roche-Genentech, Merck Sharp & Dohme, Novartis, Array, Merck Serono, Pierre-Fabre, Incyte, Medimmune, AstraZeneca, Syndax, Sun Pharma, Sanofi, Idera, Ultimovacs, Sandoz, Immunocore, 4SC, Alkermes, Italfarmaco, Nektar, Boehringer-Ingelheim, Eisai, Regeneron, Daiichi Sankyo, Pfizer, Oncosec, Nouscom, Takis, Lunaphore, Seagen. He also received research funding from Bristol Myers Squibb, Roche-Genentech, Array, Sanofi, and travel support from MSD. JL declares Scientific Advisory Board: (no stock) 7 Hills, Spring bank (stock) Actym, Alphamab Oncology, Arch Oncology, Kanaph, Mavu, Onc.AI, Pyxis, Tempest. Consultancy with compensation: Abbvie, Array, Bayer, Bristol-Myers Squibb, Checkmate, Cstone, Eisai, EMD Serono, KSQ, Janssen, Merck, Mersana, Nektar, Novartis, Pfizer, Regeneron, Ribon, Rubius, Silicon, Tesaro, TRex, Werewolf, Xilio, Xencor. Research Support: (all to institutions for clinical trials unless noted) AbbVie, Agios (IIT), Array (IIT), Astellas, Bristol-Myers Squibb (IIT & industry), Corvus, EMD Serono, Immatics, Incyte, Kadmon, Macrogenics, Merck, Moderna, Nektar, Numab, Replimmune, Rubius, Spring bank, Synlogic, Takeda, Trishula, Tizona, Xencor. Travel: Pyxis. Patents: (both provisional) Serial #15/612,657 (Cancer Immunotherapy), PCT/US18/36052 (Microbiome Biomarkers for Anti-PD-1/PD-L1 Responsiveness: Diagnostic, Prognostic, and Therapeutic Uses Thereof).

The remaining author declares that the research was conducted in the absence of any commercial or financial relationships that could be construed as a potential conflict of interest.

Advantages of publishing in Frontiers

OPEN ACCESS
Articles are free to read for greatest visibility and readership

FAST PUBLICATION
Around 90 days from submission to decision

HIGH QUALITY PEER-REVIEW
Rigorous, collaborative, and constructive peer-review

TRANSPARENT PEER-REVIEW
Editors and reviewers acknowledged by name on published articles

Frontiers
Avenue du Tribunal-Fédéral 34
1005 Lausanne | Switzerland

Visit us: www.frontiersin.org
Contact us: frontiersin.org/about/contact

REPRODUCIBILITY OF RESEARCH
Support open data and methods to enhance research reproducibility

DIGITAL PUBLISHING
Articles designed for optimal readership across devices

FOLLOW US
@frontiersin

IMPACT METRICS
Advanced article metrics track visibility across digital media

EXTENSIVE PROMOTION
Marketing and promotion of impactful research

LOOP RESEARCH NETWORK
Our network increases your article's readership